Synthetic and Mechanistic Studies into the Activation of Terminal Alkynes by a Ruthenium Acetate Complex

Christine E. Welby

PhD

University of York

Chemistry

2011

Abstract

A variety of novel organometallic complexes have been easily prepared from the ruthenium precursor complex **1** (*cis*-[Ru(κ^2-OAc)$_2$(PPh$_3$)$_2$]. This complex itself is synthesised from readily available starting materials. The family of organometallic complexes derived from complex **1** include carbonyl, nitrosyl, carbene, vinylidene and acetylide derivatives. A number of these complexes share a common structure, as evidenced by X-Ray crystallographic studies, as well as several spectroscopic features. The differing donor/acceptor properties of these ancillary ligands may be detected by a comparison of these common structural and spectroscopic features.

The addition of terminal alkynes (HC≡CR) to complex **1** results in the rapid formation of vinylidene complexes [Ru(κ^1-OAc)(κ^2-OAc)(=C=CHR)(PPh$_3$)$_2$], whilst the addition of propargylic alcohols (HC≡C{R}{R'}OH) results in the equally rapid formation of hydroxy-vinylidene complexes [Ru(κ^1-OAc)(κ^2-OAc)(=C=CHC{R}{R'}OH)(PPh$_3$)$_2$]. The rapid formation of these vinylidene complexes has been attributed to the assistance provided by a coordinated acetate ligand. A comprehensive DFT study has shown how the acetate ligand is able to behave as both acid and base, acting as a proton shuttle, to facilitate the alkyne-to-vinylidene tautomerisation. This process has been termed a **L**igand-**A**ssisted **P**roton **S**huttle (**LAPS**), which is related to the AMLA/CMD process that also facilitates the formation of acetylide complexes

The novel hydroxy-vinylidene complexes are not observed to undergo the typical dehydration process to form an allenylidene derivative. Instead, a conversion to a carbonyl complex with the concomitant formation of an alkene is observed. An experimental investigation using ^{18}O-labelling, kinetic and stoichiometric studies into the mechanism of this conversion has once more demonstrated the chemically non-innocent behaviour of an acetate ligand.

List of Contents

List of Tables and Illustrations

Chapter 1: Introduction

Chapter 2: Synthesis and Characterisation of novel Ruthenium Vinylidene complexes

Chapter 4: Mechanistic Studies on the Formation of Ruthenium Vinylidene and Acetylide complexes

Chapter 6: Mechanistic Studies on the Decarbonylation of Propargylic Alcohols

Chapter 7: Synthesis and Characterisation of novel Ruthenium Oxacyclocarbene complexes.

Chapter 8: A Comparison of Structural and Spectroscopic Features of Acetate-Containing Complexes derived from $[Ru(\kappa^2\text{-}OAc)_2(PPh_3)_2]$.

List of Accompanying Material

1. **CD-ROM Containing .cif files of crystal structures**

Acknowledgements

I would firstly like to thank my supervisor Dr. Jason Lynam, whose unrelenting enthusiasm over the past 5 years has been such an inspiration. Working in his lab for my undergraduate final year project made me realise that real research is nothing like teaching labs (thank goodness). Thank you also for being the first to believe that I could do this PhD.

To the past and present members of the SLUGs; Tracy – who taught me to treat everything as air-sensitive, Mike – for always being interested in what I was working on, and David Zhang – my organic chemistry guru. Lee, Tony, Luisa, Aimee, Ollie, Lizzie, Sharifa, Neets, Rich, Dave – it was wonderful to work alongside such a brilliant, lovely bunch of people these past few years. I will miss being a part of this group very much. A significant thank you also to David Johnson and Dr. John Slattery for all the computational work that has gone into this thesis – thank you for giving me answers my experiments couldn't and for being patient with such a DFT newb, particularly when the 'computer said no.' Thanks also to the undergraduate students who have passed through the group; especially Luke, Thomas and Nick whose results have contributed to this thesis.

Thanks also to Emma – for making sure I had my tea/coffee/chocolate break on time and to Maria, Abeda, Stephen, Cath and Áine who made break times essential. Thanks to Amanda, for being a wonderful conference companion, and Joby, who has been such a great friend for 8 years.

I'd also like to thank the experimental technicians who essentially run this department; to Heather Fish and Dave Williamson for help with NMR; Trevor Dransfield and Karl Heaton for Mass Spec; Phil Helliwell and Graeme McAllister for CHN and especially Adrian Whitwood and Rob Thatcher for XRD. Special thanks also to Naser whose ability to find/fix almost anything in this department is renowned.

Finally to my family, who have supported me throughout my time in York, both in my undergrad and postgrad courses. To my Mum and Dad, who are always interested even if they don't quite understand what I'm talking about; Vicki – who is just plain awesome in every possible way; and Ben, who has competed with this PhD for my time for so long, thank you for being so patient, so supportive and so wonderful. This thesis is dedicated to you four.

Author's Declaration

I hereby declare that the work described in this thesis was conducted in the Department of Chemistry at the University of York between October 2007 and January 2011 under the supervision of Dr. Jason M. Lynam. The work described was conducted by myself. The research presented here is, to the best of my knowledge, original except where due credit has been given to other authors or my collaborators.

Christine E. Welby

1: Introduction

1.1: Preamble

Since the discovery of the first vinylidene and allenylidene complexes in the mid 1960-70s, their importance in the field of organometallic chemistry has become well-established. The chemistry of both ligands has been extensively probed and a number of reviews[1-6], a journal special issue[7] and book[8] have been devoted to their formation, reactivity and catalytic applications. This apparent depth of understanding should not, however, preclude further investigation; novel discoveries in the field of vinylidene and allenylidene chemistry are still being made and their relevance to the catalytic transformation of small organic molecules necessitates further study.

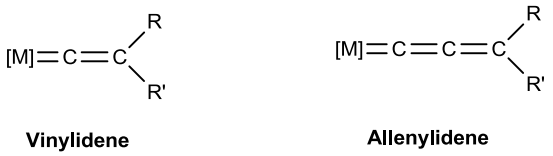

Figure 1.1.1: The vinylidene and allenylidene ligands coordinated to a transition-metal complex.

It has been shown that vinylidene in the gas phase ($:C=CH_2$) is approximately 188 kJ mol^{-1} less stable that its tautomer acetylene[1,9] ($HC\equiv CH$). Coordination to a transition metal reverses this stability and Hoffmann has shown that $[MnCp(=C=CH_2)(CO)_2]$ is 146 kJ mol^{-1} more stable than the corresponding form containing a η^2-bound acetylene ligand.[10] Both vinylidene and allenylidene ligands are Fischer carbene ligands.

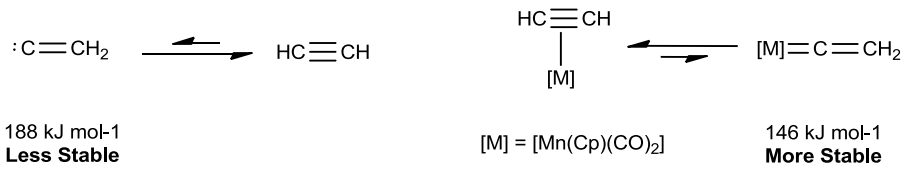

Figure 1.1.2: Comparative energies of vinylidene and acetylene tautomers.

The relative energies of the three tautomeric forms of the allenylidene ligand have been investigated computationally by a number of groups using different levels of theory.[11-13] It has been consistently shown that the singlet cyclopropenylidene form is the lowest in energy of the three.[2] The next highest in energy is the triplet propynylidene form, which has been shown to adopt a 'W' shape.[13] The singlet allenylidene form is generally highest in energy of the three, although the relative energies of each vary depending on the level of theory used.

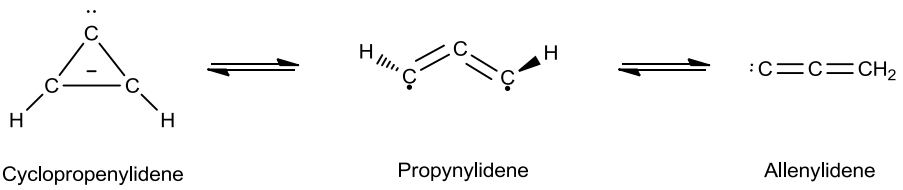

Figure 1.1.3: Three tautomeric forms of allenylidene.

The first vinylidene complex was isolated by Redhouse and Mills in 1966,[14, 15] who irradiated a solution of diphenylketene with $Fe(CO)_5$ in benzene. The orange crystals obtained were structurally characterised and revealed that the vinylidene ligand was bridging two Fe centres as $[Fe_2(\mu\text{-}C{=}CPh_2)(CO)_8]$. The majority of vinylidene complexes reported contain terminal vinylidenes, rather than bridging, with the first such example reported by King and Saran in 1972.[16] They demonstrated how the reaction of $[MoCp(CCl{=}C(CN)_2(CO)_2]$ with PPh_3 in boiling octane resulted in the formation of $[MoClCp(=C{=}C\{CN\}_2)(PPh_3)]$.

The groups of Fischer[17] and Berke[18] simultaneously and independently reported the synthesis and characterisation of the first allenylidene complexes in 1976 (Figure 1.1.4). Fischer reported that the complexes $[M(=C{=}C{=}C\{NMe_2\}\{Ph\})(CO)_5]$ (M = Cr, W) form by the stepwise reaction of the precursor $[M(=C\{OEt\}CH{=}C\{NMe_2\}\{Ph\})(CO)_5]$ with a Lewis Acid (BX_3) and a weak base (THF). Berke reported that addition of ^{t}BuLi to the precursor complex $[MnCp(\eta^2\text{-}HC{\equiv}CCO_2Me)(CO)_5]$ resulted in the formation of the allenylidene complex $[MnCp(=C{=}C{=}C^tBu_2)(CO)_2]$.

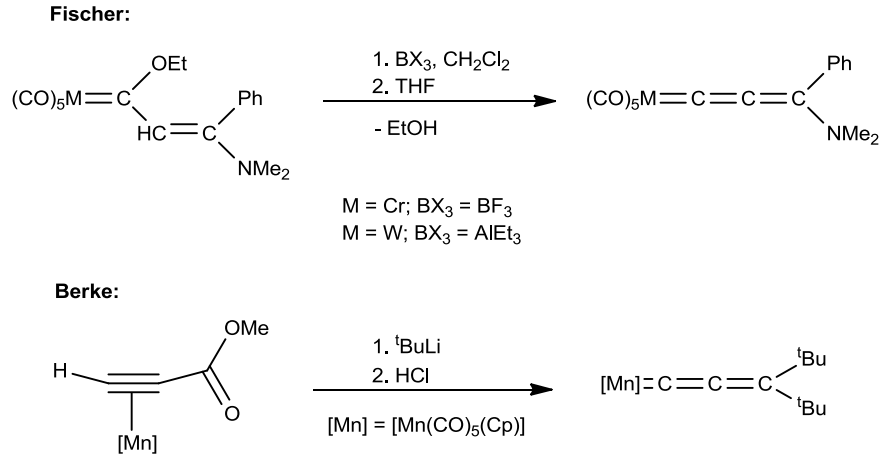

Figure 1.1.4: The first reported examples of allenylidene complexes made in 1976.

Although these authors reported the first examples of complexes containing terminal vinylidene and allenylidene ligands, the routes used are not the most common or facile. It has since been demonstrated that vinylidene ligands are most easily prepared by the isomerisation of a terminal alkyne at a transition metal complex whilst allenylidene ligands are more readily formed upon the dehydration of propargylic alcohols at a transition metal centre. In both cases a vacant metal site is a prerequisite, and the mechanisms of formation are related, as the formation of an allenylidene ligand is thought to proceed *via* a hydroxy-vinylidene intermediate. The synthesis (Section 1.3) and mechanism of formation (Section 1.4) of vinylidene and allenylidene ligands will be addressed fully later in this chapter.

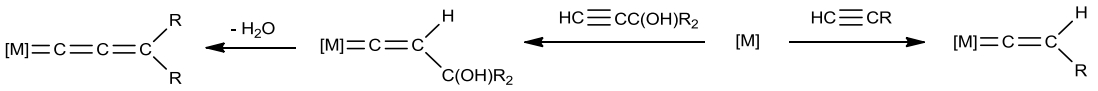

Figure 1.1.5: Formation of vinylidene and allenylidene complexes.

1.2: Bonding in Transition-Metal Vinylidene and Allenylidene complexes

Much of the reactivity of vinylidene and allenylidene ligands can be rationalised upon examining the molecular orbitals involved in the bonding of these ligands to a transition-metal centre. As mentioned earlier, the majority of vinylidene and allenylidene complexes reported are Fischer carbene ligands; the implication of which is that the carbene (C_α) carbon atom is electrophilic. It is well-established experimentally[19] that nucleophilic addition preferentially occurs at the C_α of a vinylidene ligand. A simplified molecular orbital diagram constructed for a typical vinylidene ligand coordinated to a transition-metal centre is shown in Figure 1.2.1.[19] It can be seen that the LUMO (π4) is localised mainly on the p(π)-orbital of the vinylidene ligand, which accounts for the preference for nucleophiles to attack at this position. Conversely, the HOMO (π3) consists of an antibonding interaction between the filled metal d(π)-orbital and the filled p(π)-orbital of the C=C moiety, meaning electrophilic additions may occur at either the C_β or at the metal centre. In the case of some low valent late transition metal complexes, the HOMO may have more non-bonding character.[20] In their calculations into the orbital interactions between $:C=CH_2$ and different transition-metal fragments, Kostić and Fenske[21] reported that for the $[FpCCH_2]^+$ system, the HOMO is 30 % localised on the C_β atom whilst the LUMO is 60 % localised on the C_α. For the $[Fp'CCH_2]^+$ system, the HOMO is 25 % localised on the C_β atom whilst the LUMO is again 60 % localised on the C_α (Fp = $[FeCp(CO)_2]$; Fp' = $[FeCp(PH_3)_2]$).

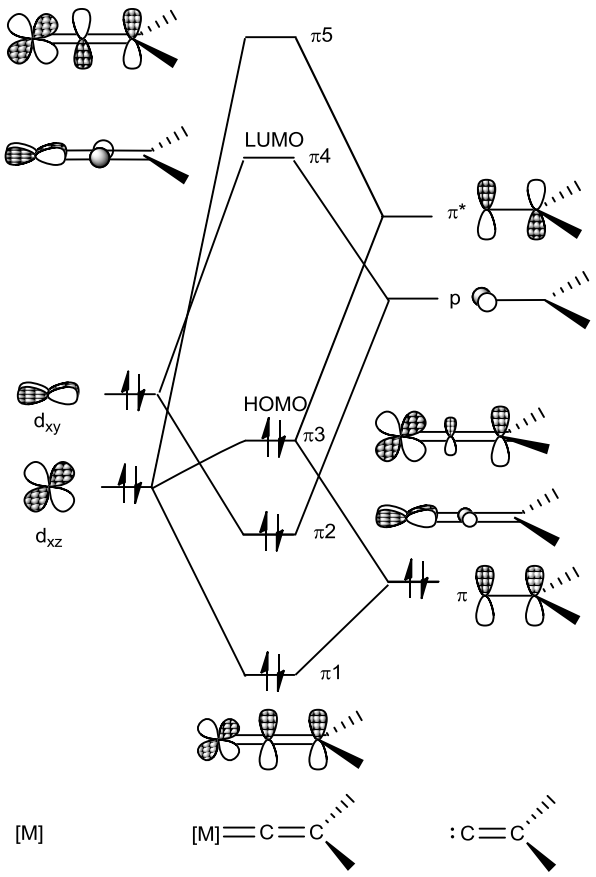

Figure 1.2.1: Simplified molecular orbital diagram for a transition-metal vinylidene complex.[19]

A well-known example of nucleophilic attack at the C_α position can be found in the reaction of a vinylidene ligand with oxygen nucleophiles such as water or alcohols to give hydroxy- or alkoxy-carbene ligands. A number of groups have shown that the addition of water to a vinylidene complex results in the formation of a carbonyl-complex and the production of the corresponding aldehyde,[22] which is thought to occur *via* the mechanism shown in Figure 1.2.2. The reaction with an alcohol proceeds in a similar fashion, although the alkoxy-carbene fragment is not eliminated.[23,24]

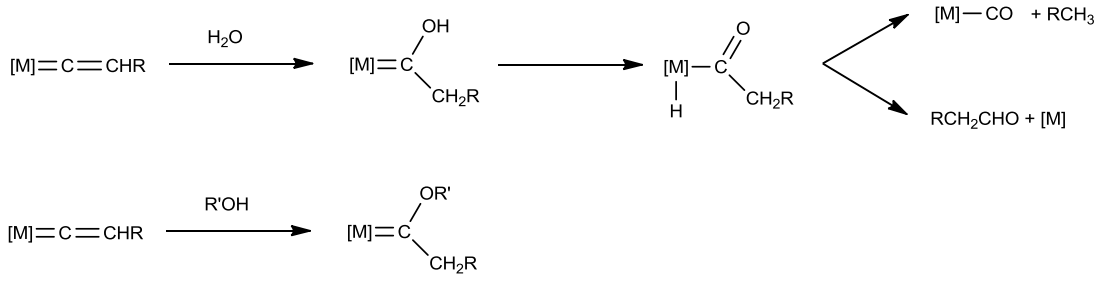

Figure 1.2.2: Reaction of a vinylidene complex with water and an alcohol.

Exceptions to this preference for nucleophiles to attack C_α and electrophiles to attack C_β are known. Werner has reported that a number of different electrophiles will add to the C_α of [RhCp(=C=CHR)(P^iPr_3)] as shown in Figure 1.2.3. Protonation of [RhCp(=C=CH_2)(P^iPr_3)] at C_α occurs upon addition of the acids CF_3CO_2H, HCl and HI to give the vinyl complex [RhCpX(CH=CH_2)(P^iPr_3)], where X = CF_3CO_2, Cl or I. In the case of X = Cl, I; a second equivalent of HCl may add to C_α resulting in the formation of the α-chloroethyl complex [RhCpX(CHClCH_3)(P^iPr_3)].[25] Addition of diazomethane in the presence of $CuSO_4$ results in the formation of the allene complex [RhCp(η^2-CH_2=C=CH_2)(P^iPr_3)],[26] whilst addition of [RhCl(P^iPr_3)$_2$] results in the formation of the dinuclear complex [RhCp(P^iPr_3)(μ-η^1,η^2-C=CH_2)RhCl(P^iPr_3)].[27] This reactivity has been justified by Delbecq[28], who performed molecular orbital calculations based on Extended Hückel Theory. He has proposed that the presence of the electron-donating P^iPr_3 and Cp ligands makes the Rh-centre particularly electron-rich. This in turn leads to an increase in electron-density donation through a π-acceptor interaction to the vinylidene C_α. In terms of the orbitals shown in Figure 1.2.1, there is a stronger contribution from the p-orbital of the vinylidene in the π2 orbital.

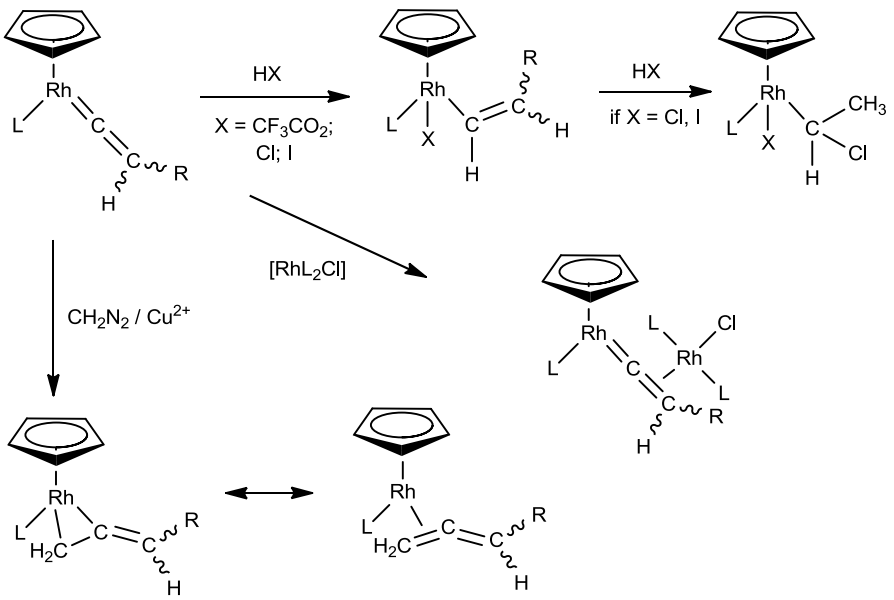

Figure 1.2.3: Summary of Werner's additions of electrophiles to [RhCp(=C=CHR)(L)] (L = P^iPr_3; R = H, Me, Ph).

Electrophilic attack at the metal centre is also known (Figure 1.2.4). In a kinetic study performed by Richards *et. al*. in 1989 on the formation of the carbyne complex *trans*-[ReCl(≡CCH$_2$Ph)(dppe)]$^+$ from the vinylidene complex *trans*-[ReCl(=C=CHPh)(dppe)], a rate law consistent with a mechanism involving protonation of the metal was observed.[29] In a related reaction, Werner also reported the protonation of the square-planar vinylidene complex [IrCl(=C=CHR)(P^{i}Pr$_3$)$_2$]$^+$ to give the carbyne complex [IrCl(≡CCH$_2$R)(P^{i}Pr$_3$)$_2$]$^+$ occurs *via* the short-lived species [IrCl(H)(=C=CHR)(P^{i}Pr$_3$)$_2$]$^+$ (R = H, Me, Ph).[30]

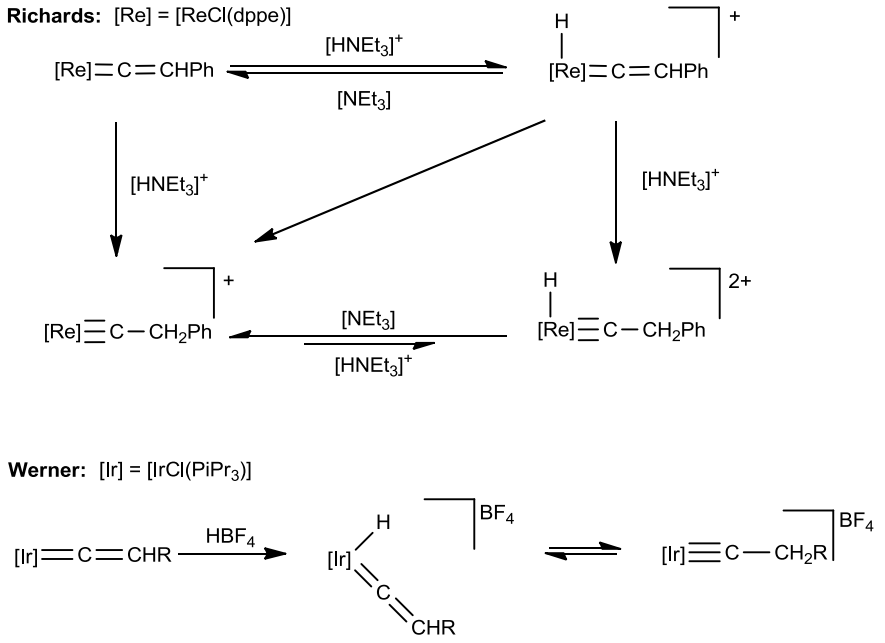

Figure 1.2.4: Literature examples of electrophilic addition to the metal centre of a vinylidene complex in preference to C$_\beta$.

Contradictory reports exist concerning the π-acceptor character of the vinylidene ligand. In 1977, Antonova *et. al*. reported that the C=CHPh moiety is a better π-acceptor than CO.[46] This conclusion was based on a comparison of force constants (K_{CO}) calculated from the CO stretching frequencies of the [MnCp(CO)$_2$(L)] fragment. This suggestion concurs with the results obtained by Kostić and Fenske,[21] who found that the extensive back-bonding inherent in the Mn – C$_\alpha$ bond of [MpCCH$_2$] meant that this bond has a multiplicity between 2 and 3 (Mp = [MnCp(CO)$_2$]). Conversely, in 2002 Werner[31] reported that the CO ligand is a better π-acceptor ligand than the vinylidene ligand based on DFT, IR and Raman

spectroscopic studies of the square-planar complex $[RhX(L)(P^iPr_3)_2]$ (X = halide; L = CO, $=C=CH_2$), with particular emphasis placed on the Rh-carbon stretch.

For half sandwich complexes, two conformational isomers of the vinylidene ligand exist, in which the two substituents may adopt a vertical or horizontal orientation relative to the metal-ligand plane. Kostić and Fenske[21] calculated that for $[MpCCH_2]$, the horizontal orientation of the vinylidene ligand is more stable than the vertical by 16.7 kJ mol^{-1}. Schilling calculated that the barrier to conversion for $[FpCCH_2]$ is similar at 15.1 kJ mol^{-1}, and that again the horizontal orientation is energetically preferred.[32] The orientation of the vinylidene ligand is thought to be governed by the orientation of the metal d-orbital involved in the back-bonding interaction into the vacant p-orbital (d_{xy} as shown in Figure 1.2.1). From a crystallographic perspective, a larger number of structurally characterised vinylidene complexes have been reported to contain a horizontal vinylidene ligand.[33-36]

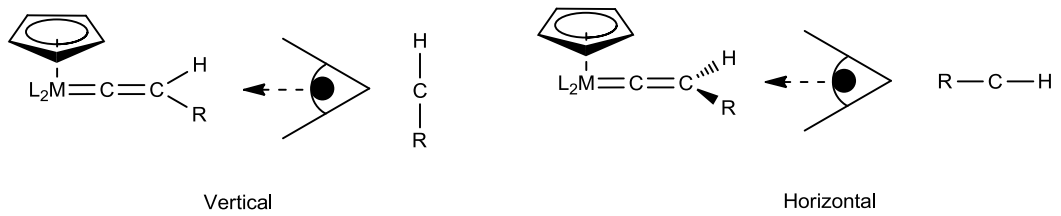

Figure 1.2.5: Vertical and Horizontal orientations of a vinylidene ligand.

One exception to this was reported by Whiteley for the $[Mo(\eta^7\text{-}C_7H_7)]$ system.[37] This fragment is isoelectronic with [RuCp] and [FeCp] fragments, whose vinylidene complexes have been shown to adopt a horizontal orientation of the vinylidene ligand. The crystal structure of $[Mo(=C=CHPh)(\eta^7\text{-}C_7H_7)(dppe)]BF_4$ demonstrated that the vinylidene ligand of this complex adopts a vertical orientation. Low-temperature solution NMR studies showed that the barrier to conversion ($\Delta G^{\ddagger}$) between the vertical and horizontal forms for $[Mo(=C=CH_2)(\eta^7\text{-}C_7H_7)(dppe)]BF_4$ is 51.9 ± 1 kJ mol^{-1} at -5 °C. This is significantly higher than the barriers reported for similar complexes $[MCp(=C=CHPh)(diphos)]^+$ (M = Ru, Fe) described by Morandini and Consiglio, which contain a variety of diphosphine ligands of the general form $Ph_2PCHRCHR'PPh_2$.[38] The barrier to rotation of the vinylidene ligand in the iron complexes was reported to be 39.3 kJ mol^{-1} whilst those of the ruthenium complexes were slightly lower at 38.1 kJ mol^{-1}. Very little difference in these values was observed for the differing diphosphine ligands.

Jia and Lin[39] have conducted a DFT study (at the B3LYP level of theory) on the five-coordinate system $[MClX(=C=CHR)(L)_2]$, where M = Ru or Os; L = phosphine, X = SiF_3, SiH_3, H, $CH=CH_2$, CH_3, Cl and R = SiF_3, SiH_3, H, Ph. They found that the barrier to rotation of the vinylidene ligand increased with the increasing π-donor properties of the X ligand. For example, the ruthenium complexes where X = SiF_3, H, Cl and L = PH_3 were calculated to have rotational barriers of 14.6, 18.0 and 30.5 kJ mol^{-1} respectively. This is thought to be due to the π-acceptor ligands having a stabilising effect on the π2 orbital (Figure 1.2.1) in transition states by interacting with the metal d(π)-orbital. Smaller rotational barriers were observed for vinylidene complexes containing a silyl substituent, attributed to the ability of these π-acceptor ligands to stabilise the π3 (HOMO) orbital of transition states. It was also found that the ruthenium complexes had a smaller rotational energy barrier than the osmium analogues, thought to be due to the more diffuse nature of the d-orbitals of osmium.

This was followed by a second DFT study (at the BP86 level of theory) by Ariafard,[40] who sought to establish the effect of phosphine ligand on the barrier to rotation of a vinylidene ligand in the complexes $[OsCl(H)(=C=CH_2)(L)_2]$ where L = PMe_3, PH_3 and PF_3. It was shown that the largest rotational barrier (37.7 kJ mol^{-1}) is calculated for the most electron-withdrawing phosphine ligand PF_3. The more electron-donating ligand PMe_3 gave an energy barrier of 23.8 kJ mol^{-1} while an intermediate value was obtained for PH_3 (28.5 kJ mol^{-1}). They attribute this to the greater competition between a more electron-withdrawing phosphine ligand and the vinylidene ligand for the electron density at the metal in the rotational transition state.

The bonding of the allenylidene ligand is similar in many respects to that of a vinylidene ligand. Figure 1.2.6 shows a simplified molecular orbital diagram for a transition-metal allenylidene complex. The LUMO (π2) is localised mainly on the C_α and C_γ atoms whilst the HOMO (π3) is localised on C_β. This implies that nucleophilic attack may occur at either the C_α or C_γ position whilst electrophilic attack is most likely to occur at C_β.[19] DFT calculations performed on a number of systems have demonstrated that the LUMO is typically localised approximately equally on the C_α and C_γ atoms.[6] Esteruelas[41] has used EHT-MO calculations to show that the LUMO of $[RuCp(=C=C=CH_2)(CO)(PH_3)]^+$ was localised between the three carbons (C_α, C_β, C_γ) of the allenylidene ligand in a distribution of 23 %, 6 %

and 31 %. The HOMO is 20 % localised on the C_β atom. This has meant that the preference for nucleophilic attack at either of these positions is generally determined by electronic and steric properties of the substituents of the allenylidene ligand and of ancillary ligands. It was also shown that the allenylidene ligand is a σ-donor, π-acceptor ligand. The σ-donor interaction occurs between the HOMO of the allenylidene (π3 in Figure 1.2.6) and the LUMO of the transition-metal fragment. A charge transfer of 0.44 e is produced from this interaction whilst the π-acceptor interaction, between HOMO of the transition-metal fragment and the LUMO of the allenylidene ligand (π2 in Figure 1.2.6), produces 0.93 e. This results in a net acceptor interaction between the allenylidene ligand and the transition-metal fragment of 0.45 e.

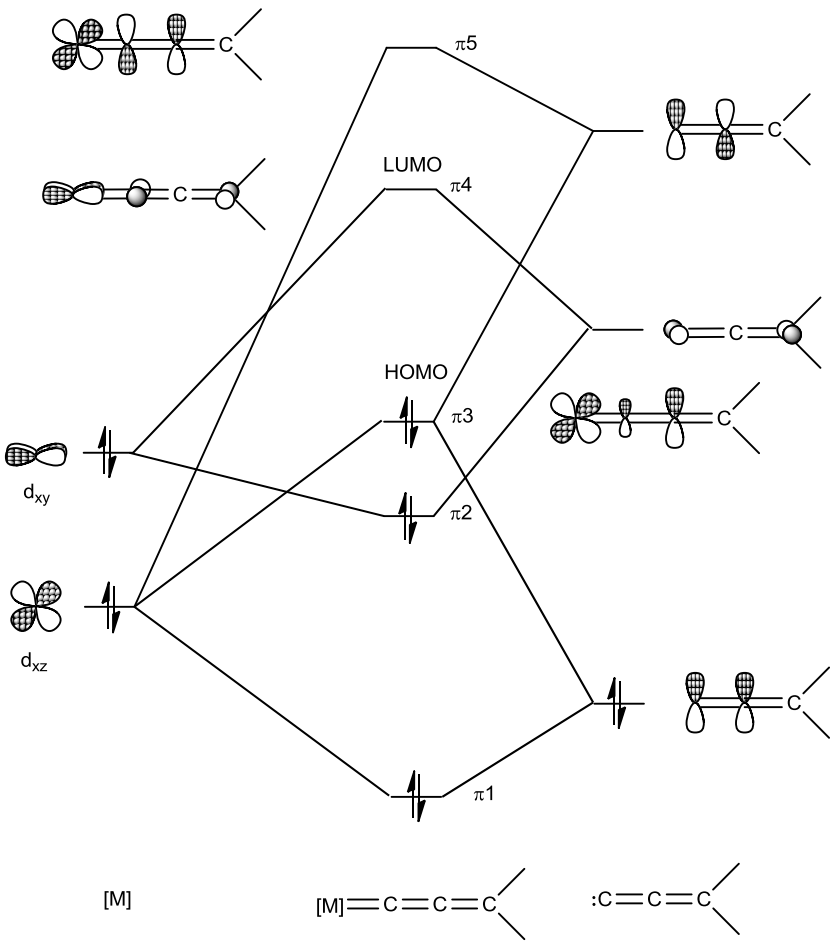

Figure 1.2.6: Simplified molecular orbital diagram for a transition-metal allenylidene complex.[19]

In 1997, Gimeno[42] demonstrated how the addition of nucleophiles to $[Ru(=C=C=CPh_2)(\eta^5\text{-}C_9H_7)L_2]^+$ was determined by the steric properties of the ligands L. When L = PPh_3 or L_2 = dppe, addition of methoxide, alkyl, alkynyl and phosphine nucleophiles occurred at the C_γ position to give the acetylide complexes $[Ru(C\equiv CC(Nu)Ph_2)(\eta^5\text{-}C_9H_7)L_2]^+$. However, when L_2 = dppm, the addition of PMe_3 or PMe_2Ph occurred at C_α to give the allene complexes $[Ru(C(PR_3)=C=CPh_2)(\eta^5\text{-}C_9H_7)(dppm)]^+$. It was also shown that the thermodynamic product of nucleophilic attack is the allene complex $[Ru(C(PR_3)=C=CPh_2)(\eta^5\text{-}C_9H_7)(dppm)]^+$, as the formation of the acetylide complex $[Ru(C\equiv CC(PR_3)Ph_2)(\eta^5\text{-}C_9H_7)(dppm)_2]^+$ was detected as an intermediate, (Figure 1.2.7). The regioselectivity observed was attributed to the bulkier phosphine ligands PPh_3 and dppe, in combination with the orientation of the indenyl ligand in these complexes, prohibiting nucleophilic attack at C_α. EHMO calculations on the model system $[Ru(=C=C=CH_2)(\eta^5\text{-}C_9H_7)(PH_3)_2]^+$ indicated that the LUMO was 25 % localised on the C_α and 33 % on C_γ.

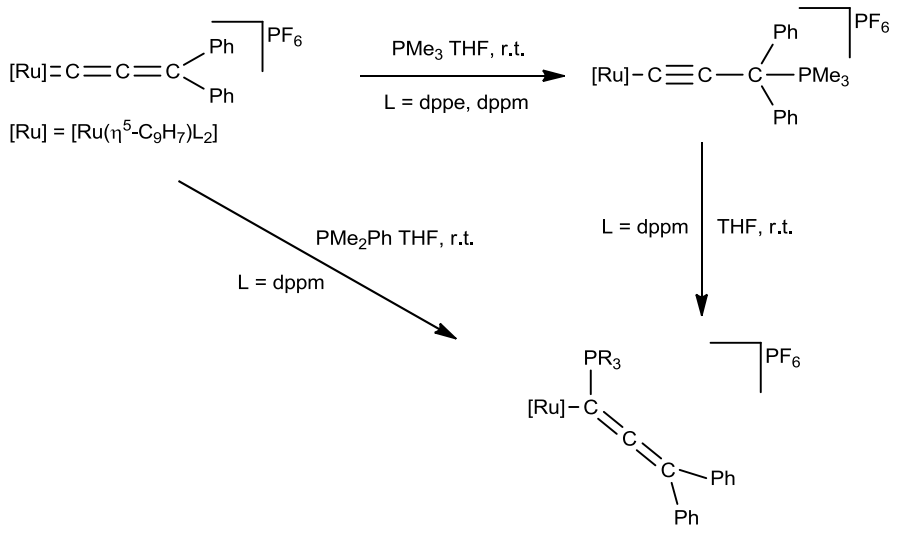

Figure 1.2.7: Addition of phosphine nucleophiles to $[Ru(=C=C=CPh_2)(\eta^5\text{-}C_9H_7)L_2]PF_6$.

Three resonance structures may be used to describe the bonding in the allenylidene ligand, as shown in Figure 1.2.8. It has been shown that complexes containing allenylidene ligands with heteroatom substituents show a greater deviation in the M=C and C=C distances reported, as there is a greater contribution from resonance form **1C**.[6] Examination of the bond distances of several allenylidene complexes has demonstrated that neutral complexes typically exhibit a structure best described by resonance form **1B**, with a short C_α-C_β bond length.

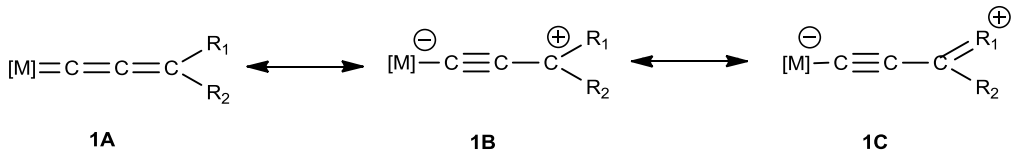

Figure 1.2.8: Three resonance structures that contribute to the bonding of an allenylidene ligand.

As is the case for the vinylidene ligand, the allenylidene ligand may adopt either a vertical or horizontal orientation. Whilst the vinylidene ligand is generally characterised in the horizontal orientation, it has been shown that allenylidene ligands, like carbene ligands (:CH_2), typically adopt a vertical orientation.[32] This preference is thought to result from orientation of the back-donation interaction between the HOMO of the transition metal fragment (a d_{xy}-orbital) and the p(π)-orbital of the allenylidene ligand (π4 in Figure 1.2.6). The barrier to rotation in the [FeCp(=C=C=CH_2)$(CO)_2$] system is 11.3 kJ mol^{-1}, smaller than for the corresponding vinylidene complex (15.1 kJ mol^{-1}). Whiteley once more demonstrated that the [Mo(η^7-C_7H_7)] system produces an exception to this preference as the crystal structure of [Mo(=C=C=CPh_2)(η^7-C_7H_7)(dppe)]PF_6 exhibits a horizontal allenylidene ligand.[43] For the analogous complex [Mo(=C=C=CMePh)(η^7-C_7H_7)(dppe)]PF_6, the barrier to rotation of the allenylidene ligand was calculated to be 57.8 kJ mol^{-1} using low temperature $^{31}P\{^1H\}$ NMR studies. This barrier compares favourably with that calculated for the related vinylidene complex mentioned previously (51.9 ± 1 kJ mol^{-1}). DFT calculations on the appropriate fragments have suggested that the HOMO of the [Mo(η^7-C_7H_7)] system has significant d_{z^2} character, rather than d_{xy}, as indicated in Figure 1.2.6. As mentioned above, the orientation of the cumulenylidene ligand is determined by the orbitals involved in the back-donation interaction (π4).

The bonding descriptions involved in the interactions between the vinylidene and allenylidene ligands and the transition-metal fragments explain the reactivities observed. The reactivity of some transition-metal vinylidene and allenylidene complexes will be elaborated on in section 1.5.

1.3: Synthesis of Transition-Metal Vinylidene and Allenylidene complexes

The most common method employed in the synthesis of transition-metal vinylidene and allenylidene complexes involves the addition of a terminal alkyne to a transition-metal complex. More specifically, the most common route to an allenylidene ligand involves the dehydration of a propargylic alcohol of general form HC≡CC(R)(R')OH. The formation of an allenylidene ligand has been shown to occur *via* a hydroxy-vinylidene ligand.

1.3.1: Addition of a Terminal Alkyne: Vinylidene complexes

The formation of transition-metal vinylidene complexes has been the focus of significant experimental and computational interest. The mechanism by which the terminal alkyne undergoes an isomerisation to a vinylidene ligand varies with the metal-ligand system involved, and will be discussed in Section 1.4.

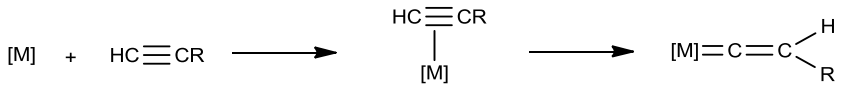

Figure 1.3.1.1: Formation of a vinylidene complex upon addition of HC≡CR.

Vinylidene complexes of a variety of metal-ligand centres are known, chiefly involving metals from Groups 4 – 9. It would be unfeasible for this thesis to attempt to detail the numerous different syntheses of vinylidene complexes reported in the literature. Instead, specific examples relevant to this thesis will be discussed. In order for alkyne-to-vinylidene isomerisation to occur, a vacant site must be available for alkyne coordination at the metal centre. This may be achieved by the loss of an ancillary ligand, or by a chelating ligand altering its mode of coordination. The loss of a halide ligand is a common strategy employed by Bruce and Dixneuf in the synthesis of ruthenium-vinylidene complexes.

In 1978, Bruce[44] reported the first example of the addition of a terminal alkyne to a ruthenium complex to afford a vinylidene complex. Inspired by the then-recent successes in the formation of vinylidene complexes by addition of a terminal alkyne to the precursors $[MCp(CO)_3]$ (M = Mn[45,46], Re[47]) and *trans*-$[FeCl_2(depe)_2]$;[48] Bruce added terminal alkynes HC≡CR (R = Me, Ph, C_6F_5, CO_2Me) to the ruthenium

precursor complex $[RuClCp(PPh_3)_2]$ in the presence of either NH_4PF_6 or $NaBPh_4$. This resulted in the formation of vinylidene complexes $[RuCp(=C=CHR)(PPh_3)_2]PF_6$ (or BPh_4). The reactions were conducted at room temperature in methanol, and the products characterised by their IR and NMR spectroscopic data. He later expanded on this work reporting the formation of analogous complexes $[RuCp(=C=CHR)(PMe_3)_2]PF_6$ (R = H, Me, Ph) from the related complex $[RuClCp(PMe_3)_2]$[49] using the conditions shown in Figure 1.3.1.2. This work was revisited by Bullock in 1989,[50] who demonstrated that the η^2-alkyne complex could be identified in the synthesis of the methyl-substituted vinylidene complex $[RuCp(=C=CHMe)(PMe_3)_2]PF_6$. Formation of the vinylidene ligand was also shown to be reversible, and that heating $[RuCp(=C=CHMe)(PMe_3)_2]PF_6$ at 80 – 110 °C in MeCN resulted in the liberation of propyne. Bullock also showed that the same precursor complex will react with $HC{\equiv}CSiMe_3$ to give the parent vinylidene complex $[RuCp(=C=CH_2)(PMe_3)_2]PF_6$.

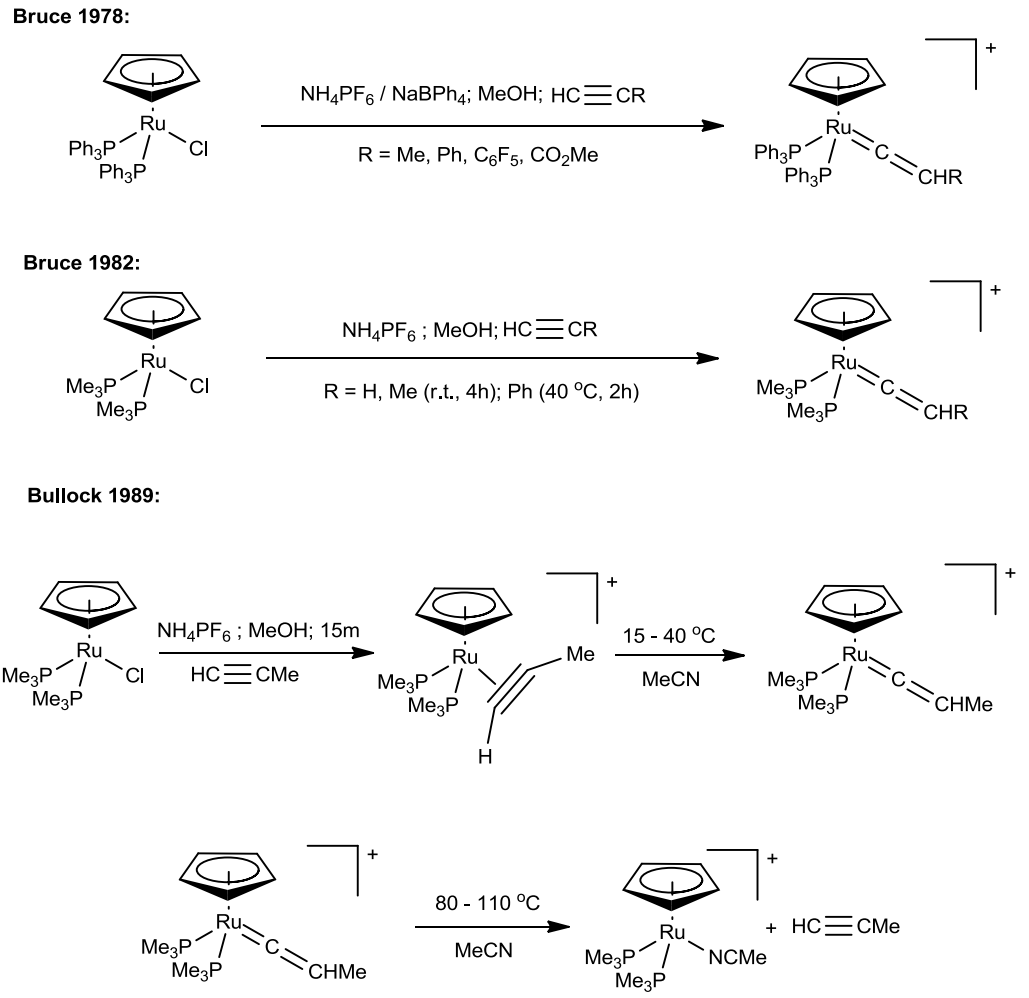

Figure 1.3.1.2: Synthesis of ruthenium-vinylidene complexes by halide ligand loss.

Dixneuf has used a similar method in the synthesis of a range of vinylidene complexes of the form *trans*-[RuCl(=C=CHR)(P)$_2$] (P = dppm, dppe). The addition of two equivalents of terminal alkyne and $NaPF_6$ to the precursor complexes *cis*-[$RuCl_2(P)_2$] in DCM solution resulted in the formation of the appropriate vinylidene complexes after 4 hours (P = dppm)[51] or 12 hours (P = dppe).[52]

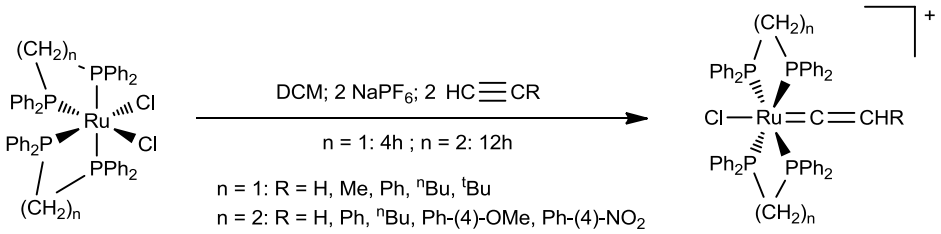

Figure 1.3.1.3: Formation of vinylidene complexes by addition of terminal alkynes.

Bruce has demonstrated that the complex [RuClCp*(PPh_3)$_2$], analogous to the one described above, may undergo either phosphine or halide ligand loss in the formation of a vinylidene complex, depending on the choice of solvent.[53,54] The addition of terminal alkynes to this complex in MeOH results in the formation of both the cationic complex [RuCp*(=C=CHR)(PPh_3)$_2$]$^+$, in which the counter-ion is presumably Cl^-, and the neutral complex [RuClCp*(=C=CHR)(PPh_3)]. Conducting the reaction in benzene gives only the neutral complex obtained by the loss of PPh_3.

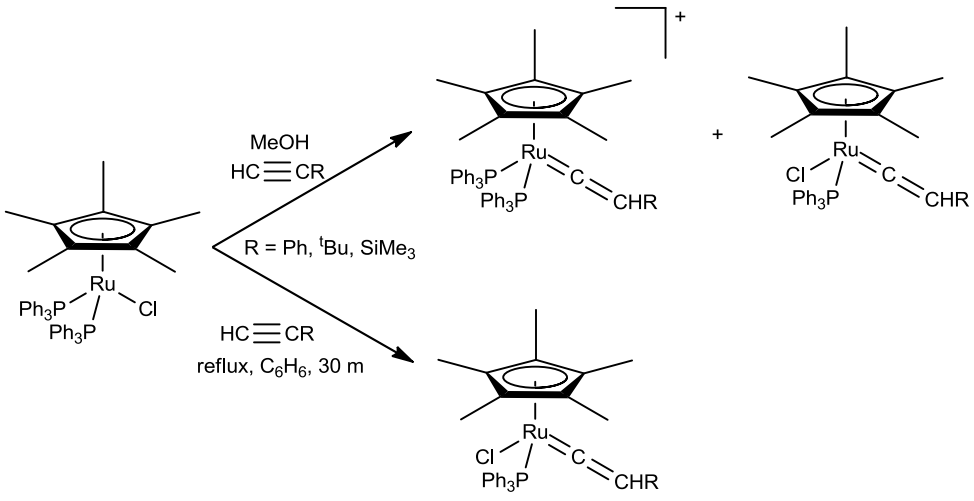

Figure 1.3.1.4: Competing reaction pathways in the formation of vinylidene complexes from [RuClCp*(PPh_3)$_2$].

Wakatsuki has shown that the formation of the vinylidene complex $[RuCl_2(=C=CH^tBu)(PPh_3)_2]$ from $[RuCl_2(PPh_3)_3]$ occurs *via* phosphine ligand loss.[55] The reaction shown in Figure 1.3.1.5 occurs over a period of 24 hours, and can be conveniently monitored by ^1H and $^{31}P\{^1H\}$ NMR spectroscopy. This reaction will be examined in more detail later in this thesis.

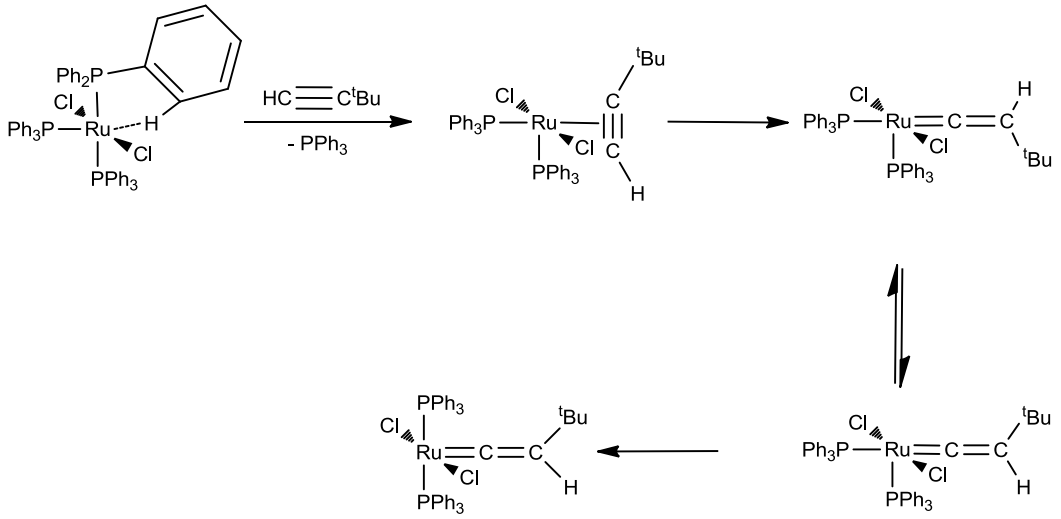

Figure 1.3.1.5: Proposed mechanism for the formation of $[RuCl_2(=C=CH^tBu)(PPh_3)_2]$.

An alternative to vinylidene formation that is dependent on ancillary ligand loss is the use of chelating ligands which may alter their coordination mode. The use of hemi-labile ligands to stabilise reactive intermediates has found uses in a number of catalytic processes including hydrogenation, carbonylation and ring-opening metathesis polymerization (ROMP).[56] Werner has demonstrated the use of phosphino-ether ligands in the formation of ruthenium vinylidene complexes.[57] The addition of terminal alkynes to the precursor complex $[RuCl(H)(CO)(P^iPr_3)_2]$ did not result in the generation of the corresponding vinylidene complexes. Instead, insertion of the alkyne occurred to give the vinyl complexes $[RuCl(CH=CHR)(CO)(P^iPr_3)_2]$. However, addition of HC≡CPh to the precursor complex $[RuCl_2(\kappa^2\text{-}^iPr_2PCH_2CH_2OMe)_2]$ resulted in the formation of the corresponding vinylidene complex shown in Figure 1.3.1.6. It appeared that the oxygen-bound 'arm' of the phosphino-ether ligand is coordinated more loosely to the ruthenium centre than the phosphorus-bound. Consequently, it is able to readily dissociate and allow for alkyne binding and vinylidene tautomerisation. A low-temperature $^{31}P\{^1H\}$ NMR spectroscopy study revealed that the phosphino-ether ligands are fluxional, the free energy of exchange calculated to be 41 kJ mol^{-1} at – 55

°C. A similar reaction was also observed for the octahedral iridium complex [IrCl(H)(κ^2-{O,P}^{i}Pr$_2$PCH$_2$CH$_2$OMe)(κ^2-{C,P}^{i}Pr$_2$PCH$_2$CH$_2$OCH$_2$)]. Upon addition of a terminal alkyne to this complex at room temperature in benzene solution, the formation of the alkynyl-hydride complex [IrCl(C≡CR)(H)(κ^2-{O,P}^{i}Pr$_2$PCH$_2$CH$_2$OMe)(κ^1-{P}^{i}Pr$_2$PCH$_2$CH$_2$OMe)] was observed. These complexes gradually evolved upon heating at 80 °C in benzene into the square-planar vinylidene complex [IrCl(=C=CHR)(κ^1-{P}^{i}Pr$_2$PCH$_2$CH$_2$OMe)$_2$].

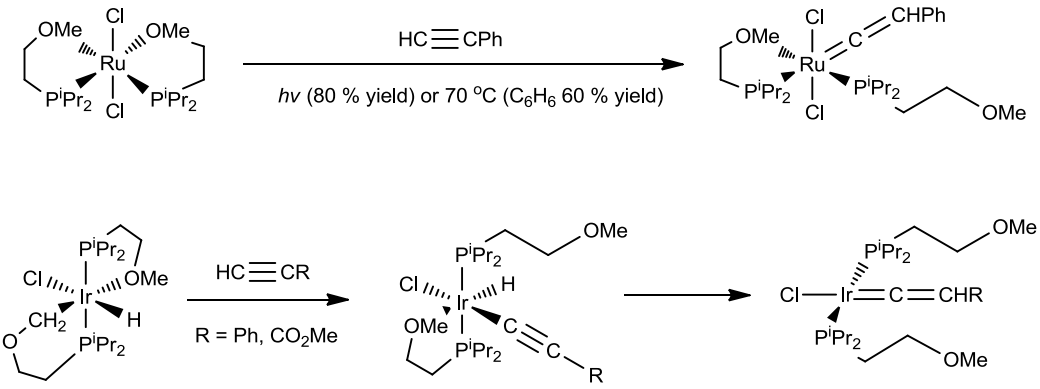

Figure 1.3.1.6: Formation of Ru- and Ir-vinylidene complexes utilising a hemi-labile ligand.

1.3.2: Addition of a Terminal Alkyne: Allenylidene complexes

The most effective synthesis of allenylidene complexes was first reported by Selegue in 1982.[58] The addition of HC≡CCPh$_2$OH to [RuClCp(PMe$_3$)$_2$] in the presence of NH_4PF_6 resulted in the formation of the allenylidene complex [RuCp(=C=C=CPh$_2$)(PMe$_3$)$_2$]PF$_6$. It was postulated that the reaction proceeds *via* the hydroxy-vinylidene complex [RuCp(=C=CHCPh$_2$OH)(PMe$_3$)$_2$]PF$_6$, which undergoes the loss of H_2O to generate the allenylidene ligand. The mechanism by which the hydroxy-vinylidene ligand forms is thought to be similar to that of a typical vinylidene ligand (see Section 1.4). Since Selegue's report was published, this route has become favoured among organometallic chemists wishing to synthesise allenylidene complexes.

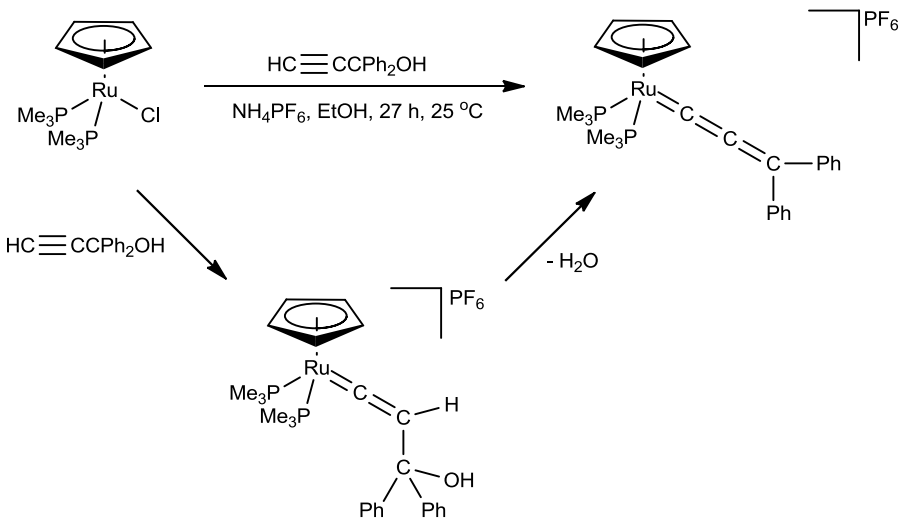

Figure 1.3.2.1: Selegue's preparation of an allenylidene complex from a propargylic alcohol substrate.

For complexes of Group 8 metals, Selegue's method typically works well and the dehydration of the hydroxy-vinylidene intermediate occurs spontaneously. However, some complexes have shown a reluctance to undergo dehydration, whilst others undergo a competing process to form the vinylvinylidene ligand. This ligand may also form *via* the dehydration of a hydroxy-vinylidene when an additional C–H bond in a β-position to the OH on an R group[59-63] is present, as illustrated in Figure 1.3.2.2.

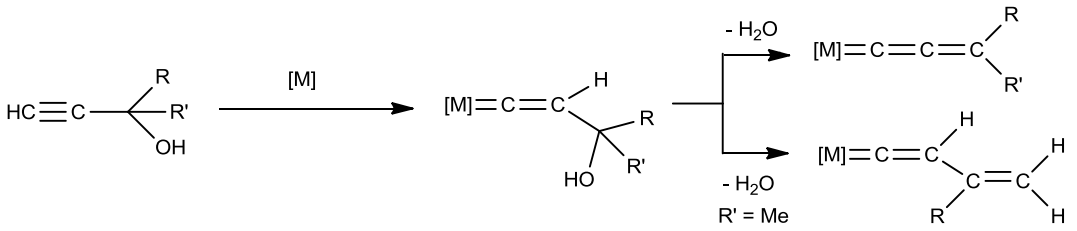

Figure 1.3.2.2: Isomerisation of a propargylic alcohol to either an allenylidene or vinylvinylidene.

On occasions when an apparently stable hydroxy-vinylidene complex is obtained, dehydration may be promoted by the addition of acid, or by passage of the complex through acidic alumina.[64] Werner has demonstrated the latter method in the synthesis of the allenylidene complex in Figure 1.3.2.3.

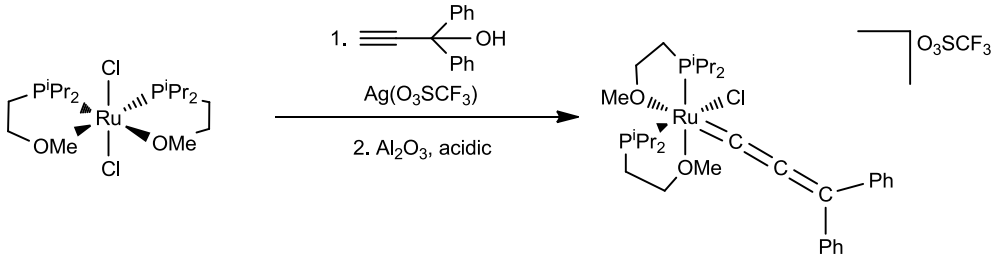

Figure 1.3.2.3: Formation of an allenylidene complex assisted by acidic alumina.

Cadierno and Gimeno's group have proposed that the allenylidene and vinylvinylidene forms exist in equilibrium. They have investigated this equilibrium[61] using the reaction of the indenyl-derivative $[RuCl(\eta^5\text{-}C_9H_7)L_2]$. They initially demonstrated that the reaction of propargylic alcohols $HC{\equiv}CCR_2OH$, where R_2 = 2 Ph or $C_{12}H_8$ (fluorenyl), with their precursor complexes $[RuCl(\eta^5\text{-}C_9H_7)L_2]$ (L = PPh_3, L_2 = dppe) results exclusively in the formation of the allenylidene complexes $[Ru(=C=C=CR_2)(\eta^5\text{-}C_9H_7)L_2]^+$. However, when the propargylic substrate HC≡CC(OH)(Ph)(Me) is used, a mixture of allenylidene $[Ru(=C=C=C\{Ph\}\{Me\})(\eta^5\text{-}C_9H_7)L_2]^+$ and vinylvinylidene $[Ru(=C=CHC\{Ph\}=CH_2)(\eta^5\text{-}C_9H_7)L_2]^+$ complexes were obtained, which could not be successfully separated.[61] They later demonstrated that the reaction of their precursor complexes with 1-ethynylcyclopentanol resulted only in the formation of the vinylvinylidene derivatives. Whilst probing this reaction further, they noted how the acetylide complex shown in Figure 1.3.2.4 is generated when the reaction is conducted in the presence of PPh_3, suggesting that an unstable allenylidene intermediate is involved.[65] Further investigation into this reaction used the related biologically-active propargylic alcohols ethisterone, 17α-ethnylestradiol and mestranol. Reaction of these substrates with the precursor complexes resulted in mixtures of allenylidene and vinylvinylidene complexes, which again could not be separated.[66]

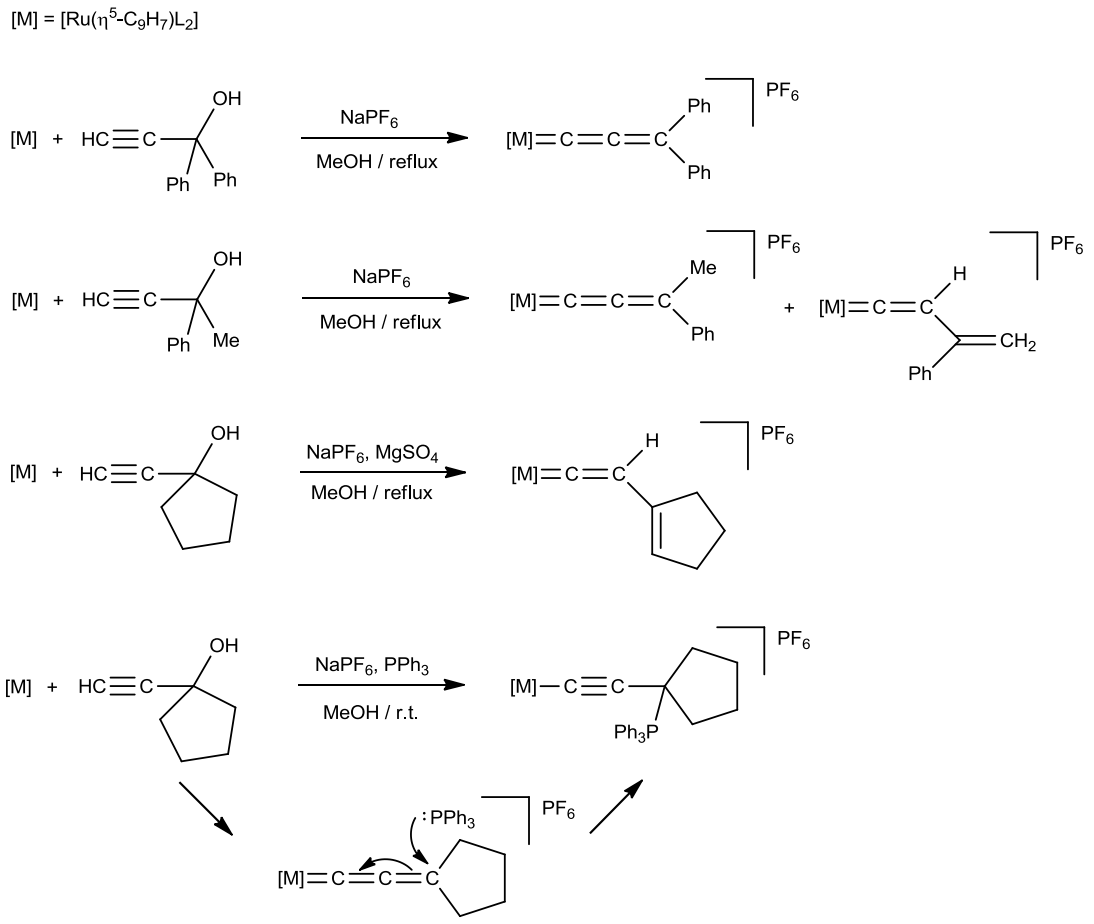

Figure 1.3.2.4: Gimeno and Cadierno's work investigating the equilibrium between allenylidene and vinylvinylidene complexes.

DFT calculations on the model complexes $[RuCp(=C=C=C\{H\}\{Me\})(PH_3)_2]^+$ and $[RuCp(=C=CHCH=CH_2)(PH_3)_2]^+$ using the B3LYP/DZV(d,p) level of theory showed how the two complexes interconvert through a 1,3-hydrogen sigmatropic rearrangement.[66] They found their vinylvinylidene model complex to be 8.79 kJ mol^{-1} more stable than the allenylidene form, an energy gap that they suspect would decrease in reality as endocyclic cyclopentenes (i.e. the vinylvinylidene form) are more strained than the exocyclic form (i.e. allenylidene). The activation energy calculated for the model transition state was found to be 278.2 kJ mol^{-1}. The authors stipulate that this barrier is higher than anticipated due to an overestimation by the level of theory chosen.

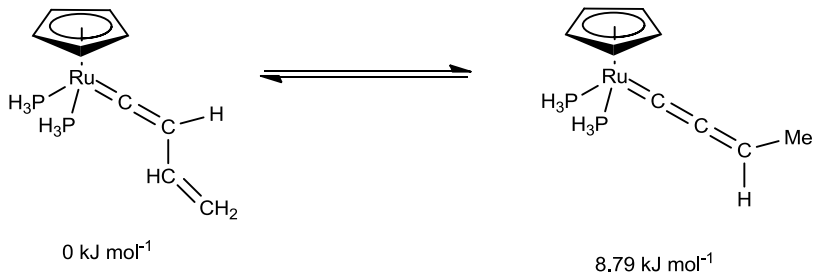

Figure 1.3.2.5: Equilibrium between vinylvinylidene and allenylidene complexes of $[Ru(Cp)(PH_3)_2]$.

Unfortunately, Selegue's method cannot be applied to every transition-metal complex. For example, the procedure is unsuitable for $[M(CO)_5]$ fragments (M = Cr, W) when the propargylic alcohol contains alkyl or aryl substituents, due to the thermal instability of the resulting complexes. Fischer[67,68] has developed an alternative route, also based on terminal alkynes. It involves the initial synthesis of functionalised acetylide complexes which undergo an abstraction to give the appropriate allenylidene complexes. For example, the allenylidene complex $[M(=C=C=C(OR)(NR'_2)(CO)_5]$ (M = Cr, W) may be generated by the addition of the propynoic acid amide $HC{\equiv}CCONR'_2$. This alkyne is first deprotonated by Li^nBu to form the acetylide anion which subsequently reacts with *in situ* generated $[M(CO)_5(THF)]$ to generate $[M(C{\equiv}CCONR'_2)(CO)_5]^-$. This is subsequently reacted with $[R_3O]BF_4$ to give the product, as shown in Figure 1.3.2.6. Other alternatives to the use of terminal alkynes to give vinylidene and allenylidene complexes directly are explored in the following section.

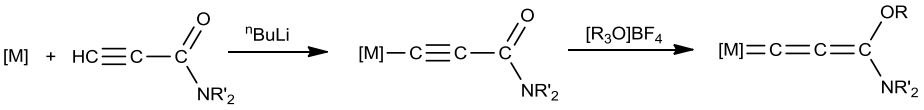

[M] = $[Cr(CO)_5]$, $[W(CO)_5]$

Figure 1.3.2.6: Fischer's alternative synthesis to allenylidene complexes of Cr and W.

1.3.3: Alternative Preparations of Vinylidene and Allenylidene complexes

Whilst the routes discussed in section 1.3.1 and 1.3.2 are the most common for the preparation of transition-metal vinylidene and allenylidene complexes, others are possible. Vinylidene complexes may also be synthesised by the protonation of acetylide derivatives or by the deprotonation of carbyne ligands. Disubstituted vinylidene ligands may be generated either by the isomerisation of an internal alkyne at the transition-metal, or by the addition of electrophiles to the C_β of an acetylide ligand. Examples of synthetic alternatives to Selegue's methodology for the production of allenylidene ligands include the oxidation of acetylides to generate cationic allenylidene radicals. Again, a number of examples of these alternative strategies are contained in the literature, however only a select few will be discussed.

1.3.3.1: Alternative Preparations of Transition-metal Vinylidene complexes

Like the vinylidene ligand, an acetylide ligand is electron-deficient at C_α while C_β is electron-rich and so the preferential sites for electrophilic and nucleophilic additions to these ligands are the same. Consequently, protonation of the C_β of an acetylide ligand will generate a vinylidene ligand. It has also been shown that acetylide complexes may be synthesised by the deprotonation of a vinylidene ligand. The interconversion of these ligands was demonstrated by Bruce in 1979[69] who showed that the addition of the acids HBF_4 or HPF_6 to the vinylidene complexes $[RuCp(=C=CHR)(PPh_3)_2]^+$ resulted in the acetylide derivatives $[RuCp(C\equiv CR)(PPh_3)_2]$. The reaction could be reversed by the addition of a base such as NaOMe. He also stated that the "deprotonation/protonation cycle could be repeated many times without apparent loss of complex."

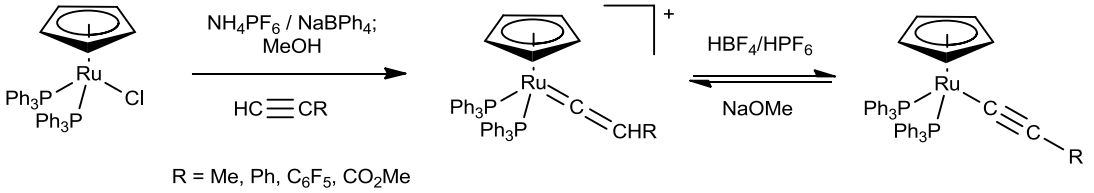

Figure 1.3.3.1.1: Interconversion of vinylidene and acetylide ligands by protonation/deprotonation.

Rheingold[70] also demonstrated this method in the synthesis of the neutral vinylidene complex [MnCp'(=C=CHMe)(CO)(PPh_3)] *via* [MnCp'(C≡CMe)(CO)(PPh_3)]$^-$. The anionic acetylide complex is protonated *in situ* by H_2O when the precursor carbene complex [MnCp'(=C{OMe}CH_2R)(CO)(PPh_3)] is treated with two equivalents of ^{n}BuLi in THF at 0 °C.

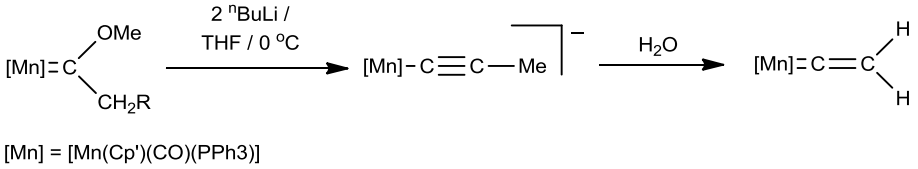

Figure 1.3.3.1.2: Synthesis of a Mn-vinylidene complex by addition of H_2O to an acetylide complex.

The deprotonation of a carbyne ligand is the formal reverse of the protonation of a vinylidene ligand.[71] This method of synthesising a vinylidene complex has been exploited by Esteruelas,[72] who has shown that the deprotonation of the carbyne complex [OsCp(H)(≡CCH_2Ph)(P^iPr_3)] by KOH results in the generation of an equilibrium mixture of the corresponding vinylidene complex and its cyclometalated isomer as shown in Figure 1.3.3.1.3.

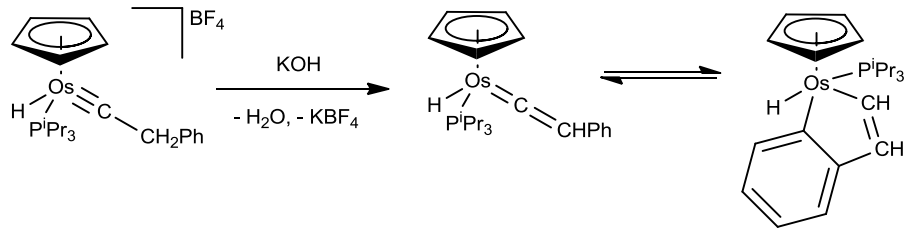

Figure 1.3.3.1.3: Deprotonation of an Os-carbyne complex to the corresponding vinylidene complex.

Disubstituted vinylidene complexes may result from either addition of an internal alkyne to a suitable transition-metal precursor or from the addition of an electrophile to the C_β of an acetylide ligand. The latter procedure is analogous to the protonation of an acetylide complex to give a mono-substituted vinylidene ligand. The formation of vinylidene ligands *via* the rearrangement of heteroatom-substituted internal alkynes is relatively well-known. One such example was reported by Werner[73] who showed that the addition of the trimethylsilyl-substituted alkyne RC≡C$SiMe_3$ to [RhCl(P^iPr_3)$_2$]$_n$ gave the vinylidene complexes [RhCl(=C=C{R}{$SiMe_3$})(P^iPr_3)$_2$] *via* the η^2-alkyne complex shown in Figure 1.3.3.1.4. Ozawa[74] has investigated the kinetics of the transformation from the η^2-

alkyne complex to the vinylidene using $FcC{\equiv}CSiMe_3$, who showed that the mechanism proceeds *via* a 1,2-sigmatropic migration of the $SiMe_3$ group.

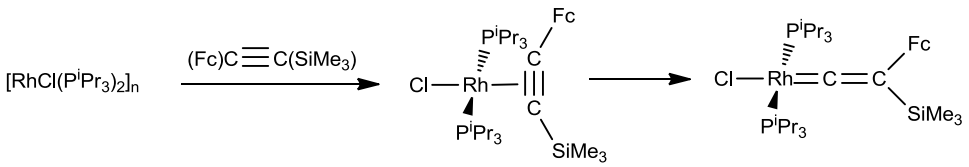

Figure 1.3.3.1.4: Formation of $[RhCl(=C=C\{Fc\}\{SiMe_3\})(P^iPr_3)_2]$.

Other examples involving heteroatom groups such as $SiMe_3$,[73-78] $SnMe_3$,[79,80] SR[81] and I[82] have also been reported. More recently, Ishii has demonstrated that internal alkynes bearing unfunctionalised substituents may also be used to produce disubstituted vinylidene complexes.[83] Heating a DCE solution of [RuClCp(dppe)] with PhC≡CAr (Ar = *para*-substituted phenyl groups) at 70 °C in the presence of $NaBAr^F$ was shown to give the vinylidene complexes $[RuCp(=C=C\{Ph\}\{Ar\})(dppe)]BAr^F$ in good yields.[84] The authors have since demonstrated that the reaction is reversible, and that the mechanism proceeds *via* an uncommon 1,2-electrophilic migration of either carbon substituent. A ^{13}C-labelling experiment suggested that the preference for migration is based on the electron-withdrawing properties of the Ar group: a more electron-donating substituent is less likely to migrate.[85]

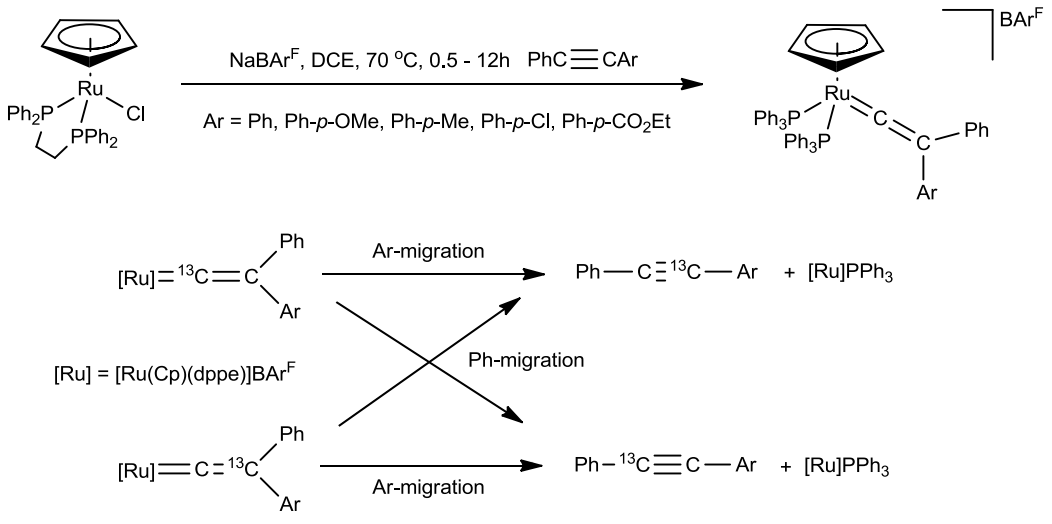

Figure 1.3.3.1.5: A summary of Ishii's study into the formation of disubstituted vinylidene complexes.

One example of electrophilic addition to the C_β atom of an acetylide to produce a disubstituted vinylidene complex was reported by Lin.[86] He synthesised a variety of such complexes using haloalkanes as shown in Figure 1.3.3.1.6.

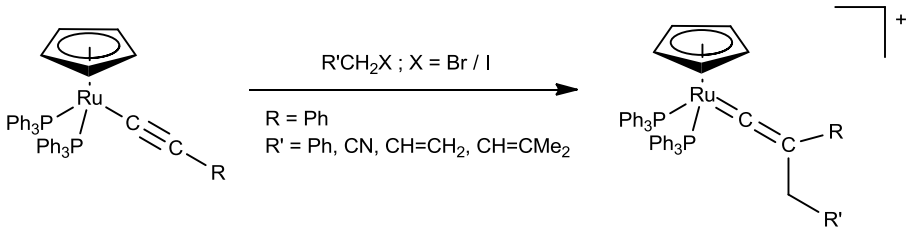

Figure 1.3.3.1.6: A disubstituted vinylidene complex from electrophilic addition to an acetylide ligand.

1.3.3.2: Alternative Preparations of Transition-metal Allenylidene complexes

A number of synthetic procedures, other than Selegue's, have been reported to produce allenylidene complexes and one such example will be discussed here. Sato has demonstrated that the chemical oxidation of a ruthenocenylacetylide complex afforded a, "kind of allenylidene"[87] as shown in Figure 1.3.3.2.1. The presence of an allenylidene ligand was evidenced by a stretch in the IR spectrum at 1980 cm^{-1}, indicative of a C=C=C moiety. Sato has demonstrated that this procedure is also possible for a number of analogous complexes containing ruthenocenylacetylide ligands.[88,89]

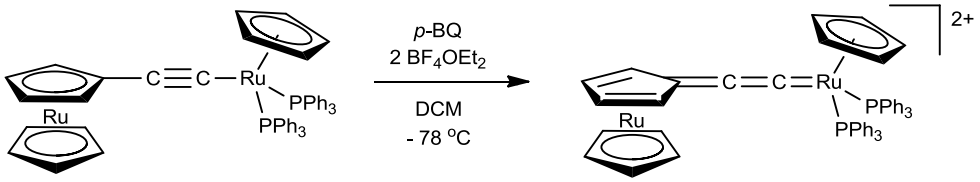

Figure 1.3.3.2.1: Oxidation of a ruthenocenylacetylide complex to give the allenylidene derivative.

1.4: Mechanism of Formation of Transition-Metal Vinylidene and Allenylidene complexes

A significant number of theoretical and experimental studies have sought to fully comprehend the exact process by which a terminal alkyne tautomerises to a vinylidene ligand at a transition-metal centre.[1,5,19,20] Computational techniques have become more important in understanding the mechanism of rearrangement particularly when the reaction is too rapid to monitor experimentally.[90,91] The precise mechanism has been shown to vary depending on the metal-ligand system involved; however the initial step in all cases has been shown to involve the coordination of the alkyne in an η^2-fashion. From this point the mechanism may diverge down one of three major pathways to give the vinylidene complex, as illustrated in Figure 1.4.1. These include Path **I**, a concerted 1,2-hydrogen shift; Path **II**, involving a formal oxidative addition to give the acetylide derivative followed by a 1,3-hydrogen shift, and Path **III**, in which alkyne insertion into a hydride ligand to give a vinyl ligand is followed by α-H migration. Relevant examples from the literature containing evidence for each mechanism will be discussed in this section.

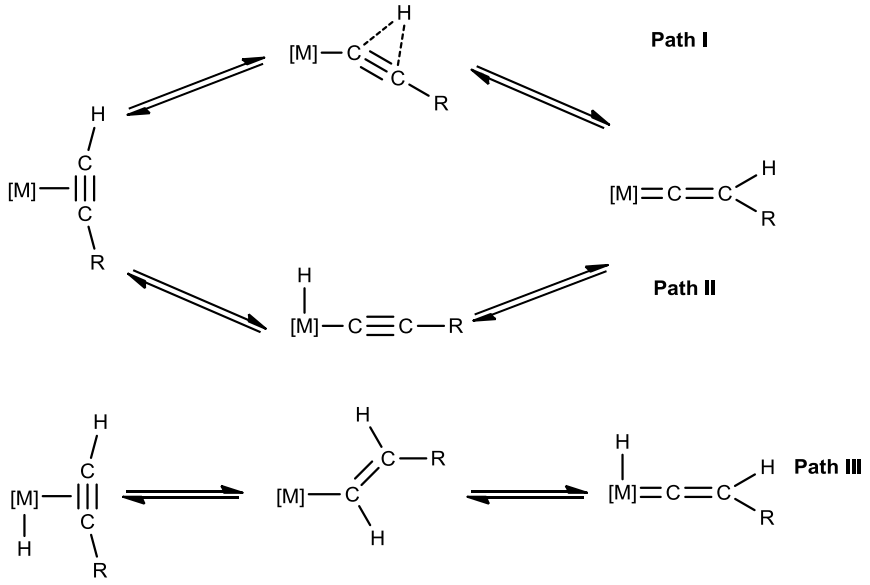

Figure 1.4.1: Three general pathways for alkyne-vinylidene isomerisation.

The formation of allenylidene complexes has not been investigated theoretically to the same extent as vinylidene complexes. They are known to form *via* the spontaneous dehydration of hydroxy-vinylidene intermediates, which in turn are

thought to form by the same processes involved in the formation of simple vinylidene ligands. To the best of the author's knowledge, the dehydration step has not been successfully computationally modelled.

1.4.1: Path I – A concerted 1,2-hydrogen shift

One of the first theoretical studies published on the alkyne-to-vinylidene tautomerisation was reported by Hoffmann and Silvestre in 1986.[10] Their extended Hückel calculations suggested that the 1,2-hydrogen shift for the [$MnCp(CO)_2$] fragment was the lowest energy pathway, and that the alternative oxidative addition pathway (Path **II**) involved a higher activation barrier. The authors felt that "…the hydrido-acetylide channel is a dead end, as far as eventual vinylidene production is concerned. We think the expenditure of energy to promote the migration from the metal to C_β of the acetylide is prohibitive."

This study was followed up some years later by Sgamelotti[92] who used static DFT methods on the same system to show that the lowest energy pathway proceeded by an intermediate in which the η^2-alkyne ligand 'slips' into a η^2-C–H interaction before undergoing a 1,2-hydrogen shift. Three mechanistic pathways were considered in this study; a direct 1,2-hydrogen shift, which was found to involve an unusual η^2-bound vinylidene intermediate, a 1,2-hydrogen shift *via* a η^2-C–H σ complex, and an oxidative addition pathway, involving a 1,3-hydrogen shift from a hydride-acetylide intermediate. The three pathways are illustrated in Figure 1.4.1.1. The highest energy barrier was calculated for the oxidative addition pathway, at 190.4 kJ mol^{-1} while the next highest was found for the direct 1,2-hydrogen shift at 189.5 kJ mol^{-1}. The highest energy barrier for the preferred route *via* the C-H agostic species was found to be 114.2 kJ mol^{-1}; significantly lower than the two alternatives.

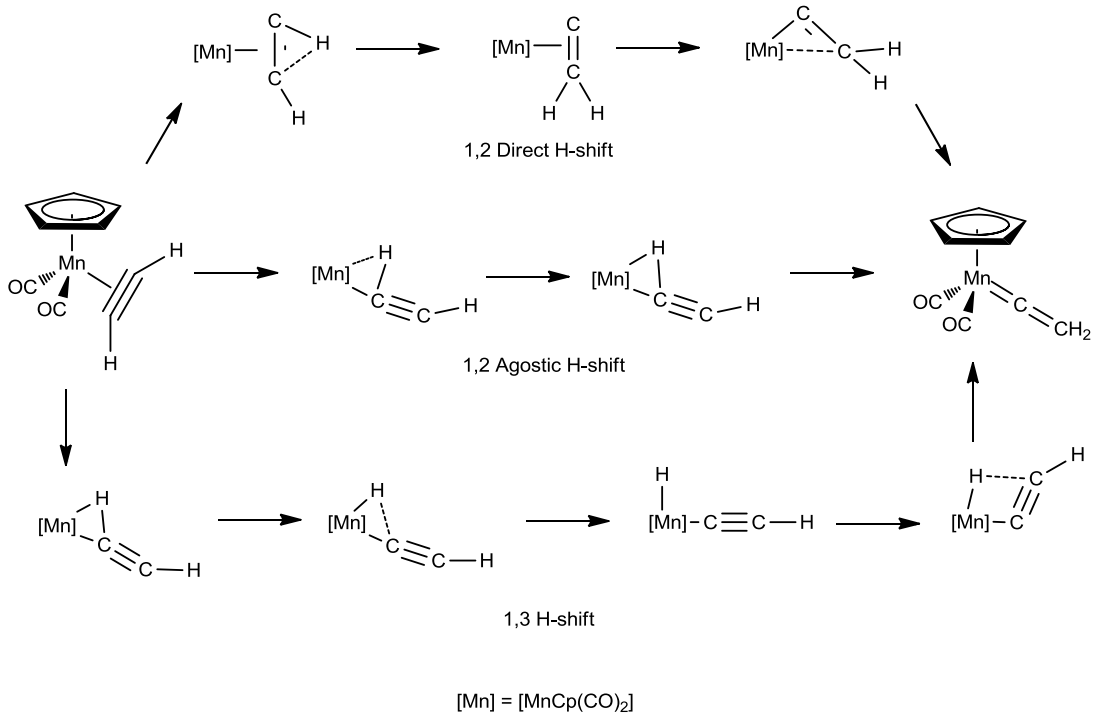

Figure 1.4.1.1: Three pathways considered by Sgamalotti for vinylidene formation at $[MnCp(CO)_2]$.

The same group have also published a study of the isomerisation of HC≡CH and HC≡CMe at the $[RuCp(PMe_3)_2]$ fragment to identify the energy barriers for the same three mechanistic pathways using a gradient-corrected DFT approach.[93] Again they were able to show that the 1,2-hydrogen shift involving an intermediate with a C–H agostic interaction had the lowest energy barrier at 112.1 and 77.8 kJ mol^{-1} for HC≡CH and HC≡CMe respectively. The oxidative addition pathway for the conversion of HC≡CMe had a barrier of 121.3 kJ mol^{-1} however for HC≡CH the barrier is only 132.6 kJ mol^{-1}. This is not significantly higher than the barrier to the preferred pathway, indicating that for this alkyne the processes may compete.

Wakatsuki's group performed *ab initio* molecular orbital calculations on the $[RuCl_2(PH_3)]$ fragment, and their findings again indicated that a 1,2-hydrogen shift proceeding *via* a η^1-C–H agostic alkyne derivative was favoured.[55] Analysis of the oxidative addition pathway required the use of a different method of geometry optimisations, so energetic comparisons could not be made. However, it was clear that the 1,3-hydrogen shift pathway involving a hydride-acetylide intermediate was thermodynamically unfavourable.

These reports, among others, have found that for the systems studied, a concerted 1,2-hydrogen shift pathway (Path **I**) is preferred to an oxidative addition pathway (Path **II**). However, a number of theoretical studies on metal-ligand systems deemed to be more electron-rich have reported that Path **II** is favoured.

1.4.2: Path II – Oxidative Addition and 1,3-hydrogen shift

A number of experimental and theoretical reports have suggested that this pathway occurs for vinylidene ligand formation at a number of transition-metal centres. The experimental observation of, or the implication of, intermediate complexes containing hydride-acetylide ligands has provided significant support to proponents of this pathway. One of the earliest reports on the synthesis of transition-metal vinylidene complexes by the reaction with terminal alkynes was made by Antonova's group in 1976.[45,46] The addition of alkynes $PhC{\equiv}CEPh_3$ (E = Ge, Sn) to the precursor $[MnCp(CO)_2(THF)]$ was observed to result in the formation of both the η^2-alkyne complex $[MnCp(\eta^2\text{-}PhC{\equiv}CEPh_3)(CO)_2]$ and the mono-substituted vinylidene complex $[MnCp(=C=CHPh)(CO)_2]$. A mechanism for this reaction was proposed, based on these observations in which oxidative addition of the terminal alkyne occurs first to give an acetylide complex as illustrated in Figure 1.4.2.1. The proton required for the formation of $[MnCp(=C=CHPh)(CO)_2]$ was suggested to come from the solvent (THF).

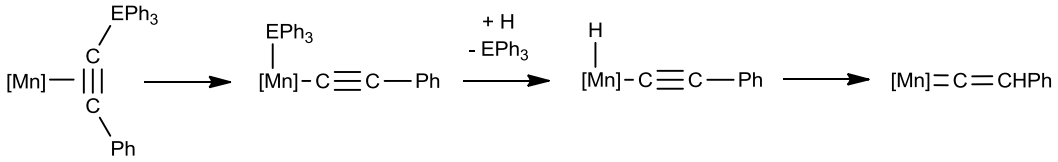

Figure 1.4.2.1: Antonova's proposed mechanism for alkyne-to-vinylidene tautomerism.

Werner subsequently demonstrated[73] that reaction of $[RhCl(P^iPr_3)_2]_n$ with $HC{\equiv}CSiMe_3$ at -30 °C results in the formation of the hydride-acetylide complex $[RhCl(H)(C{\equiv}CSiMe_3)(P^iPr_3)_2]$. This complex may rearrange in either solution or the solid state to give the vinylidene complex $[RhCl(=C=CHSiMe_3)(P^iPr_3)_2]$. Some $^{31}P\{^1H\}$ NMR spectroscopic evidence for the η^2-bound alkyne complex was detected in the formation of the hydride-acetylide derivative.

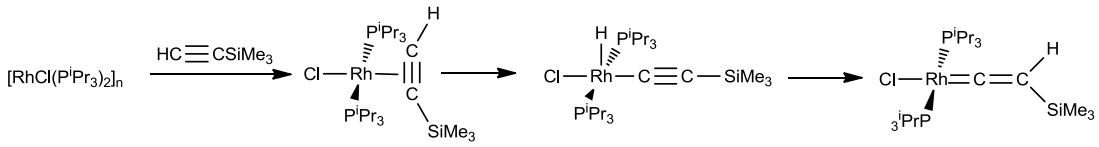

Figure 1.4.2.2: Formation of a Rh-vinylidene complex *via* a hydride-acetylide species.

The molecularity of this mechanism has been the focus of some debate over the past 20 years. A report by Werner in 1990[94] seemed to suggest that a bimolecular process may in fact be occurring, owing to some circumstantial experimental evidence. However, when Bianchini's group in 1991[95] conducted a kinetic study into the isomerisation of a hydride-acetylide species to a vinylidene complex of the [Co(PP_3)] fragment (PP_3 = P{$CH_2CH_2PPh_2$}$_3$), they found it to be unimolecular. They also concluded that the process occurred *via* a dissociative intramolecular 1,3-hydrogen shift pathway. A significant theoretical study was carried out into the question of molecularity by Wakatsuki in 1997,[96] whose results appeared to suggest that the bimolecular pathway was preferred over the unimolecular for the [RhCl(η^2-HC≡CH)(PH_3)$_2$] to [RhCl(=C=CH_2)(PH_3)$_2$] process. Using *ab initio* molecular orbital calculations, they report that $\Delta H^{\ddagger}$ for the unimolecular process to be 140.2 kJ mol^{-1}, indicating that the value of $\Delta G^{\ddagger}$ will be higher than this with a negative value of $\Delta S^{\ddagger}$. The bimolecular pathway is estimated to have a $\Delta G^{\ddagger}$ of approximately 71.1 kJ mol^{-1}, even when the larger P^{i}Pr$_3$ ligands are incorporated into the model.

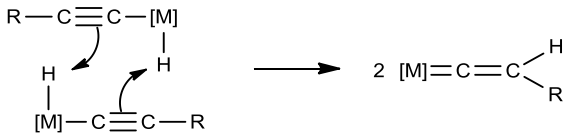

Figure 1.4.2.3: Proposed bimolecular pathway for the formation of vinylidene complexes.

Experimental and theoretical studies conducted more recently have discredited the bimolecular pathway. An isotopic-labelling study conducted by Grotjahn's group concluded that the conversion must be unimolecular.[97,98] A 1:1 mixture of the complexes [RhCl(η^2-HC≡CH)(P^{i}Pr$_3$)$_2$] and [RhCl(η^2-D^{13}C≡^{13}CD)(P^{i}Pr$_3$)$_2$] was allowed to convert to the corresponding vinylidene complexes whilst monitored by NMR spectroscopy. No crossover of the isotopes was observed in this reaction, indicating a unimolecular process must be occurring.

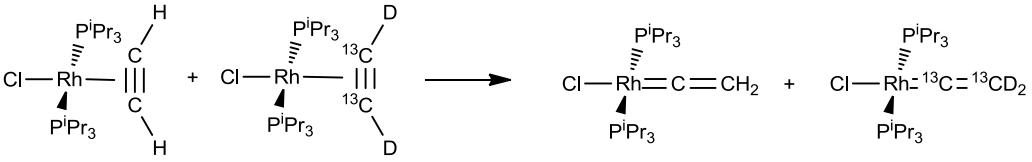

Figure 1.4.3.4: Isotopic labelled crossover experiment conducted by Grotjahn's group.

Lynam *et. al.* have probed this question further by conducting a kinetic study into the conversion of the complex in question.[99] A rate model of A ⇄ B → C (A = [RhCl(η^2-HC≡CR)(P^iPr_3)$_2$]; B = [RhCl(H)(C≡CR)(P^iPr_3)$_2$]; C = [RhCl(=C=CHR)(P^iPr_3)$_2$]) was found to fit the data best, whilst attempts to fit the data to a rate law involving a bimolecular conversion of B to C failed.

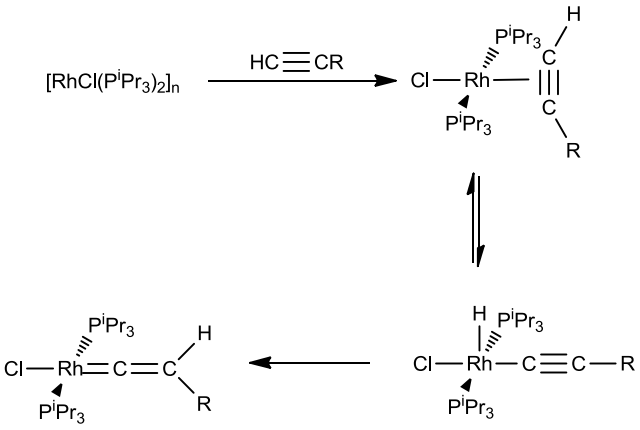

Figure 1.4.3.5: Kinetic reaction monitored by NMR spectroscopy.

These results were corroborated further by a full quantum mechanical DFT study on the full metal-ligand system by De Angelis.[100] Wakatusuki's initial report was based on the model system [RhCl(PH_3)$_2$], which gives a very different potential energy surface for the conversion than the 'more true' model [RhCl(P^iPr_3)$_2$]. For example, in Wakatsuki's study, the hydride-acetylide complex [RhCl(H)(C≡CH)(PH_3)$_2$] was found to be 39.3 kJ mol^{-1} higher in energy than the η^2-alkyne complex [RhCl(η^2-HC≡CH)(PH_3)$_2$]. De Angelis computes that this difference in energy is significantly smaller for the two equivalent complexes incorporating the P^iPr_3 ligand, a factor attributed to the different phosphine ligands involved rather than the differing levels of theory utilised. De Angelis also reported that "…the transition state for the bimolecular pathway…is calculated to be 41.1 kcal/mol (172.0 kJ mol^{-1}) above twice the energy of the alkyne complex, therefore, 15.0 kcal/mol (62.8 kJ mol^{-1}) higher than the transition state for the unimolecular

pathway…" This study was able to conclude that a bimolecular pathway for this mechanism of vinylidene formation was unlikely and emphasised the importance of performing calculations on a model system that is as close to reality as possible.

When comparing transition-metal complexes that undergo an alkyne-to-vinylidene isomerisation, it is interesting to note the characteristics of those that tend to follow Path **I**, the concerted 1,2-hydrogen shift; and those that proceed *via* Path **II**. It was noted that the Rh (I) d^8 centre may easily oxidise to Rh (III) d^6, whereas this transition is more difficult, but not impossible, for a Ru (II) d^6 to Ru (IV) d^4 system.

De Angelis and Re performed an interesting[101] theoretical study by investigating the mechanism of tautomerisation at Ru d^6 centres with varying degrees of electron-richness. The model fragments involved were $[RuCp^*(dippe)]^+$, $[RuCp^*(dmpe)]^+$, $[RuCp(PMe_3)_2]^+$, $[RuClCp'(PMe_3)]^+$, $[RuCp(CO)(PPh_3)]^+$, $[RuCl(\eta^6\text{-}C_6H_6)(PMe_3)]^+$. For each fragment, the two isomerisation pathways were calculated and the resulting energy barriers compared. A linear correlation was found between the C=C stretching frequency of the vinylidene moiety and the HOMO energy of each fragment which provided a good estimate of the degree of electron-richness for the alkyne/vinylidene derivatives. It was discovered that increasing the electron-richness of the metal-centre led to an increase in the energy gap between the alkyne and vinylidene complexes of each fragment whilst also leading to the stabilisation of the hydride-acetylide complex. This feature was illustrated best by the most electron-rich fragment sampled; $[RuCp^*(dippe)]^+$. For this fragment, the η^2-alkyne and hydride-acetylide complexes were almost isoenergetic with only an energy difference of 7.95 kJ mol^{-1} between them. Puerta was able to experimentally observe the formation of the hydride-acetylide complex $[RuCp^*(C{\equiv}CR)(H)(dippe)]^+$ as a metastable intermediate in the formation of the corresponding vinylidene complexes.[102] However, the experimental evidence also indicated that the formation of the vinylidene ligand occurred *via* an unusual deprotonation/reprotonation route and that the alkyne and hydrido-acetylide derivatives of acetylene were in equilibrium.

De Angelis and Re suggest that the formation of the vinylidene complex $[RuCp^*(=C=CH_2)(dippe)]^+$ proceeds *via* an oxidative addition/1,3-hydrogen shift pathway (Path **II**), as this system is able to readily access the hydride-acetylide

complex due to its electron-rich nature. A comparison of the two pathways calculated for this fragment showed that the η^2-C–H agostic intermediate is common to both pathways, as illustrated in Figure 1.4.3.6.

The barrier to the subsequent formation of the hydride-acetylide complex from the η^1-C–H intermediate in the 1,3-hydrogen shift pathway is only 10.0 kJ mol^{-1} while the barrier to the subsequent formation of the vinylidene complex in the direct 1,2-hydrogen shift pathway is larger at 47.3 kJ mol^{-1}. It therefore became apparent that the 1,3-hydrogen shift pathway for alkyne-to-vinylidene tautomerisation is favoured for electron-rich fragments, such as Rh complexes or Ru complexes with strong electron-donor ligands.

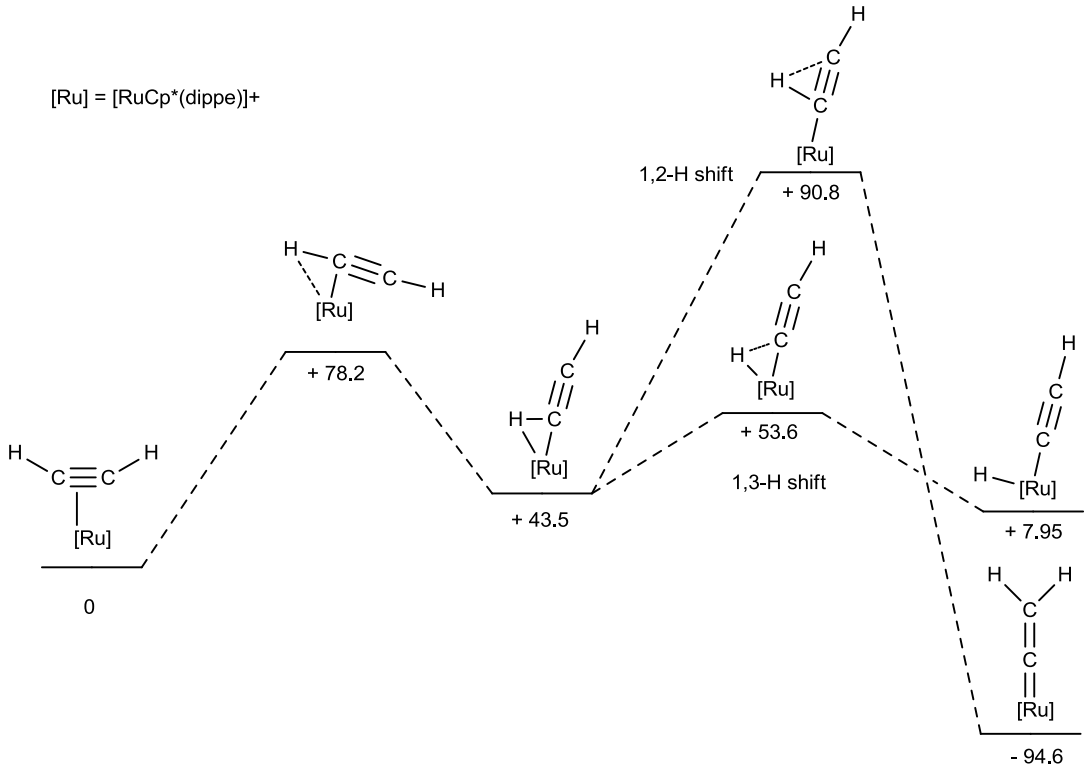

Figure 1.4.3.6: A comparison of two competing reaction pathways for vinylidene formation at $[RuCp^*(dippe]^+$ (energies in kJ mol^{-1}).

1.4.3: Path III – Alkyne Insertion into Hydride ligand

This particular mechanism of vinylidene formation is less common than the two pathways detailed in the preceding sections.[5,90,103] It was first described by Eisenstein and Caulton in 1998.[90] They observed how the addition of two

equivalents of the terminal alkyne HC≡CR (R = Ph, $SiMe_3$) to the complex $[RuX(H)(H_2)(P^tBu_2Me)_2]$ (X = Cl, I) led to the formation of the vinylidene complex $[RuX(H)(=C=CHR)(P^tBu_2Me)_2]$ and $H_2C=CHR$. A deuterium isotope labelling study conducted using DC≡CPh gave $[RuX(D)(=C=CHR)(P^tBu_2Me)_2]$ and HDC=CHPh as the only products and ^2H NMR spectroscopy confirmed the presence of the Ru–D moiety. These results were consistent with a mechanism in which the alkyne initially inserts into the ruthenium-hydride to give a vinyl ligand. This step is followed by the selective migration of the H_α of the vinyl ligand onto the metal. An *ab initio* computational study using the fragment $[RuCl(H)(PH_3)_2]$ as a model complex confirmed that this mechanism of vinylidene formation was a lower energy pathway than the 1,2-hydrogen shift pathway.

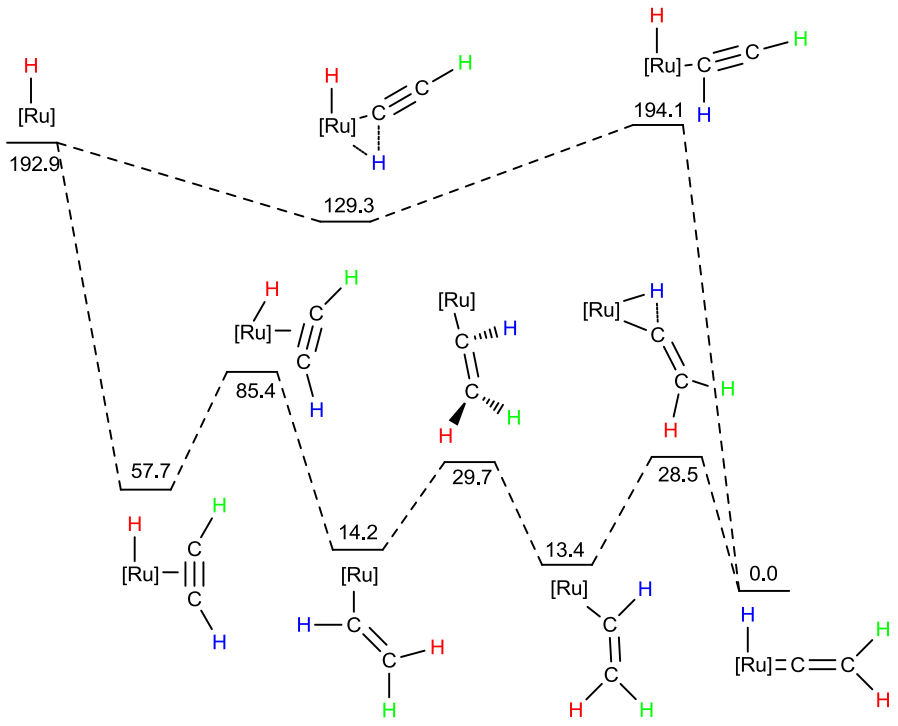

Figure 1.4.3.1: Computational results for the formation of a vinylidene ligand at [Ru] = $[RuCl(H)(PH_3)_2]$ using the B3LYP functional (all energies in kJ mol^{-1}).

The three mechanistic pathways discussed in this section are considered the predominant pathways by which alkyne-to-vinylidene tautomerisation occurs at a transition-metal centre. The majority of examples discussed in the literature fall into one of these three categories. However, it will be shown in this thesis that a fourth alternative pathway may operate when an appropriate ligand able to act as an intramolecular base is present.

1.5: Reactivity of Transition-Metal Vinylidene and Allenylidene complexes

The reactivity of transition-metal vinylidene and allenylidene complexes towards electrophiles and nucleophiles has been discussed in Section 1.2. The current section will deal with two specific examples of the reactive behaviour of these ligands which are particularly relevant to this thesis.

1.5.1: Formation of Oxacyclocarbene complexes

The preference for nucleophiles to attack at C_α has been attributed to an electron-deficiency at this atom. This feature has been exploited in the formation of oxacyclocarbene ligands, which form upon addition of ω-alkynols of the general form $HC{\equiv}C(CH_2)_nOH$ *via* a hydroxy-vinylidene ligand.[104,105,106] The most common forms of these ligands, which are technically Fischer-carbenes, consist of the five-, six- and seven-membered ring types, although reports of seven-membered ring systems are rarer.

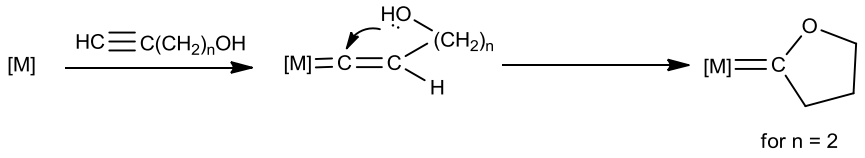

Figure 1.5.1.1: Formation of an oxacyclocarbene complex.

In 1996, Bianchini, Peruzzini and Rossi[107] demonstrated that the addition of the β- and γ-alkynols ($HC{\equiv}C(CH_2)_nOH$, n = 2, 3) to the rhenium precursor complex $[Re(CO)_2(H_2)(triphos)]^+$ (triphos = $MeC\{CH_2PPh_2\}_3$) resulted in the formation of the five- and six-membered oxacyclocarbene complexes respectively, as illustrated in Figure 1.5.1.2. The authors also reported one of the first examples of a oxacycloheptylidene ligand obtained from the reaction of $[Re(CO)_2(H_2)(triphos)]^+$ with 5-hexyn-1-ol ($HC{\equiv}C\{CH_2\}_4OH$), as shown in Figure 1.5.1.3.

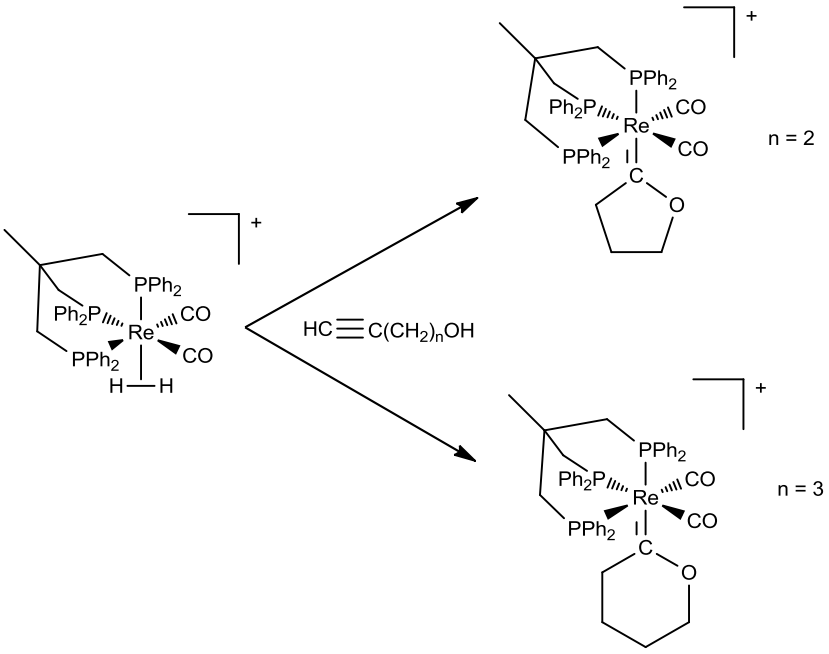

Figure 1.5.1.2: Formation of oxacyclocarbene complexes derived from $[Re(CO)_2(H_2)(triphos)]^+$.

The formation of the seven membered oxacyclocarbene ligand was observed to occur *via* an intermediate hydroxybutylvinylidene complex, which was identified and spectroscopically characterised at temperatures below – 10 °C. At temperatures above – 10 °C, the thermodynamic product containing the seven-membered oxacyclocarbene ligand formed. The authors also noted that in their case "…the intramolecular attack by the hydroxy group is increasingly disfavoured as the number of CH_2 spacers between the triple bond and the OH group in the alkynol increases." This statement has been confirmed by a number of reports recording the synthesis of complexes containing oxacyclocarbene ligands.[107,108]

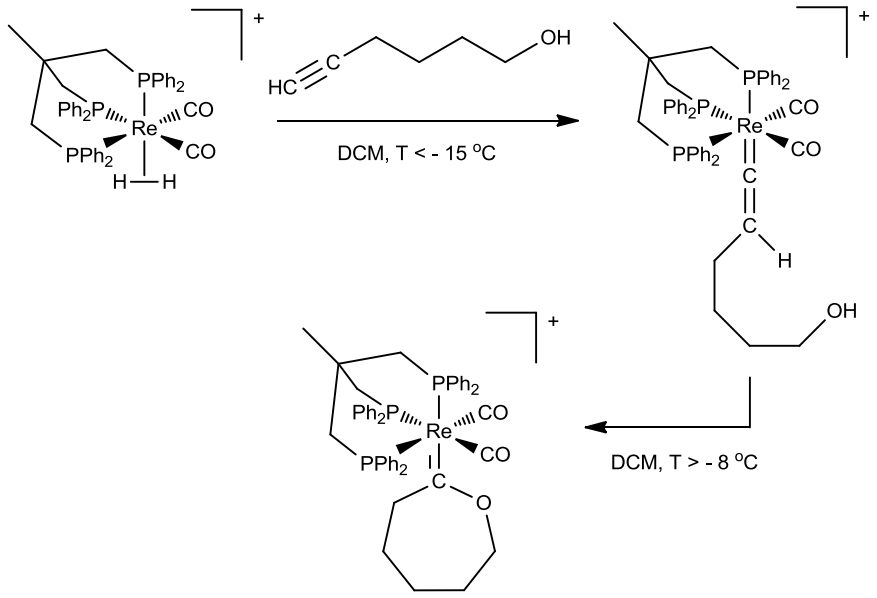

Figure 1.5.1.3: Formation of an oxacycloheptylidene complex.

Other research groups have also reported the identification of hydroxy-vinylidene intermediates in the formation of these oxacyclocarbene complexes. One such example was reported by Whiteley[109] in 1996 who successfully isolated and structurally characterised the relatively stable hydroxypropylvinylidene complex [Mo(=C=CH{CH_2}$_3$OH)(η^7-C_7H_7)(dppe)] obtained by the reaction of the *in situ*-generated complex [Mo(η^7-C_7H_7)(dppe)($OCMe_2$)] with 4-pentyn-1-ol. The hydroxy-vinylidene complex could then be converted into the six-membered oxacyclocarbene complex by heating in methanol at reflux for 18 hours, as shown in Figure 1.5.1.4. This reactivity contrasted with the analogous reaction utilising dppm as a chelating phosphine ligand which resulted instead in the direct formation of the oxacyclocarbene derivative.

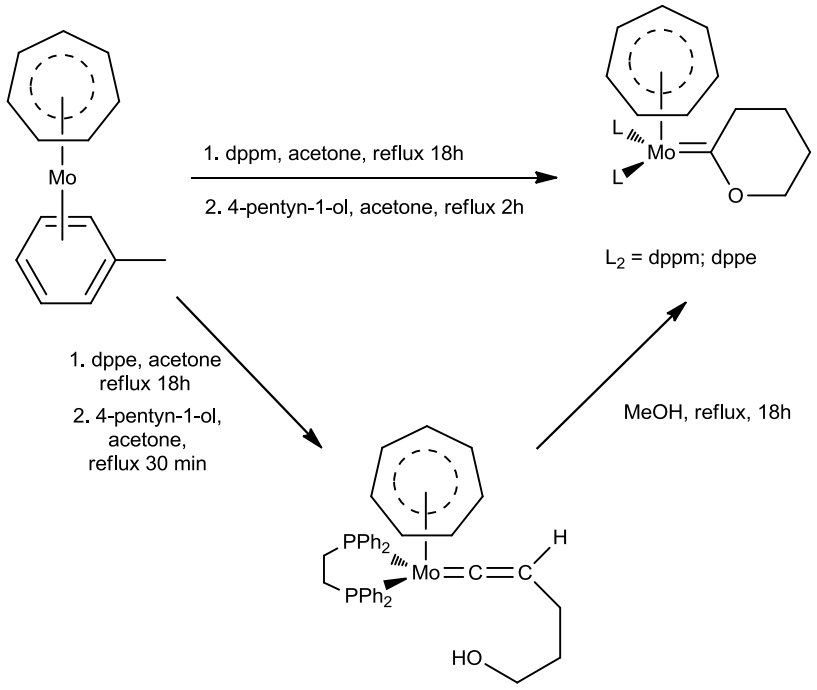

Figure 1.5.1.4: Formation of a Mo-oxacyclocarbene complex *via* a hydroxypropylvinylidene intermediate.

The cycloisomerisation process may be conducted in a catalytic manner and has been exploited to produce a range of compounds including furan and pyran derivatives. An example of the catalytic cycloisomerisation of aromatic alkynols to give the seven-membered oxepines[110] is illustrated in Figure 1.5.1.5.

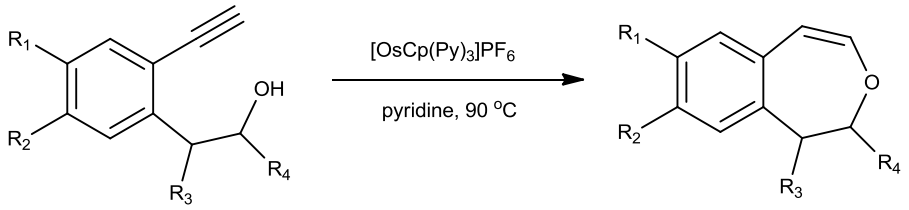

Figure 1.5.1.5: 7-*endo* cycloisomerisation of aromatic alkynols to benzoxepines.

1.5.2: Allenylidene to Indenylidene Rearrangement

The synthesis of allenylidene complexes by the dehydration of a propargylic alcohol substrate at a suitable transition-metal centre was a well-known process when Hill[111] reported the formation of what was initially thought to be the allenylidene complex $[RuCl_2(=C=C=CPh_2)(PPh_3)_2]$ from $[RuCl_2(PPh_3)_3]$ and $HC{\equiv}CCPh_2OH$ upon heating at reflux in THF. A preparation of this complex had been attempted by Dixneuf's group in 1996,[112] however they reported instead the formation of the dinuclear allenylidene complex shown in Figure 1.5.2.1 by conducting the reaction at room temperature and in the presence of $NaPF_6$.

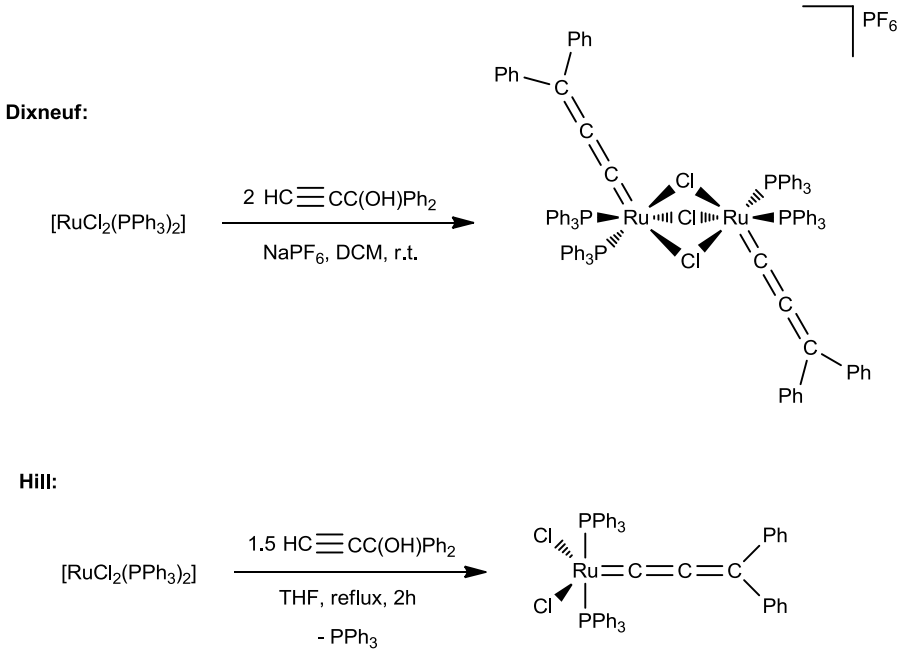

Figure 1.5.2.1: Reaction of $HC{\equiv}CC(OH)Ph_2$ with $[RuCl_2(PPh_3)_3]$.

The product Hill obtained could undergo ligand exchange with PCy_3 to give what was thought to be $[RuCl_2(=C=C=CPh_2)(PCy_3)_2]$, shown to be a good catalyst for olefin metathesis.[113] However, it was soon noticed that the analytical and spectroscopic data of the product obtained by Hill's synthetic procedure did not match the molecular structure proposed.[114,115] In particular, it was noted that the $^{13}C\{^1H\}$ NMR data of the product was inconsistent with the presence of an allenylidene ligand. Careful analysis by 2D-NMR techniques by Fürstner's group[115] revealed that a phenylindenylidene ligand was instead formed, as illustrated in Figure 1.5.2.2.

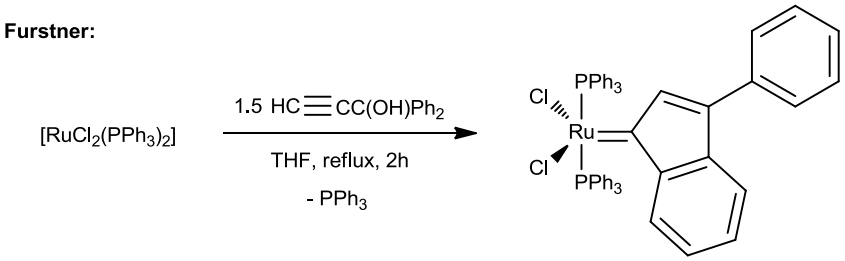

Figure 1.5.2.2: Formation of the phenylindenylidene complex; the true product of the reaction of $HC{\equiv}CC(OH)Ph_2$ with $[RuCl_2(PPh_3)_3]$.

A number of phenylindenylidene complexes have proven to be excellent catalysts for olefin metathesis,[116,117] which will be discussed further in Section 1.6.2. The mechanism by which the rearrangement is thought to occur has been extensively probed by Dixneuf.[118,119] He was able to observe an alkenylcarbyne species by low temperature NMR studies as an intermediate in the allenylidene-to-indenylidene isomerisation. Addition of triflic acid to the diphenylallenylidene complex $[RuCl(=C=C=CPh_2)(PCy_3)(\eta^6\text{-}p\text{-cymene})]^+$ at – 40 °C in CD_2Cl_2 led to the observation of resonances due to the alkenylcarbyne complex shown in Figure 1.5.2.3. Allowing the temperature to rise above – 20 °C saw this species convert to the phenylindenylidene derivative.

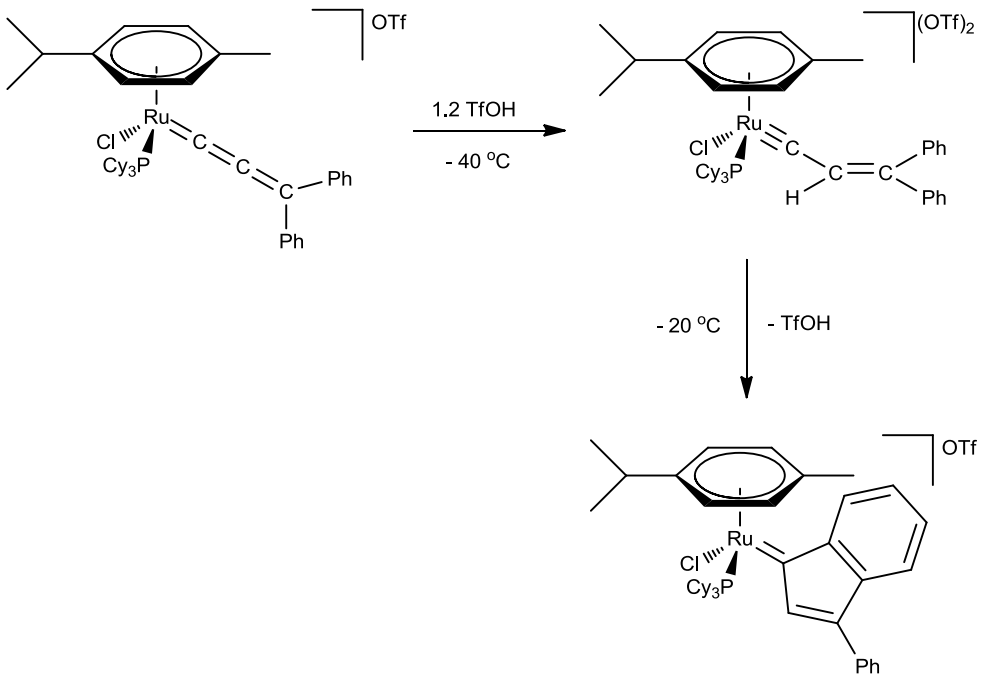

Figure 1.5.2.3: Observation of an intermediate alkenylcarbene species in the formation of a phenylindenylidene complex.

Mechanistic studies reported by Schanz[120] also corroborated Dixneuf's findings. A crystal structure of the alkenylcarbene complex $[RuCl_3(\equiv CCH{=}CPh_2)(PPh_3)_2]$, proposed as in intermediate in indenylidene ligand formation was obtained from this study. It was proposed that the rearrangement occurs *via* a phenyl substitution onto the electrophilic C_α atom which is favoured if a canonical form of the alkenylcarbyne shown in Figure 1.5.2.4 is considered.

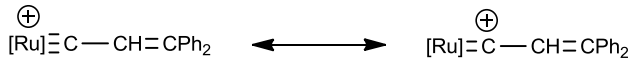

Figure 1.5.2.4: Two canonical forms of the Ru-alkenylcarbene complex.

The protonation of ruthenium allenylidene ligands had been previously demonstrated to give rise to unstable cationic alkenylcarbyne complexes,[121-124] however none had been observed to undergo this rearrangement to the indenylidene form.

1.6: Catalytic Applications of Transition-Metal Vinylidene and Allenylidene complexes

A large number of transition-metal vinylidene and allenylidene complexes have been implicated as intermediates in the catalytic transformations of small organic molecules and different transition-metals[8] have been utilised for different transformations. For example, a vinylidene derivative of $Pd(OAc)_2$ has been implicated in the catalytic coupling of norbornene and $HC{\equiv}CPh$[125] whilst the synthesis of pyrrole-fused heterocycles has been shown to involve an alkyne-to-vinylidene tautomerisation at the $AuBr_3$ catalyst.[126] DFT calculations performed on the catalytic copper-mediated alkyne-azide "click" coupling reaction (CuAAC) have proposed the involvement of a strained copper-vinylidene species.[127] These reactions are illustrated in Figure 1.6.1.

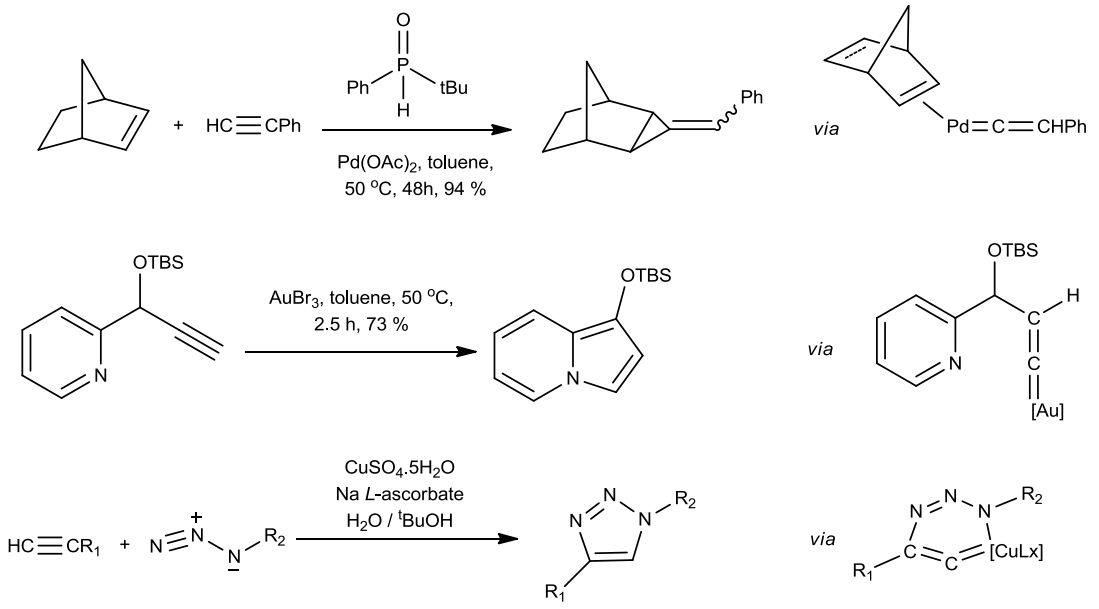

Figure 1.6.1: Examples of catalytic transformations of small organic molecules mediated by transition metal vinylidene complexes.

Nishibayashi has shown that a ruthenium allenylidene complex is a key component of the propargylic substitution of propargylic alcohols with a variety of nucleophiles[128] by $[RuClCp^*(\mu_2\text{-}SR)]_2$. Further select examples of catalytic processes that are relevant to this thesis involving ruthenium vinylidene and allenylidene complexes will be discussed in more detail in the next two sections.

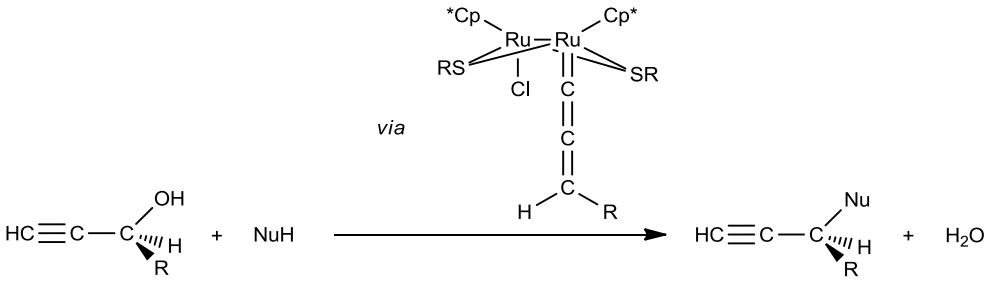

Figure 1.6.2: Propargylic substitution reaction mediated by a ruthenium-allenylidene complex.

1.6.1: Ruthenium Vinylidene complexes

The involvement of a vinylidene ligand in the catalytic transformations of terminal alkynes often makes use of the properties imposed on it upon coordination; namely, that the C_α atom becomes susceptible to nucleophilic attack. This feature has been exploited in the *anti*-Markovnikov addition of nucleophiles to alkynes.

Examples of this have been demonstrated by the groups of Dixneuf[129,130] and Kirchner[131] who have shown that the coupling of carboxylic acids to terminal alkynes to give enol esters proceeds *via* vinylidene intermediates.

The coupling of carboxylic acids with terminal alkynes may result in the formation of three isomeric products; (*E*)- and (*Z*)-enol esters are obtained by an *anti*-Markovnikov addition of the acid whilst the geminal isomer results from Markovnikov addition. Dixneuf[130] has demonstrated that the complex [Ru(methallyl)$_2$(dppb)] will preferentially produce the (*Z*)-enol esters when used to catalyse the coupling between carboxylic acids and terminal alkynes with a wide range of substituents. Kirchner's group[131] screened a number of tris(pyrazolylborate) complexes and found that [RuCl(HBpz)(COD)] gave the highest proportion of the (*E*)-enol ester (a product distribution of 1.63:1:0 for the (*E*):(*Z*):(*gem*)-enol esters).

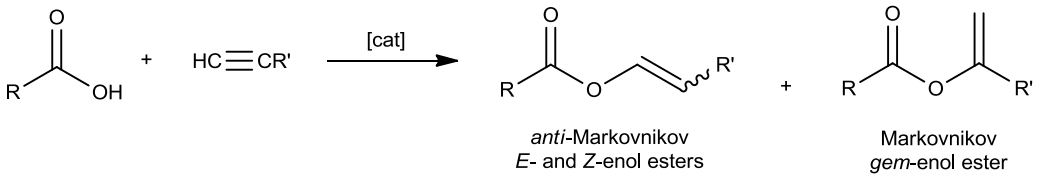

Figure 1.6.1.1: Catalytic coupling of carboxylic acids and terminal alkynes.

The mechanism proposed by Dixneuf[130] for the coupling of these substrates is shown in Figure 1.6.1.2. His group demonstrated that in the presence of a carboxylic acid, the two methallyl ligands are lost and replaced by two carboxylate ligands coordinated in a κ^2-fashion, indicating that this is likely to be an initial step in the overall mechanism. Furthermore, the bis(carboxylate) complex [Ru(κ^2-OBz)$_2$(dppb)] could be isolated at the end of the catalytic coupling reaction between benzoic acid and hexyne, supporting the idea that this is the active form of the catalyst. Once the active species is generated, it is proposed that one of the carboxylate ligands may then alter its coordination mode to monodentate, thus creating a vacant site for alkyne-to-vinylidene tautomerisation. The vinylidene ligand may then undergo nucleophilic attack by the acid in an intermolecular fashion, to give the coordinated form of the enol ester which can be liberated upon protonation. This mechanism is illustrated in Figure 1.6.1.2.

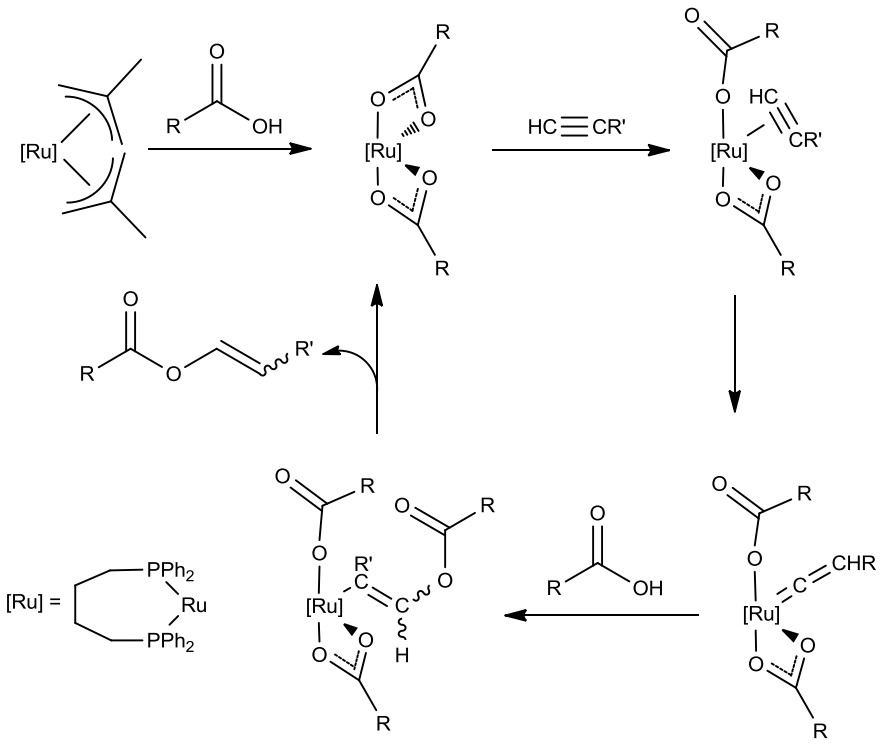

Figure 1.6.1.2: Proposed mechanism for the catalytic production of *E*- and *Z*-enol esters.

Dixneuf also suggests that the nucleophilic attack of the carboxylate to the alkyne is an intermolecular process: that is, the carboxylate ligands coordinated to the metal in its active form do not react with the vinylidene ligand to give the enol ester. This claim is based on the results of a coupling reaction between HC≡CPh (four equivalents) and PhCOOH (two equivalents) by the catalyst [Ru(κ^2-$OCOCF_3$)$_2$(dppb)] which selectively produced (*Z*)-styryl benzoate whilst the catalyst was recovered unchanged, as shown in Figure 1.6.1.3.

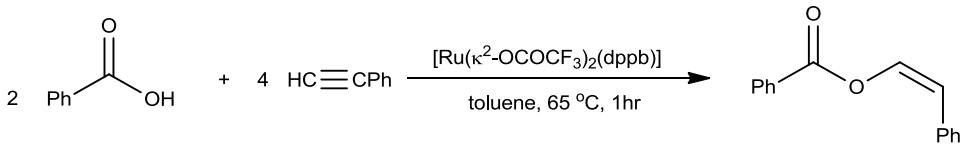

Figure 1.6.1.3: Catalytic coupling of benzoic acid and phenylacetylene by [Ru(κ^2-$OCOCF_3$)$_2$(dppb)].

Ruthenium complexes have also been shown to promote the formation of the (*gem*)-enol ester. The formation of this isomer is thought to occur *via* a different mechanistic pathway, which does not involve the formation of a vinylidene ligand. Mitsudo and Watanabe[132] showed that the selective production of the *gem*-enol ester was facilitated by the [Ru(η^5-COD)$_2$]/PR_3/maleic anhydride system.

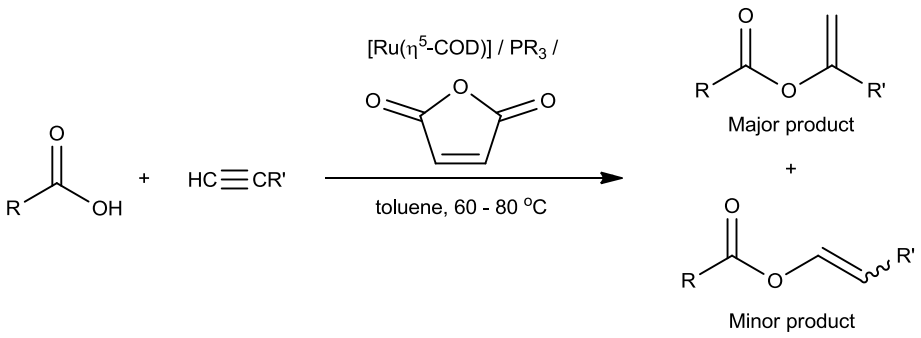

Figure 1.6.1.4: Selective formation of a (*gem*)-enol ester.

The mechanism by which these geminal products may be obtained is shown in Figure 1.6.1.5. The alkyne coordinates to the metal in a η^2-fashion, however it does not subsequently undergo tautomerisation to the corresponding vinylidene. Instead, the carboxylic acid is thought to attack the alkyne at this point, to generate a metalloenolester derivative. The organic product may then be liberated by protonation.[133,134] The regioselectivity of product distribution is thought to be affected by the steric and electronic properties of ancillary ligands and substrate substituents.

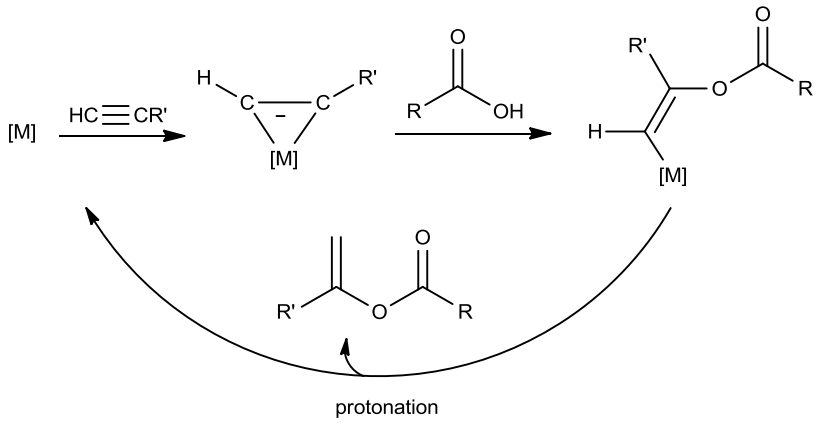

Figure 1.6.1.5: Markovnikov addition of a carboxylic acid to a terminal alkyne.

Other catalytic *anti*-Markovnikov P-, N- and O-nucleophilic additions are also thought to proceed *via* mechanisms similar to that shown in Figure 1.6.1.2.[133] As mentioned earlier, (Section 1.2) the addition of water to terminal alkynes to yield aldehydes is thought to proceed *via* the intermolecular attack of water onto the vinylidene C_α. The resulting acyl derivative can then be liberated from the metal as an aldehyde.[103,135,136]

Related to these reactions is the production of β-oxo esters by the coupling of carboxylic acids with propargylic alcohols. Watanabe used the same catalytic system described above for the coupling of acetic acid with 1-ethynylcyclohexanol giving the β-oxopropyl ester in 54 % yield.[132] Dixneuf's group were subsequently able to demonstrate that their catalytic systems using $[RuCl_2(p\text{-cymene})(PR_3)]$[137,138] and $[Ru(\mu\text{-}O_2CH)(CO)_2(PPh_3)]_2$[139] were also able to catalyse the coupling of carboxylic acids and propargylic alcohols with a range of substituents. More recently, Bauer[140] showed that novel ruthenium-phosphoramidite complexes were also efficient catalysts for this process.

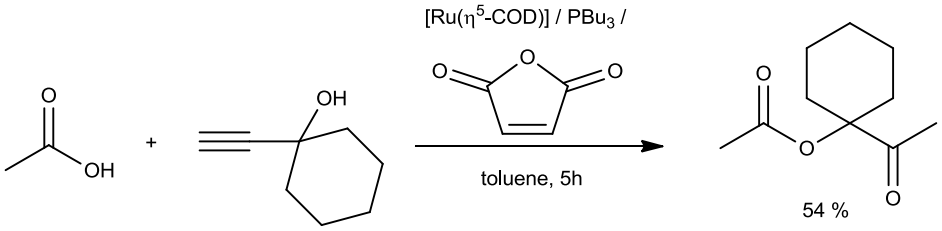

Figure 1.6.1.6: Catalytic coupling of acetic acid with 1-ethynylhexanol to give a β-oxo ester.

The mechanism proposed for the formation of these compounds is very similar to that for the Markovnikov addition of carboxylic acids to terminal alkynes in that the acid again reacts with the alkyne electophilically when it is coordinated in a η^2-fashion. This is followed by an intramolecular transesterification and then a keto-enol tautomerisation to give the coordinated form of the β-oxopropyl ester. Dixneuf[139] has used $[Ru(\mu\text{-}O_2CH)(CO)_2(PPh_3)]_2$ to couple the steroids mestranol, norethindrone and levonorgestrel with carboxylic acids with full retention of configuration. However, it has not been indicated whether a different mechanism may operate for the bimetallic system.

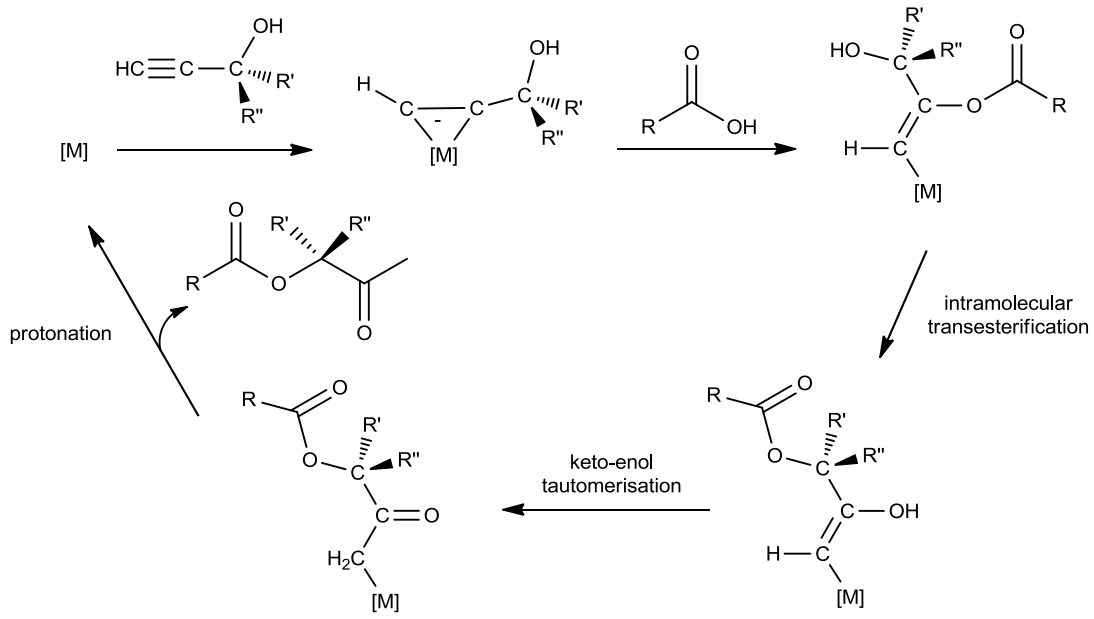

Figure 1.6.1.7: Proposed mechanism for the formation of β-oxopropyl esters.

1.6.2: Ruthenium Allenylidene complexes

The role of ruthenium allenylidene complexes in propargylic substitution reactions has been referred to earlier in this section. This catalytic transformation is thought to exploit the inherent electrophilic properties of the C_γ of the cumenylidene chain. Nishibayashi's group have made significant progress in this field using their bimetallic $[RuClCp^*(\mu_2\text{-}SR)]_2$ system. The mechanism by which this catalyst operates was derived from stoichiometric studies[128,141] and is illustrated in Figure 1.6.2.1. It is thought to involve the initial formation of a hydroxy-vinylidene ligand which undergoes dehydration to form an allenylidene ligand. Nucleophilic attack then occurs at the C_γ position to regenerate a vinylidene ligand. This may then tautomerise back to its alkyne form and then dissociate from the ruthenium centre. It was also shown that a diruthenium system is essential for successful transformations. The ruthenium that is not involved in the formation of the allenylidene ligand is thought to act as an 'electron pool' to facilitate the ligand exchange step (i.e. in the exchange of one η^2-bound alkyne for another in the final step of the mechanism). DFT calculations performed at the B3LYP level of theory also support this proposal.[142]

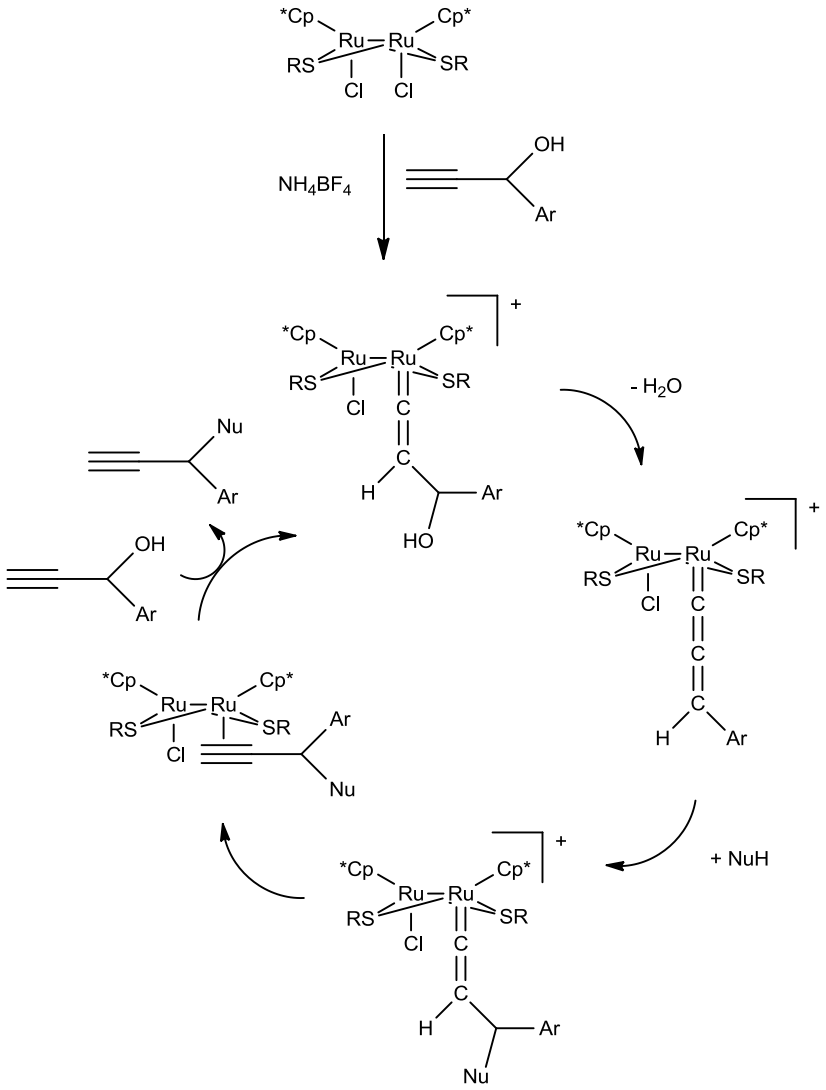

Figure 1.6.2.1: Proposed mechanism for propargylic substitution mediated by $[Ru(Cp^*)(Cl)(\mu_2\text{-}SR)]_2$.

Another significant field of catalysis in which ruthenium allenylidene complexes feature heavily is olefin metathesis. Fürstner first demonstrated in 1998 that the ruthenium allenylidene complex $[RuCl(arene)(=C=C=CAr_2)(PR_3)]X$ could be used as a catalyst for RCM of a variety of substrates.[143,144] Since then, it has been demonstrated that this class of complexes will also catalyse ROMP and enyne metathesis reactions.[145-147] The choice of ligands has been shown to be important to the activity of the complex, the optimum combination being $[RuCl(=C=C=CPh_2)(PCy_3)(p\text{-cymene})]OTf$,[117] as the allenylidene form is not the active species. Instead, these complexes have been shown to undergo a rearrangement to their indenylidene forms, with concomitant loss of the arene ligand. This generates the active form of the catalyst: $[RuCl(indenylidene)(PR_3)(OTf)]$.[117] The mechanism by which the allenylidene-indenylidene rearrangement occurs was

discussed in Section 1.5.2. It is presumed that the *p*-cymene ligand is the most easily displaced arene ligand, and that the OTf counterion is able to weakly interact with the ruthenium centre to give the active form,[119] as shown in Figure 1.6.2.2. Kinetic studies have demonstrated that the choice of solvent is also an important factor; Dixneuf has shown that the rearrangement occurs faster in benzene than in DCM, which is thought to be due to a stronger interaction between the OTf counterion and the cationic rearranging species in the less polar solvent.[148]

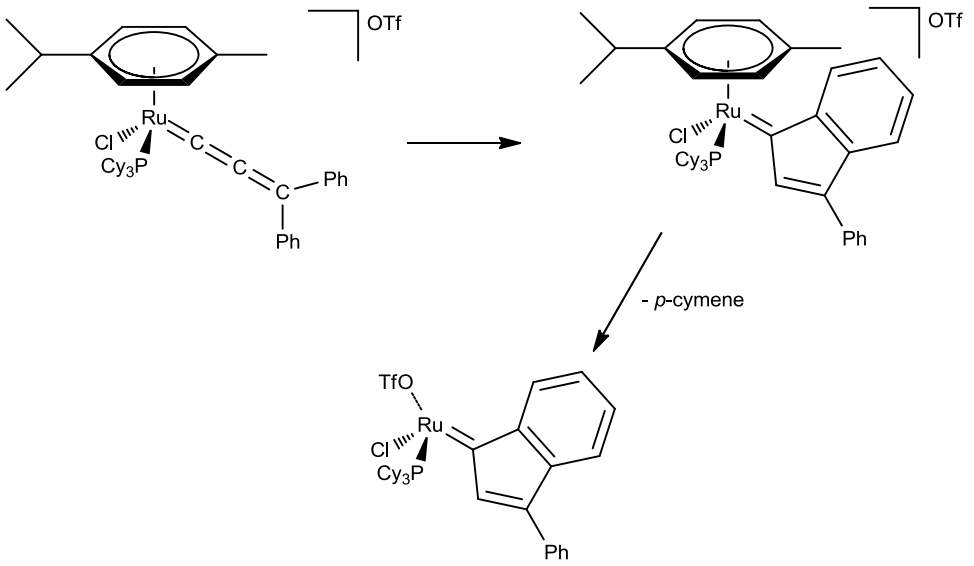

Figure 1.6.2.2: Formation of the active catalytic species containing an indenylidene ligand.

The ruthenium-indenylidene complexes have been described as 'attractive alternatives'[116] to the Grubbs-type benzylidene catalysts as they are easily synthesised and have robust thermal stability. Consequently, significant efforts have been made to optimise the activity of these complexes in various forms of metathesis reactions. The improvements made to the indenylidene complexes have mimicked the improvements made to the original Grubbs first generation catalysts of the form $[RuCl_2(=CHPh)(PR_3)_2]$; in that more electron-donating ligands such as PCy_3 or a *N*-heterocyclic carbene (NHC) ligand have been included within the coordination sphere of the metal. In 2004, Nolan's group[149] reported a high yielding one-pot synthesis of $[RuCl_2(3\text{-phenylindenylidene})(PCy_3)_2]$. This complex, and its PPh_3-containing analogue, are used as precursors to the NHC-containing complexes $[RuCl_2(3\text{-phenylindenylidene})(PR_3)(NHC)]$ (NHC = IMes or IPr: see Figure 1.6.2.3).[150]

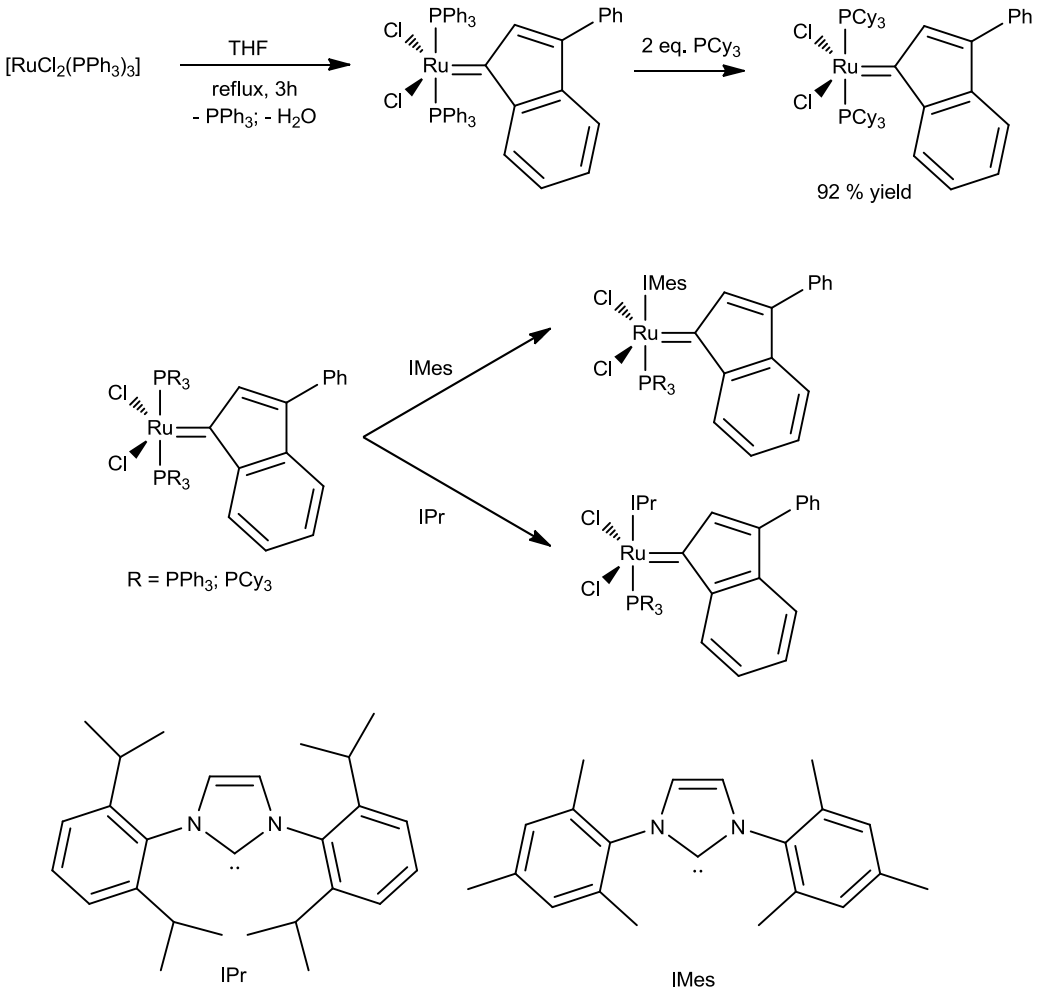

Figure 1.6.2.3: Formation of PR_3 and NHC-containing ruthenium-indenylidene catalysts.

1.7: Conclusions

As has been shown, the chemistry of transition metal vinylidene and allenylidene complexes is well understood. There have been numerous investigations undertaken; first to establish their structure and coordination chemistry, then to understand their reactivity and potential catalytic application. The precise mechanism of their formation has also occupied a number of researchers in this field, and the use of computational modelling methods in this area has been particularly important. This thesis uses the groundwork laid by these researchers to understand the reactive behaviour of vinylidene complexes derived from ruthenium carboxylate complexes.

1.8: Project Aims

A variety of ruthenium-precursors containing a range of ligands within the coordination sphere have been used to synthesise vinylidene and allenylidene complexes. This thesis is concerned with exploring the reactive behaviour of the easily synthesised complex $[Ru(\kappa^2\text{-}OAc)_2(PPh_3)_2]$, **1**. This complex was first synthesised by Wilkinson[151] in 1973, however has received little subsequent attention. Despite the simplicity of the procedure reported by Wilkinson, an improved procedure for its synthesis was developed giving the orange-red air stable complex in 92 % yield from $[RuCl_2(PPh_3)_3]$. A crystal structure of this complex was also obtained, confirming the mutually *cis*-arrangement of the two PPh_3 ligands. A full discussion of its crystallographic features is provided elsewhere.[152,153]

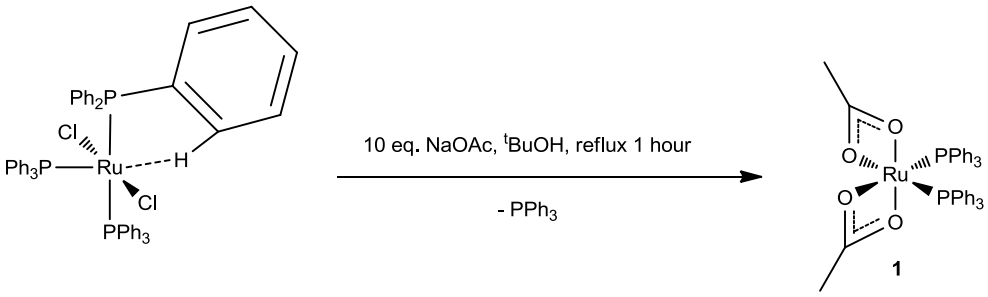

Figure 1.8.1: Synthesis of $[Ru(\kappa^2\text{-}OAc)_2(PPh_3)_2]$, **1**.

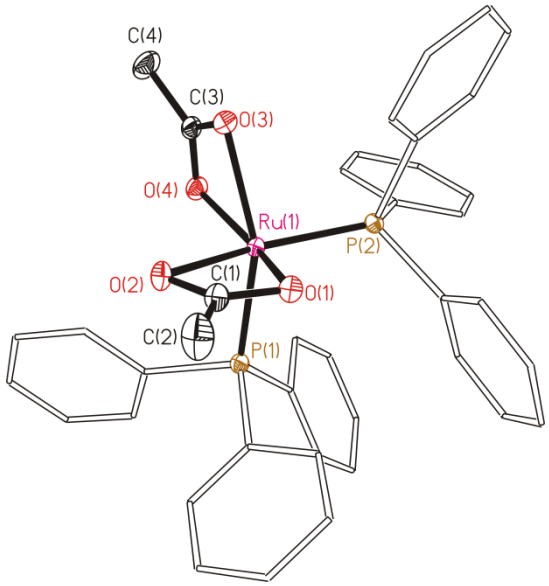

Figure 1.8.2: ORTEP structure of complex 1, with thermal ellipsoids, where shown, at the 50 % probability level. Hydrogen atoms and CH_2Cl_2 of crystallisation are omitted for clarity.

The fluxional properties of carboxylate ligands have been well-established, so it was with a view to exploiting this inherent property that it was reacted with a number of terminal alkynes containing substituents with widely varying steric and electronic properties. Simple terminal alkynes of the general form HC≡CR were expected to react to form vinylidene complexes. Propargylic alcohols, HC≡CCRR'OH, may form either hydroxy-vinylidene, allenylidene or vinylvinylidene derivatives and ω-alkynols, $HC{\equiv}C(CH_2)_nOH$, may give hydroxy-vinylidene or oxacyclocarbene complexes. The possible formation of an indenylidene complex upon the reaction of **1** with the diphenyl-substituted propargylic alcohol $HC{\equiv}CC(OH)Ph_2$ was also considered. The formation of vinylidene complexes may also lead to the synthesis of novel acetylide complexes, which could be obtained upon deprotonation of the vinylidene ligand. As such, it may be envisioned that a library of complexes may be derived from this ruthenium precursor, which would provide an understanding of the reactive behaviour of complex **1**.

Mechanistic studies into the formation of the above-mentioned complexes would also be interesting, particularly with regard to the alkyne-to-vinylidene tautomerisation pathway. It may be expected that a 1,2-hydrogen shift pathway appears most plausible for this complex, given that the ruthenium centre is unlikely to be electron-rich enough to support an oxidative addition pathway. The isolation and characterisation of any intermediate species in the formation of these complexes would also be vital.

Whilst this complex has been known in the literature for almost 40 years, it has received very little attention, particularly with regards to it catalytic application. A notable exception to this is a report by Sharpless in 2005[154] who was investigating the possibility for ruthenium complexes to promote the formation of 1,5-substituted 1,2,3-triazole compounds *via* a 'click' coupling reaction between a terminal alkyne and a substituted azide compound. Complex **1** was found to promote the formation of the 1,4-substituted 1,2,3-triazole compounds, whilst the η^5-ring complexes $[RuClCp(PPh_3)_2]$ and $[RuClCp^*(PPh_3)_2]$ complexes gave the desired 1,5-substituted 1,2,3-triazole compounds exclusively. Thus, complex **1** was found to give the same regioisomers produced by copper catalysts which are typically employed in the CuAAC process.

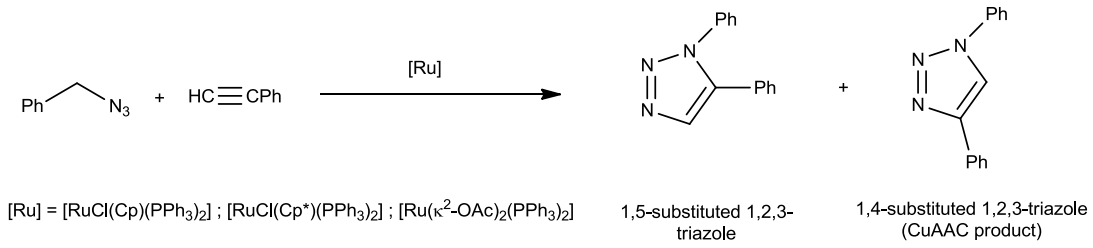

Figure 1.8.3: 'Click' coupling reaction between phenylacetylene and benzyl azide mediated by ruthenium complexes.

Consequently, this thesis intends to explore the chemistry of the neglected ruthenium complex **1** with particular regard to its reactivity towards terminal alkynes.

1.9: References

1. Bruce, M. I. *Chem. Rev*. **1991**, *91*, 197.

2. Bruce, M. I. *Chem. Rev*. **1998**, *98*, 2797.

3. Bruneau, C.; Dixneuf, P. H. *Acc. Chem. Res*. **1999**, *32*, 311.

4. Katayama, H.; Ozawa, F. *Coord. Chem. Rev*. **2004**, *248*, 1703.

5. Lynam, J. M., *Chem. Eur. J*. **2010**, *16*, 8238.

6. Cadierno, V., Gimeno, J., *Chem. Rev*. **2009**, *109*, 3512.

7. King, R. B. (ed). Coord. *Chem. Rev*. **2004**, *248*, 1531.

8. Bruneau, C., Dixneuf, P. H., Eds. *Metal Vinylidenes and Allenylidenes in Catalysis: From Reactivity to Applications in Synthesis*, **2008**, Wiley VCH: Weinheim, Germany.

9. Dykstra, C. E.; Schaefer, H. F., III, *J. Am. Chem. Soc*. **1978**, *100*, 1378.

10. Silvestre, J., Hoffmann, *Helv. Chim. Acta*. **1985**, *68*, 1461.

11. Stanton, J. F.; DePinto, J. T.; Seberg, R. A.; Hodges, J. A.; McMahon, R. J. *J. Am. Chem. Soc*. **1997**, *119*, 429.

12. Sherrill, C. D.; Brandow, C. G.; Allen, W. D.; Schaefer, H. F., III *J. Am. Chem. Soc*. **1996**, *118*, 7158.

13. Hehre, W. J.; Pople, J. A.; Lathan, W. A.; Radom, L.; Wasserman, E.; Wasserman, Z. R. *J. Am. Chem. Soc*. **1976**, *98*, 4378.

14. Mills, O. S.; Redhouse, A. D. *Chem. Commun*. **1966**, 444.

15. Mills, O. S.; Redhouse, A. D. *J. Chem. Soc. A*. **1968**, 1282.

16. King, R. B.; Saran, M. S. *Chem. Commun*. **1972**, 1053.

17. Fischer, E. O.; Kalder, H. J.; Frank, A.; Köhler, F. H.; Huttner, G. *Angew. Chem. Int. Ed*. **1976**, *15*, 623.

18. Berke, H. *Angew. Chem. Int. Ed.* **1976**, *15*, 624.

19. Zhu, J.; Lin, Z. Theoretical Aspects of Metal Vinylidene and Allenylidene Complexes (Chapter 4) *Metal Vinylidenes and Allenylidenes in Catalysis: From Reactivity to Applications in Synthesis*, (Bruneau, C., Dixneuf, P. H., Eds.) **2008**, Wiley VCH: Weinheim, Germany.

20. Wakatsuki, Y. *J. Organomet. Chem*. **2004**, *689*, 4092.

21. Kostić, N. M.; Fenske, R. F. *Organometallics* **1982**, *1*, 974.

22. Bianchini,C.; Casares, J. A.; Peruzzini, M.; Romerosa, A.; Zanobini, F. *J. Am. Chem. Soc*. **1996**, *118*, 4585.

23. Bruce, M. I.; Swincer, A. G.; Wallis, R. C. *J. Organomet. Chem*. **1979**, *171*, C5.

24. Jiménez-Tenorio, M. A.; Jiménez-Tenorio, M.; Puerta, M. C.; Valerga, P. *Organometallics* **1997**, *16*, 5528.

25. Wolf, J.; Werner, H. *J. Organomet. Chem*. **1987**, *336*, 413.

26. Wolf, J.; Zolk, R.; Schubert, U.; Werner, H. *J. Organomet. Chem*. **1988**, *340*, 161.

27. Werner, H.; Wolf, J.; Muller, G.; Kruger, C. *J. Organomet. Chem*. **1988**, *342*, 381.

28. Delbecq, F. *J. Organomet. Chem*. **1991**, *406*, 171.

29. Carvalho, M. F. N. N.; Henderson, R. A.; Pombeiro, A. J. L.; Richards, R. L. *J. Chem. Soc. Chem. Commun*. **1989,** 1796.

30. Hohn, A.; Werner, H. *Angew. Chem. Int. Ed*. **1986**, *25*, 737.

31. Moigno, D.; Callejas-Gasper, B.; Gil-Rubio, J.; Werner, H.; Kiefer, W. *J. Organomet. Chem*. **2002**, *661*, 181.

32. Schilling, B. E. R.; Hoffmann, R.; Lichtenberger. D. L. *J. Am. Chem. Soc*. **1979**, *101*, 585.

33. Gamasa, M. P.; Gimeno, J.; Lastra, E.; Martin, B. M.; Anillo, A.; Tiripicchio, A. *Organometallics* **1992**, *11*, 1373.

34. Miller, D. C.; Angelici, R. J. *Organometallics* **1991**, *10*, 79.

35. Bruce, M. I.; Dean, C.; Duffy, D. N.; Humphrey, M. G.; Koustsantonis, G. A. *J. Organomet. Chem*. **1986**, *314*, 213.

36. Consiglio, G.; Morandini, F.; Ciani, G. F.; Sironi, A. *Organometallics* **1986**, *5*, 1976.

37. Beddoes, R. L.; Bitcon, C.; Grime, R. W.; Ricalton A.; Whiteley, M. W. *J. Chem. Soc. Dalton Trans*. **1995**, 2873.

38. Consiglio, G.; Morandini, F. *Inorg. Chim. Acta*. **1987**, *127*, 79.

39. Yang, S. Y.; Wen, T. B.; Jia, G.; Lin, Z. *Organometallics* **2000**, *19*, 5477.

40. Ariafard, A.; Zare, K. *Inorg. Chem. Commun*. **2004**, *7*, 999.

41. Esteruelas, M. A.; Gómez, A. V.; López, A. M.; Modrego, J.; Oñate, E. *Organometallics* **1997**, *16*, 5826.

42. Cadierno, V.; Gamasa, M. P.; Gimeno, J.; López-González, M. C.; Borge, J.; García-Granda, S. *Organometallics* **1997**, *16*, 4453.

43. Grime, R. W.; Helliwell, M.; Hussain, Z. I.; Lancashire, H. N.; Mason, C. R.; McDouall, J. J. W.; Mydlowski, C. M.; Whiteley, M. W. *Organometallics* **2008**, *27*, 857.

44. Bruce, M. I.; Wallis, R. C. *J. Organomet.Chem*. **1978**, *161*, C1.

45. Nesmeyanov, A. N.; Aleksandrov, G.G.; Antonova, A.B.; Anisimov, K.N.; Kolobova, N.E.; Struchkov, Y.T. *J. Organomet. Chem*. **1976**, *110*, C36.

46. Antonova, A.B.; Kolobova, N.E.; Petrovsky, P.V.; Lokshin B.V.; Obezyuk, N.S. *J. Organomet. Chem*. **1977**, *137*, 55.

47. Kolobova, N.E.; Antonova, A.B.; Khitrova, O.M.; Antipin M.Y.; Struchkov, Y.T. *J. Organomet. Chem*. **1977**, *137*, 69.

48. Bellerby, J.M.; Mays, H. J. *J. Organomet. Chem*. **1976**, *117*, C21.

49. Bruce, M. I., Wong, F. S., Skelton, B. W., White, A. H., *J. Chem. Soc. Dalton. Trans*. **1982**, 2203.

50. Bullock, R. M., *J. Chem. Soc. Chem. Commun*. **1989**, 165.

51. Haquette, P., Pirio, N., Touchard, D., Toupey, L., Dixneuf, P. H., *J. Chem. Soc. Chem. Commun*. **1993**, 163.

52. Touchard, D., Haquette, P., Pirio, N., Toupet, L., Dixneuf, P. H., *Organometallics* **1993**, *12*, 3132.

53. Bruce, M. I., Hall, B. C., Zaitseva, N. N., Skelton, B. W., White, A. H., *J. Organomet. Chem*. **1996**, *522*, 307.

54. Bruce, M. I., Hall, B. C., Zaitseva, N. N., Skelton, B. W., White, A. H., *Dalton Trans*. **1998**, 1793.

55. Wakatsuki, Y., Koga, N., Yamazaki, H., Morokuma, K., *J. Am. Chem. Soc*. **1994**, *116*, 8105.

56. Braunstein, P.; Naud, F. *Angew. Chem. Int. Ed*. **2001**, *40*, 680.

57. Werner, H., Stark, A., Schulz, M., Wolf, J., *Organometallics* **1992**, *11*, 1126.

58. Selegue, J. P., *Organometallics* **1982**, *1*, 217.

59. Bustelo, E., Jiménez-Tenorio, M., Puerta, M. C., Valerga, P., *Organometallics* **1999**, *18*, 4563.

60. Aneetha, H., Jiménez-Tenorio, M., Puerta, M. C., Valerga, P., *Organometallics* **2003**, *22*, 2001.

61. Cadierno, V., Gamasa, M. P., Gimeno, J., González-Cueva, M., Lastra, E., Borge, J., García-Granda, S., Pérez-Carreño, E., *Organometallics* **1996**, *15*, 2137.

62. Werner, H., Rappert, T., Wiedemann, R., Wolf, J., Mahr, N., *Organometallics* **1994**, *13*, 2721.

63. Bustelo, E., Jiménez-Tenorio, M., Puerta, M. C., Valerga, P., *Eur. J. Inorg. Chem*. **2001**, 2391.

64. Martín, M.; Gevert. O.; Werner, H. *Dalton Trans.* **1996**, 2275.

65. Cadierno, V.; Gamasa, M. P.; Gimeno, J.; Borge, J.;García-Granda, S. *Organometallics* **1997**, *16*, 3178.

66. Cadierno, V.; Conejero, S.; Gamasa, M. P.; Gimeno, J.; Rodríguez, M. A. *Organometallics* **2002**, *21*, 203.

67. Fischer, H.; Szesni, N. *Coord. Chem. Rev*. **2004**, *248*, 1659.

68. Cadierno, V.; Crochet, P.; Gimeno, J. Preparation and Stoichiometric Reactivity of Metal Allenylidene Complexes (Chapter 2) *Metal Vinylidenes and Allenylidenes in Catalysis: From Reactivity to Applications in Synthesis*, (Bruneau, C., Dixneuf, P. H., Eds.) **2008**, Wiley VCH: Weinheim, Germany.

69. Bruce, M. I., Wallis, R. C., *Aust. J. Chem*. **1979**, *32*, 1471.

70. Kelley, C.; Lugan, N.; Terry, M. R.; Geoffroy, G. L.; Haggerty, B. S.; Rheingold, A.L. *J. Am. Chem. Soc*. **1992**, *114*, 6735.

71. Bruce, M.I. Preparation and Stoichiometric Reactivity of Mononuclear Metal Vinylidene Complexes (Chapter 1) *Metal Vinylidenes and Allenylidenes in Catalysis: From Reactivity to Applications in Synthesis*, (Bruneau, C., Dixneuf, P. H., Eds.) **2008**, Wiley VCH: Weinheim, Germany.

72. Baya, M.; Esteruelas, M. A. *Organometallics* **2002**, *21*, 2332.

73. Werner, H.; Baum, M.; Schneider, D.; Windmiiller, B. *Organometallics*, **1994**, *13*, 1089.

74. Katayama, H.; Onitsuka, K.; Ozawa, F. *Organometallics* **1996**, *15*, 4642.

75. Connelly, N. G.; Geiger, W. E.; Lagunas, M. C.; Metz, B.; Rieger, A. L.; Rieger, P. H.; Shaw, M. J. *J. Am. Chem. Soc*. **1995**, *117*, 12202.

76. Sakurai, H.; Fujii, T.; Sakamoto, K. *Chem. Lett*. **1992**, 339.

77. Naka, A.; Okazaki, S.; Hayashi, M.; Ishikawa, M. *J. Organomet. Chem*. **1995**, *499*, 35.

78. Ilg, K.; Paneque, M.; Poveda, M. L.; Rend_on, N.; Santos, L. L.; Carmona, E.; Mereiter, K. *Organometallics* **2006**, *25*, 2230.

79. Venkatesan, K.; Blacque, O.; Fox, T.; Alfonso, M.; Schmalle, H. W.; Kheradmandan, S.; Berke, H. *Organometallics* **2005**, *24*, 920.

80. Venkatesan, K.; Fox, T.; Schmalle, H. W.; Berke, H. *Eur. J. Inorg. Chem*. **2005**, 901.

81. Miller, D. C.; Angelici, R. J. *Organometallics* **1991**, *10*, 79.

82. Miura, T.; Iwasawa, N. *J. Am. Chem. Soc*. **2002**, *124*, 518.

83. Ikeda, Y.; Yamaguchi, T.; Kanao, K.; Kimura, K.; Kamimura, S.; Mutoh,Y.; Tanabe,Y.; Ishii, Y. *J. Am. Chem. Soc*. **2008,** *130*, 16856.

84. Mutoh,Y.; Ikeda,Y.;Kimura,Y.; Ishii,Y. *Chem.Lett*. **2009,** *38*, 534.

85. Mutoh, Y.; Imai, K.; Kimura, Y.; Ikeda, Y.; Ishii, Y. *Organometallics* **2011**, *30*, 204.

86. P. C. Ting, Y. C. Lin, G. H. Lee, M. C. Cheng, Y. Wang, *J. Am. Chem. Soc*. **1996**, *118*, 6433.

87. Sato, M.; Kawata, Y.; Shintate, H.; Habata, Y.; Akabori, S.; Unoura, K.; *Organometallics* **1997**, *16*, 1693.

88. Sato, M.; Shintate, H.; Kawata, Y.; Sekino, M.; Katada, M.; Kawata, S. *Organometallics* **1994**, *13*, 1956.

89. Sato, M.; Iwai, A.; Watanabe, M. *Organometallics* **1999**, *18*, 3208.

90. Olivan, M.; Clot, E.; Eisenstein, O.; Caulton, K. G. *Organometallics* **1998**, *17*, 3091.

91. Johnson, D. G.; Lynam, J. M.; Slattery, J. M.; Welby, C. E. *Dalton Trans*. **2010**, *39*, 10432.

92. De Angelis, F.; Sgamellotti, A.; Re, N. *Organometallics* **2002**, *21*, 2715.

93. De Angelis, F.; Sgamellotti, A.; Re, N. *Organometallics* **2002**, *21*, 5944.

94. Höhn, A.; Werner, H. *J. Organomet. Chem*. **1990**, *382*, 255.

95. Bianchini, C.; Peruzzini, M.; Vacca, A.; Zanobini, F. *Organometallics* **1991**, *10*, 3697.

96. Wakatsuki, Y.; Koga, N.; Werner, H.; Morokuma, K. *J. Am. Chem. Soc*. **1997**, *119*, 360.

97. Grotjahn, D. B.; Zeng, X.; Coosky, A. L. *J. Am. Chem. Soc*. **2006**, *128*, 2798.

98. Grotjahn, D. B.; Zeng, X.; Cooksy, A. L.; Kassel, W. S.; DiPasquale, A. G.; Zakharov, L. N.; Rheingold, A. L. *Organometallics* **2007**, *26*, 3385.

99. Cowley, M. J.; Lynam, J. M.; Slattery, J. M. *Dalton Trans*. **2008**, 4552.

100. De Angelis, F.; Sgamellotti, A.; Re, N. *Organometallics* **2007**, *26*, 5285.

101. De Angelis, F.; Sgamellotti, A.; Re, N. *Dalton Trans*. **2004**, 3225.

102. de Los Ríos, I.; Jiménez-Tenorio, M.; Puerta, M. C.; Valerga, P. *J. Am. Chem. Soc*. **1997**, *119*, 6529.

103. Tokunaga, M.; Suzuki,T.; Koga, N.; Fukushima, T.;Horiuchi, A.; Wakatsuki, Y. *J. Am. Chem. Soc*. **2001**, *123*, 11917.

104. Weyershausen, B.; Dötz, K. H. *Eur. J. Inorg. Chem*. **1999**, 1057.

105. Bruce, M. I.; Swincer, A. G.; Thomson, B. J.; Wallis, R. C.; *Aust. J. Chem*. **1980**, *33*, 2605.

106. Dötz, K. H.; Sturm, W. *Organometallics* **1987**, *6*, 1424.

107. Bianchini, C.; Marchi, A.; Mantovani, N.; Marvelli, L.; Masi, D.; Peruzzini, M.; Rossi, R. *Eur. J. Inorg. Chem*. **1998**, 211.

108. Gamasa, M. P.; Gimeno, J.; Martín-Vaca, B. M.; Isea, R.; Vegas, A. *J. Organomet. Chem*. **2002**, *651*, 22.

109. Hussain, Z. I.; Whiteley, M. W. *J. Chem. Soc. Dalton. Trans*. **1996**, 3893.

110. Varela-Fernández, A.; García-Yebra, C.; Varela, J. A.; Esteruelas, M. A.; Saá, C. *Angew. Chem. Int. Ed*. **2010**, *49*, 4278.

111. Harlow, K. J.; Hill, A. F.; Wilton-Ely, J. D. E. T. *J. Chem. Soc. Dalton Trans.* **1999**, 285.

112. Touchard, D.; Guesmi, S.; Bouchaib, M.; Haquette, P.; Daridor, A.; Dixneuf, P. H. *Organometallics* **1996**, *15*, 2580.

113. Fürstner, A.; Hill, A. F.; Liebl, M.; Wilton-Ely, J. D. E. T. *Chem. Commun.* **1999**, 601.

114. Schanz, H-J.; Jafarpour, L.; Stevens, E. D.; Nolan, S. P. *Organometallics* **1999**, *18*, 5187.

115. Fürstner, A.; Guth, O.; Düffels, A.; Seidel, G.; Liebl, M.; Gabor, B.; Mynott, R. *Chem. Eur. J.* **2001**, *7*, 4811.

116. Boeda, F.; Clavier, H.; Nolan, S. P. *Chem. Commun*. **2008**, 2726.

117. Malacea, R.; Dixneuf, P. H. Ruthenium Allenylidenes and Indenylidenes as Catalysts in Alkene Metathesis (Chapter 8) *Metal Vinylidenes and Allenylidenes in Catalysis: From Reactivity to Applications in Synthesis*, (Bruneau, C., Dixneuf, P. H., Eds.) **2008**, Wiley VCH: Weinheim, Germany.

118. Castarlenas, R.; Dixneuf, P. H. *Angew. Chem. Int. Ed.* **2003**, *42*, 4524.

119. Castarlenas, R.; Vovard, C.; Fischmeister, C.; Dixneuf, P. H. *J. Am. Chem. Soc*. **2006**, *128*, 4079.

120. Shaffer, A.; Chen, C-L.; Beatty, A. M.; Valente, E. J.; Schanz, H-J. *J. Organomet. Chem.* **2007**, *692*, 5221.

121. Jung, S.; Brandt, C. D.; Werner, H. *New J. Chem.* **2001**, *25*, 1101.

122. Bustelo, E.; Jiménez-Tenorio, M.; Mereiter, K.; Puerta, M. C.; Valerga, P. *Organometallics* **2002**, *21*, 1903.

123. Cadierno, V.; Diéz, J.; García-Garrido, S. E.; Gimeno, J. *Organometallics* **2005**, *24*, 3111.

124. Rigaut, S.; Touchard, D.; Dixneuf, P. H. *Organometallics* **2003**, *22*, 3980.

125. Bigeault, J.; Giodano, L.; Buono, G. *Angew. Chem. Int. Ed.* **2005**, *44*, 4753.

126. Seregin, I. V.; Gevorgyan, V. *J. Am. Chem. Soc.* **2006**, *128*, 12050.

127. Himo, F.; Lovell, T.; Hilgraf, R.; Rostostsev, V. V.; Noodleman, L.; Sharpless, K. B.; Fokin, V. V. *J. Am. Chem. Soc.* **2005**, *127*, 210.

128. Nishibayashi, Y.; Milton, M. D.; Inada, Y.; Yoshikawa, M.; Wakiji, I.; Hidai, M.; Uemura, S. *Chem. Eur. J.* **2005**, *11*, 1433.

129. Doucet, H.; Höfer, J.; Bruneau, C.; Dixneuf, P. H. *J. Chem. Soc. Chem. Commun.* **1993**, 850.

130. Doucet, H.; Matin-Vaca, B.; Bruneau, C.; Dixneuf, P. H. *J. Org. Chem.* **1995**, *60*, 7247.

131. Gemel, C; Trimmel, G.; Slugovc, C.; Kremel, S.; Mereiter, K.; Schmid, R.; Kirchner, K. *Organometallics* **1996**, *15*, 3998.

132. Mitsudo, T.; Hori, Y.; Yamazaki, Y.; Watanabe, Y. *J. Org. Chem.* **1987**, *52*, 2230.

133. Bruneau, C. *Anti*-Markovnikov Additions of *O*-, *N*-, *P*-Nucleophiles to Triple Bonds with Ruthenium Catalysts (Chapter 10) *Metal Vinylidenes and Allenylidenes in Catalysis: From Reactivity to Applications in Synthesis*, (Bruneau, C., Dixneuf, P. H., Eds.) **2008**, Wiley VCH: Weinheim, Germany.

134. Alonso, F.; Beletskaya, I. P.; Yus, M. *Chem. Rev.* **2004**, *104*, 3079.

135. Tokunaga, M.; Wakatsuki, Y. *Angew. Chem. Int. Ed.* **1998**, *37*, 2867.

136. Suzuki, T.; Tokunaga, M.; Wakatsuki, Y. *Org. Lett.* **2001**, *3*, 735.

137. Devanne, D.; Ruppin, C.; Dixneuf, P. H. *J. Org. Chem.* **1988**, *53*, 925.

138. Bruneau, C.; Kabouche, Z.; Neveux, M.; Seiller, B.; Dixneuf, P. H. *Inorg. Chim. Acta.* **1994**, *222*, 154.

139. Darcel, C.; Bruneau, C.; Dixneuf, P. H.; Neef, G. *J. Chem. Soc. Chem. Commun.* **1994**, 333.

140. Costin, S.; Rath, N. P.; Bauer, E. B. *Adv. Synth. Catal.* **2008**, *350*, 2414.

141. Nishibayashi, Y.; Wakiji, I.; Hidai, M. *J. Am. Chem. Soc.* **2000**, *122*, 11019.

142. Ammal, S. C.; Yoshikai, N.; Inada, Y.; Nishibayashi, Y.; Nakamura, E. *J. Am. Chem. Soc.* **2005**, *127*, 9428.

143. Fürstner, A.; Picquet, M.; Bruneau, C.; Dixneuf, P. H. *Chem. Commun.* **1998**, 1315.

144. Picquet, M.; Touchard, D.; Bruneau, C.; Dixneuf, P. H. *New. J. Chem.* **1999**, *23*, 141.

145. Picquet, M.; Bruneau, C.; Dixneuf, P. H. *Chem. Commun.* **1998**, 2249.

146. Sémeril, D.; Le Nôtre, J.; Bruneau, C.; Dixneuf, P. H.; Kolomiets, A. F.; Osipov, S. *New. J. Chem.* **2001**, *25*, 16.

147. Castarlenas, R.; Sémeril, D.; Noels, A. F.; Demnoceau, A, Dixneuf, P. H. *J. Organomet. Chem.* **2002**, *663*, 235.

148. Antonucci, A.; Bassetti, M.; Bruneau, C.;Dixneuf, P. H.; Pasquini, C. *Organometallics* **2010**, *29*, 4524.

149. Dorta, R.; Kelly III, R. A.; Nolan, S. P. *Adv. Synth. Catal.* **2004**, *346*, 917.

150. Jafarpour, L.; Schanz, H-J.; Stevens, E. D.; Nolan, S.P. *Organometallics* **1999**, *18*, 5416.

151. Mitchell, R. W.; Spencer, A.; Wilkinson, G. *J. Chem. Soc., Dalton Trans.* **1973**, 846.

152. Lynam, J. M.; Welby, C. E.; Whitwood, A. C. *Organometallics* **2009**, *28*, 1320.

153. Ford, C. E.; Final Year MChem report, *Synthesis and Reactivity of an η^3-Butenynyl Towards CO, ^{t}BuNC and XylNC. Formation of a Novel Diacetate-Substituted Vinylidene Compound*, University of York, **2007**.

154. Zhang, L.; Chen, X.; Xue, P.; Sun, H. H. Y.; Williams, I. D.; Sharpless, K. B.; Fokin, V. V.; Jia, G. *J. Am. Chem. Soc.* **2005**, *127*, 15998.

2: Synthesis and Characterisation of novel Ruthenium Vinylidene complexes

2.1: Introduction

The importance of transition-metal vinylidene complexes to a number of catalytic transformations of small organic molecules is well-established. A number of experimental and theoretical studies have been conducted into their reactivity,[1-4] which is dominated by the susceptibility of C_α to nucleophilic attack. This feature has been exploited in many processes including *anti*-Markovnikov additions to alkynes,[5,6] C-C bond formations[7,8] and olefin metathesis.[9,10]

Vinylidene ($:C=CH_2$) is a high energy tautomer of acetylene ($HC\equiv CH$), and gas phase calculations have shown this energy gap to be approximately 188 kJ mol^{-1}.[1] However, their relative stability may be reversed upon coordination to a transition metal; Hoffmann has shown that vinylidene ($:C=CH_2$) when coordinated to the $[MnCp(CO)_2]$ fragment is 146 kJ mol^{-1} more stable than acetylene (C_2H_2).[11] Transition-metal vinylidene complexes are most readily obtained by the addition of an alkyne to an appropriate transition-metal precursor. The exact mechanism of their formation varies depending on the metal centre and ancillary ligands present,[12,13] however it is generally agreed that the initial step involves the coordination of the alkyne in a η^2-fashion. The alkyne may then rearrange to its vinylidene form in a number of ways. Therefore, to allow for alkyne-coordination a vacant site must be made available at the transition metal centre. This may be achieved by the loss of an ancillary ligand, such as a phosphine or halide,[14-17] or utilising the hemi-labile properties of a chelating ligand.[18-22]

It is proposed that the acetate ligands of **1** may be able to alter their coordination mode from κ^2 to κ^1 to generate a vacant site, so as to allow for alkyne binding and the formation of a vinylidene complex. This is illustrated in Figure 2.1.1 below. To this end, terminal alkynes were selected that had varying steric and electronic properties to react with **1**, and this chapter details the outcomes of these reactions.

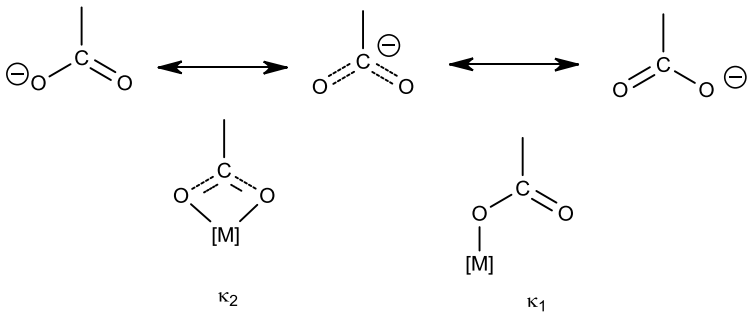

Figure 2.1.1: Modes of coordination for an acetate ligand.

2.2: Reaction of 1 with HC≡CPh

Werner has previously shown that the phosphino-ethers of $[RuCl_2(\eta^2\text{-}^iPr_2PCH_2CH_2OMe)_2]$ are able to act as hemi-labile ligands to enable the formation of the corresponding vinylidene complex.[18] It was shown that the oxygen atom of the η^2-coordinate $^iPr_2PCH_2CH_2OMe$ ligand is able to readily dissociate to create a vacant site for alkyne coordination.

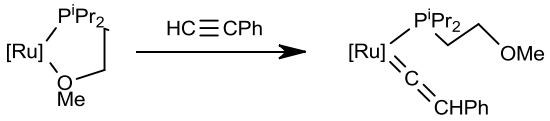

Figure 2.2.1: Displacement of the O-bound arm of a phosphine-ether to generate a vacant site for vinylidene formation.

In order to probe the ability of the acetate ligand to behave in a similar way, one equivalent of HC≡CPh was added to a solution of **1** in DCM. After stirring for one hour, a slight colour change was observed from orange-red to red. The product was isolated as a pink precipitate by trituration with pentane or hexane, and was shown by subsequent analysis to be spectroscopically pure.

In the ^1H NMR spectrum of this product recorded in CD_2Cl_2, a triplet at δ_H 5.14 with a splitting of $^4J_{PH}$ = 3.7 Hz was observed consistent with a vinylidene proton that is coupled to two equivalent ^{31}P nuclei. This resonance becomes a singlet in the $^1H\{^{31}P\}$ NMR spectrum, further confirming this assignment. A singlet at δ_H 0.81 with a relative integration of six suggests that both CH_3 groups of the acetate ligands are equivalent, or undergoing rapid exchange on the NMR timescale. The $^{13}C\{^1H\}$ NMR spectrum displays two distinctive triplet resonances at δ_C 355.6 ($^2J_{PC}$ = 16.8

Hz) and 112.1 ($^3J_{PC}$ = 4.4 Hz) characteristic of a vinylidene C_α and C_β, each coupling to two equivalent ^{31}P nuclei. These values are typical of the C_α and C_β atoms of a vinylidene ligand; in Bruce's extensive review of vinylidene complexes,[1] he states that "C_α is strongly deshielded and resonates in the range δ_C 258 – 382…while the resonance for C_β is found between δ_C 87 – 143 ppm" Changes in the resonances due to the carbon atoms of the PPh_3 ligands suggest that the phosphine ligands are now mutually *trans*, rather than mutually *cis* as in **1**. For complex **1**, the *ipso*-C of the PPh_3 ligand is observed as a complex resonance due to virtual coupling at δ_C 137.3 with a $^1J_{PC}$ + $^3J_{PC}$ coupling of 44.4 Hz. For complex **2a**, the corresponding resonance is observed as a virtual triplet at δ_C 129.6 with a $^1J_{PC}$ + $^3J_{PC}$ = 43.6. Complex **1** was modelled as an AA'X_3X_3' system which demonstrated that the phosphine ligands are chemically the same but magnetically inequivalent, resulting in the multiplicity observed.

In the $^{31}P\{^1H\}$ NMR spectrum, a singlet resonance at δ_P 34.1 again suggests the two phosphines are equivalent, and as the peak has shifted significantly relative to **1** (δ_P 63.5) implies that they are no longer in a *cis* orientation.[23] Consequently, the structure shown in Figure 2.2.2 is proposed for this novel vinylidene complex **2a**.

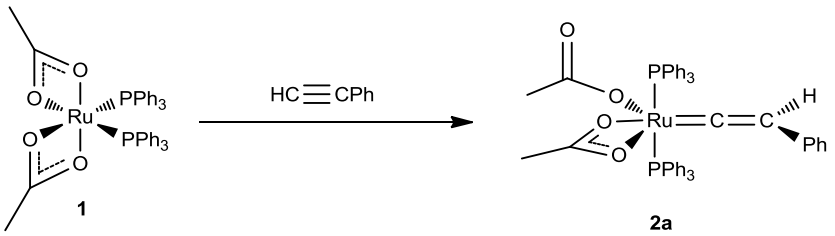

Figure 2.2.2: Reaction of HC≡CPh with **1** to give **2a**.

IR spectra recorded in both solid (KBr) and solution (DCM) phase provided further evidence for the proposed structure, which indicate the presence of both κ^1- and κ^2-coordination modes of the acetate ligand. Examples of these spectra are given in Figure 2.2.3 and 2.2.4. The $\upsilon(OCO)_{sym}$ and $\upsilon(OCO)_{asym}$ bands occur at different frequencies depending upon the mode of coordination and the difference in their frequencies $\Delta\upsilon$, is also indicative of their coordination mode.[24] The $\Delta\upsilon$ of the symmetric and asymmetric stretches of a unidentate carboxylate is generally larger than that of a chelate; typically in the region of 210 – 270 cm^{-1} for monodentate coordination and 40 – 120 cm^{-1} for chelate. Monodentate coordination of a

carboxylate ligand involves two inequivalent CO moieties with different bond orders; one single and one double as in an ester. This results in an increase in the ν_{asym} and a decrease in ν_{sym} with a net increase in $\Delta\upsilon$ relative to the ionic value (e.g. for NaOAc $\Delta\upsilon$ = 164 cm^{-1}). When the carboxylate is chelated, no change in the bond orders should occur so the $\Delta\upsilon$ should be similar to the ionic value, although experimental investigations have suggested that a $\Delta\upsilon$ smaller than the ionic value is indicative of a κ^2-coordinated carboxylate.[25] However, assignments are always considered tentative as P–Ph stretches occur in the same region. In the solid phase, a peak at 1360 cm^{-1} is assigned to the symmetric stretch of the κ^1-OAc ligand, whilst the asymmetric stretch is at 1595 cm^{-1}. This gives a $\Delta\upsilon_{uni}$ value of 235 cm^{-1}, a large value in the typical range[25] for a monodentate carboxylate ligand. For the κ^2-OAc ligand; the symmetric stretch occurs at 1459 cm^{-1}, whereas the asymmetric occurs at 1534 cm^{-1}; giving a $\Delta\upsilon_{chelate}$ of 75 cm^{-1}. A stretch at 1635 cm^{-1} is assigned to the C=C stretch of the vinylidene. Similar stretches are observed in the solution phase. This serves to demonstrate the difference in timescales between the NMR and IR experiments. The acetate ligands are fluxional in solution, and appear equivalent on the NMR timescale, whereas in the faster IR experiment, both coordination modes are clearly observed. For a comparison of the IR data of all acetate-containing complexes described in this thesis, see Chapter 8.

	P–Ph	**C=C**	**κ^1-OCO_{sym}**	**κ^1-OCO_{asym}**	**κ^1-$\Delta\upsilon$**	**κ^2-OCO_{sym}**	**κ^2-OCO_{asym}**	**κ^2-$\Delta\upsilon$**
2a KBr / cm^{-1}	1434	1635	1360	1595	235	1459	1534	75
2a DCM / cm^{-1}	1435	1630	1366	1594	228	1462	1531	69

Table 2.2.1: Summary of IR stretches observed for **2a** in both DCM and KBr.

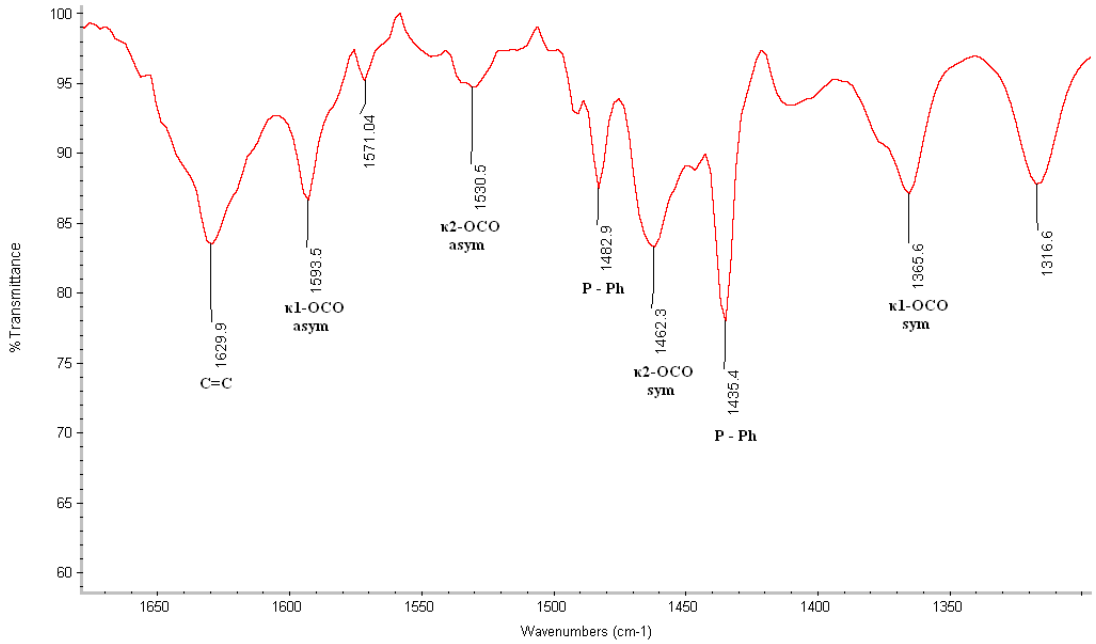

Figure 2.2.3: IR spectrum of **2a** in DCM.

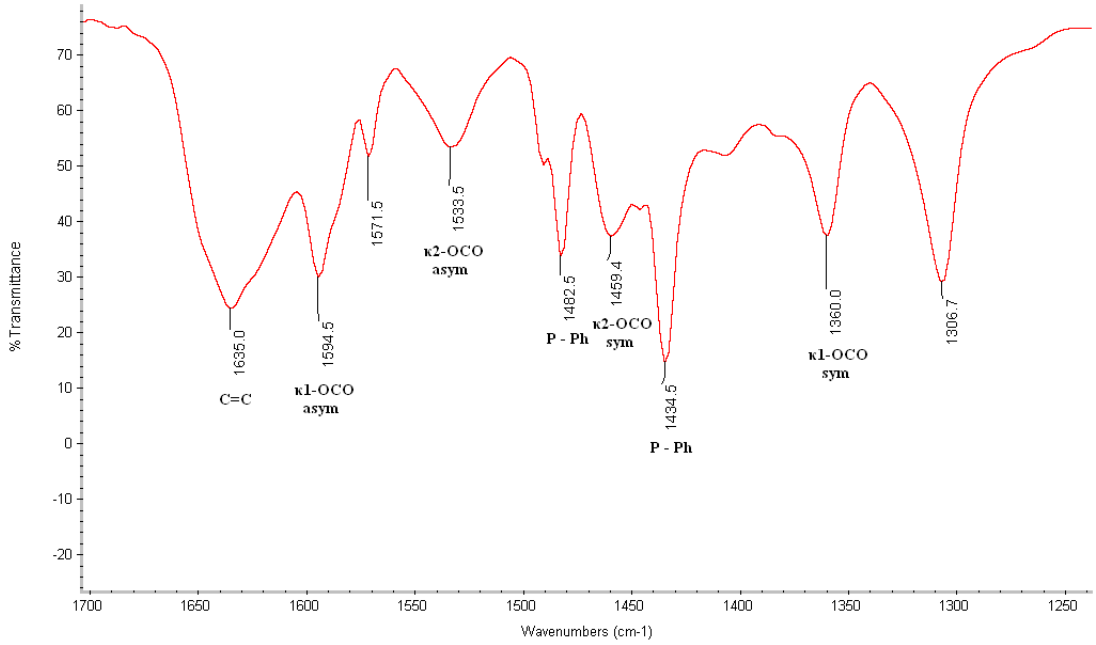

Figure 2.2.4: IR spectrum of **2a** in KBr.

A FAB Mass Spectrum of **2a** displayed a peak at *m/z* 846 for the molecular ion that displays the ruthenium isotope pattern. Crystals suitable for X-ray Diffraction were obtained from a solution of **2a** in CD_2Cl_2 and the structure obtained confirms the one proposed in Figure 2.2.2. An ORTEP representation and significant bond lengths and angles are given in Figure 2.2.5 and Table 2.2.1 respectively.

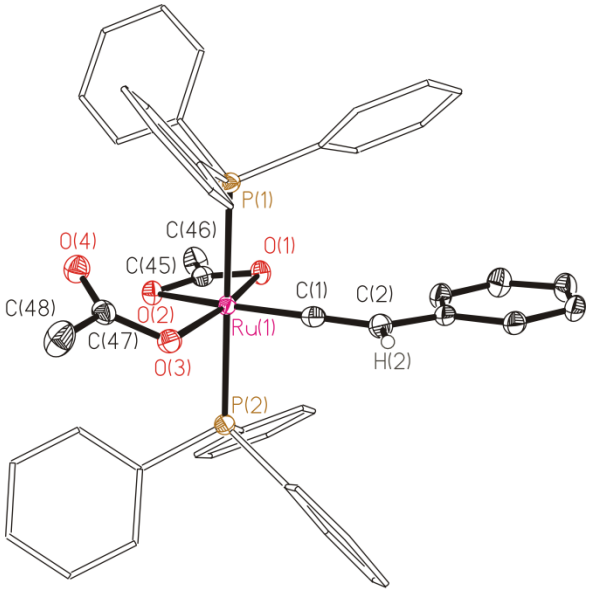

Figure 2.2.5: ORTEP diagram of **2a**, thermal ellipsoids, where shown, at the 50 % probability level. Hydrogen atoms, except for H(6), and two molecules of CH_2Cl_2 of crystallization omitted for clarity.

Bond Length	**(Å)**	**Bond Angle**	**(deg / °)**
Ru – P(1)	2.3853(7)	P(1) – Ru – P(2)	178.89(3)
Ru – P(2)	2.3910(7)	P(1) – Ru – O(1)	89.08(5)
Ru – O(1)	2.1139(17)	P(1) – Ru – O(2)	98.59(5)
Ru – O(2)	2.2863(18)	P(1) – Ru – O(3)	93.06(5)
Ru – O(3)	2.0699(17)	O(1) – Ru – O(2)	59.08(6)
Ru – C(1)	1.786(3)	O(1) – Ru – O(3)	168.17(7)
C(1) – C(2)	1.318(4)	O(2) – Ru – O(3)	109.09(7)
		P(1) – Ru – C(1)	87.77(8)
		P(2) – Ru – C(1)	91.58(8)
		O(1) – Ru – C(1)	97.81(9)
		O(2) – Ru – C(1)	155.65(9)
		O(3) – Ru – C(1)	93.90(9)
		Ru – C(1) – C(2)	176.5(2)

Table 2.2.2: Selected Bond Lengths and Angles for **2a**.

The structure obtained shows that **2a** adopts a distorted octahedral structure. The majority of the angles about the ruthenium are close to that of an ideal octahedron; however significant distortions arise due to the constraints of a κ^2-OAc ligand. The P(1) – Ru – P(2) angle is close to linear at 178.89(2) ° whereas the O(2) – Ru – C(5) is significantly deviated at 155.65(9) °. Bruce has reported that the M=C=C bond should be "essentially linear, the angle at C_α being in the range 167-180 °".[1] He also suggests the M=C moiety has a bond order of two whilst the bond order of C=C is typically between two and three, in a range of 1.25-1.41 Å. The Ru – C(1) – C(2) angle of **2a** is almost linear at 176.5(2) °, and the bond lengths of the vinylidene moiety are typical; both Ru – C(1) and C(1) – C(2) are short at 1.786(3) Å and 1.318(4) Å respectively. The crystal data also reveals that the Ru – O(3) bond length of 2.0699(17) Å of the monodentate acetate ligand is marginally shorter than of Ru – O(1) and Ru – O(2) the chelate OAc at 2.1139(17) Å and 2.2863(18) Å.

This structure can be contrasted with two complexes which can be considered 'analogues' of this system; $[RuCl_2(=C=CHPh)(PR_3)]$, where R = ^{i}Pr,[26] Cy.[27] Both are considered to have a distorted square pyramid structure, with the vinylidene ligand in an apical position. In both, the Ru – C(1) – C(2) angle is close to linear at 177.1(3) ° and 178.2(6) ° for the isopropyl- and cyclohexylphosphine-containing complexes respectively and the Ru – C(1) and C(1) – C(2) bond lengths are typical of vinylidene complexes. The phosphine and chloride ligands in the basal plane of the complexes also appear to be bent away from the vinylidene ligand.

The structure confirms the interpretation of the IR spectra in that both κ^1- and κ^2- coordinated acetate ligands are present, and that they must undergo an exchange process that is rapid on the NMR timescale. To probe this exchange, a low temperature ^{1}H NMR study was conducted, whereby a sample of **2a** in CD_2Cl_2 was cooled to 195 K. Although the peak due to the acetate protons broadens, it does not coalesce, so the energy barrier to exchange could not be determined for this complex, although it is assumed to be very low.

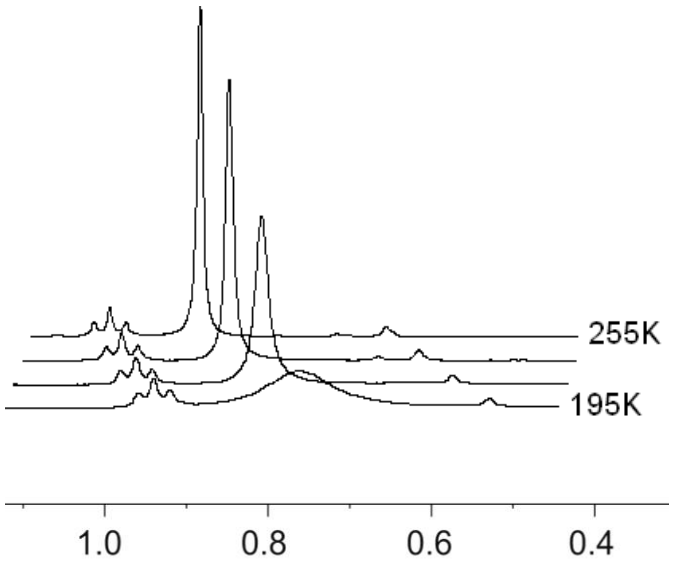

Figure 2.2.6: ^{1}H NMR of **2a** at 255 – 195K.

Werner[28] has synthesised the analogous complexes [Ru(=C=CHR)(κ^2-OAc)(κ^1-OAc)(PCy_3)$_2$] where R = Ph, CO_2Me *via* an alternative route. The addition of PCy_3 to the binuclear precursor [{Ru(η^1-OAc)(Sb^{i}Pr$_3$)$_2$}$_2$(μ-OAc)$_2$(μ-OH$_2$)] results in the formation of a complex of formula [Ru(OAc)$_2$(PCy_3)$_2$], whose structure cannot be unambiguously determined. Addition of HC≡CPh to this intermediate species gives the vinylidene complex, as shown in Figure 2.2.7. The structure proposed for this complex indicates the phosphine ligands are mutually *cis*. Werner suggests that the vinylidene complex is fluxional in solution; resonances ascribed to the *P*Cy_3 and *C*O_2CH_3 ligands undergo coalescence at 203 K in the ^{31}P and ^{13}C NMR spectra respectively. The resonance assigned to the acetate protons also undergoes coalescence at low temperature; however he is unable to specify an exact coalescence temperature as resonances due to the protons of the Cy moiety occur in a similar region. The IR spectra of this complex recorded in KBr also indicate the presence of both κ^1- and κ^2-coordination modes for the acetate ligands.

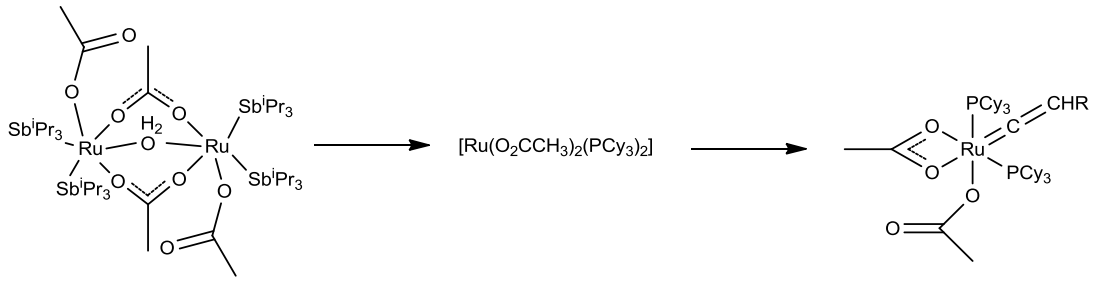

Figure 2.2.7: Synthesis of analogous vinylidene complexes by Werner.

It was noted that the formation of **2a** from **1** and HC≡CPh is extremely fast at room temperature; when the reaction was conducted on an NMR scale the reaction had reached completion by the time spectra could be recorded. Consequently, no intermediates have been observed to suggest a particular pathway for the alkyne-to-vinylidene isomerisation. This is particularly interesting in light of comparisons with the analogous complex $[RuCl_2(PPh_3)_3]$. This complex is reported by Wakatsuki[29] to require 30 hours to react with HC≡C^{t}Bu to give $[RuCl_2(PPh_3)_2(=C=CH^tBu)]$. This reaction was repeated independently using HC≡CPh and a similar timescale was found to be necessary for the reaction to reach completion. The mechanism for this process is given in Figure 2.2.8 below. Wakatsuki proposes that the loss of a phosphine ligand is necessary to create a vacant site for the alkyne to bind in a η^2-fashion. Once it has done so, isomerisation to the vinylidene occurs to give a mixture of intermediates **2B** and **2C**, where both phosphine ligands are mutually *cis*. A final isomerisation step to give the product **2D** in which the phosphine ligands are ultimately *trans*. Experimental and theoretical evidence for this mechanism will be discussed in more detail in Chapter 4.

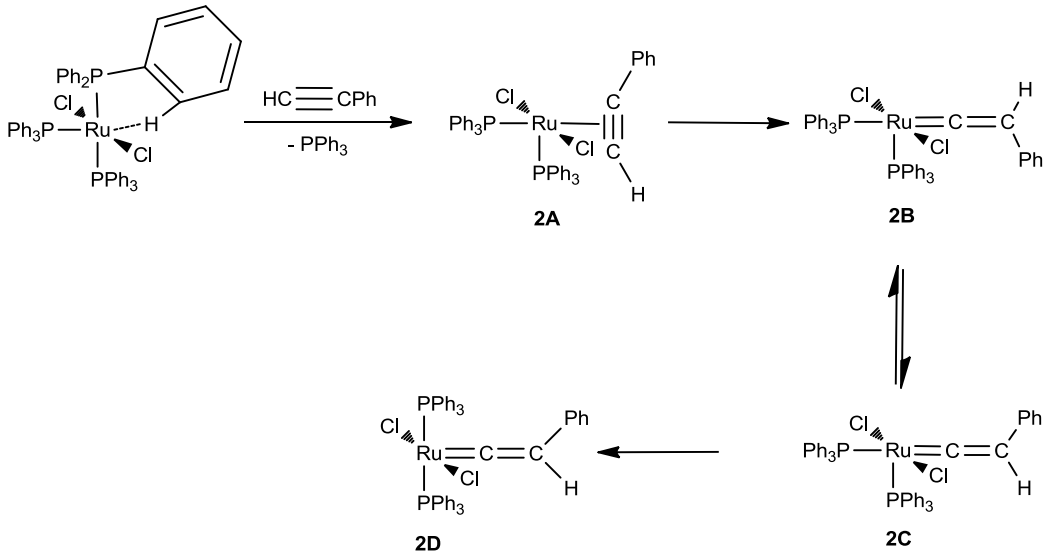

Figure 2.2.8: Proposed mechanism for the formation of $RuCl_2(PPh_3)_2(=C=CHPh)$.

It is proposed that a different mechanism is operating for complex **1**, as the loss of a phosphine ligand has been rendered unnecessary for this system by the hemi-labile properties of the acetate ligand. Recent investigations into the mechanism of C-H activation pathways have shown that an acetate ligand is able to assist the

process by acting as an internal base to remove a proton. This has been termed an AMLA[30] (**A**mphiphilic **M**etal-**L**igand **A**ctivation) or CMD[31] (**C**oncerted **M**etalation-**D**eprotonation) process. It is therefore proposed that the rapidity of the formation of vinylidene complex **2a** is due to the assistance of an acetate ligand. A mechanism for this process is proposed in Figure 2.2.5 below.

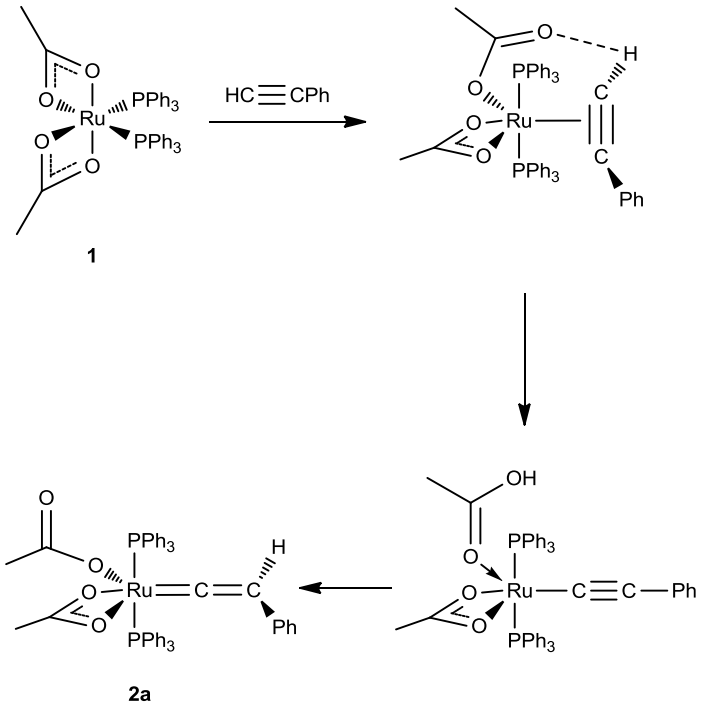

Figure 2.2.5: Proposed mechanism for the formation of **2a**.

It is suggested that upon addition of HC≡CPh, one of the oxygen atoms of an acetate ligand dissociates to generate a vacant site and allow the alkyne to bind in a η^2-fashion. This oxygen atom is then able to interact with the alkyne proton resulting in deprotonation of the alkyne and formation of an acetylide complex. The coordinated acetic acid then reprotonates the acetylide at C_β to generate the vinylidene complex **2a**. Whilst no direct experimental evidence has been found for this pathway, a significant computational effort has shown that this route is the lowest energy pathway for the formation of a vinylidene complex for this system. This type of pathway, where the acetate ligand is acting as a shuttle for the proton between the C_α and C_β has been termed a **L**igand-**A**ssisted **P**roton **S**huttle (LAPS). A full account of the experimental and theoretical investigation into this mechanism is given in Chapter 4.

In conclusion, it has been shown that the reaction of **1** with HC≡CPh results in the formation of the novel vinylidene complex **2a**. This complex has been characterised fully by NMR and IR spectroscopic methods, and a single crystal X-ray structure has been successfully obtained. The formation of this vinylidene complex is remarkably fast and may proceed *via* a new mechanistic pathway where the acetate ligand is acting as a proton shuttle.

2.3: Reaction of 1 with additional alkynes

The reactivity of **1** towards terminal alkynes has been demonstrated by its reaction with HC≡CPh. This was subsequently extended to include additional terminal alkynes with different steric and electronic properties; HC≡CCO_2Me, HC≡C(pyrene) and HC≡CTMS. The products obtained from reaction of **1** with HC≡CCO_2Me and 1-ethynylpyrene, **2b** and **2c** respectively, have been successfully characterised and will be discussed in this section. The synthesis and characterisation of the product obtained from reaction of **1** with HC≡CTMS (**2d**) was conducted in collaboration with an Erasmus student, Thomas Eschemann, and whilst this product was not characterised to the same full extent as **2b** and **2c**, the complex is still relevant to this discussion.

As 1-ethynylpyrene is not commercially available, it was synthesised *via* a Sonagashira coupling of HC≡CTMS and 1-bromopyrene, in a procedure recently reported by Zhao and Guo.[32] The route taken is shown in Figure 2.3.1, and involves the initial formation of a TMS-substituted ethynylpyrene. The $SiMe_3$ group is subsequently removed in a deprotection step and the desired product purified by column chromatography. It was interesting to note that whilst the alkyne was fluorescent under long-wave UV radiation, the resulting vinylidene complex **2c** was not.

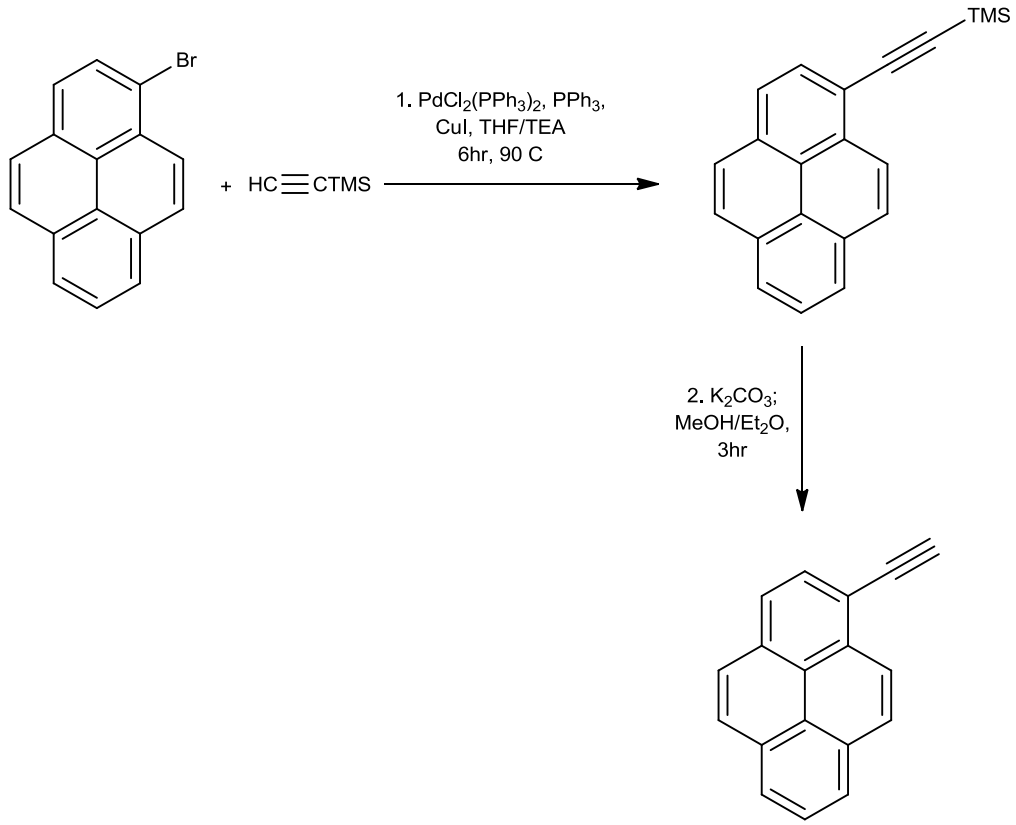

Figure 2.3.1: Synthetic route used for the preparation of 1-ethynylpyrene.

The addition of HC≡CCO_2Me, 1-ethynylpyrene and HC≡CTMS to **1** was carried out in the same way as for the reaction of HC≡CPh with **1**. A single equivalent of the alkyne was added to a solution of **1** in DCM and the reaction stirred for one hour at room temperature. The subsequent trituration with hexane or pentane afforded a bright yellow powder for **2b**, a red powder for **2c** and a yellow powder for **2d**. Similarly to **2a**, when carried out on an NMR scale, the formation of the vinylidene complex was fast, and no intermediates could be detected. It is therefore proposed that a LAPS mechanism is again facilitating the rapid isomerisation of the alkynes to the corresponding vinylidene complexes. Spectroscopic analysis of the three complexes by NMR and IR techniques show that they share many common characteristic features with **2a**. Singlet resonances for the acetate ligand protons are observed in the ^{1}H NMR spectrum, whilst IR spectra recorded in both DCM and KBr media indicates the presence of both κ^1- and κ^2-OAc coordination modes.

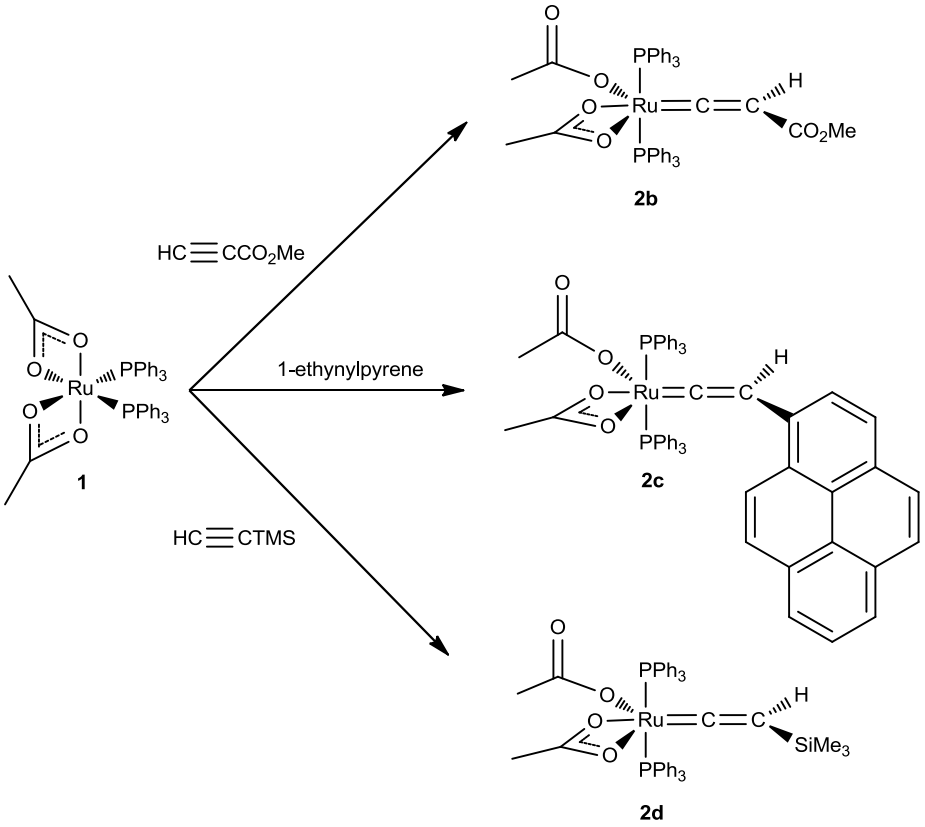

Figure 2.3.2: Formation of vinylidene complexes **2b, 2c** and **2d**.

The pertinent NMR and IR spectroscopic features that demonstrate the formation of these vinylidene complexes are summarised in Tables 2.3.1 and 2.3.2. For **2c**, the protons of the acetate ligands are again observed as a singlet resonance at δ_H 0.95, which only broadens, and does not coalesce, when cooled to 195 K. Furthermore, a resonance for C_α could not be distinguished in the $^{13}C\{^1H\}$ NMR spectrum, even in a saturated sample. The peak for C_α of **2b** is observed as a multiplet, so the $^2J_{CP}$ coupling could not be resolved. The δ_C values of C_α and C_β fall into the range suggested by Bruce;[1] these and the other spectroscopic features characteristic of a vinylidene complex are comparable to those obtained for **2a**. Bruce has also suggested that it is difficult to conclude a significant amount from the value of δ_C for C_α as "the sign and magnitude of the paramagnetic contributions to nuclear shielding, which are related to differences in energies of filled and unfilled orbitals on C_α, are more significant in determining this chemical shift than the electron deficient nature of C_α."

	^{1}H δ_H [Ru]=C=C*H*	^{1}H $^{4}J_{HP}$/Hz	^{1}H δ_H C*H*$_3$COO	^{31}P δ_P PPh_3	^{13}C δ_C C_α	^{13}C $^{2}J_{CP}$/Hz	^{13}C δ_C C_β	^{13}C $^{3}J_{CP}$/Hz
2b	5.41	3.2	0.78	34.8	345.2	-	104.4	3.9
2c	6.20	3.6	0.95	33.8	-	-	109.4	4.6
2d	3.74	3.7	0.74	35.5	337.6	15.4	94.0	3.9

Table 2.3.1: Common characteristic NMR features of complexes **2b**, **2c** and **2d** recorded in CD_2Cl_2.

	2b KBr / cm^{-1}	**2b DCM / cm^{-1}**	**2c KBr / cm^{-1}**	**2c DCM / cm^{-1}**	**2d KBr / cm^{-1}**	**2d DCM / cm^{-1}**
P–Ph	1433	1435	1434	1434	1433	1433
C=C	1696	1684	1610	1607	1633	1636
κ^1-OCO$_{sym}$	1365	1365	1360	1366	1361	1366
κ^1-OCO$_{asym}$	1600	1600	1587	1590	1611	1616
κ^1-$\Delta\upsilon$	235	235	227	224	250	250
κ^2-OCO$_{sym}$	1460	1466	1458	1462	1463	1459
κ^2-OCO$_{asym}$	1533	1535	1536	1530	1521	1531
κ^2-$\Delta\upsilon$	73	69	78	68	58	72

Table 2.3.2: Summary of IR stretches observed for **2b**, **2c** and **2d** in both DCM and KBr.

As for **2a**, the $\Delta\upsilon$ values calculated for the κ^1- and κ^2-OAc ligands of **2b**, **2c** and **2d** obey the limits proposed by Robinson.[24] However, there seems to be a greater deviation in the values of κ^2-$\Delta\upsilon$ recorded in DCM and KBr than for κ^1-$\Delta\upsilon$. For **2b** and **2c**, the value of κ^2-$\Delta\upsilon$ in KBr is larger than in DCM; however for **2d** the reverse is true. A full comparison of common NMR and IR and structural features of the complete family of ruthenium-vinylidene complexes also bearing acetate ligands reported in this thesis are discussed in Chapter 8.

Crystals of both **2b** and **2c** were obtained and their structures solved by X-ray Diffraction. ORTEP representations are shown in Figures 2.3.4 and 2.3.5 for **2b** and **2c** respectively, and Tables 2.3.3 and 2.3.4 give relevant bond lengths and angles.

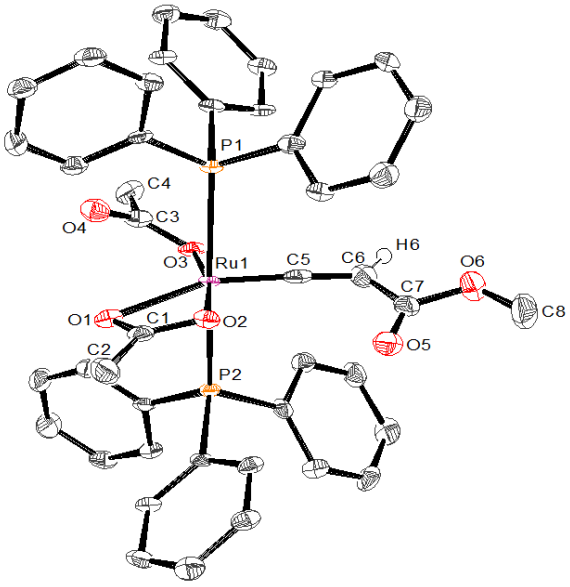

Figure 2.3.3: ORTEP diagram of **2b**, thermal ellipsoids, where shown, at the 50 % probability level. Hydrogen atoms, except for H(6), and two molecules of CH_2Cl_2 of crystallization omitted for clarity.

Bond Length	**(Å)**	**Bond Angle**	**(deg / °)**
Ru – P(1)	2.3788(14)	P(1) – Ru – P(2)	178.20(6)
Ru – P(2)	2.3762(14)	P(1) – Ru – O(1)	99.24(10)
Ru – O(1)	2.282(4)	P(1) – Ru – O(2)	88.78(11)
Ru – O(2)	2.102(4)	P(1) – Ru – O(3)	92.45(11)
Ru – O(3)	2.063(4)	O(1) – Ru – O(2)	58.78(14)
Ru – C(5)	1.766(6)	O(1) – Ru – O(3)	109.67(15)
C(5) – C(6)	1.296(8)	O(2) – Ru – O(3)	168.40(15)
		P(1) – Ru – C(5)	88.08(17)
		P(2) – Ru – C(5)	90.65(17)
		O(1) – Ru – C(5)	154.7(2)
		O(2) – Ru – C(5)	97.5(2)
		O(3) – Ru – C(5)	94.1(2)
		Ru – C(5) – C(6)	173.6(5)

Table 2.3.3: Selected Bond Lengths and Angles for **2b**.

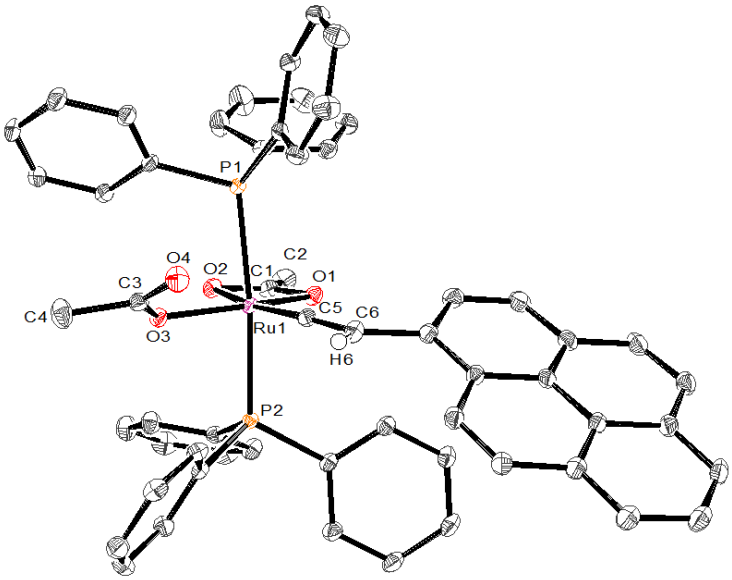

Figure 2.3.4: ORTEP diagram of **2c**, thermal ellipsoids, where shown, at the 50 % probability level. Hydrogen atoms, except for H(6), and two molecules of CH_2Cl_2 of crystallization omitted for clarity.

Bond Length	**(Å)**	**Bond Angle**	**(deg / °)**
Ru – P(1)	2.4195(5)	P(1) – Ru – P(2)	174.126(15)
Ru – P(2)	2.3720(5)	P(1) – Ru – O(1)	92.86(3)
Ru – O(1)	2.1116(11)	P(1) – Ru – O(2)	84.48(3)
Ru – O(2)	2.2465(12)	P(1) – Ru – O(3)	89.16(3)
Ru – O(3)	2.0160(11)	O(1) – Ru – O(2)	59.86(4)
Ru – C(5)	1.7863(16)	O(1) – Ru – O(3)	154.87(5)
C(5) – C(6)	1.325(2)	O(2) – Ru – O(3)	95.49(4)
		P(1) – Ru – C(5)	96.53(5)
		P(2) – Ru – C(5)	88.70(5)
		O(1) – Ru – C(5)	101.92(6)
		O(2) – Ru – C(5)	161.77(6)
		O(3) – Ru – C(5)	102.72(6)
		Ru – C(5) – C(6)	174.72(14)

Table 2.3.4: Selected Bond Lengths and Angles for **2c**.

The structural characterisation of complexes **2b** and **2c** has revealed that, as for **2a**, they adopt a distorted octahedron structure. The distortion is attributed to the constraints enforced by the κ^2-OAc ligand. Again, it is confirmed that the PPh_3 ligands adopt a mutually *trans* orientation with the two acetate ligands and the vinylidene ligand occupying the remaining coordination sites. The majority of bond lengths and angles are similar to those observed in **2a**. The bond lengths of Ru – C_α and C_α – C_β are typical of a vinylidene ligand. For all three complexes the Ru – C_α bond length is remarkably similar; for **2a** it is 1.786(3) Å, **2b** 1.766(6) Å and for **2c** 1.7863(16) Å. The C=C bond lengths are also similar and short at around 1.3 Å; for **2a** it is 1.318(4) Å, 1.296(8) Å for **2b** and at 1.325(2) Å for **2c**. The angle of the M=C=C moiety is again nearly linear for complexes **2b** and **2c**; the greatest deviation is observed for **2b** at 173.6(5) ° whilst for **2c** (174.72(14) °) and **2a** (176.5(2) °) the deviation is slightly smaller. In **2a**, the phenyl substituent of the vinylidene ligand is in the same plane as the ligand, however for **2c** the 'tilt' of the pyrene substituent is noticeable at 30.3 °.

Complex **1** has been shown to react rapidly with terminal alkynes to give vinylidene complexes; this was now extended towards internal alkynes. In terminal alkynes, the migration of hydrogen is relatively facile. The migration of a heteroatom group such as $SiMe_3$ or SnR_3 has been reported,[33-38] but it was only very recently that the formation of vinylidene complexes derived from unfunctionalised internal alkynes, such as PhC≡CMe,[39,40] have been reported.[4] For example, Ishii has demonstrated that the reaction of (PPN)[Ru(P_3O_9)(MeOH)(dppe)] (PPN = $N^+(PPh_3)_2$) with PhC≡CMe at 70 °C in DCE affords the vinylidene complex (PPN)[Ru(P_3O_9)(=C=C{Ph}Me)(dppe)] after 3 days.[39]

The reactivity of **1** towards PhC≡CPh, MeC≡CMe, PhC≡CTMS and EtC≡CEt was therefore probed. The reactions were conducted on an NMR scale, in an initial test of their reactivity. As for the reactions with terminal alkynes, one equivalent of the alkyne (PhC≡CPh, MeC≡CMe and PhC≡CTMS) was added to a solution of **1** in CD_2Cl_2 and the mixture monitored by NMR spectroscopy over a period of several days. Unfortunately, no significant reaction was observed to occur between **1** and the alkyne even after this time. For the reaction of **1** with PhC≡CTMS, the sample was heated at 40 °C for three hours, however this produced no change. The addition of EtC≡CEt to **1** was conducted in d_8-toluene and the mixture heated at 80 °C for 22

hours. After this time, no significant change could be observed in the $^{31}P\{^{1}H\}$ NMR spectrum. Consequently, this avenue of investigation was not explored further. If the acetate ligand is in fact assisting the proton migration step in vinylidene formation then the lack of reactivity by these internal alkynes is not surprising.

Despite this apparent inertness towards internal alkynes, it has still been shown that **1** is remarkably reactive and selective for terminal alkynes. This has been extended towards propargylic alcohols ($HC{\equiv}CCR_2OH$), which will be discussed further in Chapter 5.

2.4: Conclusions

This chapter has described the syntheses, isolation and full spectroscopic characterisation of a number of novel ruthenium vinylidene complexes based on the precursor **1**. One of the simplest routes to the formation of vinylidene complexes is by isomerisation of terminal alkynes at the transition-metal centre, and this particular route has proved extremely effective. The reaction to form complexes **2a**, **2b**, **2c** and **2d** is rapid in solution at room temperature and intermediates could not be identified.

It has been shown that all complexes share common spectroscopic features that are characteristic of this class of compound. The ^{1}H and $^{13}C\{^{1}H\}$ NMR spectra in particular indicate the presence of a vinylidene ligand due to the observation of distinctive resonances attributed to C_{α}, C_{β} and [Ru]=C=C*H*. It has been shown that the acetate ligands are fluxional in solution, and IR spectroscopy has been significant in confirming the presence of both κ^1- and κ^2-coordination modes.

Structural characterisation by X-ray diffraction has shown that these complexes share a common structural motif, whereby the two PPh_3 ligands are mutually *trans* and the remaining two acetate and vinylidene ligands occupy the remaining sites around the ruthenium, building a complex that appears to be a distorted octahedron.

It is proposed that the rapid isomerisation of alkyne to vinylidene at ruthenium in this particular system is due to the presence of the fluxional acetate ligands. It is suggested that these acetates are able to act as a proton shuttle and facilitate the fast formation of the vinylidene product. They would initially act as a base to remove the terminal alkyne proton, and then as an acid to reprotonate an acetylide ligand resulting in the formation of a vinylidene ligand. This mechanism has been termed a LAPS process (**L**igand-**A**ssisted **P**roton **S**huttle), and will form the basis of Chapter 4.

Unfortunately, **1** appears to be inert towards internal alkynes under the conditions employed. Nevertheless, the selectivity it shows towards terminal alkynes has been exploited further in testing its activity towards a wider range of substrates; most notably with propargylic alcohols $HC{\equiv}CCR_2OH$. These reactions form the basis of Chapter 5 and have led to the revelation that the acetate ligand again is pivotal in determining the behaviour of this family of ruthenium complexes.

2.5: References

1. Bruce, M. I. *Chem. Rev*. **1991**, *91*, 197.
2. Bruneau, C.; Dixneuf, P. H. *Acc. Chem. Res*. **1999**, *32*, 311.
3. Katayama,H.; Ozawa, F. *Coord. Chem. Rev*. **2004**, *248*, 1703.
4. Lynam, J. M., *Chem. Eur. J.* **2010**, *16*, 8238.
5. Tokunaga, M.; Suzuki, T.; Koga, N.; Fukushima, T.; Horiuchi, A.; Wakatsuki, Y. *J. Am. Chem. Soc.* **2001**, *123*, 11917.
6. Bruneau, C.; Dixneuf, P. H. *Angew. Chem. Int. Ed*. **2006**, *45*, 2176.
7. Puerta, M. C.; Valerga, P. *Coord. Chem. Rev.* **1999**, *193-195*, 977.
8. Jiménez Tenorio, M. A.; Jiménez Tenorio, M.; Puerta, M. C.; Valerga, P. *Organometallics* **2000**, *19*, 1333.
9. Katayama, H.; Ozawa, F.; *Chem. Lett*. **1998**, 67.
10. Opstal, T.; Verpoort, T. *J. Mol. Catal. A*. **2003**, *200*, 49.
11. Silvestre, J., Hoffmann, *Helv. Chim. Acta.* **1985**, *68*, 1461.
12. Y. Wakatsuki, *J. Organomet. Chem*., **2004**, *689*, 4092.
13. Johnson, D. J., Lynam. J. M., Slattery, J. M., Welby, C. E., *Dalton Trans*. **2010**, *39*, 10432.
14. Le Lagadec, R.; Roman, E.; Toupet, L.; Muller, U.; Dixneuf, P. H. *Organometallics* **1994**, *13*, 5030.
15. Touchard, D.; Haquette, P.; Daridor, A.; Romero, A.; Dixneuf, P. H. *Organometallics* **1998**, *17*, 3844.
16. Bruce, M. I.; Hall, B. C.; Zaitseva, N. N.; Skelton, B. W.; White, A. H. *J. Organomet. Chem*. **1996**, *522*, 307.
17. Bruce, M. I.; Hall, B. C.; Zaitseva, N. N.; Skelton, B. W.; White, A. H.; *Dalton Trans*. **1998**, 1793.

18. Werner, H.; Stark, A.; Schulz, M.; Wolf, J. *Organometallics* **1992**, *11*, 1126.

19. Werner, H.; Schulz, M.; Windmuller, B. *Organometallics* **1995**, *14*, 3659.

20. Bader, A.; Linder, E. *Coord. Chem. Rev*. **1991**, *108*, 27.

21. Slugovc, C.; Mauthner, K.; Kacetl, M.; Mereiter, K.; Schmid, R.; Kirchner, K. *Chem. Eur. J*. **1998**, *4*, 2043.

22. Lynam, J. M.; Welby, C. E.; Whitwood, A. C. *Organometallics* **2009**, *28*, 1320.

23. All complexes reported in this thesis found to contain mutually *trans* phosphine ligands have δ_P values in the range 30-40 ppm; for those in which the phosphines are mutually *cis*, this range is higher, typically between δ_P 45-70.

24. Robinson, S.D.; Uttley, M.F. *J. Chem. Soc. Dalton. Trans.* **1973**, 1912.

25. Deacon, G.B., Phillips, R.J., *Coord. Chem. Rev.* **1980**, *33*, 227.

26. Katayama, H.; Ozawa, F. *Organometallics* **1998**, *17*, 5190.

27. Wolf, J. Stüer, W; Grünwald, C.; Gevert, O; Laubender, M.; Werner, H. *Eur. J. Inorg. Chem.* **1998**, 1827.

28. Grunwald, C., Laubender, M., Wolf, J., Werner, H., *J. Chem. Soc. Dalton. Trans.* **1998**, 833.

29. Wakatsuki, Y., Koga, N., Yamazaki, H., Morokuma, K., *J. Am. Chem. Soc.* **1994**, *116*, 8105.

30. Boutadla, Y.; Davies, D. L.; Macgregor, S. A.; Poblador-Bahamonde, A. I. *Dalton Trans.* **2009**, 5820.

31. Lapointe, D.; Fagnou, K. *Chem. Lett*. **2010**, *39*, 1118.

32. Wu, W., Wu, W., Ji, S., Guo, H., Zhao, J., *Eur. J. Inorg. Chem.* **2010**, 4470.

33. Werner, H.; Baum, M.; Schneider, D.; Windmuller, B. *Organometallics* **1994**, *13*, 1089.

34. Connelly, N. G.; Geiger, W. E.; Lagunas, M. C.; Metz, M.; Rieger, A. L.; Rieger, P. H.; Shaw, M. J.; *J. Am. Chem. Soc*. **1995**, *117*, 12202.

35. Katayama, H.; Onitsuka, K.; Ozawa, F. *Organometallics* **1996**, *15*, 4642.

36. Werner, H.; Lass, R. W.; Gevert, O.; Wolf, J. *Organometallics* **1997**, *16*, 4077.

37. Venkatesan, K.; Blacque, O.; Fox, T.; Alfonso, M.; Schmalle, H. W.; Kheradmandan, S.; Berke, H. *Organometallics* **2005**, 24, 920.

38. Venkatesan, K.; Fox, T.; Schmalle, H. W.; Berke, H. *Eur. J. Inorg. Chem*. **2005**, 901.

39. Ikeda, Y.; Yamaguchi, T.; Kanao, K.; Kimura, K.; Kamimura, S.; Mutoh, Y.; Tanabe, Y.; Ishii, Y. *J. Am. Chem. Soc*. **2008**, *130*, 16856.

40. Mutoh, Y.; Ikeda, Y.; Kimura, Y.; Ishii, Y. *Chem. Lett*. **2009**, *38*, 534.

41. Sheldrick, G. *Acta Crystallographica Section A* **2008**, *64*, 112-122.

42. Dolomanov, O. V.; Bourhis, L. J.; Gildea, R. J.; Howard J. A. K.; Puschmann, H. *J. Appl. Cryst*. **2009**, *42*, 339.

2.6 Experimental

General:

All experimental procedures were performed under an atmosphere of dinitrogen or argon using standard Schlenk Line and Glove Box techniques. DCM, pentane and hexane were purified with the aid of an Innovative Technologies anhydrous solvent engineering system. THF was distilled under N_2 from Na/benzophenone. The CD_2Cl_2 used for NMR experiments was dried over CaH_2 and degassed with three freeze-pump-thaw cycles. The solvent was then vacuum transferred into NMR tubes fitted with PTFE Young's taps. NMR spectra were acquired on a Bruker AVANCE 500 (Operating Frequencies ^{1}H 500.23 MHz, ^{31}P 202.50 MHz, ^{13}C 125.77 MHz). ^{31}P and ^{13}C spectra were recorded with proton decoupling. Mass spectrometry measurements were performed on a Thermo-Electron Corp LCQ Classic (ESI) instrument or a Fisons Analytical (VG) Autospec instrument (FAB). IR spectra were acquired on a Thermo-Nicolet Avatar 370 FTIR spectrometer using either CsCl solution cells or as KBr discs. CHN measurements were performed using an Exeter Analytical Inc. CE-440 analyser. The proportion of DCM in CHN samples was confirmed by recording a ^{1}H NMR spectrum of a sample used for CHN analysis in d_8-toluene. Relative integration of the peak at δ_H 4.31 (CH_2Cl_2) to that of the vinylidene proton indicated the proportion of DCM in that sample.

Structural characterisation of complexes **2a** and **2b** was conducted using a Bruker Smart Apex diffractometer with Mo K_α radiation (λ = 0.71073 Å) at 110 K with a SMART CCD camera. Diffractometer control, data collection and initial unit cell determination was performed using SMART. Frame integration and unit-cell refinement software was carried out with Saint+. Absorption corrections were applied by SADABS (v 2.03, Sheldrick). Structures were solved by direct methods using SHELXS-97,[41] and refined by full-matrix least-squares using SHELX-97. All non-hydrogen atoms were refined anisotropically. Hydrogen atoms were placed using a "riding model" and included in the refinement at calculated positions.

Structural characterisation of complex **2c** was collected at 110 K on an Agilent SuperNova diffractomer with MoK_α radiation (λ = 0.71073Å). Data collection, unit cell determination and frame integration were carried out with "CrysalisPro". Absorption corrections were applied using crystal face-indexing and the ABSPACK

absorption correction software within CrysalisPro. The structure was solved and refined using Olex2[42] implementing SHELX algorithms. It was solved by direct methods using SHELXS-97 and refined by full-matrix least squares using SHELXL-97. All non-hydrogen atoms were refined anisotropically. Hydrogen atoms were placed using a "riding model" and included in the refinement at calculated positions or otherwise found by difference map.

Complex **1** was prepared by the published literature methods.[22] HC≡CPh was obtained from Acros Organics and purified by passage through an alumina column and degassed by three freeze-pump-thaw cycles. HC≡CCO_2Me, 1-bromopyrene, PhC≡CTMS (Sigma-Aldrich) PPh_3, MeC≡CMe (Fluka), EtC≡CEt (Acros Organics), PhC≡CPh (Avocado Research Chemicals) and CuI, HC≡CTMS (Alfa Aesar) were used as supplied without further purification. Triethylamine was obtained from Aldrich and degassed by flushing through N_2 prior to use.

Key to NMR shorthand:

s (singlet); br s (broad singlet); d (doublet); dd (doublet of doublets); ad (apparent doublet); t (triplet); dt (doublet of triplets); tt (triplet of triplets); at (apparent triplet); q (quartet); aq (apparent quartet); qn (quintet), aqn (apparent quintet); sp (septet); asp (apparent septet); m (multiplet)

(H_2-Ph) or (H_2-PPh_3) refers to the proton in the *ortho*-position of a phenyl ring

(H_3-Ph) or (H_3-PPh_3) refers to the proton in the *meta*-position of a phenyl ring

(H_4-Ph) or (H_4-PPh_3) refers to the proton in the *para*-position of a phenyl ring

2.6.1: Synthesis of [Ru(κ^2-OAc)(κ ^{1}-OAc)(PPh$_3$)$_2$(=C=CHPh)] 2a

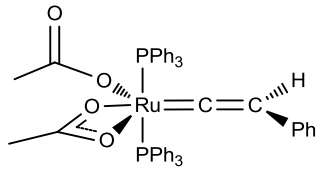

2a

HC≡CPh (31.0 μL, 0.28 mmol) was added to a stirred solution of **1** (0.21 g, 0.28 mmol) in 15 mL DCM and was stirred for one hour. The volume was reduced slightly *in vacuo* before addition of 20 mL hexane or pentane resulting in the formation of a pink precipitate. The solid was isolated by filtration and washed with 2 x 20 mL portions of hexane or pentane, and dried under vacuum. If required, the product could be further purified from a DCM/hexane or DCM/pentane solution. Crystals for X-ray diffraction were obtained from a CD_2Cl_2 solution of **2a**. Yield 0.32 g (71 %).

NMR Spectra CD_2Cl_2:

^{1}H δ_H 0.81 (s, 6.0H, C*H*$_3$COO), 5.14 (t, $^4J_{PH}$ = 3.7 Hz, 1H, Ru=C=C*H*Ph), 6.77 (d, 7.7 Hz, 2H, *ortho*-H of CH*Ph*), 6.83 (at, 7.4 Hz, 1.0H, *para*-H of CH*Ph*), 7.04 (t, 7.7 Hz, 2H, *meta*-H of CH*Ph*), 7.27, (t, 7.4 Hz, 12H, *meta*-H of P*Ph*$_3$), 7.35 (t, 7.4 Hz, 6H, *para*-H of P*Ph*$_3$), 7.46 (m, 12H, *ortho*-H of P*Ph*$_3$)

^{31}P δ_P 34.1 (s, *P*Ph$_3$)

^{13}C δ_C 21.9, (s, *C*H$_3$COO), 112.1 (t, $^3J_{PC}$ = 4.4 Hz, Ru=C=*C*), 123.7 (s, CH*Ph-C$_4$*), 124.7, (s, CH*Ph-C$_2$/C$_3$*), 127.9 (vt, $^3J_{PC}$+$^5J_{PC}$ = 9.1 Hz, PPh$_3$-*C$_3$*), 129.6 (vt, $^1J_{PC}$+$^3J_{PC}$ = 43.6 Hz, PPh$_3$-*C$_1$*), 130.0 (s, PPh$_3$, C$_4$), 133.4 (t, $^4J_{PC}$ = 2.9 Hz, CH*Ph*, C$_1$), 134.9 (t, $^2J_{PC}$+$^4J_{PC}$ = 12.4 Hz, PPh$_3$-*C$_2$*), 179.6 (s, CH$_3$*C*OO), 355.6 (t, $^2J_{PC}$ = 16.8 Hz, Ru=*C*)

IR (KBr) 1360.0 cm^{-1} (κ^1-OCO$_{sym}$), 1434.5 cm^{-1} (P-Ph), 1459.4 cm^{-1} (κ^2-OCO$_{sym}$), 1533.5 cm^{-1} (κ^2-OCO$_{asym}$), 1594.5 cm^{-1} (κ^1-OCO$_{asym}$), 1635.0 cm^{-1} (C=C), $\Delta\nu_{(uni)}$ 234.5 cm^{-1}, $\Delta\nu_{(chelate)}$ 74.1 cm^{-1}; (DCM) 1365.6 cm^{-1} (κ^1-OCO$_{sym}$), 1435.4 cm^{-1} (P-Ph), 1462.3 cm^{-1} (κ^2-OCO$_{sym}$), 1530.5 cm^{-1} (κ^2-OCO$_{asym}$), 1593.5 cm^{-1} (κ^1-OCO$_{asym}$), 1629.9 cm^{-1} (C=C), $\Delta\nu_{(uni)}$ 227.9 cm^{-1}, $\Delta\nu_{(chelate)}$ 68.2 cm^{-1}

MS (FAB), 846 m/z (Expected for $^{101}RuP_2O_4C_{48}H_{42}$ $[M]^+$ = 846.1), 787 m/z ($[Ru(OAc)(=C=CHPh)(PPh_3)_2]^+$), 727 m/z ($[Ru(=C=CHPh)(PPh_3)_2]^+$), 685 m/z ($[Ru(OAc)(PPh_3)_2]^+$), 625 m/z ($[Ru(PPh_3)_2]^+$), 584 m/z ($[Ru(OAc)_2(=C=CHPh)(PPh_3)]^+$), 524 m/z ($[Ru(OAc)(=C=CHPh)(PPh_3)]^+$)

CHN Anal for $RuP_2O_4C_{48}H_{42}$: (calc) % C 68.15, % H 5.02; (found) % C 67.79, % H 4.99

Crystal data and structure refinement for 2a.

Identification code	jml0706m	
Empirical formula	$RuP_2O_4Cl_4C_{50}H_{46}$	
Formula weight	1015.68	
Temperature	110(2) K	
Wavelength	0.71073 Å	
Crystal system	Triclinic	
Space group	P-1	
Unit cell dimensions	a = 11.4131(8) Å	α= 73.9130(10)°.
	b = 14.0888(10) Å	β= 89.8290(10)°.
	c = 15.2752(10) Å	γ = 84.941(2)°.
Volume	2350.2(3) $Å^3$	
Z	2	
Density (calculated)	1.435 Mg/m^3	
Absorption coefficient	0.673 mm^{-1}	
F(000)	1040	
Crystal size	0.12 x 0.11 x 0.05 mm^3	
Theta range for data collection	1.39 to 28.34°.	
Index ranges	-15<=h<=15, -18<=k<=18, -20<=l<=20	
Reflections collected	24318	
Independent reflections	11571 [R(int) = 0.0328]	
Completeness to theta = 28.34°	98.6 %	
Absorption correction	Semi-empirical from equivalents	
Max. and min. transmission	0.970 and 0.865	
Refinement method	Full-matrix least-squares on F^2	
Data / restraints / parameters	11571 / 8 / 582	
Goodness-of-fit on F^2	1.018	
Final R indices [I>2sigma(I)]	R1 = 0.0442, wR2 = 0.0976	
R indices (all data)	R1 = 0.0612, wR2 = 0.1046	
Largest diff. peak and hole	1.097 and -0.844 $e.Å^{-3}$	

2.6.2: Formation of 2a on an NMR scale

One equivalent (2.8 μL, 2.55 μmol) HC≡CPh was added to a CD_2Cl_2 solution of complex **1** (19.1 mg, 25.7 μmol) and ^1H and $^{31}P\{^1H\}$ NMR spectra were recorded as soon after addition of the alkyne as possible. The NMR features observed matched those reported for complex **2a**; complex **1** and HC≡CPh were completely consumed.

2.6.3: Reaction of $RuCl_2(PPh_3)_3$ with HC≡CPh

$RuCl_2(PPh_3)_3$ (34.0 mg, 35.5 μmol) was dissolved in 0.05 mL CD_2Cl_2. To this was added HC≡CPh (3.90 μL, 35.5 μmol) and the mixture monitored by ^1H and ^{31}P NMR spectroscopy over a period of 3 days.

$^{31}P\{^1H\}$ NMR spectrum after 1 day CD_2Cl_2: ^{31}P δ_P –5.47 (s, free *P*Ph_3), 27.1 (s, O=*P*Ph_3), 28.9 (s, [Ru(=C=CHPh)Cl_2(*P*Ph_3)$_2$]), 34.1 (AB-type d, $^2J_{PP}$ = 25.3 Hz), 40.7 (br s, [$RuCl_2$(*P*Ph_3)$_3$]), 47.3 (AB-type d, $^2J_{PP}$ = 39.0 Hz)

2.6.4: Synthesis of [Ru(κ^2-OAc)(κ^1-OAc)(PPh$_3$)$_2$(=C=CHCO$_2$CH$_3$)] 2b.

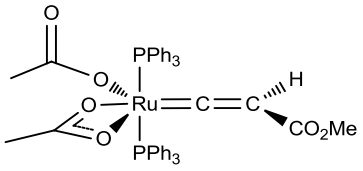

2b

The pale yellow complex [Ru(κ^2-OAc)(κ^1-OAc)(PPh$_3$)$_2$(=C=CHCO$_2$CH$_3$)] could be prepared in a similar manner to that described for **2a** using **1** (0.20 g, 0.27 mmol), HC≡CCO$_2$CH$_3$ (24.0 μL, 0.27 mmol) and 20 mL DCM. Crystals for X-ray diffraction were obtained from a DCM/hexane solution. Yield 0.13 g (59 %).

NMR Spectra CD_2Cl_2:

^{1}H δ_H 0.78 (s, 6H, C*H*$_3$COO) 3.46 (s, 3H, Ru=C=CHCO$_2$C*H*$_3$), 4.51, (t, $^4J_{PH}$ = 3.2 Hz, 1.H, Ru=C=C*H*), 7.33-7.47, (m, 38.5H, P*Ph*$_3$)

^{31}P δ_P 34.8 (s, *P*Ph$_3$)

^{13}C δ_C 21.8 (s, *C*H$_3$COO), 50.5 (s, Ru=C=CH−*C*), 104.4 (t, $^3J_{PC}$ = 3.9 Hz, Ru=C=*C*), 128.0 (t, $^3J_{PC}$+$^5J_{PC}$ = 9.6 Hz, PPh$_3$-*C*$_3$), 128.9, (t, $^1J_{PC}$+$^3J_{PC}$ = 44.4 Hz, PPh$_3$-*C*$_1$), 130.3 (s, PPh$_3$-*C*$_4$), 134.9 (t, $^2J_{PC}$+$^4J_{PC}$ = 12.2 Hz, PPh$_3$-*C*$_2$), 167.7 (s, Ru=C=CHCO$_2$*C*H$_3$), 179.8 (s, CH$_3$*C*OO), 345.2 (m, Ru=*C*)

IR (KBr) 1365.4 cm^{-1} (κ^1-OCO$_{sym}$), 1433.0 cm^{-1} (P-Ph), 1459.8 cm^{-1} (κ^2-OCO$_{sym}$), 1533.4 cm^{-1} (κ^2-OCO$_{asym}$), 1600.3 cm^{-1} (κ^1-OCO$_{asym}$), 1696.2 cm^{-1} (C=C), $\Delta\nu_{(uni)}$ 234.9 cm^{-1}, $\Delta\nu_{(chelate)}$ 73.6 cm^{-1}; IR (DCM) 1365.4 cm^{-1} (κ^1-OCO$_{sym}$), 1434.7 cm^{-1} (P-Ph), 1465.7 cm^{-1} (κ^2-OCO$_{sym}$), 1535.1 cm^{-1} (κ^2-OCO$_{asym}$), 1599.7 cm^{-1} (κ^1-OCO$_{asym}$), 1684.3 cm^{-1} (C=C), $\Delta\nu_{(uni)}$ 234.3 cm^{-1}, $\Delta\nu_{(chelate)}$ 80.1 cm^{-1}

MS (ESI) m/z 851.1269 (Expected for [^{101}RuP$_2$O$_6$C$_{45}$H$_{44}$Na]$^+$ = 851.1241)

CHN Anal for RuP$_2$O$_6$C$_{45}$H$_{44}$ + (0.75 CH$_2$Cl$_2$) (calc), % C 60.62, % H 4.63; (found) % C 60.74, % H 4.70.

Crystal data and structure refinement for 2b.

Identification code	jml0808m	
Empirical formula	$RuP_2O_6Cl_4C_{46}H_{44}$	
Formula weight	997.62	
Temperature	110(2) K	
Wavelength	0.71073 Å	
Crystal system	Triclinic	
Space group	P-1	
Unit cell dimensions	a = 11.1010(14) Å	α= 105.694(3)°.
	b = 13.9967(17) Å	β= 92.102(2)°.
	c = 15.1277(19) Å	γ = 97.559(3)°.
Volume	2236.8(5) $Å^3$	
Z	2	
Density (calculated)	1.481 Mg/m^3	
Absorption coefficient	0.708 mm^{-1}	
F(000)	1020	
Crystal size	0.14 x 0.05 x 0.04 mm^3	
Theta range for data collection	1.40 to 28.42°.	
Index ranges	-14<=h<=14, -18<=k<=18, -20<=l<=20	
Reflections collected	22964	
Independent reflections	11014 [R(int) = 0.0706]	
Completeness to theta = 28.42°	97.8 %	
Absorption correction	Semi-empirical from equivalents	
Max. and min. transmission	0.972 and 0.742	
Refinement method	Full-matrix least-squares on F^2	
Data / restraints / parameters	11014 / 4 / 533	
Goodness-of-fit on F^2	1.007	
Final R indices [I>2sigma(I)]	R1 = 0.0722, wR2 = 0.1620	
R indices (all data)	R1 = 0.1345, wR2 = 0.1884	
Largest diff. peak and hole	1.373 and -1.625 $e.Å^{-3}$	

2.6.5: Synthesis of 1-ethynylpyrene

Following procedure reported by Guo and Zhao[32]

Under a N_2 atmosphere, a Schlenk tube with inbuilt condenser and stirrer bar was charged with 1-bromopyrene (0.47 g, 1.67 mmol), $[PdCl_2(PPh_3)_2]$ (46.0 mg, 0.07 mmol), PPh_3 (37.0 mg, 0.14 mmol) and CuI (29.2 mg, 0.15 mmol). 25 mL TEA and 15 mL THF were then introduced and the mixture stirred vigorously to give an orange-yellow solution. HC≡CTMS (285 μL, 2.01 mmol) was then added and the mixture heated at 90 °C for 6.5 hours. After allowing to cool to room temperature, the solution was filtered *via* cannula wire into another Schlenk tube and the solvent removed *in vacuo*. Hexane (approx. 40 mL) was added to the yellow-orange powder and the remaining solid was removed by filtration. The solvent was removed from the filtrate and the resulting yellow oil dissolved in Et_2O (10 mL), followed by the addition of MeOH (20 mL) and a stirrer bar. K_2CO_3 (1.60 g) was added and the mixture stirred for 3 hours at room temperature. After this time, the mixture was filtered and the solvent evaporated. At this point, the orange-yellow residue was purified by column chromatography, however the residue was not completely soluble in either DCM or hexane. A concentrated solution of the products in hexane was loaded onto the column (additional DCM increases the solubility of the products but leads to bleaching and incomplete separation) and the products eluted with a 50:1 hexane:DCM solvent system. The proportion of DCM was gradually increased until 4 products had eluted – they can be clearly identified using long-wave UV light. The third fraction was collected and the solvent removed to give 1-ethnylpyrene as a grey powder. Yield 20 mg (5.3%).

^{1}H NMR $CDCl_3$ (400 MHz): δ_H 3.55 (s, 1H, *H*C≡C(pyrene)), 7.97 (m, 2H), 8.04 (m, 2H), 8.13 (m, 4H), 8.52 (d, J = 9.1 Hz, 1H)

MS (EI): m/z 226.0779 $[M]^+$; predicted for $C_{18}H_{10}$: 226.0783

2.6.6: Synthesis of [Ru(κ^2-OAc)(κ^1-OAc)(PPh_3)$_2$(=C=CH(pyrene)] 2c.

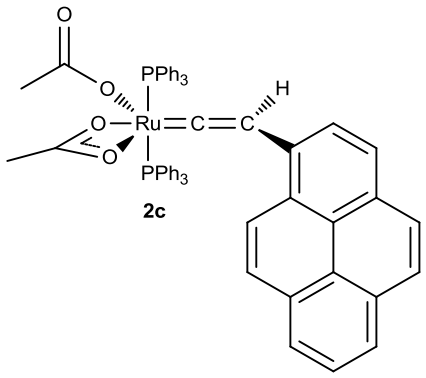

2c

20.0 mg 1-ethynylpyrene (0.09 mmol) was dissolved in 7mL DCM in a degassed round-bottomed flask. This solution was then transferred *via* cannula wire under a N_2 atmosphere to a Schlenk tube containing 66.7 mg **1** (0.09 mmol) with a stirrer bar. The mixture was stirred under N_2 for 1 hour. After this time, the solution was concentrated *in vacuo* and 25 mL pentane added to precipitate the product as a bright red powder. The liquid was removed by a cannula, fitted with a filter-paper tip, and the product washed with two further portions of pentane (10 mL) before finally drying *in vacuo*. Yield 34.7 mg (40.5 %)

NMR Spectra CD_2Cl_2:

^{1}H δ_H 0.95 (s, 6H, C*H*$_3$COO), 6.20 (t, $^4J_{HP}$ = 3.6 Hz, 1H, [Ru]=C=C*H*), 7.27-7.33 (m, 18H, P*Ph*$_3$), 7.54-7.58 (m, 12H, P*Ph*$_3$), 7.77-7.87 (m, 3H, pyrene), 7.91-8.00 (m, 4H, pyrene), 8.09 (t, *J* = 7.55 Hz, 2H, pyrene)

^{31}P δ_P 33.8 (*P*Ph$_3$)

^{13}C δ_C 22.0 (s, *C*H$_3$COO), 109.4 (t, $^3J_{PC}$ = 4.6 Hz, Ru=C=*C*Ph), 124.0, 124.2, 124.3, 124.5, 124.8, 125.2, 125.2, 125.3, 125.5, 125.7, 127.6, 127.9 (t, $^3J_{CP}$ + $^5J_{CP}$ = 9.24 Hz, PPh$_3$-*C*$_3$), 128.1, 128.7, 129.4 (t, $^1J_{CP}$ + $^3J_{CP}$ = 43.1 Hz, PPh$_3$-*C*$_1$), 130.0 (s, PPh$_3$-*C*$_4$), 131.4, 131.8, 134.9 (t, $^2J_{CP}$ + $^4J_{CP}$ = 10.9 Hz, PPh$_3$-*C*$_2$), 179.8 (s, CH$_3$*C*OO).

IR (KBr) 1360 cm^{-1} (κ^1-OAc$_{sym}$), 1434 cm^{-1} (P-Ph), 1458 cm^{-1} (κ^2-OAc$_{sym}$), 1536 cm^{-1} (κ^2-OAc$_{asym}$), 1587 cm^{-1}(κ^1-OAc$_{asym}$), 1610 cm^{-1} (C=C), $\Delta\nu_{(uni)}$ = 227 cm^{-1}, $\Delta\nu_{(chelate)}$ 78 cm^{-1}; (DCM) 1366 cm^{-1} (κ^1-OAc$_{sym}$), 1434 cm^{-1} (P-Ph), 1462 cm^{-1} (κ^2-OAc$_{sym}$), 1530 cm^{-1} (κ^2-OAc$_{asym}$), 1590 cm^{-1}(κ^1-OAc$_{asym}$), 1607 cm^{-1} (C=C), $\Delta\nu_{(uni)}$ = 224 cm^{-1}, $\Delta\nu_{(chelate)}$ 68 cm^{-1}

MS (ESI) m/z 971.1968 (Expected for $^{101}RuP_2O_4C_{58}H_{47}$ $[MH]^+$ = 971.1993), 952.2034 (Expected for $^{101}RuP_2O_2NC_{58}H_{46}$ = 952.2047 [M] - OAc^- + MeCN)

CHN Analysis for $RuP_2O_4C_{58}H_{46}$ + (0.30 CH_2Cl_2): (calc) C 70.34, H 4.72; (found) C 69.89, 4.82

Crystal data and structure refinement for 2c.

Identification code	jml1025
Empirical formula	$RuP_2O_4Cl_4C_{60}H_{50}$
Formula weight	1139.81
Temperature / K	383.15
Crystal system	triclinic
Space group	P-1
a / Å, b / Å, c / Å	13.5902(10), 13.9934(10), 16.6038(8)
α/°, β/°, γ/°	98.866(5), 106.633(5), 115.860(7)
Volume / $Å^3$	2576.1(3)
Z	2
ρ_{calc} / mg mm^{-3}	1.469
μ / mm^{-1}	0.623
F(000)	1168
Crystal size / mm^3	0.2437 × 0.1686 × 0.1268
2Θ range for data collection	6.08 to 64.3°
Index ranges	$-20 \le h \le 19$, $-19 \le k \le 16$, $-23 \le l \le 19$
Reflections collected	25341
Independent reflections	16076[R(int) = 0.0206]
Data/restraints/parameters	16076/12/649
Goodness-of-fit on F^2	1.046
Final R indexes [I>2σ (I)]	R_1 = 0.0337, wR_2 = 0.0751
Final R indexes [all data]	R_1 = 0.0416, wR_2 = 0.0803
Largest diff. peak/hole / e $Å^{-3}$	1.296/-0.943

2.6.7: Reaction of 1 with PhC≡CPh

One equivalent of PhC≡CPh (5.13 mg, 0.03 mmol) was added to a solution of **1** (21.4 mg, 0.03 mmol) in 0.5 mL CD_2Cl_2. This solution was monitored by ^{1}H and ^{31}P NMR spectroscopy over 11 days. The ^{31}P NMR data indicates that even after this time, the major component of this mixture continues to be **1**.

2.6.8: Reaction of 1 with MeC≡CMe

One equivalent of MeC≡CMe (2.49 μL , 0.03 mmol) was added to a solution of **1** (23.6 mg, 0.03 mmol) in 0.5 mL CD_2Cl_2. This solution was monitored by ^{1}H and ^{31}P NMR spectroscopy over 3 days. The ^{31}P NMR data indicates that even after this time, the major component of this mixture continues to be **1**.

2.6.9: Reaction of 1 with PhC≡CTMS

One equivalent of PhC≡CTMS (4.00 μL, 0.02 mmol) was added to a solution of **1** (15.0 mg, 0.02 mmol) in 0.5 mL CD_2Cl_2. This solution was monitored by ^{1}H and ^{31}P NMR spectroscopy over 2 days. After this time the mixture was heated at 40 °C for 3 hours and again NMR spectra were recorded. The ^{31}P NMR data indicates that even after this time, the major component of this mixture continues to be **1**.

2.6.10: Reaction of 1 with EtC≡CEt

One equivalent of EtC≡CEt (2.14 μL, 0.02 mmol) was added to a solution of **1** (14.0 mg, 0.02 mmol) in 0.5 mL d_8-toluene. The solution was degassed by five freeze-pump-thaw cycles using an ultra-high vacuum line and the mixture analysed by ^{1}H and ^{31}P NMR spectroscopy. The solution was then heated at 80 °C for 22 hours and NMR spectra were re-recorded. The ^{31}P NMR data indicates that even after this time, the major component of this mixture continues to be **1**.

3: Synthesis and Characterisation of novel Ruthenium Acetylide complexes

3.1: Introduction

Transition-metal acetylide, or alkynyl, complexes have been the focus of significant attention due mainly to their luminescent properties, electrical conductivity, optical non-linearity and liquid crystallinity.[1-7] These properties are attributed to the extensive overlap of metal orbitals with the π-orbitals of the acetylide.[7,8] Acetylide copper complexes are essential to the well-known Sonagashira cross-coupling reaction, where a terminal alkyne is coupled with a vinyl halide. The copper-acetylide forms *via* deprotonation of the corresponding terminal alkyne bound in an η^2-fashion to the metal, and undergoes a subsequent transmetallation to palladium.[9] Transition-metal acetylides can also be synthesised from the transmetallation of a highly reactive lithium acetylide (LiC≡CR), generated from the terminal alkyne and a Li base such as LiBu.

An alternative route to metal acetylide complexes was demonstrated by Bruce in 1979, who showed that a ruthenium-acetylide $[RuCp(PPh_3)_2(C{\equiv}CPh)]$ could be generated by deprotonation of the vinylidene ligand of $[RuCp(PPh_3)_2(=C=CHPh)]PF_6$ with sodium methoxide.[10,11] Since then, a number of research groups who have interests in vinylidene and acetylide chemistry have used this method to generate acetylide-complexes using a variety of transition-metal precursors and bases. The reverse reaction, the reprotonation of the acetylide to produce a vinylidene, has also become a well-established procedure.[11-19]

The reaction of terminal alkynes with **1** to form vinylidene complexes is remarkably facile, as detailed in Chapter 2. It is therefore appropriate to probe the ability of this system to support acetylide ligands, by attempting to remove the vinylidene proton.

3.2: Unsuccessful attempts to deprotonate 2a and 2c

The removal of a proton from a nucleophilic vinylidene C_β by a suitable base to produce an acetylide ligand is considered to be relatively facile. However, attempts to generate the corresponding acetylide complexes from **1** *via* this method proved surprisingly unsuccessful.

Addition of one equivalent of the base $Na[N(SiMe_3)_2]$ to a solution of **2a** in THF resulted in a mixture of components, none of which could be successfully isolated. Analysis of this mixture by ^1H and $^{31}P\{^1H\}$ NMR spectroscopy showed that in addition to the starting material, two other PPh_3-containing complexes were present, which were thought to correspond to complexes **3A** and **3** shown in Figure 3.2.1 below. A triplet resonance at δ_P 52.3 and a doublet at δ_P 31.5 with a mutual coupling constant of 26.5 Hz, and a relative integration ratio of 1:2 respectively were observed, coupled with the lack of resonances for a new vinylidene complex in the ^1H NMR spectrum, suggests that a complex with structure **3** was formed. If this were the case, it is reasonable to suggest that this compound might form *via* an intermediate in the form of structure **3A**. This would give rise to a singlet in the $^{31}P\{^1H\}$ NMR spectrum, and such a singlet is observed at δ_P 30.5. It should also be noted that the addition of an excess of PPh_3 did not alter to the outcome of this reaction.

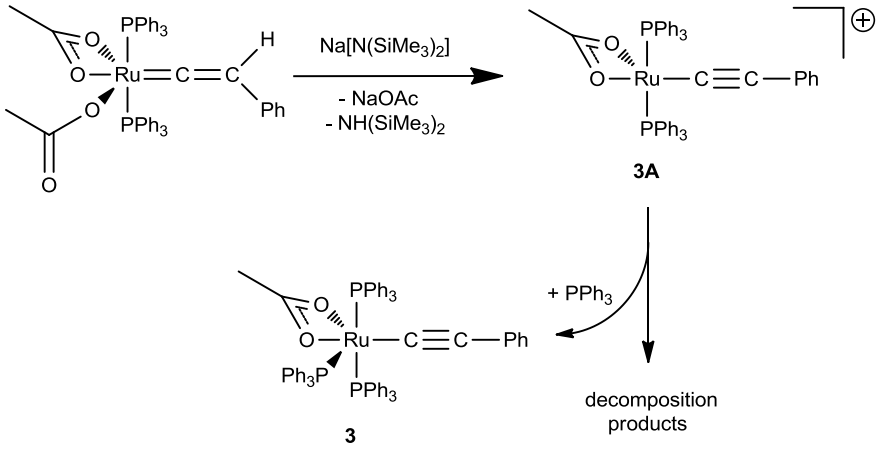

Figure 3.2.1: Reaction of **2a** with $Na[N(SiMe_3)_2]$.

A series of similar experiments were conducted by Erasmus student Thomas Eschermann on the analogous complex [Ru(κ^1-OAc)(κ^2-OAc)(=C=CHTMS)(PPh_3)$_2$] (**2d**).[20] Addition of CsF to a solution of **2d** resulted not in the expected desilylation to give [Ru(κ^1-OAc)(κ^2-OAc)(=C=CH_2)(PPh_3)$_2$], but in a mixture of products. Analysis by ^{1}H and ^{31}P{^{1}H} NMR spectroscopy showed that a complex apparently analogous to **3** is part of the mixture. A triplet resonance at δ_P 50.7, and a doublet resonance at δ_P 32.3 were observed in the ^{31}P{^{1}H} NMR spectrum, coupled by 25.0 Hz, and have a relative integration ratio of 1:2. A single crystal of this species suitable for study by X-ray diffraction was obtained from this mixture by the slow diffusion of pentane into the DCM solvent. This confirmed the proposed structure [Ru(PPh_3)$_3$(κ^2-OAc)(C≡C$SiMe_3$)], **3**, shown in the ORTEP figure below (Figure 3.2.2), with selected bond lengths and angles given in Table 3.2.1. The IR spectrum of the crystals exhibited a band at 1998 cm^{-1}, which was assigned to the C≡C stretching mode.

The reaction of **2d** with CsF was also conducted in the presence of an excess of triphenylphosphine in an attempt to form the acetylide complex **3** exclusively, however this was unsuccessful. An identical mixture of products was also generated when Na[N($SiMe_3$)$_2$] was used as an alternative base. Both NaOAc and DBU, a base also used by Dixneuf to generate an acetylide from a vinylidene-complex,[13] did not exhibit any reaction, and *n*-BuLi was also unsuccessful. It seems that both desilylation and deprotonation are competing reactions for the TMS-substituted vinylidene complex, so deprotonation of **2a** was attempted using DBU. Unfortunately, this reaction was again unsuccessful, no reaction between the two occurred as shown by ^{1}H and ^{31}P{^{1}H} NMR spectroscopy.

The route most commonly used to generate an acetylide in ruthenium-vinylidene chemistry has been applied to vinylidene derivatives of complex **1**, it was however unsuccessful. Consequently, investigations were extended to consider alternative ruthenium precursors, which are closely related to this system.

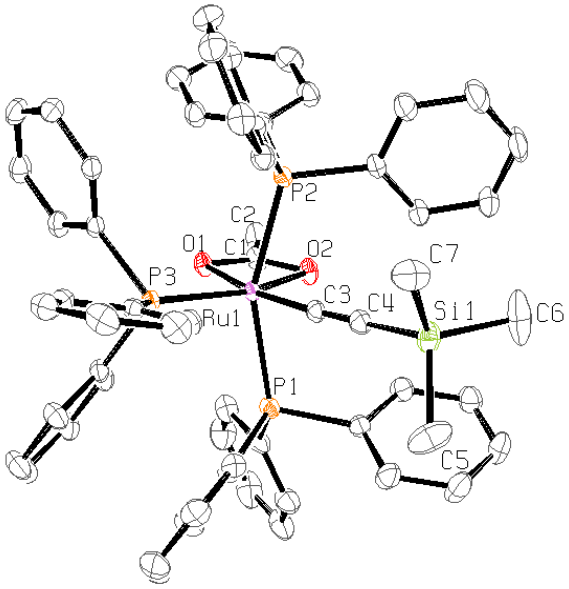

Figure 3.2.2: ORTEP diagram of **3**, thermal ellipsoids at the 50 % probability level. Hydrogen atoms omitted for clarity.

Bond Length	**(Å)**	**Bond Angle**	**(deg / °)**
Ru – P(1)	2.3877(5)	P(1) – Ru – P(2)	156.432(17)
Ru – P(2)	2.3673(5)	P(1) – Ru – P(3)	98.097(17)
Ru – P(3)	2.2833(5)	P(2) – Ru – P(3)	101.739(17)
Ru – C(3)	1.9835(18)	P(1) – Ru – C(3)	81.78(5)
Ru – O(1)	2.1996(12)	P(1) – Ru – O(1)	99.26(4)
Ru – O(2)	2.2375(13)	P(1) – Ru – O(2)	87.20(4)
C(3) – C(4)	1.222(3)	P(2) – Ru – C(3)	83.19(5)
C(4) – Si(1)	1.807(2)	P(2) – Ru – O(1)	92.14(4)
		P(2) – Ru – O(2)	81.09(4)
		P(3) – Ru – C(3)	97.31(5)
		P(3) – Ru – O(1)	93.51(3)
		P(3) – Ru – O(2)	152.45(4)
		Ru – C(3) – C(4)	176.31(16)
		C(3) – C(4) – Si(1)	178.98(18)

Table 3.2.1: Selected Bond Lengths and Angles for **3**.

3.4 Preparation of [Ru(κ^1-OAc)(κ^2-OAc)(CO)(PPh$_3$)$_2$]

In the 1960-80's, a significant amount of work was done by the groups of Wilkinson and Robinson, amongst others, into the synthesis, characterisation and behaviour of a range of different acetato- and trifluoroacetato- complexes of ruthenium. We have drawn upon these works to provide new inspiration for easily prepared ruthenium precursors.

In 1974, Wilkinson reported the synthesis of the CO-containing derivative of complex **1**, Ru(κ^1-OAc)(κ^2-OAc)(CO)(PPh$_3$)$_2$. His procedure involved bubbling CO through a solution of **1** in MeOH for one hour, followed by isolation of the resulting pale yellow-green precipitate which was washed with MeOH and Et_2O.[21] We have found that this complex can also be prepared by vigorously stirring a solution of **1** in DCM under an atmosphere of CO until a colour change from red-orange to a pale yellow-green is observed. Removal of the solvent *in vacuo* affords a pale yellow-green residue which can be used without further purification. The latter method is used to conveniently generate this compound (**4**) *in situ*, whilst Wilkinson's method was used to prepare the complex on a large scale.[22]

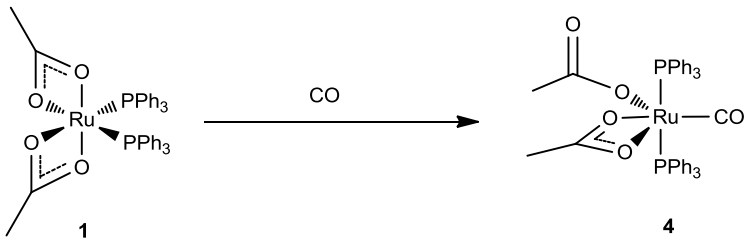

Figure 3.3.1: Addition of CO to **1**.

Complex **4** is readily identified by characteristic spectroscopic features, most notably in the IR spectrum where a band assigned to υ_{CO} was observed at 1946 cm^{-1}. A single resonance in the ^{1}H NMR spectrum at δ_H 0.64 assigned to the acetate protons decoalesces when cooled to 195 K, indicating that the acetate ligands have adopted a fluxional κ^1- κ^2 coordination mode. The rate and energy barrier for this fluxional exchange can be described by k_{coal} and $\Delta G^{\ddagger}$ using the expressions below. The rate constant at coalescence (k_{coal}) is given by Equation 3.3.1:

$$k_{coal} = \frac{\pi\delta\nu}{\sqrt{2}} = 2.22\delta\nu \tag{3.3.1}$$

This can be combined with a rearrangement (Equation 3.3.2) of the Eyring Equation (Equation 5.2.3) to give an expression for $\Delta G^{\ddagger}$ (Equation 3.3.4 see also Section 5.2)

$$k = \kappa \frac{k_B T}{h}\left(-\Delta G^{\ddagger} / RT\right) \tag{3.3.2}$$

$$\Delta G^{\ddagger} = RT[23.76 - \ln(k/T)] \tag{3.3.3}$$

$$\Delta G^{\ddagger} = RT_c\left[22.96 + \ln\left(\frac{T_c}{\delta\nu}\right)\right] Jmol^{-1} \tag{3.3.4}$$

Ideally, the value of δ_ν in Equation 3.3.4 used to calculate the energy barrier to exchange should be recorded at the low temperature limit when the two individual proton environments can be clearly distinguished. Unfortunately, it was not possible to reach this low temperature limit so the values of $\Delta G^{\ddagger}$ and k_{coal} are the lower limits. The values of T_c were uncalibrated and it is estimated that the values have a ± 5 K error associated with them as spectra were recorded every 5 K at these low temperatures. Consequently, the rate constant (k_{coal}) for complex **4** is ≤ 385.6 s^{-1}, and $\Delta G^{\ddagger} \leq 37.4$ kJ mol^{-1}.

Stretches for both coordination modes are also evident in the IR spectrum. The $^{31}P\{^1H\}$ NMR spectrum displays a singlet at δ_P 39.1, indicating a *trans*-orientation of the PPh_3 ligands, as noted for the vinylidene complexes. In the $^{13}C\{^1H\}$ NMR spectrum, a triplet resonance at δ_C 207.4 ($^2J_{PC}$ = 13.2 Hz) was observed which corresponds to the CO ligand. Crystals of **4** obtained from a separate reaction mixture (see Section 5.3) were subjected to a structural characterisation, which revealed that the compound crystallises in the P–1 space group. This confirmed that the PPh_3 ligands are mutually *trans*, whilst the CO and acetate ligands occupy the remaining sites of the octahedral complex. An ORTEP representation of **4** is shown in Figure 3.3.2 and a table of selected bond lengths and angles is included in Table 3.3.1.

The structure obtained is that of a distorted octahedron and most bond angles about the ruthenium atom are close to 90 °. However the κ^2-OAc ligand has a constraining angle of 60.42(4) ° (O(1) – Ru – O(2)) which results in the observed distortion. The structure is similar to that obtained for the vinylidene complexes **2a-c** reported in Chapter 2; a comparison with other acetate-containing complexes reported in this thesis is included in Chapter 8. As expected, the Ru – C(5) – O(5) ° angle is close to linear at 175.01(15) °. Hocking and Hambley[23] have recently surveyed thousands of crystal structures of transition metal complexes reported in the CSD to contain terminal CO ligands. They have found that for ruthenium complexes the average CO bond length is approximately 1.138 Å with a range of values from 1.07 – 1.19 Å reported. For complex **4**, the C(5) – O(5) bond length is 1.146(2) Å, which is well within this range and close to the average. Hocking and Hambley also report that for ruthenium CO complexes, the Ru–C bond length ranges from 1.75 – 2.03 Å, and that a shorter Ru–C bond length is often associated with a longer C≡O bond length. For complex **4**, the Ru – C(5) bond length is 1.8318(17) Å, which is within the expected range.

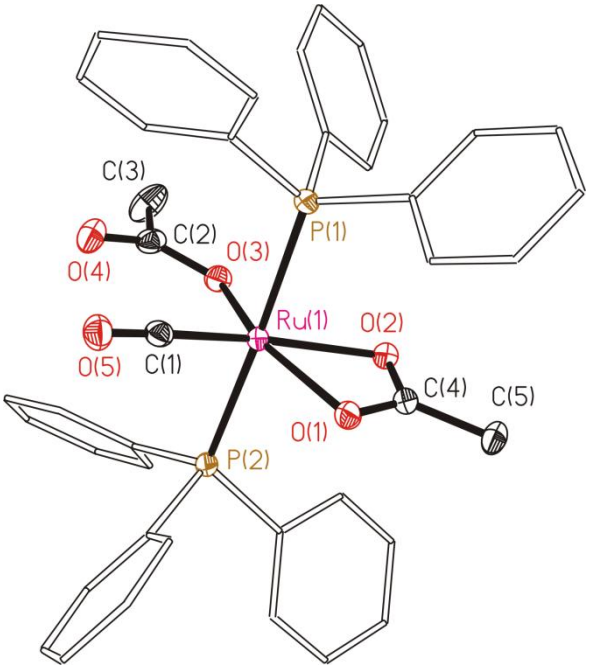

Figure 3.3.2: ORTEP diagram of **4**, thermal ellipsoids, where shown, at the 50 % probability level. Hydrogen atoms omitted for clarity.

Bond Length	**(Å)**	**Bond Angle**	**(deg / °)**
Ru – P(1)	2.4060(4)	P(1) – Ru – P(2)	176.545(15)
Ru – P(2)	2.3873(4)	P(1) – Ru – O(1)	95.14(3)
Ru – O(1)	2.1466(11)	P(1) – Ru – O(2)	86.12(3)
Ru – O(2)	2.1897(11)	P(1) – Ru – O(3)	87.52(3)
Ru – O(3)	2.0365(11)	P(1) – Ru – C(5)	91.24(5)
Ru – C(5)	1.8318(17)	P(2) – Ru – C(5)	88.21(5)
C(5) – O(5)	1.146(2)	O(1) – Ru – O(2)	60.42(4)
		O(1) – Ru – O(3)	155.62(5)
		O(2) – Ru – O(3)	95.71(5)
		O(1) – Ru – C(5)	104.71(6)
		O(2) – Ru – C(5)	164.49(6)
		O(3) – Ru – C(5)	99.45(6)
		Ru – C(1) – O(5)	175.02(15)

Table 3.3.1: Selected Bond lengths and Angles for **4**.

The *trans*-orientation of the PPh_3 ligands in **4** contrasts with work reported by Robinson in 1979 on his preparation of **4**, who claims the two phosphine ligands adopt a non-equivalent mutually *cis*-orientation.[24-27] Whilst not describing the synthesis of *cis*-**4** explicitly, he has referred to the preparation of the analogous complexes $[Ru(OCOR)_2(CO)(PPh_3)_2]$, where R is *p*-$C_6H_4Cl$ or *p*-$C_6H_4NO_2$ from addition of the appropriate carboxylic acid to $[RuH_2(CO)(PPh_3)_3]$ in boiling 2-methoxyethanol (125 °C).[25] He provides evidence for the fluxional behaviour of *cis*-**4** and describes how a singlet at δ_P 47.0 in the $^{31}P\{^1H\}$ NMR spectrum decoalesces at 243 K to afford an AB pattern (δ_P 48.7 and 45.4 $^2J_{PP}$ = 24.4 Hz), whilst a singlet at δ_H 1.29 in the ^1H NMR spectrum corresponding to the acetate protons decoalesces to two sharp peaks at δ_H 1.44 and 1.14 at a temperature of 270 K. From these results, he has concluded that there are two separate rate processes, with distinct activation parameters governing the equilibration of the phosphine ligands and interchange of the acetate groups. The mechanisms Robinson proposes for these processes are given in Figure 3.3.3 below:

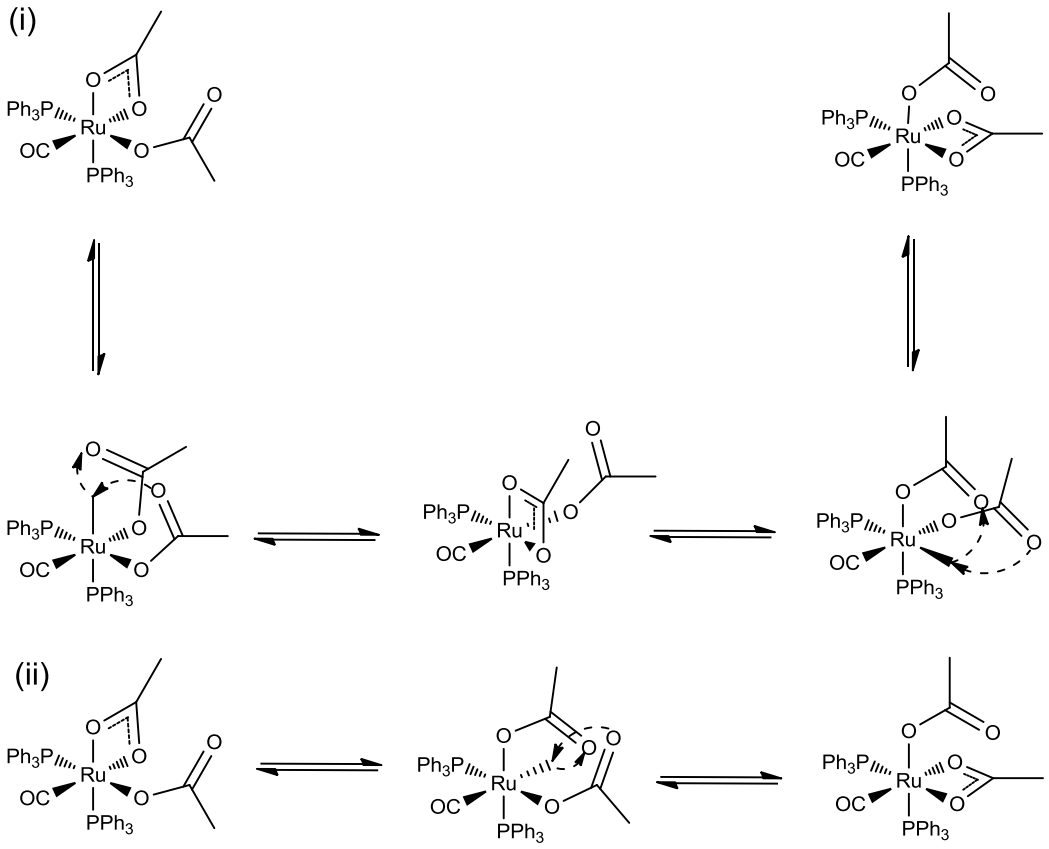

Figure 3.3.3: (i) Robinson's proposed mechanism for the interchange of phosphine but not acetate ligands in *cis*-**4** and (ii) Mechanism for interchange of both acetate and phosphine ligands in *cis*-**4**.

The two different processes account for the two different activation parameters obtained; the exchange of the acetate ligands was calculated to have an energy barrier of $\Delta G^{\ddagger}$ = 55.6 ± 2 kJ mol^{-1} whilst that of the phosphine ligands was calculated to be $\Delta G^{\ddagger}$ = 46.0 ± 2 kJ mol^{-1}. Figure 3.3.3 (i) demonstrates how the phosphine ligands remain equivalent whilst the interchange of the acetate ligands occurs. This involves cleavage of the Ru-O bonds *trans* to a phosphine ligand whilst the coordination site *trans* to the CO is retained throughout. Figure 3.3.3 (ii) suggests how cleavage of the Ru-O bond *trans* to the carbonyl ligand means both acetate ligands and phosphine ligands are equilibrated. At high temperatures, both mechanisms are operating, however as the temperature is lowered, the distinct environments of the acetate ligands can first be observed *via* the mechanism given in Figure 3.3.3 (ii), and further cooling resolves the different phosphine environments (i).

Variable temperature NMR experiments were therefore conducted on a sample of **4** prepared using our conditions. This showed that the singlet peak at δ_P 39.1 in the $^{31}P\{^1H\}$ NMR spectrum only broadens at 195 K, and as stated earlier, the singlet due to the CH_3 protons of the OAc ligand decoalesces at 195 K. It was also noted from this experiment that a trace amount of a compound at δ_P 47.8 present at 300 K as a broad singlet, decoalesces at 235 K to two doublets at δ_P 45.7 and 49.0 ($^2J_{PP}$ = 25.0 Hz) in an AB pattern, corresponding to Robinson's *cis*-**4** complex. Observations matching those of Robinson's were also made in the corresponding ^1H NMR spectrum. The same NMR sample was then heated at 50 °C for an extended period of time. Over the course of 50 days, resonances matching those of *cis*-**4** gradually increased in intensity, indicating that **4** prepared by our method results in the formation of the *trans*-isomer as the single kinetic product of the reaction, whereas Robinson's *cis*-**4** is the ultimate thermodynamic product.

The relative energies of these complexes were calculated at the PBE0/TZVPP level of theory by David Johnson and are shown in Figure 3.3.4 below.

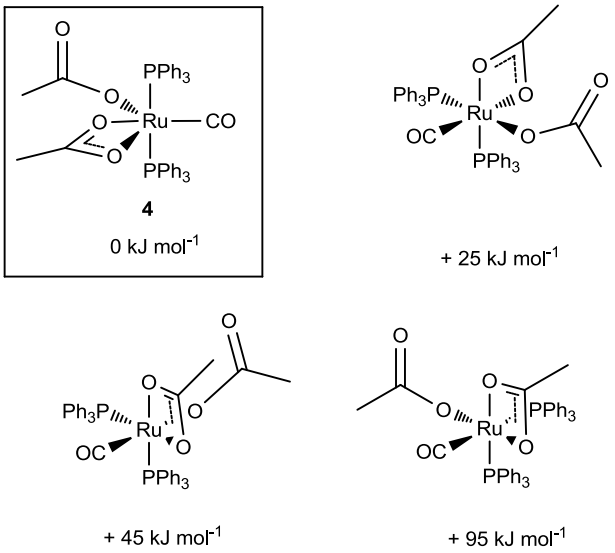

Figure 3.3.4: The relative energies of the four isomeric forms of $[Ru(\kappa^1\text{-OAc})(\kappa^2\text{-OAc})(CO)(PPh_3)_2]$.

The Gibbs energies have been calculated relative to *trans*-**4** and show that, confusingly, the three isomers of *cis*-**4** are all higher in energy than *trans*-**4**. This is counter to our expectations, as we have demonstrated experimentally that *cis*-**4** should be the thermodynamically preferred isomer as heating a sample of *trans*-**4** results in the gradual formation of *cis*-**4**.

3.4 Preparation of $[Ru(\kappa^1\text{-OAc})(\kappa^2\text{-OAc})(NO)(PPh_3)_2]BF_4$

In a similar manner to the preparation of **4**, the analogous, but novel, complex $[Ru(\kappa^1\text{-OAc})(\kappa^2\text{-OAc})(NO)(PPh_3)_2]BF_4$ (**5**) was prepared by addition of one equivalent of $NOBF_4$ to a solution of **1** in DCM. After stirring for one hour at room temperature the solution was concentrated and the product precipitated out of solution upon addition of toluene. Filtration and further washing with toluene gave the product as a light brown powder that can be recrystallized further by the slow diffusion of pentane into a DCM solution of **5**.

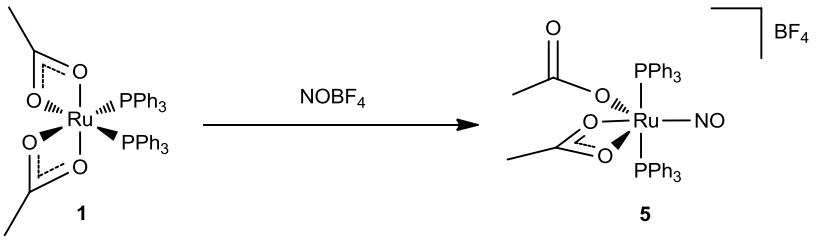

Figure 3.4.1: Addition of $NOBF_4$ to **1**.

Complex **5** displays a singlet in the $^{31}P\{^{1}H\}$ NMR spectrum at δ_P 34.7, once more consistent with a *trans*-orientation of the phosphine ligands. The ^{1}H NMR spectrum shows only a singlet resonance for the acetate ligands, however it is noticeably broader than that of **4**. Cooling to 235 K saw this peak decoalesce ($\Delta G^{\ddagger} \leq$ 45.3 kJ mol^{-1} see Section 3.3), although no change is observed in the $^{31}P\{^{1}H\}$ NMR, even at 215 K. This behaviour is somewhat similar to that observed for complex **4**, in that coalescence is observed for the signal due to the acetate protons in the ^{1}H NMR spectrum, whilst the resonance in the $^{31}P\{^{1}H\}$ NMR spectrum only broadens at 195 K.

The IR spectrum of **5** in DCM shows a sharp peak at 1874 cm^{-1} attributed to the NO ligand in a linear orientation.[28] A similar peak at 1865 cm^{-1} is present in the IR spectrum recorded in the solid state (KBr disc). Unusually however, the IR spectra recorded in both solid and solution state exhibit stretches that could only be assigned to monodentate OAc ligands; little evidence for the chelating mode could be observed. The IR spectra for both **4** and **5** in DCM are included for comparison in Figure 3.4.2. This contrasts with the crystallographically determined structure, which shows that complex **5** contains acetate ligands in both coordination modes. The crystals of **5** were obtained by the slow diffusion of pentane into a DCM solution of the complex. An ORTEP representation is shown in Figure 3.4.3 and a table of selected bond lengths and angles is included in Table 3.4.1.

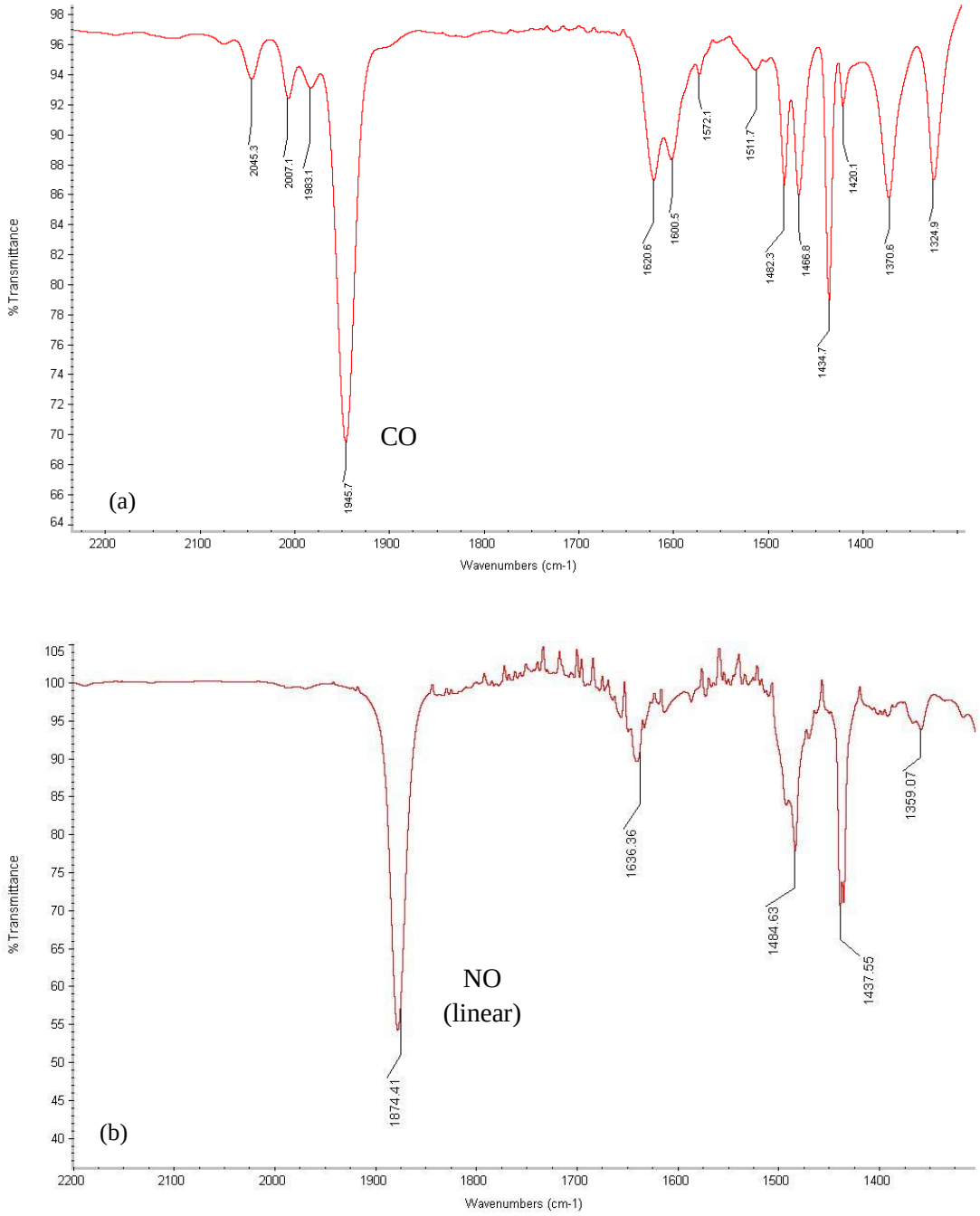

Figure 3.4.2: (a) IR spectra of **4** in DCM, (b) IR spectra of **5** in DCM.

The additional trace peaks in the 'CO region' of the IR spectrum of complex **4** can be assigned to two di-carbonyl species $[Ru(\kappa^1\text{-}OAc)_2(CO)_2(PPh_3)_2]$ (υ_{CO} = 2045 and 1983 cm^{-1}) and $[Ru(\kappa^2\text{-}OAc)(CO)_2(PPh_3)_2]OAc$ (υ_{CO} = approx. 2070 and 2007 cm^{-1}) that form upon prolonged exposure to CO. Evidence for the formation of these complexes was discovered by Mr Nicholas Hiett and experimental detail may be found in the appropriate publication.[39]

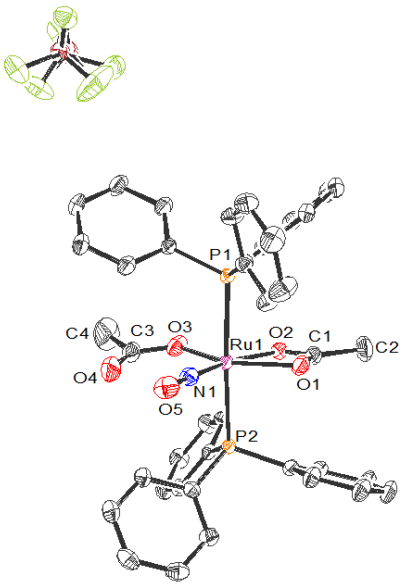

Figure 3.4.3: ORTEP diagram of **5**, thermal ellipsoids, where shown, at the 50 % probability level. Hydrogen atoms and two molecules of DCM of crystallization removed omitted for clarity.

Bond Length	**(Å)**	**Bond Angle**	**(deg / °)**
Ru – P(1)	2.4336(8)	P(1) – Ru – P(2)	176.05(2)
Ru – P(2)	2.4466(8)	P(1) – Ru – O(1)	86.79(6)
Ru – O(1)	2.1336(19)	P(1) – Ru – O(2)	90.64(5)
Ru – O(2)	2.0744(19)	P(1) – Ru – O(3)	88.08(6)
Ru – O(3)	1.9966(19)	P(1) – Ru – N(1)	91.36(7)
Ru – N(1)	1.739(2)	P(2) – Ru – N(1)	92.50(7)
N(1) – O(5)	1.137(3)	O(1) – Ru – O(2)	61.55(8)
		O(1) – Ru – O(3)	150.64(9)
		O(2) – Ru – O(3)	89.64(8)
		O(1) – Ru – N(1)	106.75(9)
		O(2) – Ru – N(1)	168.00(9)
		O(3) – Ru – N(1)	102.25(10)
		Ru – N(1)– O(5)	176.5(2)

Table 3.4.1: Selected Bond Lengths and Angles for **5**.

The structural characterisation revealed that the NO ligand is linear in the solid state, but in contrast to the IR spectrum recorded in both DCM and KBr media, both κ^1- and κ^2-coordination modes are present. The angle of the Ru – N(1) – O(5) group is very close to 180 ° at 176.5(2) °, implying that the NO ligand is acting as an isoelectronic analogue of CO. A survey of crystallographically characterised structures in the CSD containing linear NO ligands has reported that the average bond length for the N – O ligand is 1.176 Å and the average Ru – N distance is 1.743 Å.[29] For complex **5** a length of 1.137 Å is observed for N(1) – O(5), and 1.739(2) Å for Ru – N(1). Both values are fairly close to the averages reported. It should also be noted that the Ru – O(2) distance is the shortest reported for the ruthenium-acetate complexes in this thesis, a feature ascribed to the strong *trans*-influence of the NO ligand. Peter Legzdins[28] has surveyed a number of six-coordinate mononitrosyl complexes and has concluded that "…the *trans* M–L bonds appear to be "long and weak" when the υ_{NO} of the complexes are less than 1800 cm^{-1}. On the other hand, these *trans* M–L bonds appear to be "short and strong" when the υ_{NO} of the complexes are greater than *ca.* 1800 cm^{-1}." As complex **5** exhibits a υ_{NO} of 1878 cm^{-1}, it is unsurprising to observe that the Ru – O(2) distance is short (see also Chapter 8).

Both complexes **4** and **5** are easily prepared ruthenium precursors that have their OAc and PPh_3 ligands arranged in the same orientation as in the vinylidene derivatives of complex **1**. The use of these compounds as a convenient starting material for the preparation of acetylide complexes was subsequently investigated.

3.5: Successful syntheses of acetylides

Initial attempts detailed in Section 3.2 to synthesise an acetylide complex *via* the typical route of deprotonating a vinylidene ligand met with little success. Consequently, alternative precursors were sought, and found, in the forms of the readily prepared complexes **4** and **5**.

3.5.1: Synthesis of [Ru(C≡CPh)(κ^2-OAc)(CO)(PPh$_3$)$_2$]

It was initially proposed that addition of HC≡CPh to **4** would result in the formation of a vinylidene complex similar to **2a** where both OAc ligands are coordinated in a κ^1-mode and the remaining coordination site is occupied by the CO ligand. It was hoped that attempts to deprotonate the vinylidene ligand of such a complex may prove more successful. However, the addition of 1.4 equivalents of HC≡CPh to a solution of **4** in CD_2Cl_2 resulted in the extremely slow evolution of CH_3COOH and a new PPh_3-containing complex, **6**. The reaction was monitored by ^1H and $^{31}P\{^1H\}$ NMR spectroscopy for 8 days at room temperature, and from the observations made, the reaction scheme shown in Figure 3.5.1.1 proposed. It is suggested that the new complex **6** forms over the course of several days, and contains a single OAc ligand, a CO ligand and acetylide ligand in addition to two mutually *trans* PPh_3 ligands. Over the course of this time, the appearance and disappearance of CH_3COOH is also observed, along with the ultimate formation of another organic compound (*Z*)-*β*-styryl acetate. However, this reaction did not go to completion, as residual **4** remains even after 8 days.

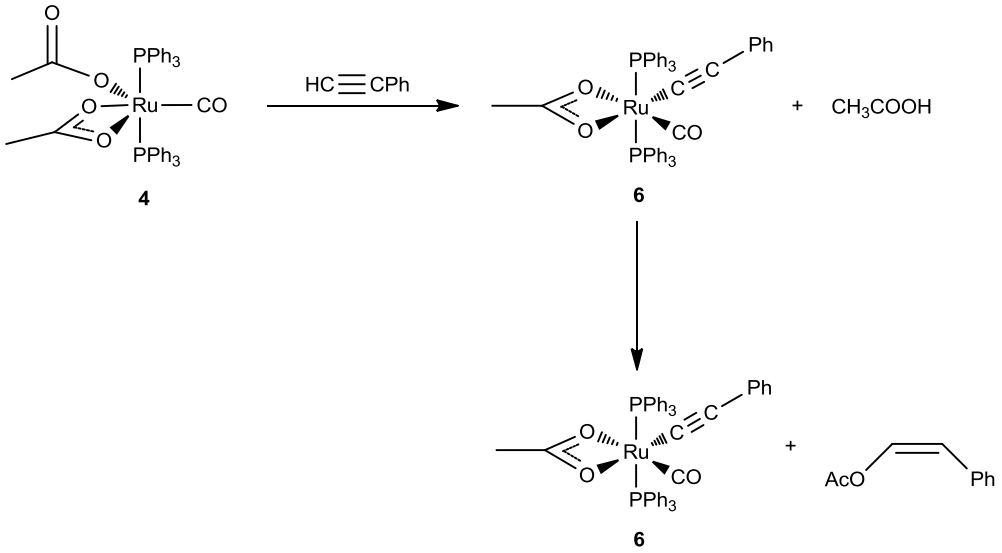

Figure 3.5.1.1: Reaction of HC≡CPh with **4**

The $^{31}P\{^{1}H\}$ NMR spectra recorded over this time showed that the concentration of the new complex **6** (δ_P 38.6) gradually increases whilst that of **4** (δ_P 39.1) decreases, but does not disappear entirely. The ^{1}H NMR spectrum shows that a new singlet peak associated with the CH_3 resonances of an OAc ligand (δ_H 0.61) grows in at a comparable rate with new resonances associated with a Ph group. It was also noted that the resonance associated with CH_3COOH (δ_H 2.09)[29] begins to diminish after 2 days, whilst simultaneously another resonance attributed to the CH_3 of (*Z*)-*β*-styryl acetate grows in (δ_H 2.30). One of the alkene protons of this species is observed at δ_H 5.76 as a doublet resonance ($^{3}J_{HH}$ = 7.3 Hz), whilst the other is presumably obscured by other phenyl resonances. The identity of (*Z*)-*β*-styryl acetate was further confirmed by comparison with literature data.[30] Comparison of the integrations of peaks attributed to (*Z*)-*β*-styryl acetate and the OAc ligand after 8 days revealed that the two are present in equal concentration. This implies that of the two OAc ligands present in **4**, one has become associated with **6** whilst the other is associated with the organic by-product (*Z*)-*β*-styryl acetate.

This reaction was repeated using 1.7 equivalents $H^{13}C{\equiv}CPh$, which provided further evidence to support the formation of a complex with the structure of **6**. In the $^{31}P\{^{1}H\}$ NMR spectrum, the resonance for complex **6** now appeared as a doublet due to additional coupling to the ^{13}C-label (δ_P 38.6, d, $^{2}J_{CP}$ = 16.4 Hz), whilst the $^{13}C\{^{1}H\}$ NMR spectrum showed a corresponding triplet resonance for $^{13}C_\alpha$ at δ_C 107.7 ($^{2}J_{CP}$ = 16.3 Hz). The proposed mechanism for this process is shown in Figure 3.5.1.2 below:

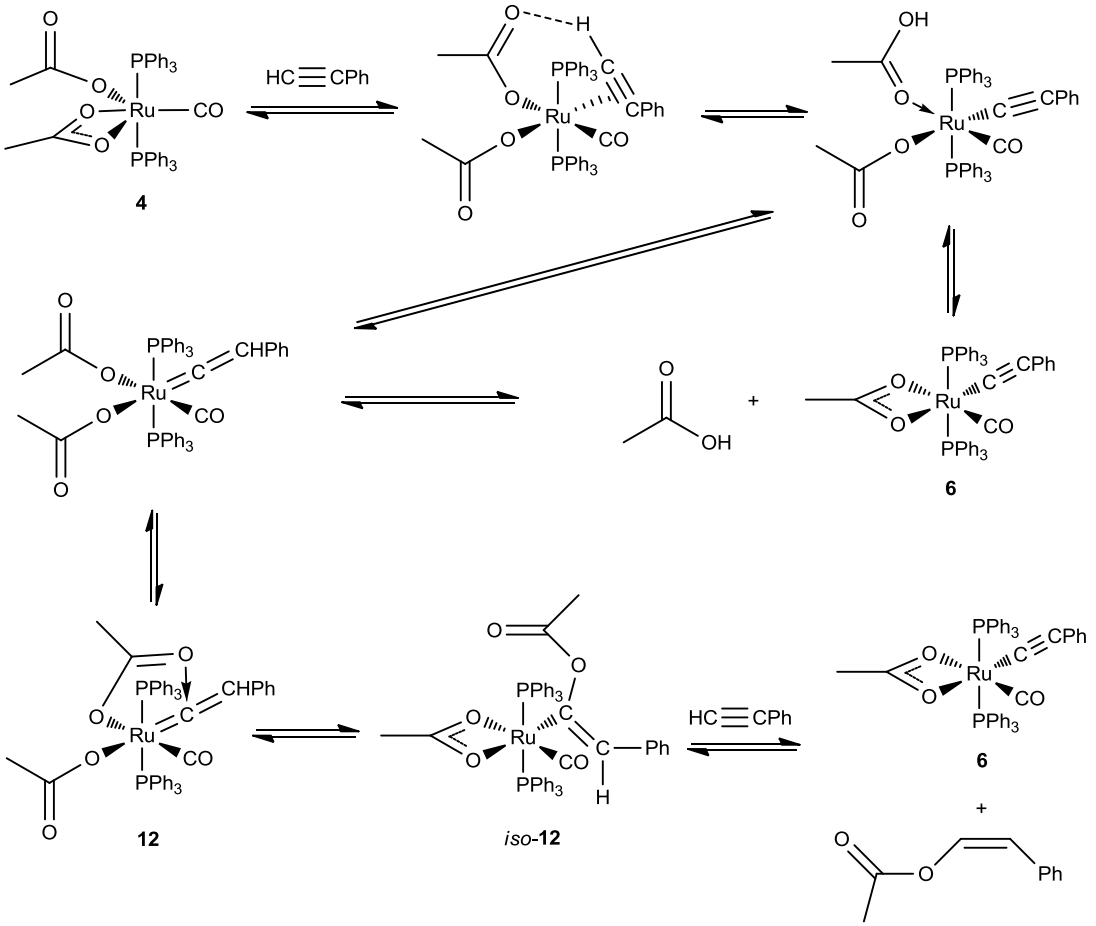

Figure 3.5.1.2: Proposed mechanism for the reaction of **4** with two HC≡CPh.

It is proposed that the fluxional nature of the OAc ligands allows for the initial coordination of HC≡CPh in an η^2-fashion. One of the κ^1-OAc ligands is then able to deprotonate the alkyne to give an acetylide ligand, before the protonated OAc ligand dissociates as CH_3COOH to generate **6**. However, the CH_3COOH is also able to re-protonate the acetylide at the nucleophilic C_β to give a vinylidene. Alternatively, the coordinated acetic acid molecule may re-protonate the acetylide in an intramolecular fashion to generate the vinylidene complex. This is followed by nucleophilic attack of the uncoordinated O-atom of a κ^1-OAc ligand onto the C_α of the vinylidene to give complex **12**. Another molecule of HC≡CPh is then able to protonate the coordinated (*Z*)-*β*-styryl acetate to regenerate **6**. Further experimental and computational evidence for this mechanism, with particular regard to the presence of complex **12** will be discussed in more detail in Section 4.4.

According to the proposed mechanism, two equivalents of HC≡CPh are required for the reaction to go to completion. In light of this, and considering the reaction takes several days to reach partial completion at room temperature, attempts were made to improve the synthesis of **6**. One such attempt involved the addition of DBU to a mixture of **4** and $H^{13}C{\equiv}CPh$ so as to avoid the accumulation of CH_3COOH and disfavour the secondary reaction. However, this resulted in some unwanted side-reactions giving a mixture of unidentified products. The optimised conditions were found to involve addition of two equivalents of HC≡CPh to a DCM solution of **4** that was then heated at 50 °C for 48 hours. Upon cooling, the solvent was evaporated and the residue washed with pentane to remove the organic by-product to leave a yellow-green residue. The product was purified further by the slow diffusion of pentane into a DCM solution of this residue to afford yellow crystals of **6**. Using this method, a crystal suitable for study by X-Ray diffraction was grown. An ORTEP representation of the complex is shown in Figure 3.5.1.3.

The IR spectrum of **6** recorded in DCM solution shows a band at 2105 cm^{-1} assigned to the C≡C stretch, and one at 1947 cm^{-1} assigned to υ_{CO}. When monitoring the progress of the reaction by IR spectroscopy, it became apparent that the υ_{CO} stretches of complexes **4** and **6** are coincident. The IR spectrum also shows that the dominant species contains an κ^2-OAc ligand; the symmetric stretch was observed at 1463 cm^{-1} whilst the asymmetric was observed at 1521 cm^{-1} ($\Delta\nu_{(chelate)}$ 58 cm^{-1}).

Attempts were also made to adapt this synthesis to HC≡C^{t}Bu, however these met with little success. A reaction between **4** and two equivalents HC≡C^{t}Bu was performed on an NMR scale. Analysis by $^{31}P\{^1H\}$ NMR spectroscopy showed that in addition to what may be the acetylide-containing product (δ_P 37.8) an additional $^{31}PPh_3$-containing complex (δ_P 36.7) also formed, which may be related to complex **12**. The persistent nature of this impurity meant that the acetylide complex could not be isolated.

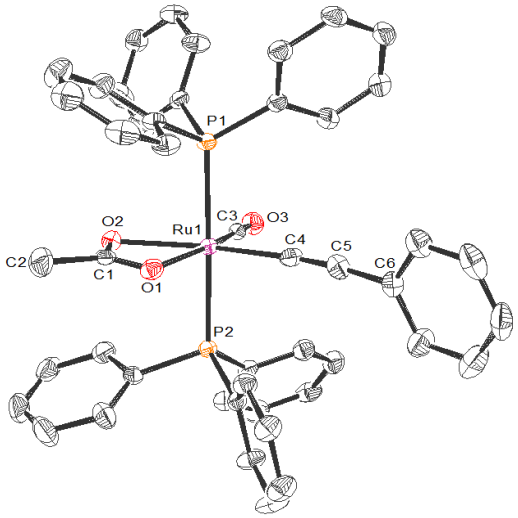

Figure 3.5.1.3: ORTEP diagram of **6**, thermal ellipsoids, where shown, at the 50 % probability level. Hydrogen atoms omitted for clarity.

Bond Length	**(Å)**	**Bond Angle**	**(deg / °)**
Ru – P(1)	2.3839(7)	P(1) – Ru – P(2)	178.15(3)
Ru – P(2)	2.3677(7)	P(1) – Ru – O(1)	93.14(5)
Ru – O(1)	2.1829(18)	P(1) – Ru – O(2)	86.30(5)
Ru – O(2)	2.1959(18)	P(1) – Ru – C(3)	89.79(8)
Ru – C(3)	1.824(3)	P(1) – Ru – C(4)	93.16(8)
Ru – C(4)	2.002(3)	P(2) – Ru – C(3)	91.82(8)
C(3) – O(3)	1.138(3)	P(2) – Ru – C(4)	87.69(8)
C(4) – C(5)	1.200(4)	O(1) – Ru – O(2)	59.91(7)
C(5) – C(6)	1.444(4)	O(1) – Ru – C(3)	166.69(9)
		O(1) – Ru – C(4)	100.37(10)
		O(2) – Ru – C(4)	160.16(10)
		C(3) – Ru – C(4)	92.42(12)
		C(3) – Ru – O(2)	107.40(9)
		Ru – C(3) – O(3)	178.3(2)
		Ru – C(4) – C(5)	170.7(3)
		C(4) – C(5) – C(6)	173.0(3)

Table 3.5.1.1: Selected Bond Lengths and Angles for **6**.

By virtue of the presence of a κ^2-OAc ligand, the structure obtained is again one of a distorted octahedron. The O(1) – Ru – O(2) of the κ^2-OAc ligand is constrained to 59.91(7) °, which leads to the bond angles of C(3) – Ru – O(2) and O(1) – Ru – C(4) being > 90 ° at 107.40(9) ° and 100.37(10) ° respectively. The majority of angles between the acetate, acetylide and CO ligands and the phosphine ligands are close to 90 °. The angle of the CO ligand to the metal is once more close to linear at 178.3(2) ° whilst the Ru – C(3) and C(3) – O(3) bond lengths are close to the averages at 1.824(3) Å and 1.138(3) Å respectively. For the acetylide ligand, the average C≡C distance reported is approximately 1.201(13) Å[32] and the distance obtained for C(4) – C(5) is close to this at 1.200(4). The Ru – C(4) observed (2.002(3) Å) is similar to those observed for the acetylide complexes [RuCp(C≡CPh)(PPh_3)$_2$] at 2.016(3) Å[33] and [RuCp(C≡CPh)(dppe)] at 2.009(3) Å.[34] A significant feature of this complex resides in the angle of the acetylide moiety of 170.7(3) °. This is an unexpected deviation from the expected 180 ° and it is proposed that this results from the effects of crystal packing, rather than from any intrinsic property of the molecule. Figure 3.5.1.4 shows the packing environment around the phenyl ring of the acetylide ligand, it seems to 'sit' in a pocket created by the positioning of two neighbouring molecules.

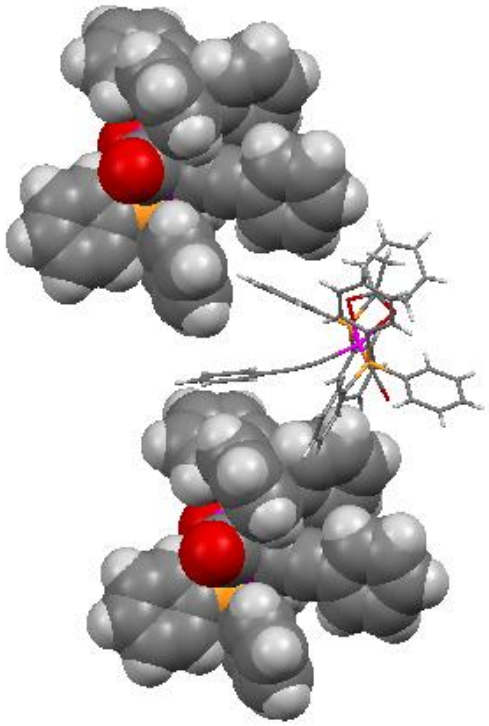

Figure 3.5.1.4: Illustration of the packing environment of the acetylide ligand of **6**.

Complex **6** has been previously synthesised, though not structurally characterised, by another research group led by Echavarren and Santos.[35] Their procedure involves a ligand exchange reaction from $[Ru(C{\equiv}CPh)(CO)(PPh_3)_2(Py)_2]PF_6$ with NaOAc to give **6**. The spectroscopic features reported by Echavarren and Santos compare favourably with those obtained for our preparation of complex **6**. For example, they report a C≡C stretch at 2100 cm^{-1} in the IR spectrum recorded as KBr discs, whereas we observed it at 2101 cm^{-1}.

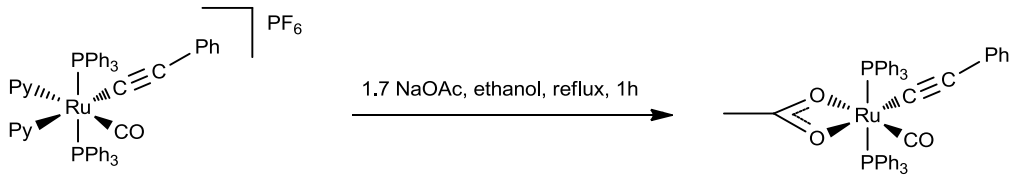

Figure 3.5.1.5: Synthesis of **6** by ligand exchange from $[Ru(PPh_3)_2(CO)(Py)_2(C{\equiv}CPh)]PF_6$.

The overall synthetic procedure used to produce **6** in this way rather than *via* **1** requires an additional step. In our procedure, the OAc ligands are pre-coordinated and thought to play a significant active role in the formation of the acetylide. However, Echavarren *et. al.* have also demonstrated that the synthesis of their precursor $[Ru(C{\equiv}CPh)(CO)(PPh_3)_2(Py)_2]PF_6$ requires two molecules of HC≡CPh, and produces a terminal alkene, in this case styrene, as a by-product.[36,37] This appears to mirror in part the synthesis of **6** from **4**, although in no instance was the formation of styrene observed in the reaction of **4** with HC≡CPh when it was monitored by NMR spectroscopy. Their proposed mechanism is shown in Figure 3.5.1.6 below. The initial insertion of HC≡CPh into the Ru-H bond of $[Ru(H)(CO)(PPh_3)_2(Py)_2]PF_6$, and the simultaneous dissociation of a Py ligand results in the formation of a 16-electron intermediate (**3C**). This is then able to undergo addition of another molecule of HC≡CPh which coordinates in a η^2-fashion before undergoing an oxidative addition to give the hydride complex. The final step involves reductive elimination to generate styrene and the acetylide complex $[Ru(C{\equiv}CPh)(CO)(PPh_3)_2(Py)_2]PF_6$.

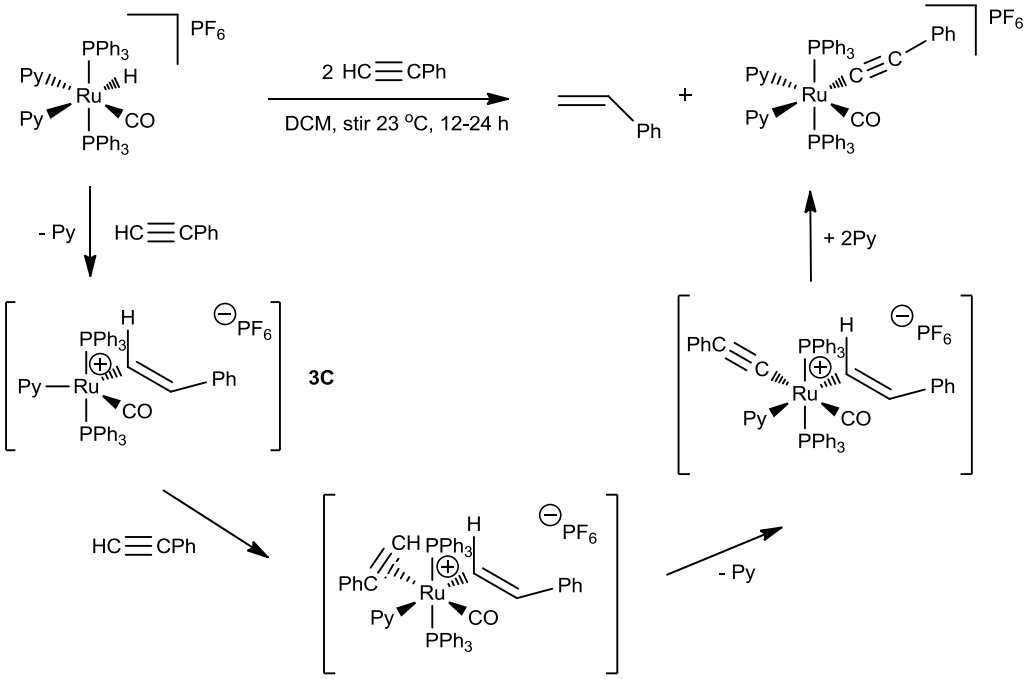

Figure 3.5.1.6: Synthesis of $[Ru(C{\equiv}CPh)(CO)(PPh_3)_2(Py)_2]PF_6$.

Echavarren's procedure for acetylide formation is notably milder than our method; the reaction occurs at room temperature within 16 hours whereas our method requires heating at reflux for 2 days to reach completion. It is also noted that no reaction occurs when hydride complexes bearing chelating ligands, such as $[Ru(H)(CO)(bpy)(PPh_3)_2]ClO_4$ and $[Ru(H)(CO)(phen)(PPh_3)_2]ClO_4$ are used, even when forcing conditions are employed. Furthermore, attempts by Echavarren to react complex **6** with alkynes in 1,2-dichloroethane under reflux conditions resulted in the recovery of the complex unchanged.[35]

3.5.2: Synthesis of $[Ru(C{\equiv}CPh)(\kappa^2\text{-}OAc)(NO)(PPh_3)_2]BF_4$

In order to further test the scope of our procedure for synthesising acetylide derivatives of complex **1**, it was applied to complex **5**. Under similar conditions (two equivalents of HC≡CPh and heating at 50 °C were again necessary however purification of the product required toluene in the place of pentane), the corresponding acetylide complex (**7**) was obtained. It is important to note however, that whilst complex **4** can be generated and used *in situ* by reaction of $CO_{(g)}$ with **1**, complex **5** must be isolated and purified prior to use owing to the presence of a number of impurities in the crude product mixture (including *cis*-**5**).

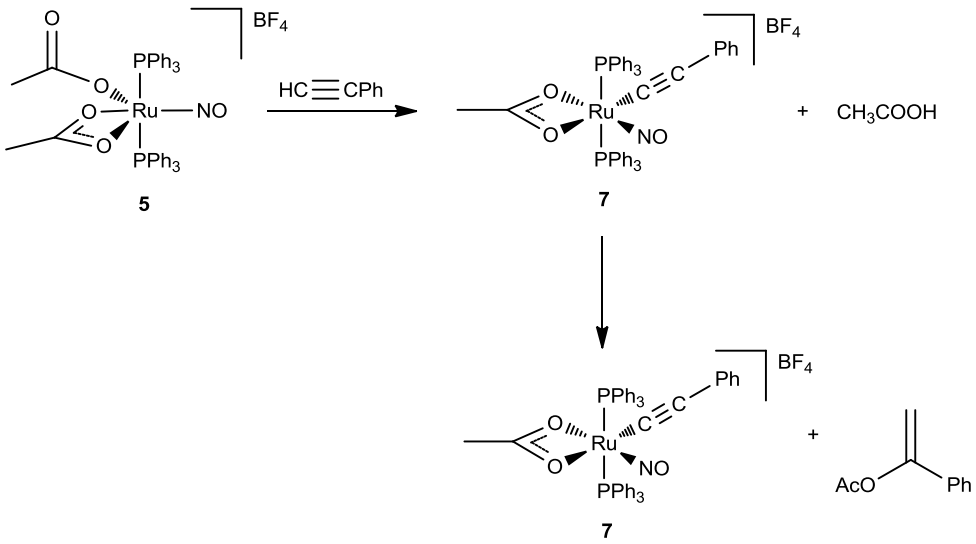

Figure 3.5.2.1: Reaction of HC≡CPh with **5**.

The IR spectrum of complex **7** in DCM indicates that the NO ligand is in a linear orientation due to presence of a sharp band at 1866 cm^{-1}. However, the corresponding stretch in the KBr IR spectrum is at 1880 cm^{-1}, but with a shoulder at 1860 cm^{-1}. Ambiguity also exists in determining the coordination mode of the OAc ligand as stretches for both κ^1- and κ^2-OAc ligands are observed in both solution and solid state IR. A relatively weak peak for the C≡C moiety is observed at 2122 cm^{-1} (KBr) and 2123 cm^{-1} (DCM). Difficulties were also encountered in the analysis of the IR spectra of **5**. The ^1H NMR spectrum of compound **7** contains similar features to those observed for **6**, and the $^{31}P\{^1H\}$ NMR spectrum displays a singlet resonance at δ_P 32.8. In the $^{13}C\{^1H\}$ NMR spectrum, the resonance for the acetylide C_α is observed at δ_C 99.2 ($^2J_{CP}$ = 15.4 Hz) whilst C_β is observed as a singlet at δ_C 102.0. The ESI MS displays a m/z peak at 816.14 ($[M]^+$ - loss of BF_4) that displays the appropriate isotope splitting pattern for Ru.

The reaction of **5** with 1.6 equivalents $H^{13}C{\equiv}CPh$ in CD_2Cl_2 was also conducted, and monitored by ^1H, $^{31}P\{^1H\}$ and $^{13}C\{^1H\}$ NMR spectroscopy. The expected additional coupling was observed in the $^{31}P\{^1H\}$ NMR, the resonance at δ_P 32.8 becoming a doublet ($^2J_{CP}$ = 15.2 Hz). This experiment also showed that acetic acid is evolved during the course of the reaction, in addition to an organic by-product. However, as this reaction involved the use of **5** generated *in situ*, the reaction mixture contains a number of other impurities. It has already been noted that the synthesis of **5** requires an additional purification step owing to the formation of

impurities, which were not observed for **4**. Crystals were grown by the slow diffusion of pentane into a solution of **7** in DCM, however they were not of sufficient quality for a good diffraction pattern to be obtained.

Interestingly, the organic by-product from the reaction of **5** with HC≡CPh was not (*Z*)-*β*-styryl acetate, but its geminal isomer 1-phenylvinyl acetate. This was evidenced by the presence of two doublet resonances at δ_H 5.05 and 5.52 with a mutual $^2J_{HH}$ coupling of 2.2 Hz. These protons integrate to one each respective to the three acetate protons observed as a singlet at δ_H 2.30. Further confirmation of the identity of this compound was provided by comparison with literature data.[38] Consequently, the mechanism proposed in Figure 3.5.1.2 for the formation of **6** and (*Z*)-*β*-styryl acetate does not stand for the formation of **7**. Instead, an alternative has been proposed in Figure 3.5.2.2.

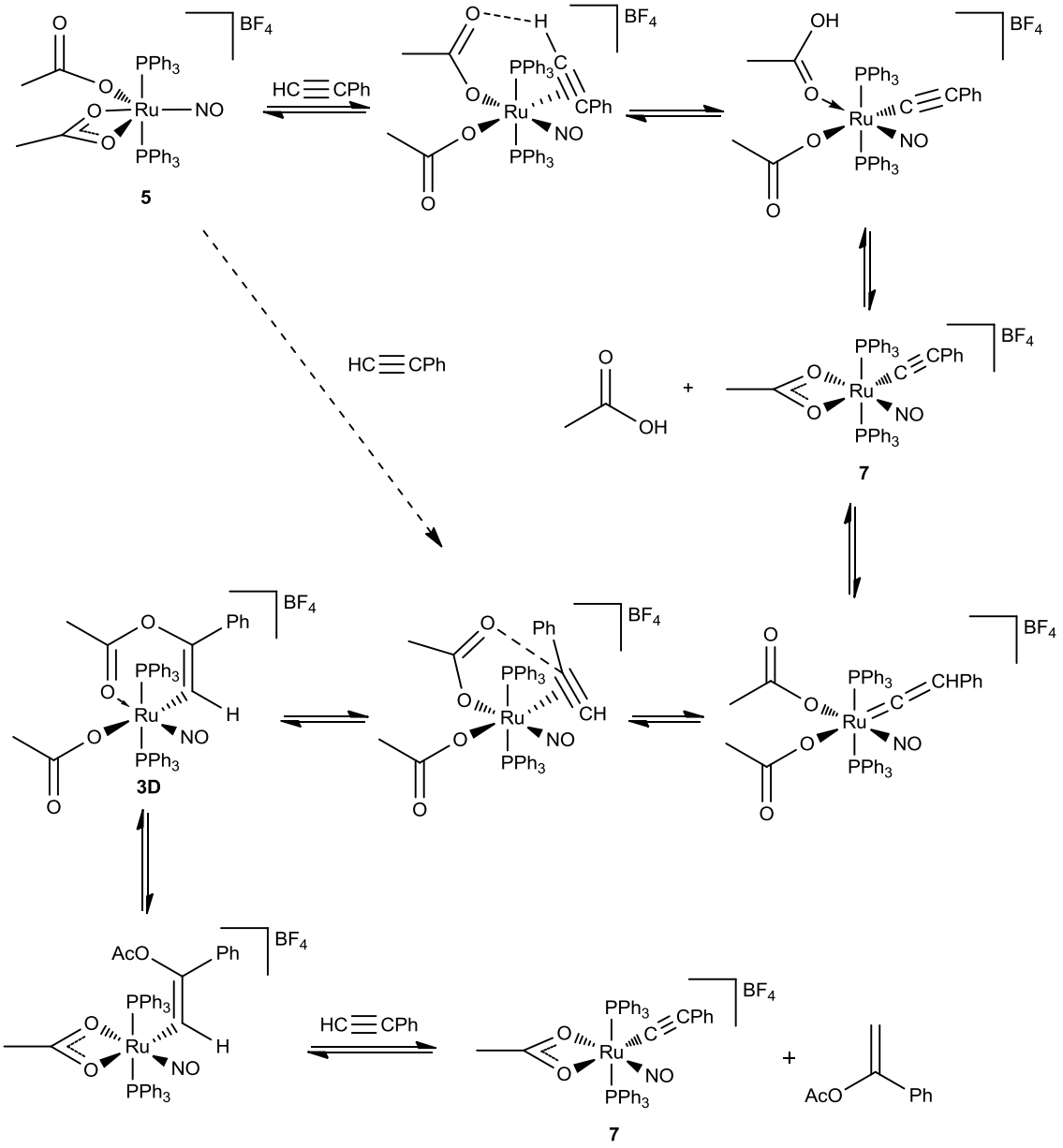

Figure 3.5.2.2: Proposed mechanism for the reaction of **5** with HC≡CPh.

The reaction of **5** with 1.6 equivalents $H^{13}C{\equiv}CPh$ in CD_2Cl_2 shows that complex **7** and CH_3COOH begin to form immediately after addition of the alkyne, as per the reaction of **4** with HC≡CPh. After one day, trace amounts of $H_2C{=}C(OAc)(Ph)$ can be observed in the ^1H NMR spectrum. Consequently, it is proposed that the first stage of the reaction proceeds as for **4**. Upon formation of **7** and CH_3COOH, it is proposed that the acid reprotonates the acetylide ligand to give a vinylidene complex, which exists in an equilibrium with the η^2-alkyne isomer. Computational evidence has been discovered for the formation of a complex analogous to **3D** (as

shown in Figure 3.5.2.2), which may account for the formation of the geminal isomer of styryl acetate (see Section 4.6). This compound is liberated from the complex by the addition of another equivalent of HC≡CPh to regenerate **7**. It is conceivable that **7** and 1-phenylvinyl acetate form *via* the shorter pathway indicated by the dashed arrow, which bypasses the evolution of acetic acid. This appears to conflict with the NMR evidence whereby the formation of CH_3COOH is observed prior to the formation of 1-phenylvinyl acetate, however the possibility that the two pathways proceed at very different rates cannot be dismissed. As for the proposed mechanism for the formation of **6**, this will be discussed in more detail in Chapter 4.

Two acetylide complexes **6** and **7** have been successfully synthesised from precursors **4** and **5** respectively that both derive from the parent complex **1**. It is proposed that the acetate ligands play an essential role in the synthesis of the acetylide ligands, a role that will be explored in more detail in the following chapter.

3.6: Conclusions

This chapter has described attempts to form acetylide complexes derived from complex **1**. It has been shown that methods typically employed to generate an acetylide, such as deprotonation of a suitable vinylidene precursor complex were largely unsuccessful. Despite the use of a variety of commonly employed bases, the deprotonation of **2a** and **2c** did not proceed smoothly, and mixtures of components were generally obtained. Amongst these components however, was evidence for a novel TMS-substituted acetylide **3**, which also contained three PPh_3 ligands and one acetate ligand coordinated to the ruthenium centre. These compounds could not be synthesised pure, however the structure of **3** was successfully determined by X-Ray crystallography. This is an example of when the deprotonation of a neutral vinylidene species is more difficult than that of a charged one.[10,11]

Consequently, alternative precursors were sought, and found, in the form of **4** and **5**. Complex **4** has been reported previously by the groups of Robinson and Wilkinson, however debate existed surrounding the orientation of ligands in its coordination sphere. It has been shown that when **4** is prepared by Wilkinson's or our modified procedure *via* the addition of CO to **1**, the product with mutually *trans* PPh_3 ligands is obtained. Robinson's alternative route involved the boiling of $[RuH_2(CO)(PPh_3)_3]$ with the appropriate acid at 125 °C in 2-methoxyethanol. This produced the thermodynamic product, in which the two PPh_3 ligands are *cis*. The analogous complex **5**, containing the fluxional NO ligand, is obtained by a similar addition of $NOBF_4$ to **1**.

The synthesis of **4** and **5** mirrors the synthesis of the vinylidene complexes **2a-d**, whereby the additional ligand is introduced to a solution of **1** in DCM, and a rapid rearrangement of the coordination sphere occurs. The resulting complex contains two mutually *trans* PPh_3 ligands, and the remaining ligands occupy the other octahedral coordination sites. The two acetate ligands of **4** and **5** undergo rapid exchange in solution, as evidenced by variable temperature NMR studies, in a similar fashion to the vinylidene complexes **2a-d**.

Complexes **4** and **5** were used to successfully obtain acetylide complexes **6** and **7** respectively, which have been successfully isolated and characterised fully. The synthesis requires addition of two equivalents of HC≡CPh and also produces an

organic by-product. The two different precursors **4** and **5** give rise to two different isomers of the same compounds, (*Z*)-*β*-styryl acetate and 1-phenylvinyl acetate respectively. The reason for this change in selectivity is currently unclear, and further studies are required to better understand this reactivity.

The mechanisms suggested for the formation of complexes **6** and **7** also mirror those of the vinylidene complexes **2a-d**, in that it appears that the non-innocent acetate ligands are essential to the formation of the products. The involvement of an acetate ligand is also hinted at by the evidence surrounding the formation of the styryl acetate product. In order to deconvolute the behaviour of the acetate ligands in these acetylide and vinylidene complexes, a series of combined computational and experimental investigations has been undertaken. These experiments will be described in the following chapter.

3.7 References

1. Yam, V. W. W. *Acc. Chem. Res.* **2002**, *35*, 555.
2. Long, N. J.; Williams, C. K. *Angew. Chem. Int. Ed.* **2003**, *42*, 2586.
3. Szafert, S.; Gladsyz, J. A. *Chem. Rev.* **2003**, *103*, 4175.
4. Yam, V. W. W. *J. Organomet. Chem.* **2004**, *689*, 1393.
5. D'Alessandro, D. M; Keene, F. R. *Chem. Rev*. **2006**, *106*, 2270.
6. Aguire-Etcheverry, P.; O'Hare, D. *Chem. Rev.* **2010**, *110*, 4839.
7. Hartwig, J. F. *Organotransition Metal Chemistry: From Bonding to Catalysis*, **2010**, University Science Books.
8. Manna, J.; John, K. D.; Hopkins, M. D. *Adv. Organomet. Chem.* **1995**, *38*, 79.
9. Chinchilla, R.; Nájera, C. *Chem. Rev.* **2007**, *107*, 874.
10. Bruce, M. I.; Wallis, R. C. *J. Organomet. Chem.* **1978**, *161*, C1.
11. Bruce, M. I.; Wallis, R. C. *Aust. J. Chem*. **1979**, *32*, 1471.
12. Bullock, R. M. *J. Chem. Soc. Chem. Commun.* **1989**, 165.
13. Touchard, D.; Hacquette, P.; Pirio, N.; Toupet, L.; Dixneuf, P. H.; *Organometallics* **1993**, *12*, 3132.
14. Hacquette, P.; Pirio, N.; Touchard, D.; Toupet, L.; Dixneuf, P. H. *J. Chem. Soc. Chem. Commun.* **1993**, 163.
15. Faulkner, C. W.; Ingham, S. L.; Khan, M. S.; Lewis, J.; Long, N. J.; Raithby, P. R. *J. Organomet. Chem*. **1994**, *482*, 139.
16. Touchard, D.; Marice, C.; Cadierno, V.; Hacquette, P.; Toupet, L.; Dixneuf, P. H. *J. Chem. Soc. Chem. Commun.* **1994**, 859.
17. Martín, M.; Gevert, O.; Werner, H.; *J. Chem. Soc. Dalton. Trans.* **1996**, 2275.

18. Touchard, D.; Hacquette, P.; Guesmi, S.; Le Pichon, L.; Doridor, A.; Toupet, L.; Dixneuf, P. H.; *Organometallics* **1997**, *16*, 3640.

19. Olivier, C.; Kim, B.; Touchard, D.; Rigaut, S., *Organometallics* **2008**, *27*, 509.

20. Experimental information is provided in Thomas Eschermann's Erasmus report.

21. Spencer, A.; Wilkinson, G. *J. Chem. Soc. Dalton. Trans*. **1974**, 786.

22. Lynam, J. M.; Welby, C. E.; Whitwood, A. C. *Organometallics* **2009**, *28*, 1320.

23. Hocking, R. K.; Hambley, T. W. *Organometallics* **2007**, 26, 2815.

24. Robinson, S. D.; Uttley, M. F. *J. Chem. Soc. Chem. Commun*. **1972**, 1047.

25. Robinson, S. D.; Uttley, M. F. *J. Chem. Soc. Dalton. Trans*. **1973**, 1912.

26. Dobson, A.; Robinson, S. D.; Uttley, M. F.; *J. Chem. Soc. Dalton. Trans*. **1975**, 370.

27. Creswell, C. J.; Dobson, A.; Moore, D. S. Robinson, S. D. *Inorg. Chem.* **1979**, *18*, 2055.

28. Richter-Addo, G. B.; Legzdins, P. *Metal Nitrosyls*, **1992**, Oxford University Press.

29. Orpen, A. G.; Brammer, L.; Allen, F. H.; Kennard, O.; Watson, D. G.; Taylor, R. *J. Chem. Soc. Dalton Trans.* **1989**, S1.

30. Literature data for ^{1}H NMR CH_3COOH (authentic sample in CD_2Cl_2).

31. Doucet, H.; Martin-Vaca, B.; Bruneau, C.; Dixneuf, P. H. *J. Org. Chem.* **1995**, *60*, 7247.

32. Manna, J.; John, K. D.; Hopkins, M. D. *Adv. Organomet. Chem.* **1995**, *38*, 79.

33. Wisner, J. M.; Bartczak, T. J.; Ibers, J. A. *Inorg. Chim. Acta.* **1985**, *100*, 115.

34. Bruce, M. I.; Hinterding, P.; Tiekink, E. R. T.; Skelton, B. W.; White, A. H. *J. Organomet. Chem.* **1993**, *450*, 209.

35. Santos, A.; López, J.; Matas, L.; Ros, J.; Galán, A.; Echavarren, A. M. *Organometallics* **1993**, *12*, 4215.

36. Echavarren, A. M.; López, J.; Santos, A.; Romero, A.; Hermoso, J. A.; Vegas, A.; *Organometallics* **1991**, *10*, 2371.

37. Romero, A.; Vegas, A.; Santos, A.; Martinez-Ripoll, M. *J. Organomet. Chem.* **1987**, *319*, 103.

38. Panella, L; Feringa, B. L; de Vries, J. G; Minaard, A. J; *Org. Lett*. **2005**, *7*, 4177.

39. Hiett, N. P.; Lynam, J. M.; Welby, C. E.; Whitwood, A. C. *J. Organomet. Chem.* **2011**, *696*, 378.

3.8 Experimental

General:

All experimental procedures were performed under an atmosphere of dinitrogen or argon using standard Schlenk Line and Glove Box techniques. DCM, pentane, hexane and toluene were purified with the aid of an Innovative Technologies anhydrous solvent engineering system. MeOH was dried over a combination of Mg/I_2 and then distilled under N_2. THF was distilled under N_2 from Na/benzophenone. The CD_2Cl_2 used for NMR experiments was dried over CaH_2 and degassed with three freeze-pump-thaw cycles. The solvent was then vacuum transferred into NMR tubes fitted with PTFE Young's taps. NMR spectra were acquired on a Bruker AVANCE 500 (Operating Frequencies ^{1}H 500.23 MHz, ^{31}P 202.50 MHz, ^{13}C 125.77 MHz). ^{31}P and ^{13}C spectra were recorded with proton decoupling. Mass spectrometry measurements were performed on a Thermo-Electron Corp LCQ Classic (ESI) instrument. IR spectra were acquired on a Thermo-Nicolet Avatar 370 FTIR spectrometer using either CsCl solution cells or as KBr discs. CHN measurements were performed using an Exeter Analytical Inc. CE-440 analyser. The proportion of DCM in CHN samples was confirmed by recording a ^{1}H NMR spectrum of a sample used for CHN analysis in d_8-toluene. Relative integration of the peak at δ_H 4.31 (CH_2Cl_2) to that of the vinylidene proton indicated the proportion of DCM in that sample. Structural characterisation of complexes **4**, **5** and **6** was conducted using a Bruker Smart Apex diffractomer with Mo K_α radiation (λ = 0.71073 Å) with a SMART CCD camera. Diffractometer control, data collection and initial unit cell determination was performed using SMART. Frame integration and unit-cell refinement software was carried out with Saint+. Absorption corrections were applied by SADABS (v 2.03, Sheldrick). Structures were solved by direct methods using SHELXS-97, and refined by full-matrix least-squares using SHELX-97. All non-hydrogen atoms were refined anisotropically. Hydrogen atoms were placed using a "riding model" and included in the refinement at calculated positions. Complex **1** was prepared by the published literature method.[22] $H^{13}C{\equiv}CPh$, $HC{\equiv}C^{t}Bu$, $NOBF_4$ (Sigma-Aldrich) and HC≡CPh, DBU (Acros Organics) were used as supplied without further purification. $Na[N(SiMe_3)_2]$ was synthesised by Dr. Charlotte Willans.

Key to NMR shorthand:

s (singlet); br s (broad singlet); d (doublet); dd (doublet of doublets); ad (apparent doublet); t (triplet); dt (doublet of triplets); tt (triplet of triplets); at (apparent triplet); q (quartet); aq (apparent quartet); qn (quintet), aqn (apparent quintet); sp (septet); asp (apparent septet); m (multiplet)

(H_2-Ph) or (H_2-PPh_3) refers to the proton in the *ortho*-position of a phenyl ring

(H_3-Ph) or (H_3-PPh_3) refers to the proton in the *meta*-position of a phenyl ring

(H_4-Ph) or (H_4-PPh_3) refers to the proton in the *para*-position of a phenyl ring

3.8.1: Reaction of 2a with Na[N(SiMe$_3$)$_2$]

One equivalent of Na[N(SiMe$_3$)$_2$] (7.00 mg, 35.5 μmol) was added to a solution of **2a** (30.0 mg, 35.5 μmol) in 15 mL THF and the mixture stirred for 15 minutes. After this time, the mixture had changed colour from pale orange to dark orange-red. The solvent was then removed *in vacuo* to leave a dark brown residue that was analysed by ^{1}H and ^{31}P NMR spectroscopy.

NMR Spectra CD_2Cl_2: ^{31}P (121.40 MHz) δ_P –6.11 (s, free *P*Ph$_3$), 26.7 (s, O=*P*Ph$_3$), 30.5 (s, (**3A**), PPh$_3$), 31.6 (d, $^2J_{PP}$ = 26.5 Hz, 2P, (**3B**), *P*Ph$_3$), 33.7 (s, **2a**, *P*Ph$_3$), 52.2 (t, $^2J_{PP}$ = 26.5 Hz, 1P, (**3B**), *P*Ph$_3$)

3.8.2: Synthesis of [Ru(κ^1-OAc)(κ^2-OAc)(CO)(PPh$_3$)$_2$], 4.

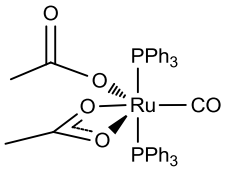

4

50 mg **1** (0.07 mmol) was suspended in 20 mL MeOH in a Schlenk tube equipped with a stirrer bar. The reaction mixture was then placed under an atmosphere of CO and stirred for 5 minutes. Over the course of this time the suspension changed colour from red to pale yellow. The product was isolated by filtration and washed with 10 mL MeOH and 10 mL Et_2O and dried *in vacuo*. Yield 20 mg, 38.4 %.

NMR Spectra CD_2Cl_2:

^{1}H δ_H 0.64 (s, 6H, C*H*$_3$COO), 7.35-7.49 (m, 30H, P*Ph*$_3$)

^{31}P{^{1}H} δ_P 39.1 (s, *P*Ph$_3$)

^{13}C{^{1}H} δ_C 29.1 (s, *C*H$_3$COO), 128.2 (t, $^3J_{PC}$+$^5J_{PC}$ = 9.7 Hz, PPh$_3$-*C*$_3$), 130.0 (t, $^1J_{PC}$+$^3J_{PC}$ = 43.0 Hz, PPh$_3$-*C*$_1$), 130.3 (s, PPh$_3$-*C*$_4$), 134.7 (t, $^2J_{PC}$+$^4J_{PC}$ = 11.8 Hz, PPh$_3$-*C*$_2$), 181.4 (s, CH$_3$*C*OO), 207.4 (t, $^2J_{PC}$ = 13.2 Hz, Ru***C***O).

IR (KBr) 1366 cm^{-1} (κ^1-OCO$_{sym}$), 1435 cm^{-1} (P-Ph), 1466 cm^{-1} (κ^2-OCO$_{sym}$), 1520 cm^{-1} (κ^2-OCO$_{asym}$), 1607 cm^{-1} (κ^1-OCO$_{asym}$), 1941 cm^{-1} (CO), $\Delta\nu_{(uni)}$ 239 cm^{-1}, $\Delta\nu_{(chelate)}$ 54 cm^{-1}; (CH_2Cl_2) 1373 cm^{-1} (κ^1-OCO$_{sym}$), 1437 cm^{-1} (P-Ph), 1468 cm^{-1} (κ^2-OCO$_{sym}$), 1520 cm^{-1} (κ^2-OCO$_{asym}$), 1603 cm^{-1} (κ^1-OCO$_{asym}$), 1946 cm^{-1} (CO), $\Delta\nu_{(uni)}$ 230 cm^{-1}, $\Delta\nu_{(chelate)}$ 52 cm^{-1}

MS (ESI) m/z 754.1 (Expected for $^{101}RuP_2O_3NC_{41}H_{36}$ [M] – OAc$^-$ + MeCN = 754.1292)

Crystal data and structure refinement for 4

Identification code	jml0816a	
Empirical formula	$RuP_2O_5C_{41}H_{36}$	
Formula weight	771.71	
Temperature	110(2) K	
Wavelength	0.71073 Å	
Crystal system	Triclinic	
Space group	P-1	
Unit cell dimensions	a = 9.4889(9) Å	α = 100.934(2)°.
	b = 10.7254(10) Å	β = 104.233(2)°.
	c = 18.505(2) Å	γ = 102.280(2)°.
Volume	1724.6(3) $Å^3$	
Z	2	
Density (calculated)	1.486 Mg/m^3	
Absorption coefficient	0.593 mm^{-1}	
F(000)	792	
Crystal size	0.26 x 0.16 x 0.06 mm^3	
Theta range for data collection	1.17 to 30.04°.	
Index ranges	-13<=h<=13, -15<=k<=14, -26<=l<=26	
Reflections collected	19579	
Independent reflections	9681 [R(int) = 0.0159]	
Completeness to theta = 30.04°	95.9 %	
Absorption correction	Semi-empirical from equivalents	
Max. and min. transmission	0.965 and 0.842	
Refinement method	Full-matrix least-squares on F^2	
Data / restraints / parameters	9681 / 0 / 444	
Goodness-of-fit on F^2	1.035	
Final R indices [I>2sigma(I)]	R1 = 0.0269, wR2 = 0.0652	
R indices (all data)	R1 = 0.0350, wR2 = 0.0691	
Largest diff. peak and hole	0.508 and -0.418 $e.Å^{-3}$	

3.8.3: Synthesis of $[Ru(\kappa^1\text{-}OAc)(\kappa^2\text{-}OAc)(NO)(PPh_3)_2]BF_4$ 5

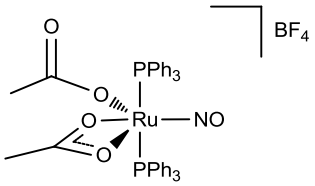

5

0.20 g **1** (0.27 mmol) was dissolved in 15 mL DCM in a Schlenk tube with a stirrer bar. One equivalent $NOBF_4$ was added (31.6 mg, 0.27 mmol) and the solution allowed to stir for one hour. After this time, the solution was concentrated to approximately 5mL and the product titurated by addition of 40 mL toluene. The solution was filtered to leave a light brown powder product which was dried *in vacuo*.

NMR Spectra CD_2Cl_2:

^1H δ_H 0.82 (s, 6H, C*H*$_3$COO), 7.48 (aq, 6.6 Hz, 12H, *ortho*-H of P*Ph*$_3$), 7.60 (at, 7.7 Hz, 12H, *meta*-H of P*Ph*$_3$), 7.71 (at, 7.5 Hz, 6H, *para*-H of P*Ph*$_3$)

$^{31}P\{^1H\}$ δ_P 34.7 (*P*Ph$_3$)

$^{13}C\{^1H\}$ δ_C 21.1 (s, *C*H$_3$COO), 122.9 (t, $^1J_{CP}$ + $^3J_{CP}$ = 52.0 Hz, PPh$_3$-*C*$_1$), 129.6 (t, $^3J_{CP}$ + $^5J_{CP}$ = 10.7 Hz, PPh$_3$-*C*$_3$), 133.0 (s, PPh$_3$-*C*$_4$), 134.7 (t, $^2J_{CP}$ + $^4J_{CP}$ = 10.8 Hz, PPh$_3$-*C*$_2$), unobserved, presumed broad (s, CH$_3$*C*OO)

IR (KBr) 1364 cm^{-1} (κ^1-OAc$_{sym}$), 1435 cm^{-1} (P-Ph), 1483 cm^{-1} (P-Ph), 1636 cm^{-1} (κ^1-OAc$_{asym}$), 1865 cm^{-1} (NO), $\Delta\nu_{(uni)}$ = 271 cm^{-1}, (CH_2Cl_2) 1359 cm^{-1} (κ^1-OAc$_{sym}$), 1438 cm^{-1} (P-Ph), 1485 cm^{-1} (P-Ph), 1636 cm^{-1} (κ^1-OAc$_{asym}$), 1874 cm^{-1} (NO), $\Delta\nu_{(uni)}$ = 277 cm^{-1}

MS (ESI) m/z 774.1094 (Expected for $^{101}RuP_2O_5NC_{40}H_{36}$ $[M]^+$ = 774.1112)

CHN Anal for $RuP_2O_5NBF_4C_{40}H_{36}$ + (1.00 CH_2Cl_2): (calc) C 52.08, H 4.05, N 1.48; (found) C 51.89, H 4.20, N 1.60

Crystal data and structure refinement for 5

Identification code	jml1020m	
Empirical formula	$RuP_2O_5NF_4Cl_4BC_{42}H_{40}$	
Formula weight	1030.37	
Temperature	110(2) K	
Wavelength	0.71073 Å	
Crystal system	Monoclinic	
Space group	P2(1)/n	
Unit cell dimensions	a = 14.592(4) Å	α= 90°.
	b = 20.189(6) Å	β= 100.348(6)°.
	c = 15.770(5) Å	γ = 90°.
Volume	4570(2) $Å^3$	
Z	4	
Density (calculated)	1.498 Mg/m^3	
Absorption coefficient	0.707 mm^{-1}	
F(000)	2088	
Crystal size	0.24 x 0.17 x 0.06 mm^3	
Theta range for data collection	1.74 to 28.36°.	
Index ranges	-19<=h<=19, -26<=k<=26, -21<=l<=20	
Reflections collected	46131	
Independent reflections	11370 [R(int) = 0.0377]	
Completeness to theta = 28.36°	99.6 %	
Absorption correction	Semi-empirical from equivalents	
Max. and min. transmission	0.958 and 0.748	
Refinement method	Full-matrix least-squares on F^2	
Data / restraints / parameters	11370 / 33 / 593	
Goodness-of-fit on F^2	1.029	
Final R indices [I>2sigma(I)]	R1 = 0.0433, wR2 = 0.1080	
R indices (all data)	R1 = 0.0625, wR2 = 0.1187	
Largest diff. peak and hole	1.317 and -0.743 e.$Å^{-3}$	

3.8.4: Reactions of 4 with HC≡CPh/H^{13}C≡CPh

General procedure for NMR scale reactions involving *in situ* preparation of 4:

1 was dissolved in DCM in a Schlenk tube under N_2 with a stirrer bar. The N_2 atmosphere was removed *in vacuo* and replaced with CO. After stirring for 5-15 minutes, the solution had changed colour from red-orange to pale yellow-green. The CO atmosphere was removed in vacuo and replaced with N_2. The solution was then transferred *via* cannula wire into an NMR tube fitted with a PTFE Young's tap and the solvent removed under a stream of N_2. The pale-yellow residue was then redissolved in CD_2Cl_2 transferred into the tube *via* vacuum distillation. Additional reagents were subsequently introduced under an N_2 atmosphere.

3.8.3.1: Addition of 1 eq. HC≡CPh to 4 (NMR scale)

The general procedure for an NMR scale reaction was followed using 25.3 mg **1** (34.0 μmol) and 3.8 μL HC≡CPh (34.6 μmol).

3.8.3.2: Addition of 1 eq. H^{13}C≡CPh to 4 (NMR scale)

The general procedure for an NMR scale reaction was followed using 27.0 mg **1** (36.3 μmol) and 4.0 μL H^{13}C≡CPh (36.4 μmol).

3.8.3.3: Addition of 1 eq. H^{13}C≡CPh and DBU to 4 (NMR scale)

The general procedure for an NMR scale reaction was followed using 25.0 mg **1** (33.6 μmol), 3.7 μL H^{13}C≡CPh (33.7 μmol) and 5.0 μL DBU (33.5 μmol) .

3.8.3.4: Addition of 2 eq. HC≡C^{t}Bu to 4

The general procedure for an NMR scale reaction was followed using 25.0 mg **1** (33.6 μmol) and 8.2 μL HC≡C^{t}Bu (67.2 μmol).

3.8.5: Synthesis of [Ru(κ^2-OAc)(C≡CPh)(CO)(PPh$_3$)$_2$] 6.

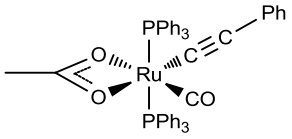

6

0.20 g **1** (0.27 mmol) was dissolved in 15 mL DCM in a Schlenk tube with an inbuilt condenser. The N_2 atmosphere was removed *in vacuo* and replaced with CO and the mixture stirred vigorously for 15 minutes, until the solution had changed colour from orange-red to green. The CO atmosphere was removed *in vacuo* and replaced with N_2. Two equivalents of HC≡CPh (60 μL, 0.54 mmol) was added and the mixture heated at 50 °C for 2 days. After cooling, the solvent was removed *in vacuo* and the yellow-green residue washed with 2 x 20 mL portions of pentane. The product was dried *in vacuo.* Yield 0.09 g (41.1 %)

^{1}H δ_H 0.61 (s, 3H, C*H*$_3$COO), 6.38 (m, 2H, C≡C*Ph*), 6.91 – 6.98 (m, 3H, C≡C*Ph*), 7.42 – 7.51 (m, 18H, P*Ph*$_3$), 7.63 – 7.67 (m, 12H, P*Ph*$_3$)

^{31}P{^{1}H} δ_P 38.6 (*P*Ph$_3$)

^{13}C{^{1}H} δ_C 22.5 (s, *C*H$_3$COO), 107.8 (t, $^2J_{CP}$ = 16.8 Hz, Ru-*C*≡CPh), 115.5 (s, Ru-C≡*C*Ph), 124.2 (s, *Ph*), 127.4 (s, *Ph*), 128.2 (t, $^3J_{CP}$ + $^5J_{CP}$ = 9.4 Hz, PPh$_3$-*C*$_3$), 129.0 (s, *Ph*), 130.2 (s, PPh$_3$-*C*$_4$), 130.6 (s, *Ph*), 131.4, (t, $^1J_{CP}$ + $^3J_{CP}$ = 44.1 Hz, PPh$_3$-*C*$_1$), 134.7 (t, $^2J_{CP}$ + $^4J_{CP}$ = 12.4 Hz, PPh$_3$-*C*$_2$), 185.4 (s, CH$_3$*C*OO), 204.9 (t, $^2J_{CP}$ = 13.9 Hz, Ru-*C*O)

IR (KBr) 1434 cm^{-1} (P–Ph), 1463 cm^{-1} (κ ^{2}-OCO$_{sym}$), 1521 cm^{-1} (κ ^{2}-OCO$_{asym}$), 1947 cm^{-1} (CO), 2101 cm^{-1} (C≡C), $\Delta\nu_{(chelate)}$ 58 cm^{-1}; (CH_2Cl_2) 1435 cm^{-1} (P–Ph), 1464 cm^{-1} (κ ^{2}-OCO$_{sym}$), 1521 cm^{-1} (κ ^{2}-OCO$_{asym}$), 1947 cm^{-1} (CO), 2105 cm^{-1} (C≡C), $\Delta\nu_{(chelate)}$ 57 cm^{-1};

MS (ESI) m/z 815.1400 (Expected for $RuP_2O_3C_{47}H_{39}$ $[M]^+$ = 815.1418)

CHN Anal for $RuP_2O_3C_{47}H_{39}$ + (0.50 CH_2Cl_2): (calc) C 66.55, H 4.70; (found) C 66.45, H 4.91

Crystal data and structure refinement for 6

Identification code	jml1019m	
Empirical formula	$RuP_2O_3C_{47}H_{38}$	
Formula weight	813.78	
Temperature	110(2) K	
Wavelength	0.71073 Å	
Crystal system	Monoclinic	
Space group	P2(1)/c	
Unit cell dimensions	a = 9.8259(8) Å	α= 90°.
	b = 14.5847(12) Å	β= 91.845(2)°.
	c = 27.166(2) Å	γ = 90°.
Volume	3891.1(6) $Å^3$	
Z	4	
Density (calculated)	1.389 Mg/m^3	
Absorption coefficient	0.527 mm^{-1}	
F(000)	1672	
Crystal size	0.25 x 0.09 x 0.05 mm^3	
Theta range for data collection	1.50 to 28.36°.	
Index ranges	-13<=h<=13, -19<=k<=19, -36<=l<=36	
Reflections collected	39677	
Independent reflections	9700 [R(int) = 0.0672]	
Completeness to theta = 28.36°	99.7 %	
Absorption correction	Semi-empirical from equivalents	
Max. and min. transmission	0.974 and 0.862	
Refinement method	Full-matrix least-squares on F^2	
Data / restraints / parameters	9700 / 0 / 479	
Goodness-of-fit on F^2	1.014	
Final R indices [I>2sigma(I)]	R1 = 0.0434, wR2 = 0.0897	
R indices (all data)	R1 = 0.0695, wR2 = 0.0998	
Largest diff. peak and hole	0.726 and -0.435 $e.Å^{-3}$	

3.8.6: Synthesis of $[Ru(\kappa^2\text{-}OAc)(C{\equiv}CPh)(NO)(PPh_3)_2]BF_4$ 7.

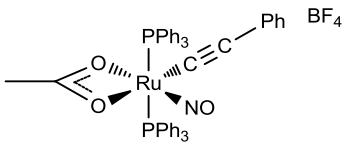

7

0.15 g $[Ru(NO)(\kappa^2\text{-}OAc)(\kappa^2\text{-}OAc)(PPh_3)_2]BF_4$ (0.17 mmol) was dissolved in 15 mL DCM in a Schlenk tube with an inbuilt condenser. Two equivalents of HC≡CPh (38.5 μL, 0.35 mmol) was then added and the mixture heated at 50 °C under N_2 for 2 days. After cooling, the solvent was removed *in vacuo* and the yellow-green residue washed with 2 x 20 mL portions of toluene and the product was dried *in vacuo.* Yield 0.08 g (50.0 %)

^1H δ_H 0.70 (s, 3H, C*H*$_3$COO), 6.27 (m, 2H, C≡C*Ph*), 7.09 (m, 3H, C≡C*Ph*), 7.55-7.61 (m, 30H, P*Ph*$_3$)

$^{31}P\{^1H\}$ δ_P 32.8 (*P*Ph$_3$)

$^{13}C\{^1H\}$ δ_C 22.4 (s, *C*H$_3$COO), 99.2 (t, $^2J_{CP}$ = 15.4 Hz, Ru-*C*≡CPh), 102.0 (s, Ru-C≡*C*Ph), 125.0 (t, $^1J_{CP} + {}^3J_{CP}$ = 53.1 Hz, PPh$_3$-C_1), 128.0, 128.3, 129.1 (s, *Ph*), 129.5 (t, $^3J_{CP} + {}^5J_{CP}$ = 11.4 Hz, PPh$_3$-C_3), 132.8 (s, PPh$_3$-C_4), 134.6 (t, $^2J_{CP} + {}^4J_{CP}$ = 12.4 Hz, PPh$_3$-C_2), 138.1 (s, *Ph*), 191.7 (s, CH$_3$*C*OO)

IR assignments are tentative owing to ambiguity in assignment

IR (KBr) 1394 cm^{-1} (κ^1-OCO$_{sym}$), 1436 cm^{-1} (P–Ph), 1463 cm^{-1} (κ^2-OCO$_{sym}$), 1483 cm^{-1} (P–Ph), 1506, 1559, 1570 cm^{-1} (κ^2-OCO$_{asym}$), 1586, 1594 cm^{-1} (κ^1-OCO$_{asym}$), 1880 cm^{-1} with shoulder 1860 cm^{-1} (NO), 2122 cm^{-1} (C≡C), $\Delta\nu_{(uni)}$ 192 cm^{-1}; (CH_2Cl_2) 1391 cm^{-1} (κ^1-OCO$_{sym}$), 1434 cm^{-1} (P–Ph), 1464 cm^{-1} (κ^2-OCO$_{sym}$), 1481 cm^{-1} (P–Ph), 1513 cm^{-1} (κ^2-OCO$_{asym}$), 1603 cm^{-1} (κ^1-OCO$_{asym}$), 1866 cm^{-1} (NO), 2123 cm^{-1} (C≡C), $\Delta\nu_{(chelate)}$ 49 cm^{-1}, $\Delta\nu_{(uni)}$ 212 cm^{-1}

MS (ESI) m/z 816.1360 (Expected for $^{101}RuP_2O_3NC_{46}H_{38}$ $[M]^+$ = 816.1370)

CHN Anal for $RuP_2NO_3BF_4C_{46}H_{38}$ + (1.1 CH_2Cl_2): (calc) C 56.80, H 4.07, N 1.41; (found) C 56.87, H 4.19, N 1.57

3.8.7: Addition of 1 eq. $H^{13}C{\equiv}CPh$ to 5

15.0 mg **1** (20.2 μmol) and 2.4 mg $NOBF_4$ (20.5 μmol) were added to an NMR tube fitted with a PTFE Young's tap. Approximately 0.6 mL CD_2Cl_2 was transferred into the tube *via* vacuum distillation and the mixture shaken vigorously. After standing for 1 hour, 2.3 μL $H^{13}C{\equiv}CPh$ (20.9 μmol) was introduced under a N_2 atmosphere, the sample sealed and the mixture periodically monitored by NMR spectroscopy.

4: Mechanistic Studies on the Formation of Ruthenium Vinylidene and Acetylide complexes

4.1: Introduction

Over the past 30 years, a significant number of experimental and theoretical investigations have been conducted into the precise mechanism by which transition-metal vinylidene complexes form.[1-4] As methods of computational sophistication have developed, so too has their ability to accurately predict and model experimental results.[5] Recently, the technique has been exploited to provide insight into reactions for which little experimental evidence can be provided due to their rapid nature.[6,7]

There are three typical mechanistic pathways proposed for the isomerisation of a terminal alkyne to a vinylidene ligand at a transition metal centre. These are illustrated in Figure 4.1.1 below.

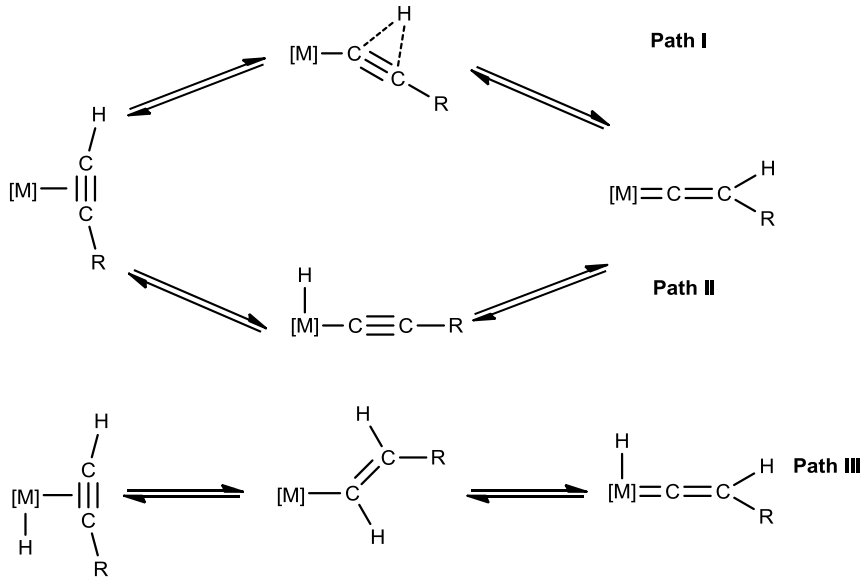

Figure 4.1.1: Three general pathways for alkyne-vinylidene isomerisation.

The initial coordination of the alkyne to the metal in a η^2-fashion is common to all three pathways. After this step, the reaction may proceed *via* Path **I**, where the alkyne undergoes a concerted 1,2-hydrogen shift to generate the vinylidene.[8-14] Alternatively, it may undergo an oxidative addition to generate an acetylide complex, which then undergoes a 1,3-hydrogen shift to form the vinylidene[15-23] (Path

II). Path **II** is generally preferred for more electron-rich complexes, which can more readily tolerate an oxidative addition.[3,4] For example, a Rh (I) d^8 centre, such as $[RhCl(P^iPr_3)_2]_n$, may easily oxidise to Rh (III) d^6 to give $[RhCl(H)(C{\equiv}CR)(P^iPr_3)_2]$,[17,23] whereas this transition is more difficult for a Ru (II) d^6 to Ru (IV) d^4 system.[i] In the case of Path **III**, where a hydride ligand is already present on the metal, an insertion of the alkyne may occur to give a vinyl complex. A subsequent α-H migration then gives rise to the ultimate hydrido-vinylidene product.[3,6,25]

The formation of complex **2a** from **1** and HC≡CPh has been shown to be rapid at room temperature, and no intermediates could be detected using NMR spectroscopy. In an attempt to discern the mechanism by which the alkyne-to-vinylidene isomerisation was occurring in this system, a series of experiments were conducted at low temperature. These experiments were accompanied by a comprehensive theoretical study conducted in collaboration with David Johnson and Dr. John Slattery.

4.2: Experimental study of formation of 2a

A number of literature studies have reported the identification of intermediates in the formation of vinylidene complexes at low temperatures using NMR spectroscopy.[26-29] For example, Puerta[28] has shown that the hydroxyalkynylhydrido complex $[RuCp^*(H)(C{\equiv}CC\{OH\}H_2)(PEt_3)_2]BPh_4$ forms upon addition of propargyl alcohol and an excess of $NaBPh_4$ to the precursor $[RuClCp^*(PEt_3)_2]$ at 0 °C in MeOH. Increasing the temperature to room temperature leads to the conversion of this intermediate to the hydroxyvinylidene form $[RuCp^*(=C=CHC\{OH\}H_2)(PEt_3)_2]BPh_4$.

Consequently, the reaction between **1** and HC≡CPh was monitored *in situ* in an NMR spectrometer cooled to 205 K. A single equivalent of the alkyne was added to the lip of a Young's NMR tube containing a solution of **1** in CD_2Cl_2 frozen in liquid N_2. The solution was warmed until the solution had just thawed and the reagents

[i] Unless the ruthenium system is particularly electron rich, in which case Path **II** is favoured.

mixed immediately before transferring the tube to the spectrometer. At this temperature the $^{31}P\{^{1}H\}$ NMR spectrum indicated that the major component of the mixture was **1** as a resonance at δ_P 63.8 dominates the spectrum. A minor resonance at δ_P 34.2 indicated the formation of a small amount of **2a**, either formed whilst the mixing of reactants occurred outside the spectrometer, or that formation of **2a** can occur even at 205 K. As the mixture was gradually warmed to 245 K, the resonance due to **2a** increased in intensity. At the same time, an additional species was detected which exhibited two new doublet resonances at δ_P 66.6 and 30.7, with a mutual coupling constant of $^{2}J_{PP}$ = 17.1 Hz. The magnitude of this coupling constant suggests this novel species contains mutually *cis*-PPh_3 ligands. In the ^{1}H NMR spectrum at this temperature, a broad singlet resonance, also thought to correspond to this intermediate at δ_H 5.94, was also detected. Warming the mixture to 255 K saw these resonances diminish in intensity. These additional resonances had not been previously observed in the $^{31}P\{^{1}H\}$ NMR spectrum when **2a** was cooled to 195 K. However, as mentioned in Chapter 2, the vinylidene proton (δ_H 5.14) moves to a higher chemical shift value (approximately δ_H 5.31 at 215 K), comparable to that observed for this intermediate complex.

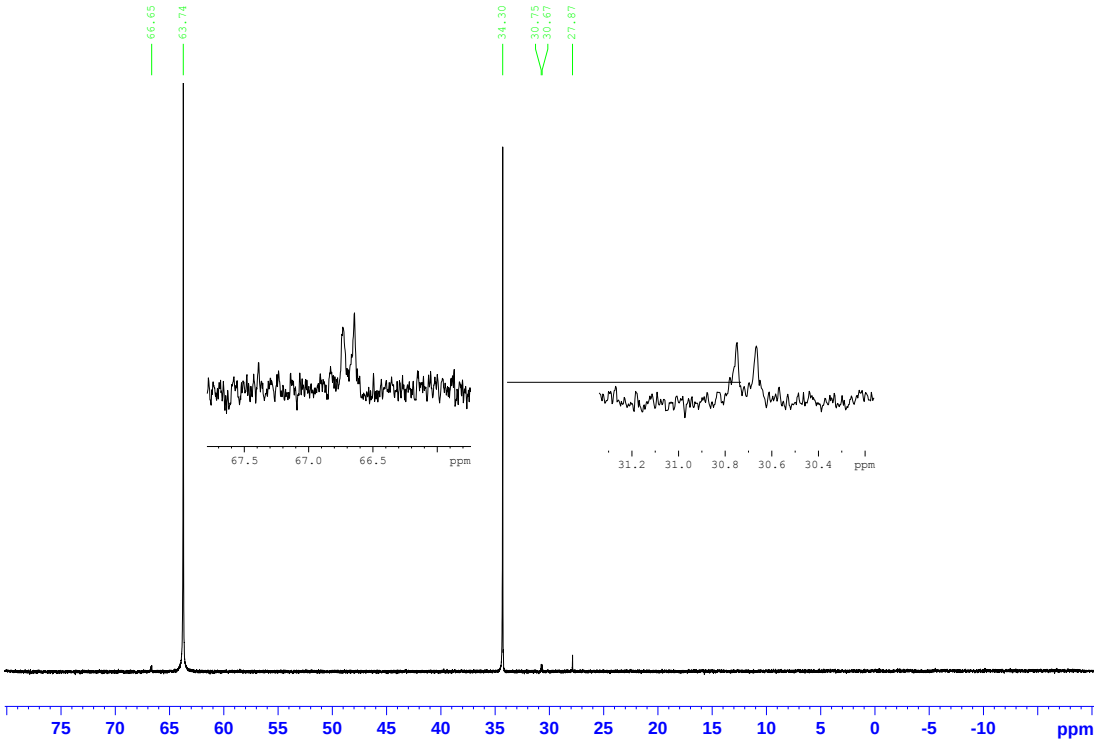

Figure 4.2.1: ^{31}P NMR spectrum of reaction between **1** and HC≡CPh recorded at 245 K.

In order to provide greater insight on the nature of this reaction pathway, a series of experiments were performed using $H^{13}C{\equiv}CPh$. In the first instance, [Ru(κ^1-OAc)(κ^2-OAc)(=^{13}C=CHPh)(PPh_3)$_2$] (**2a-^{13}C**) was prepared from the reaction between **1** and $H^{13}C{\equiv}CPh$ at room temperature. The expected ^{13}C-coupling was observed for the vinylidene proton at δ_H 5.20. For **2a**, this resonance was observed as a triplet, however for **2a-^{13}C** the resonance appeared as an apparent quartet with a $^2J_{HC}$ coupling of 3.11 Hz and $^4J_{HP}$ of 3.60 Hz. These couplings were resolved with the assistance of the $^1H\{^{31}P\}$ NMR spectrum. This $^2J_{HC}$ value is typical of this system; in 2008 Cadierno reported that the vinylidene proton of [Ru(=^{13}C=CHPh)(η^5-C_9H_7)(PPh_3)$_2$]PF_6 had a $^2J_{HC}$ coupling of 3.4 Hz.[14] In the $^{31}P\{^1H\}$ NMR spectrum of **2a-^{13}C**, a doublet resonance is observed at δ_P 34.2 with a $^2J_{CP}$ of 16.7 Hz. The corresponding resonance for $^{13}C_\alpha$ is observed at δ_C 355.6 as a triplet, as for **2a**, however the intensity of this resonance is enhanced due to the presence of the ^{13}C label. This complex was also characterised in solution (DCM) IR spectroscopy. This showed the presence of both κ^1- and κ^2-coordination modes, with stretches comparable to those observed for **2a**. The $^{13}C{=}^{12}C$ stretch is predicted to occur at 1599 cm^{-1}, as shown using Equations 4.2.1 – 4.2.4. However, it is presumed that this stretch may be obscured by that of the strong asymmetric stretch of the κ^1-OAc ligand, which is observed at 1589 cm^{-1}. A small shoulder peak on this stretch is observed at 1601 cm^{-1} which may account for the $^{13}C{=}^{12}C$ stretch.

$$\mu_{C^{(i)}C} = \frac{m_1 m_2}{m_1 + m_2} \qquad \text{(Eqn 4.2.1)}$$

$$\upsilon_{C^{(i)}C} = \frac{1}{2\pi c}\sqrt{\frac{k}{\mu_{C^{(i)}C}}} \qquad \text{(Eqn 4.2.2)}$$

$$\frac{\upsilon_{^{12}C^{13}C}}{\upsilon_{^{12}C^{12}C}} = \sqrt{\frac{\mu_{^{12}C^{12}C}}{\mu_{^{12}C^{13}C}}} = \sqrt{\frac{6}{6.24}} = 0.981 \qquad \text{(Eqn 4.2.3)}$$

$$\upsilon_{^{12}C^{13}C} = \frac{\upsilon_{^{12}C^{12}C}}{0.981} = 1599 cm^{-1} \qquad \text{(Eqn 4.2.4)}$$

	P–Ph	C=C	κ^1-OCO_{sym}	κ^1-OCO_{asym}	κ^1-$\Delta\upsilon$	κ^2-OCO_{sym}	κ^2-OCO_{asym}	κ^2-$\Delta\upsilon$
2a / cm^{-1}	1435	1630	1366	1594	228	1462	1531	69
2a-^{13}C / cm^{-1}	1435	n.d.	1365	1589	224	1460	1528	68

Table 4.2.1: Summary of IR stretches observed for **2a** and **2a-^{13}C** in DCM (n.d. = not detected).

The low temperature reaction of **1** with H^{13}C≡CPh was conducted in the same manner as for the reaction with HC≡CPh. The $^{31}P\{^1H\}$ NMR spectrum recorded at 245 K once more showed the presence of the intermediate complex exhibiting additional coupling to the ^{13}C label: at δ_P 66.7 an apparent triplet is observed, with presumably coincident coupling of $^2J_{PP} \approx {}^2J_{PC} \approx 16.7$ Hz and at δ_P 30.8, a doublet of doublets resonance is observed ($^2J_{PP}$ = 16.8 Hz, $^2J_{PC}$ = 94.5 Hz). The large $^2J_{PC}$ coupling suggests that the ^{13}C-label is *trans* to the PPh_3 ligand responsible for the resonance at δ_P 30.8. In the ^1H NMR spectrum, the resonance at δ_H 5.94 appeared as an apparent doublet ($^2J_{HC}$ = 10.9 Hz). This coupling is larger than observed for **2a-^{13}C**, suggesting that this intermediate species does not contain a vinylidene ligand. It is also inconsistent with that of an η^2-alkyne ligand, which would exhibit a much larger $^1J_{HC}$ coupling. For example, Grotjahn reports that the η^2-alkyne complex [RhCl(η^2-H^{13}C≡^{13}CH)(PPh^{i}Pr$_2$)$_2$] exhibits a $^1J_{HC}$ coupling of 233.2 Hz, in addition to couplings to ^{103}Rh and ^{31}P.[20] It is therefore proposed that this intermediate has the structure *cis*-**12** shown in Figure 4.2.1. Further insight into the structure of *cis*-**12** was provided from the reaction of **2a** with CO. As will be discussed in Chapter 6 (Section 6.2), this results in the formation of complex **12** (Scheme 4.2.2) containing a metallo-enolester ligand, presumably formed by nucleophilic attack of a κ^1-OAc ligand on the C_α of the vinylidene.

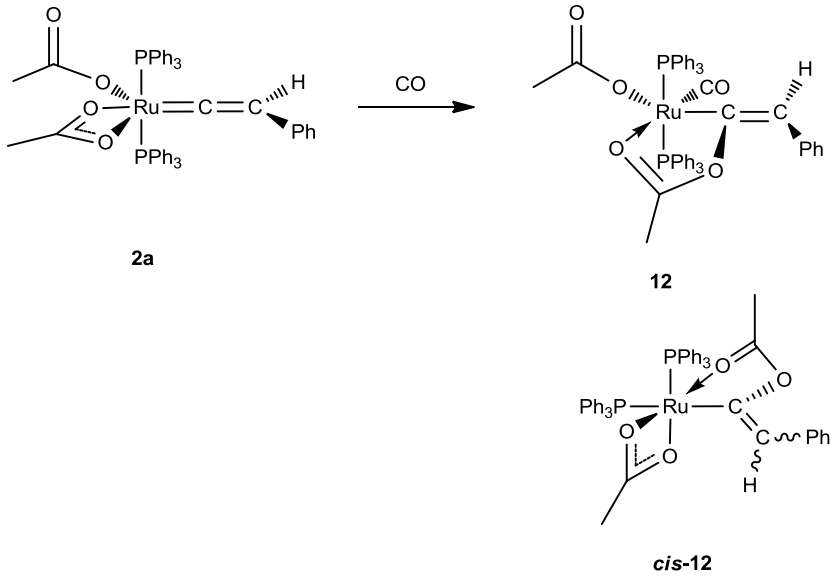

Figure 4.2.2: Proposed structure of intermediate *cis*-**12**.

Complex **12** exhibits similar spectroscopic features to those observed for *cis*-**12**. A triplet resonance at δ_H 6.25 ($^4J_{HP}$ = 2.8 Hz) in the ^{1}H NMR spectrum of *cis*-**12** has been assigned to the proton attached to C_β of the coordinated enol-ester, whilst a singlet is observed at δ_P 30.7 for the phosphine ligands. The two acetate ligands no longer display fluxional behaviour and are therefore observed as two singlet resonances each with a relative integration of three at δ_H 1.15 and 1.63. Additional evidence is provided by the synthesis and characterisation of **12-^{13}C**. This was carried out in the same manner as for **12** using H^{13}C≡CPh in the place of HC≡CPh. The 'vinylic' proton resonance at δ_H 6.24 (dt, $^4J_{HP}$ = 2.6 Hz) exhibits an additional coupling of 11.1 Hz due to a $^2J_{HC}$ coupling, comparable in magnitude to the corresponding coupling observed for *cis*-**12**, and greater than the $^2J_{HC}$ observed in **2a-^{13}C**. The ^{31}P NMR spectrum of **12-^{13}C** displays a doublet resonance at δ_P 30.7 ($^2J_{PC}$ = 17.8 Hz) whilst in the ^{13}C NMR spectrum, a triplet resonance is observed at δ_P 193.3 ($^2J_{PC}$ = 17.6 Hz) for the $^{13}C_\alpha$ of the enol ester ligand.

The NMR spectra recorded at 255 K showed that the resonances due to *cis*-**12** had disappeared. Upon warming to room temperature, resonances due to **2a** increased in intensity and those due to **1** decreased in both the ^{1}H and ^{31}P{^{1}H} NMR spectra.

The detection of complex *cis*-**12** did not appear to be particularly useful in determining the mechanism by which vinylidene formation takes place, as the proton

migration has already occurred. It has been shown that the isomerisation of HC≡CPh to its vinylidene form mediated by **1** is facile even at 255 K. As a result, it is unlikely that further experimental studies will provide conclusive evidence for the pathway of vinylidene formation. Consequently, a thorough computational investigation was conducted. This will be detailed in Section 4.3.

It was noted in Chapter 2 that the similar complex $[RuCl_2(PPh_3)_3]$ had been reported to require approximately 30 hours to react with HC≡C^{t}Bu to give the corresponding vinylidene complex by Wakatsuki. This provides an interesting mechanistic contrast to our system. Our independent study of the reaction of $[RuCl_2(PPh_3)_3]$ with HC≡CPh confirmed that at least 24 hours was required for the formation of $[RuCl_2(=C=CHPh)(PPh_3)_2]$. Wakatsuki had shown that a number of intermediate species, shown in Figure 4.2.3 could be detected over the course of the reaction, using $^{31}P\{^1H\}$ NMR spectroscopy, and analogous species were detected in our investigation. However, when the reaction was repeated using $H^{13}C\equiv CPh$, it became apparent that one of the intermediates detected could not have the structure proposed by Wakatsuki.

In his original report, Wakatsuki analysed the reaction mixture by IR and NMR spectroscopies 15 minutes after the addition of the alkyne HC≡C^{t}Bu to $[RuCl_2(PPh_3)_3]$. No evidence for a C≡C moiety, either of a η^2-alkyne or acetylide ligand could be detected by IR spectroscopy, however a peak at 1638 cm^{-1} was indicative of a vinylidene species. The $^{31}P\{^1H\}$ NMR spectrum of the mixture at this point showed that, in addition to resonances assigned to the starting complex, free PPh_3 and the expected vinylidene product $[Ru(=C=CH^tBu)Cl_2(PPh_3)_2]$ (δ_P 27.2); two AB-type quartets are present centred at δ_P 46.5 (J = 38 Hz) and δ_P 34.4 (J = 25 Hz). These species were observed to disappear at a 'rate almost equal' to that of the formation of the vinylidene product complex.[9] These two species were assigned to the intermediate forms **4B** and **4C** shown in Figure 4.2.3. The mechanism proposed involves the initial loss of a PPh_3 ligand to provide a vacant site for the alkyne to bind. The η^2-bound alkyne then isomerises to its vinylidene form, which is suggested to exist in the two isomeric forms **4B** and **4C**. A *cis-trans* isomerisation of the phosphine ligands then results in the formation of the ultimate vinylidene product.

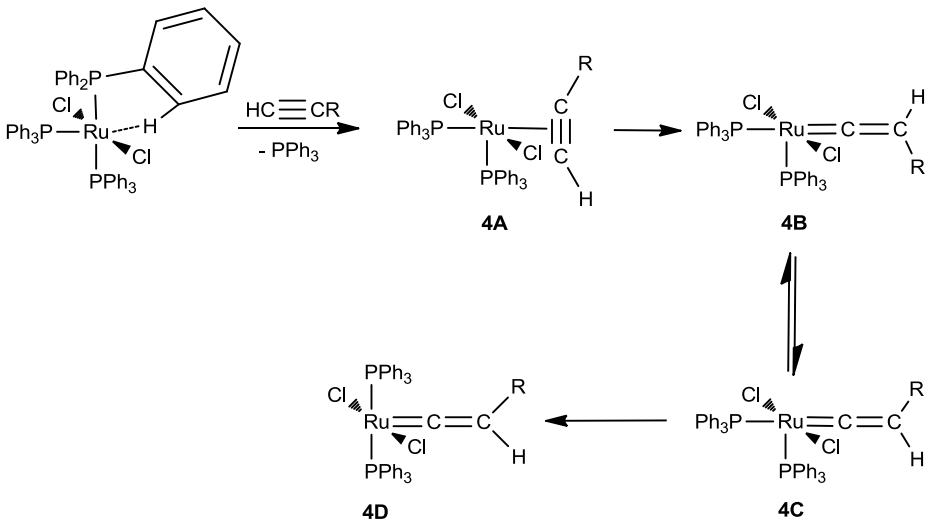

Figure 4.2.3: Proposed mechanism for the formation of $[RuCl_2(PPh_3)_2(=C=CHR)]$.

To complement his experimental investigation, Wakatsuki also conducted a theoretical study on the isomerisation of the model complex $[RuCl_2(PH_3)_2(\eta^2\text{-}HC{\equiv}CH)]$ to $[RuCl_2(PH_3)_2(=C=CH_2)]$ using the MP2 level of theory. The lowest energy pathway appeared to proceed *via* a 1,2-hydrogen shift pathway, in which a η^2-CH agostic species is also implicated. An oxidative addition pathway was found to be highly unfavourable. It was also shown that two rotational isomers of a vinylidene complex in which the two PH_3 ligands are mutually *cis*, analogues of **4B** and **4C**, are local minima on the potential energy surface. The energy difference between the two was found to be 40.2 kJ mol^{-1}. These are illustrated in Figure 4.2.4. It is proposed that these intermediates are observed experimentally as, for the full ligand system, steric repulsion exists between the PPh_3 ligand and the ^{t}Bu substituent of the vinylidene.

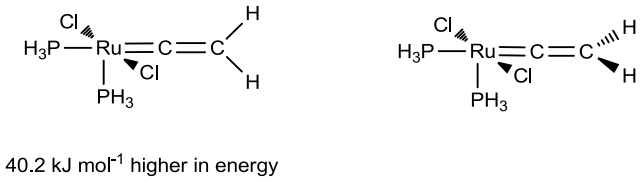

Figure 4.2.4: Rotational isomers of the model complex *cis*-$[RuCl_2(PH_3)_2(=C=CH_2]$.

Our repetition of Wakatsuki's experiment using HC≡CPh gave similar results. A single equivalent of HC≡CPh was added to a CD_2Cl_2 solution of $[RuCl_2(PPh_3)_3]$ under N_2 and the composition of the mixture monitored by NMR spectroscopy. Soon after addition of the alkyne, evidence for species analogous to **4B** and **4C** were

observed. In addition to resonances at δ_P -5.5 (PPh_3), δ_P 27.1 ($O{=}PPh_3$), δ_P 28.9 ([Ru(=C=CHPh)$Cl_2(PPh_3)_2$]) and δ_P 40.7 ([$RuCl_2(PPh_3)_3$]), two AB-quartet resonances centred on δ_P 34.1 ($^2J_{PP}$ = 25.3) and δ_P 47.3 ($^2J_{PP}$ = 39.0) were observed in the $^{31}P\{^1H\}$ NMR spectrum. These are illustrated by the blue spectrum in Figure 4.2.5. In the ^1H NMR spectrum, resonances due to unreacted HC≡CPh (δ_H 3.12) and the vinylidene proton of the product (δ_H 4.94, $^4J_{HP}$ = 4.1 Hz) were observed. Furthermore, two broad singlets that were thought to correspond to the vinylidene protons of intermediates **4B** and **4C** were observed at δ_H 3.34 and δ_H 4.04. Approximate relative integrations indicate that the peak at δ_H 4.04 is associated with the complex which displays an AB-doublet at δ_P 34.1, and the resonance at δ_H 3.34 is associated with the AB-doublet at δ_P 47.3.

After one day, the $^{31}P\{^1H\}$ NMR spectrum shows that the resonances assigned to these two species **4B** and **4C** have diminished and the resonance due to the product complex has increased in intensity. Other minor resonances due to other phosphorus-containing species are also present in the reaction mixture at this point, however their identities are unknown.

In order to 'shed more light' on this reaction, it was conducted in an identical fashion using $H^{13}C{\equiv}CPh$. The resulting vinylidene complex [$RuCl_2(={}^{13}C{=}CHPh)(PPh_3)_2$] exhibited a characteristic doublet resonance at δ_P 29.0 ($^2J_{PC}$ = 17.0 Hz) in the $^{31}P\{^1H\}$ NMR spectrum and a corresponding triplet at δ_C 340.5 ($^2J_{CP}$ = 17.0 Hz) in the $^{13}C\{^1H\}$ NMR spectrum. The vinylidene proton is observed as an apparent quartet at δ_H 5.00 ($^3J_{HC}$ = 2.4 Hz; $^4J_{HP}$ = 4.0 Hz). Resonances assigned to the two proposed intermediate species are also observed soon after addition of the alkyne. Two additional broad singlet resonances are observed at δ_H 3.45 and δ_H 4.11 in the ^1H NMR spectrum whilst resonances at δ_P 34.1 and δ_H 47.3 are again observed in the $^{31}P\{^1H\}$ NMR spectrum. However, surprisingly, only the multiplicity of the resonance at δ_P 34.1 is altered by the presence of the ^{13}C-label. The coupling is difficult to accurately discern from the $^{31}P\{^1H\}$ NMR spectrum obtained however the $^{13}C\{^1H\}$ NMR spectrum at this stage also exhibits an additional resonance at very high field indicative of a vinylidene C_α (δ_C 362.3, $^2J_{PC}$ = 18.1 Hz). Figure 4.2.5 provides an overlay of the labelled and unlabelled $^{31}P\{^1H\}$ NMR spectra recorded soon after addition of the alkyne.

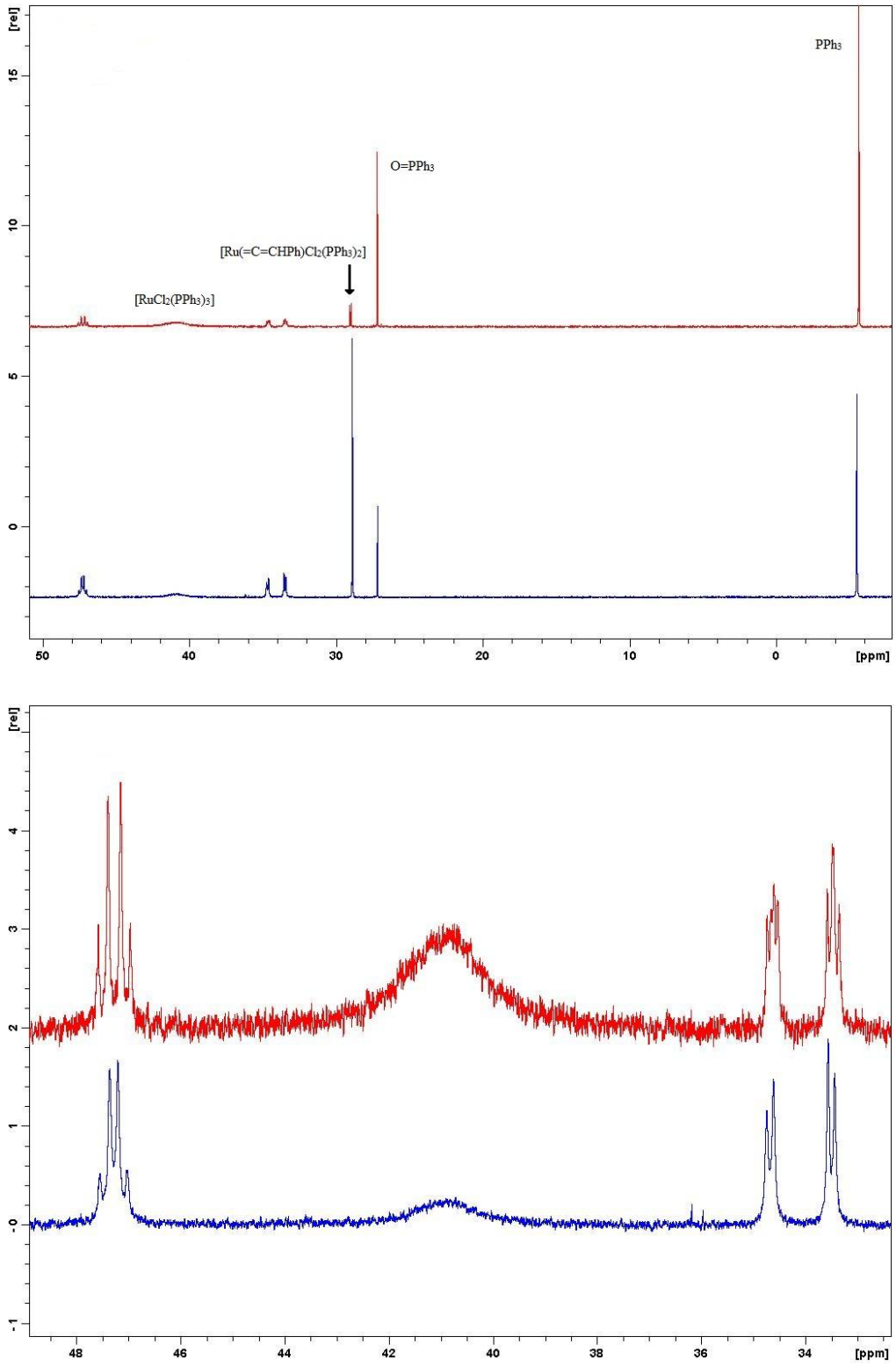

Figure 4.2.5: Overlay of $^{31}P\{^{1}H\}$ NMR spectra for the reaction between $[RuCl_2(PPh_3)_3]$ and HC≡CPh (blue) and $[RuCl_2(PPh_3)_3]$ and $H^{13}C{\equiv}CPh$ (red).

Again, after one day, resonances due to the product increase in intensity whilst those of the intermediate species diminish or disappear entirely. It is therefore proposed that only one of the intermediates proposed by Wakatsuki is a vinylidene

complex. We suggest that the proposed intermediate species **4B** and **4C** are undergoing a conversion that is rapid on the NMR timescale and corresponds to the species which exhibits an AB-quartet resonance at δ_P 34.1. This also contrasts with Wakatsuki's theoretical study. However, the model complexes employed did not take into account the full ligand substituents, so it is uncertain how this would affect the potential energy surface for the reaction. We also cannot discount that the use of HC≡CPh as an alternative to HC≡C^{t}Bu may affect the reaction mechanism, though the steric differences between the two are not as great as between H and ^{t}Bu.

The identity of the second intermediate species we observe remains unclear at this point. Wakatsuki has shown that no evidence for a C≡C moiety is detected by IR spectroscopy soon after addition, and the absence of a large $^1J_{HC}$ or $^2J_{PC}$ coupling in our ^{13}C-labelled experiment appears to confirm that this intermediate is not a η^2-alkyne or acetylide complex. It should also be noted that in our hands, the unknown intermediate species disappears entirely after one day, whilst the second vinylidene complex can be detected after one day in trace quantities.

This example serves to highlight the mechanistic differences between the formation of vinylidene complexes in the similar complexes **1** and [$RuCl_2(PPh_3)_3$]. The reaction of complex **1** with a terminal alkyne appears to proceed *via* a different mechanistic pathway, one which the acetate ligand apparently facilitates, which contrasts with the similar complex [$RuCl_2(PPh_3)_3$], which is likely to proceed *via* a 1,2-hydrogen shift pathway.

4.3: Computational (DFT) study of 2a formation

An extensive theoretical study using DFT methods was conducted by David Johnson and Dr. John Slattery (University of York) in an effort to determine the mechanism by which vinylidene formation occurs for **2a**.[7] Three potential pathways were investigated for this system; these include the concerted 1,2 H-migration and oxidative addition pathways represented by paths **I** and **II** respectively in Figure 4.1.1. An additional pathway was also considered whereby an acetate ligand facilitates the formation of the vinylidene ligand. For this route, it is proposed that once the alkyne is bound to the ruthenium centre in the usual η^2-fashion, it may be

deprotonated by an acetate ligand to give an acetylide ligand. The coordinated acetic acid may then reprotonate the acetylide at C_β resulting in the formation of the vinylidene complex, as shown in Figure 4.3.1 below:

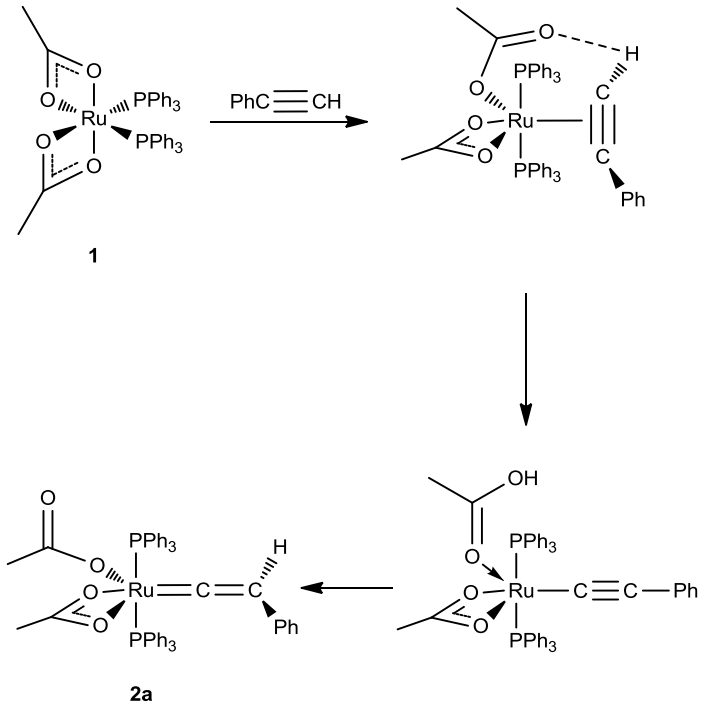

Figure 4.3.1: Proposed mechanism for the formation of **2a**.

Inspiration for this proposed pathway arose from recent investigations by the Fagnou[30] and MacGregor/Davies[31] groups into the mechanism by which carboxylate and carbonate ligands may assist C-H activation at Pd-centres by acting as an internal base. Fagnou initially proposed the use of the term CMD[32] (**C**oncerted **M**etalation **D**eprotonation) to describe such heteroatom-assisted C-H activations; however McGregor and Davies have since suggested the term AMLA (**A**mbiphilic **M**etal **L**igand **A**ctivation) be used to truly distinguish the process from SBM (**S**igma-**B**ond **M**etathesis) which also involves a deprotonation step.[33]

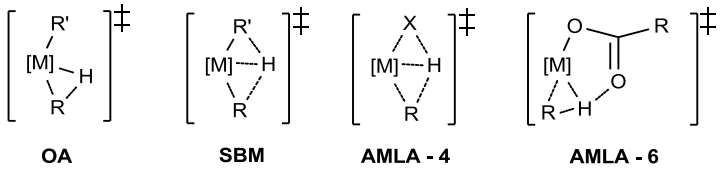

Figure 4.3.2: Transition states involved in C-H activation mechanisms: OA = oxidative addition; SBM = σ-bond metathesis; R' = H, hydrocarbyl, boryl; X = heteroatom with lone pair(s)[34]

The alkyne-to-vinylidene isomerisation process for this system is accompanied by an isomerisation of the phosphine ligands; complex **1** contains a *cis*-phosphine manifold whereas in the product **2a** they are *trans*. Consequently, for the three potential pathways considered three possible isomers of each transition state (**TS**) and intermediate (**I**) exist. One isomer was considered for the *trans*-manifold and two for the *cis* (*cis* and *cis*'), where *cis*-$_{XX}$ indicates that the vacant site for alkyne coordination has been generated *trans* to an acetate ligand and *cis*'-$_{XX}$ denotes an isomer where the alkyne is coordinated *trans* to a phosphine ligand. Furthermore, several confomers of each isomer had to be considered at each point on the potential energy surface (PES), full details are provided in the experimental section.

Two model systems were chosen for study; the first (**i**) used structurally smaller ligands such as PH_3 and a Me-substituted alkyne in the place of PPh_3 and HC≡CPh. This model was used in order to generate an approximate idea of the PES using computationally 'cheaper' ligands with fewer atoms that are easier to calculate. The second model (**ii**) calculated the PES for the 'full' system that was investigated experimentally.

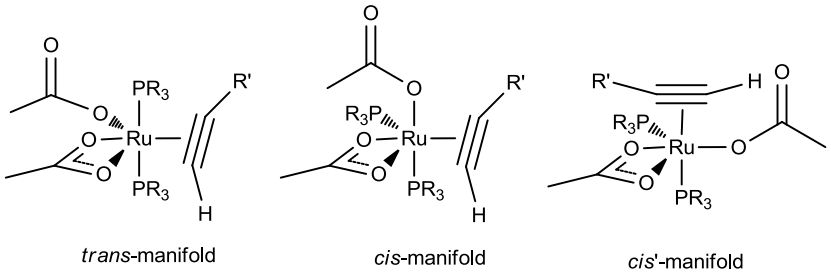

Figure 4.3.3: The structures of isomers used for model (**i**) R = H, R' = Me and model (**ii**) R = R' = Ph.

The potential energy surface generated for model (**i**) is shown in Figure 4.3.1.1 below. All Gibbs energies for both models are given in kJ mol^{-1} relative to the energy of *cis*-***a*** (equivalent to complex **1**) + free alkyne. The lowest energy pathway of the three mechanisms considered is shown for each isomer; for the *cis*-manifold this is indicated by the black route, for the *cis*'-manifold this is pale blue and for the *trans*-manifold, dark blue.

4.3.1: Model (i) $Ru(\kappa^2\text{-}OAc)_2(PH_3)_2$ + HC≡CMe

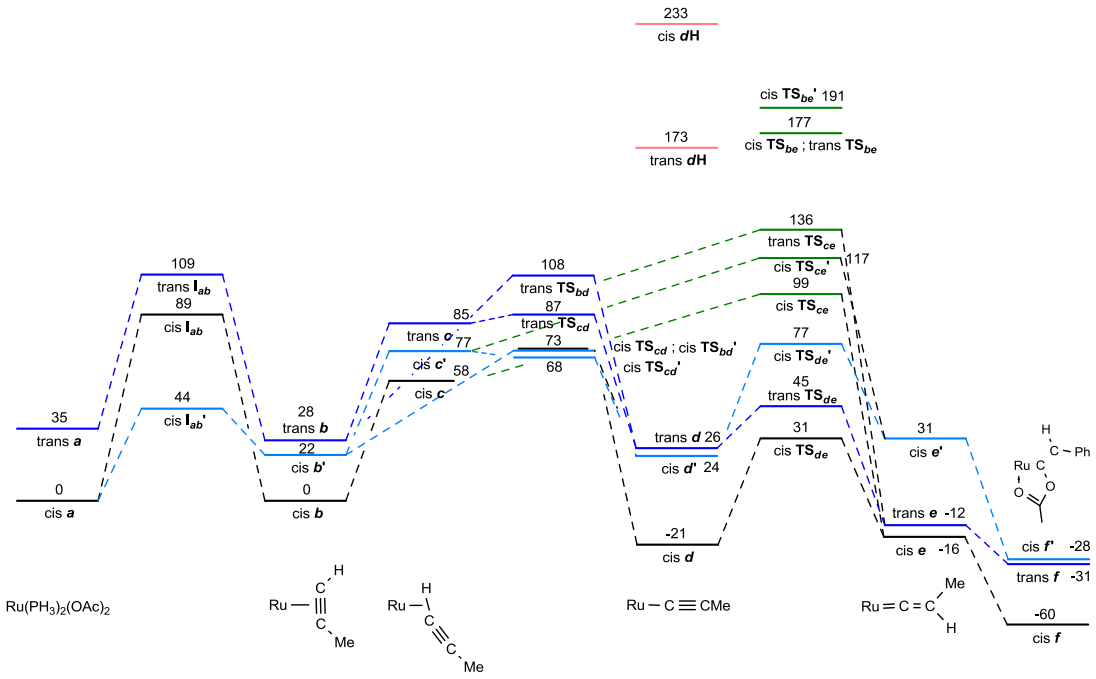

Figure 4.3.1.1: Potential Energy Surface calculated for model system (**i**).

The calculations confirm what has been demonstrated experimentally, that the *cis* isomer of ***a*** is lower in energy than the *trans*, which is calculated to be 35 kJ mol^{-1} higher in energy. The next stationary point encountered on the PES is the intermediate between ***a*** and ***b***, in which a vacant site is generated and alkyne coordination occurs. This intermediate, denoted $\mathbf{I}_{ab}$, is formed by dissociation of one oxygen atom of the two acetate ligands. From this point onwards on the PES, the three isomers *trans*-XX, *cis*-XX and *cis*'-XX described above must be considered. The difference in energy between the optimised structures of intermediates *cis*-$\mathbf{I}_{ab}$ and *trans*-$\mathbf{I}_{ab}$, and *cis*-***a*** and *trans*-***a*** is larger than may be considered reasonable for a reaction that appears rapid at 245 K. It is suggested that this may be a consequence of performing these calculations in the gas-phase, which does not consider the stabilising effect solvation may have on this intermediate. Continuum-based solvation models were not used in this instance as specific metal-solvent interactions could not be ruled out. The energy of the *cis'*-$\mathbf{I}_{ab}$ isomer is notably lower than that of the *cis*-$\mathbf{I}_{ab}$ and *trans*-$\mathbf{I}_{ab}$ isomers which may be due to the more favourable

positioning of the vacant site *trans* to PH_3, which has a stronger *trans*-labilising effect compared to the acetate ligand.

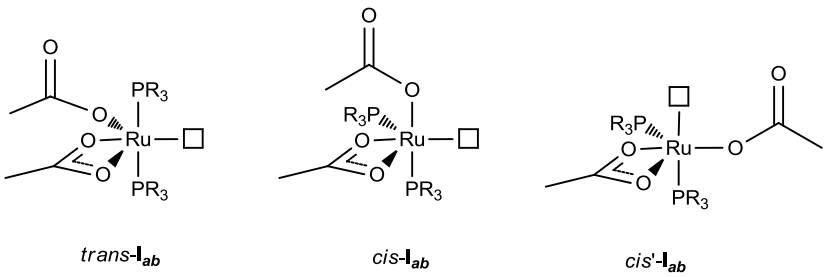

Figure 4.3.1.2: Three isomers of intermediate $\mathbf{I}_{ab}$.

A number of computational investigations have determined that alkyne-to-vinylidene isomerisation occurs *via* a σ-complex of the type ***c***, rather than directly from the π-bound alkyne form ***b***.[6,9,12,24] This structure was also found to be a local minimum on the PES. From ***c***, an oxidative addition pathway would proceed *via* a hydride-acetylide complex, represented as ***d*H** and the red route in Figure 4.3.1.1. The isomers *cis*-***d*H** and *trans*-***d*H** were calculated to be very high energy at 233 and 173 kJ mol^{-1} above the energy of *cis*-***a*** + HC≡CMe respectively. It is therefore highly unlikely that this mechanism occurs at the temperatures demonstrated experimentally.

A concerted 1,2-hydrogen shift mechanism may proceed from either the alkyne complex ***b*** or σ-complex ***c*** *via* the transition states $\mathbf{TS}_{be}$ and $\mathbf{TS}_{ce}$ respectively. However, the calculated energies of the $\mathbf{TS}_{be}$ isomers are prohibitively high at 177 kJ mol^{-1} and 191 kJ mol^{-1} and it is therefore unlikely that this mechanism proceeds at the temperatures observed. The energies of $\mathbf{TS}_{ce}$ however are more accessible at 136, 117 and 99 kJ mol^{-1} for the *trans*, *cis* and *cis*' isomers respectively, though are still higher in energy than the lowest energy pathway.

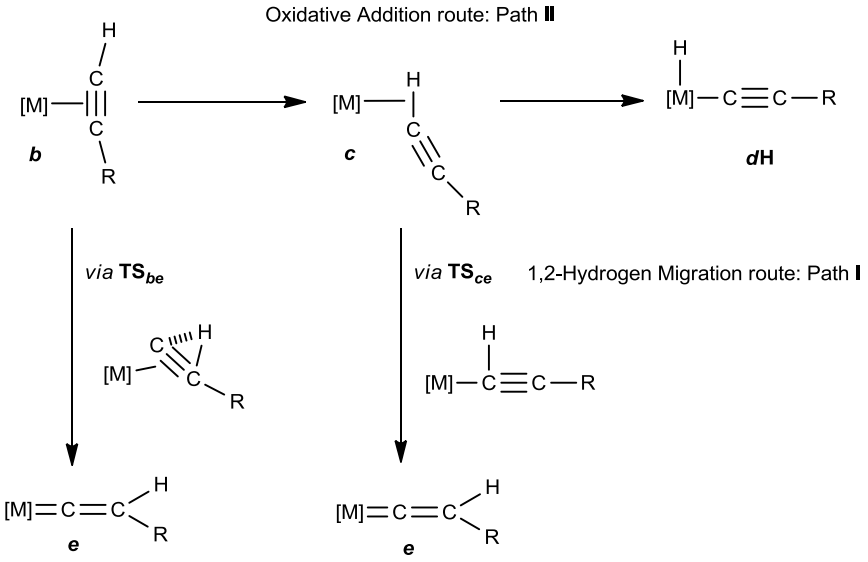

Figure 4.3.1.3: Possible alkyne-to-vinylidene isomerisation mechanisms for model (**i**).

The potential for the alkyne proton to form a hydrogen bond with the uncoordinated oxygen of the κ^1-acetate ligand in structures ***b*** and ***c*** was investigated computationally, however in the cases of the two *cis*-***b*** isomers and the three isomers of ***c*** the structures converged to the acetylide-complex ***d***. In the case of *trans*-***b***, optimised structures converge to one where the uncoordinated oxygen of the κ^1-acetate ligand forms a contact with the phosphorus atom of a PH_3 ligand. These convergences occur regardless of the choice of convergence and optimisation parameters for a number of input geometries.

An alternative pathway also considered the assistance of an acetate ligand in the formation of the vinylidene complex ***e***. For this pathway, an initial deprotonation of the alkyne by an acetate ligand may occur from either ***b*** or ***c***, resulting in the formation of the acetylide complex ***d***, also containing a protonated acetic acid ligand. Consequently, transition states $\mathbf{TS}_{\boldsymbol{bd}}$ and $\mathbf{TS}_{\boldsymbol{cd}}$ were identified as minima on the PES. Unfortunately, the structure of *cis*-$\mathbf{TS}_{\boldsymbol{bd}}$ could not be found and convergence to ***d*** was observed for all starting geometries. However, the energies calculated for the isomers of $\mathbf{TS}_{\boldsymbol{bd}}$ indicate that this pathway is more accessible than the concerted 1,2-hydrogen shift *via* $\mathbf{TS}_{\boldsymbol{be}}$. The energies of $\mathbf{TS}_{\boldsymbol{cd}}$ indicate that this transition is particularly facile. For the *cis*-manifold, there is a barrier of 15 kJ mol^{-1}, whereas for the *trans*- and *cis*'-manifold the transition is virtually barrier-less at +2 and –9 kJ mol^{-1} respectively.

The next step in this proposed acetate-assisted pathway is the protonation of C_β by the coordinated acetic acid ligand of ***d*** to generate the vinylidene complex ***e***. This transition appears to have a relatively low energy barrier, particularly for the *trans*-manifold where $\Delta G^{\ddagger} = 19$ kJ mol^{-1}.

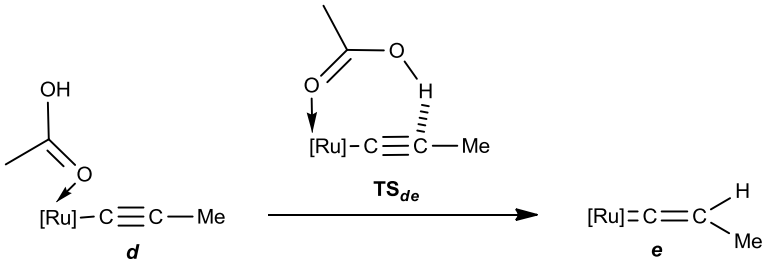

Figure 4.3.1.4: Formation of ***e*** *via* protonation by coordinated acetic acid of **TS$_{de}$**.

At this point on the PES of model (**i**), there is a significant deviation from experimental observations, in that the three isomers of the metallo-enolester analogue of *cis*-**12** (***f***) are the apparent thermodynamic products of the reaction. This is unlikely as it has been observed that the metallo-enolester complex *cis*-**12** is a kinetic product that decays before the complete formation of the vinylidene complex **2a**.

This acetate-assisted pathway appears to provide a lower energy route for the isomerisation of the alkyne HC≡CMe to its vinylidene form for the model complex Ru(κ^2-OAc)$_2$(PH$_3$)$_2$ than the alternative oxidative addition and concerted 1,2-hydrogen shift mechanisms. Across the entire PES, it appears that the *cis*-manifold is often the lowest energy isomer of the three considered. However, this does not mean that this is the most favourable pathway, as the energy barriers for the transition between these local minima are often high. It is also unclear at which point on the PES the isomerisation of the phosphine ligands from the *cis*-manifold of the starting material to the *trans* of the product occurs. This model also places the experimentally observed thermodynamic product **2a**/***e*** higher in energy than a kinetic product (*cis*-**12**/***f***). Furthermore, the model suggests that the *cis*-isomer of ***e*** is lower in energy than the experimental analogue of **2a**, *trans*-***e***. Consequently, despite the computational expense of using the 'full' ligand substituents, the model generated warrents further investigation.

4.3.2: Model (ii) $Ru(\kappa^2\text{-}OAc)_2(PPh_3)_2$ + HC≡CPh

The PES for the model (**ii**) system is shown in Figure 4.3.2.1, where the phosphine and alkyne ligand substituents are the same as those used experimentally. Using the larger substituents in this model meant that the calculations required a longer processing time; however the expense appears to be worthwhile. For example, in this model the thermodynamic product is the vinylidene complex *trans*-***e*** and the metallo-enolester complex ***f***; a kinetic product. As for model (**i**), the *cis*-isomer of the starting material ***a*** is lower in energy than the *trans*, but this time by 8 kJ mol^{-1} rather than 35 kJ mol^{-1}calculated in model (**i**).

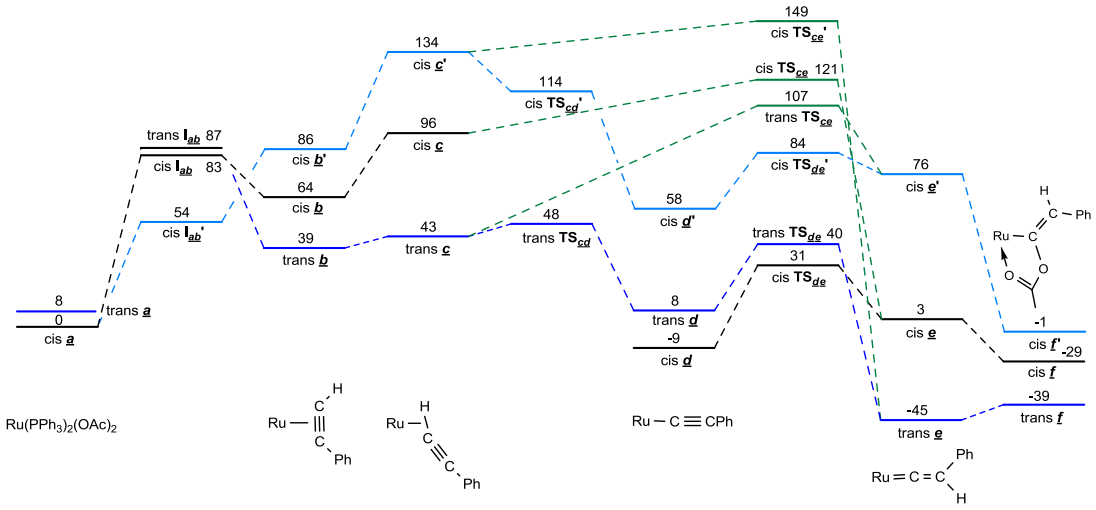

Figure 4.3.2.1: Potential Energy Surface calculated for model system (**ii**).

The initial step involving the creation of a vacant site again proceeds *via* the $\mathbf{I}_{ab}$ intermediate, and as for model (**i**), the *cis*'-isomer in which a vacant site is generated *trans* to a phosphine ligand is lower in the energy. The energies of ***b*** are higher than observed for the model (**i**) system; however this may be attributed to the differing steric or electronic effects of the larger ligand substituents.

From this point the various mechanistic pathways may be considered once more. The stationary points involved in the oxidative addition pathway are not shown on Figure 4.3.2.1 as the energy of the ground state for the hydride-acetylide complex ***d*H** was calculated to be very high (151 kJ mol^{-1}). Consequently, this pathway was

not considered further. The concerted 1,2-hydrogen shift pathway *via* $\mathbf{TS}_{\underline{\boldsymbol{be}}}$ is also excluded from the above Figure 4.3.2.1 due to the extremely high energy of these transition states; *cis*-$\mathbf{TS}_{\underline{\boldsymbol{be}}}$ at 291 kJ mol^{-1}, *cis*'-$\mathbf{TS}_{\underline{\boldsymbol{be}}}$ at 280 kJ mol^{-1} and *trans*-$\mathbf{TS}_{\underline{\boldsymbol{be}}}$ at 235 kJ mol^{-1}. It is therefore highly unlikely that either of these mechanisms operate at the low temperatures demonstrated experimentally. The energies of the structures calculated for the concerted 1,2-hydrogen shift pathway proceeding from the σ-complex ***c*** *via* $\mathbf{TS}_{\underline{\boldsymbol{ce}}}$ are low enough in energy to be considered feasible, however as for model (**i**) the lowest energy pathway is one which proceeds with the assistance of an acetate ligand.

In the acetate-assisted pathway, deprotonation of the alkyne was once more considered from both the alkyne complex ***b*** and the σ-complex ***c***. However optimised geometries of $\mathbf{TS}_{\underline{\boldsymbol{bd}}}$ could not be located; in all instances convergence to ***d*** was observed regardless of the choice of convergence and optimisation parameters. This was also found to be the case for *cis*-$\mathbf{TS}_{\underline{\boldsymbol{cd}}}$; however the isomers *cis*'-$\mathbf{TS}_{\underline{\boldsymbol{cd}}}$ and *trans*-$\mathbf{TS}_{\underline{\boldsymbol{cd}}}$ were located. The reprotonation of the acetylide by the coordinated acetic acid ligand then proceeds *via* $\mathbf{TS}_{\underline{\boldsymbol{de}}}$, which can be calculated for all three isomers, despite the difficulty in accessing *cis*-***d***. The ultimate generation of the vinylidene complex ***e*** as the thermodynamic product demonstrates the worth of the extra computational effort, as these results appear to provide a more accurate description of reality. The metallo-enolester complex *cis*'-***f*** is the computational analogue to the experimentally observed *cis*-**12**, where the vinyl ligand is situated *trans* to a phosphine ligand and is calculated to be 44 kJ mol^{-1} higher in energy than ***e***. It has also been determined that the *E*-isomer of *cis*'-***f*** is 18 kJ mol^{-1} lower in energy than the *Z*-isomer, suggesting that this form is observed experimentally. The energy of *trans*-***f*** is not significantly higher than *trans*-***e***; the difference is only 6 kJ mol^{-1}. This feature will become important in Chapter 6, and will be discussed further in Section 6.6.

Across the PES, the *trans*-manifold of the acetate-assisted pathway of the model (**ii**) system is generally the lowest in energy whereas for the model (**i**) system, the *cis*-manifold is generally lower in energy. In *trans*-***c***, there is evidence of a stabilising hydrogen bonding effect between the uncoordinated oxygen atom of the κ^1-OAc ligand and the alkyne proton, which could not be found in the *cis* or *cis*'-manifolds. The molecular structures of these three isomers are shown in Figure

4.3.2.2. Attempts to model structures in which such a hydrogen bond exists for these two manifolds resulted in the convergence of the starting geometries to ***d***. The general stabilisation of the *trans*-manifold across the PES may be due to the steric preference to have the two PPh_3 ligands in this position.

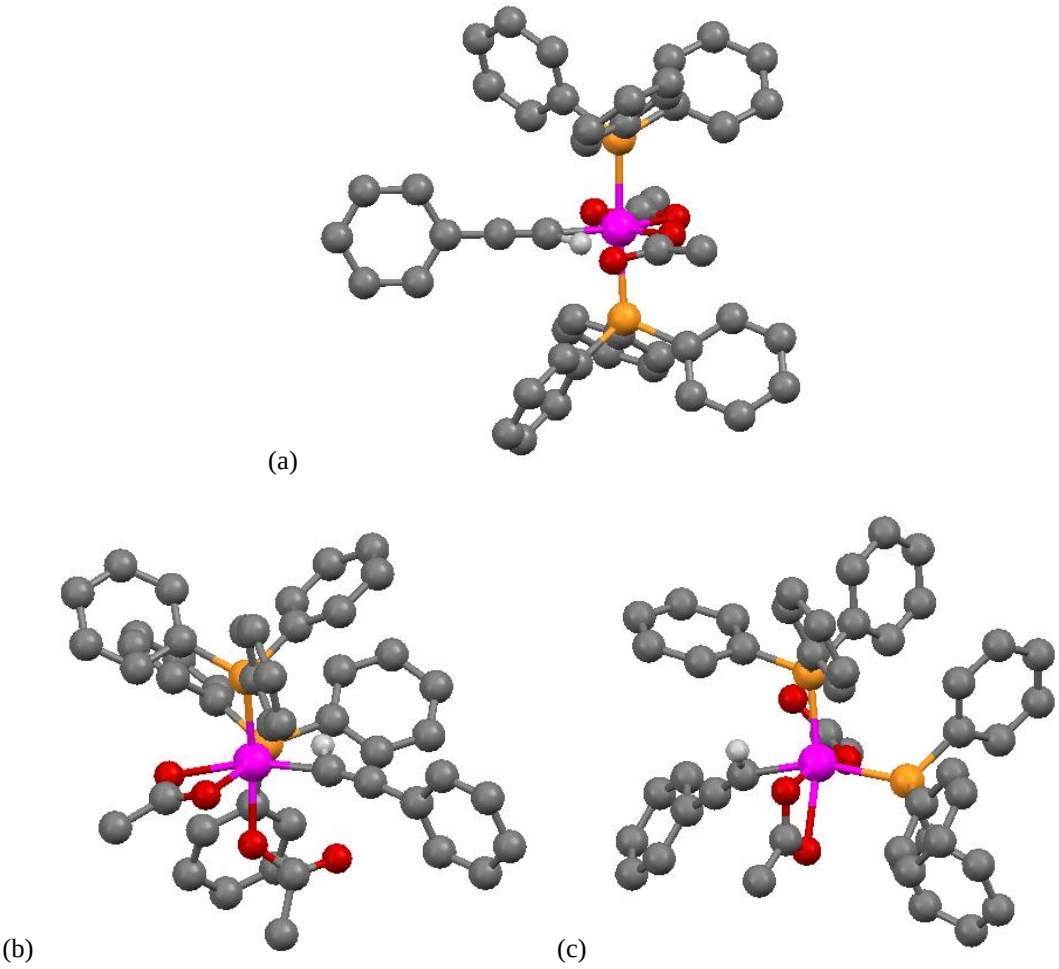

(a) (b) (c)

Figure 4.3.2.2: (a) *trans*-**c**; (b) *cis*-**c**; (c) *cis*'-**c**.

It is clear that the acetate-assisted pathway provides the lowest energy route for the alkyne-to-vinylidene tautomerisation to take place at this particular metal centre, as shown by both model systems investigated. Specifically, model (**ii**) has demonstrated that the *trans*-manifold is the most likely route followed at the low temperatures used. However, the position at which the *cis*/*trans* isomerisation occurs is still uncertain as there is no obvious point on the PES at which this takes place. The observation of the metallo-enolester *cis*-**12**/*cis*'-***f*** at 245 K also contradicts the theoretical findings that the *trans*-manifold of the acetate-assisted pathway is operating as it is lowest in energy.

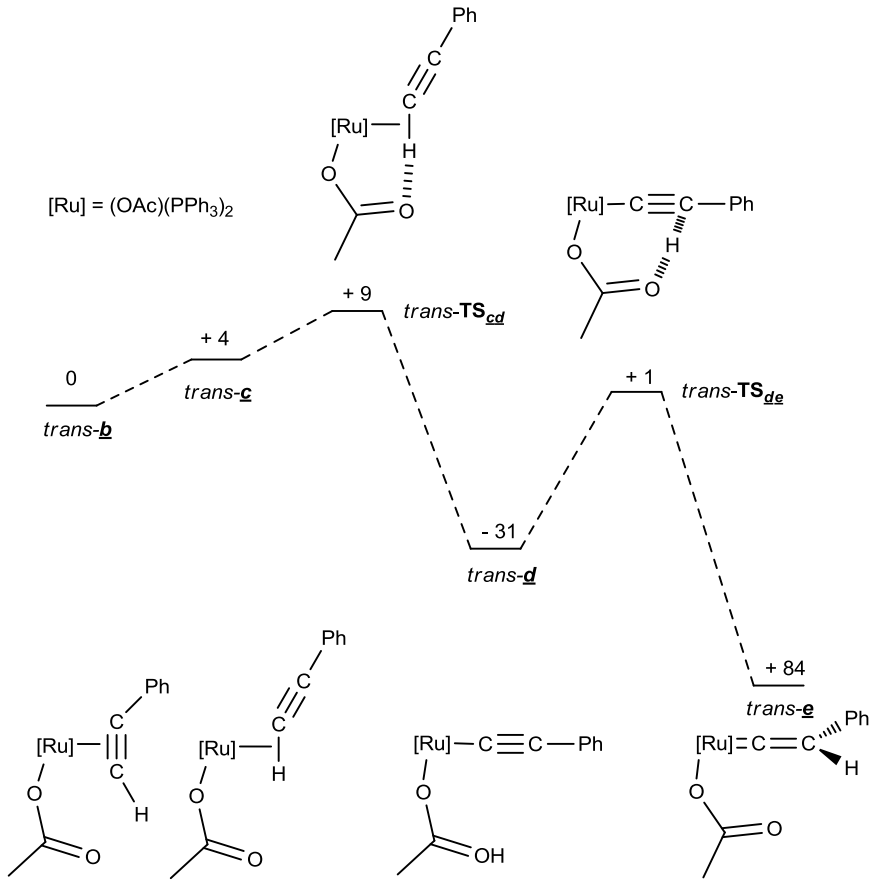

Figure 4.3.2.3: *trans*-manifold of the model (**ii**) system, all energies relative to *trans*-***b***.

This acetate-mediated isomerisation pathway is distinct from the CMD/AMLA processes, which involve only the deprotonation of a ligand by acetate or a related intramolecular base. In this system the acetate ligand is able to act as both Lewis acid and base, essentially as a proton shuttle. Consequently, this process has been termed a **L**igand-**A**ssisted **P**roton **S**huttle (LAPS) to reflect the dual nature of the acetate ligand. It was also proposed in Chapter 3 that the acetate ligand has a part to play in the formation of the acetylide complexes **6** and **7**. The mechanism by which this process occurs has also been probed both experimentally and computationally.

4.4: Experimental investigation into the mechanism of the formation of 6 and 7

In Section 3.5, the synthesis and characterisation of the acetylide complexes **6** ([Ru(C≡CPh)(κ^2-OAc)(CO)(PPh_3)$_2$]) and **7** ([Ru(C≡CPh)(κ^2-OAc)(NO)(PPh_3)$_2$]BF_4) was discussed. A general procedure was found in which two equivalents of HC≡CPh was added to a solution of **4** ([Ru(κ^1-OAc)(κ^2-OAc)(CO)(PPh_3)$_2$]) or **5** ([Ru(κ^1-OAc)(κ^2-OAc)(NO)(PPh_3)$_2$]BF_4) in DCM which was then heated at 50 °C for 2 days. After this time, two products were obtained; the organometallic complexes **6** or **7** and an organic product. A crucial difference between the formation of these acetylide complexes arises in the form of the organic product; for the CO-complex **4** the product arising from *anti*-Markovnikov addition (*Z*)-*β*-styryl acetate is observed whereas for the NO-complex **5**, the Markovnikov product 1-phenylvinyl acetate is obtained.

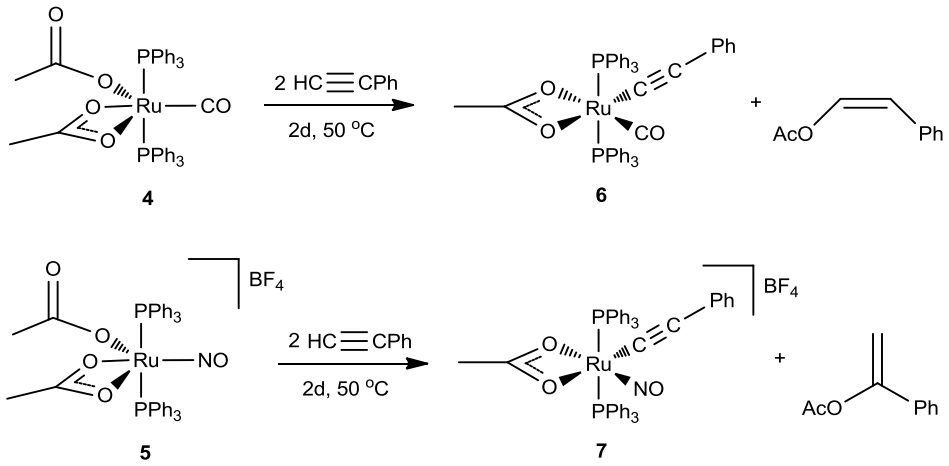

Figure 4.4.1: Formation of complexes **6** and **7**.

Stoichiometric reactions were monitored by NMR and showed that a minimum of two equivalents of HC≡CPh are required for the complete formation of the acetylide complexes. These also showed that acetic acid is observed as a transient species over the course of the reaction; it is detected soon after addition of the alkyne along with the initial formation of the acetylide complex and begins to decay once the formation of the organic product begins. In light of the role the acetate ligand plays in the LAPS mechanism discussed above, a route was proposed whereby the acetate ligand acts again as a proton shuttle. The mechanism suggested in Chapter 3 for the formation of the acetylide complex **6** and (*Z*)-*β*-styryl acetate is shown in Figure 4.4.2 below:

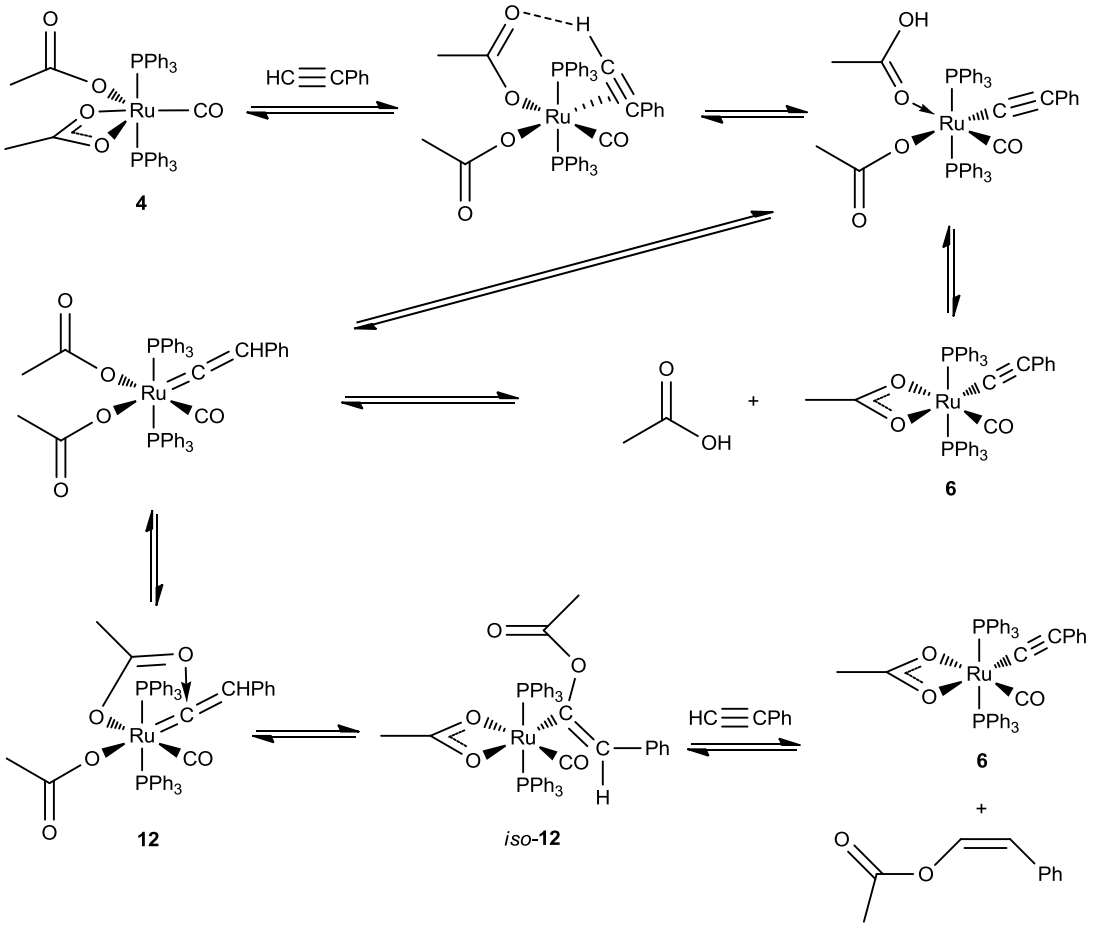

Figure 4.4.2: Proposed mechanism for the reaction of **4** with two HC≡CPh.

The initial coordination of the alkyne is enabled by the fluxional nature of the acetate ligands, which both become monodentate to create a vacant site. One of the uncoordinated oxygen atoms of an acetate ligand then deprotonates the alkyne and dissociates as acetic acid. The other acetate ligand switches to a chelate coordination mode to form the 18-electron complex **6**. However, the acetic acid may then reprotonate the acetylide at the nucleophilic C_β to generate a vinylidene complex. Nucleophilic attack of an uncoordinated oxygen atom of one κ^1-OAc ligand onto the C_α of the vinylidene results in the formation of the intermediate complex (*iso*-**12**) which contains the coordinated form of (*Z*)-*β*-styryl acetate. Protonation of this ligand by the second molecule of HC≡CPh results in its liberation and the regeneration of the acetylide complex **6**.

Whilst monitoring the reaction of **4** with 1.7 equivalents of $H^{13}C{\equiv}CPh$ (see section 3.5.1) by NMR spectroscopy, evidence for the presence of an additional transient organometallic component (*iso*-**12**) was detected. In addition to the doublet resonance due to **6**, another doublet resonance in the ^{31}P NMR spectrum was observed after one day at δ_P 34.2 ($^2J_{CP}$ = 13.3 Hz) which is thought to be associated with a triplet resonance in the ^{13}C NMR spectrum at δ_C 188.2 ($^2J_{CP}$ = 13.1 Hz). In the ^1H NMR spectrum, a resonance at δ_H 5.19 (dt, $^2J_{CH}$ = 11.4 Hz, $^4J_{HP}$ = 1.8 Hz) appears to correspond to H_A, whilst two distinct equivalent singlet resonances can be observed at δ_H 1.15 and 1.30, which have a relative integration of three with respect to the single proton H_A. These are attributed to the two CH_3 groups of the different acetate group environments. At first glance, these spectroscopic features may fit either complex (**12**) or (*iso*-**12**) as shown in Figure 4.4.2. However, the NMR features of complex **12** are quite different to those observed for this complex. For example, the corresponding resonance for H_A of **12** is observed at δ_H 6.25 (t, $^4J_{HP}$ = 2.8 Hz) in the ^1H NMR spectrum whilst in the ^{31}P NMR spectrum a singlet at δ_P 30.7 is observed. The C_α of the vinyl ligand is observed as a triplet at δ_C 193.2 ($^2J_{PC}$ = 17.8 Hz); consequently it is proposed that this observed intermediate has the structure shown for (*iso*-**12**). A full discussion of all characterising features of complex **12** is provided in Section 6.2.

Literature precedence for the second part of the mechanism proposed in Figure 4.4.2 exists;[35-38] in 1994 Esteruelas[35] performed a number of experiments involving the addition of acids to the P^iPr_3 analogue of **6**. A scheme depicting the reactivity he observed is shown in Figure 4.4.3 below. He demonstrated that the addition of HBF_4 to a solution of **4E** in acetone resulted in the formation of the vinyl ester complex **4G**. He postulated that this process occurred by the initial protonation of the acetylide ligand to give the vinylidene complex **4H**, which then underwent a nucleophilic attack of the acetate at C_α. Addition of another equivalent of acetic acid to **4G** resulted in the formation of the di-carbonyl complex **4H** and (*Z*)-*β*-styryl acetate. It is proposed that the additional carbonyl ligand of **4H** originates from the decarbonylation of acetic acid.[35,38] Esteruelas was able to isolate and structurally characterise the vinyl ester complex **4G**, which is analogous to complex **12**.

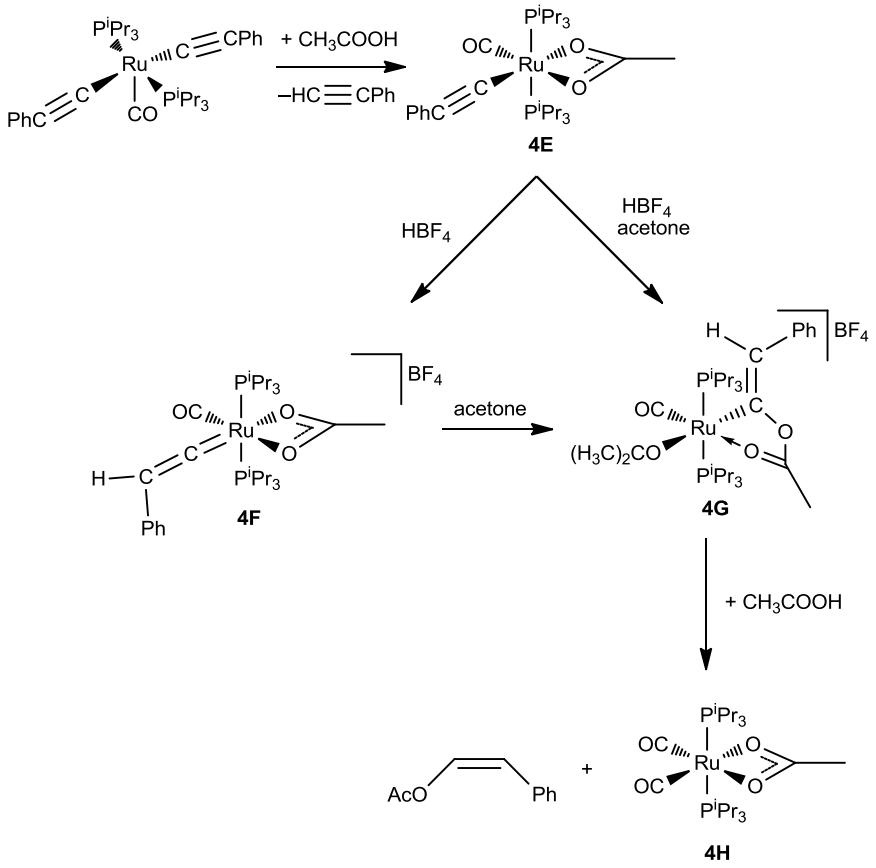

Figure 4.4.3: Reaction scheme proposed by Esteruelas for the addition of HBF_4 to **4E**.

The formation of 1-phenylvinyl acetate in the synthesis of **7** from **5** suggests that a different mechanism is operating. In Section 3.4, an alternative mechanism was proposed, also shown in Figure 4.4.4 below. The formation of geminal alkenes from terminal alkynes is thought to proceed *via* η^2-alkyne rather than vinylidene intermediates, as nucleophilic attack occurs at the more substituted carbon in a Markovnikov addition.[39-41] It is therefore suggested that the mechanism initially proceeds in the same manner as for the formation of **6**. Reprotonation of the acetylide complex **7** by acetic acid generates a vinylidene complex, which exists in equilibrium with the η^2-alkyne. The uncoordinated oxygen of a κ^1-OAc ligand then attacks the substituted alkyne carbon atom to generate the coordinated form of 1-phenylvinyl acetate. This is liberated upon protonation by the second equivalent of HC≡CPh which simultaneously regenerates **7**.

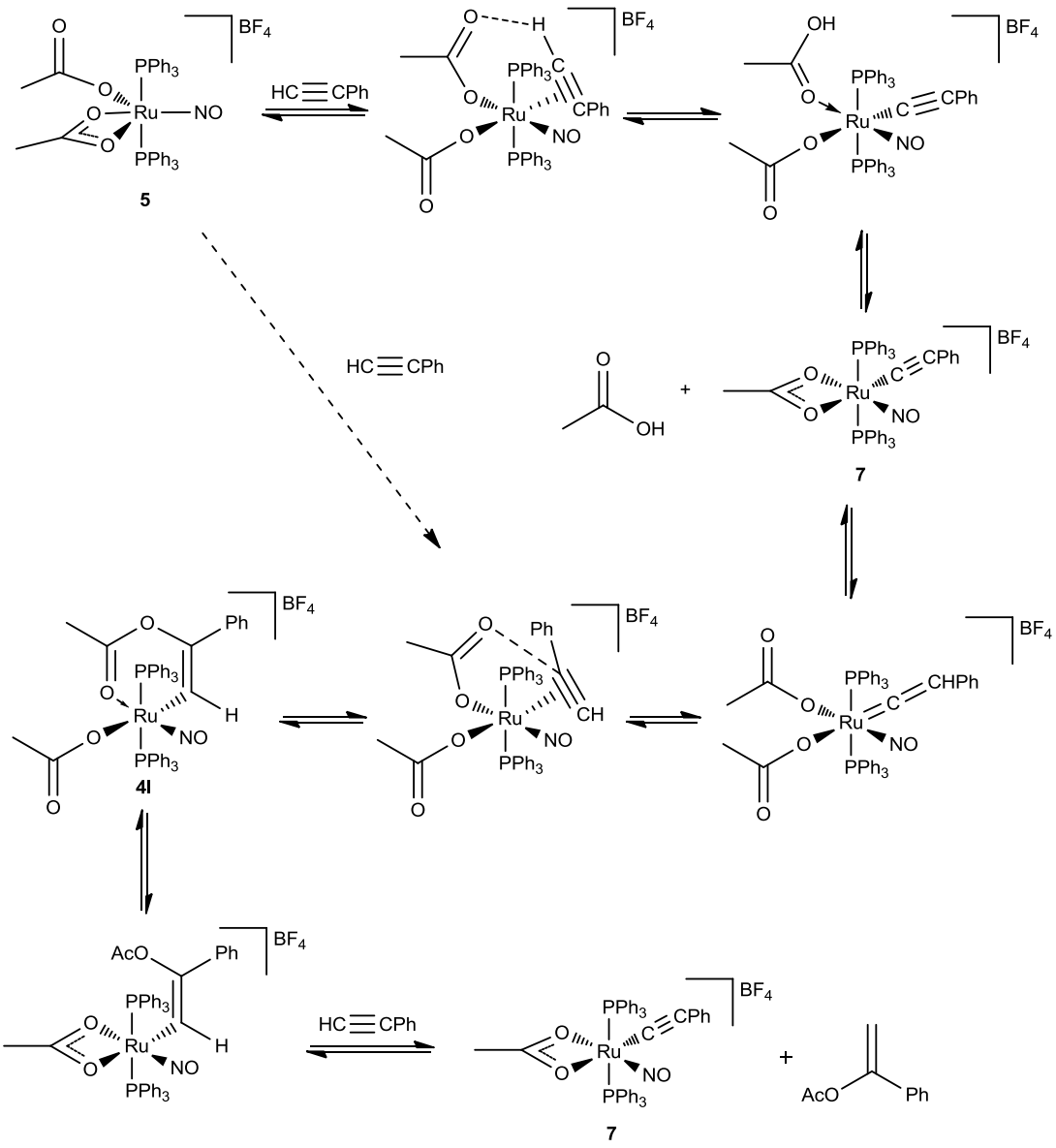

Figure 4.4.4: Proposed mechanism for the reaction of **5** with two HC≡CPh.

A feasible alternative exists where **7** and 1-phenylvinyl acetate form *via* the shorter pathway indicated by the dashed arrow, which bypasses the evolution of acetic acid. However, the NMR evidence detailed in Section 3.4 indicates that acetic acid is observed prior to the formation of the alkene. An explanation for this may be that the two pathways operate at different rates. Unfortunately, no experimental evidence could be detected for any intermediates. Computational evidence has been discovered for the formation of a complex analogous to **4I**, which will be discussed further in Section 4.5.

These mechanisms have been suggested based on the experimental evidence and knowledge of the LAPS and AMLA/CMD processes. Further evidence was sought from a computational investigation. Unfortunately, the structure of complex **7** obtained by structural characterisation could not be successfully modelled computationally. Complex **7** may potentially exist in two forms in which the NO ligand is either linear or bent, which are shown in Figure 4.4.5. Only the linear form has been crystallographically characterised, however the IR spectrum recorded in DCM hints at some interconversion. It is thought that the PES for the interconversion of these two isomers is very flat, so ground state structures could not be located. Consequently, a DFT study was pursued only for the CO-complex **4**.

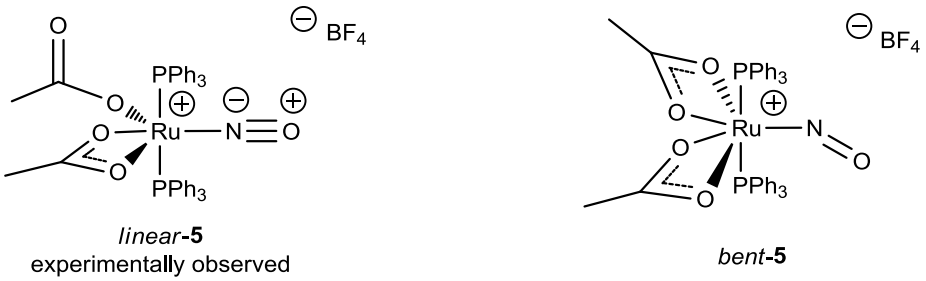

Figure 4.4.5: Two isomers of complex **5**, in which the NO ligand may be either linear or bent.

4.5: Computational investigation into the formation of 6.

A DFT investigation into the mechanism of formation of the acetylide complex **6** was conducted by David Johnson. The PES for the system mapped is shown in Figure 4.5.1 below. The numbering system used is similar to that established for the two LAPS models discussed in Section 4.3; the computational analogue of acetylide complex **6** is referred to as ***d*neg**. The PES calculated for this process was simpler than those modelled for the LAPS process; only the *trans*-manifold required consideration. A comparison of the two model systems used in the previous investigation demonstrated the importance of using the same ligand substituents as those used experimentally. Consequently, the structures calculated did not contain any ligand approximations, although this required longer computing time. All Gibbs energies are again provided in kJ mol^{-1} relative to **4**/***a*** + HC≡CPh. As for the model (**i**) and model (**ii**) systems calculated in Section 4.3, solvation effects were not considered.

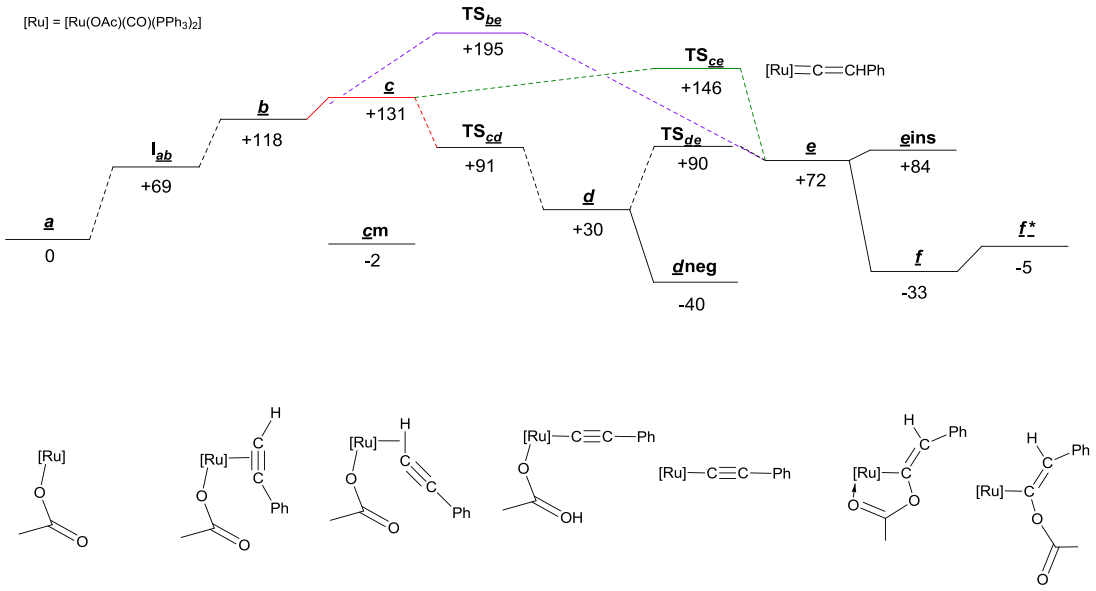

Figure 4.5.1: Potential Energy Surface calculated for the formation of acetylide complex **6**/***d*neg**.

As for the LAPS process, the initial step utilises the fluxional nature of the acetate ligands to create a vacant site for alkyne coordination which proceeds *via* the intermediate complex $\mathbf{I}_{\underline{ab}}$. Once the η^2-alkyne complex ***b*** has formed, the alkyne may slip into a σ-coordination mode to give ***c***. An alternative isomer of ***c***, ***c*m** was also located as a local minimum on the PES. This structure incorporates an acetate ligand that has cyclised onto the C_β atom of the alkyne, analogous to that postulated as an intermediate **4I** in the formation of complex **7** and 1-phenylvinyl acetate. Complex ***c*m** is found to be 133 kJ mol^{-1} lower in energy than ***c***, so it would initially appear that the formation of the *anti*-Markovnikov product (*Z*)-*β*-styryl acetate is unfavourable. However, what has not been determined is the energy barrier to the formation of this complex. It could therefore be suggested that the energy barrier to the formation of the *anti*-Markovnikov product is lower for complex **6**, but higher for complex **7**.

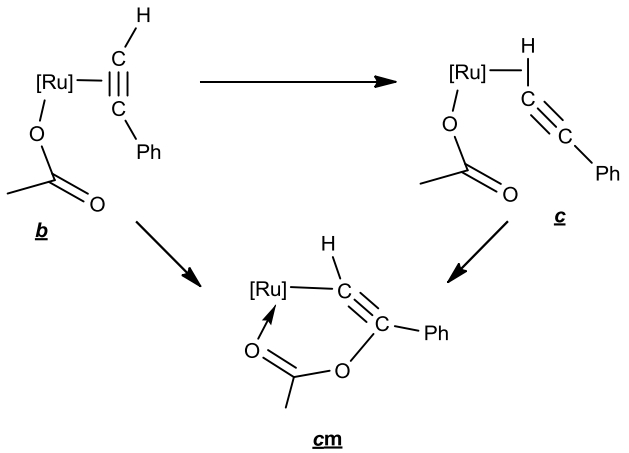

Figure 4.5.2: Proposed formation of ***c*m** from ***b*** and ***c***.

From this point on the PES, the deprotonation of the alkyne by a κ^1-OAc ligand occurs to generate the acetylide complex ***d*** in which the acetic acid ligand is still coordinated. This stationary point on the PES precedes a branching position between two processes; either the acetic acid may dissociate from ***d***, resulting in the experimentally observed complex **6**/***d*neg** (also the thermodynamic product) or the acetic acid may reprotonate the acetylide complex to give the vinylidene complex ***e***.

Alternative pathways for the formation of the vinylidene complex ***e*** were also considered. The oxidative addition pathway is not considered for this system as complexes ***b*** and ***c*** are coordinatively saturated so a hydride complex is unlikely to form. The concerted 1,2-hydrogen shift pathway may occur from either the alkyne complex ***b*** or the σ-complex ***c*** *via* the transition states $\mathbf{TS}_{\boldsymbol{be}}$ and $\mathbf{TS}_{\boldsymbol{ce}}$ respectively. However, the energy barriers to these pathways are significantly higher (195 kJ mol^{-1} and 146 kJ mol^{-1} respectively) than the barrier to the LAPS pathway for this system, which essentially proceeds downhill from complex ***c***.

As previously noted for **2a**, the vinylidene ligand may undergo nucleophilic attack at the C_α by an uncoordinated oxygen atom of a κ^1-OAc ligand. In this pathway this results in the metallo-enolester complex ***f***, which is also analogous to complex **12**. An exchange in the coordination modes of the two acetate ligands results in the isomer ***f****, which is thought to be a kinetic product also observed experimentally (*iso*-**12**). Interestingly, the PES mapped for this system shows that ***f*** is 28 kJ mol^{-1} lower in energy than ***f****. The protonation of the styryl acetate ligand by the second molecule of HC≡CPh would then result in the regeneration of the acetylide complex ***d*neg**/**6**. The relative energy of ***d*neg** and (*Z*)-*β*-styryl acetate is –

195 kJ mol^{-1}, indicating that these are the thermodynamic products. The initial formation of ***d*neg**/**6** and acetic acid is therefore due to kinetic effects.

Another structure located on the PES showed that attack of an uncoordinated oxygen atom of an acetate ligand may also occur onto the CO ligand (***e*ins**). This complex is accessed *via* the vinylidene complex ***e***. No experimental evidence has been detected for such a complex; however it is interesting to compare the alternative points of intramolecular attack of the acetate ligand. The complex ***e*ins** is calculated to be 117 kJ mol^{-1} higher in energy than ***f***, and 89 kJ mol^{-1} higher in energy than ***f****. This suggests that the vinylidene C_α is more electrophilic than the carbon atom of the CO ligand.

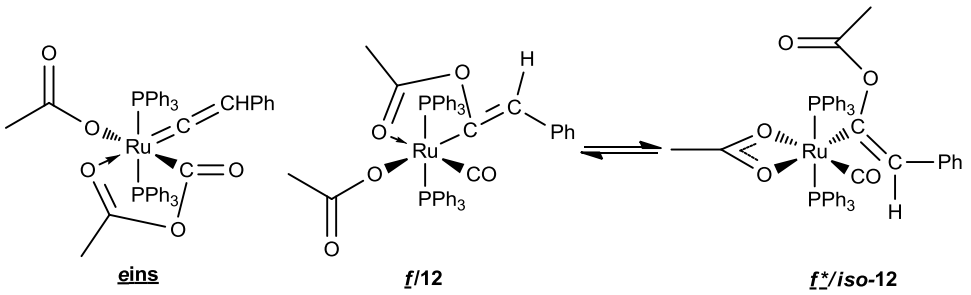

Figure 4.5.3: The isomeric forms of the metallo-enolester complex ***f***.

A significant assumption this model has made is in the intramolecular attack of coordinated acetic acid in the formation of the intermediate ***e*** complex. An alternative pathway may involve an intermolecular reaction, as uncoordinated acetic acid is observed in the ^{1}H NMR spectrum. However, this reaction could not be so easily modelled due to basis set superposition error.

This model demonstrates once more that the acetate ligand plays an integral part in the formation of the acetylide complexes **6** and **7**, and in the formation of the Markovnikov and anti-Markovnikov products 1-phenylvinyl acetate and (*Z*)-*β*-styryl acetate respectively. It suggests the mechanism proposed in Figure 4.4.2 and explains why two equivalents of HC≡CPh are necessary. It is again acting as a proton shuttle in the formation of the vinylidene complex ***e***, an essential part in the formation of (*Z*)-*β*-styryl acetate and regeneration of the acetylide complex ***d*neg**/**6**.

4.6: Conclusions

In this chapter, the hemi-labile nature of the acetate ligand has been highlighted as a significant advantage in the reactivity of these ruthenium complexes. Computational methods have been crucial to understanding the precise role of the acetate ligand when experimental efforts have been exhausted. The importance of undertaking a full DFT study involving the 'real' ligand substituents used experimentally was also emphasised.

It has been shown that the formation of the vinylidene complex **2a** is rapid, even at 255 K, so a comprehensive DFT study was undertaken. This demonstrated that of all the pathways known to operate for alkyne-to-vinylidene isomerisation at a transition metal centre, the route in which the acetate ligand acted as a proton shuttle was lowest in energy. This isomerisation pathway (**IV**) has been termed a **L**igand-**A**ssisted **P**roton **S**huttle (LAPS) and bears some resemblance to the AMLA/CMD pathways proposed for the activation of C-H bonds. The crucial difference between these pathways is the reprotonation step in the LAPS mechanism. It is therefore proposed that the rapid nature of vinylidene formation in complexes **2a-d** is due to the fluxional nature of the acetate ligand and its inherent ability to act as both a Lewis acid and base.

The assistance of an acetate ligand was also proposed in the formation of the acetylide complexes **6** and **7**. Unfortunately, the ground state of complex **7** could not be located so a computational investigation could not be conducted into this system. However, the formation of complex **6** was shown to proceed again *via* a LAPS-type (or AMLA/CMD-type) mechanism in the formation of an intermediate vinylidene complex (***e***). This has been termed a CO-LAPS mechanism (**V**). The intramolecular attack of the acetate ligand onto the C_α and subsequent liberation of (*Z*)-*β*-styryl acetate results in the regeneration of complex **6**. The relatively low energy barriers calculated for this second stage of the mechanism may explain why two equivalents of HC≡CPh are required for the reaction to go to completion. Alternatively, the second equivalent may be acting as a base in order to sequester the acetic acid formed.

The ability of acetate ligands to alter their coordination mode and behave as both Lewis acid and base will also become relevant in the decarbonylation of propargylic alcohols, which will be discussed in Chapter 6.

4.7: References

1 Bruce, M. I. *Chem. Rev*. **1991**, *91*, 197.

2 Zhu, J.; Lin, Z. Theoretical Aspects of Metal Vinylidene and Allenylidene Complexes (Chapter 4) *Metal Vinylidenes and Allenylidenes in Catalysis: From Reactivity to Applications in Synthesis*, (Bruneau, C., Dixneuf, P. H., Eds.) **2008**, Wiley VCH: Weinheim, Germany.

3 Lynam, J. M. *Chem. Eur J.* **2010**, *16*, 8238.

4 Wakatsuki, Y. *J. Organometal. Chem*. **2004**, *689*, 4092.

5 Jensen, F. *Introduction to Computational Chemistry* (2nd Ed.) **2007**, Wiley.

6 Olivan, M.; Clot, E.; Eisenstein, O.; Caulton, K. G. *Organometallics* **1998**, *17*, 3091.

7 Johnson, D. G.; Lynam, J. M.; Slattery, J. M.; Welby, C. E. *Dalton Trans*. **2010**, *39*, 10432.

8 Silvestre, J.; Hoffmann, R. *Helv. Chim. Acta* **1985**, *68*, 1461.

9 Wakatsuki, Y.; Koga, N.; Yamazaki, H.; Morokumal, K. *J. Am. Chem. Soc.* **1994**, *116*, 8105.

10 Cadierno, V.; Gamasa, M. P.; Gimeno, J. Pérez-Carreño, E.; García-Granda, S. *Organometallics* **1999**, *18*, 2821.

11 Cadierno, V.; Gamasa, M. P.; Gimeno, J.; González-Bernardo, C.; Pérez-Carreño, E.; García-Granda, S. *Organometallics* **2001**, *20*, 5177.

12 De Angelis, F.; Sgamellotti, A.; Re, N. *Organometallics* **2002**, *21*, 2715.

13 De Angelis, F.; Sgamellotti, A.; Re, N. *Organometallics* **2002**, *21*, 5944.

14 Bassetti, M.; Cadierno, V.; Gimeno, J.; Pasquini, C. *Organometallics* **2008**, *27*, 5009.

15 Nesmeyanov, A. N.; Aleksandrov, G. G; Antonova, A. B.; Anisimov, K. N.; Kolobova, N. E.; Struchkov, Yu. T. *J.Organomet. Chem.* **1976**, *110*, C36.

16 Antonova, A. B.; Kolobova, N. E.; Petrovsky, P. V.; Lokshin, B. V.; Obezyuk, N. S. *J. Organomet. Chem.* **1977**, *137*, 55.

17 Werner, H.; Baum, M.; Schneider, D.; Windmüller, B. *Organometallics* **1994**, *13*, 1089.

18 Wakatsuki, Y.; Koga, N.; Werner, H.; Morokuma, K. *J. Am. Chem. Soc.* **1997**, *119*, 360.

19 Grotjahn, D. B.; Zeng, X.; Coosky, A. L. *J. Am. Chem. Soc.* **2006**, *128*, 2798.

20 Grotjahn, D. B.; Zeng, X.; Cooksy, A. L.; Kassel, W. S.; DiPasquale, A. G.; Zakharov, L. N.; Rheingold, A. L. *Organometallics* **2007**, *26*, 3385.

21 De Angelis, F.; Sgamellotti, A.; Re, N. *Organometallics* **2007**, *26*, 5285

22 Vastine, B. A.; Hall, M. B. *Organometallics* **2008**, *27*, 4325.

23 Cowley, M. J.; Lynam, J. M.; Slattery, J. M. *Dalton Trans.* **2008**, 4552.

24 De Angelis, F.; Sgamellotti, A.; Re, N. *Dalton Trans.,* **2004**, 3225.

25 Tokunaga, M.; Suzuki,T.; Koga, N.; Fukushima, T.;Horiuchi, A.; Wakatsuki, Y. *J. Am. Chem. Soc.* **2001**, *123*, 11917.

26 Grotjahn,D. B.; Miranda-Soto, V.; Kragulj, E. J.; Lev, D. A.; Erdogan, G.; Zeng, X.; Cooksy, A. L. *J. Am. Chem. Soc*. **2008**, *130*, 20.

27 Bustelo, E.; Jiménez-Tenorio, M.; Puerta, M. C.; Valerga, P. *Organometallics* **1999**, *18*, 4563.

28 Bustelo, E.; Jiménez-Tenorio, M.; Puerta, M. C.; Valerga, P. *Organometallics* **1999**, *18*, 950.

29 Aneetha, H.; Jiménez-Tenorio, M.; Puerta, M. C.; Valerga, P.; Mereiter, K. *Organometallics* **2003**, *22*, 2001.

30 Lafrance, M.; Rowley, C. N.; Woo, T. K.; Fagnou, K. *J. Am. Chem. Soc.* **2006**, *128*, 8754.

31 Davies, D. L.; Donald, S. M. A.; Macgregor, S. A.*J. Am. Chem. Soc.* **2005**, *127*, 13754.

32 Lapointe, D.; Fagnou, K. *Chem. Lett*. **2010**, *39*, 1118.

33 Boutadla, Y.; Davies, D. L.; Macgregor, S. A.; Poblador-Bahamonde, A. I. *Dalton Trans.*, **2009**, 5820.

34 Adapted from Davies, D. L.; Macgregor, S. A.; Poblador-Bahamonde, A. I. *Dalton Trans.* **2010**, 10520.

35 Esteruelas, M. A., Lahoz, F. J., López, A. M., Oñate, Oro, L. A., *Organometallics* **1994**, *13*, 1669.

36 Shaffer, A.; Chen, C-L.; Beatty, A. M.; Valente, E. J.; Schanz, H-J. *J. Organomet. Chem.* **2007**, *692*, 5221.

37 Daniel, T.; Mahr, N.; Braun, T.; Werner, H. *Organometallics*, **1993**, *12*, 1475.

38 Ropp, J. *J. Am. Chem. Soc*. **1960**, *82*, 842.

39 Mitsudo, T.; Hori, Y.; Yamazaki, Y.; Watanabe, Y. *J. Org. Chem.* **1987**, *52*, 2230.

40 Bruneau, C. *Anti*-Markovnikov Additions of *O*-, *N*-, *P*-Nucleophiles to Triple Bonds with Ruthenium Catalysts (Chapter 10) *Metal Vinylidenes and Allenylidenes in Catalysis: From Reactivity to Applications in Synthesis*, (Bruneau, C., Dixneuf, P. H., Eds.) **2008**, Wiley VCH: Weinheim, Germany.

41 Alonso, F.; Beletskaya, I. P.; Yus, M. *Chem. Rev.* **2004**, *104* , 3079.

42 Lynam, J. M.; Welby, C. E.; Whitwood, A. C. *Organometallics* **2009**, *28*, 1320.

43 Ahlrichs, R.; Baer, M.; Haeser, M.; Horn, H.; Koelmel, C. *Chem. Phys. Lett.*, **1989**, *162*, 165.

44 Arnim M. V.; Ahlrichs, R. *J. Chem. Phys.* **1999**, *111*, 9183.

45 Császár, P.; Pulay, P. *J. Mol. Struct.*, **1984**, *114*, 31.

46 Koga, T.; Kobayashi, H. *J. Chem. Phys.* **1985**, *82*, 1437.

47 Pulay, P. *Chem. Phys. Lett.* **1980**, *73*, 393.

48 Deglmann, P.; May, K.; Furche, F.; Ahlrichs, R. *RI-J Implementation*, **2004**, *384*, 103.

49 Deglmann, P.; Furche, F.; Ahlrichs, R. *Chem. Phys. Lett.* **2002**, *362*, 511.

50 Deglmann, P.; Furche, F. *J. Chem. Phys.* **2002**, *117*, 9535.

51 Treutler, O.; Ahlrichs, R. *J. Chem. Phys.* **1995**, *102*, 346.

52 Eichkorn, K.; Treutler, O.; Oehm, H.; Haeser, M.; Ahlrichs, R. *Chem. Phys. Lett*. **1995**, 240, 283.

53 Eichkorn, K.; Weigend, F.; Treutler, O.; Ahlrichs, R. *Theo. Chem. Acc*. **1997**, 97, 119.

54 Weigend, F. *Phys. Chem. Chem. Phys.* **2006**, *8*, 1057.

4.8: Experimental

General:

All experimental procedures were performed under an atmosphere of dinitrogen or argon using standard Schlenk Line and Glove Box techniques. CH_2Cl_2 and pentane were purified with the aid of an Innovative Technologies anhydrous solvent engineering system. ^{t}BuOH was degassed by purging with dinitrogen prior to use. The CD_2Cl_2 used for NMR experiments was dried over CaH_2 and degassed with three freeze-pump-thaw cycles. The solvent was then vacuum transferred into NMR tubes fitted with PTFE Young's taps. NMR spectra were acquired on a Bruker AVANCE 500 (Operating Frequencies ^{1}H 500.23 MHz, ^{31}P 202.50 MHz, ^{13}C 125.77 MHz). ^{31}P and ^{13}C spectra were recorded with proton decoupling. *cis*-Ru(κ^2-OAc)$_2$(PPh_3)$_2$ **1**[42] was prepared by the published literature methods. HC≡CPh (Acros Organics) and purified by passage through an alumina column and degassed by three freeze-pump-thaw cycles. H^{13}C≡CPh (Sigma-Aldrich) was used as supplied without any purification.

Key to NMR abbreviations:

s (singlet); br s (broad singlet); d (doublet); dd (doublet of doublets); ad (apparent doublet); t (triplet); dt (doublet of triplets); tt (triplet of triplets); at (apparent triplet); q (quartet); aq (apparent quartet); qn (quintet), aqn (apparent quintet); sp (septet); asp (apparent septet); m (multiplet)

4.8.1: Synthesis of [Ru(κ^1-OAc)(κ^2-OAc)(=^{13}C=CHPh)(PPh$_3$)$_2$]; ^{13}C-2a

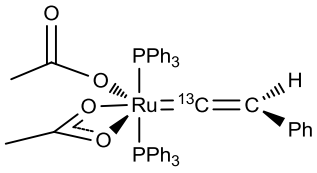

^{13}C-2a

H^{13}C≡CPh (22.2 μL, 0.202 mmol) was added to a Schlenk vessel containing a solution of **1** (0.15 g, 0.202 mmol) in 10 mL CH_2Cl_2. After stirring for 1 hour the solution had changed from a red suspension to a dark pink solution. The volume of the solution was partially reduced *in vacuo* and the product precipitated as a pink powder by addition of pentane. The powder was filtered and washed with two further 15 mL portions of pentane and dried *in vacuo*. Yield 0.10 g (58.5 %)

NMR Spectra CD_2Cl_2:

^{1}H δ_H 0.87 (s, 6H, C*H*$_3$COO), 5.20 (aq, $^4J_{HP}$ = 3.6 Hz, $^2J_{HC}$ = 3.1 Hz, 1H, ^{13}C=C*H*), 6.83 (d, 7.5 Hz, 2H, *H*$_2$-CH*Ph*), 6.89 (at, 7.4 Hz, 1H, *H*$_4$-CH*Ph*), 7.10 (at, 7.7 Hz, 2H, *H*$_3$-CH*Ph*), 7.33 (at, 7.7 Hz, 12H, *H*$_3$-P*Ph*$_3$), 7.41 (t, 7.4 Hz, 6H, *H*$_4$-P*Ph*$_3$), 7.51 (m, 12H, *H*$_2$-P*Ph*$_3$)

^{31}P δ_P 34.2 (d, $^2J_{CP}$ = 16.7 Hz, 2.0P, *P*Ph$_3$)

^{13}C δ_c 21.9 (s, *C*H$_3$COO), 127.9 (t, $^3J_{PC}$ + $^5J_{PC}$ = 9.3 Hz, PPh$_3$–*C*$_3$), 129.6 (t, $^1J_{PC}$ + $^3J_{PC}$ = 43.2 Hz, PPh$_3$–*C*$_1$), 130.0 (s, PPh$_3$–*C*$_4$), 134.9 (t, $^2J_{PC}$ + $^4J_{PC}$ = 12.3 Hz, PPh$_3$–*C*$_2$), 355.6 (t, $^2J_{PC}$ = 16.3 Hz, Ru=^{13}*C*)

IR (CH_2Cl_2) 1365 (κ^1-OCO$_{sym}$), 1435 cm^{-1} (P–Ph), 1460 (κ^2-OCO$_{sym}$), 1528 (κ^2-OCO$_{asym}$), 1589 cm^{-1} (κ^1-OCO$_{asym}$), 1627 cm^{-1} (^{13}C=C), $\Delta\nu_{(chelate)}$ 68 cm $\Delta\nu_{(uni)}$ 224 cm^{-1}.

4.8.2: Synthesis of [Ru(κ^1-OAc)(=^{13}C(OAc)=CHPh)(CO)(PPh$_3$)$_2$]; ^{13}C-12

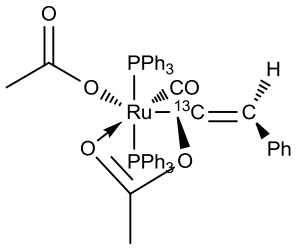

^{13}C-12

29.7 mg (0.04 mmol) of Ru(κ^2-OAc)(κ^1-OAc)(=^{13}C=CHPh)(PPh$_3$)$_2$ was dissolved in 5 mL CH_2Cl_2 in a Schlenk vessel under N_2 with a stirrer bar. The vessel was placed under a vacuum before being backfilled with a CO atmosphere. The solution was allowed to stir for 5 min, during which time the mixture changed from pink to pale-yellow/green. The solvent was then removed *in vacuo* to leave the product as a yellow residue.

NMR Spectra CD_2Cl_2:

^{1}H δ_H 1.15 (s, 3H, C*H*$_3$COO), 1.62 (s, 3H, C*H*$_3$COO), 6.24 (dt, $^4J_{HP}$ = 2.6 Hz, $^2J_{HC}$ = 11.1 Hz, 1H, ^{13}C=C*H*Ph), 7.09 (at, 7.3 Hz, 1H, *H*$_4$-CH*Ph*), 7.11 (ad, 7.9 Hz, 2H, *H*$_2$-CH*Ph*), 7.24 (at, 7.6 Hz, 2H, *H*$_3$-CH*Ph*), 7.33 (at, 7.5 Hz, 12H, *H*$_2$-P*Ph*$_3$), 7.40 (at, 7.3 Hz, 6H, *H*$_4$-P*Ph*$_3$), 7.63 (m, 12H, *H*$_3$-P*Ph*$_3$)

^{31}P δ_P 30.7 (d, $^2J_{PC}$ = 17.8 Hz, 2.0P, *P*Ph$_3$)

^{13}C δ_C 18.5 (s, *C*H$_3$COO), 24.0 (s, *C*H$_3$COO), 127.9 (t, $^3J_{PC}$ + $^5J_{PC}$ = 9.2 Hz, PPh$_3$–*C*$_3$), 129.7 (s, PPh$_3$–*C*$_4$), 132.6 (t, $^1J_{PC}$ + $^3J_{PC}$ = 41.6 Hz, PPh$_3$–*C*$_1$), 134.4 (t, $^2J_{PC}$ + $^4J_{PC}$ = 11.7 Hz, PPh$_3$–*C*$_2$), 193.3 (t, $^2J_{PC}$ = 17.6 Hz, Ru–^{13}*C*=*C*HPh)

IR (CH_2Cl_2) 1372 (κ^1-OCO$_{sym}$) 1435 cm^{-1} (P–Ph), 1592 cm^{-1} (κ^1-OCO$_{asym}$), 1609 cm^{-1} (^{13}C=C), 1962 cm^{-1} (CO), $\Delta\nu_{(uni)}$ 220 cm^{-1}.

4.8.3: Variable Temperature NMR experiments

Procedure:

NMR-scale experiments were performed in tubes fitted with PTFE Young's taps using 20 mg **1** dissolved in approx. 5 mL CD_2Cl_2. Samples were frozen in liquid nitrogen and the alkyne (one equivalent; 3 μL) added to the mouth of the NMR tube under a N_2 atmosphere. Samples were then sealed and transported to the NMR spectrometer where they were warmed until thawing had just completed, rapidly shaken, and immediately transferred to the pre-cooled NMR spectrometer.

4.8.3.1: Reaction of 1 with HC≡CPh: *cis*-12

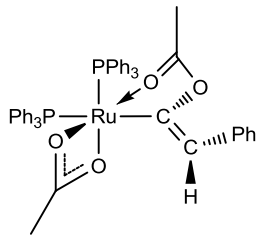

At 245 K:

^{1}H δ_H 5.90 (br s)

^{31}P δ_P 66.6 (d, $^{2}J_{PP}$ = 17.2 Hz), 30.7 (d, $^{2}J_{PP}$ = 17.0 Hz)

4.8.3.1: Reaction of 1 with H^{13}C≡CPh: *cis*-12

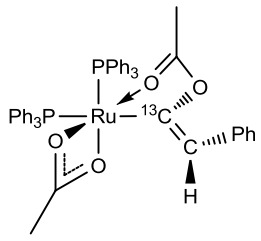

At 245 K:

^{1}H δ_H 5.94 (ad, $^{2}J_{HC}$ = 10.9 Hz)

^{31}P δ_P 66.7 (t, $^{2}J_{PP}$ = 16.7 Hz), 30.8 (dd, $^{2}J_{PP}$ = 16.8 Hz, $^{2}J_{PC}$ = 94.5 Hz)

4.8.4: Quantum-chemical Calculations

Provided by Dr. John Slattery:

Initial optimisations were performed at the (RI-)BP86/SV(P) level, followed by frequency calculations at the same level. Transition states were located by initially performing a constrained minimisation (by freezing internal coordinates that change most during the reaction) of a structure close to the anticipated transition state. This was followed by a frequency calculation to identify the transition vector to follow during a subsequent transition state optimisation. A final frequency calculation was then performed on the optimised transition-state structure. All minima were confirmed as such by the absence of imaginary frequencies and all transition states were identified by the presence of only one imaginary frequency.

Single-point calculations on the (RI-)BP86/SV(P) optimised geometries were performed using the hybrid PBE0 functional and the flexible def2-TZVPP basis set. The (RI-)PBE0/def2-TZVPP SCF energies were corrected for their zero point energies, thermal energies and entropies (obtained from the (RI-)BP86/SV(P)-level frequency calculations) and the resulting Gibbs energies are shown here. In all calculations, a 28 electron quasi-relativistic ECP replaced the core electrons of Ru. No symmetry constraints were applied during optimisations. All calculations were performed using the TURBOMOLE V5.10 package using the resolution of identity (RI) approximation.[43-54]

In our previous work on alkyne-vinylidene tautomerisations at Rh we were able to compare a similar theoretical methodology *{*(RI-)PBE0/TZVP//(RI-)BP86/SV(P) level*}* to the one used in this study to a comprehensive experimental kinetic study.[20] The agreement between experimentally determined and calculated kinetic parameters was very good in this system and the calculations were even able to reproduce the trends in substituent effects seen in the experimental study. Although a similarly close comparison between experiment and theory was not possible in the system described here, these previous results give us some confidence that the PBE0 functional in combination with a flexible basis set is likely to be appropriate for calculation of energies in this system. Studies are currently underway in our group to assess the effects of dispersive interactions, which are not well described by conventional functionals, on this system. These effects are expected to be more

significant when the full ligand periphery is included. Preliminary results suggest that the use of dispersion corrected functionals may only have a relatively small effect on the relative energies in this system. The main conclusion presented here, that an acetate-mediated LAPS mechanism is the lowest energy route across the PES, is unlikely to be affected by the lack of dispersion-correction in the functionals used.

Solvation effects were not considered during the study reported here. However, as the majority of stationary points involve coordinatively saturated, neutral metal complexes we consider that the effects of solvation on the relative energies on the PES will be quite small. The exceptions to this are the energies of the $\mathbf{I_{12}}$ isomers, which will likely be destabilised by the lack of solvation and one should bear this in mind when assessing the PES around $\mathbf{I_{12}}$.

4.8.5: NMR scale reactions of complexes 4 and 5 with HC≡CPh/H^{13}C≡CPh

For reactions of complex **4**; see section 3.8.4

For reaction of complex **5**, see section 3.8.7

5: Synthesis and Characterisation of novel Ruthenium Hydroxy-Vinylidene complexes

5.1: Introduction

It has been shown that **1** is highly reactive towards terminal alkynes, readily facilitating their isomerisation to vinylidene at the ruthenium centre. This study was extended to include propargylic alcohols (HC≡CCRR'OH), which are well-known to react with transition metal centres to give allenylidene complexes *via* the spontaneous dehydration of a hydroxy-vinylidene intermediate.[1-8] Often, the formation of the allenylidene is fast, and the hydroxy-vinylidene intermediate remains undetected. However, it has been possible to isolate and study a number of these types of complexes when the electronic environment of the metal is favourable.[9,10] The formation of an allenylidene ligand is occasionally in competition with the formation of a vinylvinylidene ligand. This also forms *via* the dehydration of a hydroxy-vinylidene, in instances where there is an additional C–H bond in a β-position to the OH on a R group.[11-15]

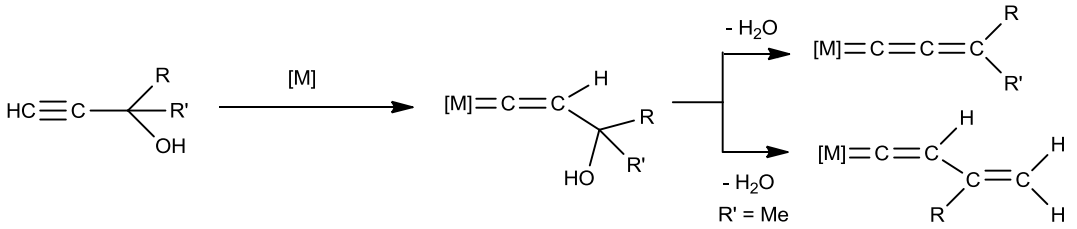

Figure 5.1.1: Isomerisation of a propargylic alcohol to either an allenylidene or vinylvinylidene.

An additional rearrangement has been shown to occur for the reaction between $[RuCl_2(PPh_3)_3]$ and the diphenyl-substituted propargylic alcohol $HC{\equiv}CCPh_2OH$. Instead of observing the formation of the allenylidene complex $[RuCl_2(=C=C=CPh_2)(PPh_3)_2]$, the indenylidene complex shown in Figure 5.1.2 is formed.[16,17] This complex is thought to form *via* a rearrangement of the allenylidene ligand which is promoted in the presence of acid. It has also been shown that the rearrangement of the analogous complex $[RuCl(=C=C=CPh_2)(PCy_3)]OTf$ proceeds *via* an alkenylcarbene ligand.[18,19]

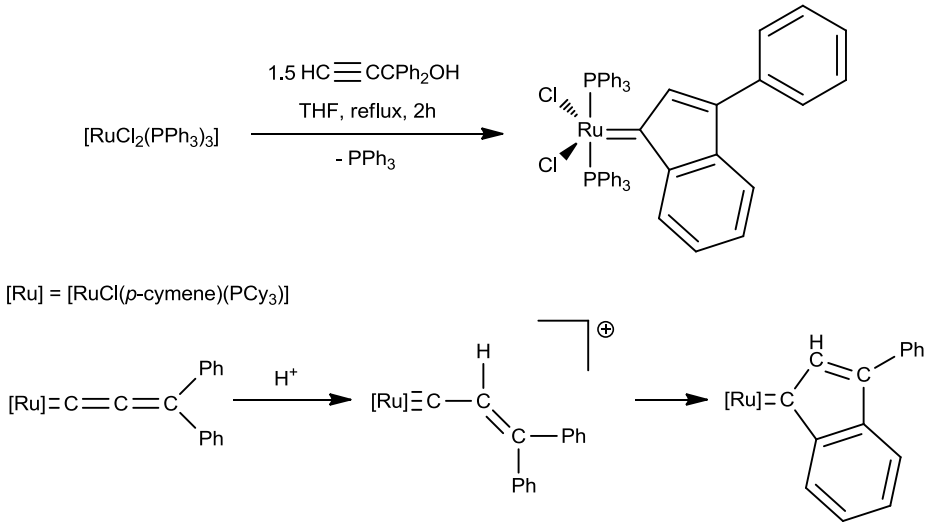

Figure 5.1.2: Rearrangement of an allenylidene ligand to the indenylidene form.

Significant interest in allenylidene complexes arose upon the discovery of this convenient synthetic methodology, and the number of allenylidene complexes reported in the literature is vast. A number of studies have demonstrated that the allenylidene moiety has an electrophilic C_α and nucleophilic C_β, as for a vinylidene, and that C_γ is also electrophilic.[2,20] Calculations have shown that the distribution of this electrophilic character of C_α and C_γ is approximately equal, so the regioselectivity of additions is often controlled by steric factors.[2]

These properties have been exploited in a number of catalytic processes, such as alkene metathesis[21-25] and propargylic substitution.[26,27] The electrophilic nature of C_γ, coupled with the fact that it is generally more accessible than C_α due to steric factors means that propargylic substitutions of the OH group for another nucleophile generally occurs at this point.

In a further test of the reactivity and catalytic potential of **1**, it was proposed to explore its reaction with a number of propargylic alcohols containing a range of differing steric and electronic properties. The formation and stability of an allenylidene ligand may then act as an indicator of this complex's potential to act as a catalyst for propargylic transformations. We were also interested to see whether the hydroxy-vinylidene intermediate could be detected.

5.2: Synthesis and Characterisation of $Ru(\kappa^1\text{-}OAc)(\kappa^2\text{-}OAc)(=C=CHCRR'OH)(PPh_3)_2$

The addition of propargylic alcohols **8a-i** to **1** was carried out in an identical manner as for the simple terminal alkynes **2a-d**. This resulted in the formation of the hydroxy-vinylidene complexes **9a-i**, rather than the expected allenylidenes. These complexes have been successfully isolated and characterised.

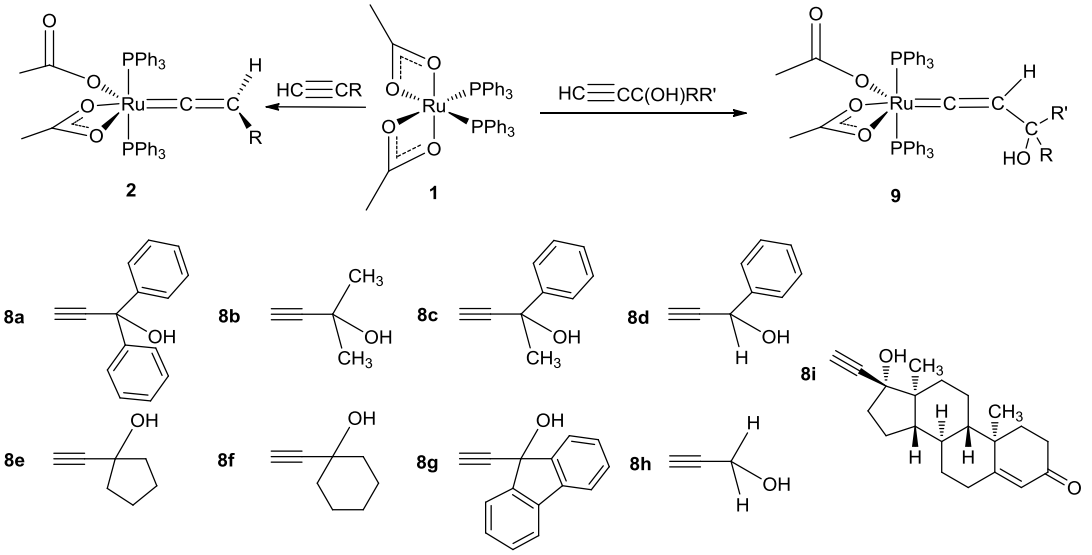

Figure 5.2.1: Reaction of **1** to form vinylidene complexes **2** and hydroxy-vinylidene complexes **9a-i**.

The mechanism of hydroxy-vinylidene formation is thought to be analogous to that of vinylidene formation. The groups of Werner *et. al.*[14] and Puerta *et. al.*[11] have detected the initial formation of an η^2-bound alkyne which subsequently undergoes isomerisation to the corresponding hydroxy-vinylidene complex. This isomerisation can occur *via* two pathways as shown in Figure 5.2.2 below. Either a direct 1,2 H-shift may occur (Path **I**), or an oxidative addition to give a 3-hydroxyalkynyl hydride complex, which subsequently undergoes a 1,3 H-shift to give the hydroxy-vinylidene (Path **II**).[2,15] In our case, no intermediates could be observed in the formation of any of the hydroxy-vinylidene complexes **9a-i**, even when monitored by NMR spectroscopy as complete conversion was observed in the time taken to record the spectra at room temperature. It is proposed that as for **2a-d**, the formation of these complexes is aided by an acetate ligand in a LAPS mechanism; however alternative mechanisms cannot be ruled out as an extensive experimental and theoretical investigation has not been conducted on the OH-substituted case.

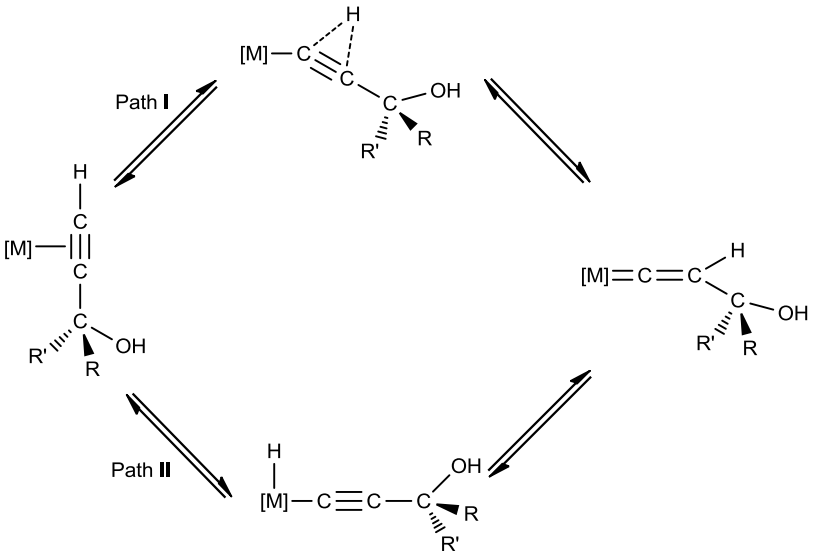

Figure 5.2.2: Proposed mechanisms for the isomerisation of a propargylic alcohol to a hydroxy-vinylidene at a transition metal centre.

Further comparisons can be drawn with complexes **2a-d** in that these hydroxy-vinylidene complexes also display similar characteristic spectroscopic features. A summary of these is provided in Table 5.2.1 below. It was also important to confirm that the products obtained were hydroxy-vinylidenes and not allenylidenes. The possibility of vinylvinylidene formation must also be considered for complexes **9b**,**c**,**e**,**f** and **9i**.

	^{1}H δ_H **[Ru]=C=C*H***	^{1}H $^{4}J_{HP}$/Hz	^{1}H δ_H **O*H***	^{1}H δ_H **CH_3COO**	^{31}P δ_P **PPh_3**
9a	4.73	3.9	4.88	0.71	34.0
9b	4.32	3.9	0.93	0.77	34.1
9c	4.56	3.9	2.79	0.81	34.3
9d	4.14	3.8	2.87	0.86	34.9
9e	4.38	3.8	1.35	0.83	34.3
9f	4.39	3.7	1.17	0.82	34.4
9g	4.56	3.8	2.77	0.82	33.9
9h	4.11	3.7	1.26	0.85	35.1
9i	4.48	3.7	n.d.	0.75	35.5

	^{13}C δ_C C_α	^{13}C $^2J_{CP}$/Hz	^{13}C δ_C C_β	^{13}C $^3J_{CP}$/Hz	^{13}C δ_C C_γ
9a	347.6	16.2	117.2	4.7	74.0
9b	352.0	16.3	118.4	4.8	67.9
9c	350.4	16.0	117.6	4.3	71.1
9d	345.1	16.2	112.5	4.7	67.0
9e	352.0	16.3	116.3	4.6	70.7
9f	352.2	16.5	117.5	4.7	69.6
9g	349.3	16.1	113.7	4.6	77.2
9h	345.7	16.3	106.5	5.0	54.9
9i	352.0	16.2	114.4	4.6	81.6

Table 5.2.1: Common characteristic NMR features of complexes **9a-i**.

The $^{31}P\{^1H\}$ NMR spectra of complexes **9a-i** display singlet resonances due to the PPh_3 ligands at approximately δ_P 34, similar to that observed for **2a-d**, suggesting the phosphines are again mutually *trans*. A triplet resonance assigned to a vinylidene proton is observed in a narrow δ_H range of 4 – 5 ppm for these complexes, with a consistent coupling to the PPh_3 ligands of 3.7 – 3.9 Hz. The use of $^1H\{^{31}P\}$ NMR spectra was required to resolve the couplings to PPh_3 in the case of **9d** and **9h**, as these exhibit additional proton couplings, and was often used to confirm assignments of resonances expected to show coupling to ^{31}P nuclei. The hydroxy resonance is observed as a broad singlet in most cases and over a much wider spectral range; 1 – 5 ppm. (For **9i**, the hydroxy resonance is indistinguishable from other resonances due to the ethisterone substituent in this region). The presence of these two resonances endorses the identification of complexes **9a-i** as hydroxy-vinylidenes rather than allenylidenes or vinylvinylidenes – for an allenylidene complex, both resonances would be absent whereas for the vinylvinylidene the hydroxy resonance would be absent. These features are also very similar to those observed for the vinylidene complexes **2a-d**.

It should be noted that the absence of an individual spectroscopic feature does not confirm the absence of a vinylvinylidene or allenylidene. In many respects the three exhibit similar spectroscopic features. It is the consideration of all spectroscopic features which suggests that the complexes obtained contain hydroxy-vinylidene ligands, rather than allenylidene or vinylvinylidene.

Further confirmation that these complexes do not contain allenylidene or vinylvinylidene ligands can be drawn from inspection of the $^{13}C\{^{1}H\}$ NMR data. For an allenylidene ligand, the value and trend in δ_C for C_α, C_β and C_γ is dependent on the coordinated metal and its associated ligands. The largest review of such features was provided by Bruce in 1998,[6] who showed that the variation in chemical shift for C_α, C_β and C_γ can be large. For C_α a resonance may occur in the range δ_C 200-320; for C_β the range is δ_C 130-250 and for C_γ δ_C 130-170, with outlying exceptions in all cases. Assignment of the peaks to a particular carbon atom of the allenylidene chain is often based on the magnitude of P-C coupling; the assumption being the value of J_{CP} diminishes with distance.[28] The chemical shift of C_α can also be affected by the electron density on C_α and is thought to be an indication of the mesomeric form of allenylidene that has the most significant contribution in that molecule. Crystallographic data is typically required to fully validate such findings.

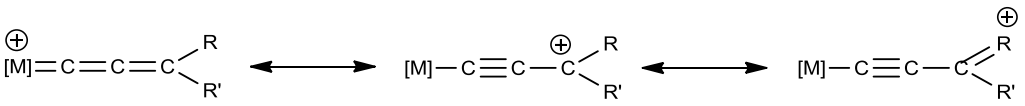

Figure 5.2.3: Mesomeric forms of a coordinated allenylidene.

For complexes **9a-i**, triplet resonances evident at very low field ~ δ_C 350 with $^{2}J_{CP}$ values of approximately 16 Hz were consistent with a vinylidene C_α coupling to two PPh_3 ligands, whilst a triplet assigned to C_β and a singlet assigned to C_γ were ~ δ_C 110 and 70 respectively. The resonance for C_β exhibits a smaller $^{3}J_{CP}$ value of around 4.7 Hz, consistent with C_β of a vinylidene. The resonance assigned to C_γ in all complexes **9a-i** is very different to that predicted for C_γ of an allenylidene or a vinylvinylidene ligand. The chemical shift value observed is significantly lower than expected, indicating that C_γ in **9a-i** has stronger sp^3 character. Furthermore, coupling is often observed to ancillary phosphine ligands for C_γ of an allenylidene, whereas in all cases of **9a-i**, the resonance is a singlet with no evidence of additional coupling.

In complexes **9b,c,e,f** and **9i** there is no additional methylene resonance for C_{δ}, which would be expected for a vinylvinylidene.

Unequivocal confirmation of these complexes containing hydroxy-vinylidene ligands was obtained upon the growth of crystals suitable for X-Ray Diffraction for complexes **9a**, **9c** and **9e**. Crystals were obtained by the slow diffusion of pentane or hexane into a solution of the complexes in DCM. Interestingly, structural characterisation of **9a** revealed the presence of an intramolecular hydrogen bond between the hydroxy proton and the uncoordinated oxygen atom of the κ^1-OAc ligand. On the other hand, this intramolecular hydrogen bond was not observed in the crystal structure of **9c** or **9e**; however an intermolecular hydrogen bond was observed between the hydroxyl-proton of the vinylidene and the uncoordinated oxygen atom of a κ^1-OAc ligand belonging to an adjacent molecule.

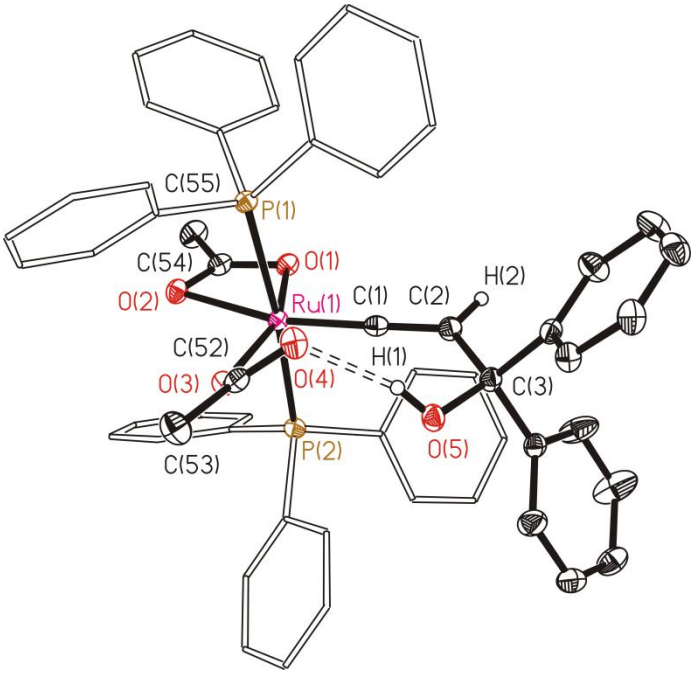

Figure 5.2.4: ORTEP diagram of **9a**, thermal ellipsoids at the 50 % probability level. Hydrogen atoms (except for H(5) and H(6)) and one molecule of DCM omitted for clarity

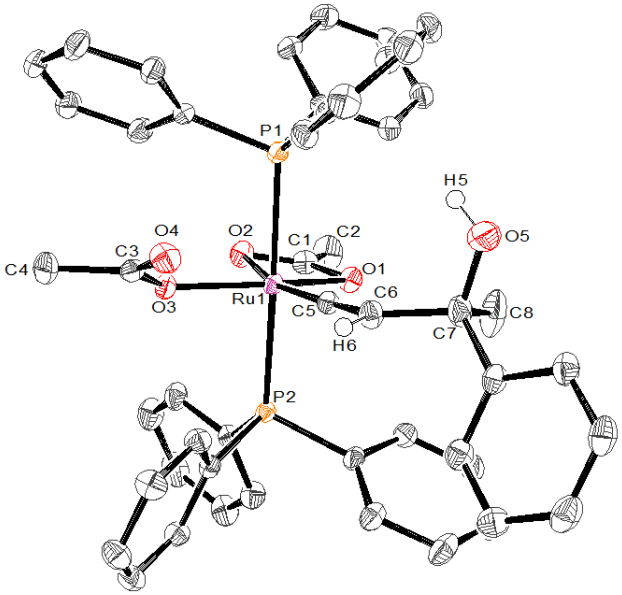

Figure 5.2.5: ORTEP diagram of **9c**, thermal ellipsoids at the 50 % probability level. Hydrogen atoms (except for H(5) and H(6)) omitted for clarity

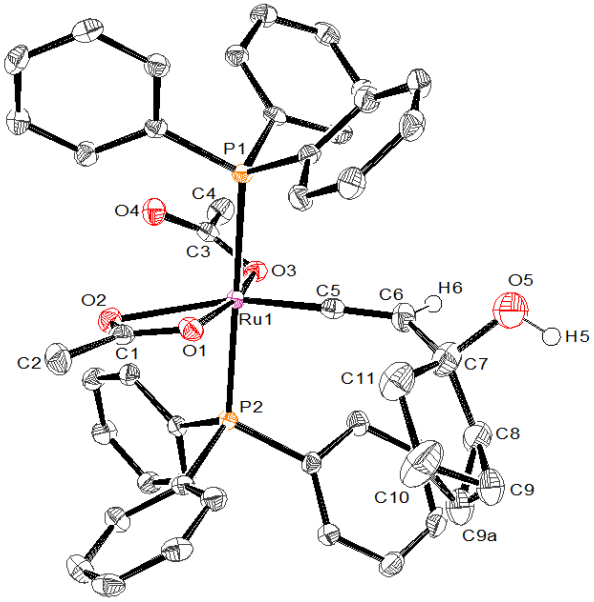

Figure 5.2.6: ORTEP diagram of **9e**, thermal ellipsoids at the 50 % probability level. Hydrogen atoms (except for H(5) and H(6)) and one molecule of DCM omitted for clarity.

Bond Length	**9a / Å**	**9c / Å**	**9e / Å**
Ru – P(1)	2.4178(4)	2.4040(5)	2.3734(7)
Ru – P(2)	2.3652(4)	2.3757(5)	2.3850(7)
Ru – O(1)	2.1100(11)	2.1141(13)	2.1119(19)
Ru – O(2)	2.2588(11)	2.2620(13)	2.3259(19)
Ru – O(3)	2.0344(11)	2.0179(12)	2.088(2)
Ru – C_α	1.8027(15)	1.7959(18)	1.805(3)
C_α – C_β	1.312(2)	1.316(2)	1.297(4)
C_β – C_γ	1.530(2)	1.520(3)	1.517(5)

Bond Angle	**9a / °**	**9c / °**	**9e / °**
P(1) – Ru – P(2)	173.647(14)	177.844(17)	178.45(3)
P(1) – Ru – O(1)	92.02(3)	93.75(4)	88.79(6)
P(1) – Ru – O(2)	82.82(3)	85.78(4)	99.45(5)
P(1) – Ru – O(3)	89.31(3)	90.36(4)	92.14(6)
O(1) – Ru – O(2)	59.79(4)	59.78(5)	58.45(7)
O(1) – Ru – O(3)	156.68(4)	151.04(5)	168.47(7)
O(2) – Ru – O(3)	97.36(4)	92.05(5)	110.09(7)
P(1) – Ru – C_α	96.95(5)	90.72(6)	88.78(9)
P(2) – Ru – C_α	89.29(5)	88.43(6)	92.12(9)
O(1) – Ru – C_α	101.35(6)	103.64(6)	98.99(10)
O(2) – Ru – C_α	161.05(6)	162.68(6)	155.45(10)
O(3) – Ru – C_α	101.59(6)	104.95(7)	92.52(10)
Ru – C_α – C_β	175.16(13)	178.10(16)	178.2(3)
C_α – C_β – C_γ	124.00(14)	127.42(17)	129.0(3)

Table 5.2.2: Bond Lengths and Angles for complexes **9a**, **9c** and **9e**.

As for all other complexes reported thus far to contain a κ^2-OAc ligand, the structures obtained of complexes **9a**, **9c** and **9e** are that of a distorted octahedron. The majority of bond lengths and angles are very similar across these four complexes, with deviations caused by the constraining O(1) – Ru – O(2) angle at approximately 60 °. The angle associated with the vinylidene moiety is close to linear for each, with the largest deviation from 180 ° observed for complex **9a** at 175.16(13) °. The distances of the Ru=C and C=C bonds observed are very similar to one another and are characteristic of a vinylidene ligand. Bruce[29] suggests that a typical C=C distance ought to be within the range of 1.25-1.41 Å and the bond lengths observed fit into this range. The intramolecular hydrogen bond located in complex **9a** is unique to this structure; such a feature was not observed in the structures of the other hydroxy-vinylidene complexes **9c** and **9e**. The full O–H---O distance of 2.691 Å is reported, indicative of a strong interaction.[30] There are no detectable hydrogen bonds in the crystal structure of complex **9c**, although it appears that the hydroxyl-proton is directed towards the π-electron density of a phenyl ring of a PPh_3 ligand. The distance between the oxygen atom and the *ipso*-carbon of the phenyl ring is 3.699 Å, which would comprise a weak interaction; although the position of the hydrogen of the OH group could not be located on the electron difference map. A strong intermolecular hydrogen bond of 2.802 Å is observed in the crystal structure of **9e** between the hydroxyl-proton of the vinylidene ligand and the uncoordinated oxygen atom of a κ^1-OAc ligand of an adjacent molecule. There is significant disorder of the cyclopentanol ring of the vinylidene ligand, so the ring positions were modelled in a ratio of 76:24.

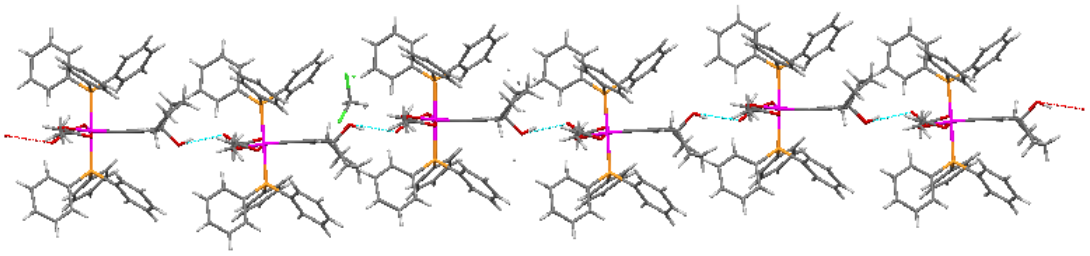

Figure 5.2.7: A chain of molecules of complex **9e** bonded *via* an intermolecular hydrogen bond.

In Chapter 2, it was shown that the two acetate ligands in complex **2a** are fluxional. This exchange process was shown to be rapid on the NMR timescale even at 195 K, yet slow on the IR timescale. It was postulated that the presence of a hydrogen bond between the hydroxy-proton of **9a** and the uncoordinated oxygen atom of the κ^1-OAc ligand may affect the rate of this exchange. Consequently, a variable temperature NMR experiment was conducted and showed that coalescence occurred for **9a** at 235 K.

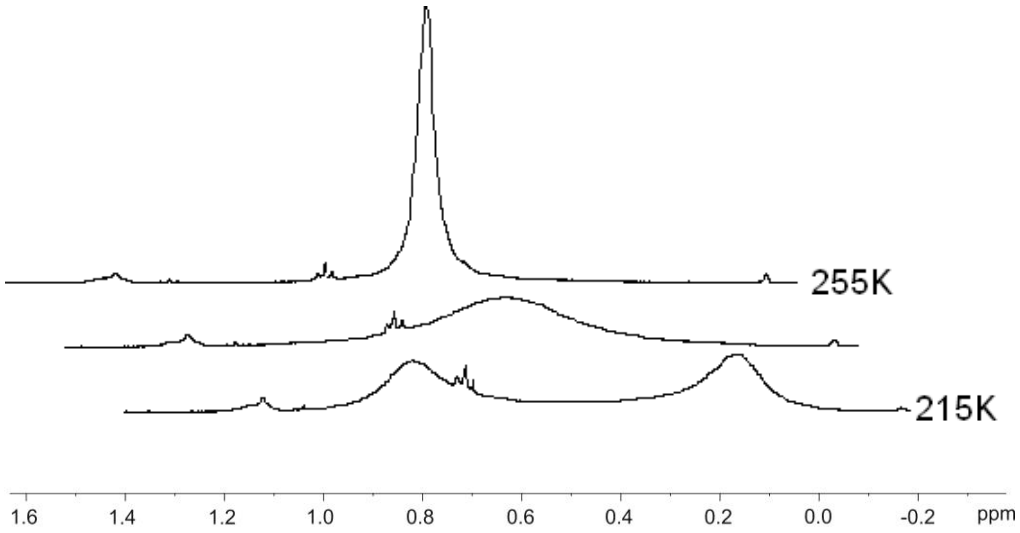

Figure 5.2.8: ‘H NMR Spectrum of **9a** at 215, 235 and 255K.

The rate and energy barrier for this fluxional exchange can be described by k_{coal} and $\Delta G^{\ddagger}$ using the expressions below (see also Section 3.3). The rate constant at the coalescence temperature T_c is given by Equation 5.2.1:

$$k_{coal} = \frac{\pi \delta \nu}{\sqrt{2}} = 2.22 \delta \nu \tag{5.2.1}$$

This can be combined with a rearrangement (Equation 5.2.2) of the Eyring Equation (Equation 5.2.3) to give an expression for $\Delta G^{\ddagger}$ (Equation 5.2.4)[31]

$$k = \kappa \frac{k_B T}{h} \left(-\Delta G^{\ddagger} / RT \right) \tag{5.2.2}$$

$$\Delta G^{\ddagger} = RT[23.76 - \ln(k/T)] \tag{5.2.3}$$

$$\Delta G^{\ddagger} = RT_c \left[22.96 + \ln\left(\frac{T_c}{\delta \nu} \right) \right] Jmol^{-1} \tag{5.2.4}$$

As noted in Section 3.3, the values of $\Delta G^{\ddagger}$ and k_{coal} reported here are the lower limits as δ_ν was not recorded at the low temperature limit. The values of T_c reported here are uncalibrated and have an error of at least ± 5 K associated. Similar low

temperature experiments were subsequently conducted on all complexes **9**, except for **9f** and **9i**. The resonance assigned to the acetate protons for these complexes is in a region of the spectrum that contains a number of resonances, it was therefore suggested that the broadening of the acetate resonance and the extent of its coalescence would be difficult to determine. Whilst coalescence was observed for **9d**, **9e** and **9g**, this occurred at markedly lower temperatures than for **9a**. A summary of these results is given in Table 5.2.3 below. This has shown that the energy barrier ($\Delta G^{\ddagger}$) for the exchange of the acetate ligands is small, and comparable for each complex for which coalescence was successfully observed. The values are also comparable to those obtained for complexes **4** ($\Delta G^{\ddagger}$ = 37.4 kJ mol^{-1} at 195 K) and **5** ($\Delta G^{\ddagger}$ = 45.3 kJ mol^{-1} at 235 K). It is very difficult to determine whether the presence of the hydrogen bond observed in the solid state for **9a** is a significant factor, as these results were obtained in solution.

Complex	**δ_v / s^{-1}**	**T_c / K**	**$k_{coal} \leq$ / s^{-1}**	**$\Delta G^{\ddagger} \leq$ / kJ mol^{-1}**
9a	291.3	215	646.7	40.5
9b	n.d.	n.d.	n.d.	n.d.
9c	n.d.	n.d.	n.d.	n.d.
9d	270.4	190	600.2	35.7
9e	175.8	195	390.2	37.4
9f				
9g	138.7	195	307.8	37.8
9h	n.d.	n.d.	n.d.	n.d.
9i				

Table 5.2.3: Temperature of coalescence, rate and free energy of exchange for compounds **9a-i**. Those marked '–' did not show signs of coalescence even at 195K. (n.d. = not detected).

IR spectra of complexes **9a-i** were recorded in both solution (DCM) and the solid (KBr) state. In both media, as for vinylidenes **2a-d**, the presence of κ^1- and κ^2-OAc coordination modes was observed. In addition, peaks due to the OH stretch of the hydroxy-vinylidene ligand were also detected. The presence of an allenylidene ligand is often confirmed by the presence of a characteristic υ(C=C=C) stretch[6] at 1800 – 2100 cm^{-1}. In no instances was such a stretch observed for complexes **9a-i**.

Complex	P–Ph	C=C	OH	κ^1-OCO_{sym}	κ^1-OCO_{asym}	κ^1-$\Delta\upsilon$	κ^2-OCO_{sym}	κ^2-OCO_{asym}	κ^2-$\Delta\upsilon$
9a (DCM)	1435	1649	3276	1371	1598	227	1463	1531	68
9a (KBr)	1434	1654	3260	1378	1595	217	1465	1527	62
9b(DCM)	1435	1653	3563	1366	1623	257	1459	1539	80
9b (KBr)	1434	1648	3572	1362	1619	257	1460	1533	73
9c (DCM)	1434	1652	3565	1367	1601	234	1463	1533	70
9c (KBr)	1434	1649	3574	1361	1601	240	1458	1536	78
9d (DCM)	1435	1647	3610	1373	1596	223	1455	1538	83
9d (KBr)	1435	1648	3571	1369	1592	223	1454	1537	83
9e (DCM)	1431	1656	3569	1364	1584	220	1457	1533	76
9e (KBr)	1434	1654	3564	1364	1590	226	1458	1536	78
9f (DCM)	1434	1648	3571	1368	1600	232	1461	1536	75
9f (KBr)	1434	1646	3571	1366	1591	225	1458	1538	80
9g (DCM)	1435	1646	3554	1367	1606	239	1463	1531	68
9g (KBr)	1433	1636	3542	1367	1597	230	1463	1534	71
9h (DCM)	1434	1651	3573	1368	1605	237	1456	1538	82
9h (KBr)	1433	1655	3575	1372	1595	223	1457	1533	76
9i (DCM)	1433	1652	3564	1372	1616	244	1458	1538	80
9i (KBr)	1433	1649	3573	1374	1620	246	1456	1530	74

Table 5.2.4: Summary of IR stretches for complexes **9a-i**, all values in cm^{-1}

The OH peak in the IR for **9a** is markedly lower than that of any other in both solution and solid state which we have tentatively ascribed to the presence of an intramolecular hydrogen bond revealed in the crystal structure. It appears that the remainder of the stretches obtained show very little variation. They are also comparable to those obtained for the vinylidenes **2a-d**. A full comparison of IR and NMR spectroscopic and structural features of all complexes included in this thesis containing acetate ligands is given in Chapter 8.

Two mass spectrometry methods were employed for the characterisation of complexes **9a-i**. The use of ESI was often found to be too 'hard' a technique for these compounds – a frequent observation was a peak with the appropriate ruthenium isotope pattern that had either lost a mass equal to OH^- (**9c**, **9e**, **9f**), or gained a mass equal to Na^+ (**9a**, **9b**, **9i**) or H^+ (**9h**). Alternatively, there is a mass difference equal to the loss of an OAc^- ligand and gain of a MeCN group, as shown for **9g**. This is presumably observed as trace amounts of MeCN are always present within the mass spectrometer due to its popularity as an appropriate solvent[32] (all complexes **9a-i** were dissolved in DCM). The use of accurate mass spectra was required in order to make these assignments. In his original paper on the synthesis of an allenylidene ligand from a propargylic alcohol, Selegue[1] refers to a report[33] by Burke whereby dehydration of the stable hydroxy-vinylidene complex $[MnCp(=C=CHC\{OH\}\{CMe_3\}_2)(CO)_2]$ occurs within the mass spectrometer. It is not clear if this is happening in the cases of complexes **9a-i** as a variety of results were obtained.

An alternative technique was found in the form of LIFDI, (Liquid-Injection Field Desorption Ionisation) which is considered to be a 'softer' ionisation technique, and more appropriate for air-sensitive complexes. This was able to give more accurate molecular ion peaks for those complexes it was employed for (**9d**, **9g**, **9h**). However, difficulties were again encountered. It seemed that in the process of ionisation, decomposition of these complexes occurred on the graphite filament which resulted in the build-up of a deposit on the surface of the filament. This led to a gradual loss of sensitivity and ultimately required the filament to be replaced.

It has been shown that the addition of a range of propargylic alcohols with varying steric and electronic properties results in the rapid formation of hydroxy-vinylidene complexes **9a-i**. The following section will detail attempts to encourage dehydration of these ligands to give allenylidene complexes, and the unexpected reactivity that was ultimately observed.

5.3: Reactivity of [Ru(κ^1-OAc)(κ^2-OAc)(=C=CHCRR'OH)(PPh$_3$)$_2$]

Hydroxy-vinylidene complexes, such as **9a-i**, are often observed as intermediates in the formation of allenylidene complexes. It was expected that the loss of H_2O from these complexes would be observed over time. When this did not occur, methods typically used to encourage allenylidene formation were employed, such as addition of acid and passage through an acidic alumina column.[34] However, despite these attempts to promote dehydration, an allenylidene complex could not be successfully detected. Addition of an excess of HBF_4 to a solution of **9a** in CD_2Cl_2 led to the formation of liberated PPh_3 and additional, unassigned resonances as observed in the $^{31}P\{^1H\}$ NMR spectrum. Similar observations were made upon the addition of CF_3COOH. Werner showed that the formation of the allenylidene complex shown in Figure 5.3.1 was promoted by the passage of the hydroxy-vinylidene precursor down an acidic alumina column. When a solution of **9a** was treated in a similar manner, rapid decomposition was observed.

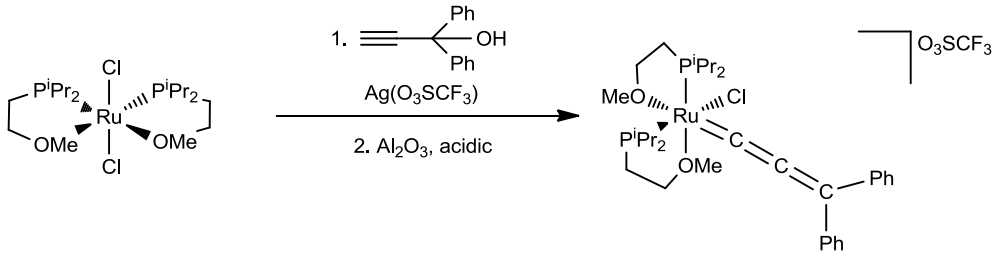

Figure 5.3.1: Formation of an allenylidene complex assisted by acidic alumina.

Monitoring solutions of complexes **9a-i** by NMR spectroscopy over time led to the observation that an alternative process was occurring. Resonances assigned to the CO-containing complex **4** were observed to form at a comparative rate to those due to an alkene H_2C=CRR'; where the propargylic alcohol used was HC≡CCRR'OH. A crystal of complex **4** used for structural characterisation was first isolated from a CD_2Cl_2 solution of **9a** that had been allowed to stand for several days before diffusion into a hexane solution. The formation of **4** may be accounted for by the presence of either H_2O or O_2; it has been shown that a vinylidene ligand may be oxidised by O_2 to give a CO-containing complex,[10] although this results in the formation of aldehydes or ketones as organic by-products rather than alkenes. This is not the case for complexes **9a-i**, as will be shown in Chapter 6. The identity of these alkenes was confirmed by either comparison with literature data or an authentic sample where possible.

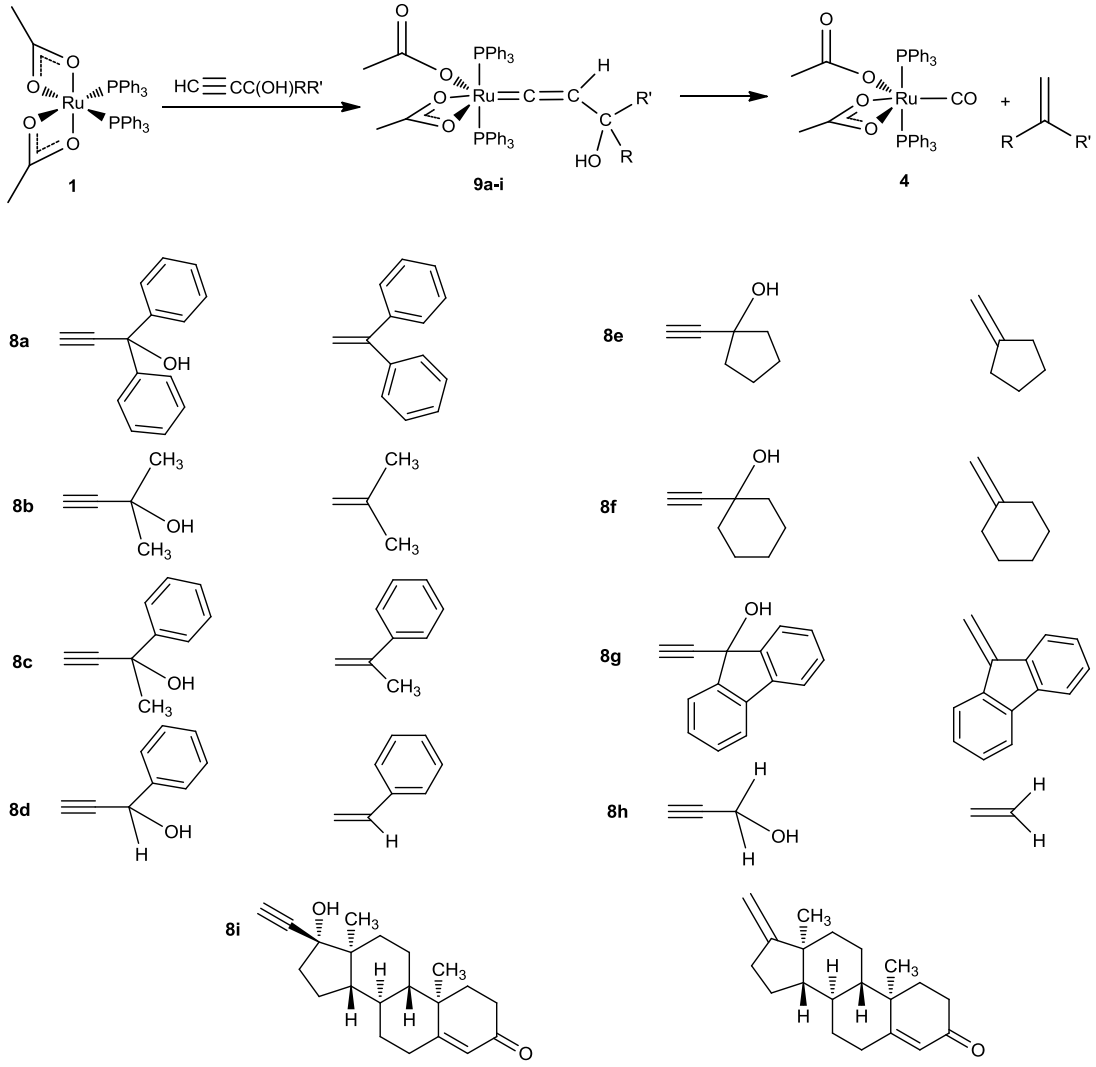

Figure 5.3.2: Formation of complex **4** and an alkene from **1** and HC≡CC(OH)(R)(R') *via* hydroxy-vinylidene complexes **9a-i**.

The rate of this process varies slightly with the substrate; bulkier R groups react over longer periods of time whereas smaller R groups react faster. The fastest example is **9h**, which decays to **4** and ethene in a sealed Young's NMR tube in CD_2Cl_2 at room temperature over 48 hours. For **9i**, this stoichiometric reaction takes approximately 1 month to reach completion. This conversion is not without precedent – Dixneuf *et. al.* previously demonstrated[35,36] that the addition of HC≡CCH(OH)Ph to [RuCl(*p*-cymene)(PCy_3)][$B(Ar_F)_4$] resulted in the formation of [RuCl(*p*-cymene)(PCy_3)(CO)][$B(Ar_F)_4$] and styrene. They also demonstrated that this process occurred *via* complexes containing a hydroxycarbene ligand, and suggested that an allenylidene ligand was also involved.

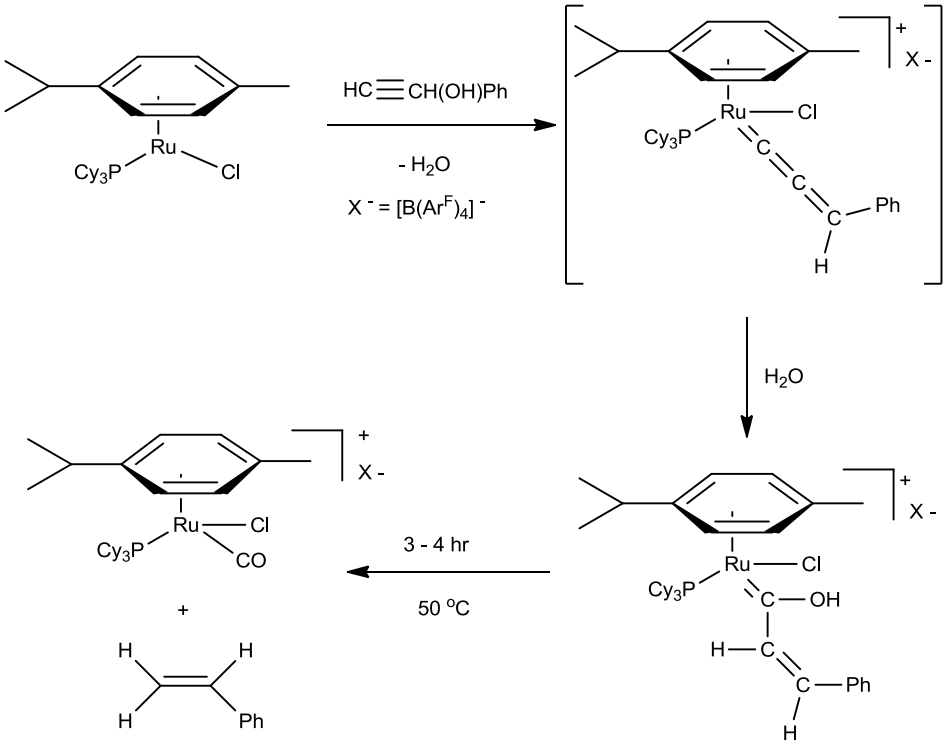

Figure 5.3.3: Dixneuf's proposed mechanism to account for propargylic alcohol to alkene conversion.[35]

A key spectroscopic feature of hydroxy-carbene complexes is a resonance for the OH proton at ~ δ_H 14 – 16,[35] however no such resonances were observed in this region of the ^{1}H NMR spectra when the formation of **4** from complexes **9a-i** was monitored over time. Given that the formation of an allenylidene ligand has also gone undetected, a series of further experiments were conducted to provide insight into the mechanism involved in this conversion. This involved a series of stoichiometric reactions as well as kinetic, ^{18}O-labelling and DFT studies (the latter conducted in collaboration with Dr. John Slattery and David Johnson), which will be discussed in the following chapter.

5.4 Catalytic Studies

Although Dixneuf[35,36] has reported that the stoichiometric reaction of the propargylic alcohol **8d** with [RuCl(*p*-cymene)(PCy_3)][$B(Ar_F)_4$] produced $H_2C{=}CPh_2$, no attempt was made to produce the alkene catalytically. However, Liu reported the catalytic equivalent of this reaction in 2003,[37] using a range of ruthenium complexes containing a Tp ligand. Optimal conditions were found using the [Ru(Tp)(PPh_3)(CH_3CN)$_2$]PF_6 complex in the presence of LiOTf as a Lewis acid and the concomitant production of CO was confirmed by GC-MS. It is proposed that the catalytic cycle proceeds as shown in Figure 5.4.1; initial coordination of the alkyne in a η^2-fashion is followed by the formation of an acetylide-hydride complex. In the presence of LiOTf, ionisation of this species occurs to generate an allenylidenium species which undergoes nucleophilic attack at C_α by LiOH to give an acyl species. The subsequent decarbonylation process results in the formation of both CO and vinyl ligands coordinated to the ruthenium centre and a subsequent reductive elimination reaction regenerates the active catalyst.

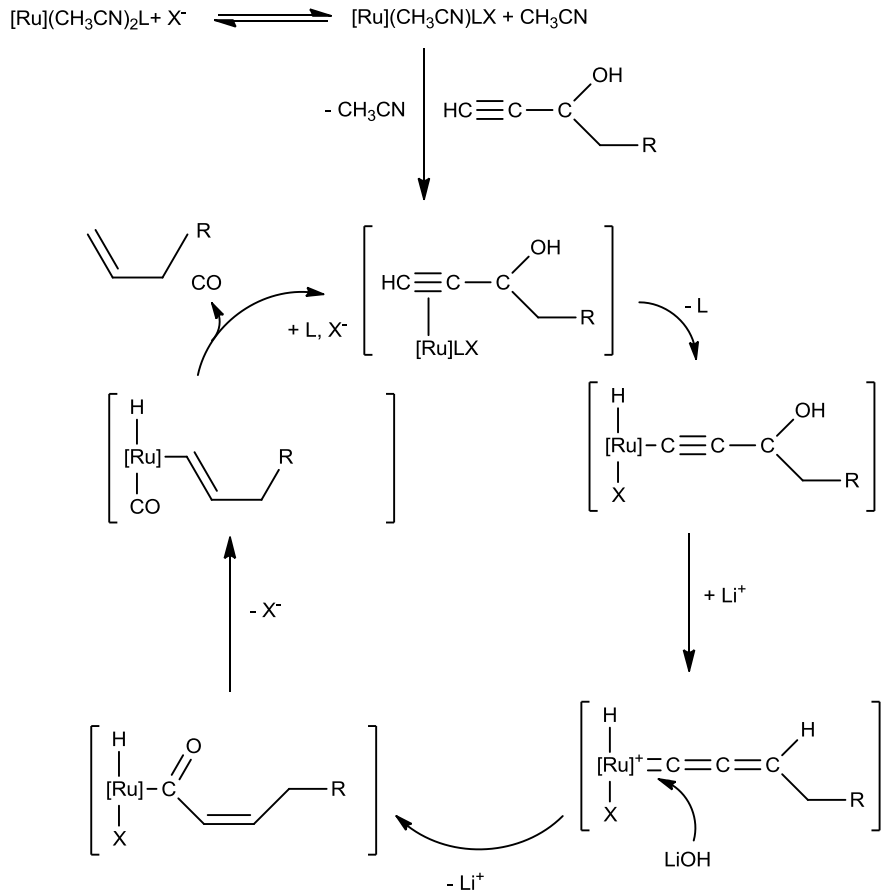

Figure 5.4.1: Catalytic cycle proposed by Liu for the decarbonylation of propargylic alcohols.

Consequently, a series of experiments were conducted in an attempt to mimic the success of Liu's system, using the precursor complex **1** to catalytically produce the corresponding alkene from propargylic alcohols **8a-i**.

5.4.1 Catalytic conversion of Propargylic Alcohols to Alkenes.

Initially, conditions for the conversion of **8a** to $H_2C{=}CPh_2$ were optimised, and then these conditions were applied to the remaining propargylic alcohol substrates. Unfortunately, these reactions resulted in the formation not only of the alkene, but in a number of additional products including an enal, and three isomers resulting from alkyne dimerisation processes. These different products are illustrated in Figure 5.4.1.1. Efforts to isolate and characterise these different organic products individually by column chromatography failed. Consequently the identification of these compounds is based on a comparison of the ^{1}H NMR spectrum of the crude reaction mixture with that of literature data (where available). In cases where literature data was not available, structural assignments were made based on the observation of comparable resonances in other reaction mixtures. It was also shown that the product distribution varied for each substrate.

For example, the dimerization of propargylic alcohols is relatively rare in the literature, however, by analysing the NMR features of the reported examples[38-42] (**8a**, **8b**, **8e**, **8g**) and of dimerization products of terminal alkynes,[43-51] it was noted that there are characteristic resonances for the two protons of the alkene moiety for the three different isomers of the enyne. For the (*E*)-dimer, two doublet resonances at approximately δ_H 5.9 and δ_H 6.5 exhibit a coupling constant of ~ 16 Hz, whilst the (*Z*)-dimer exhibits two doublet resonances around δ_H 5.5 and δ_H 6.0 with a mutual coupling of ~ 12 Hz. Only one example of a (*gem*)-dimer of a propargylic alcohol (**8b**) could be found in the literature,[43] which is characterised by two singlet resonances at δ_H 5.32 and δ_H 5.37. However, for (*gem*)-dimer isomers of other terminal alkynes, two doublet resonances with a small coupling constant of around 2 Hz are observed at similar chemical shifts.

Table 5.4.1.1 summarises the product distributions from the initial experiments to optimise the conditions for the selective production of the alkene $H_2C{=}CPh_2$ from **8a**. These yields are calculated from the relative integrations of the appropriate peaks in the ^{1}H NMR spectrum of the crude mixture using a characteristic resonance of the (*Z*)-dimer as a 'standard' integrated to 1. The numbers in brackets below this indicate the percentage composition of this component in the overall mixture. All reactions were carried out over 16 hours.

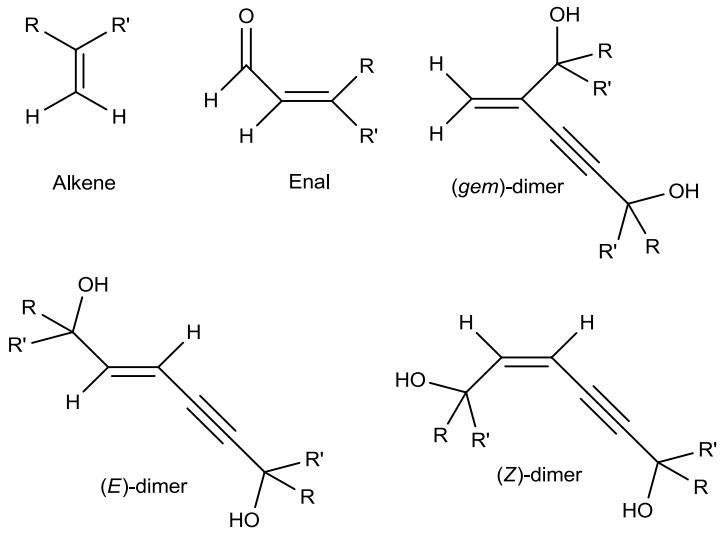

Figure 5.4.1.1: The range of products from attempts to catalytically generate alkenes from **8a-i**.

Catalytic Run	Reaction conditions			Alkene (%)	Enal (%)	(*gem*)-dimer (%)	(*E*)-dimer (%)	(*Z*)-dimer (%)	Remaining SM (%)
	Mol %	T / K	mL toluene						
1	5	383	10	11.4 (12.2)	2.28 (2.46)	-	4.53 (4.86)	1.00 (1.08)	74.0 (79.4)
2	5	383	5	17.4 (8.91)	2.22 (1.13)	-	4.44 (2.26)	1.00 (0.50)	170 (87.2)
3	10	383	10	18.5 (26.2)	2.82 (4.00)	-	3.25 (4.60)	1.00 (1.40)	45.0 (63.8)
4	10	403	10	15.3 (52.5)	3.39 (11.6)	-	3.45 (11.8)	1.00 (3.50)	6.00 (20.6)

Table 5.4.1.1: Product distribution for the catalytic production of $H_2C{=}CPh_2$ from **8a**.

The conditions used in run 4 gave the highest conversion of starting material to alkene, although significant amounts of side products were still obtained. Nevertheless, these conditions were applied to catalytic runs using propargylic alcohols **8a-i** and the results are summarised in Table 5.4.1.2 and Figure 5.4.1.2.

In those instances where no (*Z*)-dimer was detected; the lowest yielding product was given an integral of 1. The assignments of product peaks are tentative due to the complex nature of the crude mixture and, as mentioned earlier, assignments have been based on the best possible comparison with available literature data. In the case of substrates **8b** and **8h**, the alkenes expected are gaseous. Therefore, although observation of the alkenes was not expected, a catalytic run was conducted to discern the nature of other products that may be observed. The reaction of **8h** has been excluded from analysis as none of the expected products could be identified from the ^{1}H NMR spectrum of the crude reaction mixture. An attempt to isolate the individual products, from the crude reaction mixture of **8e** by silica-gel chromatography was made, however the only identifiable product obtained was a small amount of $O{=}PPh_3$.

Substrate	Reaction conditions			Alkene (%)	Enal (%)	(*gem*)-dimer (%)	(*E*)-dimer (%)	(*Z*)-dimer (%)	Remaining SM (%)
	Mol %	T / K	mL toluene						
8a	10	403	10	15.3 (52.5)	3.39 (11.6)	n.d.	3.45 (11.8)	1.00 (3.50)	6.00 (20.6)
8b	10	403	10	n.d. (g)	0.04 (2.60)	1.00 (65.0)	0.50 (32.4)	n.d.	n.d.
8c	10	403	10	4.93 (12.9)	3.67+1.03* (12.3)	n.d.	3.62 (9.50)	1.00 (2.60)	24.0 (62.7)
8d	10	403	10	1.10 (52.3)	1.00 (47.7)	n.d.	n.d.	n.d.	n.d.
8e	10	403	10	n.d.	0.22 (1.90)	1.91 (16.9)	1.20 (10.6)	1.00 (8.80)	7.00 (61.7)
8f	10	403	10	2.65 (20.0)	0.36 (2.60)	2.27 (17.2)	1.95 (14.8)	1.00 (7.60)	54.0 (37.8)
8g	10	403	10	0.60 (22.2)	1.10 (40.7)	1.00 (37.1)	n.d.	n.d.	n.d.
8i	10	403	10	10.1 (80.2)	n.d.	n.d.	1.50 (11.9)	1.00 (7.90)	n.d.

Table 5.4.1.2: Product distribution for the attempted catalytic production of alkenes from **8a-i** (excluding **8h**); n.d. = not detected; (g) = gas; * = both *E* and *Z* isomers detected.[52]

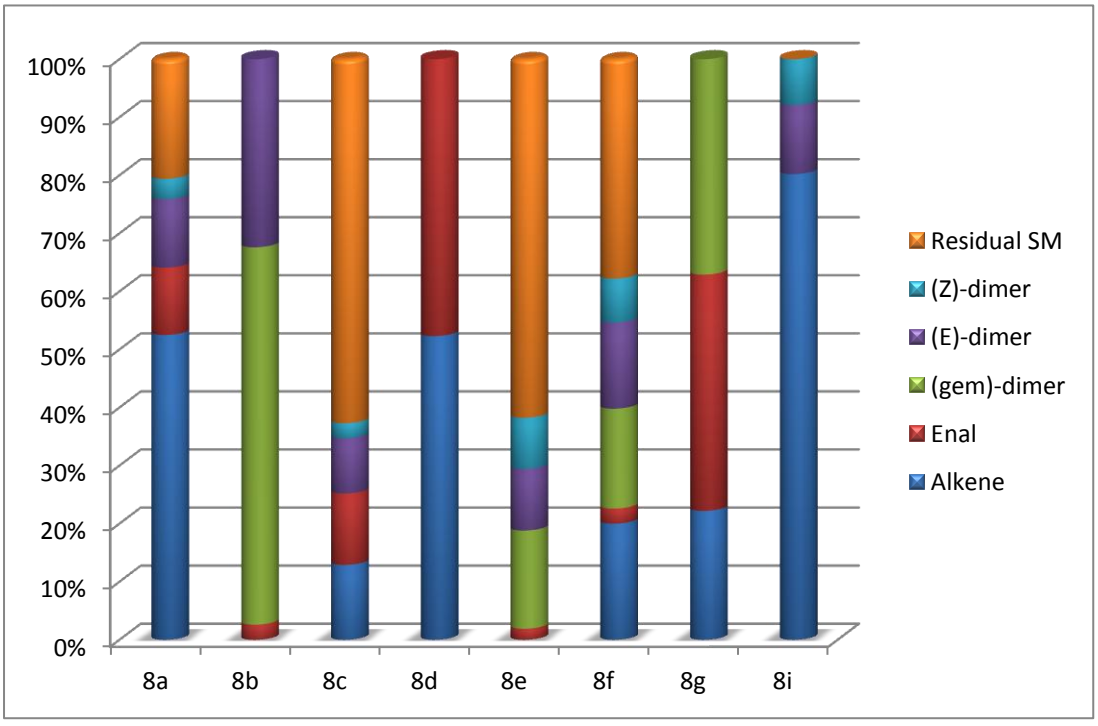

Figure 5.4.1.2: Bar Chart illustrating the product distribution in Table 5.4.1.2.

The presence of enals and alkyne dimerisation products in the reaction mixtures is unsurprising as the use of ruthenium-based complexes for the catalytic production of these species from propargylic alcohols is well-established.[27,35,36,38,53,54] Gimeno and Cadierno have used the 16-electron species [Ru(η^3-2-C_3H_4Me)(CO)(dppf)][SbF_6] to catalyse the regioselective isomerisation of propargylic alcohols into enals and ketones *via* the Meyer-Schuster and Rupe rearrangements. They propose that their products form *via* the mechanism shown in Figure 5.4.1.3 and involve allenylidene and hydroxy-carbene species as intermediates.[55]

An attempt was made to selectively produce the enal (cinnamaldehyde; PhHC=CHCHO) from **8d** following the procedure used by Gimeno[55] (10 mol % **1** in 10mL 'wet, degassed' THF heated to 75°C for 16 hours). However virtually no conversion was observed and the major component at the end of the reaction was residual starting material.

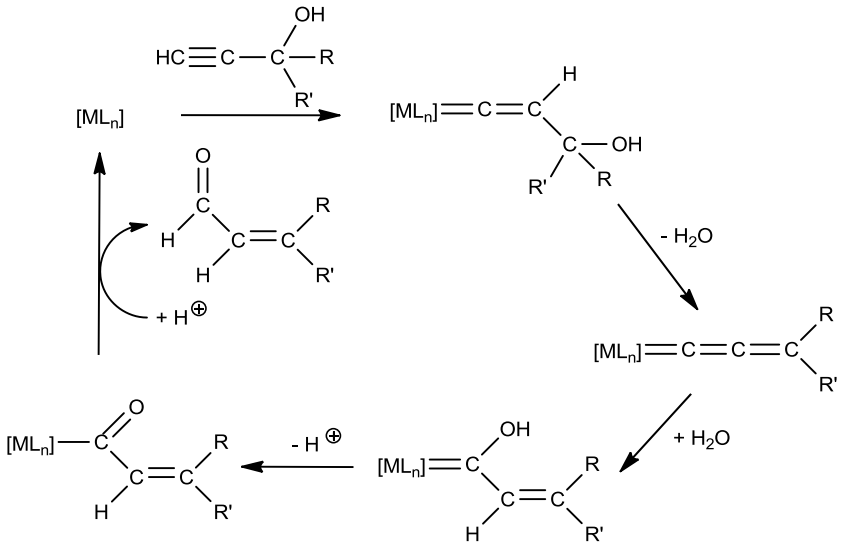

Figure 5.4.1.3: Gimerno's proposed mechanism for the Meyer-Schuster rearrangement of propargylic alcohols.

A number of ruthenium complexes have been shown to catalyse the dimerisation of terminal alkynes with varying degrees of selectivity.[42,45,56-68] The mechanism believed to apply to the majority of alkyne dimerisations involving *anti*-Markovnikov addition of the alkyne is given in Figure 5.4.1.4. After the initial formation of the vinylidene ligand, it may be deprotonated to the acetylide form. Another terminal alkyne may then coordinate as a vinylidene ligand so the two are ideally placed for intramolecular C-C bond formation to give the η^3-enyne species. A further terminal alkyne is then involved, whose acidic proton liberates the dimer and coordinates to the metal as an acetylide ligand.

The stereoselectivity of the dimer formed (*E*:*Z*) is thought to depend on the metal-ligand system used,[57,63-66] in addition to the substituents on the terminal alkyne.[42,45,67,68] Yi was able to demonstrate how bulky ligands on $[RuCp^*(H)_3L]$, such as when L = PCy_3, promotes the formation of (*Z*)-PhCH=CHC≡CPh, whereas a smaller phosphine, like PMe_3, gives the (*E*)-isomer.[50,57] This is thought to be due to the greater steric demand of bulky ligands that direct the η^3-butenyne intermediate to adopt an (*E*)-configuration. However, it has also been noted that bulky ligands may also promote the formation of a butatrienyl product.[62,69]

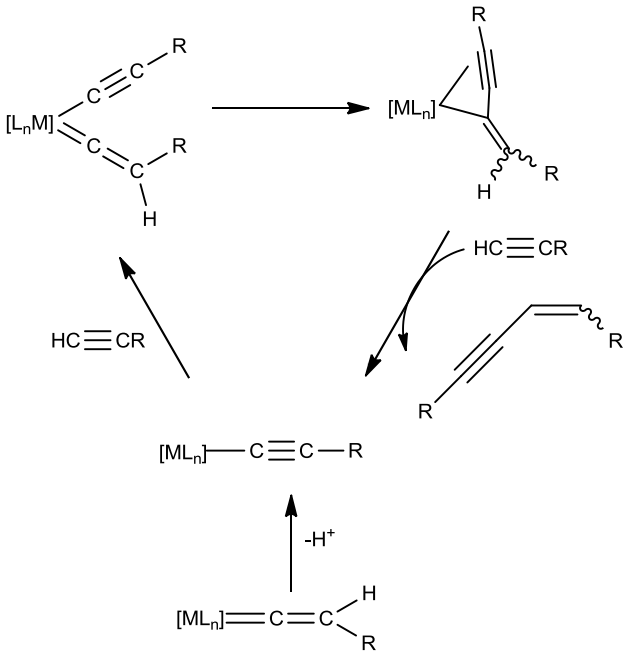

Figure 5.4.1.4: Mechanism for the dimerisation of terminal alkynes.

The mechanism proposed for the formation of a (*gem*)-dimer of a terminal alkyne is thought to involve the Markovnikov addition of a terminal alkyne to a second η^2-bound alkyne.[47] For our system, we have proposed an alternative mechanism based on the LAPS mechanisms proposed for vinylidene and acetylide ligand formation (Figure 5.4.1.5). It is thought that an acetate ligand may act as an internal base to deprotonate the vinylidene ligand to an acetylide. A second equivalent of the alkyne may then coordinate in a η^2-fashion so as to facilitate C-C bond formation to give the enyne. This may then be protonated by the liberated acetic acid and another alkyne may coordinate as a vinylidene.

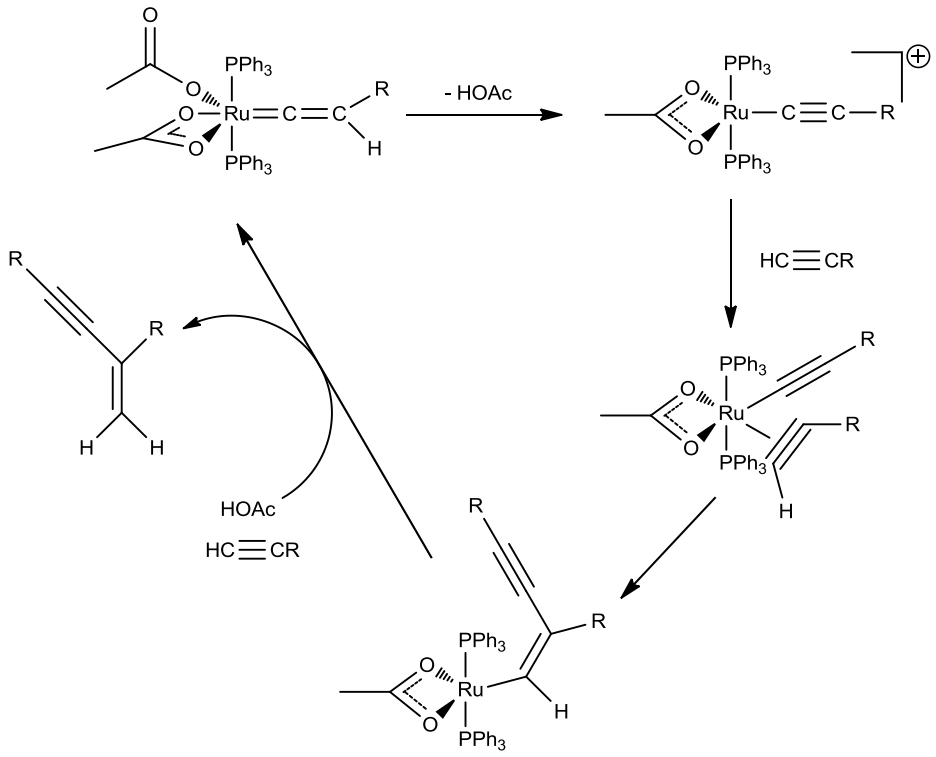

Figure 5.4.1.5: Mechanism proposed for the formation of a geminal-isomer of an alkyne dimer.

Analysis of the crude catalytic reaction mixtures by ^{31}P NMR spectroscopy led to the observation that in most cases one of the major phosphine-containing products had a chemical shift around δ_P 38, similar to the vinyl complex [Ru(CH=CH$_2$)(κ^2-OAc)(CO)(PPh$_3$)$_2$] (**10**), discussed further in Section 6.2.1. Protonation of this complex by acetic acid has been shown to result in the formation of complex **4** and ethene (Section 6.2.4). The other major peak often observed may correspond to [H-PPh$_3$]$^+$ at δ_P 31.5; a resonance at a similar chemical shift (δ_P 30.5) was identified upon addition of acetic acid to a solution of PPh$_3$ in CD_2Cl_2. Peaks thought to

correspond to analogues of complex **10** [Ru(CH=CRR')(κ^2-OAc)(CO)(PPh_3)$_2$] detected whilst monitoring stoichiometric reactions of the conversion of **9a-i** to **4** and an alkene by NMR spectroscopy are given in Table 5.4.1.3. The major and minor components detected in the crude $^{31}P\{^1H\}$ NMR spectra of the catalytic runs are also given. In the cases of **8d** and **8i**, two resonances are observed at similar chemical shifts. These resonances may be doublets, however the coupling distances are inconsistent (**8d** is 2.02 Hz, **8i** is 6.36 Hz). A more plausible explanation is that two isomers of the complex **10** analogue are formed, presumably (*E*) and (*Z*).

Substrate	**δ_P of '[Ru(CH=CRR')(κ^2-OAc)(CO)(PPh_3)$_2$]' analogue**	**δ_P of catalytic run Major & (minor)**
8a	38.7	38.7 (-)
8b	38.6	38.6 (31.5)
8c	38.7	- (38.7)
8d	38.7(2); 38.7(1)	31.6 (38.8)
8e	38.6	38.7 (-)
8f	38.8	38.4 (40.7)
8g	38.3	38.0 (41.9)
8h	38.5	31.5 (38.3, 38.9)
8i	38.5(7); 38.6(0)	38.57, 38.60

Table 5.4.1.3: Significant δ_P values of peaks observed in the monitored stoichiometric reactions of **9a-i** attributed to intermediates **10** and **11**, and the major and minor peaks observed in the crude mixture of catalytic products.

Although **1** has proven to be a poor catalyst for the conversion of a propargylic alcohol into an alkene, greater success was achieved when complex **1** was applied to the catalytic coupling of propargylic alcohols with carboxylic acids to give β-oxopropyl esters.

5.4.2 Catalytic conversion of Propargylic Alcohols to β-oxopropyl esters.

As noted in the introduction to this thesis (Section 1.6.1), the coupling of carboxylic acids with propargylic alcohols has been explored by the groups of Watanabe,[70] Dixneuf[71-73] and Bauer.[74] As for the coupling of carboxylic acids with terminal alkynes,[75] the mechanism is thought to involve the Markovnikov addition of the carboxylic acid to the alkyne when it is coordinated to the metal centre in a η^1-fashion. This electrophilic addition is then followed by an intramolecular transesterification to give the β-oxopropyl esters.

The following reactions were predominantly performed by Mr Nicholas Hiett and experimental detail may be found in the appropriate publication.[76] Initially, the catalytic coupling of HC≡CPh with benzoic acid was attempted using 5 mol % complex **1**. This resulted in the formation of four products; the (*E*)-, (*Z*)- and (*gem*)-isomers of the alk-1-en-1-yl esters and alkyne dimerisation products (Figure 5.4.2.1). The alk-1-en-1-yl esters result from the Markovnikov (geminal) and *anti*-Markovnikov (*cis*/*trans*) additions of the benzoic acid to the alkyne. When the reaction was performed at 60 °C, a mixture of components was obtained consisting mainly of alkyne dimerisation products. Repeating the reaction at 120 °C resulted in the formation of the four products indicated in a 6:1:10:1 ratio.

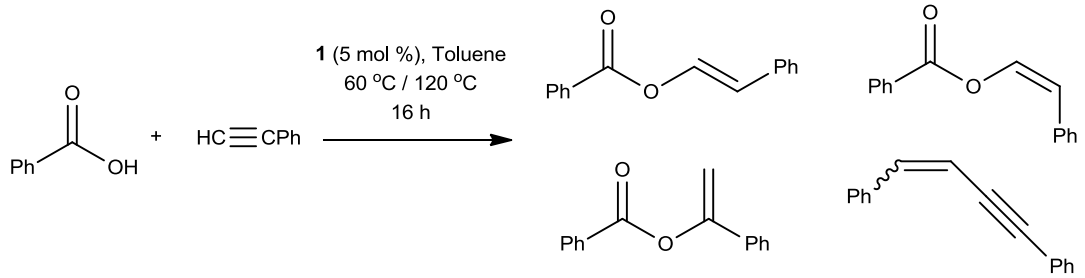

Figure 5.4.2.1: Catalytic coupling of HC≡CPh with benzoic acid by complex **1**.

The same conditions were employed for the catalytic coupling of the propargylic alcohols **8a-i** (excluding **8g**) with both benzoic and acetic acids to give β-oxopropyl esters. This process is illustrated in Figure 5.4.2.2 and Table 5.4.2.1 summarises the results obtained.

High isolated yields were obtained for this coupling across a range of substituted-propargylic alcohols, most notably including the steroid ethisterone (**8i**), with NMR conversion near 100 % in most cases. Unfortunately, the coupling of the diphenyl-substituted propargylic alcohol with benzoic acid failed, possibly due to the steric hindrance of two Ph-substituents on C_γ. A reaction of substrate **8d** with PhCOOH conducted in the absence of complex **1** (entry 4) resulted in zero conversion to the expected β-oxopropyl ester product, indicating that the presence of a ruthenium complex is essential.

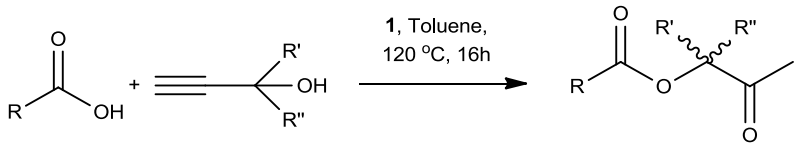

Figure 5.4.2.1: Catalytic coupling of **8d** with benzoic acid to give a β-oxopropyl ester.

Entry	Substrate HC≡C(R')(R'')(OH)	Acid (RCOOH)	Catalyst	Isolated Yield (%)
1	**8a**	PhCOOH	**1**	0
2	**8b**	PhCOOH	**1**	79
3	**8c**	PhCOOH	**1**	72
4	**8d**	PhCOOH	**-**	0
5	**8d**	PhCOOH	**1**	81
6	**8d**	PhCOOH	**4**	81
7	**8d**	PhCOOH	**13**	68
8	**8b**	MeCOOH	**1**	79
9	**8e**	PhCOOH	**1**	89
10	**8f**	PhCOOH	**1**	78
11	**8h**	PhCOOH	**1**	77
12	**8i**	PhCOOH	**1**	53

Table 5.4.2.1: Summary of yields obtained on coupling propargylic alcohols with benzoic/acetic acid.

The reaction also gave good yields when the CO-complex **4** (entry 6) or the benzoate-containing analogue (entry 7) $[Ru(\kappa^2\text{-}OBz)_2(PPh_3)_2]$ (**13** – Section 6.3) were used in the place of complex **1**. Trace amounts of an aldehyde product was often detected as a reaction component, which was thought to result from a competitive Meyer-Schuster rearrangement of the propargylic alcohol (see Section 5.4.1)

A catalytic coupling was also attempted between the phenoxy-substituted substrate **8j** and benzoic acid. This resulted in the formation of three products in a ratio of 0.7:1:1.6. As for the simple coupling of HC≡CPh and benzoic acid (Figure 5.4.2.1), it is clear that the three products result from the Markovnikov and *anti*-Markovnikov additions of the acid to the terminal alkyne.

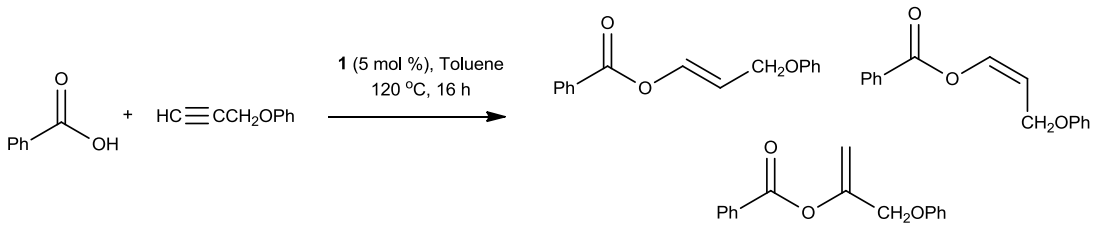

Figure 5.4.2.3: Catalytic Markovnikov and anti-Markovnikov addition of benzoic acid to **8j**.

Two proposed mechanisms are illustrated in Figure 5.4.2.3; (a) shows the *anti*-Markovnikov additions of an acid to a terminal alkyne and (b) shows the accepted mechanism for the formation of the β-oxopropyl esters from propargylic alcohols and an acid. In (a), it is proposed that the electrophilic C_α undergoes attack by an uncoordinated oxygen of a carboxylate ligand in an *anti*-Markovnikov reaction. The (*E*)- and (*Z*)-isomers are obtained depending on the orientation of the R' substituent. For mechanism (b), the η^2-bound alkyne undergoes attack by a carboxylate nucleophile in a Markovnikov-type addition. A keto-enol tautomerisation followed by an intramolecular transesterification to generate the coordinated form of the β-oxopropyl ester may occur, and the organic product may be liberated by protonation.

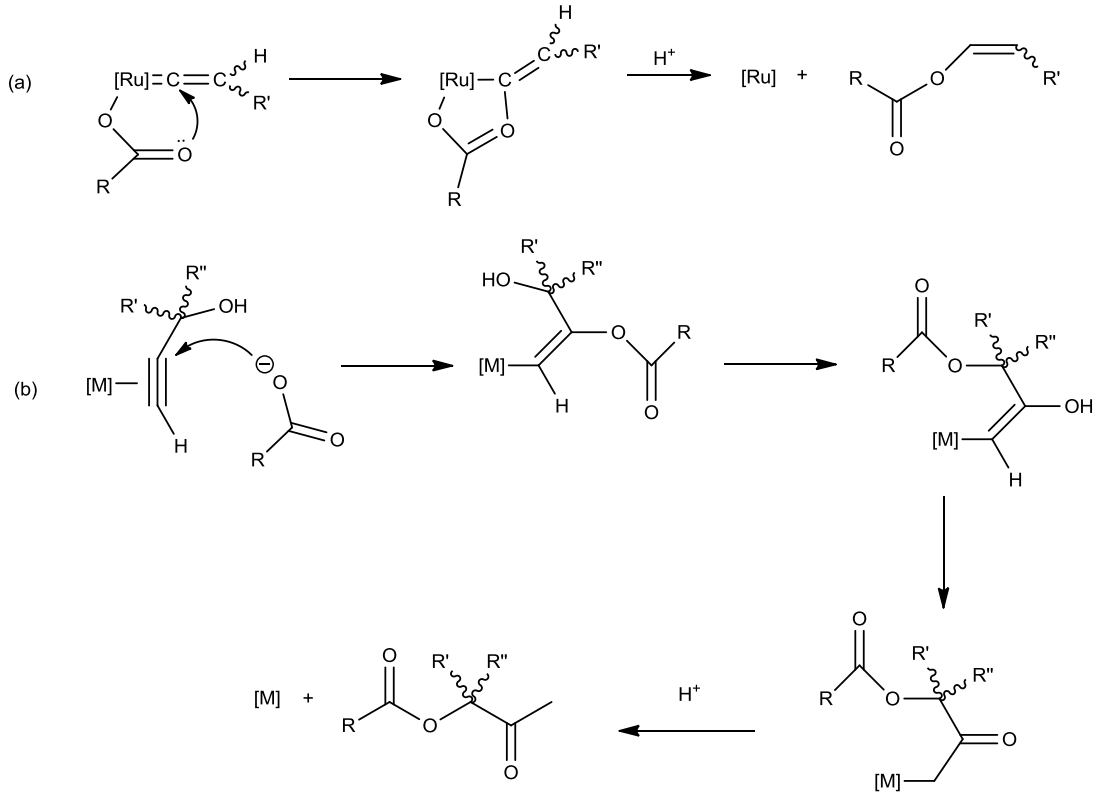

Figure 5.4.2.3: Mechanisms proposed for (a) the *anti*-Markovnikov addition of acid to a terminal alkyne; (b) catalytic formation of β-oxopropyl esters.

Unfortunately, the conversion of propargylic alcohols to alkenes could not be made catalytic using complex **1**, under the conditions employed. However, a greater degree of success was achieved in the catalytic coupling of propargylic alcohols with carboxylic acids.

5.5: Conclusions

A library of novel ruthenium hydroxy-vinylidene complexes has been successfully synthesised by the addition of commercially available propargylic alcohols to **1**. These complexes **9a-i** have been isolated and characterised by a range of spectroscopic techniques, including NMR, IR and MS. Careful analysis of this data provided overwhelming evidence that the complexes obtained contained hydroxy-vinylidene ligands, and had not undergone dehydration to the allenylidene or vinylvinylidene forms. In some cases, crystals suitable for study by X-ray diffraction were obtained, providing conclusive proof that these were hydroxy-vinylidene complexes.

These complexes have been shown to possess similar NMR and IR spectroscopic features to those observed for the vinylidene complexes **2a-d**. A full comparison of these features for all acetate-containing complexes described in this thesis is provided in Chapter 8.

Surprisingly, it has not been possible to observe the formation of an allenylidene ligand *via* the dehydration of these hydroxy-vinylidenes. Instead, solutions of these complexes **9a-i** were observed to convert in time through to the CO-containing complex **4**, previously reported in Chapter 3, and the corresponding alkene. A significant amount of theoretical and experimental work was conducted in order to understand the mechanism by which this process occurs, which is the focus of the following chapter. Attempts to make this conversion catalytic met with little success, with the conditions employed giving rise to a range of products including dimerisation products. Efforts could be made in the future to optimise this process, for example by varying the reaction conditions. However, the catalytic coupling of propargylic alcohols with carboxylic acids by complex **1** was more successful, with products obtained in good to excellent yields.

5.6: References

1. Selegue, J. P. *Organometallics* **1982**, *1*, 217.
2. Cadierno, V., Gimeno, J., *Chem. Rev.* **2009**, *109*, 3512.
3. Bruneau, C., Dixneuf, P. H., Eds. *Metal Vinylidenes and Allenylidenes in Catalysis: From Reactivity to Applications in Synthesis*, **2008**, Wiley VCH: Weinheim, Germany.
4. Selegue, J. P., *Coord. Chem. Rev.* **2004**, 248, 1543.
5. Rigaut, S., Touchard, D., Dixneuf, P. H., *Coord. Chem. Rev.* **2004**, *248*, 1585.
6. Bruce, M. I., *Chem. Rev.* **1998**, *98*, 2797.
7. Cadierno, V., Gamasa, M. P., Gimeno, J., *Eur. J. Inorg. Chem.* **2001**, 571.
8. Touchard, D., Dixneuf, P. H., *Coord. Chem. Rev.* **1998**, *178-180*, 409.
9. Bustelo, E., Jiménez-Tenorio, M., Puerta, M. C., Valerga, P., *Organometallics* **1999**, *18*, 950.
10. Le Lagadac, R., Roman., E., Toupet, L., Müller, U., Dixneuf, P. H., *Organometallics* **1994**, *13*, 5030.
11. Bustelo, E., Jiménez-Tenorio, M., Puerta, M. C., Valerga, P., *Organometallics* **1999**, *18*, 4563.
12. Aneetha, H., Jiménez-Tenorio, M., Puerta, M. C., Valerga, P., *Organometallics* **2003**, *22*, 2001.
13. Cadierno, V., Gamasa, M. P., Gimeno, J., González-Cueva, M., Lastra, E., Borge, J., García-Granda, S., Pérez-Carreño, E., *Organometallics* **1996**, *15*, 2137.
14. Werner, H., Rappert, T., Wiedemann, R., Wolf, J., Mahr, N., *Organometallics* **1994**, *13*, 2721.

15. Bustelo, E., Jiménez-Tenorio, M., Puerta, M. C., Valerga, P., *Eur. J. Inorg. Chem.* **2001**, 2391.

16. Schanz, H-J.; Jafarpour, L.; Stevens, E. D.; Nolan, S. P. *Organometallics* **1999**, *18*, 5187.

17. Fürstner, A.; Guth, O.; Düffels, A.; Seidel, G.; Liebl, M.; Gabor, B.; Mynott, R. *Chem. Eur. J.* **2001**, *7*, 4811.

18. Castarlenas, R.; Dixneuf, P. H. *Angew. Chem. Int. Ed.* **2003**, *42*, 4524.

19. Castarlenas, R.; Vovard, C.; Fischmeister, C.; Dixneuf, P. H. *J. Am. Chem. Soc*. **2006**, *128*, 4079.

20. Rigaut, S., Touchard, D., Dixneuf, P. H., *Coord. Chem. Rev.***2004**, *248*, 1585.

21. Fürstner, A.; Picquet, M.; Bruneau, C.; Dixneuf, P. H. *Chem. Commun.* **1998**, 1315.

22. Picquet, M.; Touchard, D.; Bruneau, C.; Dixneuf, P. H. *New. J. Chem.* **1999**, *23*, 141.

23. Picquet, M.; Bruneau, C.; Dixneuf, P. H. *Chem. Commun.* **1998**, 2249.

24. Sémeril, D.; Le Nôtre, J.; Bruneau, C.; Dixneuf, P. H.; Kolomiets, A. F.; Osipov, S. *New. J. Chem.* **2001**, *25*, 16.

25. Castarlenas, R.; Sémeril, D.; Noels, A. F.; Demnoceau, A, Dixneuf, P. H. *J. Organomet. Chem.* **2002**, *663*, 235.

26. Bruneau, C., Dixneuf, P. H., *Angew. Chem. Int. Ed.* **2006**, *45*, 2176.

27. Castarlenas, R., Fischmeister, C., Bruneau, C., Dixneuf, P. H., *J. Mol. Catal. A: Chem.* **2004**, *213*, 31.

28. Winter, R. F., Záliš, S., *Coord. Chem. Rev.* **2004**, *248*, 1565.

29. Bruce, M. I. *Chem. Rev*. **1991**, *91*, 197.

30. Desiraju, G. R.; Steiner, T. *The Weak Hydrogen Bond: In Structural Chemistry and Biology*; **1999**, Oxford Science Publications.

31. Günther, H., *NMR Spectroscopy: Basic Principles, Concepts and Applications*, 2nd Ed., **1995**, Wiley.

32. Personal communication from T.A.D. Former MS service Technician, University of York.

33. Berke, H. *Z. Naturforsch., B: Anorg Chem., Org. Chem.* **1980**, *35B*, 86.

34. Martín, M.; Gevert. O.; Werner, H. *Dalton Trans.* **1996**, 2275.

35. Bustelo, E., Dixneuf, P. H., *Adv. Synth. Catal.* **2005**, *347*, 393.

36. Bustelo, E., Dixneuf, P. H., *Adv. Synth. Catal.* **2007**, *349*, 933.

37. Datta, S.; Chang, C-L.; Yeh, K-L.; Liu, R-S. *J. Am. Chem. Soc.* **2003**, *125*, 9294.

38. Haak, E. *Eur. J. Org. Chem.* **2007**, 2815.

39. Schmitt, H. J.; Singer, H. *J.Organomet. Chem.* **1978**, *153*, 165.

40. Chen, X.; Xue, P.; Sung, H. H. Y.; Williams, I. D.; Peruzzini, M.; Bianchini, C.; Jia, G. *Organometallics* **2005**, *24*, 4330.

41. Trost, B. M.; Chan, C.; Rühter, G. *J. Am. Chem. Soc.* **1987**, *109*, 3486.

42. Trost, B. M.; Sorum, M. T.; Chan, C.; Harms, A. E.; Rühter, G. *J. Am. Chem. Soc.***1997**, *119*, 698.

43. Daniels, M.; Kirss, R. U. *J. Organomet. Chem.* **2007**, *692*, 1716.

44. Ohshita, J.; Furumori, K.; Matsuguchi, A.; Ishikawa, M. *J. Org. Chem.* **1990**, *55*, 3277.

45. Slugovc, C.; Mereiter, K.; Zobetz, E.; Schmid, R.; Kirchner, K. *Organometallics* **1996**, *15*, 5275.

46. Katayama, H.; Nakayama, M.; Nakano, T.; Wada, C.; Akamatsu, K.; Ozawa, F. *Macromolecules*, **2004**, *37*, 13.

47. Katayama, H.; Yari, H.; Tanaka, M.; Ozawa, F. *Chem. Commun*. **2005**, 4336.

48. Echavarren, A. M.; López, J.; Santos, A.; Montoya, J. *J. Organomet. Chem.* **1991**, *414*, 393.

49. Ohmura, T.; Yorozuya, S-i.; Yamamoto, Y.; Miyaura, N.; *Organometallics* **2000**, *19*, 365.

50. Yi, C. S.; Liu, N. *Organometallics* **1996**, *15*, 3968.

51. Fossatelli, M.; van der Kerk, A. C. T. H. M.; Vasilevsky, S. F.; Brandsma, L. *Tett. Lett.* **1992**, *33*, 4229.

52. Provencal, D. P.; Leahy, J. W. *J. Org. Chem.* **1994**, *59*, 5496.

53. Bruneau, C., Dixneuf, P. H., *Chem. Commun.* **1997**, 1201.

54. Suzuki, T., Tokunaga, M., Wakatsuki, Y., *Tett. Lett.*, **2002**, *43*, 7531.

55. Cadierno, V., García-Garrido, S. E., Gimeno, J., *Adv. Synth. Catal.* **2006**, *348*, 101.

56. Puerta, M. C.; Valerga, P. *Coord. Chem. Rev.* **1999**, *193-195*, 977.

57. Katayama, H., Ozawa, F., *Coord. Chem. Rev*. **2004**, *248*, 1703.

58. Katayama, H., Ozawa, F., Tanaka, M., Yari, H., *Chem. Commun*. **2004**, *248*, 1703.

59. Olivier, C., Kim, B-S., Touchard, D., Rigaut, S., *Organometallics* **2008**, *27*, 509.

60. Bianchini, C., Peruzzini M., Zanobini, F., Frediani, P., Albinati, A., *J. Am. Chem. Soc*. **1991**, *113*, 5453.

61. Bianchini, C., Frediani, P., Masi, D., Peruzzini, M., Zanobini, F., *Organometallics* **1994**, *13*, 4616.

62. Bianchini, C., Innocenti, P., Peruzzini, M., Romerosa, A., Zanobini, F., *Organometallics*. **1996**, *15*, 272.

63. Nolan, S. P., Yang, C., *J. Org. Chem*. **2002**, *67*, 591.

64. Hou, Z., Nishiura, M., Miyayoto, T., Wakatsuki, Y., Yamaki, T., *J. Am. Chem. Soc*. **2003**, *125*, 1184.

65. Trost, B. M., Crawley, M. L., *Chem. Rev*. **2003**, *103*, 2921.

66. Ishii, Y., Hirabayashi, T., Sakaguchi, S., *Adv. Synth. Catal*. **2005**, *347*, 872.

67. Yi, C. S., Jiu, N., *Organometallics* **1998**, *17*, 3158.

68. Katayama, H., Ozawa, F., Taniguchi, K., Wada, C., *Organometallics* **2002**, *21*, 3285.

69. Wakatsuki, Y., Yamazaki, H., Kumegawa, N., Satoh, T., Satoh, J. Y., *J. Am. Chem. Soc*. **1991**, *113*, 9604.

70. Mitsudo, T.; Hori, Y.; Yamazaki, Y.; Watanabe, Y. *J. Org. Chem.* **1987**, *52*, 2230.

71. Devanne, D.; Ruppin, C.; Dixneuf, P. H. *J. Org. Chem.* **1988**, *53*, 925.

72. Bruneau, C.; Kabouche, Z.; Neveux, M.; Seiller, B.; Dixneuf, P. H. *Inorg. Chim. Acta.* **1994**, *222*, 154.

73. Darcel, C.; Bruneau, C.; Dixneuf, P. H.; Neef, G. *J. Chem. Soc. Chem. Commun.* **1994**, 333.

74. Costin, S.; Rath, N. P.; Bauer, E. B. *Adv. Synth. Catal.* **2008**, *350*, 2414.

75. Bruneau, C. *Anti*-Markovnikov Additions of *O*-, *N*-, *P*-Nucleophiles to Triple Bonds with Ruthenium Catalysts (Chapter 10) *Metal Vinylidenes and Allenylidenes in Catalysis: From Reactivity to Applications in Synthesis*, (Bruneau, C., Dixneuf, P. H., Eds.) **2008**, Wiley VCH: Weinheim, Germany.

76. Hiett, N. P.; Lynam, J. M.; Welby, C. E.; Whitwood, A. C. *J. Organomet. Chem.* **2011**, *696*, 378.

77. Comparison with authentic sample of diphenylethylene.

78. Comparison with simuated spectrum provided by Scifinder.

79. Pondey, S. K., Greene, A. E., Poisson, J-F., *J. Org. Chem.* **2007**, *72*, 7769.

80. Styrene: ALDRICH online NMR library.

81. Methylenecyclopentane: ALDRICH online NMR library.

82. Methylenecyclohexane: ALDRICH online NMR library.

83. Cho, B. P., *Tett. Lett.* **1995**, *36*, 2403.

84. Ethene: Comparison with simulated NMR spectrum in ALDRICH online NMR library.

85. Macdonald, B. S., Sykes, P. J., Adhikary, P. M., Harkness, R. A., *Steroids* **1971**, *18:6,* 753.

86. Templeton, J. F., Jackson, C. J. C., *Steroids* **1983**, *41*, 485.

87. Shimizu, I., Sugiura, T., Tsuji, J., *J. Org. Chem.* **1985**, *50*, 537.

88. Pettigrew, J. D., Cadieux, J. A., So, S. S. S., Wilson, P. D., *Org. Lett.* **2005**, *7*, 467.

89. Ye, J., Ge, J., Chen, X., Zhao, Z., Lu, P., *Tetrahedron* **2007**, *63*, 11040.

5.7: Experimental

General:

All experimental procedures were performed under an atmosphere of dinitrogen or argon using standard Schlenk Line and Glove Box techniques. DCM, pentane and hexane were purified with the aid of an Innovative Technologies anhydrous solvent engineering system. The CD_2Cl_2 used for NMR experiments was dried over CaH_2 and degassed with three freeze-pump-thaw cycles. The solvent was then vacuum transferred into NMR tubes fitted with PTFE Young's taps. NMR spectra were acquired on a Bruker AVANCE 500 (Operating Frequencies ^{1}H 500.23 MHz, ^{31}P 202.50 MHz, ^{13}C 125.77 MHz). ^{31}P and ^{13}C spectra were recorded with proton decoupling. Mass spectrometry measurements were performed on a Thermo-Electron Corp LCQ Classic (ESI) instrument or Waters GCT Premier Acceleration TOF MS (LIFDI). IR spectra were acquired on a Thermo-Nicolet Avatar 370 FTIR spectrometer using either CsCl solution cells or as KBr discs. CHN measurements were performed using an Exeter Analytical Inc. CE-440 analyser. The proportion of DCM in CHN samples was confirmed by recording a ^{1}H NMR spectrum of a sample used for CHN analysis in d_8-toluene. Relative integration of the peak at δ_H 4.31 (CH_2Cl_2) to that of the vinylidene proton indicates the proportion of DCM in that sample. Structural characterisation of complexes **9a**, **9c**, and **9e** was conducted using a Bruker Smart Apex diffractomer with Mo-K_α radiation (λ = 0.71073 Å) with a SMART CCD camera. Diffractometer control, data collection and initial unit cell determination was performed using SMART. Frame integration and unit-cell refinement software was carried out with Saint+. Absorption corrections were applied by SADABS (v 2.03, Sheldrick). Structures were solved by direct methods using SHELXS-97, and refined by full-matrix least-squares using SHELX-97. All non-hydrogen atoms were refined anisotropically. Hydrogen atoms were placed using a "riding model" and included in the refinement at calculated positions. Substrates **8a-f**, **h** and **i** (Sigma-Aldrich), and **g** (Lancaster Synthesis) were used as supplied without further purification. Complex **1** was prepared according to the published literature method.[76]

Key to NMR shorthand:

s (singlet); br s (broad singlet); d (doublet); dd (doublet of doublets); ad (apparent doublet); t (triplet); dt (doublet of triplets); tt (triplet of triplets); at (apparent triplet); q (quartet); aq (apparent quartet); qn (quintet), aqn (apparent quintet); sp (septet); asp (apparent septet); m (multiplet)

(H_2-Ph) or (H_2-PPh_3) refers to the proton in the *ortho*-position of a phenyl ring

(H_3-Ph) or (H_3-PPh_3) refers to the proton in the *meta*-position of a phenyl ring

(H_4-Ph) or (H_4-PPh_3) refers to the proton in the *para*-position of a phenyl ring

General Procedure for the synthesis of complexes 9a-i

Approximately one equivalent of the alkyne was added to a Schlenk vessel containing a solution of **1** in CH_2Cl_2. After stirring for one hour the product was precipitated by addition of pentane/hexane. After filtration of the solvent by a cannula wire fitted with a filter-paper tip, the solid powder was washed twice more with pentane/hexane and dried *in vacuo*.

5.7.1: Synthesis of [Ru(κ^1-OAc)(κ^2-OAc)(=C=CHC(Ph)$_2$OH)(PPh$_3$)$_2$], 9a.

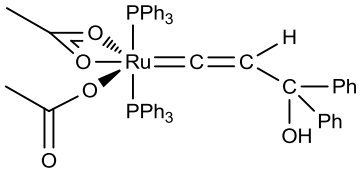

0.55 g **9a** (85.9 %) was obtained as a bright yellow powder from 0.50 g (0.67 mmol) **1** and 0.14 g (0.67 mmol) HC≡CCPh$_2$OH in 30 mL DCM. After reducing the volume of the solution by half *in vacuo*, 40 mL hexane was used to precipitate the product, and it was washed further with 2 x 30 ml portions of hexane. Crystals for X-ray diffraction were obtained from a CH_2Cl_2/hexane solution.

NMR Spectra CD_2Cl_2:

^{1}H δ_H 0.71 (s, 6H, C*H*COO$_3$), 4.73 (t, $^4J_{PH}$ = 3.9 Hz, 1H, Ru=C=C*H*C{OH}Ph$_2$), 4.88 (s, 1H, Ru=C=CHC{O*H*}Ph$_2$), 6.93-7.03 (m, 10H, Ru=C=CHC{OH}*Ph*$_2$), 7.24-7.37 m, (30H, P*Ph*$_3$)

^{31}P δ_P 34.0 (s, *P*Ph$_3$)

^{13}C δ_C 21.7 (s, *C*H$_3$COO), 74.0 (s, Ru=C=CH−*C*{OH}Ph$_2$), 117.2 (t, $^3J_{PC}$ = 4.7 Hz, Ru=C=*C*), 125.9, (CPh$_2$-*C$_4$*), 126.2 (s, CPh$_2$-*C$_2$*/*C$_3$*), 127.7 (s, CPh$_2$-*C$_2$*/*C$_3$*), 128.0 (t, $^3J_{PC}$+$^5J_{PC}$ = 9.8 Hz, PPh$_3$-*C$_3$*), 129.4 (t, $^1J_{PC}$+$^3J_{PC}$ 42.2 Hz, PPh$_3$-*C$_1$*), 130.1 (s, PPh$_3$-*C$_4$*), 135.0 (t, $^2J_{PC}$+$^4J_{PC}$ = 11.6 Hz, PPh$_3$-*C$_2$*), 149.8 (s, C*Ph$_2$*-*C$_1$*), 179.6 (s, CH$_3$*C*OO), 347.6 (t, $^2J_{PC}$ = 16.2 Hz, Ru=*C*)

IR (KBr) 1378 cm^{-1} (κ^1-OCO$_{sym}$), 1434 cm^{-1} (P-Ph), 1465 cm^{-1} (κ^2-OCO$_{sym}$), 1527 cm^{-1} (κ^2-OCO$_{asym}$), 1595 cm^{-1} (κ^1-OCO$_{asym}$), 1654 cm^{-1} (C=C), 3260 cm^{-1} (OH), $\Delta\nu_{(uni)}$ 217 cm^{-1}, $\Delta\nu_{(chelate)}$ 62 cm^{-1}; (CH_2Cl_2) 1371 cm^{-1} (κ^1-OCO$_{sym}$), 1435 cm^{-1} (P-Ph), 1463 cm^{-1} (κ^2-OCO$_{sym}$), 1531 cm^{-1} (κ^2-OCO$_{asym}$), 1598 cm^{-1} (κ^1-OCO$_{asym}$), 1649 cm^{-1} (C=C), 3276 cm^{-1} (OH), $\Delta\nu_{(uni)}$ 227 cm^{-1}, $\Delta\nu_{(chelate)}$ 68 cm^{-1};

MS (ESI), m/z 975.1914 (Expected for $^{101}RuP_2O_5NaC_{55}H_{48}$ [M]Na$^+$ = 975.1918), 713.1321 (Expected for $^{101}RuPO_5NaC_{37}H_{33}$ [M – PPh$_3$]Na$^+$ = 713.1007)

CHN Anal for $RuP_2O_4Cl_2C_{56}H_{50}$ (calc), % C 64.86, % H 4.86; (found) % C 64.33, % H 4.77

Crystal data and structure refinement for 9a.

Identification code	jml0804m	
Empirical formula	$RuP_2O_5Cl_2C_{56}H_{50}$	
Formula weight	1036.87	
Temperature	110(2) K	
Wavelength	0.71073 Å	
Crystal system	Monoclinic	
Space group	P2(1)/n	
Unit cell dimensions	a = 12.1131(5) Å	α= 90°.
	b = 16.5914(7) Å	β= 93.0550(10)°.
	c = 23.9945(10) Å	γ = 90°.
Volume	4815.4(3) $Å^3$	
Z	4	
Density (calculated)	1.430 Mg/m^3	
Absorption coefficient	0.553 mm^{-1}	
F(000)	2136	
Crystal size	0.24 x 0.08 x 0.08 mm^3	
Theta range for data collection	1.70 to 30.01°.	
Index ranges	-16<=h<=17, -23<=k<=23, -33<=l<=33	
Reflections collected	54123	
Independent reflections	13924 [R(int) = 0.0276]	
Completeness to theta = 30.01°	99.1 %	
Absorption correction	Semi-empirical from equivalents	
Max. and min. transmission	0.957 and 0.858	
Refinement method	Full-matrix least-squares on F^2	
Data / restraints / parameters	13924 / 0 / 601	
Goodness-of-fit on F^2	1.025	
Final R indices [I>2sigma(I)]	R1 = 0.0313, wR2 = 0.0737	
R indices (all data)	R1 = 0.0416, wR2 = 0.0780	
Largest diff. peak and hole	1.009 and -0.862 $e.Å^{-3}$	

5.7.2: Synthesis of [Ru(κ^1-OAc)(κ^2-OAc)(=C=CHC(Me)$_2$OH)(PPh$_3$)$_2$], 9b.

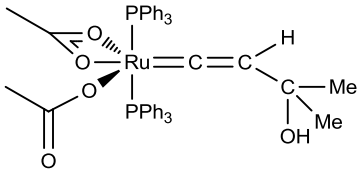

0.32 g **9b** (76.2 %) was obtained as a bright yellow powder from 0.38 g (0.51 mmol) **1** and 50.0 μL (0.51 mmol) HC≡CCMe$_2$OH in 30 mL DCM. After reducing the volume of the solution by half *in vacuo*, 20 mL hexane was used to precipitate the product, and it was washed further with 2 x 30 ml portions of hexane.

NMR Spectra CD_2Cl_2:

^{1}H δ_H 0.68 (s, 6H, Ru=C=CHC(C*H*$_3$)$_2$OH), 0.77 (s, 6H, C*H*$_3$COO), 0.93 (br s, 1H, Ru=C=CHCMe$_2$O*H*), 4.32, (t, $^4J_{PH}$ = 3.9 Hz, 1H, Ru=C=C*H*CMe$_2$OH), 7.33-7.45, (m, 30H, P*Ph*$_3$)

^{31}P δ_P 34.1 (s, *P*Ph$_3$)

^{13}C δ_C 22.0 (s, *C*H$_3$COO), 30.9 (s, Ru=C=CHC*Me*$_2$), 67.9 (s, Ru=C=CH−*C*), 118.4 (t, $^3J_{PC}$ = 4.8 Hz, Ru=C=*C*), 128.0 (t, $^3J_{PC}$+$^5J_{PC}$ = 9.3 Hz, PPh$_3$-*C*$_3$), 129.7, (t, $^1J_{PC}$+$^3J_{PC}$ = 42.6 Hz, PPh$_3$-*C*$_1$), 130.1 (s, PPh$_3$-*C*$_4$), 134.98 (t, $^2J_{PC}$+$^4J_{PC}$ = 11.0 Hz, PPh$_3$-*C*$_2$), 179.5 (s, CH$_3$*C*OO), 352.0 (t, $^2J_{PC}$ = 16.3 Hz, Ru=*C*)

IR (KBr) 1362 cm^{-1} (κ^1-OCO$_{sym}$), 1434 cm^{-1} (P-Ph), 1460 cm^{-1} (κ^2-OCO$_{sym}$), 1533 cm^{-1} (κ^2-OCO$_{asym}$), 1619 cm^{-1} (κ^1-OCO$_{asym}$), 1648 cm^{-1} (C=C), 3572 cm^{-1} (OH) $\Delta\nu_{(uni)}$ 257 cm^{-1}, $\Delta\nu_{(chelate)}$ 73 cm^{-1}; (CH_2Cl_2) 1366 cm^{-1} (κ^1-OCO$_{sym}$), 1435 cm^{-1} (P-Ph), 1459 cm^{-1} (κ^2-OCO$_{sym}$), 1539 cm^{-1} (κ^2-OCO$_{asym}$), 1623 cm^{-1} (κ^1-OCO$_{asym}$), 1653 cm^{-1} (C=C), 3563 cm^{-1} (OH), $\Delta\nu_{(uni)}$ 257 cm^{-1}, $\Delta\nu_{(chelate)}$ 80 cm^{-1};

MS (ESI) m/z 851.1612 (Expected for $^{101}RuP_2O_5NaC_{45}H_{44}$ [M]Na$^+$ = 851.1605)

5.7.3: Synthesis of [Ru(κ^1-OAc)(κ^2-OAc)(=C=CHC(Ph)(Me)OH)(PPh$_3$)$_2$], 9c.

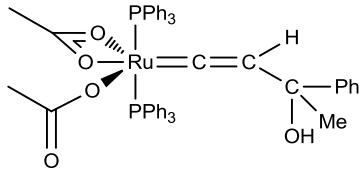

0.12 g **9c** (66.7 %) was obtained as a bright yellow powder from 0.15 g (0.20 mmol) **1** and 0.03 g (0.20 mmol) HC≡CC(Ph)(Me)OH in 10 mL CH_2Cl_2. 40 mL pentane was used to precipitate the product, and it was washed further with 2 x 15 ml portions of pentane.

NMR Spectra CD_2Cl_2:

^{1}H δ_H 0.81 (s, 6H, C*H*$_3$COO), 1.10 (s, 3H, HC≡CC(C*H*$_3$)), 2.79 (br s, 1H, [Ru]=C=CHC(O*H*)), 4.56 (t, $^4J_{HP}$ = 3.9 Hz, 1H, [Ru]=C=C*H*), 6.96 – 7.10 (m, 5H, HC≡CC(*Ph*)), 7.38 (at, *J* = 7.4 Hz, 12H, *H*$_3$-P*Ph*$_3$), 7.45 – 7.50 (m, 18H, *H*$_2$- and *H*$_4$-P*Ph*$_3$)

^{31}P δ_P 34.3 (s, 2.0P, *P*Ph$_3$)

^{13}C δ_C 21.8 (s, *C*H$_3$COO), 33.6 (s, Ru=C=C–C(*C*H$_3$)), 71.1 (s, Ru=C=CH–*C*OH), 117.6 (t, $^3J_{PC}$ = 4.3 Hz, Ru=C=*C*), 124.9 (s, Ru=C=C–CPh–*C*$_3$), 125.8 (s, Ru=C=C–CPh–*C*$_4$), 127.7 (s, Ru=C=C–CPh–*C*$_2$), 128.0 (t, $^3J_{PC}$ + $^5J_{PC}$ = 9.6 Hz, PPh$_3$–*C*$_3$), 129.4 (t, $^1J_{PC}$ + $^3J_{PC}$ = 43.2 Hz, PPh$_3$–*C*$_1$), 130.1 (s, PPh$_3$–*C*$_4$), 135.0 (t, $^2J_{PC}$ + $^4J_{PC}$ = 11.6 Hz, PPh$_3$–*C*$_2$), 150.4 (Ru=C=C–CPh–*C*$_1$), 179.6 (s, CH$_3$*C*OO), 350.4 (t, $^2J_{PC}$ = 16.0 Hz, Ru=*C*)

IR (KBr) 1361 cm^{-1} (κ^1-OCO$_{sym}$), 1434 cm^{-1} (P–Ph), 1458 cm^{-1} (κ^2-OCO$_{sym}$), 1536 cm^{-1} (κ^2-OCO$_{asym}$), 1601 cm^{-1} (κ^1-OCO$_{asym}$), 1649 cm^{-1} (C=C), 3574 cm^{-1} (OH), $\Delta\nu_{(uni)}$ 240 cm^{-1}, $\Delta\nu_{(chelate)}$ 78 cm^{-1}; (CH_2Cl_2) 1367 cm^{-1} (κ^1-OCO$_{sym}$), 1434 cm^{-1} (P–Ph), 1463 cm^{-1} (κ^2-OCO$_{sym}$), 1533 cm^{-1} (κ^2-OCO$_{asym}$), 1601 cm^{-1} (κ^1-OCO$_{asym}$), 1652 cm^{-1} (C=C), 3565 cm^{-1} (OH), $\Delta\nu_{(uni)}$ 234 cm^{-1}, $\Delta\nu_{(chelate)}$ 70 cm^{-1}.

MS (ESI) m/z 873.2074 (Expected for $^{101}RuP_2O_4C_{50}H_{45}$ $[M\text{-}OH]^+$ = 873.1837)

CHN Anal. for $RuP_2O_5C_{50}H_{46}$ + (0.40 CH_2Cl_2) (calc), C 65.52, H 5.11; (found) C 65.75, H 5.21

Crystal data and structure refinement for 9c.

Identification code	jml0825m
Empirical formula	$RuP_2O_5C_{50}H_{46}$
Formula weight	889.88
Temperature / K	110.0
Crystal system	Triclinic
Space group	P-1
a / Å, b / Å, c / Å	11.6253(5), 13.3991(6), 15.2933(6)
α/°, β/°, γ/°	87.3510(10), 68.0190(10), 71.9900(10)
Volume / $Å^3$	2094.27(15)
Z	2
ρ_{calc} / mg mm^{-3}	1.411
μ / mm^{-1}	0.499
F(000)	920
Crystal size / mm^3	0.11 × 0.10 × 0.04
2Θ range for data collection	2.88 to 60.06°
Index ranges	$-16 \leq h \leq 16$, $-18 \leq k \leq 18$, $-21 \leq l \leq 21$
Reflections collected	23951
Independent reflections	11837[R(int) = 0.0201]
Data/restraints/parameters	11837/0/527
Goodness-of-fit on F^2	1.033
Final R indexes [I>2σ (I)]	R_1 = 0.0332, wR_2 = 0.0777
Final R indexes [all data]	R_1 = 0.0449, wR_2 = 0.0830
Largest diff. peak/hole / e $Å^{-3}$	1.094/-0.847

5.7.4: Synthesis of [Ru(κ^1-OAc)(κ^2-OAc)(=C=CHC(Ph)(H)OH)(PPh$_3$)$_2$], 9d.

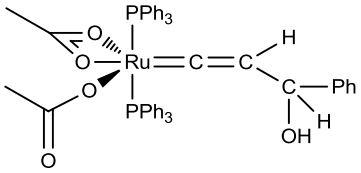

0.16 g **9d** (69.6 %) was obtained as a pale yellow powder from 0.20 g (0.27 mmol) **1** and 32.7 μL (0.27 mmol) HC≡CC(Ph)(H)OH in 15 mL CH_2Cl_2. 30 mL pentane was used to precipitate the product, and it was washed further with 2 x 15 ml portions of pentane.

NMR Spectra CD_2Cl_2:

^{1}H δ_H 0.86 (s, 6H, C*H*$_3$COO), 2.87 (br s, 1H, [Ru]=C=CHC(H)(Ph)O*H*), 4.14 (dt, $^4J_{HP}$ = 3.8 Hz, $^3J_{HH}$ = 6.4 Hz, 1H, [Ru]=C=C*H*C(H)(Ph)OH), 5.44 (d, $^3J_{HH}$ = 6.3 Hz, 1H, [Ru]=C=CHC(*H*)(Ph)OH), 6.83 (d, 7.3 Hz, 2H, *H*$_2$-Ph), 7.09 (at, 7.5 Hz, 2H, *H*$_3$-Ph), 7.14 (tt, 7.2 Hz, 1.4 Hz, 1H, *H*$_4$-Ph), 7.41 (at, 7.3 Hz, 12H, *H*$_3$-P*Ph*$_3$), 7.48 (t, 7.2 Hz, 6H, *H*$_4$-P*Ph*$_3$), 7.53 (m, 12H, *H*$_2$-P*Ph*$_3$)

^{31}P δ_P 34.9 (s, 2.0P, *P*Ph$_3$)

^{13}C δ_C 21.8 (s, *C*H$_3$COO), 67.0 (s, Ru=C=CH–*C*OH), 112.5 (t, $^3J_{PC}$ = 4.7 Hz, Ru=C=*C*), 126.3 (s, Ru=C=C–C(Ph)–*C*$_3$), 126.6 (s, Ru=C=C–C(Ph)–*C*$_4$), 127.8 (s, Ru=C=C–C(Ph)–*C*$_2$), 128.1 (t, $^3J_{PC}$ + $^5J_{PC}$ = 9.3 Hz, PPh$_3$–*C*$_3$), 129.7 (t, $^1J_{PC}$ + $^3J_{PC}$ = 42.4 Hz, PPh$_3$–*C*$_1$), 130.2 (s, PPh$_3$–*C*$_4$), 134.9 (t, $^2J_{PC}$ + $^4J_{PC}$ = 12.2 Hz, PPh$_3$–*C*$_2$), 144.9 (Ru=C=C–C(Ph)–*C*$_1$), 179.9 (s, CH$_3$*C*OO), 345.1 (t, $^2J_{PC}$ = 16.2 Hz, Ru=*C*).

IR (KBr) 1369 cm^{-1} (κ^1-OCO$_{sym}$), 1435 cm^{-1} (P–Ph), 1454 cm^{-1} (κ^2-OCO$_{sym}$), 1537 cm^{-1} (κ^2-OCO$_{asym}$), 1592 cm^{-1} (κ^1-OCO$_{asym}$), 1648 cm^{-1} (C=C), 3571 cm^{-1} (OH) $\Delta\nu_{(uni)}$ 223 cm^{-1}, $\Delta\nu_{(chelate)}$ 83 cm^{-1}; (CH_2Cl_2) 1373 cm^{-1} (κ^1-OCO$_{sym}$), 1435 cm^{-1} (P–Ph), 1455 cm^{-1} (κ^2-OCO$_{sym}$), 1538 cm^{-1} (κ^2-OCO$_{asym}$), 1596 cm^{-1} (κ^1-OCO$_{asym}$), 1647 cm^{-1} (C=C), 3610 cm^{-1} (OH) $\Delta\nu_{(uni)}$ 223 cm^{-1}, $\Delta\nu_{(chelate)}$ 83 cm^{-1}.

MS (LIFDI) m/z 876 (Expected for $^{101}RuP_2O_5C_{49}H_{44}$ $[M]^+$ = 876.1)

CHN Anal for $RuP_2O_5C_{49}H_{44}$ + (1.60 CH_2Cl_2) (calc), C 60.07, H 4.70; (found) C 60.20, H 5.00

5.7.5: Synthesis of [Ru(κ^1-OAc)(κ^2-OAc)(=C=CH(cyclopentanol))(PPh$_3$)$_2$], 9e.

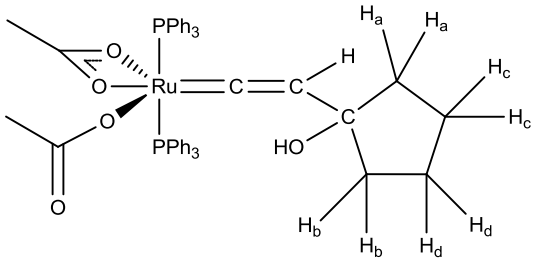

0.28 g **9e** (83.7 %) was obtained as a bright pink-orange powder from 0.25 g (0.34 mmol) **1** and 40.0 μL (0.35 mmol) 1-ethynylcyclopentanol in 15 mL CH_2Cl_2. 30 mL pentane was used to precipitate the product, and it was washed further with 2 x 15 ml portions of pentane.

NMR Spectra CD_2Cl_2:

^{1}H δ_H 0.83 (s, 6H, C*H*$_3$COO), 1.00 (m, 2H, *H*$_a$ or *H*$_b$), 1.24 (m, 4H, *H*$_c$, *H*$_d$), 1.35 (br s, 1H, [Ru]=C=CHC(O*H*)), 1.50 (m, 2H, *H*$_a$ or *H*$_b$), 4.38 (t, $^4J_{HP}$ = 3.8 Hz, 1H, [Ru]=C=C*H*), 7.41 (at, *J* = 7.1 Hz, 12H, *H*$_3$-P*Ph*$_3$), 7.46 – 7.51 (m, 18H, *H*$_2$- and *H*$_4$-P*Ph*$_3$)

^{31}P δ_P 34.3 (s, 2.0P, *P*Ph$_3$)

^{13}C δ_C 21.9 (s, *C*H$_3$COO), 23.5, 23.6, 41.5, 42.5 (all *C*H$_2$), 70.7 (s, Ru=C=CH–*C*OH), 116.3 (t, $^3J_{PC}$ = 4.6 Hz, Ru=C=*C*), 128.0 (t, $^3J_{PC}$ + $^5J_{PC}$ = 9.5 Hz, PPh$_3$–*C*$_3$), 129.1 (t, $^1J_{PC}$ + $^3J_{PC}$ = 42.3 Hz, PPh$_3$–*C*$_1$), 130.0 (s, PPh$_3$–*C*$_4$), 134.9 (t, $^2J_{PC}$ + $^4J_{PC}$ = 12.3 Hz, PPh$_3$–*C*$_2$), 179.6 (s, CH$_3$*C*OO), 352.0 (t, $^2J_{PC}$ = 16.3 Hz, Ru=*C*)

IR (KBr) 1364 cm^{-1} (κ^1-OCO$_{sym}$), 1434 cm^{-1} (P–Ph), 1458 cm^{-1} (κ^2-OCO$_{sym}$), 1536 cm^{-1} (κ^2-OCO$_{asym}$), 1590 cm^{-1} (κ^1-OCO$_{asym}$), 1654 cm^{-1} (C=C), 3564 cm^{-1} (OH), $\Delta\nu_{(uni)}$ 226 cm^{-1}, $\Delta\nu_{(chelate)}$ 78 cm^{-1}; (CH_2Cl_2) 1364 cm^{-1} (κ^1-OCO$_{sym}$), 1431 cm^{-1} (P–Ph), 1457 cm^{-1} (κ^2-OCO$_{sym}$), 1533 cm^{-1} (κ^2-OCO$_{asym}$), 1584 cm^{-1} (κ^1-OCO$_{asym}$), 1656 cm^{-1} (C=C), 3569 cm^{-1} (OH), $\Delta\nu_{(uni)}$ 220 cm^{-1}, $\Delta\nu_{(chelate)}$ 76 cm^{-1}.

MS (ESI) m/z 837.18 (Expected for $^{101}RuP_2O_4C_{47}H_{45}$ $[M\text{-}OH]^+$ = 837.1837)

CHN Anal for $RuP_2O_5C_{47}H_{46}$ + (1.40 CH_2Cl_2) (calc), C 59.76, H 5.06; (found) C 59.67, H 5.07

Crystal data and structure refinement for 9e.

Identification code	jml0910m
Empirical formula	$RuP_2O_5Cl_2C_{48}H_{48}$
Formula weight	938.77
Temperature / K	110.0
Crystal system	monoclinic
Space group	P21/n
a / Å, b / Å, c / Å	14.2578(11), 20.5627(15), 15.1557(11)
α/°, β/°, γ/°	90.00, 104.8250(10), 90.00
Volume / Å3	4295.4(6)
Z	4
ρcalc / mg mm-3	1.452
μ / mm‑1	0.611
F(000)	1936
Crystal size / mm3	0.14 × 0.08 × 0.03
2Θ range for data collection	3.42 to 56.62°
Index ranges	$-19 \leq h \leq 19$, $-27 \leq k \leq 27$, $-19 \leq l \leq 20$
Reflections collected	43320
Independent reflections	10665[R(int) = 0.0441]
Data/restraints/parameters	10665/6/538
Goodness-of-fit on F2	1.016
Final R indexes [I>2σ (I)]	R1 = 0.0435, wR2 = 0.1022
Final R indexes [all data]	R1 = 0.0732, wR2 = 0.1178
Largest diff. peak/hole / e Å-3	2.094/-0.670

5.7.6: Synthesis of [Ru(κ^1-OAc)(κ^2-OAc)(=C=CH(cyclohexanol))(PPh$_3$)$_2$], 9f.

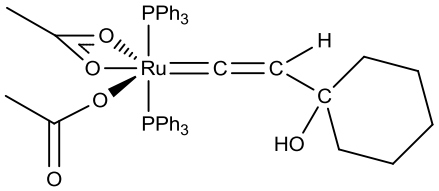

0.25 g **9f** (43.1 %) was obtained as a pale orange powder from 0.50 g (0.67 mmol) **1** and 90.0 μL (0.70 mmol) 1-ethynylcyclohexanol in 15 mL CH_2Cl_2. 25 mL pentane was used to precipitate the product, and it was washed further with 2 x 15 ml portions of pentane.

NMR Spectra CD_2Cl_2:

^{1}H δ_H 0.82 (s, 6H, C*H*$_3$COO), 0.86 – 1.09 (m, 6H, C*H*$_2$), 1.17 (br s, 1H, [Ru]=C=CHC(O*H*)), 1.23 – 1.35 (m, 4H, C*H*$_2$), 1.57 – 1.94 (m, 4H, C*H*$_2$ of unreacted alkyne), 2.38 (br s, 0.4H, HC≡C(O*H*)C$_6$H$_{10}$), 2.55 (s, 0.4H, *H*C≡C(OH)C$_6$H$_{10}$), 4.39 (t, $^2J_{HP}$ = 3.7 Hz, 1.0H, [Ru]=C=C*H*), 7.42 (at, *J* = 7.5 Hz, 12H, *H*$_3$-P*Ph*$_3$), 7.46 – 7.52 (m, 18H, *H*$_2$- and *H*$_4$-P*Ph*$_3$)

^{31}P δ_P 34.4 (s, 2.0P, *P*Ph$_3$)

^{13}C δ_C 21.9 (s, *C*H$_3$COO), 22.6, 23.2, 25.5, 39.7, 39.9 (all *C*H$_2$), 69.6 (s, Ru=C=CH–*C*OH), 117.5 (t, $^3J_{PC}$ = 4.7 Hz, Ru=C=*C*), 128.0 (t, $^3J_{PC}$ + $^5J_{PC}$ = 9.3 Hz, PPh$_3$–*C*$_3$), 129.6 (t, $^1J_{PC}$ + $^3J_{PC}$ = 43.0 Hz, PPh$_3$–*C*$_1$), 130.1 (s, PPh$_3$–*C*$_4$), 135.0 (t, $^2J_{PC}$ + $^4J_{PC}$ = 11.5 Hz, PPh$_3$–*C*$_2$), 179.5 (s, CH$_3$*C*OO), 352.2 (t, $^2J_{PC}$ = 16.5 Hz, Ru=*C*)

IR (KBr) 1366 cm^{-1} (κ^1-OCO$_{sym}$), 1434 cm^{-1} (P–Ph), 1458 cm^{-1} (κ^2-OCO$_{sym}$), 1538 cm^{-1} (κ^2-OCO$_{asym}$), 1591 cm^{-1} (κ^1-OCO$_{asym}$), 1646 cm^{-1} (C=C), 3571 cm^{-1} (OH), $\Delta\nu_{(uni)}$ 225 cm^{-1}, $\Delta\nu_{(chelate)}$ 80 cm^{-1}; (CH_2Cl_2) 1368 cm^{-1} (κ^1-OCO$_{sym}$), 1434 cm^{-1} (P–Ph), 1461 cm^{-1} (κ^2-OCO$_{sym}$), 1536 cm^{-1} (κ^2-OCO$_{asym}$), 1600 cm^{-1} (κ^1-OCO$_{asym}$), 1648 cm^{-1} (C=C), 3571 cm^{-1} (OH), $\Delta\nu_{(uni)}$ 232 cm^{-1}, $\Delta\nu_{(chelate)}$ 75 cm^{-1}.

MS (ESI) m/z 851.1927 (Expected for $^{101}RuP_2O_4C_{48}H_{47}$ [M-OH]$^+$ = 851.1993)

CHN Anal for $RuP_2O_5C_{48}H_{48}$ + (1.20 CH_2Cl_2) (calc), C 60.93, H 5.24; (found) C 61.10, H 5.29

5.7.7: Synthesis of [Ru(κ^1-OAc)(κ^2-OAc)(=C=CH(fluorenol))(PPh$_3$)$_2$], 9g.

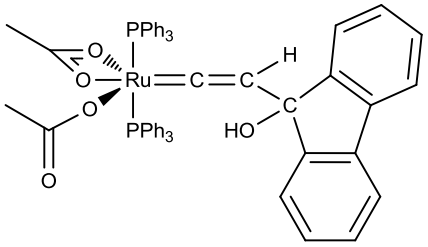

0.12 g **9g** (48.0 %) was obtained as a bright orange powder from 0.20 g (0.27 mmol) **1** and 0.06 mg (0.29 mmol) 9-ethynyl-9-fluorenol in 15 mL CH_2Cl_2. 30 mL pentane was used to precipitate the product, and it was washed further with 2 x 10 ml portions of pentane.

NMR Spectra CD_2Cl_2:

^{1}H δ_H 0.82 (s, 6H, C*H*$_3$COO), 2.77 (br s, 1H, [Ru]=C=CHC(O*H*)), 4.56 (t, $^4J_{HP}$ = 3.8 Hz, 1.0H, [Ru]=C=C*H*), 6.64 (d, *J* = 7.6 Hz, 2H, fluorenyl), 7.01 (t, *J* = 7.3 Hz, 2H, fluorenyl), 7.19 (m, 2H, fluorenyl), 7.25 (t, *J* = 7.4 Hz, 2H, fluorenyl), 7.37 (at, *J* = 7.4 Hz, 12H, *H*$_3$-P*Ph*$_3$), 7.42 – 7.48 (m, 18H, *H*$_2$- and *H*$_4$-P*Ph*$_3$)

^{31}P δ_P 33.9 (s, 2.0P, *P*Ph$_3$)

^{13}C δ_C 21.9 (s, *C*H$_3$COO), 77.2 (s, Ru=C=CH–*C*OH), 113.7 (t, $^3J_{PC}$ = 4.6 Hz, Ru=C=*C*), 119.4, 124.2, 127.8 (s, all fluorenyl), 128.0 (t, $^3J_{PC}$ + $^5J_{PC}$ = 9.3 Hz, PPh$_3$–*C*$_3$), 128.6 (s, fluorenyl), 129.3 (t, $^1J_{PC}$ + $^3J_{PC}$ = 43.1 Hz, PPh$_3$–*C*$_1$), 130.2 (s, PPh$_3$–*C*$_4$), 135.0 (t, $^2J_{PC}$ + $^4J_{PC}$ = 11.5 Hz, PPh$_3$–*C*$_2$), 138.6, 150.3, (s, all fluorenyl), 179.6 (s, CH$_3$*C*OO), 349.4 (t, $^2J_{PC}$ = 16.2 Hz, Ru=*C*)

IR (KBr) 1367 cm^{-1} (κ ^{1}-OCO$_{sym}$), 1433 cm^{-1} (P–Ph), 1463 cm^{-1} (κ ^{2}-OCO$_{sym}$), 1534 cm^{-1} (κ ^{2}-OCO$_{asym}$), 1597 cm^{-1} (κ ^{1}-OCO$_{asym}$), 1636 cm^{-1} (C=C), 3542 cm^{-1} (OH), $\Delta\nu_{(uni)}$ 230 cm^{-1}, $\Delta\nu_{(chelate)}$ 71 cm^{-1}; (CH_2Cl_2) 1367 cm^{-1} (κ ^{1}-OCO$_{sym}$), 1435 cm^{-1} (P–Ph), 1463 cm^{-1} (κ ^{2}-OCO$_{sym}$), 1531 cm^{-1} (κ ^{2}-OCO$_{asym}$), 1606 cm^{-1} (κ ^{1}-OCO$_{asym}$), 1646 cm^{-1} (C=C), 3554 cm^{-1} (OH), $\Delta\nu_{(uni)}$ 239 cm^{-1}, $\Delta\nu_{(chelate)}$ 68 cm^{-1}.

MS (ESI) m/z 932.1995 (Expected for $^{101}RuP_2O_3NC_{55}H_{46}$ [M - OAc$^-$ + MeCN]$^+$ = 932.1996

CHN Anal for $RuP_2O_5C_{55}H_{46}$ + (1.20 CH_2Cl_2) (calc), C 64.17, H 4.64; (found) C 64.33, H 4.66

5.7.8: Synthesis of [Ru(κ^1-OAc)(κ^2-OAc)(=C=CHCH$_2$OH)(PPh$_3$)$_2$], 9h.

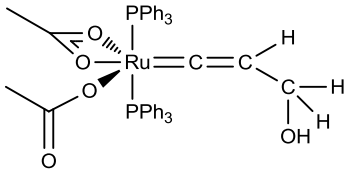

0.17 g **9h** (53.1 %) was obtained as a yellow-orange powder from 0.30 g (0.40 mmol) **1** and 22.0 μL (0.38 mmol) HC≡CCH$_2$OH in 20 mL CH$_2$Cl$_2$. 30 mL pentane was used to precipitate the product, and it was washed further with 2 x 20 ml portions of pentane.

NMR Spectra CD$_2$Cl$_2$:

^{1}H δ_H 0.85 (s, 6H, C*H*$_3$COO), 1.26 (t, $^3J_{HH}$ = 5.6 Hz, 1H, [Ru]=C=CHC(O*H*)), 3.88 (at, $^3J_{HH}$ = 6.5 Hz, 2H, [Ru]=C=CHC*H*$_2$), 4.11 (asp, $^4J_{HP}$ = 3.7 Hz, 1H, [Ru]=C=C*H*), 7.42 (at, *J* = 7.2 Hz, 12H, *H*$_3$-P*Ph*$_3$), 7.46 – 7.51 (m, 18H, *H*$_2$- and *H*$_4$-P*Ph*$_3$)

^{31}P δ_P 35.1 (s, 2P, *P*Ph$_3$)

^{13}C δ_C 21.8 (s, *C*H$_3$COO), 54.9 (s, Ru=C=CH–*C*OH), 106.5 (t, $^3J_{PC}$ = 5.0 Hz, Ru=C=*C*), 128.0 (t, $^3J_{PC}$ + $^5J_{PC}$ = 9.2 Hz, PPh$_3$–*C*$_3$), 129.8 (t, $^1J_{PC}$ + $^3J_{PC}$ = 40.3 Hz, PPh$_3$–*C*$_1$), 130.1 (s, PPh$_3$–*C*$_4$), 134.8 (t, $^2J_{PC}$ + $^4J_{PC}$ = 11.8 Hz, PPh$_3$–*C*$_2$), 179.7 (s, CH$_3$*C*OO), 345.7 (t, $^2J_{PC}$ = 16.3 Hz, Ru=*C*)

IR (KBr) 1372 cm^{-1} (κ ^{1}-OCO$_{sym}$), 1433 cm^{-1} (P–Ph), 1457 cm^{-1} (κ ^{2}-OCO$_{sym}$), 1533 cm^{-1} (κ ^{2}-OCO$_{asym}$), 1595 cm^{-1} (κ ^{1}-OCO$_{asym}$), 1655 cm^{-1} (C=C), 3575 cm^{-1} (OH), $\Delta\nu_{(uni)}$ 223 cm^{-1}, $\Delta\nu_{(chelate)}$ 76 cm^{-1}; (CH$_2$Cl$_2$) 1368 cm^{-1} (κ ^{1}-OCO$_{sym}$), 1434 cm^{-1} (P–Ph), 1456 cm^{-1} (κ ^{2}-OCO$_{sym}$), 1538 cm^{-1} (κ ^{2}-OCO$_{asym}$), 1605 cm^{-1} (κ ^{1}-OCO$_{asym}$), 1651 cm^{-1} (C=C), 3573 cm^{-1} (OH), $\Delta\nu_{(uni)}$ 237 cm^{-1}, $\Delta\nu_{(chelate)}$ 82 cm^{-1}.

MS (ESI) m/z 801.1502 (Expected for ^{101}RuP$_2$O$_5$C$_{43}$H$_{41}$ [M+H]$^+$ = 801.1473) (LIFDI) m/z 798 (^{101}RuP$_2$O$_5$C$_{43}$H$_{39}$ [M]$^+$ - 2H)

CHN: not obtained as complex found to degrade rapidly even in the solid state.

5.7.9: Synthesis of [Ru(κ^1-OAc)(κ^2-OAc)(=C=CH(ethisterone))(PPh$_3$)$_2$], 9i.

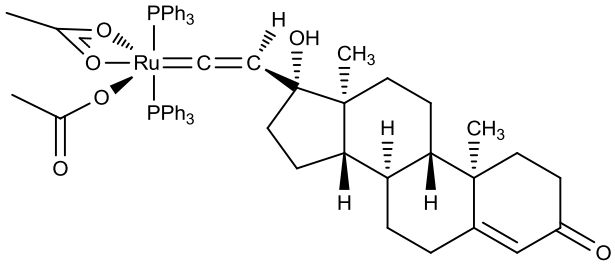

0.21 g **9i** (50.0 %) was obtained as a bright yellow powder from 0.30 g (0.40 mmol) **1** and 0.16 g (0.50 mmol) ethisterone in 30 mL CH_2Cl_2. The solvent was removed completely *in vacuo* before the product was washed with 3 x 30 ml portions of pentane. NMR Spectra CD_2Cl_2:

^{1}H δ_H 0.37 – 0.67 (m, 3H, –CH–, –CH_2–), 0.71 (s, 3H, CH_3), 0.75 (s, 6H, C*H*$_3$COO), 1.13 (s, 3H, CH_3), 1.20 – 2.04 (m, 12H, –CH–, –CH_2–), 2.16 (s, 1H, OH), 2.19 – 2.47 (m, 4H, –CH–, –CH_2–), 4.48 (t, $^4J_{HP}$ = 3.7 Hz, 1H, [Ru]=C=C*H*), 5.70 (br s, 1H, =CH–), 7.41 (at, *J* = 7.1 Hz, 12H, *H*$_3$-P*Ph*$_3$), 7.45 – 7.51 (m, 18H, *H*$_2$- and *H*$_4$-P*Ph*$_3$)

^{31}P δ_P 35.5 (s, 2.0P, *P*Ph$_3$)

^{13}C δ_C 13.3 (s, CH_3), 17.1 (s, CH_3), 20.5 (s, CH_2), 21.7 (s, *C*H$_3$COO), 24.1 (s, CH_2), 31.5 (s, CH_2), 31.8 (s, CH_2), 32.9 (s, CH_2), 34.2 (s, CH_2), 35.8 (s, CH_2), 36.1 (s, C), 38.3 (s, CH), 38.7 (s, CH_2), 46.5 (s, C), 48.7 (s, CH), 52.4 (s, CH), 81.6 (s, Ru=C=CH–*C*OH), 114.4 (t, $^3J_{PC}$ = 4.6 Hz, Ru=C=*C*), 123.5 (s, =CH–), 128.1 (t, $^3J_{PC}$ + $^5J_{PC}$ = 9.3 Hz, PPh$_3$–*C*$_3$), 129.4 (t, $^1J_{PC}$ + $^3J_{PC}$ = 42.4 Hz, PPh$_3$–*C*$_1$), 130.1 (s, PPh$_3$–*C*$_4$), 135.1 (t, $^2J_{PC}$ + $^4J_{PC}$ = 10.8 Hz, PPh$_3$–*C*$_2$), 171.8 (s, C), 179.5 (s, CH$_3$*C*OO), 199.1 (s, CO), 352.0 (t, $^2J_{PC}$ = 16.2 Hz, Ru=*C*)

IR (KBr) 1374 cm^{-1} (κ ^{1}-OCO$_{sym}$), 1433 cm^{-1} (P–Ph), 1456 cm^{-1} (κ ^{2}-OCO$_{sym}$), 1530 cm^{-1} (κ ^{2}-OCO$_{asym}$), 1620 cm^{-1} (κ ^{1}-OCO$_{asym}$), 1649 cm^{-1} (C=C), 3573 cm^{-1} (OH) $\Delta\nu_{(uni)}$ 246 cm^{-1}, $\Delta\nu_{(chelate)}$ 74 cm^{-1}; (CH_2Cl_2) 1372 cm^{-1} (κ ^{1}-OCO$_{sym}$), 1433 cm^{-1} (P–Ph), 1458 cm^{-1} (κ ^{2}-OCO$_{sym}$), 1538 cm^{-1} (κ ^{2}-OCO$_{asym}$), 1616 cm^{-1} (κ ^{1}-OCO$_{asym}$), 1652 cm^{-1} (C=C), 3564 cm^{-1} (OH) $\Delta\nu_{(uni)}$ 244 cm^{-1}, $\Delta\nu_{(chelate)}$ 80 cm^{-1}.

MS (ESI) m/z 1079.3098 (Expected for $C_{61}H_{64}NaO_6P_2Ru$ [M]Na$^+$ 1079.3119), 1039.3 (Expected for $^{101}RuP_2O_4NC_{61}H_{65}$ [MH]$^+$-OAc$^-$ + MeCN = 1039.3432)

CHN Anal for $RuP_2O_6C_{61}H_{64}$ + (0.10 CH_2Cl_2) (calc), C 68.93, H 6.08; (found) C 68.59, H 6.18

5.7.10: Stoichiometric studies of the degradation of complexes 9a-i

General procedure for monitoring the degradation of complexes 9a-i to 4 by NMR Spectroscopy:

1 (~ 20 mg) was added to a NMR tube fitted with a Young's Tap and dissolved in approximately 0.5 mL CD_2Cl_2 (transferred into the tube by vacuum distillation). One equivalent of the appropriate alkyne was then added to the sample under N_2 or Ar. The sample was immediately sealed and shaken. NMR spectra were recorded soon after addition, and were re-recorded over a number of days until the degradation was judged to have gone to completion, although in some cases a trace amount of **9** remained. The ^{1}H NMR data of the alkene degradation products are described for each complex and the integrations of the appropriate peaks are measured relative to the six acetate protons of **4** at δ_H 0.71. References 77-86 correspond to literature data for the isolated alkenes.

9a[77]

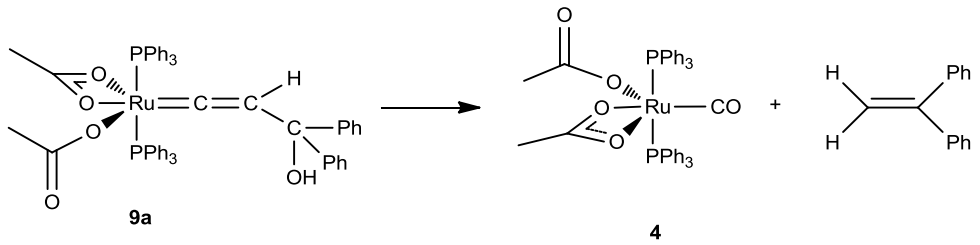

^{1}H δ_H 5.45 (s, 2H, H_2C=CPh$_2$) phenyl resonances obscured by PPh_3

9b[78]

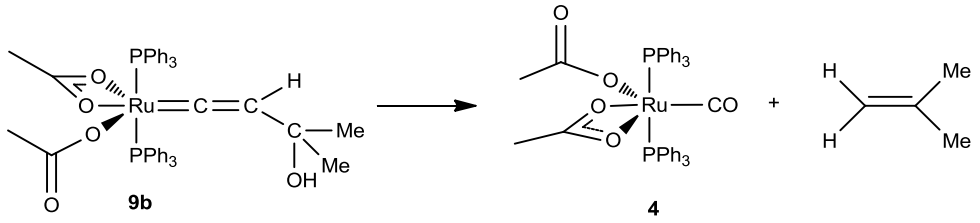

^{1}H δ_H 1.71 (t, $^4J_{HH}$ = 1.0 Hz, 6H, H_2C=CMe_2), 4.64 (sp, $^4J_{HH}$ = 1.0 Hz, 2H, H_2C=CMe$_2$)

9c[79]

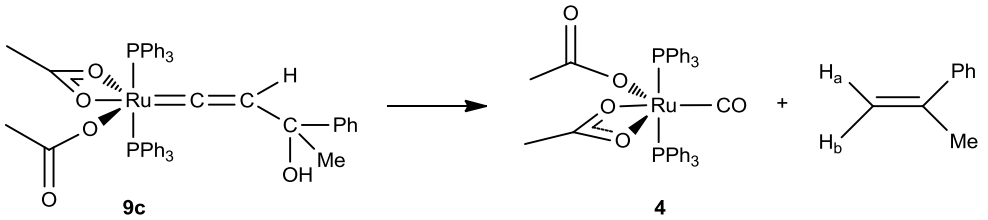

^{1}H δ_H 2.20 (br s, 3H, H_2C=C(Ph)(*Me*)), 5.13 (m, 1H, H_aH_bC=C(Ph)(Me)), 5.42 (m, 1H, H_aH_bC=C(Ph)(Me)), phenyl resonances obscured by PPh_3

9d[80]

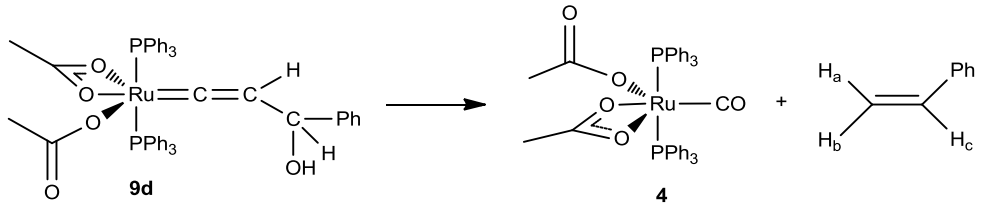

^{1}H δ_H 5.29 (dd, $^2J_{HaHb}$ = 0.7 Hz, $^3J_{HbHc}$ = 11.1 Hz, 1H, H_b), 5.81 (dd, $^2J_{HaHb}$ = 0.8 Hz, $^3J_{HaHc}$ = 17.6 Hz, 1H, H_a), 6.77 (dd, , $^3J_{HbHc}$ = 10.8 Hz, $^3J_{HaHc}$ = 17.6 Hz, 1H, H_c), phenyl resonances obscured by PPh_3

9e[81]

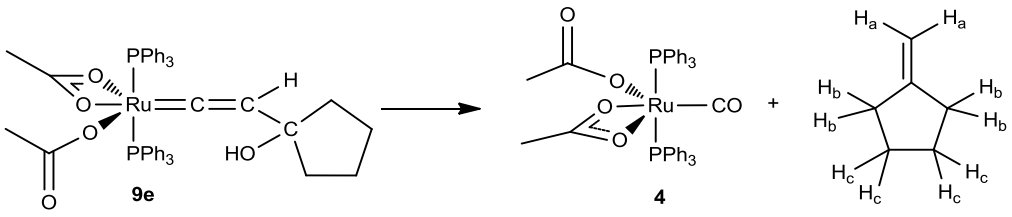

^{1}H δ_H 1.69 (aqn, 4H, $^5J_{HaHc}$ = 4.1 Hz, $^3J_{HbHc}$ = 7.5 Hz, H_c), 2.29 (tt, 4H, $^4J_{HaHb}$ = 2.4 Hz, $^3J_{HcHc}$ = 7.3 Hz, H_b), 4.87 (qn, 2H, $^5J_{HaHc}$ = 2.2 Hz, $^4J_{HaHb}$ = 4.5 Hz, H_a)

9f[82]

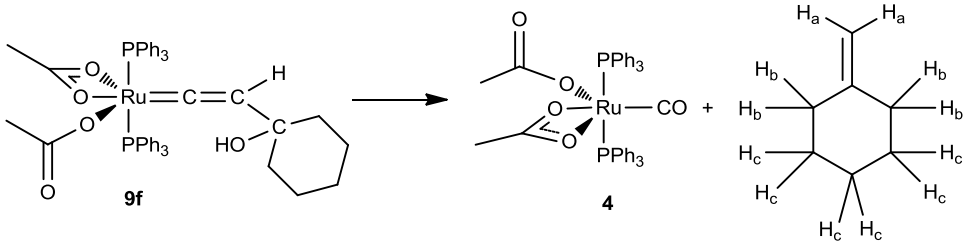

^{1}H δ_H 1.57 (m, 6H, H_c), 2.16 (m, 4H, H_b), 4.61 (t, J = 0.9 Hz, 2H, H_a)

9g[83]

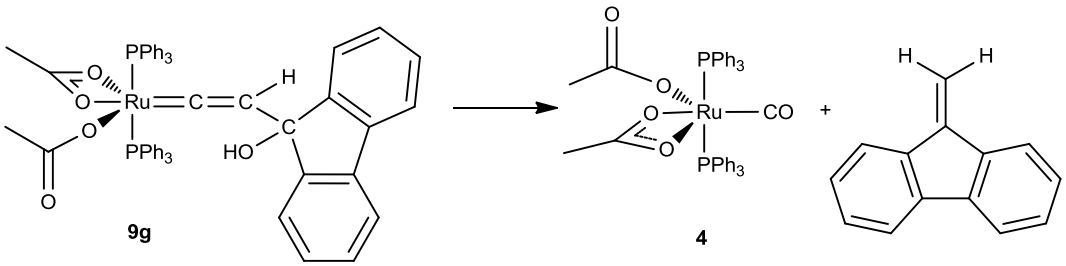

^{1}H δ_H 6.16 (s, 2H, CH_2), phenyl resonances obscured by PPh_3

9h[84]

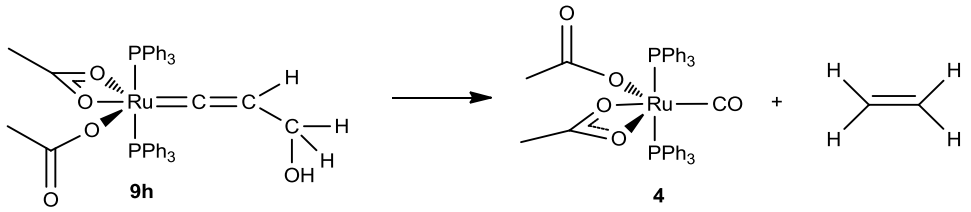

^{1}H δ_H 5.44 (s, 1H (integration likely to be inaccurate – ethene is a gas) H_2C=CH_2)

9i[85,86]

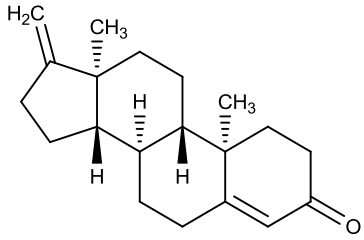

^{1}H δ_H 0.88 (s, 3H, C*H*$_3$), 1.25 (s, 3H, C*H*$_3$), 4.68 (m, 2H, C=C*H*$_2$), 5.71 (s, 1H, COC*H*=C)

5.7.11: Catalytic production of alkenes from propargylic alcohols 8a-i

General procedure:

A degassed Schlenk tube with an inbuilt reflux condenser system was charged with 10 mol % **1** and a stirrer bar. This was dissolved in 10 mL toluene and the propargylic alcohol (~ 0.20 g) added. The mixture was heated at 130 ˚C for 16 hours. After cooling the toluene was removed in vacuo and the residue redissolved in approximately 10 mL CH_2Cl_2. A small portion of this was transferred *via* cannula wire to a Young's NMR tube under N_2. The majority of the solvent was then blown off by a stream of N_2 and the remainder removed *in vacuo*. Approximately 0.5 mL CD_2Cl_2 was then transferred into the tube by vacuum distillation to dissolve the residue for NMR analysis.

Important ^{1}H NMR features are included below: in all cases phenyl resonances have been omitted for clarity. For the dimerization products, only the alkene protons are included. Integrations are relative to that of the lowest yielding product.

8a:

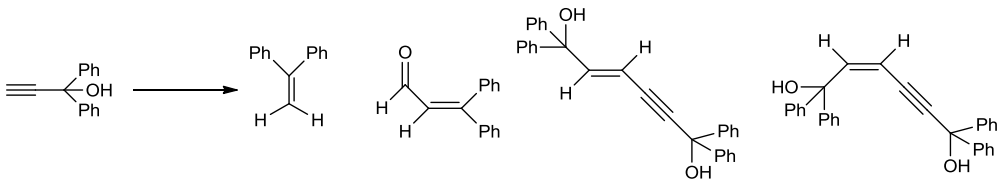

^{1}H δ_H 3.00 (s, 5.9H, *H*C≡CC(OH)Ph_2), 3.15 (s, 5.7H, HC≡CC(O*H*)Ph_2), 5.55 (s, 31H, H_2C=CPh_2), 6.03 (d, $^2J_{HH}$ = 11.7 Hz, 1.0H (*Z*)-dimer), 6.08 (d, $^2J_{HH}$ = 15.9 Hz, 3.4H (*E*)-dimer), 6.65 (d, $^2J_{HH}$ = 8.0 Hz, 6.0H, CHOC*H*=CPh_2), 6.77 (d, $^2J_{HH}$ = 11.8 Hz, 2.7H (*Z*)-dimer), 6.94 (d, $^2J_{HH}$ = 15.9 Hz, 9.7H (*E*)-dimer), 9.57 (d, $^2J_{HH}$ = 8.0 Hz, 3.4H, C*H*OCH=CPh_2)

8b:

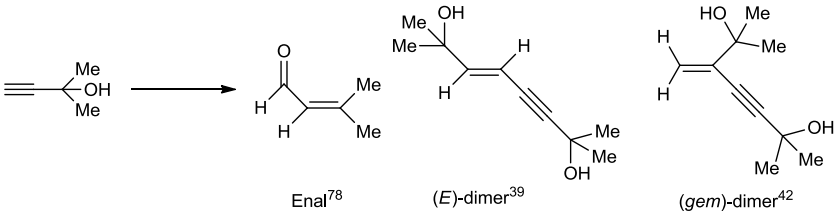

Enal[78] (*E*)-dimer[39] (*gem*)-dimer[42]

^{1}H δ_H 5.39 (d, $^{2}J_{HH}$ = 1.6 Hz, 1.1H, (*gem*)-dimer), 5.59 (d, $^{2}J_{HH}$ = 1.5 Hz, 1.0H, (*gem*)-dimer), 5.76 (d, $^{2}J_{HH}$ = 16.0 Hz, 0.5H (*E*)-dimer), 6.26 (d, $^{2}J_{HH}$ = 16.0 Hz, 0.5H (*E*)-dimer), 10.0 (s, 0.04H, C*H*OCH=CMe_2)

8c:

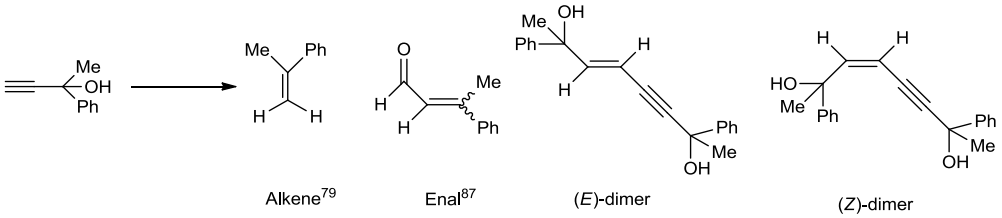

Alkene[79] Enal[87] (*E*)-dimer (*Z*)-dimer

^{1}H δ_H 5.16 (m, 4.7H, *H*HC=C(Ph)(Me)), 5.45 (br s, 4.9H, H*H*C=C(Ph)(Me)), 5.85 (d, $^{2}J_{HH}$ = 12.6 Hz, 1.0H, (*Z*)-dimer), 5.94 (d, $^{2}J_{HH}$ = 16.0 Hz, 3.6H, (*E*)-dimer), 6.52 (d, $^{2}J_{HH}$ = 15.9 Hz, 3.5H, (*E*)-dimer), 9.51 (d, $^{2}J_{HH}$ = 8.3 Hz, 1.0H, (*E*) or (*Z*)-CHOC=C(Ph)(Me)), 10.2 (d, $^{2}J_{HH}$ = 7.8 Hz, 3.7 H, (*E*)- or (*Z*)-CHOC=C(Ph)(Me)).

8d:

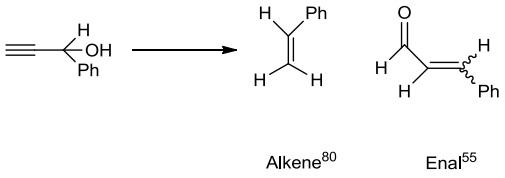

Alkene[80] Enal[55]

^{1}H δ_H 5.32 (d, $^{3}J_{HbHc}$ = 11.0 Hz, 1.1H, H_aH_bC=CH_cPh), 5.84 (dd, $^{2}J_{HaHb}$ = 0.7 Hz $^{3}J_{HaHc}$ = 17.6 Hz, 1.6H, $H_a$$H_b$C=C$H_c$Ph), 6.79 (m - overlap of 3 peaks for H_aH_bC=CH_cPh (dd) $^{3}J_{HbHc}$ = 11.3 Hz, $^{3}J_{HaHc}$ = 17.6 Hz; PhH_aC=C$H_b$$CH_c$O (dd) $^{3}J_{HbHc}$ = 7.8 Hz, $^{3}J_{HaHc}$ = 15.8 Hz; PhH_aC=C$H_b$$CH_c$O (d) $^{3}J_{HaHc}$ = 15.9 Hz), 9.76 (d, $^{3}J_{HbHc}$ = 7.7 Hz, 1H, PhH_aC=CH_bCH_cO)

8e:

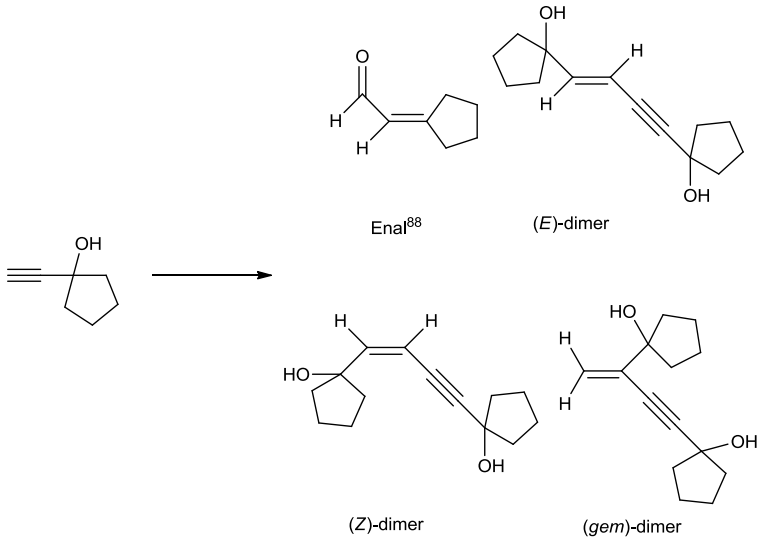

^{1}H δ_H 2.57 (s, 7.0H, *H*C≡C(C_5H_8(OH)), 5.45 (d, $^{2}J_{HH}$ = 1.6 Hz, 1.8H, (*gem*)-dimer), 5.60 (d, $^{2}J_{HH}$ = 11.7 Hz, 1.0H, (*Z*)-dimer), 5.66 (d, $^{2}J_{HH}$ = 1.6 Hz, 1.9H, (*gem*)-dimer), 5.86 (d, $^{2}J_{HH}$ = 15.9 Hz, 1.3H, (*E*)-dimer), 6.10 (d, $^{2}J_{HH}$ = 11.7 Hz, 1.3H, (*Z*)-dimer), 6.31 (d, $^{2}J_{HH}$ = 16.0 Hz, 1.2H, (*E*)-dimer), 9.89 (d, $^{3}J_{HH}$ = 8.0 Hz, 0.2H, C*H*OCH=C_5H_8

8f:

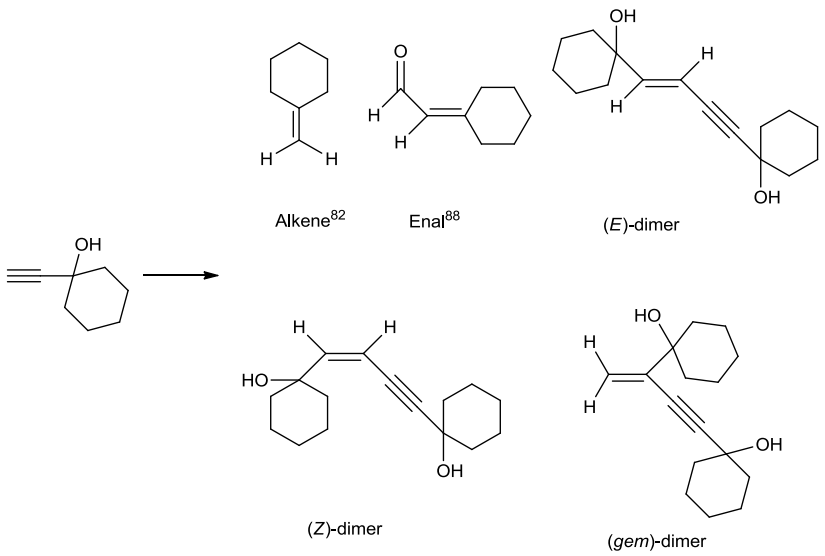

^{1}H δ_H 2.55 (s, 54H, *H*C≡C(C_6H_{10}(OH))), 4.61 (br s, 5.3H, H_2C=C_6H_{10}), 5.43 (d, $^{2}J_{HH}$ = 1.6 Hz, 3.1H, (*gem*)-dimer), 5.59 (d, $^{2}J_{HH}$ = 11.8 Hz, 0.8H, (*Z*)-dimer), 5.62 (d, $^{2}J_{HH}$ = 1.6 Hz, 2.3H, (*gem*)-dimer), 5.82 (d, $^{2}J_{HH}$ = 16.0 Hz, 2.5H, (*E*)-dimer), 6.07 (d, $^{2}J_{HH}$ = 11.8 Hz, 1.0H, (*Z*)-dimer), 6.28 (d, $^{2}J_{HH}$ = 16.0 Hz, 2.0H, (*E*)-dimer), 10.0 (d, $^{3}J_{HH}$ = 8.2 Hz, 0.2H, C*H*OCH=C_6H_{10})

8g:

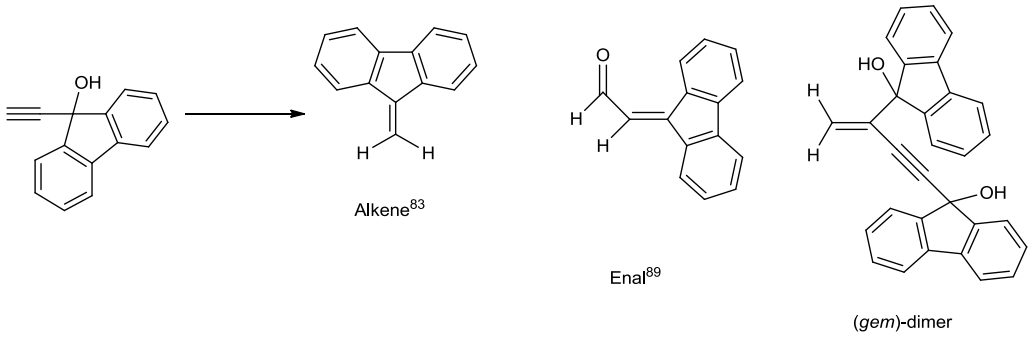

^{1}H δ_H 5.64 (d, $^{2}J_{HH}$ = 1.5 Hz, 1.0H, (*gem*)-dimer), 6.03 (d, $^{2}J_{HH}$ = 1.5 Hz, 1.0H, (*gem*)-dimer), 6.16 (s, 1.2H, H_2C=$C_{13}H_8$), 6.88 (d, $^{3}J_{HH}$ = 8.0 Hz, 1.6H CHOC*H*=$C_{13}H_8$), 10.87 (d, $^{3}J_{HH}$ = 8.0 Hz, 1.2H C*H*OCH=$C_{13}H_8$)

8i:

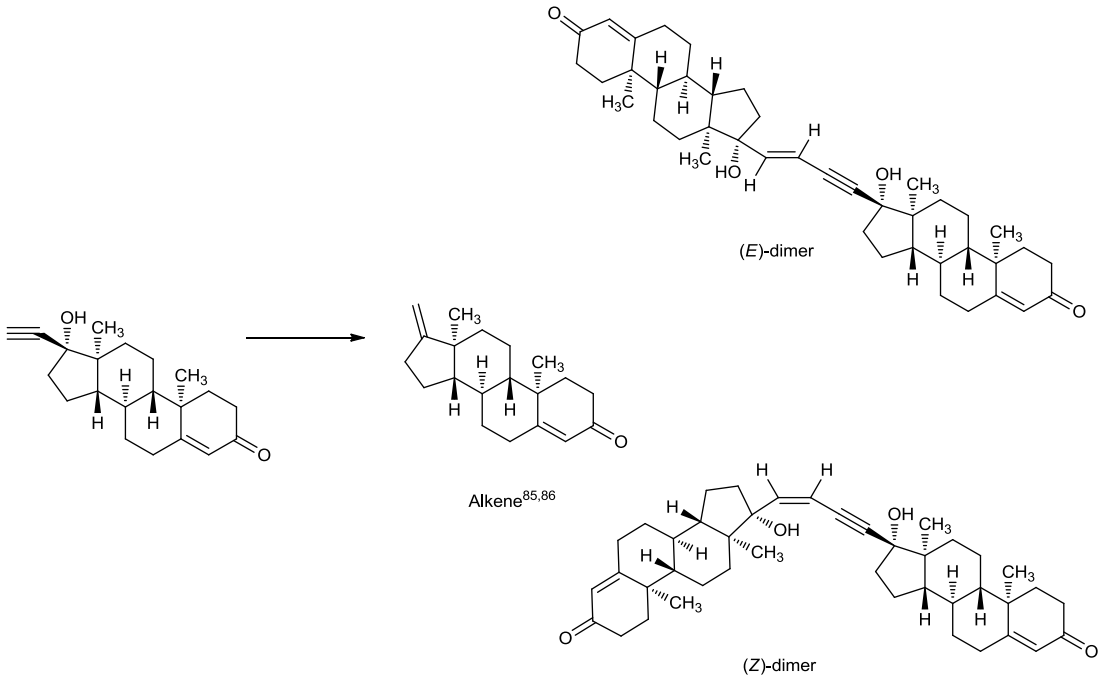

^{1}H δ_H 4.68 (m, 1.0H, H_2C=ethisterone), 6.03 (d, $^{3}J_{HH}$ = 12.1 Hz, 1.6 H, (*Z*)-dimer), 6.29 (d, $^{3}J_{HH}$ = 15.8 Hz, 1.6 H, (*E*)-dimer), 6.99 (d, $^{3}J_{HH}$ = 15.9 Hz, 1.5 H, (*E*)-dimer),

5.7.12 Addition of CH_3COOH to PPh_3

Two equivalents of CH_3COOH (6.6 μL, 0.11 mmol) was added to a solution of 15 mg PPh_3 (57.2 μmol) dissolved in CD_2Cl_2 in a Young's capped NMR tube under N_2. The mixture was monitored by ^{1}H and ^{31}P{^{1}H} NMR spectroscopy over 41 days at room temperature. Over the course of this time, resonances due to what is thought to be $[HPPh_3]^+$ slowly increased in intensity.

^{1}H NMR δ_H 7.54 (atd, *J* = 3.0 Hz, 7.74 Hz), 7.64 (at, *J* = 7.2 Hz), 7.71 (add, *J* = 7.4 Hz, 12.3 Hz).

^{31}P{^{1}H}NMR δ_P 30.5

5.7.13 Catalytic coupling of 8j with benzoic acid

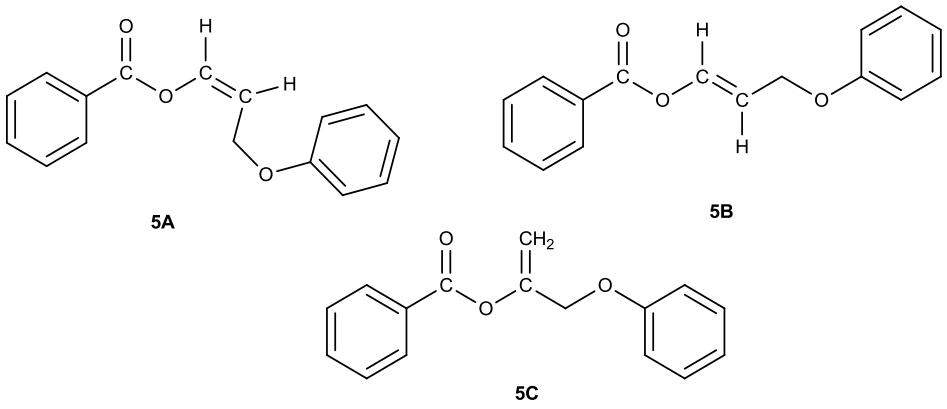

Phenyl propargyl ether (258 mg, 1.95 mmol) and benzoic acid (238 mg, 1.95 mmol) were added to a solution of **1a** (14.5 mg, 0.02 mmol) in 20 mL toluene and heated at 120 °C for 16 h. The products were purified by flash column chromatography. The column was doped with NEt_3 (5 % in hexane) and then hexane/dichloromethane used as the eluent (starting with hexane and a gradual increase in the concentration of dichloromethane). The three isomers were obtained in a ratio of 0.7:1:1.6 (**5A:5B:5C**). They could not be separated and characterised independently so yields and NMR data recorded were of a mixture. Isolated yield 160 mg (32.3 %).

NMR spectra (CD_2Cl_2) : ^1H δ_H 4.61 (dd, $^4J_{HH}$ = 1.3 Hz, $^3J_{HH}$ = 6.8 Hz, 2H, CH_2, **5A**), 4.71 (br s, 2H, CH_2, **5C**), 4.85 (dd, $^4J_{HH}$ = 1.6 Hz, $^3J_{HH}$ = 6.6 Hz, 2H, CH_2, **5B**), 5.18 (m, 1H, C=C$H_a$$H_b$, **5C**), 5.24 (m, 1H, C=C$H_a$$H_b$, **5C**), 5.35 (aq, $^3J_{HH}$ = 6.6 Hz, $^3J_{HH}$ = 6.6 Hz, 1H, =C*H*, **5A**), 5.91 (dt, $^3J_{HH}$ = 6.8 Hz, $^3J_{HH}$ = 13.5 Hz, 1H, =C*H*, **5B**) 6.93 – 7.01 (m, Ph), 7.20-7.33 (m, Ph), 7.42 – 7.72 (m, Ph, =C*H*, **5A** and =C*H*, **5B**), 8.07 – 8.24 (m, Ph); ^{13}C δ_C 61.6 (s, *C*H_2OPh, **5B**), 64.7 (s, *C*H_2OPh, **5C**), 66.7 (s, *C*H_2OPh, **5B**), 103.9 (s, C=*C*H_2, **5C**), 109.8 (s, =*C*H, **5A**), 110.3 (s, =*C*H, **5B**), 114.7, 114.8, 114.9, 120.9, 121.0, 121.4, 121.9, 128.6, 128.7, 128.8 (s, Ar-*C*H), 128.9 (s, Ar-*C*), 129.4 (s, Ar-*C*), 129.5, 129.5, 129.6, (s, Ar-*C*H), 129.7 (s, Ar-*C*), 129.9, 130.0, 130.1, 133.6, 133.7, (s, Ar-*C*H), 136.4 (s, =*C*H, **5B**), 139.4 (s, =*C*H, **5A**), 151.6 (s, *C*=CH_2, **5C**), 158.3 (s, C_1-PhCO_2, **5A**), 158.5 (s, C_1-PhCO_2, **5B**), 158.6 (s, C_1-PhCO_2, **5C**), 163.0 (s, Ph*C*O_2, **5B**), 163.4 (s, Ph*C*O_2, **5A**), 164.6 (s, Ph*C*O_2, **5C**);

EI-MS: $[M]^+$ 254.0937 ($C_{16}H_{14}O_3$)

6: Mechanistic Studies on the Decarbonylation of Propargylic Alcohols

6.1: Introduction

The preceding chapter detailed the synthesis and characterisation of a range of substituted hydroxy-vinylidene complexes prepared by the addition of propargylic alcohols to the precursor **1**. There is significant literature precedence for the dehydration of such species to give either allenylidene or vinylvinylidene complexes.[1-8] Somewhat surprisingly, this reaction was not observed for the hydroxy-vinylidene complexes **9a-i** and attempts to induce this dehydration failed. Instead, solutions of complexes **9a-i** that were allowed to stand at room temperature gradually evolved to the CO-containing complex **4** and a geminal alkene. This transformation is not without precedence and was previously reported by Dixneuf in 2005.[9,10] His proposed mechanism involves the formation of intermediate complexes containing allenylidene and hydroxy-carbene ligands (as shown in Figure 6.1.1). Yet such intermediates were elusive in attempts to understand the mechanism by which this transformation occurred in the cases of **9a-i**.

Consequently, the series of stoichiometric reactions of terminal alkynes with **1** was extended to include propargylic ethers, amine and carboxylates. On the basis of the results obtained, it was concluded that the acetate ligand was once more an important factor in the behaviour observed. A kinetic study was also performed in an attempt to understand the molecularity of the process and an ^{18}O-labelling study was used to confirm the involvement of the acetate ligand. A collaborative DFT study was also conducted with the assistance of David Johnson and Dr. John Slattery.

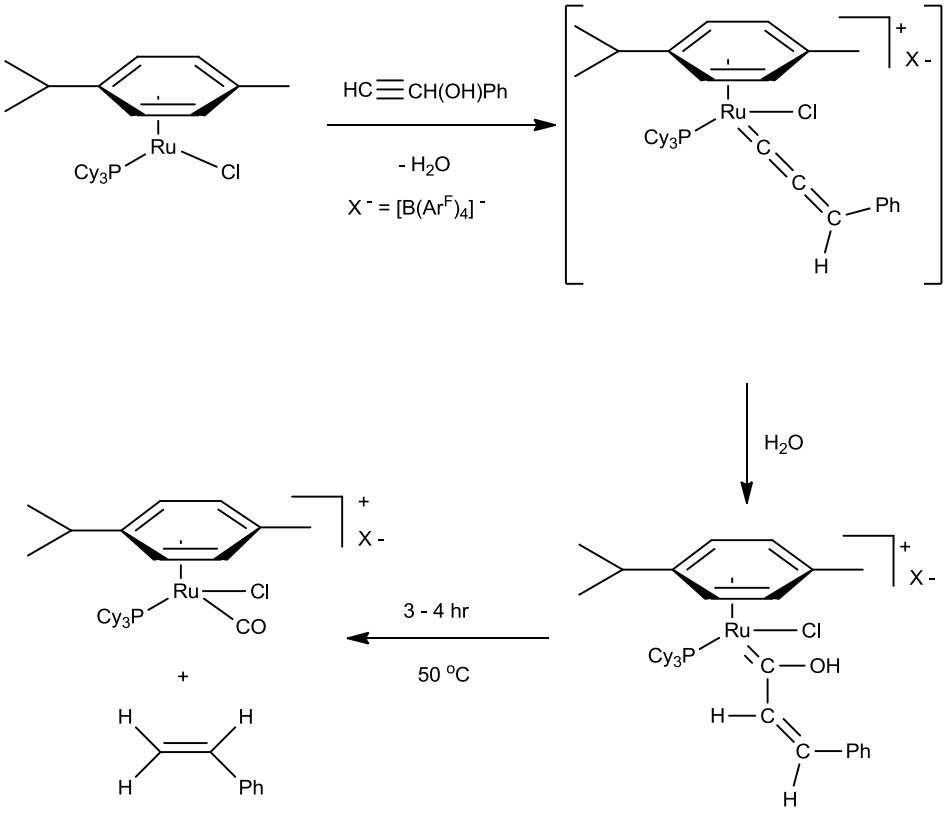

Figure 6.1.1: Dixneuf's proposed mechanism to account for propargylic alcohol to alkene conversion.

6.2: Identification of Intermediates by Stoichiometric Reactions

Initially, efforts focussed on acquiring more evidence for the fundamental steps that occur in the transformation of a propargylic alcohol to alkene. It was proposed that the hydrogen bonds identified in the crystal structures of complexes **9a**, **9c** and **9e** (discussed in Section 5.2) might play an important role in the subsequent formation of **4**. Consequently, a series of reactions were performed using propargylic substrates that could not form such hydrogen bonds.

6.2.1: Formation of a phenoxy-vinylidene complex and its subsequent conversion to phenyl acetate and $[Ru(\kappa^2\text{-}OAc)(CH{=}CH_2)(CO)(PPh_3)_2]$

The reaction of **1** with terminal alkynes was extended to the propargylic substrate $HC{\equiv}CCH_2OPh$ (**8j**). This resulted in the formation of the phenoxy-

vinylidene complex **9j**. This complex exhibits similar NMR and IR features to those observed for the hydroxy-vinylidene complexes **9a-i**. A multiplet resonance is observed in the ^{1}H NMR spectrum at δ_H 4.41 which is assigned to the vinylidene proton and a singlet resonance at δ_H 0.87 is attributed to the six acetate protons. A simulation of the vinylidene proton resonance indicates that the $^{4}J_{HP}$ coupling constant is 3.6 Hz. A singlet resonance is also observed in the $^{31}P\{^{1}H\}$ NMR spectrum at δ_P 35.2 due to the two PPh_3 ligands. Additional comments on these NMR features are made in Section 6.2.2. In the IR spectrum of this complex recorded in both DCM and KBr media, symmetric and asymmetric stretches are observed due to both κ^1- and κ^2-coordination modes of the acetate ligands.

As with complexes **9a-i**, complex **9j** was also observed to undergo a transformation process in solution. Unlike the hydroxy-vinylidene complexes, it does not convert to complex **4** and the corresponding geminal alkene. Instead, the evolution of an organometallic complex containing a vinyl ligand (**10**) and phenyl acetate is observed, as demonstrated in Figure 6.2.1.1.

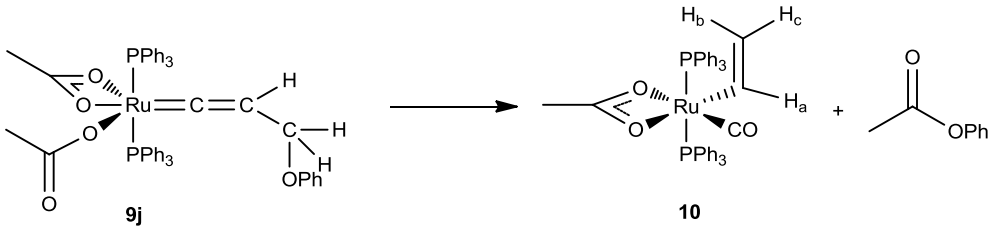

Figure 6.2.1.1: Conversion of the phenoxy-vinylidene complex **9j** to **10** and phenyl acetate.

The conversion of complex **9j** to **10** occurred significantly faster than the corresponding conversion of complexes **9a-i** to **4**; it was observed to have reached completion within 16 hours at room temperature. This is notably faster than the transformation rate of the hydroxy-vinylidene complex **9h**, which takes approximately 48 hours to fully convert to **4** and ethene. Even so, once prepared on a large scale it was stored at – 16 °C as conversion to **10** was observed in the solid state even under inert atmosphere. Unfortunately, it was impossible to grow crystals for structural characterisation as the conversion was so rapid in solution. Similar difficulties were encountered in obtaining a pure $^{13}C\{^{1}H\}$ NMR spectrum as the complex transforms as the spectrum is recorded. In the spectrum acquired,

resonances assigned to **9j**, **10** and phenyl acetate were identified but a resonance for the C_α of the vinylidene ligand could not be detected.

The vinyl complex **10** could be independently isolated on a large scale by allowing a DCM solution of **1** and $HC{\equiv}CCH_2OPh$ to stir for 22 hours. The organometallic product **10** was then separated from the organic product (phenyl acetate) by addition of pentane, which caused **10** to precipitate as a yellow-grey powder. NMR analysis of both complex **10** obtained in this way and the pentane washings indicate that the two products are successfully isolated. The identity of phenyl acetate was confirmed by comparison with an authentic sample.

The three vinyl protons of complex **10** are evident in the ^1H NMR spectrum at δ_H 4.78, 4.98 and 7.33 and can be identified based on their respective couplings. The resonance at δ_H 4.78 was an apparent doublet which corresponds to the vinyl proton H_b as shown in Figure 6.2.1.1. It displays a mutual $^3J_{HH}$ coupling of 16.5 Hz to the *trans* vinyl proton H_a, which exhibits a resonance at δ_H 7.33 as an apparent quartet of triplets. This resonance has an additional $^3J_{HH}$ mutual coupling of 8.9 Hz to the *cis* proton H_c and a $^3J_{HP}$ triplet coupling of 2.0 Hz. Finally the H_c resonance was observed as a doublet of triplets at δ_H 4.98 with a $^4J_{HP}$ coupling of 2.2 Hz. Each resonance integrates to one proton relative to the three acetate protons, observed as a singlet resonance at δ_H 0.59. In the $^{31}P\{^1H\}$ NMR spectrum, a singlet resonance was observed at δ_P 38.5 whilst in the $^{13}C\{^1H\}$ NMR spectrum, a triplet resonance at δ_C 206.7 ($^2J_{PC}$ = 15.3 Hz) corresponds to the CO ligand. A triplet resonance at δ_C 157.7 ($^2J_{PC}$ = 11.2 Hz) and a broad singlet resonance at δ_C 117.2 correspond to the C_α and C_β of the vinyl ligand respectively. In the IR spectrum of complex **10** recorded in DCM solution, a characteristic CO stretch was observed at 1914 cm^{-1}, in addition to the symmetric (1455 cm^{-1}) and asymmetric (1526 cm^{-1}) stretches for a κ^2-OAc ligand. Crystals suitable for structural characterisation by X-ray diffraction were obtained by the slow diffusion of pentane into a solution of **10** in DCM. An ORTEP figure of this complex is shown in Figure 6.2.1.2:

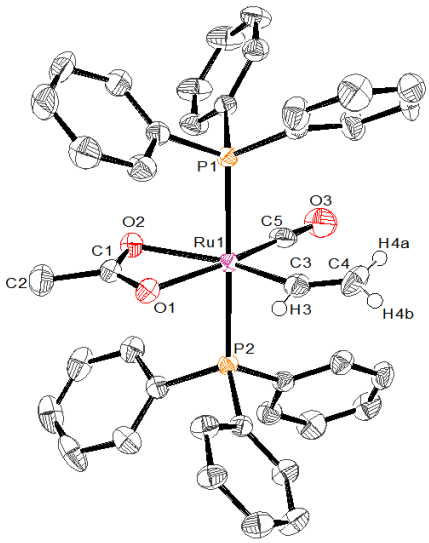

Figure 6.2.1.2: ORTEP diagram of **10**, thermal ellipsoids, where shown, at the 50 % probability level. Hydrogen atoms, except for H(3), H(4a) and H(4b), omitted for clarity.

Bond Length	**(Å)**	**Bond Angle**	**(deg / °)**
Ru – P(1)	2.3673(10)	P(1) – Ru – P(2)	179.03(4)
Ru – P(2)	2.3805(10)	P(1) – Ru – O(1)	94.56(7)
Ru – O(1)	2.190(3)	P(1) – Ru – O(2)	85.61(7)
Ru – O(2)	2.265(3)	O(1) – Ru – O(2)	58.67(10)
Ru – C(3)	1.987(4)	P(1) – Ru – C(3)	92.64(11)
C(3) – C(4)	1.227(5)	P(2) – Ru – C(3)	88.22(11)
Ru – C(5)	1.841(4)	O(1) – Ru – C(3)	98.46(14)
C(5) – O(3)	1.158(5)	O(2) – Ru – C(3)	156.74(14)
		Ru – C(3) – C(4)	144.5(4)
		C(3) – Ru – C(5)	91.92(18)
		P(1) – Ru – C(5)	86.29(12)
		P(2) – Ru – C(5)	94.14(12)
		O(1) – Ru – C(5)	169.53(14)
		O(2) – Ru – C(5)	111.08(15)
		Ru – C(5) – O(3)	172.5(4)

Table 6.2.1.1: Selected Bond Lengths and Angles for **10**.

This structural characterisation confirms that, like the acetylide complex **6**, complex **10** contains a single acetate ligand coordinated in a κ^2-fashion. The presence of a vinyl and CO ligand is also confirmed. The bond lengths and angles obtained indicate that this complex adopts a distorted octahedron structure due to the presence of the κ^2-OAc ligand. The O(1) – Ru – O(2) angle observed for this complex is 58.67(10) °, which is similar to that obtained for the acetylide complex **6** (59.91(7) °). This constraint leads to other angles in the same plane as the κ^2-OAc ligand deviating from 90 °. The C≡O bond length is 1.158(5) Å whilst the Ru–C distance is 1.841(4) Å. These values are within the expected ranges reported by Hocking and Hambley,[11] as noted in Section 3.3, and are similar to those obtained for complex **4** and **6**. Hill has surveyed 19 examples of crystallographically characterised complexes containing vinyl ligands and reports the mean M-C distance to be 2.048 Å and the mean C=C distance to be 1.356 Å. The Ru – C(3) bond length of 1.987(4) Å is close to this mean value and compares favourably to other ruthenium complexes of a similar geometry reported to contain vinyl ligands. The C=C distance reported for complex **10** is 1.227(5) Å, which is unusually short. In 1996 and 1998, Hill also reported the Ru–C and C=C bond lengths of $[Ru(CH=CH_2)(CO)(PPh_3)([9]aneS_3)]PF_6$,[12] to be 2.097(5) Å and 1.292(7) Å respectively, whilst in $[Ru(CH=CH_2)(CO)(PPh_3)_2(H_2B\{pz\}_2)]$[13] the Ru–C distance is 2.080(7) Å and the C=C is 1.345(11) Å.

6.2.2: Further examples of substituted vinylidene complexes and their subsequent conversion to $[Ru(\kappa^2\text{-}OAc)(CH=CH_2)(CO)(PPh_3)_2]$

It was postulated that the reaction of **1** with similar propargylic substrates of the form $HC{\equiv}CCH_2Y$ may also result in the formation of complex **10**, but give other organic products. The study was therefore extended to include the propargylic substrates $HC{\equiv}CCH_2OAc$ (**8k**), $HC{\equiv}CCH_2O\text{-}C_6H_4\text{-}p\text{-}OMe$ (**8l**) and $HC{\equiv}CCH_2NMe_2$ (**8m**). Addition of these substrates to a solution of **1** in CD_2Cl_2 led, unsurprisingly, to the formation of the corresponding substituted vinylidene complexes **9k-m**. These complexes exhibit similar characteristic NMR features to those observed for the phenoxy-vinylidene complex **9j** which are summarised in Table 6.2.2.1. The resonances observed in the ^1H NMR for complexes **9j-l** are very similar, however the

resonances observed for complex **9m** are slightly different. For example, the vinylidene proton is observed as a multiplet resonance in all cases but is observed at a slightly lower chemical shift in **9m** than in **9j-l**. The two resonances due to the C*H*$_2$ protons in the γ-position of the vinylidene are both broad singlets, and again are observed at a lower chemical shift in **9m** than in **9j-l**. There is very little disparity between resonances observed due to the acetate protons and PPh_3 ligands.

These complexes behave similarly to **9j**, in that they ultimately convert to the vinyl complex **10** and an organic product. In the case of **9k** this is acetic anhydride, for **9l** 4-methoxyphenylacetate, and for **9m** *N*,*N*,-dimethylacetamide is observed. For complexes **9j** and **9k**, this process was extremely selective, however in the case of **9m**, a number of unidentified products were also observed. These organic compounds (phenyl acetate, acetic anhydride *etc*.) were identified based on a comparison of their ^{1}H NMR spectra with that of either an authentic sample or literature data.

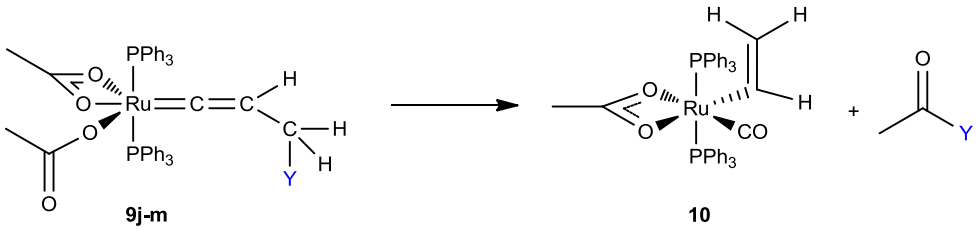

Figure 6.2.2.1: Conversion of **9j**-**m** to **10; 9j** Y = OPh; **9k** Y = OAc; **9l** Y = O-C_6H_4-OMe; **9m** Y = NMe_2.

	^{1}H δ_H **[Ru]=C=C*H***	**^{1}H δ_H** **C*H*H**	**^{1}H δ_H** **CH*H***	**^{1}H δ_H** **C*H*$_3$COO**	**^{31}P δ_P** **PPh_3**
9j	4.41	4.5	4.48	0.87	35.2
9k	4.35	4.4	4.46	0.85	35.3
9l	4.36	4.4	4.43	0.86	35.2
9m	4.07	2.9	2.93	0.83	35.3

Table 6.2.2.1: Common characteristic NMR features of complexes **9j**-**m**.

As for **9j**, the conversion of complexes **9k-m** to **10** also occurs faster than the corresponding transformation of complexes **9a-i** to **4**. Indeed, solutions of **9k** and **9m** had already undergone significant conversion by the time NMR spectra could be recorded, and appeared to take only a few hours to reach completion. The conversion of **9j** appeared to occur marginally slower than for complexes **9k** and **9l**. An attempt was made to obtain the $^{13}C\{^{1}H\}$ NMR spectrum of **9k**, however the conversion of the complex was so rapid that the major components identified were complex **10** and acetic anhydride.

6.2.3: Formation of [Ru(κ^2-OAc)(COCH=CH$_2$)(CO)(PPh$_3$)$_2$] by addition of CO to [Ru(κ^2-OAc)(CH=CH$_2$)(CO)(PPh$_3$)$_2$]

It was noted that the major carbon framework had been reduced from three to two in the formation of the vinyl complex **10** from the vinylidene complexes **9j-m**. Insertion of a CO ligand into alkyl ligands is a well-known procedure, and results in an increase in the carbon framework. Consequently, complex **11**; [Ru(κ^2-OAc)(COCH=CH$_2$)(CO)(PPh$_3$)$_2$], containing a three carbon η^1-acyl ligand, was obtained by stirring a DCM solution of **10** under an atmosphere of CO. This migratory insertion reaction between the CO and vinyl ligands resulted in the formation of another potential intermediate in the conversion of propargylic alcohols to alkenes.

This was evidenced by the evolution of a new CO stretch in the IR spectrum recorded in DCM at 1943 cm^{-1} and a stretch due to the acyl moiety at 1573 cm^{-1}. The κ^2-OAc coordination mode was also retained as shown by two stretches at 1452 cm^{-1} (κ^2-OCO$_{sym}$) and 1535 cm^{-1} (κ^2-OCO$_{asym}$).

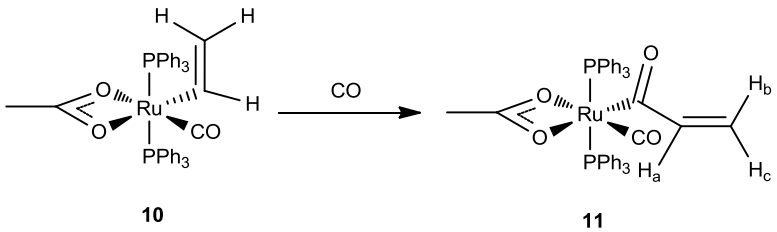

10 **11**

Figure 6.2.3.1: Addition of CO to **10**.

Analysis of this product by NMR spectroscopy revealed a singlet resonance at δ_P 36.7 in the $^{31}P\{^1H\}$ NMR spectrum. Three doublet of doublet resonances due to the three vinylic protons were evident in the ^1H NMR spectrum at δ_H 4.21 (H_c), 4.56 (H_b) and 7.21 (H_a) with mutual couplings of $^2J_{HbHc}$ = 2.6 Hz, $^3J_{HaHc}$ = 10.3 Hz and $^3J_{HaHb}$ = 17.0 Hz. These resonances each integrated to one proton relative to three of a singlet observed at δ_H 0.56 assigned to the acetate protons. In the $^{13}C\{^1H\}$ NMR, a triplet resonance for the CO ligand was observed at δ_C 204.6 ($^2J_{PC}$ = 15.0 Hz) whilst a triplet resonance at δ_C 243.6 ($^2J_{PC}$ = 7.9 Hz) is assigned to the carbon atom of the acyl ligand. Two singlet resonances at δ_C 138.4 and 111.8 were assigned to the C_α and C_β of the vinyl moiety respectively.

A similar complex was observed by Ros[14] when CO and NaO_2CCF_3 was added to the coordinatively unsaturated complex [Ru(CH=CH^{t}Bu)(Cl)(CO)(PPh_3)]. This resulted in a mixture of two complexes apparently in equilibrium, which is illustrated in Figure 6.2.3.2. The acyl-complex **6A** is analogous to **11**; it contains a trifluoroacetate ligand coordinated in a κ^2-fashion in addition to a CO ligand and two PPh_3 ligands. This complex is in equilibrium with a vinyl complex **6B**, which also contains two CO ligands and two PPh_3 ligands along with a now κ^1-O_2CCF_3 ligand.

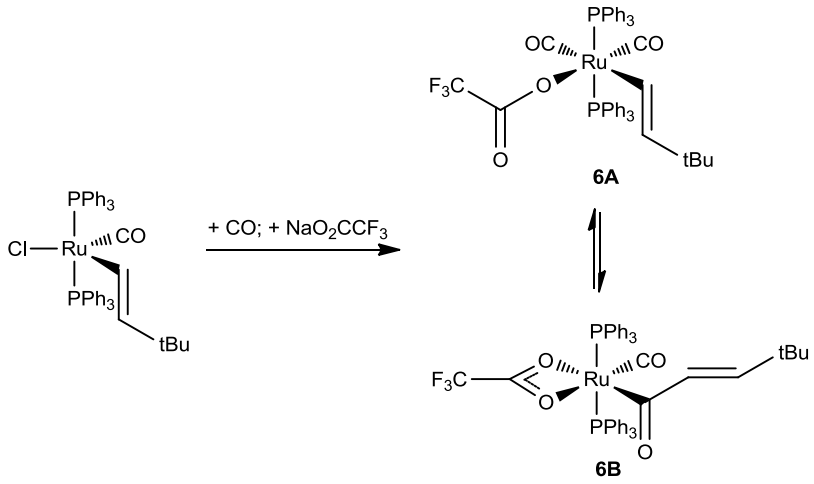

Figure 6.2.3.2: Formation of complex **6B**, an analogue of **11,** formed by addition of CO and NaO_2CCF_3 to [Ru(CH=CH^{t}Bu)(Cl)(CO)(PPh_3)].

The authors also report a crystal structure of their acyl-complex **6B** which may be compared to the structural characterisation of complex **11**, an ORTEP figure of which is shown in Figure 6.2.3.3:

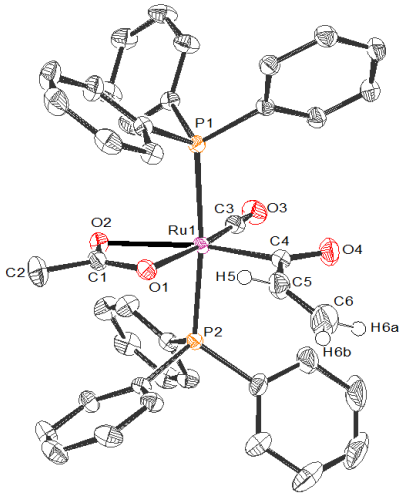

Figure 6.2.3.3: ORTEP diagram of **11**, thermal ellipsoids, where shown, at the 50 % probability level. Hydrogen atoms, except for H(5), H(6a) and H(6b), and two molecules of DCM of crystallisation omitted for clarity.

Bond Length	**(Å)**	**Bond Angle**	**(deg / °)**
Ru – P(1)	2.3856(4)	P(1) – Ru – P(2)	172.714(14)
Ru – P(2)	2.3817(4)	P(1) – Ru – O(1)	89.51(3)
Ru – O(1)	2.1612(11)	P(1) – Ru – O(2)	86.71(3)
Ru – O(2)	2.3502(11)	O(1) – Ru – O(2)	57.95(4)
Ru – C(4)	1.9935(16)	P(1) – Ru – C(4)	94.46(5)
C(4) – O(4)	1.223(2)	P(2) – Ru – C(4)	92.83(5)
C(4) – C(5)	1.504(2)	O(1) – Ru – C(4)	98.47(6)
C(5) – C(6)	1.311(3)	O(2) – Ru – C(4)	156.40(6)
Ru – C(3)	1.8344(16)	Ru – C(4) – O(4)	130.16(13)
C(3) – O(3)	1.152(2)	C(4) – Ru – C(3)	89.80(7)
		P(1) – Ru – C(3)	90.26(5)
		P(2) – Ru – C(3)	89.78(5)
		O(1) – Ru – C(3)	171.73(6)
		O(2) – Ru – C(3)	113.78(6)
		Ru – C(3) – O(3)	178.64(16)

Table 6.2.3.1: Selected Bond Lengths and Angles for **11**.

The structural features of complexes **11** and **6B** are very similar. Due to the presence of the κ^2-OAc and κ^2-O_2CCF_3 ligands, the structure exhibited by both complexes is best described as a distorted octahedron. The O(1) – Ru – O(2) angle of complex **11** (57.95(4) °) is larger than in complex **6B** (54.74(14) °). The Ru–C and C≡O bond lengths of the CO ligands are similar and conform to expected distances. In complex **11** the Ru–C and C≡O bond lengths are 1.8344(16) Å and 1.152(2) Å respectively, whilst for **6B** the Ru–C and C≡O bond distances are 1.806(5) Å and 1.148(2) Å. The Ru–C–O angle is also essentially linear in both complexes as would be expected; in complex **6B** the angle is 177.4(4) ° and in **11** 178.64(16) °. The acyl ligand is coordinated in a η^1-fashion in both complexes. Roper[15] has reported that the Ru–O distance of the η^2-acyl complex [RuI($COCH_3$)(CO)(PPh_3)$_2$] is 2.47(2) Å. The Ru – O(4) distance in complex **11** is 2.935 Å and the equivalent distance for complex **6B** is 2.725(4) Å. Both distances are considered too long to be attributed to an acyl ligand coordinated in a η^2-fashion. The Ru – C(4) and C(4) – O(4) bond lengths are similar in both complexes **11** and **6B**. In complex **11** the Ru – C(4) distance is 1.9935(16) Å and the C(4) – O(4) distance is 1.223(2) Å. For complex **6B** the corresponding distances are 1.982(5) Å and 1.230(6) Å. The C=C bond lengths are 1.311(3) Å and 1.338(7) for complexes **11** and **6B** respectively and in both complexes the alkene is in the same plane as the CO and carboxylate ligands.

6.2.4: Addition of acetic acid to [Ru(κ^2-OAc)($CH=CH_2$)(CO)(PPh_3)$_2$] and [Ru(κ^2-OAc)($COCH=CH_2$)(CO)(PPh_3)$_2$]

Upon inspection of complex **10**, it became clear that protonation with acetic acid may provide a facile pathway to complex **4** and ethene. Consequently, a stoichiometric reaction was conducted whereby one equivalent of acetic acid was added to a solution of **10** in CD_2Cl_2, the sample sealed and monitored by ^1H and $^{31}P\{^1H\}$ NMR spectroscopy. This showed the gradual liberation of ethene, as evidenced by the growth of a singlet resonance at δ_H 5.44 in the ^1H NMR spectrum, with concomitant formation of **4**; as indicated by a singlet resonance at δ_H 0.71 due to the acetate protons and a characteristic resonance at δ_P 39.1 in the $^{31}P\{^1H\}$ NMR spectrum.

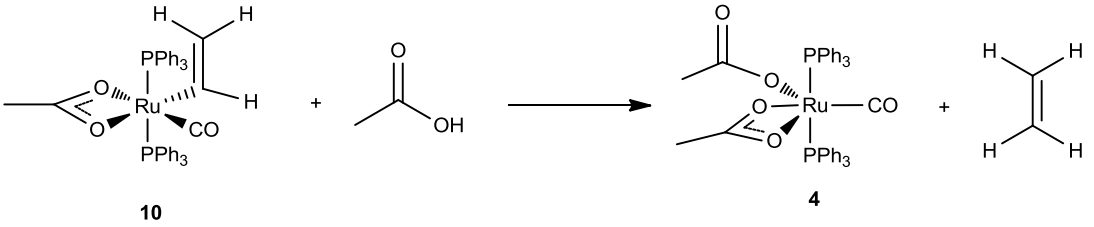

Figure 6.2.4.1: Addition of acetic acid to **10** results in the formation of **4** + ethene.

It is therefore proposed that if the conversion of the phenoxy-substituted vinylidene complex **9j** results in the formation of complex **10** and phenyl acetate, then the conversion of the hydroxy-substituted complexes **9a-i** may occur *via* a vinyl complex analogous to **10**; of the general formula [Ru(κ^2-OAc)(CH=CR_2)(CO)(PPh_3)$_2$], and acetic acid. An overall mechanism could be envisioned whereby the vinyl complex analogous to **10** forms immediately prior to the formation of **4**, which is generated by protonation of the vinyl ligand by the *in situ* acetic acid. It can also be inferred that the transformation of **9j-m** essentially 'halts' at complex **10** as the acid is no longer present *in situ* to protonate the vinyl ligand and regenerate **4**.

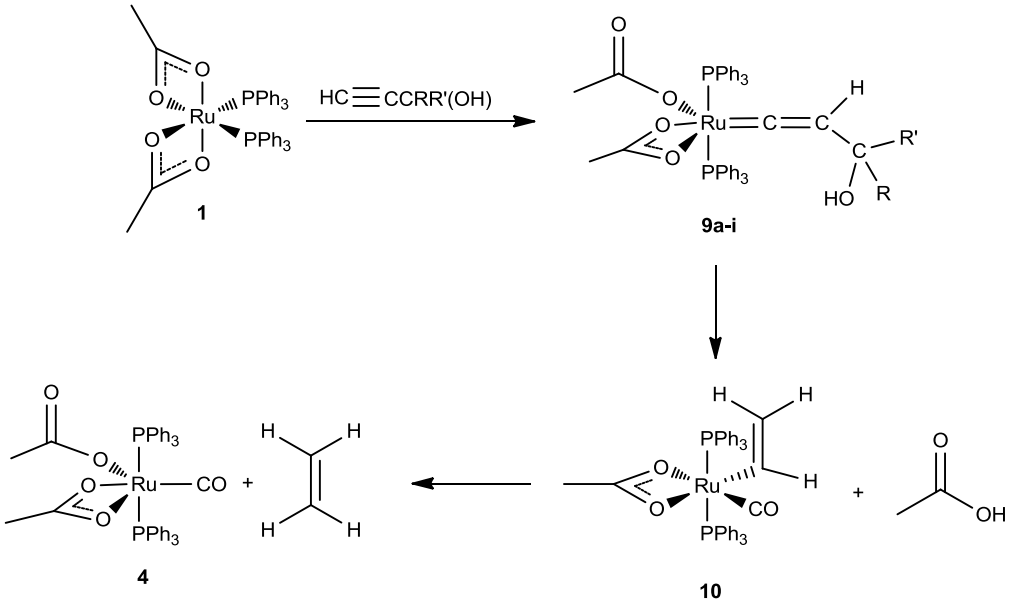

Figure 6.2.4.2: The formation of **4** + ethene is preceded by the formation of **10** + acetic acid.

It was expected that addition of acetic acid to **11** would result in the formation of **4** and the liberation of the coordinated aldehyde ligand. Instead, addition of acetic acid to a solution of **11** in CD_2Cl_2 led to the formation of ethene and another organometallic complex. The complex exhibits a singlet in the $^{31}P\{^1H\}$ NMR spectrum at δ_P 31.8 and a singlet equivalent to six acetate protons at δ_H 1.18 in the ^1H NMR spectrum. It is proposed that this complex contains two κ^1-OAc ligands, and two CO ligands. No evidence for an aldehyde product was detected by ^1H NMR spectroscopy.

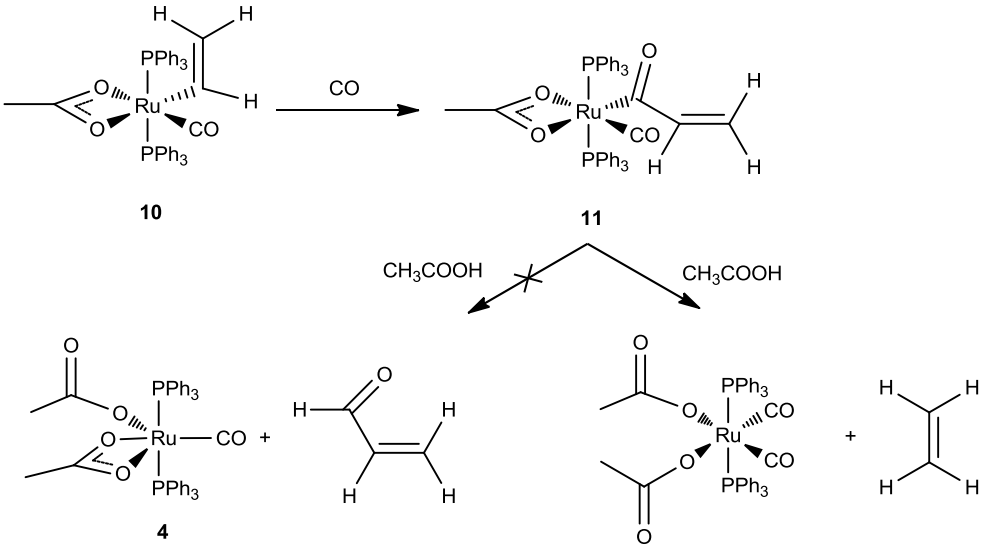

Figure 6.2.4.3: Formation of complex **11** and addition of acetic acid.

The evolution of ethene instead of acrylaldehyde on addition of acetic acid to **11** suggests that complex **10** may be an intermediary between the two. Therefore, it is implied that the conversion of the hydroxy-vinylidene complexes **9a-i** to **4** and the corresponding alkene proceeds sequentially *via* analogues of complexes **11** and **10**. Further evidence for this was discovered when the $^{31}P\{^1H\}$ NMR spectra recorded to monitor the conversion of the hydroxy-vinylidene complexes were re-examined. In some cases, minor peaks at approximately δ_P 38 and 36 could be detected. In the cases of **9d** and **9i**, two resonances are observed at similar chemical shifts, which may be due to the (*E*) and (*Z*) isomers of the complex **10** analogue.

^{31}P NMR δ_P shift	Hydroxy-vinylidene	Analogue of 10	Analogue of 11
9a	34.0	38.7	36.1
9b	34.1	38.6	36.2
9c	34.3	38.7	36.2
9d	34.9	38.7(2), 38.7(1)	36.7
9e	34.3	38.6	36.5
9f	34.4	38.8?	36.4
9g	33.9	38.3	-
9h	35.1	38.5	-
9i	35.5	38.5(7), 38.6(0)	36.9

Table 6.2.4.1: $^{31}P\{^1H\}$ NMR δ_P shifts observed whilst monitoring the degradation of complexes **9a-i**.

However, it was still unclear how the hydroxy-vinylidene complexes transformed to the acyl complex **11**. The apparent involvement of acetic acid suggested that the acetate ligands are once more behaving in a non-innocent fashion, as also observed in the LAPS mechanism.

6.2.5: Formation of [Ru(κ^1-OAc)(=C(OAc)=CHPh)(CO)(PPh_3)$_2$]

At this point a computational study was begun in collaboration with Dr John Slattery and David Johnson, the results of which will fully discussed in Section 6.6. As noted in Chapter 4, nucleophilic attack of one of the uncoordinated oxygen atoms of a κ^1-OAc ligand onto the vinylidene C_α of **2a/*e*** to give a metallo-enolester (***f***) is particularly facile. The difference in energy between the two forms is only 6 kJ mol^{-1}.

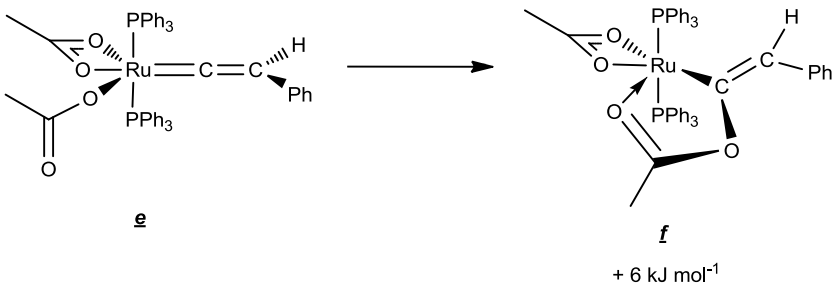

Figure 6.2.5.1: Energy difference between vinylidene complex ***e*** and metallo-enolester complex ***f***.

Consequently, attempts were made to replicate this result experimentally. It was found that a solution of the vinylidene complex **2a** in DCM underwent a rapid colour change from pink to pale-green when stirred under an atmosphere of CO. This solution exhibited a CO stretch at 1963 cm^{-1} and two distinct environments could be observed for the two different types of κ^1-OAc ligand assigned to a single product: **12**. The symmetric and asymmetric paired stretches for the 'typical' κ^1-OAc ligand are observed at 1367 cm^{-1} and 1593 cm^{-1} (these values being 'typical' for a κ^1-OAc ligand of this type of complex). The other acetate is observed as a κ^1-OAc ligand, even though it appears to be coordinated in a κ^2-fashion. The symmetric and asymmetric stretches due to this ligand are observed at 1394 cm^{-1} and 1571 cm^{-1} respectively.

Characterisation of **12** by NMR spectroscopy revealed that the vinylic proton had shifted significantly compared to the vinylidene complex **2a**; a triplet resonance was observed at δ_H 6.25 with a $^4J_{HP}$ coupling of 2.8 Hz. The two distinct environments of the two acetate ligands are again evident by the presence of two singlet resonances that have an equal integration of three protons at δ_H 1.15 and 1.63. The complex also gives rise to a singlet resonance in the $^{31}P\{^1H\}$ NMR spectrum at δ_P 30.7. In the $^{13}C\{^1H\}$ NMR spectrum a triplet resonance due to a CO ligand is observed at δ_C 205.8 ($^2J_{PC}$ = 12.7 Hz) whilst another triplet at δ_C 193.2 ($^2J_{PC}$ = 17.8 Hz) is assigned to the C_α of the vinylic moiety. The C_β is observed as a triplet resonance at δ_C 122.3 ($^3J_{PC}$ = 4.5 Hz). As in the ^1H NMR spectrum, there are also two distinct environments for the two carbon atoms of the acetate protons. Typically a singlet resonance is observed at ~ δ_C 22 when the two acetate ligands are undergoing rapid exchange on the NMR timescale, however in the case of complex **12** two singlets are observed at δ_C 18.5 and 24.0.

The ^{13}C-analogue of **12** (**^{13}C-12**) was also synthesised and characterised; its synthesis and spectroscopic features are detailed in Chapter 4 (Section 4.2). A crystal of **12** suitable for structural characterisation was grown by the slow diffusion of pentane into a solution of complex **12** in DCM. An ORTEP diagram of the resulting structure is shown in Figure 6.2.5.2:

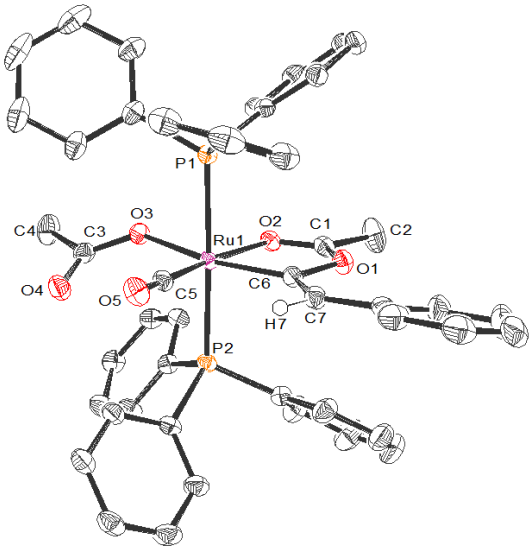

Figure 6.2.5.2: ORTEP diagram of **12**, thermal ellipsoids, where shown, at the 50 % probability level. Hydrogen atoms, except for H(7), omitted for clarity.

Bond Length	**(Å)**	**Bond Angle**	**(deg / °)**
Ru – P(1)	2.3672(5)	P(1) – Ru – P(2)	177.523(16)
Ru – P(2)	2.4116(5)	P(1) – Ru – O(3)	87.69(3)
Ru – O(2)	2.1434(12)	P(2) – Ru – O(3)	89.90(3)
Ru – O(3)	2.1378(12)	P(1) – Ru – C(5)	85.77(6)
Ru – C(5)	1.8158(18)	P(2) – Ru – C(5)	95.36(6)
C(5) – O(5)	1.161(2)	O(2) – Ru – C(5)	171.17(6)
Ru – C(6)	2.0206(17)	O(3) – Ru – C(5)	103.44(6)
C(6) – C(7)	1.346(2)	C(6) – Ru – C(5)	92.16(7)
C(6) – O(1)	1.460(2)	Ru – C(5) – O(5)	173.90(15)
		P(1) – Ru – O(2)	94.16(3)
		P(2) – Ru – O(2)	85.07(3)
		P(1) – Ru – C(6)	90.50(5)
		P(2) – Ru – C(6)	91.67(5)
		O(2) – Ru – C(6)	79.01(6)
		O(3) – Ru – C(6)	164.11(6)
		Ru – C(6) – O(1)	110.25(11)
		Ru – C(6) – C(7)	137.06(14)
		O(1) – C(6) – C(7)	112.69(15)

Table 6.2.5.1: Selected Bond Lengths and Angles for **12**.

Complexes containing a metallo-enolester have been reported previously in the literature. Some have been synthesised by the addition of a terminal alkyne to a transition-metal centre which contains a κ^2-coordinated carboxylate ligand. For example, Grubbs[16] has shown that the addition of HC≡CPh to [Ru(κ^2-O_2CCPh_2)(PPh_3)$_2$(Tp)] results in the formation of the metallo-enolester complex shown in Figure 6.2.5.3. Alternatively, Schanz[17] has reported a metallo-enolester structure resulting from the addition of acetic acid to the carbyne complex [$RuCl_3$(≡CCH=CPh_2)(PPh_3)$_2$].

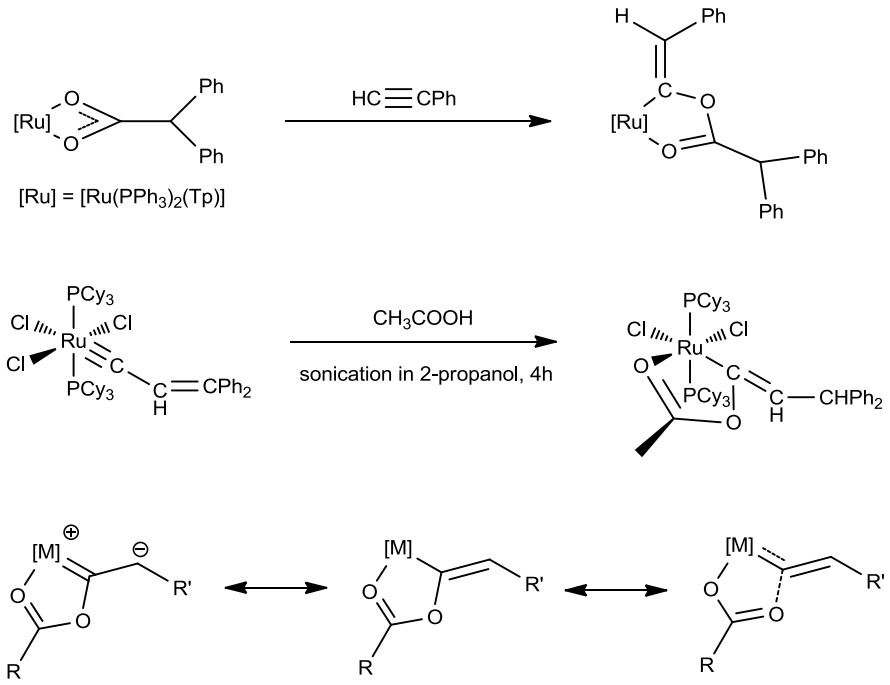

Figure 6.2.5.3: Analogues and resonance forms of the metallo-enolester complex **12**.

Both of the metallo-enolester complexes shown in Figure 6.2.5.3 have been structurally characterised and form a useful basis for comparison of the metallo-enolester ligand. Complex **12** assumes a distorted octahedron structure in the solid state, owing to the strain imposed by the five-membered metallocycle; O(2) – Ru – C(6) is 79.01(6)°. The distortion observed is similar to that seen for complexes incorporating a κ^2-OAc ligand, even though the strain may be expected to be greater in these systems as they include a smaller four-membered ring. The P(1) – Ru – P(2) angle is close to linear at 177.523(16)°, as is the Ru – C(5) – O(5) angle at 173.90(15)°. The Ru – C(5) and C(5) – O(5) distances of 1.8158(18) Å and 1.161(2) Å are also typical of a carbonyl ligand. For those complexes containing a metallo-enolester ligand which have been structurally characterised in the literature, the

coordination of the ligand may involve consideration of resonance forms, as also shown in Figure 6.2.5.3. However, little contribution is expected from the zwitterion form in the case of complex **12**, as the Ru – C(6) distance of 2.0206(17) Å is that of a single bond, and is longer even than the Ru–C distance for the vinyl ligand in complex **10** (1.987(4) Å). The C(6) – C(7) distance is also typical of a double bond at 1.346(2) Å and the Ru – O(2) distance of 2.1434(12) Å is similar to those reported in the literature for analogous compounds (for six complexes[16-21] a mean distance of 2.124 Å is calculated).

It is proposed that **12** forms by the mechanism shown in Figure 6.2.5.4, in which a vacant site is created for a CO ligand to bind by the κ^2-OAc ligand of **2a** altering its coordination mode. The C_α of the vinylidene ligand may then undergo nucleophilic attack by one of the uncoordinated oxygen atoms of a κ^1-OAc ligand to form complex **12**. An alternative suggestion is that the C_α of the vinylidene in **2a** is undergoing rapid and reversible attack by the κ^1-OAc ligand and that this form is simply trapped by the CO ligand.

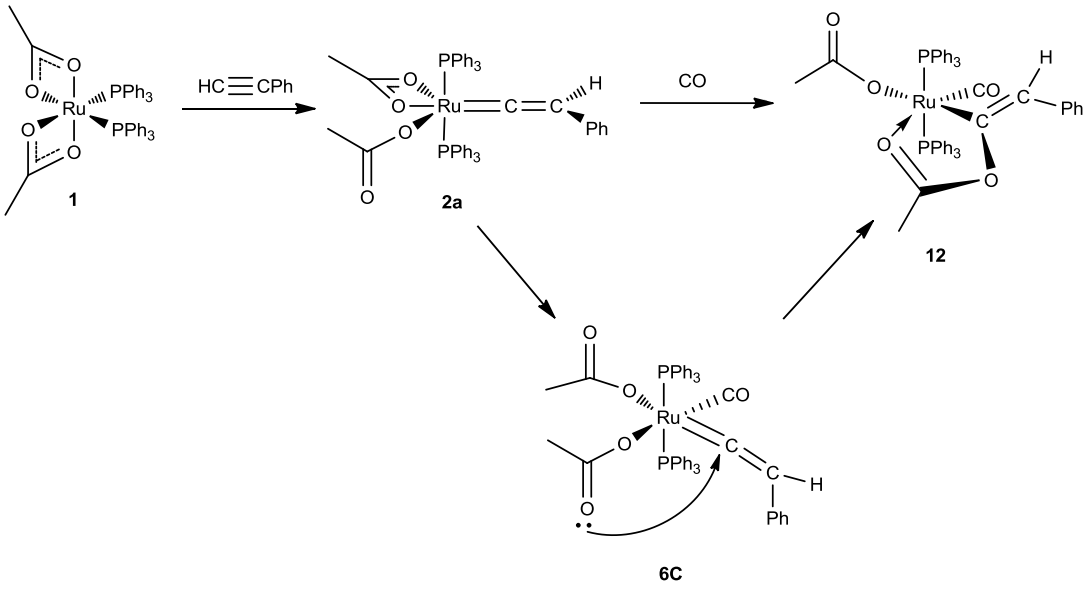

Figure 6.2.5.4: Proposed mechanism of formation for complex **12**.

Addition of one equivalent of acetic acid to a solution of **12** in CD_2Cl_2 led to the formation after one day of **4** and (*Z*)-β-styryl-acetate. This was also observed upon addition of acetic acid to **^{13}C-12**. Analysis of the mixture by $^{13}C\{^1H\}$ NMR spectroscopy indicated that the label was located on the carbon of (*Z*)-β-styryl-acetate bonded to the OAc moiety observed at δ_C 134.1.[22]

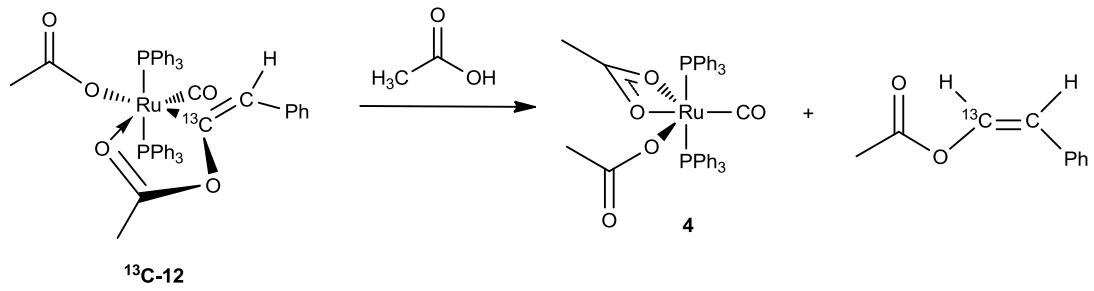

Figure 6.2.5.5: Addition of acetic acid to **^{13}C-12**.

The presence of a CO ligand has facilitated the 'trapping' of complexes **10**, **11** and **12** that are proposed intermediates in the conversion of the propargylic alcohols to alkenes. Further evidence for this was provided by monitoring the conversion of **9d** to **4** and styrene in CD_2Cl_2 by NMR spectroscopy in a sealed Young's NMR tube under an atmosphere of CO. This led to the observation that the reaction could be slowed to such an extent that the appropriate analogues of **10** and **12** could be observed in the $^{31}P\{^1H\}$ NMR spectrum. The resulting spectrum exhibited four peaks centred on δ_P 30.1. These were assigned to two doublet resonances exhibiting an AB pattern with a large $^2J_{PP}$ *trans*-coupling of 315.5 Hz consistent with the structure indicated in Figure 6.2.5.6. It is proposed that two doublets were observed as the plane of symmetry through the molecule has been broken by the stereogenic C_γ centre, meaning the two PPh_3 ligands are inequivalent.

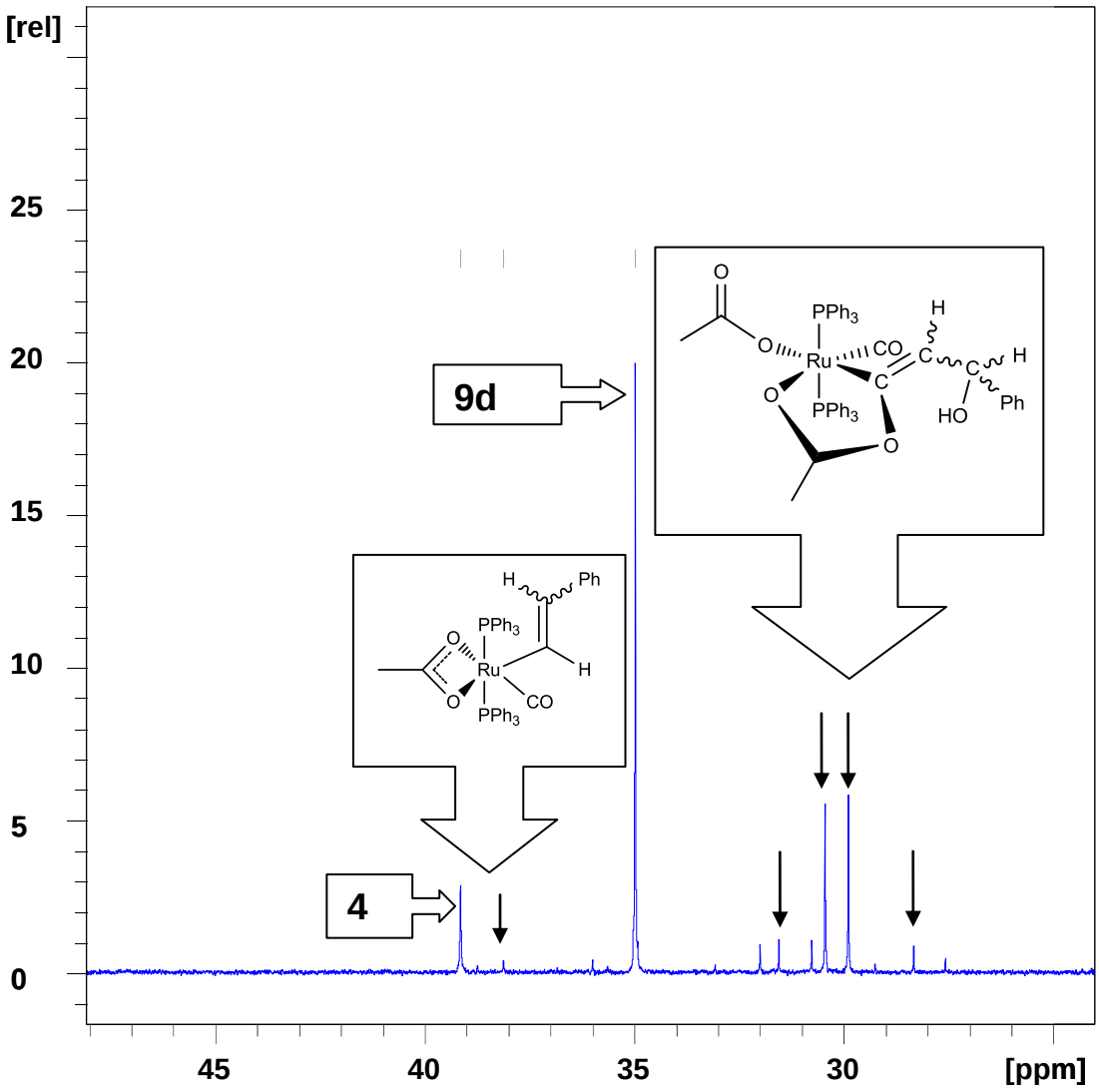

Figure 6.2.5.6: $^{31}P\{^{1}H\}$ NMR Spectrum of **9d** under an atmosphere of CO.

6.2.6: Mechanistic Implications of Complexes 10, 11 and 12

The mechanism proposed by Dixneuf for the conversion of propargylic alcohols to alkenes (see Section 6.1) involves the formation of intermediate complexes containing allenylidene and hydroxy-carbene ligands. However, no evidence for such structures has been detected experimentally in the conversion mediated by complex **1**. Instead, the independent synthesis of complexes **10**, **11** and **12** has allowed for two alternative preliminary mechanistic pathways to be proposed. The non-innocent role of the acetate ligands has already been demonstrated in the study of the LAPS pathway for the formation of vinylidene and acetylide complexes

derived from **1**. Consequently, it is suggested that the acetate ligand may again play an important role in the decarbonylation of propargylic alcohols.

One proposed pathway (**VI**) is shown in Figure 6.2.6.7 below. In this mechanism, it is suggested that after the initial formation of the vinylidene complex **9**, the C_α undergoes nucleophilic attack by an uncoordinated oxygen atom of a κ^1-OAc ligand to form a complex analogous to **12**. This may then undergo a rearrangement to give a complex containing an acyl ligand (corresponding to complex **11**). A reverse migratory insertion may then result in the formation of an analogue of the vinyl complex **10**. At this point, if R'' ≠ H the reaction halts, as for **9j-m**, but if acetic acid is present (R'' = H) the vinyl ligand is liberated by protonation to generate complex **4** and the appropriate alkene.

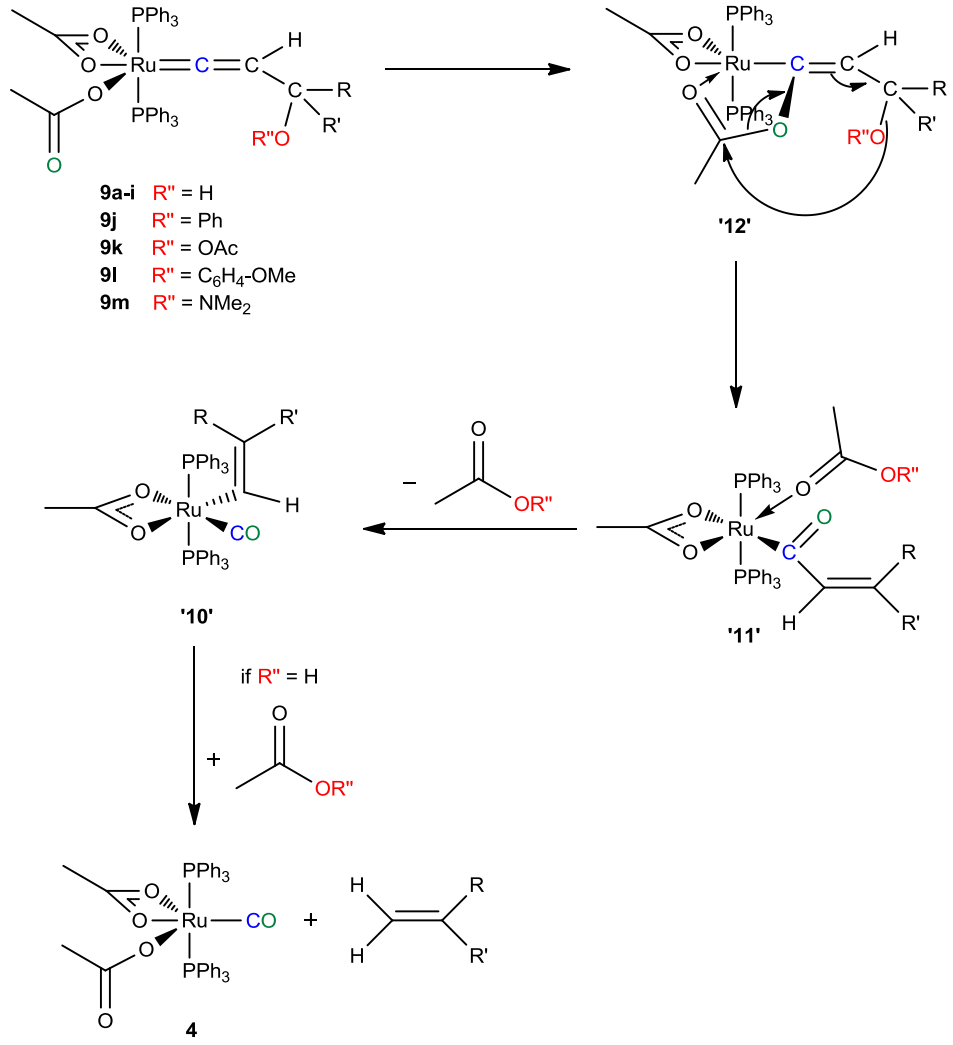

Figure 6.2.6.7: Proposed mechanism **VI**.

Alternatively, it may be proposed that instead of a concerted intramolecular rearrangement of complex **12**, the reaction may proceed *via* an intermolecular process. A scheme illustrating another possible mechanistic pathway (**VII**) is shown in Figure 6.2.6.8 below. In this route, it is proposed that an allenylidene intermediate may form upon loss of HOR'' from the metallo-enolester intermediate. Despite our apparent inability to isolate a complex containing an allenylidene ligand, we cannot presume that such a species is not involved; although to the best of our knowledge, there have been no examples of allenylidene formation *via* the loss of any other moiety other than H_2O. However, we must conclude that the absence of such evidence is not necessarily evidence of its absence.

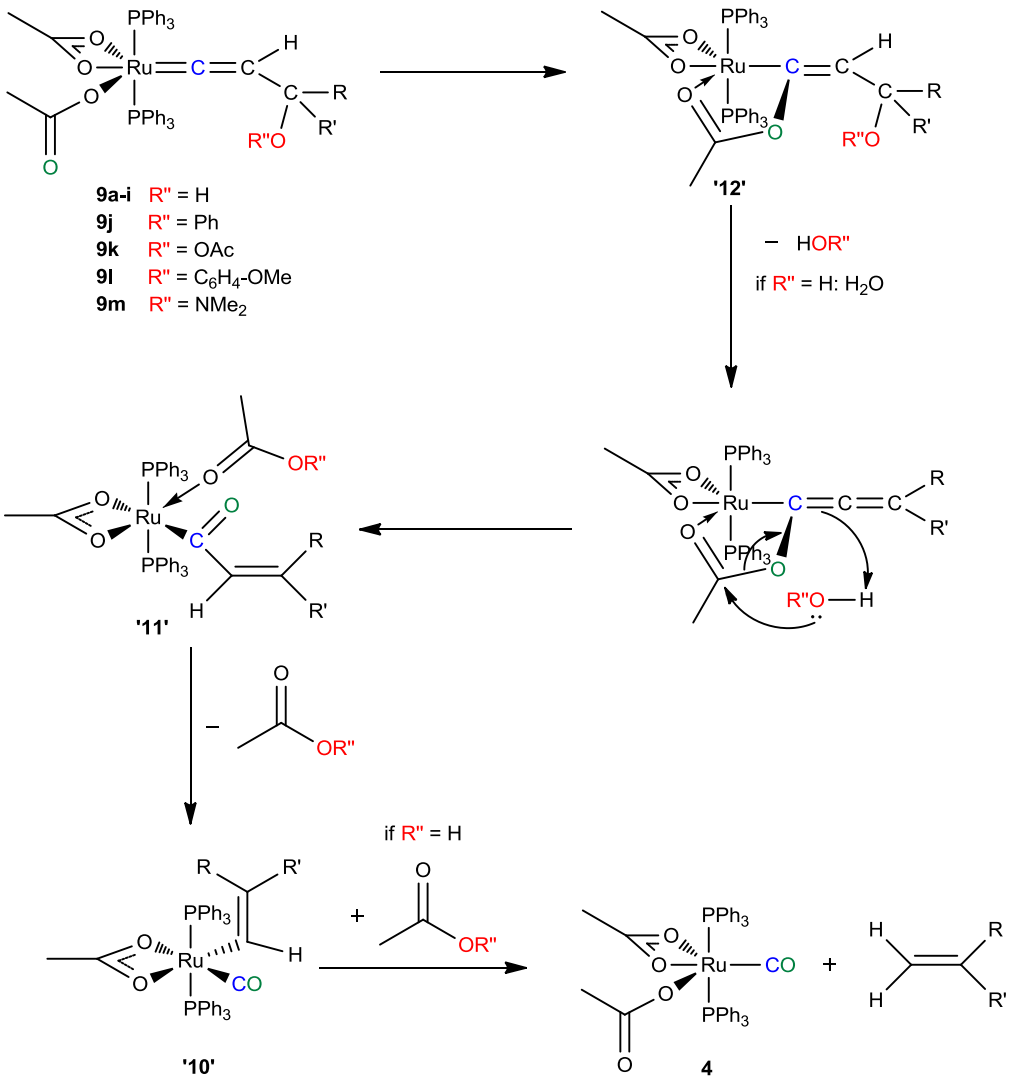

Figure 6.2.6.8: Proposed mechanism **VII**.

The importance of the acetate ligand has been demonstrated not only in the formation of vinylidene complexes **2a-d** and **9a-m** *via* the LAPS mechanism, but also in the conversion of vinylidene complexes **9a-m** into either complexes **4** or **10**, and their respective organic by-products. To probe this further, attempts were made to replicate and expand this chemistry using a benzoate analogue of **1**; $Ru(\kappa^2\text{-}OBz)_2(PPh_3)_2$ (**13**). This work was predominantly developed by Nicholas Hiett who demonstrated that this complex reacts with terminal alkynes in a similar fashion. It was proposed that cross-over experiments between acetate- and benzoate-containing complexes could also provide more mechanistic information.

6.3: Stoichiometric Reactions with a Benzoate complex

It is well-established that acetate ligands are able to act as bridging ligands between two transition metal centres. In Wilkinson's initial report on the synthesis of **1**, he also describes complexes that contain bridging acetate ligands and details the inter-conversion of these species.[23] We have noted that **1** may react with H_2O or O_2 to give one such complex (**14**) when dissolved in solvents that have not been thoroughly dried and degassed. This complex has been previously reported by Wilkinson and was synthesised by stirring a MeOH solution of $[Ru_2Cl(OAc)_4]$ and PPh_3 in air for 24 hours.[23]

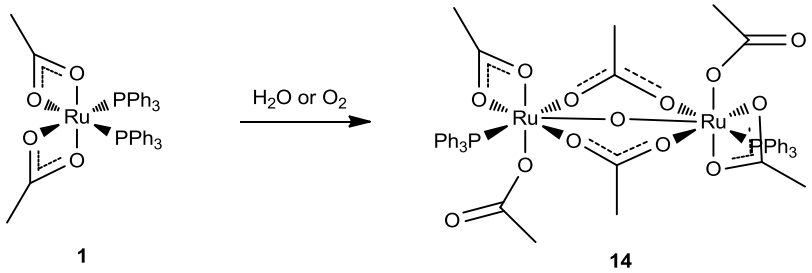

Figure 6.3.1: Reaction of **1** with H_2O to give the acetate-bridged dimer complex **14**.

The bridging ability of the acetate ligand must be considered when attempting to determine how the acetate ligands are involved in the conversion of propargylic alcohols to alkenes. Therefore, it was envisioned that a 'cross-over' experiment in which the conversion of two complexes containing different carboxylate ligands and differently substituted vinylidene ligands was monitored *in situ* by NMR spectroscopy. This would allow us to ascertain whether the acetate moiety is acting in an *inter*- or *intra*molecular fashion through analysis of the organic products obtained. An illustration of this is provided in Figure 6.3.2 below.

Towards this end, MChem student Nicholas Hiett synthesised a complex containing benzoate ligands in the place of acetate ligands (**13**) using the same procedure as for **1**, substituting NaOBz for NaOAc. A crystal structure of **13** was obtained, and the molecular structure obtained is shown in Figure 6.3.2 below.

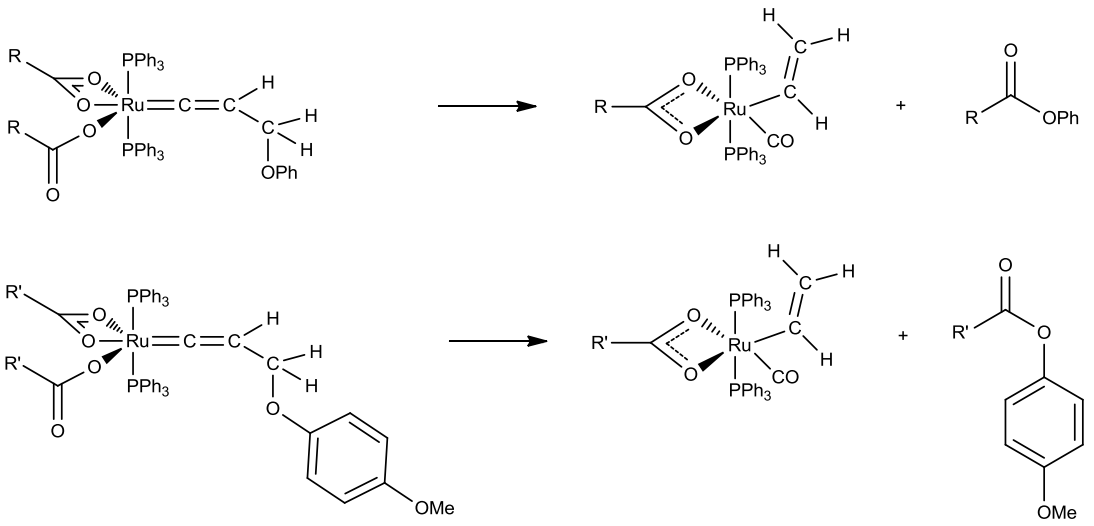

Figure 6.3.2: Cross-over experiments.

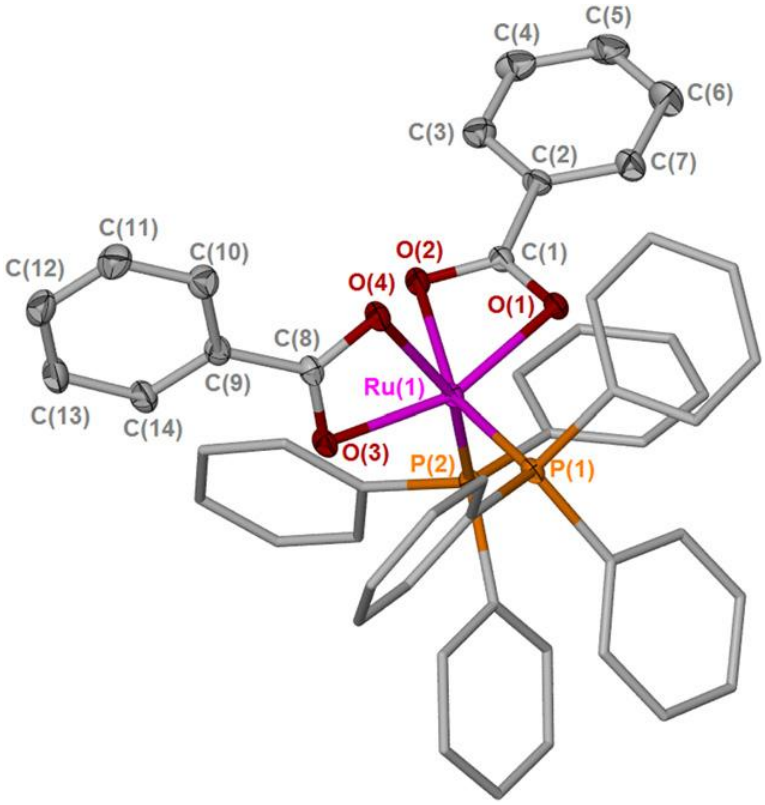

Figure 6.3.3: Molecular structure of **13**. Thermal ellipsoids (where shown) are at the 50 % probability level. Hydrogen atoms omitted for clarity.

Bond Length	**(Å)**	**Bond Angle**	**(deg / °)**
Ru – P(1)	2.2424(5)	P(1) – Ru – P(2)	104.046(17)
Ru – P(2)	2.2664(5)	P(1) – Ru – O(1)	97.82(4)
Ru – O(1)	2.1016(12)	P(1) – Ru – O(2)	156.91(4)
Ru – O(2)	2.2278(13)	P(1) – Ru – O(3)	94.92(4)
Ru – O(3)	2.1017(12)	P(1) – Ru – O(4)	91.37(4)
Ru – O(4)	2.2272(12)	P(2) – Ru – O(1)	91.35(4)
		P(2) – Ru – O(2)	86.34(4)
		P(2) – Ru – O(3)	100.06(4)
		P(2) – Ru – O(4)	156.85(4)

Table 6.3.1: Selected Bond Lengths and Angles for **13**.

As for complex **1**, the two PPh_3 ligands adopt a mutually-*cis* orientation. The overall geometry is that of a distorted octahedron which is once more ascribed to the constraints of the two κ^2-OBz ligands. Most of the bond lengths and angles are similar to those observed for complex **1**, although the two Ru – P bond lengths are more different at 2.2424(5) Å and 2.2664(5) Å for P(1) and P(2) respectively. There is evidence of π-stacking interactions between the phenyl ring of a benzoate ligand and a phenyl ring of $P(2)Ph_3$, which may account for this longer bond length.

The $^{31}P\{^1H\}$ NMR spectrum of **13** exhibited a singlet resonance at δ_P 63.1, very similar to the resonance observed for complex **1**. Characterisation of **13** by IR spectroscopy also confirmed that the two benzoate ligands are chelate; the symmetric and asymmetric stretches are observed at 1425 cm^{-1} and 1505 cm^{-1} respectively ($\Delta\upsilon$ = 80 cm^{-1}).

The vinylidene complexes **15a** and **16d** were prepared in a similar manner to their acetate-containing counterparts (**2a** and **9d**) by the addition of one equivalent of the appropriate alkyne to a solution of **13** in DCM. These complexes exhibited characteristic NMR and IR spectroscopic features typical of vinylidene and hydroxy-vinylidene complexes. These features are summarised in Table 6.3.2 below.

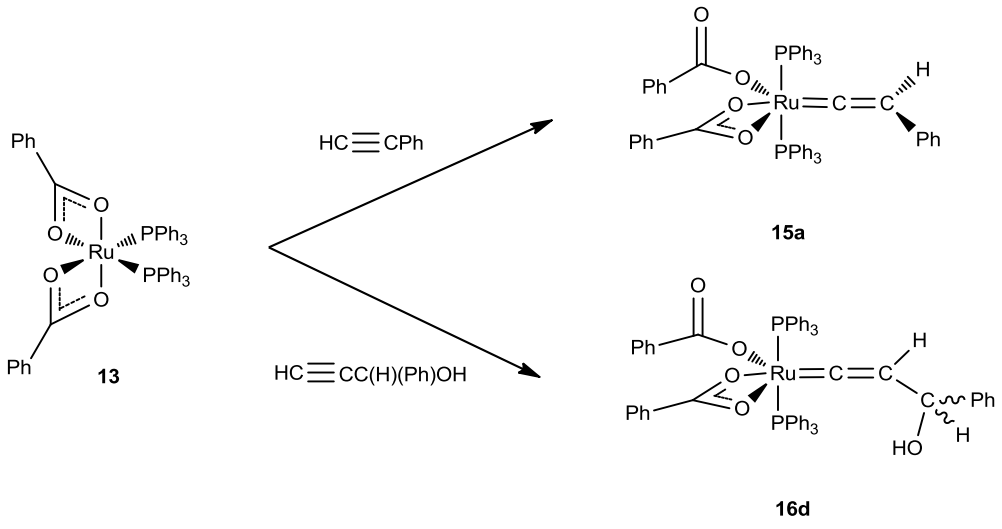

Figure 6.3.4: Formation of complexes **15a** and **16d** by addition of the appropriate alkyne to **13.**

	^{1}H δ_H [Ru]=C=C*H*	^{1}H $^{4}J_{HP}$/Hz	^{1}H δ_H O*H*	^{31}P δ_P PPh_3	^{13}C δ_C C_α	^{13}C $^{2}J_{CP}$/Hz	^{13}C δ_C C_β	^{13}C $^{3}J_{CP}$/Hz
15a	5.44	3.8	n.a.	33.5	358.2	16.8	112.8	4.6
16d	4.60	3.8	0.93	34.3	347.3	16.0	112.5	4.6

Table 6.3.2: Common NMR features of complexes **15a** and **16d**. (n.a. = not applicable).

The IR spectra of these complexes recorded in DCM show that, as for the acetate complexes, both monodentate and chelate coordination modes are present in these complexes. A summary of these IR features is included in Table 6.3.4 below. It is again presumed that the benzoate ligands are undergoing an exchange process which is rapid on the NMR timescale but slow on the IR timescale.

A crystal suitable for X-ray Diffraction was obtained for complex **15a** and its molecular structure is given in Figure 6.3.4 below. Disorder between the vinylidene ligand and the κ^2-OBz ligand was found in a ratio of 55:45 so Table 6.3.3 includes relevant bond lengths and angles that differ. The orientation of the vinylidene ligand differs significantly between the two forms; in the major form shown in Figure 6.3.4 the vinylidene ligand is significantly out of the plane with respect to the two benzoate ligands but in the minor form this deviation is less. This contrasts with the crystal structure obtained for complex **2a** (described in section 2.2), in which the vinylidene and acetate ligands are more in plane. These effects may be due to the larger steric bulk of the benzoate ligands.

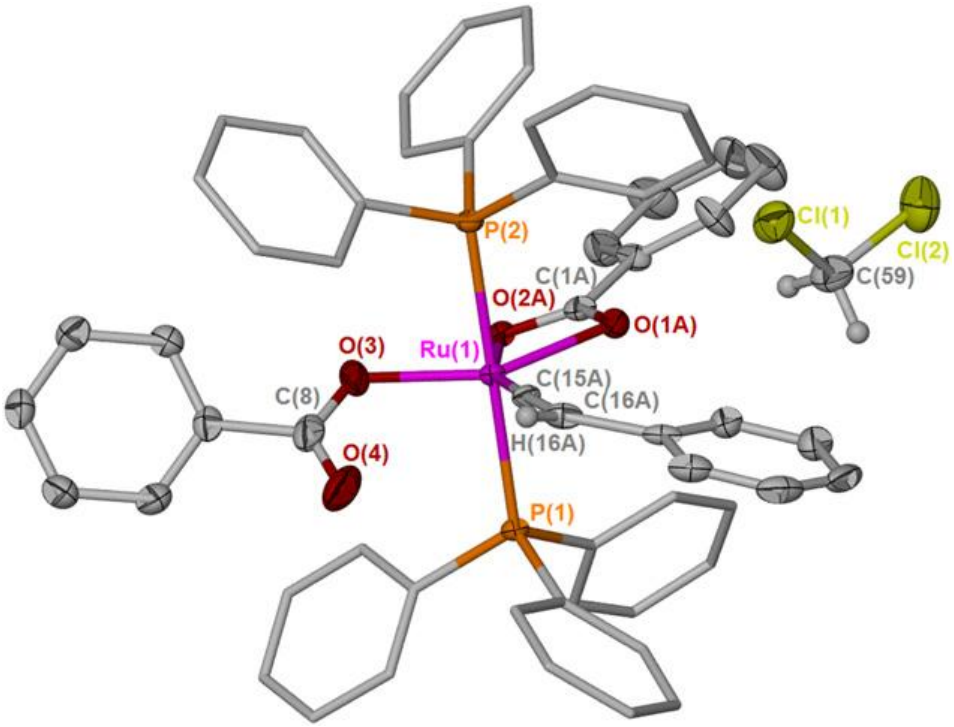

Figure 6.3.5: Molecular structure of the major form of **15a**. Thermal ellipsoids (where shown) are at the 50 % probability level. Hydrogen atoms except H(16A), H(59A) and H(59B) omitted for clarity.

Bond Length	**(Å)$_{major}$**	**(Å)$_{minor}$**	**Bond Angle**	**(deg / °) $_{major}$**	**(deg / °) $_{minor}$**
Ru – P(1)	2.4031(6)	-	P(1) – Ru – P(2)	178.08(2)	-
Ru – P(2)	2.4031(6)	-	P(1) – Ru – O(1)	82.30(7)	97.25(10)
Ru – O(1)	2.4031(6)	2.4031(6)	P(1) – Ru – O(2)	92.66(13)	89.7(2)
Ru – O(2)	2.4031(6)	2.4031(6)	P(1) – Ru – O(3)	92.66(13)	-
Ru – O(3)	2.4031(6)	-	P(2) – Ru – O(1)	92.66(13)	83.87(10)
Ru – C(15)	2.4031(6)	2.4031(6)	P(2) – Ru – O(2)	85.56(13)	92.2(2)
C(15) – C(16)	2.4031(6)	2.4031(6)	P(2) – Ru – O(3)	84.75(5)	-
			C(15) – Ru – O(1)	97.1(3)	100.5(3)
			C(15) – Ru – O(2)	155.3(3)	160.1(4)
			C(15) – Ru – O(3)	96.6(3)	110.7(3)
			Ru – C(15) – C(16)	96.6(3)	171.6(7)

Table 6.3.3: Selected Bond Lengths and Angles for **15a**.

Monitoring a solution of **16d** by NMR spectroscopy showed that this complex undergoes a conversion analogous to that of **9d** to form the corresponding CO-containing complex **17** [Ru(κ^1-OBz)(κ^2-OBz)(PPh_3)$_2$(CO)] and styrene. This was confirmed by the independent synthesis of complex **17** by stirring a MeOH solution of **13** under a CO atmosphere. A singlet resonance was observed at δ_P 38.7 in the $^{31}P\{^1H\}$ NMR spectrum whilst the carbon atom of the CO ligand is observed as a triplet resonance at δ_C 206.9 ($^2J_{PC}$ = 13.9 Hz) in the $^{13}C\{^1H\}$ NMR spectrum. The IR spectrum of this complex recorded in DCM indicated that both κ^1- and κ^2-coordination modes of the benzoate ligands are present and a sharp peak at 1947 cm^{-1} confirmed the presence of the CO ligand. The pertinent features of the IR spectra are summarised in Table 6.3.4 below.

Complex	P–Ph	C=C	CO	κ^1-OCO_{sym}	κ^1-OCO_{asym}	κ^1-$\Delta\upsilon$	κ^2-OCO_{sym}	κ^2-OCO_{asym}	κ^2-$\Delta\upsilon$
15a (DCM)	1434	n.g.	n.a.	1339	1594	255	1417	1491	74
16d (DCM)	1433	1621	n.a.	1340	1594	254	1407	1492	85
17 (DCM)	1434	n.a.	1947	1350	1616	266	1444	1505	61

Table 6.3.4: Common IR features of complexes **15a, 16d** and **17**. (n.a. = not applicable, n.g = not given).

The synthesis and characterisation of complexes **13, 15a, 16d** and **17** was conducted by Mr Nicholas Hiett and experimental details can be found in his MChem report (2008-2009).

Further insight was gained by reacting complex **13** with propargyl ethers **8j** and **8l** and propargyl benzoate (HC≡CCH_2OBz; **8n**). The addition of alkynes **8j** and **8l** to solutions of complex **13** in CD_2Cl_2 led to the initial formation of the vinylidene complexes **16j** and **16l**. In both complexes, the resonances due to the vinylidene proton and the CH_2 protons in the C_γ position are coincident in the ^1H NMR spectrum and are observed as a broad singlet at ~ δ_H 4.5. A singlet resonance is observed at δ_P 34.1 and 34.0 in the $^{31}P\{^1H\}$ NMR spectra of complexes **16j** and **16l** respectively. The conversion of these vinylidene complexes to the corresponding vinyl complex **18** (analogous to **10**) takes place at a slower rate than for the acetate complexes and does not proceed as smoothly. Resonances assigned to complex **18** include a singlet at δ_P 37.9 in the $^{31}P\{^1H\}$ NMR spectrum and two apparent doublets

observed at δ_H 4.81 (J_{HH} = 16.5 Hz) and δ_H 5.05 (J_{HH} = 9.0 Hz) in the ^{1}H NMR spectrum. Resonances due to the vinylidene complex typically disappear after five days to be replaced by those due to complex **17** (δ_P 38.2), ethene (δ_H 5.45) and **18**, although resonances due to trace quantities of unidentified organometallic species were also observed. It is presumed that the formation of complex **18** occurs with concomitant formation of PhOCOPh (phenyl benzoate) and PhOCO-C_6H_4-OMe (4-methoxyphenyl benzoate), for complexes **16j** and **16l** respectively, although resonances for these compounds cannot easily be distinguished from those of other phenyl resonances.

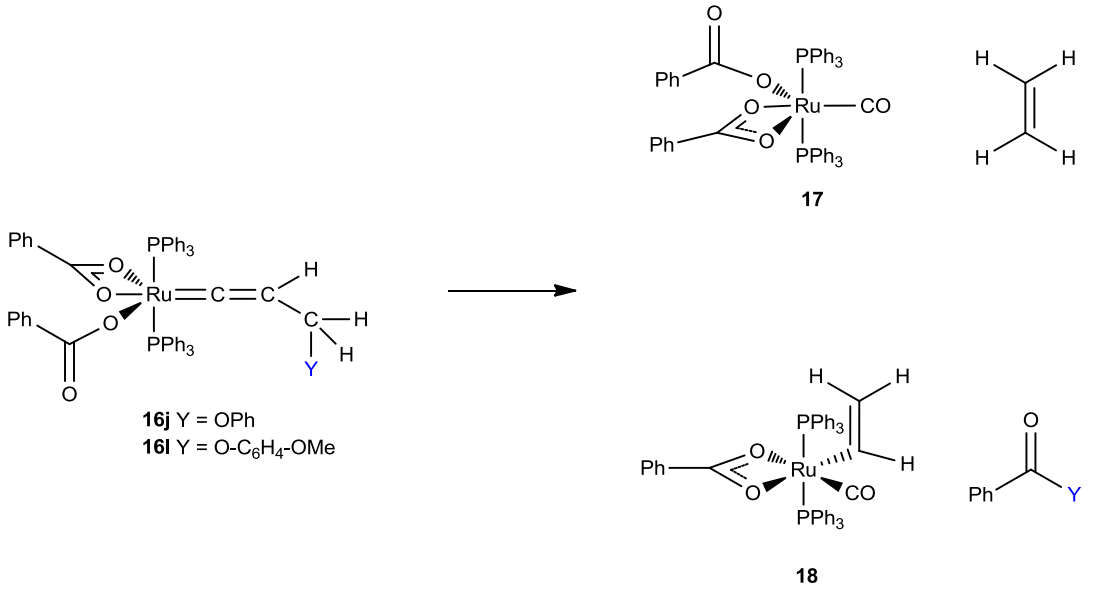

Figure 6.3.6: Products observed upon the degradation of complexes **16j** and **16l**.

The reaction of complex **13** with propargyl benzoate (**8n**) does not result in the formation of complex **18** and benzoic anhydride but in the formation of the CO-containing complex **17** and ethene. The ^{1}H and ^{31}P{^{1}H} NMR spectra recorded soon after addition of the alkyne show that the degradation of the vinylidene complex **16n** to **17** and ethene is mostly complete. One explanation for this behaviour is that the mechanism of conversion proceeds *via* mechanism **VII** proposed in Section 6.2.6. This would result in the elimination of benzoic acid in the step in which an allenylidene ligand is generated. The presence of benzoic acid in solution may then facilitate the formation of the CO-complex **17** and ethene.

At this point, it was decided that a cross-over experiment would not produce useful results as the benzoate complexes are observed to undergo a slower rate of conversion compared to the acetate analogues. Also, the benzoate complexes do not convert as smoothly to the corresponding vinyl complex. Whilst preparing for this cross-over experiment, it was also discovered that the exchange of acetate and benzoate is particularly facile. An equimolar solution of a combination of complexes **1** and **13** in CD_2Cl_2 was made up and monitored by ^1H and $^{31}P\{^1H\}$ NMR spectroscopy. Immediately, a novel complex was observed to form that contained one acetate and one benzoate ligand: $[Ru(\kappa^2\text{-}OAc)(\kappa^2\text{-}OBz)(PPh_3)_2]$ **19**. This is evidenced by the observation of a singlet resonance at δ_P 63.3 situated between the resonances for complexes **1** (δ_P 63.5) and **13** (δ_P 62.9) in the $^{31}P\{^1H\}$ NMR spectrum. In the ^1H NMR spectrum, an additional acetate resonance is observed at δ_H 1.49. After one day, this complex became the major component of the mixture.

Tentative evidence for mechanism **VII** proposed in Section 6.2.6 has already been uncovered in the addition of propargyl benzoate (**8n**) to complex **13**. This mechanism involves the generation of either H_2O or HOR''. Further confirmation for this mechanism was obtained in two stoichiometric reactions conducted between **1** and alkyne **8n**, and between **9j** and HO-C_6H_4-OMe.

In an attempt to synthesise the vinylidene complex **9n**, one equivalent of propargyl benzoate was added to a solution of **1** in CD_2Cl_2. The ^1H and $^{31}P\{^1H\}$ NMR spectra recorded 30 minutes after addition of the alkyne indicated that in addition to the presence of a complex assigned as **9n**, resonances due to another vinylidene complex were present. Two multiplet resonances, indicative of a vinylidene proton, are observed at δ_H 4.34 and 4.40 in the ^1H NMR spectrum. The multiplet resonance at δ_H 4.34 corresponds exactly to that of the vinylidene proton of complex **9k**. Two sets of two broad singlet resonances are also observed corresponding to the CH_2 protons of C_γ for both **9k** and **9n**. This is illustrated by Figure 6.3.7, which displays the overlaid spectra of complex **9k** with that obtained for the reaction of **1** with alkyne **8n**.

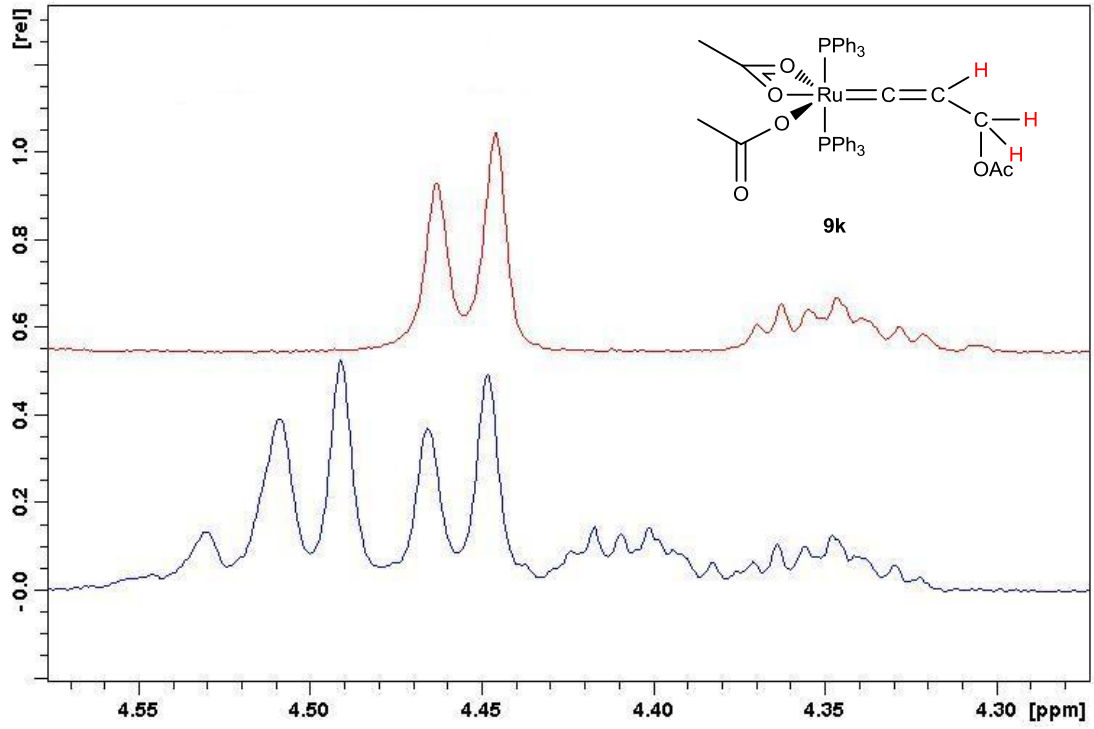

Figure 6.3.7: Overlaid ^{1}H NMR spectra of complex **9k** (red) and the reaction of **1** with **8n** (blue).

In the $^{31}P\{^{1}H\}$ NMR spectrum, a number of resonances were observed, although not all could be assigned, four singlet resonances are centred on δ_P 35.1, one of which (δ_P 35.2) is assigned to the vinylidene complex **9k**, as illustrated by Figure 6.3.9. It is proposed that the other major peak at δ_P 34.8 corresponds to the vinylidene complex **9n**. One explanation of this behaviour is that if the degradation of these vinylidene complexes is occurring *via* the route proposed in mechanism (**VII**), then HOR'' generated in this case is benzoic acid. It has already been shown that exchange of the carboxylate ligands is facile so the benzoic acid generated may initiate exchange with an acetate ligand resulting in the generation of acetic acid, as illustrated below. This may then react with the allenylidene complex (**6C**) in Figure 6.3.8 to generate a form of **9k**. In which case, it is proposed that the two minor resonances at δ_P 34.9 and 35.4 correspond to **9k'** and **9n'** which contain one OAc and one OBz ligand (as for complex **19**).

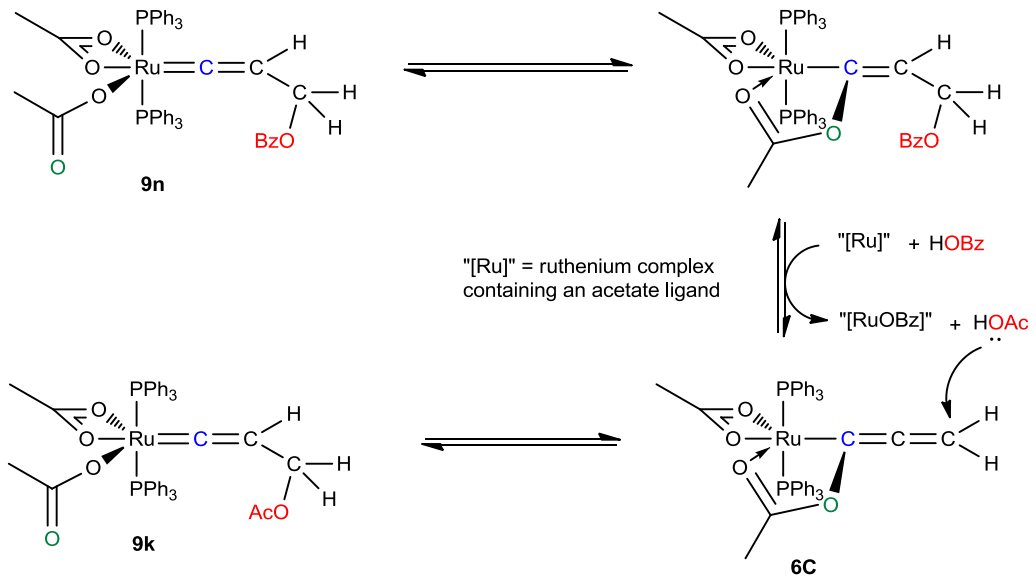

Figure 6.3.8: Proposed mechanism by which complexes **9n** and **9k** interchange.

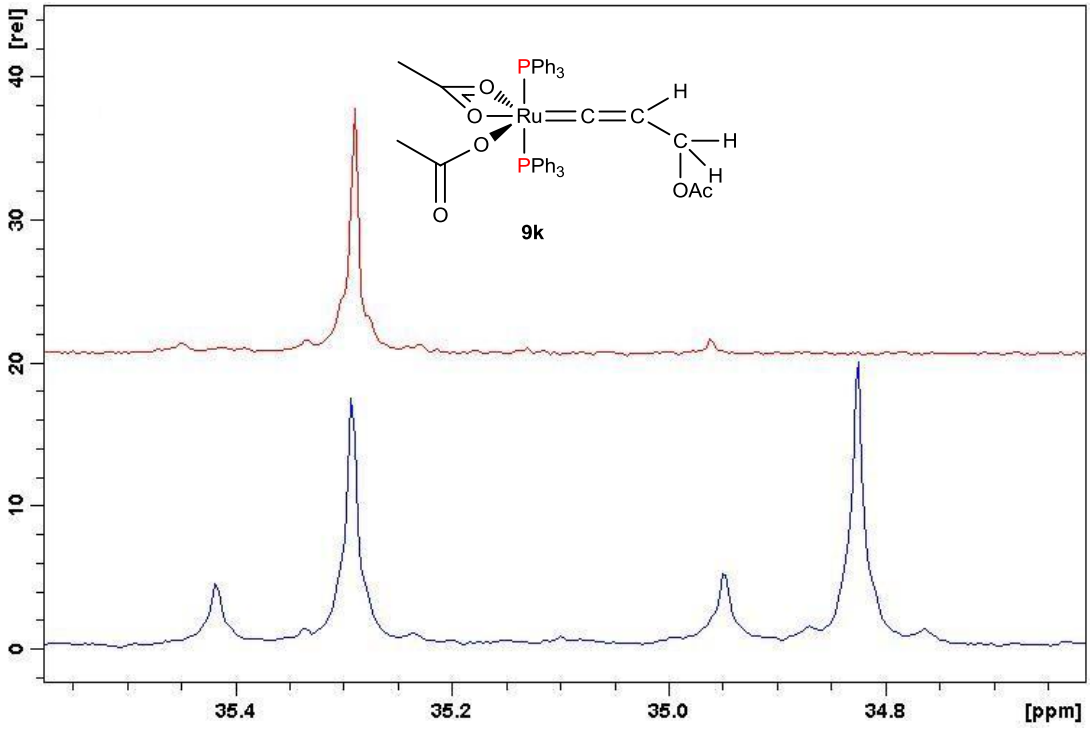

Figure 6.3.9: Overlaid $^{31}P\{^{1}H\}$ NMR spectra of complex **9k** (red) and the reaction of **1** with **8n** (blue).

Resonances due to the vinylidene complexes disappeared after two days to be replaced by those of five organometallic species, as evidenced by the blue $^{31}P\{^{1}H\}$ NMR spectrum shown in Figure 6.3.10. The red spectrum is that of **9k** after it has converted to complex **10** (with a trace of complex **4**) and the green spectrum is that of the reaction mixture after five days.

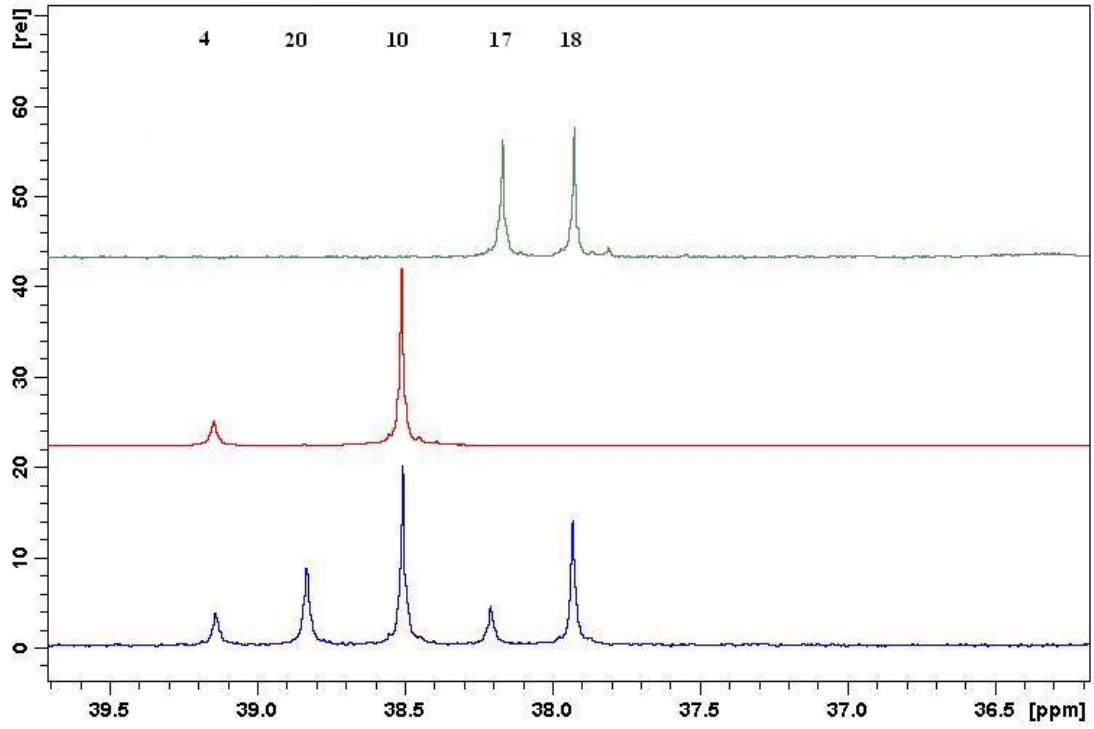

Figure 6.3.10: Overlaid $^{31}P\{^{1}H\}$ NMR spectra of complex **9k** after 20 hours (red), the reaction mixture after five days (green) and the reaction of **1** with **8n** after two days (blue).

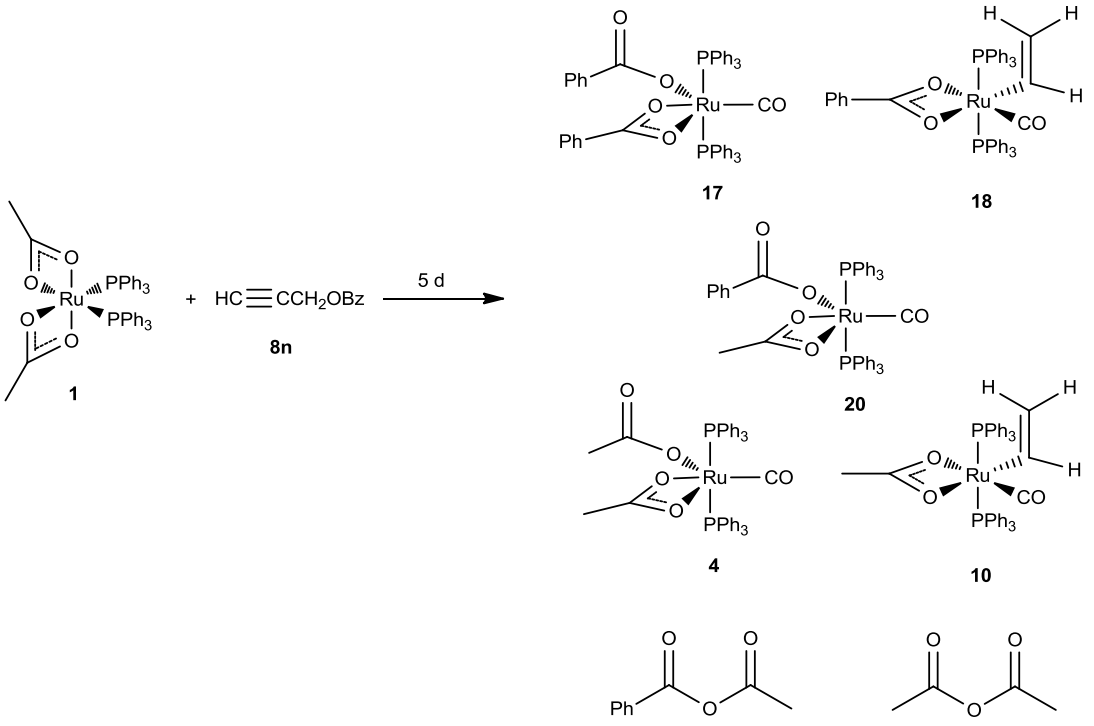

Figure 6.3.11: Multiple products are observed five days after addition of **8n** to complex **1**.

The assignments of these five species is based on the premise that complexes **9k** and **9n** should decay to the vinyl complex **10**, and as carboxylate exchange is facile, it is unsurprising to observe the formation of complex **18**, the benzoate analogue of **10**. It is also not unexpected to observe small amounts of complexes **4** and **17**, which are often observed if any proton source is present and available to remove the vinyl ligand as ethene. The remaining resonance, which has been labelled **20** has been assigned to a CO-complex containing one OAc and one OBz ligand: $[Ru(OAc)(OBz)(CO)(PPh_3)_2]$. It is presumed that the carboxylate ligands of **20** are fluxional, as in the case of **4**. The ^1H NMR spectrum recorded at this stage also confirmed the presence of complexes **10** and **18**; resonances due to the vinyl protons could be clearly observed. In addition, two resonances assigned to acetic anhydride and benzoic acetic anhydride ($CH_3COOCOPh$) were detected at δ_H 2.24 and 2.40 respectively. The resonance assigned to acetic anhydride was confirmed by comparison to an authentic sample, and that of benzoic acetic anhydride by comparison with literature data.[24] A resonance assigned to ethene was also detected at δ_H 5.45.

This reaction has provided evidence supporting mechanism **VII** shown in Figure 6.2.6.8. It has demonstrated that the elimination of a HOR'' moiety occurs and that the formation of an allenylidene ligand is reversible. To test this further, a reaction of complex **9j** with the alcohol HO-C_6H_4-OMe was performed. The ^1H and $^{31}P\{^1H\}$ NMR spectra recorded soon after the addition of an excess of the alcohol showed that two vinylidene complexes were again present in solution. In addition to **9j**, resonances due to complex **9l** were also observed. Both vinylidene complexes were observed to convert to complex **10**, phenyl acetate and 4-methoxyphenyl acetate after one day.

Experimental evidence reported thus far has pointed towards a mechanistic route involving the formation of an intermediate allenylidene complex, as proposed in mechanism **VII** in Figure 6.2.6.8. However, the role of the acetate ligand has not yet been confirmed. In both mechanisms **VI** and **VII**, an acetate ligand plays a vital role in assisting the decarbonylation of the propargylic alcohols. In order to substantiate evidence for its role, an ^{18}O-labelling study was conducted.

6.4: ^{18}O-labelling study

It was proposed in Section 6.2.5 that two mechanisms may be operating for the conversion of propargylic alcohols to alkenes. In both, it is suggested that an oxygen atom of an acetate ligand attacks the electrophilic C_α of a vinylidene ligand and is ultimately incorporated as the oxygen atom of the CO ligand of complex **4**. In order to determine if this is the case, it was proposed that an ^{18}O-labelling study be performed using the phenoxy-substituted vinylidene complex **9j**. If either of the two mechanisms proposed in Section 6.2.5 are operating, then incorporation of an ^{18}O-label into the CO ligand of complex **10** should be readily detected by IR spectroscopy. If the mechanism proposed by Dixneuf[9,10] is occurring, then no change should be detected as the oxygen of this ligand would be derived from PhOH not an acetate ligand. Towards this end, a complex equivalent to **1** in which all four oxygen atoms were ^{18}O (**^{18}O-1**) was synthesised using a adaptation of the synthesis of **1**. The typical route to complex **1** involves heating NaOAc (10 equivalents) and $[RuCl_2(PPh_3)_3]$ at 90 °C in ^{t}BuOH for one hour. The ^{18}O label was to be derived from the doubly labelled $CH_3C^{18}O^{18}OH$. Consequently, a different approach was needed to produce (**^{18}O-1**); KO^{t}Bu was used to deprotonate $CH_3C^{18}O^{18}OH$ in ^{t}BuOH to generate $K^{18}O^{18}OCCH_3$ *in situ*, which was then heated at 90 °C with 0.1 equivalents of $[RuCl_2(PPh_3)_3]$ for one hour. After cooling, the product was removed by filtration, the filtrate collected and reused in a second reaction to utilise the residual eight equivalents of $K^{18}O^{18}OCCH_3$ remaining *in situ*. The product was obtained as a red powder and could be recrystallised by the slow diffusion of pentane into a DCM solution of **^{18}O-1**.

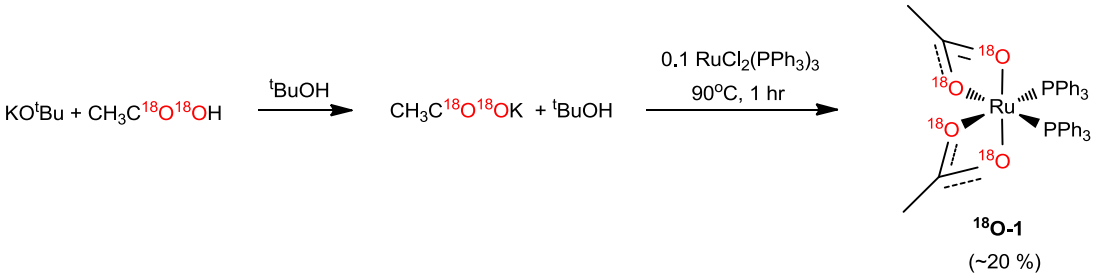

Figure 6.4.1: Synthesis of **^{18}O-1**.

Full incorporation of the label was confirmed by LIFDI-MS, which showed a molecular ion peak at 752.1 m/z as expected. A mass spectrum was also recorded using the ESI technique which exhibits a peak at m/z 730.1. As is frequently

observed for these acetate-containing complexes, this is equivalent to the m/z value predicted for **^{18}O-1** that has undergone the loss of an $^{18}O^{18}OCCH_3$ moiety and gained the mass of a molecule of MeCN. Analysis of the complex by NMR spectroscopy showed there to be no difference in the chemical shift values between the labelled and unlabelled complexes. This also confirmed that the product was free from traces of $CH_3C^{18}O^{18}OH$ which would affect subsequent reactions.

The product was also analysed by IR spectroscopy which, whilst showing the absence of the symmetric and asymmetric stretches due to the κ^2-$^{16}OC^{16}O$ ligands, showed no other bands than those typically assigned to the P-Ph stretch of the PPh_3 ligands at 1434 cm^{-1} and 1481 cm^{-1}. The expected isotopic shift of the κ^2-$^{18}OC^{18}O_{asym}$ stretch can be calculated using Equation 6.4.1 (α = 118.57 °).[25]

$$\frac{\lambda_3^{(i)}}{\lambda_3} = \left[\frac{\omega_3^{(i)}}{\omega_3}\right]^2 = \frac{m_x m_y\left(m_x^{(i)} + 2m_y^{(i)}\sin^2\alpha\right)}{m_x^{(i)} m_y^{(i)}\left(m_x + 2m_y\sin^2\alpha\right)} \qquad \text{(Eqn 6.4.1)}$$

$$\sqrt{\frac{12\times 16(12 + [\{2\times 16\}\times 0.7713\}]}{12\times 18(12 + [\{2\times 18\}\times 0.7713\}]}} = 0.982$$

The κ^2-$^{16}OC^{16}O_{asym}$ stretch is observed at 1513 cm^{-1}, and so the predicted κ^2-$^{18}OC^{18}O_{asym}$ stretch should occur at 1485 cm^{-1}. However, the peak observed in this region at 1482 cm^{-1} is typically assigned to the P-Ph stretch of the PPh_3 ligands, so it is likely that the acetate stretch is obscured.

This complex was then reacted with $HC{\equiv}CCH_2OPh$ (**j**) in an effort to synthesise **^{18}O-10**, as shown in Figure 6.4.2. One equivalent of the alkyne was added to a DCM solution of **^{18}O-1** and the mixture allowed to stir for 20 hours at room temperature.

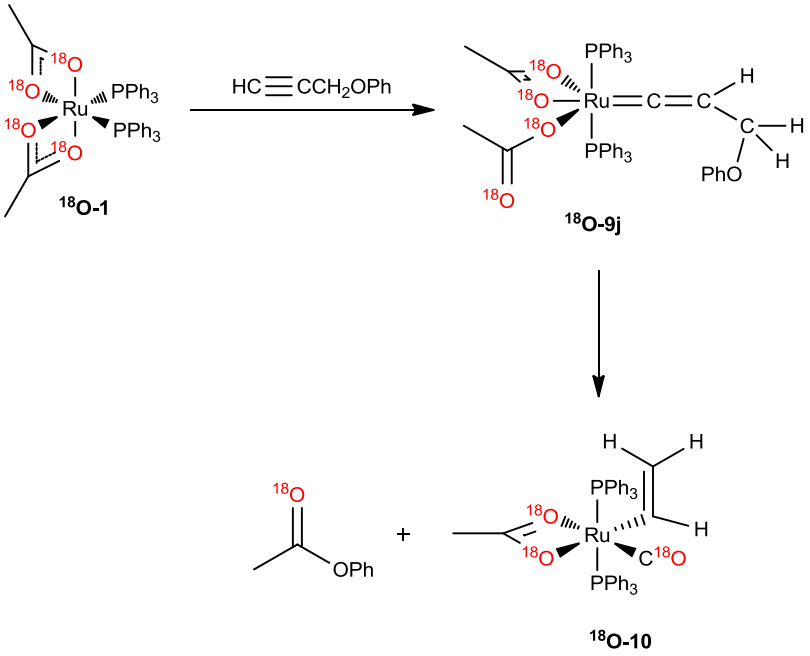

Figure 6.4.2: Formation of **^{18}O-10**.

After this time, analysis of the solution by IR spectroscopy showed a series of peaks had shifted with respect to the unlabelled complex **10** and CH_3COOPh. The most notable shift is observed for the CO stretch; the spectrum is illustrated in Figure 6.4.3.

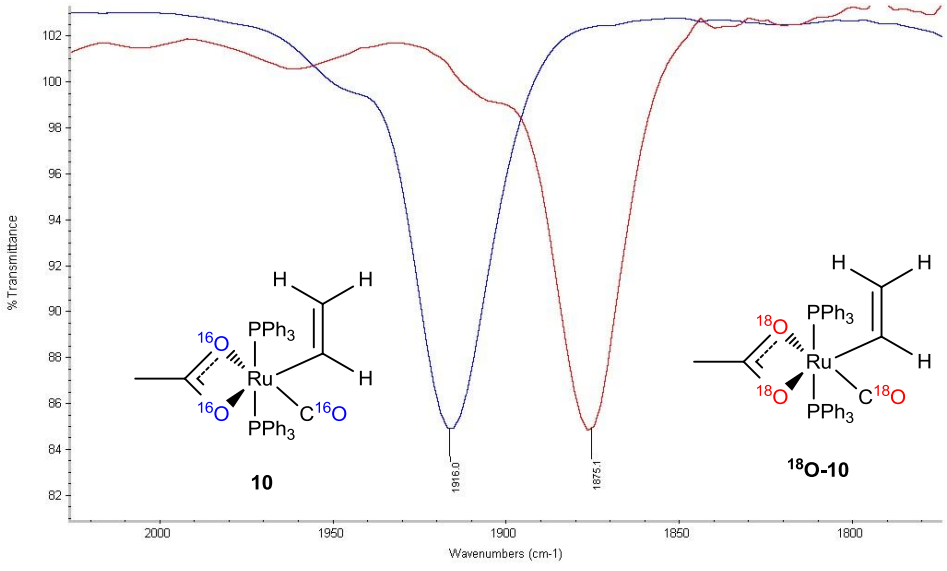

Figure 6.4.3: Overlay of IR spectra of complexes **10** and **^{18}O-10** recorded in DCM.

The expected values for the C^{18}O stretches can be predicted using Equations 6.4.2 – 6.4.5, and a comparison made with those observed. Table 6.4.1 summarises the different stretches of the labelled and unlabelled compounds.

$$\mu_{C^{(i)}O} = \frac{m_1 m_2}{m_1 + m_2} \qquad \text{(Eqn 6.4.2)}$$

$$\upsilon_{C^{(i)}O} = \frac{1}{2\pi c}\sqrt{\frac{k}{\mu_{C^{(i)}O}}} \qquad \text{(Eqn 6.4.3)}$$

$$\frac{\upsilon_{C^{16}O}}{\upsilon_{C^{18}O}} = \sqrt{\frac{\mu_{C^{18}O}}{\mu_{C^{16}O}}} = \sqrt{\frac{7.20}{6.86}} = 1.0247 \qquad \text{(Eqn 6.4.4)}$$

$$\upsilon_{C^{18}O} = \frac{\upsilon_{C^{16}O}}{1.0247} \qquad \text{(Eqn 6.4.5)}$$

IR stretch	**10** / cm^{-1}	**^{18}O-10** (predicted) / cm^{-1}	**^{18}O-10** (actual) / cm^{-1}
CO	1916	1869.8	1875
κ^2-OCO_{asym}	1531	1503	1493
CO (ester)	1763	1720.5	1722
C=C	1596	1596	1594

Table 6.4.1: Summary of notable IR spectroscopic features of **10** and **^{18}O-10** recorded in DCM.

The value obtained for the CO stretch of **^{18}O-10** is very close to that predicted using Equation 6.4.5. There is a difference of 5.2 cm^{-1} between the predicted value of the $C^{18}O$ stretch (1869 cm^{-1}) and the peak observed (1875 cm^{-1}). A very close correlation also exists between the predicted and observed $C^{18}O$ stretch of the ester $CH_3C^{18}O^{16}OPh$.

Further analysis of this solution by LIFDI-MS showed the organometallic component to have a mass of 746.1 m/z, corresponding to the mass expected for complex **^{18}O-10** containing three ^{18}O labelled atoms. A GC-EI-MS of this solution also revealed the presence of $CH_3C^{18}O^{16}OPh$, with a molecular ion of 138.1 m/z and significant peaks at 94.0 and 45.0 m/z, corresponding to the fragment ions $[^{16}OPh]^+$ and $[CH_3C^{18}O]^+$ respectively. The ^1H and $^{31}P\{^1H\}$ NMR spectra indicated that complex **10** and phenyl acetate were formed and no change was observed in the chemical shifts of these resonances.

The incorporation of the ^{18}O labels in the CO ligand of **^{18}O-10** and in the carbonyl moiety of phenyl acetate gives credence to both mechanisms proposed in Section 6.3. It also excludes the mechanism proposed by Dixneuf for this system; if

the conversion proceeded *via* this route then there would be no ^{18}O-incorporation in the CO ligand of **10**.

Further evidence was sought by performing the reaction using propargyl alcohol (HC≡CCH$_2$OH; **h**) in the place of phenyl propargyl ether (HC≡CCH$_2$OPh; **j**) in an attempt to synthesise the corresponding form of **^{18}O-4**.

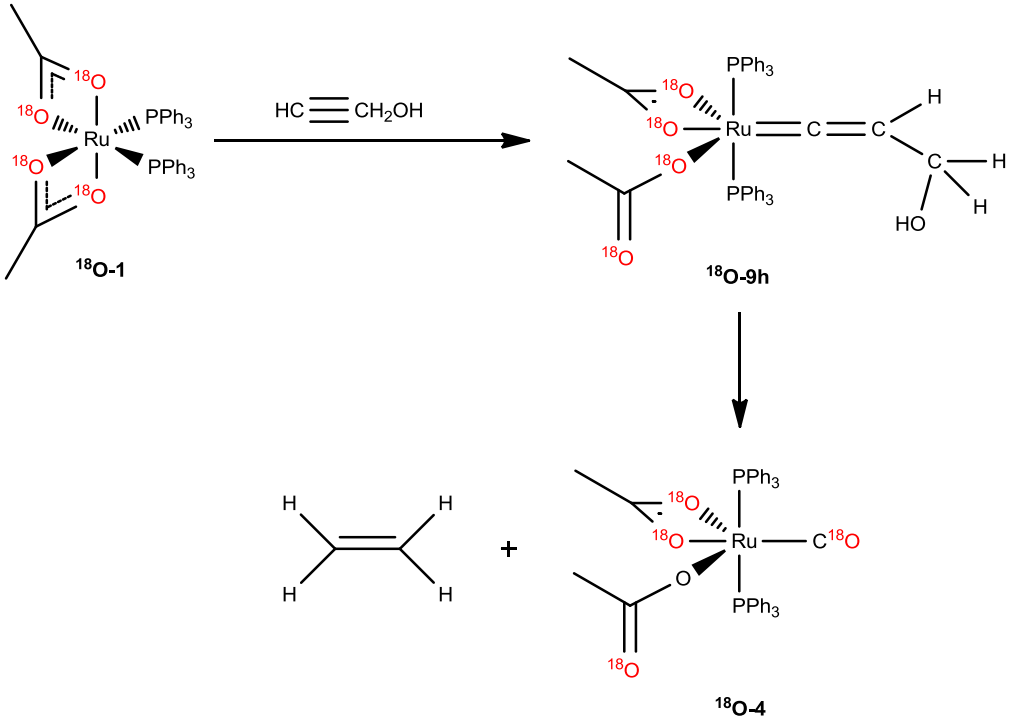

Figure 6.4.4: Formation of **^{18}O-4**.

The reaction between complex **^{18}O-1** with HC≡CCH$_2$OH should result in the formation of Ru(^{18}OC^{18}OCH$_3$)(^{16}OC^{18}OCH$_3$)(PPh$_3$)$_2$(C^{18}O), **^{18}O-4**. This reaction was carried out in the same manner as for the reaction with HC≡CCH$_2$OPh; however, analysis by IR spectroscopy and LIFDI-MS showed that a mixture of complexes **4**, **^{18}O-4** and **^{18}O-10** was present. An IR spectrum of the DCM reaction mixture recorded 16 hours after the addition of the alkyne is shown in Figure 6.4.5 below. The C^{16}O stretch in complex **4** is observed at 1946 cm^{-1}, so it is predicted that the C^{18}O stretch should occur at 1899 cm^{-1}. There are three stretches in the CO region attributed to C^{18}O of **^{18}O-10** at 1878 cm^{-1}, C^{16}O of **4** at 1946 cm^{-1}, and C^{18}O of **^{18}O-4** at 1905 cm^{-1}. The IR spectrum also indicates the presence of what may be CH$_3$C^{18}O^{16}OH with a peak due to the C^{18}O of the acid at 1723 cm^{-1}.

The presence of **4** may be accounted for by the exchange of the singly labelled acid $CH_3C^{18}O^{16}OH$ with an ^{18}OAc ligand of an unreacted molecule of ^{18}**O-1**. Exchange between carboxylate ligands has been shown to be particularly facile (see Section 6.3). The resulting conversion of **8h** would then lead to incorporation of an unlabelled (^{16}O) oxygen atom in the CO ligand of complex **4**.

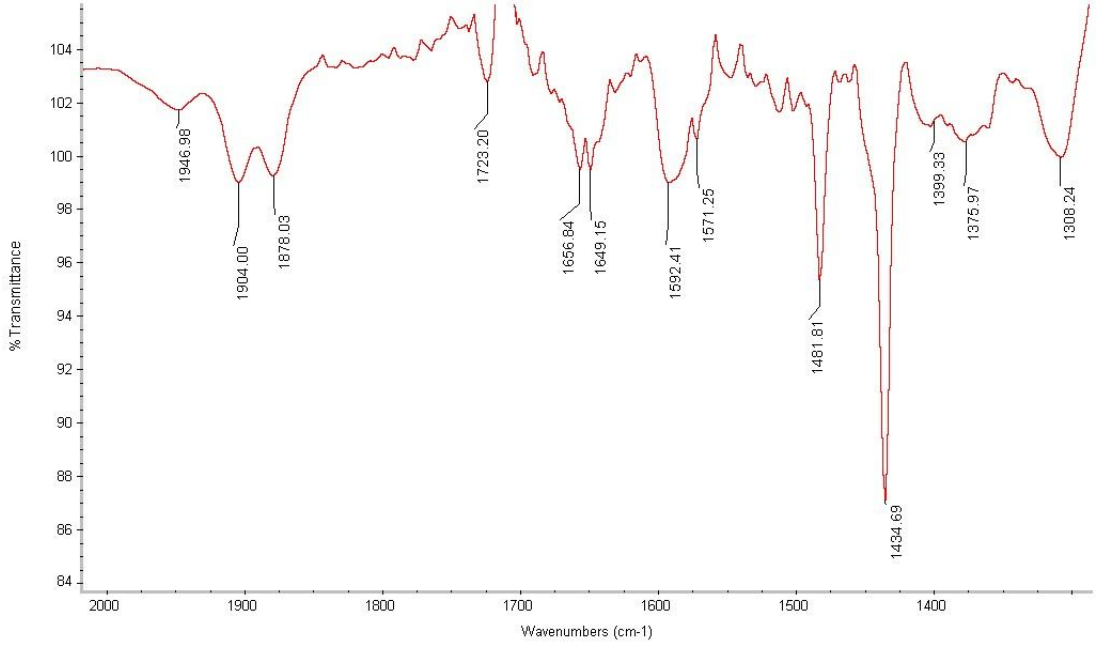

Figure 6.4.3: IR spectrum of the reaction of $HC{\equiv}CCH_2OH$ with ^{18}**O-1** after 16 hours.

The mixture was also analysed by LIFDI-MS, which showed four major peaks at m/z 818.1, 774.1, 746.1 and 718.1. The peak at 774.1 m/z can be assigned as $[M]H^+$ of complex **4**, and the peak at 746.1 can be assigned to ^{18}**O-10**. The peak at 718.1 m/z is consistent with a complex of formula $Ru(^{16}OC^{18}OCH_3)(PPh_3)_2(C^{18}O)$, which suggests that the intended product ^{18}**O-4** has formed, but has undergone fragmentation under the ionisation conditions. However it should be noted that the position of the ^{18}O labels cannot be determined from MS techniques, so the fragment of ^{18}**O-4** may incorporate the isotope at a different position than the one suggested. The species responsible for the peak at 818.1 m/z is currently unknown. It has been noted in Section 5.3 that the full conversion of **9h** to **4** and ethene requires 48 hours. It is therefore not unexpected to observe complex ^{18}**O-10** and $CH_3C^{18}O^{16}OH$ in the reaction mixture which was analysed after 16 hours.

This ^{18}O labelling study has confirmed that the acetate ligands are playing an important role in the conversion of propargylic alcohols to alkenes. The incorporation of ^{18}O labels into both the CO ligand of complex **^{18}O-10** and the carbonyl moiety of phenyl acetate provides important evidence supporting the mechanisms **VI** and **VII** proposed in Section 6.2.6. Although this labelling experiment is not able to distinguish between the two, it successfully discounts the possibility that the alternative mechanism proposed by Dixneuf is operating.

6.5: Kinetic study

The results discussed in Sections 6.3 and 6.4 have demonstrated that the carboxylate ligand plays an important role in the decarbonylation of propargylic alcohols. Both mechanisms proposed in Section 6.2 (**VI** and **VII**) involve the acetate ligand in the same way; however more experimental evidence points to mechanism **VII**. It has already been established that exchange of carboxylate ligands is facile yet the potential for a bimolecular pathway has not been discredited. It was therefore proposed that a kinetic study would confirm whether a unimolecular or bimolecular pathway is operating whilst also establishing the activation parameters of the reaction. This was achieved by monitoring the degradation of **9j** and the growth of both phenyl acetate and complex **10** by ^{1}H NMR spectroscopy at a range of temperatures (290 – 320 K). The phenoxy-vinylidene complex was chosen as the reaction is complete in 16 hours at 300 K, which is a convenient timescale to monitor by NMR spectroscopy. In addition, this reaction is thought to involve fewer elementary steps than the corresponding reaction to form **4** and a geminal alkene; only the acetate-mediated step is considered. Recording a ^{1}H NMR spectrum every 20 minutes over 15 hours at 300 K meant the rate of the disappearance of **9j**, and the growth of the products could be easily derived from the integrations of the methyl resonances of the three compounds relative to the internal TMS standard.

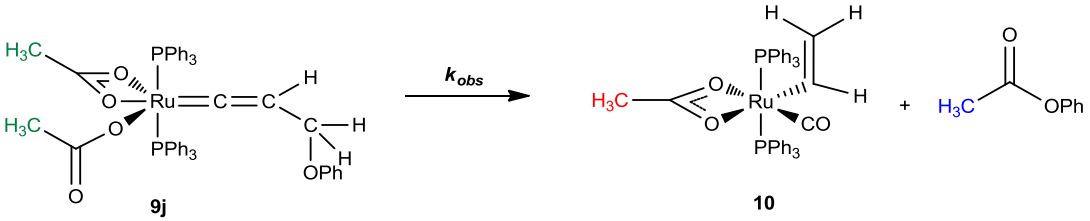

Figure 6.5.1: Reaction monitored by ^{1}H NMR spectroscopy in a kinetic study.

The rate constant (k_{obs}) calculated in this way is a combination of all the individual elementary reactions that occur in the conversion of **9j** to **10** and phenyl acetate, whether this occurs *via* mechanism **VI**, **VII** or another bimolecular pathway. Figure 6.5.2 is an example of a growth and decay plot of the overall reaction at 305 K.

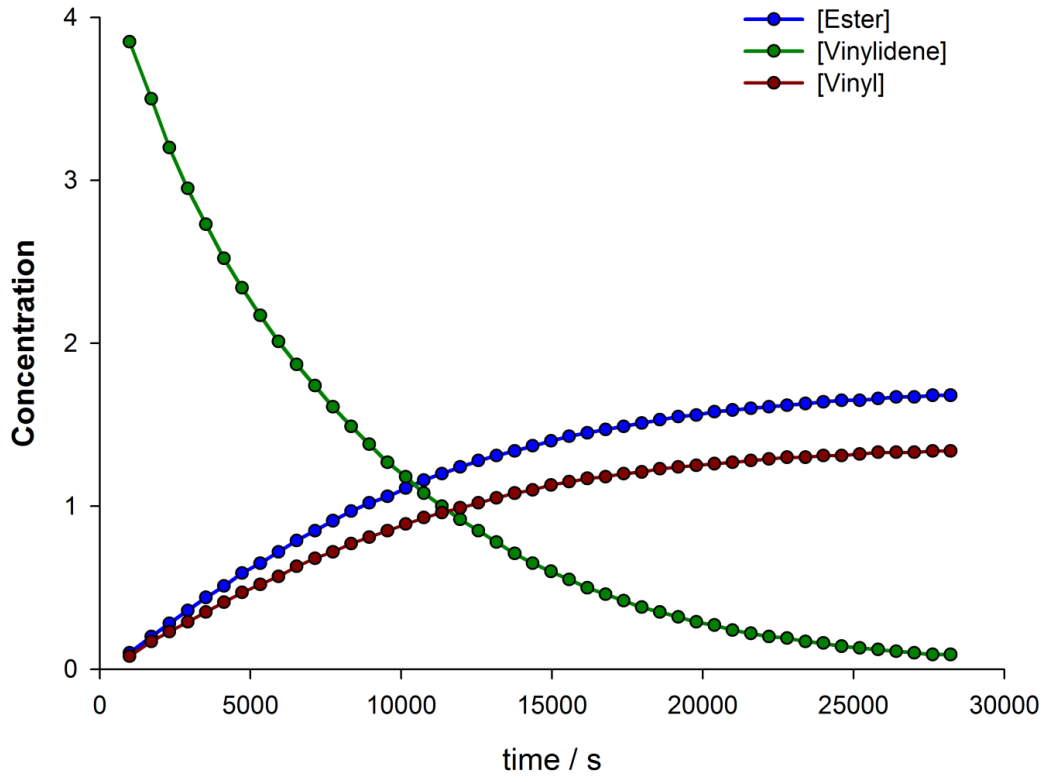

Figure 6.5.2: The change in concentration of the three species monitored in the conversion of **9j** to **10** and phenyl acetate.

Attempts were made to fit this data to zero, first and second order rate laws. Whilst the plot obtained for a first order rate law gave a straight line graph with an R^2 of 0.9988, the plots generated upon fitting the data to zero and second order rate laws did not give straight lines.

A first order rate law for this reaction is shown in Equation 6.5.1 below, and shows how ideally, the rate of the disappearance of **9j** should equal the rate of the appearance of both **10** and MeCOOPh. Analysis of the data has shown that the easiest way to deduce the rate law is to monitor the rate of the bleach of the peak due to the acetate ligands of **3j**.

$$rate = -\frac{d[9j]}{dt} = \frac{d[10]}{dt} = \frac{d[MeCOOPh]}{dt} = k_{obs}[9j] \qquad \text{(Eqn 6.5.1)}$$

This can be rearranged to give Equation 6.5.2

$$-\frac{d[9j]}{[9j]} = k_{obs}dt \qquad \text{(Eqn 6.5.2)}$$

which can then be integrated over the limits [**9j**] = [**9j**]$_0$ to [**9j**] and t = 0 to t; to give Equation 6.5.3:[26]

$$\ln[9j] - \ln[9j]_0 = -k_{obs}t \qquad \text{(Eqn 6.5.3)}$$

Consequently, if the reaction obeys first order kinetics, a plot of ln[**9j**] versus t should give a straight line, with the gradient of the slope = $-k_{obs}$. Figure 6.5.3 confirms that the data collected shows the overall conversion of **9j** to **10** obeys first order kinetics for the reaction conducted at 305 K. As the reaction mechanism is likely to involve a number of elementary steps, as illustrated by mechanisms **VI** and **VII**, and we have no indication as to which step may be rate-determining, the value of k_{obs} should be viewed tentatively.

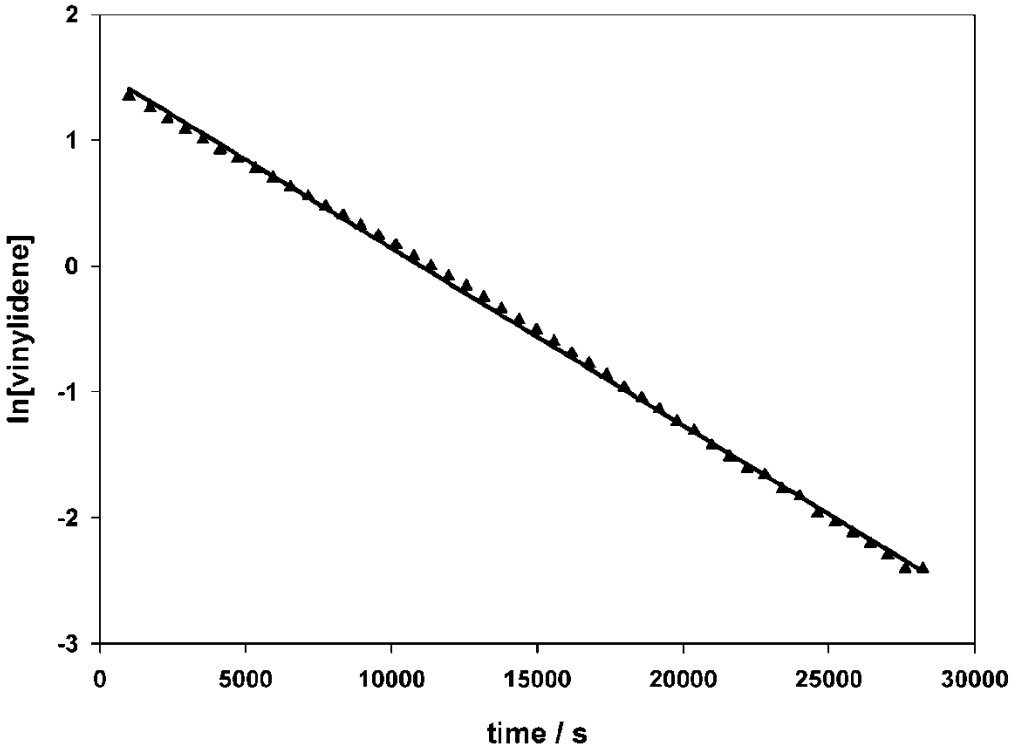

Figure 6.5.3: Plot of ln[**9j**] vs. time at 305 K.

Similar plots were generated for data obtained at other temperatures, however in some cases it was noted that early data points did not conform to a first-order regime. For example, at 300 K, there appears to be an initial period of adjustment, which may be indicative of an induction period or of temperature or solubility fluctuations. This is illustrated in Figure 6.5.4. A similar period is seen in the data collected at 295 K and 320 K. However, data collected after this stage at these temperatures gave a much better fit to a first-order rate law and so in certain cases the data set was restricted slightly to account for this. Similarly, data points near the end of the data set showed that a plateau had been reached as the reaction had gone to completion. Consequently, some of these values were also removed. An example of a resulting plot for the reaction at 300 K is shown in Figure 6.5.5. The reaction is therefore thought to obey apparent first order kinetics as the model used does not account for the induction period.

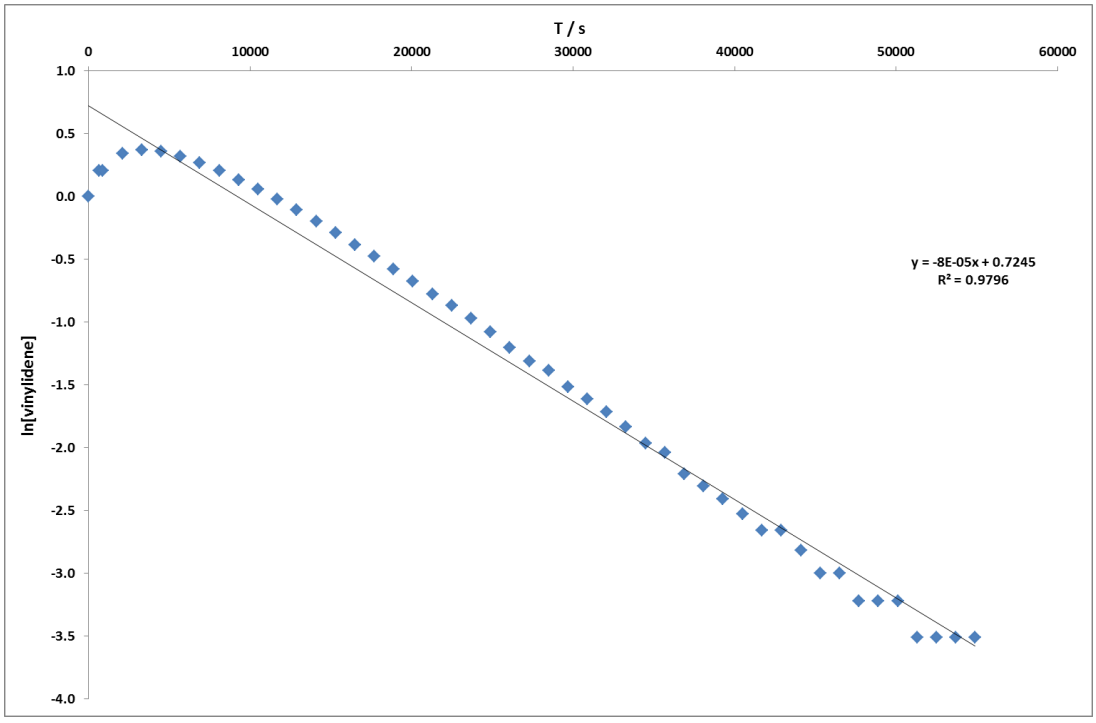

Figure 6.5.4: Plot of ln[**9j**] vs. time at 300 K obtained from the entire data set.

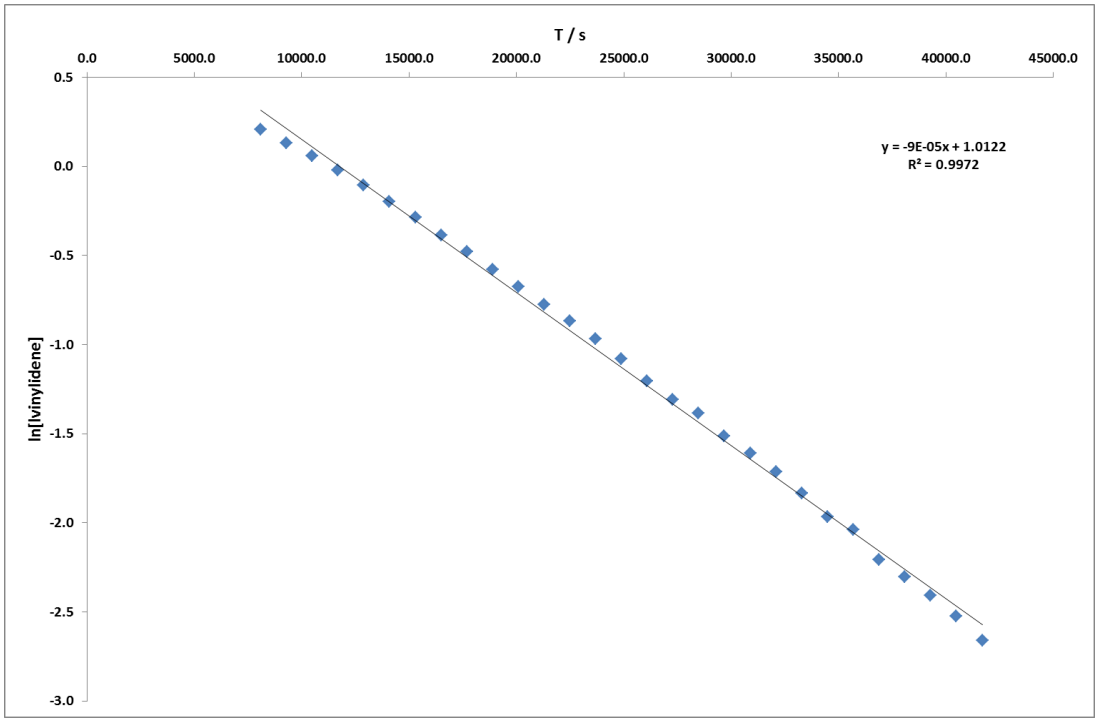

Figure 6.5.5: Plot of ln[**9j**] vs. time at 300 K obtained from restricting the data set.

A linear regression analysis was performed on these plots using Excel 2007 to calculate the values of k_{obs} given in Table 6.5.1. A rearrangement (Equation 6.5.4) of the Eyring equation (Equation 6.5.5) was used to calculate $\Delta G^{\ddagger}$ at each calibrated temperature, and the half-life $t_{1/2}$ for a first order system was determined using Equation 6.5.6 for the condition where [**9j**] = [**9j**]$_0$/2.

$$k = \kappa \frac{k_B T}{h}\left(-\Delta G^{\ddagger} / RT\right) \qquad \text{(Eqn 6.5.4)}$$

$$\Delta G^{\ddagger} = RT[23.76 - \ln(k/T)] \qquad \text{(Eqn 6.5.5)}$$

$$t_{1/2} = \frac{\ln 2}{k_{\exp}} \qquad \text{(Eqn 6.5.6)}$$

Temperature / K	k_{obs} / x 10^{-4} s^{-1}	R^2	$\Delta G^{\ddagger}$ / kJ mol^{-1}	$t_{1/2}$ / h^{-1}
290	0.251 ± 0.007	0.9978	96.5 ± 0.07	7.67
295	0.338 ± 0.01	0.9993	97.4 ± 0.07	5.57
300	0.860 ± 0.02	0.9972	96.8 ± 0.06	2.24
305	1.40 ± 0.02	0.9988	97.3 ± 0.04	1.38
310	2.20 ± 0.04	0.9970	97.7 ± 0.05	0.875
315	3.53 ± 0.08	0.9981	98.1 ± 0.06	0.545
320	5.87 ± 0.08	0.9993	98.4 ± 0.04	0.328

Table 6.5.1: Values of k_{obs}, $\Delta G^{\ddagger}$ and $t_{1/2}$ calculated for the decay of vinylidene **9j**.

These results confirm that the decay of **9j** is apparent first order in ruthenium, thus excluding a potential bimolecular pathway. Attempting to fit the data to a second order rate law failed. The results are also fairly reproducible; a repeat of the reaction at 295 K gave a k_{obs} of 0.346 x 10^{-4} s^{-1} whilst a repeat at 300 K gave a k_{obs} of 0.600 x 10^{-4} s^{-1}. As expected, the reaction rate increases with temperature. The enthalpy and entropy of activation $\Delta H^{\ddagger}$ and $\Delta S^{\ddagger}$ were then obtained for this process using a further rearrangement of the Eyring equation (Equation 6.5.7). A plot of ln(k/T) versus 1/T (Figure 6.5.6) gives a straight line with a slope of – ($\Delta H^{\ddagger}$ /R) and an intercept of [23.76 + ($\Delta S^{\ddagger}$/R)].[27]

$$\ln\left(\frac{k}{T}\right) = 23.76 - \left(\frac{\Delta H^{\ddagger}}{RT}\right) + \left(\frac{\Delta S^{\ddagger}}{R}\right) \qquad \text{(Eqn 6.5.7)}$$

From this plot, the value of $\Delta H^{\ddagger}$ was calculated to be -80.7 ± 9.7 kJ mol^{-1} and $\Delta S^{\ddagger}$ to be -54.9 ± 32 J K^{-1} mol^{-1}. The value of $\Delta S^{\ddagger}$ is both small and negative which suggests an associative mechanism is occurring. This is consistent with our observations and the mechanisms proposed. However, the error associated with the value of $\Delta S^{\ddagger}$ is rather large, so attempts were made to re-analyse the data in order to minimise such errors. This was achieved using the Dynafit program.[28] This program was used to obtain values of k_{obs} using data for all components of the reaction, namely **9j**, **10** and phenyl acetate.

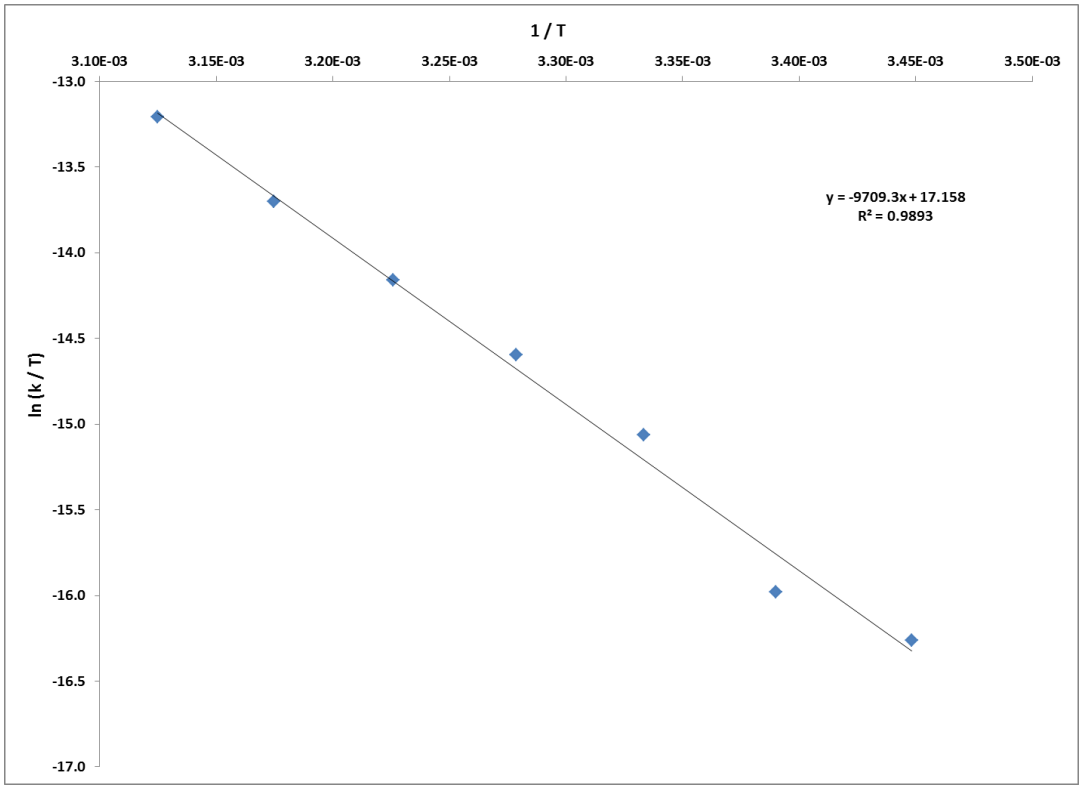

Figure 6.5.6: Eyring plot for the decay of **9j** using values of k_{obs} from Table 6.5.1 (uncalibrated T).

Two reaction profiles were used to model the data obtained. Model **1** made an assumption that the reactions are irreversible, and that in all cases there is an inevitable degree to which complex **10** decays to **4**.

$$A \rightarrow B + C \ (k1)$$

$$B \rightarrow D \ (k2) \qquad \text{(Model 1)}$$

$$Key: \ A = \mathbf{9j} \ ; B = \mathbf{10} \ ; C = phenyl \ acetate \ ; D = \mathbf{4} \ ; (k1) = k_{obs}$$

In some instances, traces of complex **1** and **j** were observed in the ^{1}H NMR spectra when beginning to monitor the reaction. This was observed at 290 and 300 K. It was therefore necessary to modify model **1** to account for the initial incomplete formation of the vinylidene:

$$A + B \rightarrow C \ (k1)$$

$$C \rightarrow D + E \ (k2)$$

$$D \rightarrow F \ (k3) \qquad \text{(Model 2)}$$

$$Key: \ A = \mathbf{1} \ ; B = \mathbf{8j} \ ; C = \mathbf{9j} \ ; D = \mathbf{10} \ ;$$
$$E = phenyl \ acetate \ ; F = \mathbf{4} \ ; (k2) = k_{obs}$$

These models were used to generate values of k_{obs} which are summarised in Table 6.5.2 shown below. These values, and those of $\Delta G^{\ddagger}$ are very similar to those obtained from the analysis of the decay of **9j**. Another Eyring plot was generated using these values of k_{obs}, as shown in Figure 6.5.7.

Temperature / K	**k_{obs} / x 10^{-4} s^{-1}**	**$\Delta G^{\ddagger}$ / kJ mol^{-1}**	**$t_{1/2}$ / h^{-1}**
290	0.159 ± 0.004	97.6 ± 0.06	12.1
295	0.270 ± 0.006	98.0 ± 0.05	7.12
300	0.548 ± 0.006	98.0 ± 0.03	3.51
305	0.876 ± 0.02	98.4 ± 0.06	2.20
310	1.58 ± 0.03	98.6 ± 0.05	1.21
315	2.46 ± 0.09	99.1 ± 0.10	0.78
320	3.63 ± 0.12	99.6 ± 0.09	0.53

Table 6.5.2: Values of k_{obs}, $\Delta G^{\ddagger}$ and $t_{1/2}$ calculated for the decay of vinylidene **9j**.

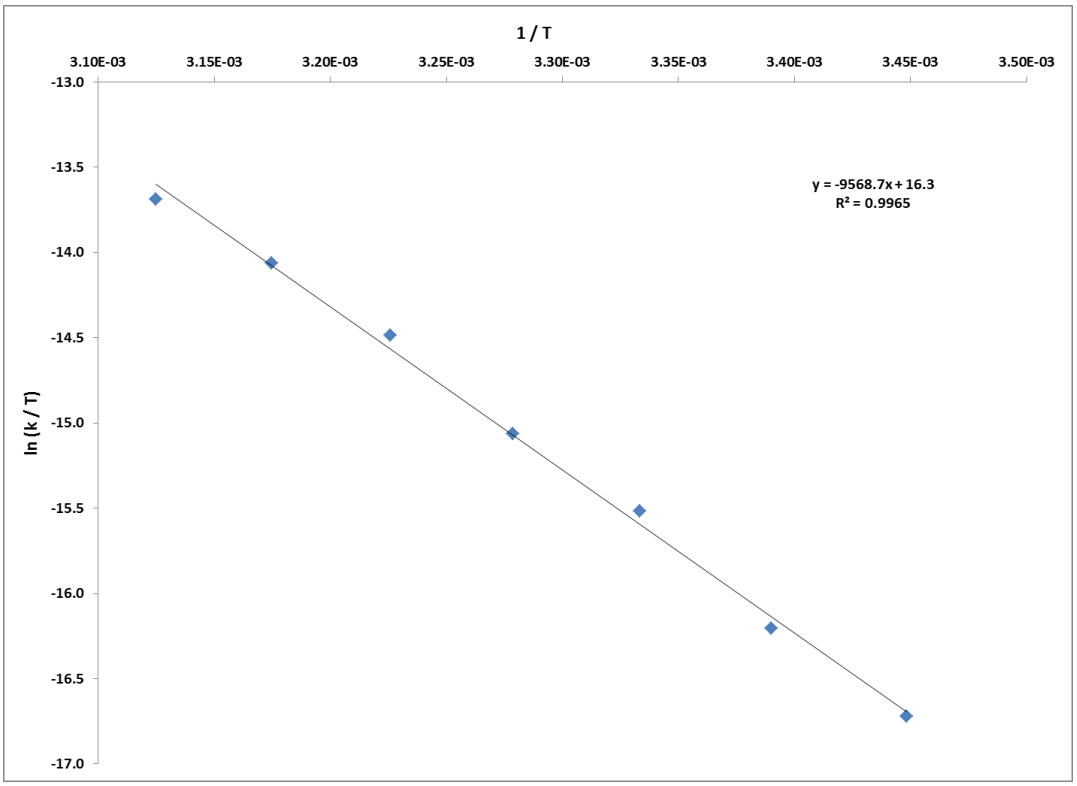

Figure 6.5.7: Eyring plot for the decay of **9j** using values of k_{obs} from Table 6.5.2 (uncalibrated T).

The values of $\Delta H^{\ddagger}$ and $\Delta S^{\ddagger}$ calculated from this plot are -79.6 ± 5.4 kJ mol^{-1} and -62.0 ± 17 J K^{-1} mol^{-1}. The magnitude of $\Delta S^{\ddagger}$ is slightly larger than that obtained previously, however the error is smaller.

The rate of conversion of the hydroxy-vinylidene complex **9h** to **4** and ethene was also monitored at 300 K over 36 hours. The reaction was also found to obey apparent first order kinetics. Simply calculating k_{obs} from the decay of **9h** gave a value of 9.64 ± 0.34 x 10^{-6} s^{-1} and $\Delta G^{\ddagger}$ of 102.3 kJ mol^{-1}. The data was also analysed using the Dynafit program and Model 3. The integration of the ethene resonance was excluded from analysis as it will be inaccurate due to ethene's gaseous nature.

$$A \rightarrow B\ (k1) \qquad \text{(Model 3)}$$

$$Key:\ A = \mathbf{9h}\,;\, B = \mathbf{4}\,;\, (k1) = k_{obs}$$

Analysis of the data in this way gave a value of k_{obs} of 5.84 ± 0.25 x 10^{-6} s^{-1} and $\Delta G^{\ddagger}$ of 103.5 kJ mol^{-1}. The value of k_{obs} is smaller than those obtained for the conversion of complex **9j** at 300 K, which concurs with experimental observations of a slower reaction.

The results discussed thus far have demonstrated that the decay of complexes **9j** and **9h** is first-order with respect to ruthenium. An attempt was made to determine if the reaction would be affected by the presence of an excess of acetate. A reaction was conducted in the presence of one equivalent of NaOAc at 300 K which returned values of k_{obs} virtually identical to those obtained in the absence of additional acetate (Excel: 0.840 ± 0.01 x 10^{-4} s^{-1}; Dynafit: 0.577 ± 0.01 x 10^{-4} s^{-1}). However, NaOAc is only sparingly soluble in CD_2Cl_2, so the rates obtained may not truly account for any effect the acetate may have. So the reaction was repeated using Bu_4NOAc, which is completely soluble in CD_2Cl_2. When just the decay of the vinylidene complex **9j** was analysed, the conversion was found to proceed at a similar rate as in the absence of acetate at 0.798 ± 0.01 x 10^{-4} s^{-1}. However, a slightly higher value was obtained using the Dynafit program (k_{obs} = 0.941 ± 0.06 x 10^{-4} s^{-1}). It seems these results suggest that the presence of additional acetate alters the rate of conversion slightly.

Experimental evidence has so far indicated that of the two possible mechanisms proposed for the conversion of propargylic alcohols to alkenes, mechanism **VII** is more likely to be occurring. If this mechanism were to operate, then in the conversion of **9j** to **10** and phenyl acetate the allenylidene-type ligand (see Figure 6.2.6.8) would form upon liberation of phenol (HOR'' = PhOH). If this were the case, it would be expected that the addition of PhOH to **9j** should induce an increase

in the rate of conversion. The rate of decay of **9j** in the presence of one equivalent of PhOH at 300 K was found to be 3.07 ± 0.07 x 10^{-4} s^{-1}; whilst a Dynafit analysis of the system gave k_{obs} to be 2.12 ± 0.12 x 10^{-4} s^{-1} (in absence of PhOH k_{obs} = 0.860 ± 0.02 x 10^{-4} s^{-1} {Excel} and k_{obs} = 0.548 ± 0.006 x 10^{-4} s^{-1} {Dynafit}). The presence of PhOH has clearly accelerated the reaction. This provides further evidence for mechanism **VII** as the more likely interpretation of the two routes proposed.

It can be concluded from these results that the conversion of the vinylidene complexes **9a-i** to **4** and ethene is a first order process, with respect to the ruthenium complex. The enthalpy and entropy of activation for the conversion were successfully obtained from an Eyring analysis, which suggested that the mechanism is dissociative. The Dynafit program was used to model the reaction profile using data for all components. Addition of PhOH to **9j** resulted in an increase in the rate of conversion, implying that mechanism **VII** is the route by which the conversion occurs.

6.6: DFT study

Thus far, experimental evidence has given some indication of the pathway by which propargylic alcohols are converted to alkenes by complex **1**. To provide further insight, a mechanistic investigation using DFT methods was undertaken by David Johnson and Dr. John Slattery. At the time of writing, this study is still on-going, so only preliminary results are reported. Initial work focused on a mechanism involving complexes that had been experimentally characterised, or their appropriate derivatives (**10**, **11** and **12**). These were optimised to their local minima geometries based on a model system using propargyl alcohol **8h**. The same DFT methodology was used as in Chapter 4; initial optimisations were calculated at the (RI-)BP86/SV(P) level before single-point energy calculations using (RI-)PBE0/def2-TZVPP were performed. Chapter 4 demonstrated the importance of using full ligand substituents when modelling this system, despite the greater computational expense. Consequently, the model complexes were derived from the experimentally observed complexes, to mirror reality as closely as possible. Figures 6.6.1 and 6.6.2 illustrate the energies of the proposed intermediates relative to complex [**1** + **8h**].

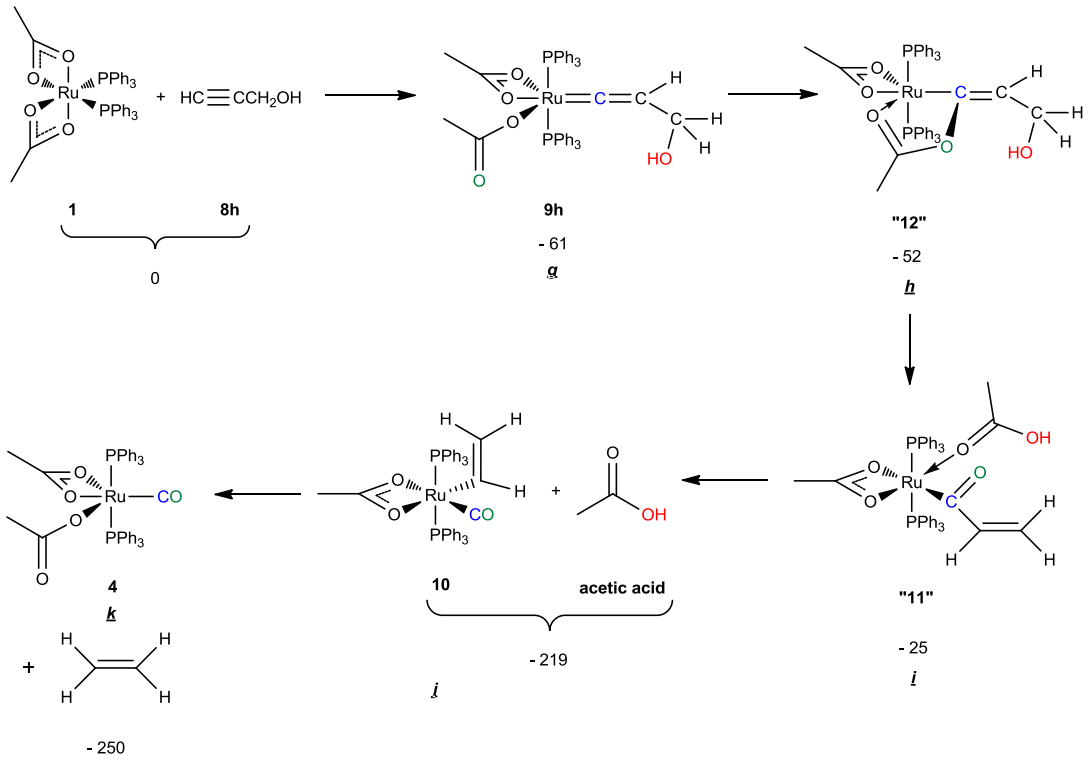

Figure 6.6.1: Proposed intermediates derived from experimentally characterised analogues and their energies relative to complex [**1** + **8h**] (Gibbs energies in kJ mol^{-1}).

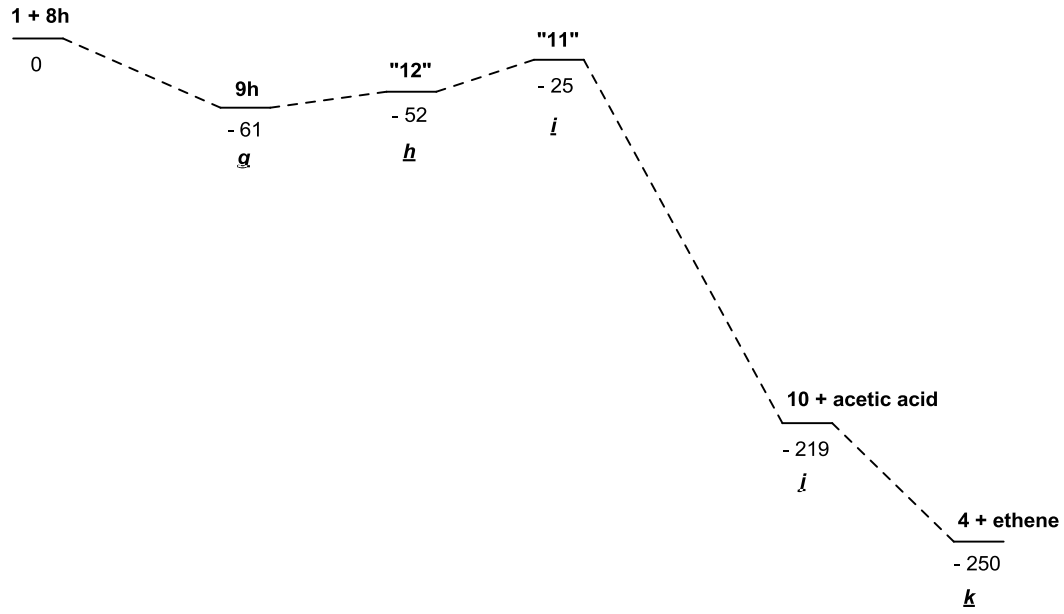

Figure 6.6.2: A simplified PES illustrating the Gibbs free energies in kJ mol^{-1} of proposed intermediates derived from experimentally characterised complexes in the conversion of **9h** to **4** + ethene.

The kinetic experiments detailed in Section 6.5 have determined activation parameters for this process, ($\Delta G^{\ddagger}$ = 102.3 kJ mol^{-1}). Consequently, a pathway may

only be considered realistic if the highest energy barrier to conversion is near this mark. The ^{18}O-labeling study has also indicated that the oxygen atom of the CO ligand must be derived from an acetate ligand. Stoichiometric experiments have also implied that the formation of an allenylidene species may occur, and that propargylic substitution of the hydroxy-vinylidene complexes is possible.

The formation of the vinylidene complex ***g*** (**9h**) is presumed to proceed *via* a LAPS mechanism. It was discovered that the conversion from complex ***i*** ("**11**") to ***k*** (**4**) + ethene is essentially a downhill process, consequently no transition states were modelled for this transition. Furthermore, this step has strong supporting experimental evidence and as migratory insertions are so well-established in organometallic chemistry, efforts focussed on understanding how the transition from the metallo-enolester derivative ***h*** ("**12**") to the acyl derivative ***i*** occurred.

The first transition examined involved the formation of the metallo-enolester derivative of **12** (***h***) from the hydroxy-vinylidene complex **9h** (***g***) *via* the transition state TS_{gh}. This transition state has an energy of -26 kJ mol^{-1} relative to [**1** + **8h**]; 35 kJ mol^{-1} higher than the hydroxy-vinylidene complex ***g***.

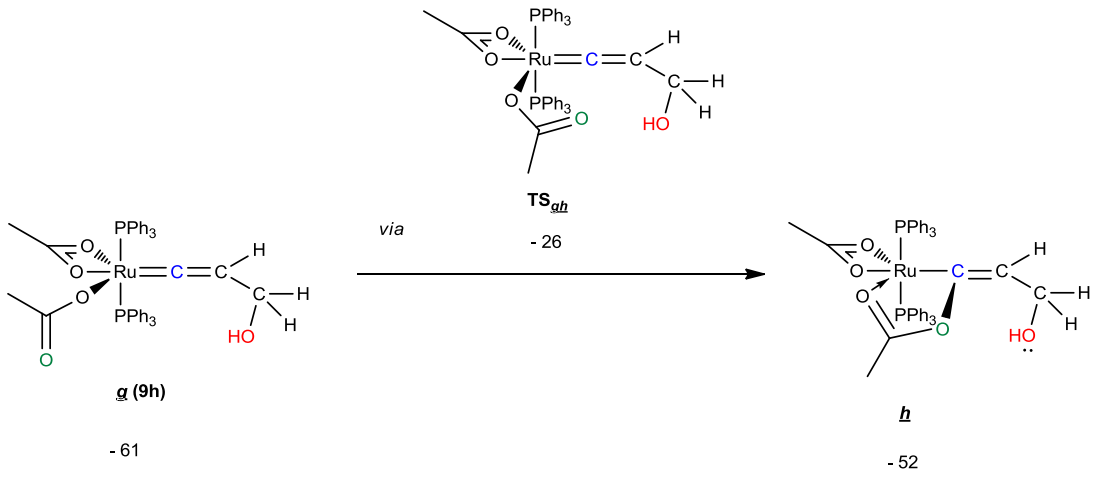

Figure 6.6.3: Conversion of ***g*** to ***h*** *via* **TS**$_{gh}$

After the formation of the metallo-enolester species, a concerted intramolecular attack of the OH moiety onto the carbon atom of the cyclised acetate ligand (Figure 6.6.4) was considered as the next step in the reaction pathway. This is analogous to

the mechanism proposed in pathway **VI** given in Figure 6.2.6.7. However, the transition state calculated for this transformation (**TS**$_{\underline{\boldsymbol{hi}}}$) is 218 kJ mol^{-1} higher in energy than the reference point **[1 + 8h]**, and 270 kJ mol^{-1} higher in energy than ***h***. An alternative transition state (**TS**$_{\underline{\boldsymbol{h'i'}}}$) was calculated based the experimental evidence which points to the possibility of nucleophilic substitution at C_γ of the cumenylidene ligand (see Section 6.3). The intramolecular attack of an acetate moiety onto the carbon atom of the cyclised acetate ligand was considered, however the barrier to this transformation is again large at 200 kJ mol^{-1} higher than the vinylidene derivative **9k**. The high energy barriers associated with these transformations has indicated that pathway **VI** is unrealistic. Consequently, efforts turned towards an evaluation of pathway **VII** (Figure 6.2.6.8)

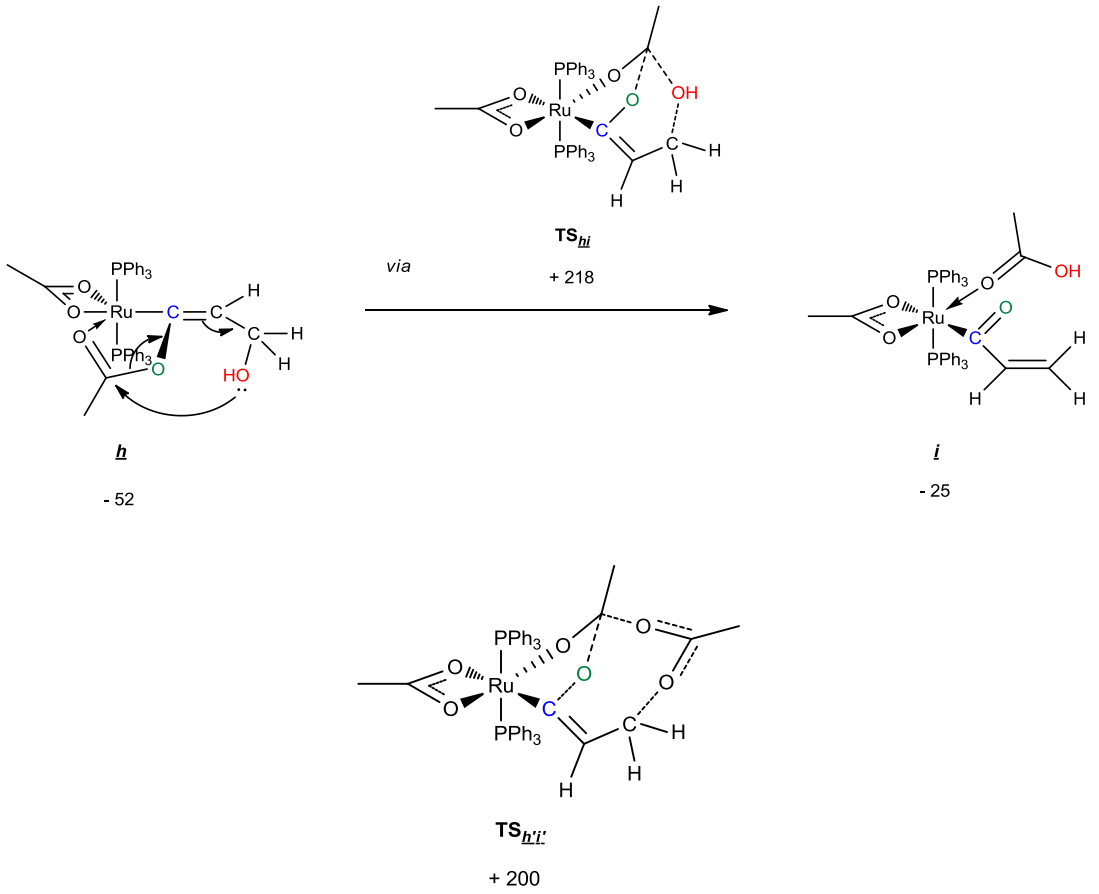

Figure 6.6.4: Conversion of ***h*** to ***i*** *via* **TS**$_{\underline{\boldsymbol{hi}}}$ and the structure of **TS**$_{\underline{\boldsymbol{h'i'}}}$

Pathway **VII** involves the formation of an allenylidene ligand by the dehydration of a hydroxy-vinylidene species. The formation of an allenylidene derivative is implied by the experimental evidence of propargylic nucleophilic

substitution (Section 6.3), as allenylidene complexes are considered to be important intermediates in catalytic propargylic substitution.[29] The allenylidene derivative ***l*** was calculated to be – 14 kJ mol^{-1} lower in energy relative to [**1** + **8h**]; 47 kJ mol^{-1} higher in energy than the hydroxy-vinylidene complex ***g*** (**9h**). However the transition state for the dehydration step (**TS**$_{gl}$) is + 181 kJ mol^{-1} relative to [**1** + **8h**], and 242 kJ mol^{-1} higher in energy than ***g***. This prohibitive energy barrier indicates that the traditional pathway for the formation of an allenylidene ligand (Figure 6.6.5) is unlikely to occur for this system.

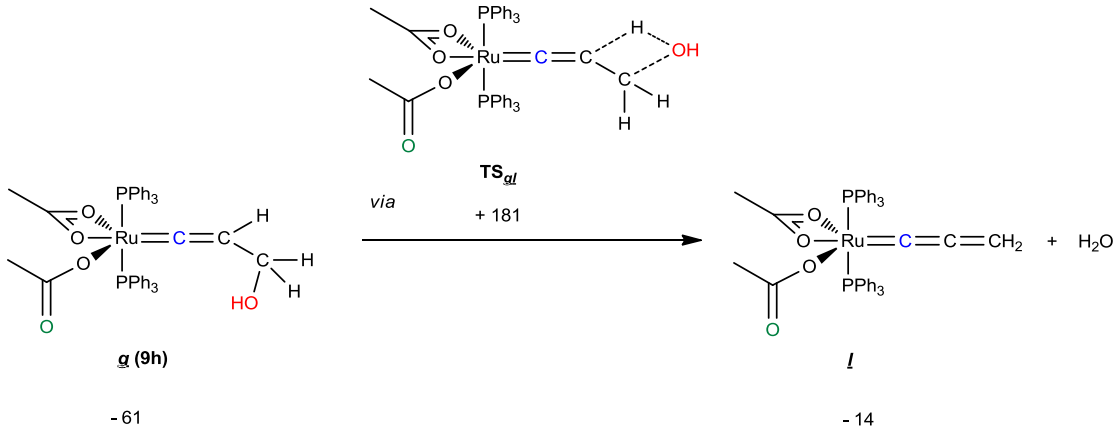

Figure 6.6.5: Conversion of ***g*** to ***l*** *via* **TS**$_{gl}$

An alternative pathway to the formation of ***l*** may arise *via* a process related to the LAPS mechanism. This involves the deprotonation of the hydroxy-vinylidene complex (***g***) to give an acetylide derivative (***m***) also containing an acetic acid ligand. This complex is 6 kJ mol^{-1} higher in energy than [**1+8h**], and 67 kJ mol^{-1} higher in energy than ***g***. The barrier to this process *via* **TS**$_{gm}$ is + 31 kJ mol^{-1} relative to [**1+8h**] and 92 kJ mol^{-1} relative to ***g***. The dehydration step may then occur *via* the transition state **TS**$_{ml}$ to give the allenylidene complex ***l***. However, this transition involves a barrier of 90 kJ mol^{-1} relative to [**1+8h**], which is 151 kJ mol^{-1} relative to the hydroxy-vinylidene complex ***g***. This route is therefore also considered to be unrealistic, as the barrier is greater than that indicated by the kinetic experiments.

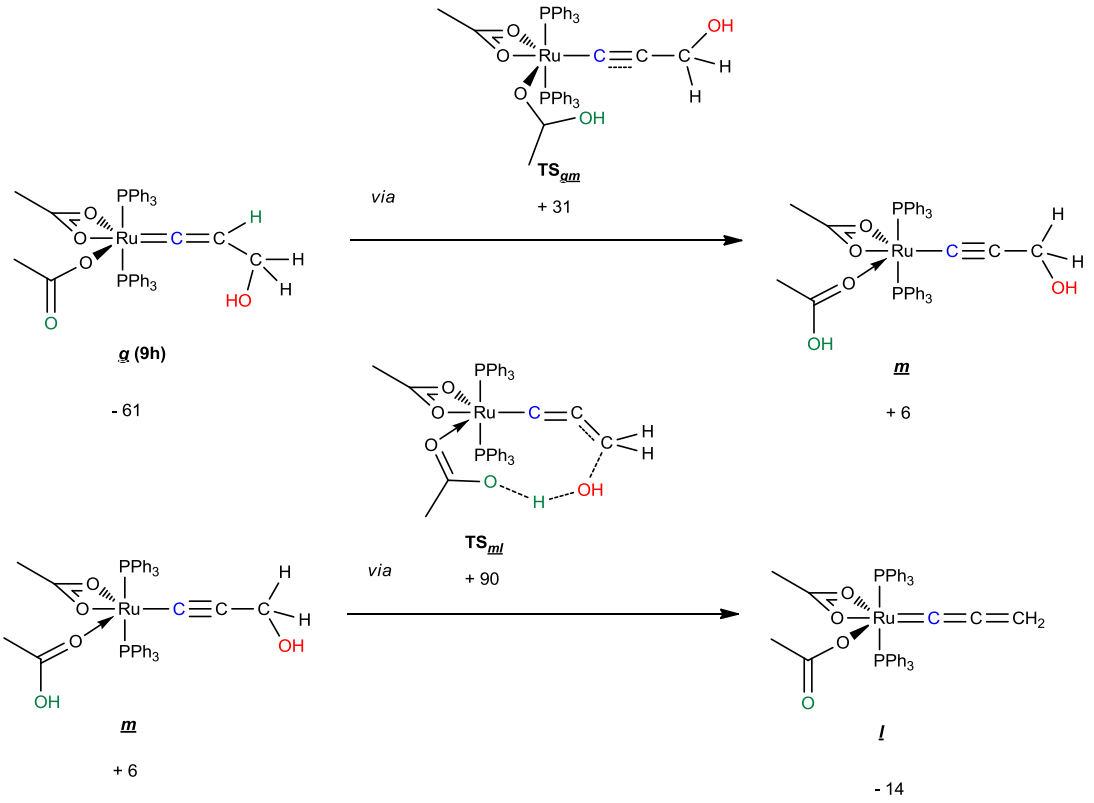

Figure 6.6.6: Alternative mechanism to formation of allenylidene complex ***l***

Another pathway considered the formation of a metallo-allenylidene-ester derivative (***n***) by the elimination of a water molecule from the metallo-enolester complex ***h***. This complex was found to have an energy of -2 kJ mol^{-1} relative to [**1**+**8h**] and +59 kJ mol^{-1} relative to ***g***. The transition state for this process however, (**TS**$_{hn}$) was found to have an energy of +250 kJ mol^{-1} relative to [**1**+**8h**]; +311 kJ mol^{-1} higher than ***g***. Again, it is clear that this pathway involves an activation barrier that is too high to occur experimentally.

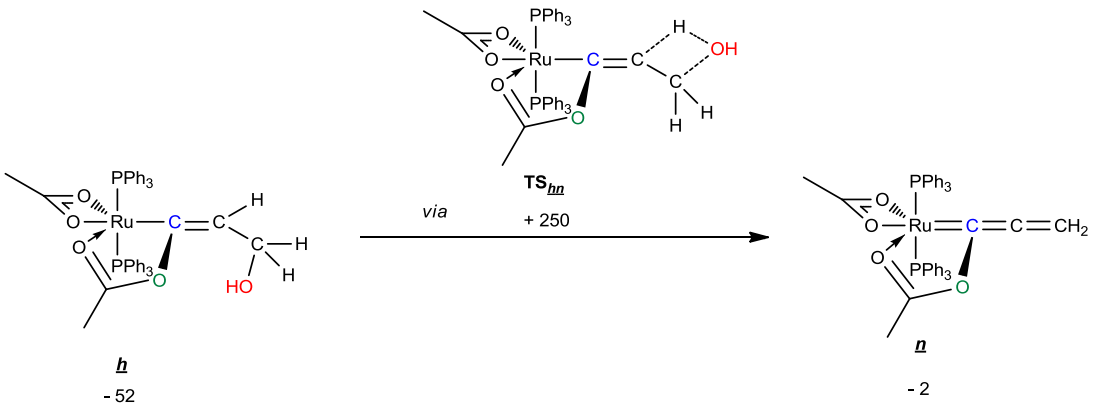

Figure 6.6.7: Conversion of ***h*** to ***n*** *via* **TS**$_{hn}$

The results discussed thus far have indicated that pathways **VI** and **VII**, as shown in Figures 6.2.6.7 and 6.2.6.8 respectively, involve activations barriers that are higher than the 102.3 kJ mol^{-1} threshold indicated by the kinetic experiments. Consequently, alternative routes must be considered which still conform to the experimental evidence obtained.

One such alternative considered the possibility of two alternative ground state structures of complex ***h*** and ***i***. These have been labelled ***h**** and ***i**** respectively and their structures are given in Figure 6.6.8. Complex ***h**** differs from ***h*** in that a bond no longer exists between the ruthenium and the cyclised acetate ligand. This complex is presumed to form from ***g*** *via* **TS**$_{gh}$ as shown in Figure 6.6.3. However ***h**** was found to have an energy of +53 kJ mol^{-1} relative to [**1**+**8h**]; 114 kJ mol^{-1} higher than ***g***. Complex ***i**** has an energy of -81 kJ mol^{-1} relative to [**1**+**8h**], which is -20 kJ mol^{-1} relative to ***g***. In this alternative structure, a coordinated molecule of acetic acid is no longer present, and the coordination sphere about the ruthenium has instead been completed by the formation of a bond between the ruthenium and oxygen atom of the acyl ligand. Indeed this alternative structure of ***i*** may be considered to be an intermediate in the formation of ***j*** from ***i*** and its discovery prompted further study. However, the conversion of ***h**** to ***i**** *via* a concerted intramolecular mechanism was found to occur *via* the high energy transition state **TS**$_{h^*i^*}$, which was found to have an energy of 208 kJ mol^{-1} relative to [**1**+**8h**]; 269 kJ mol^{-1} higher than the hydroxy-vinylidene complex ***g***.

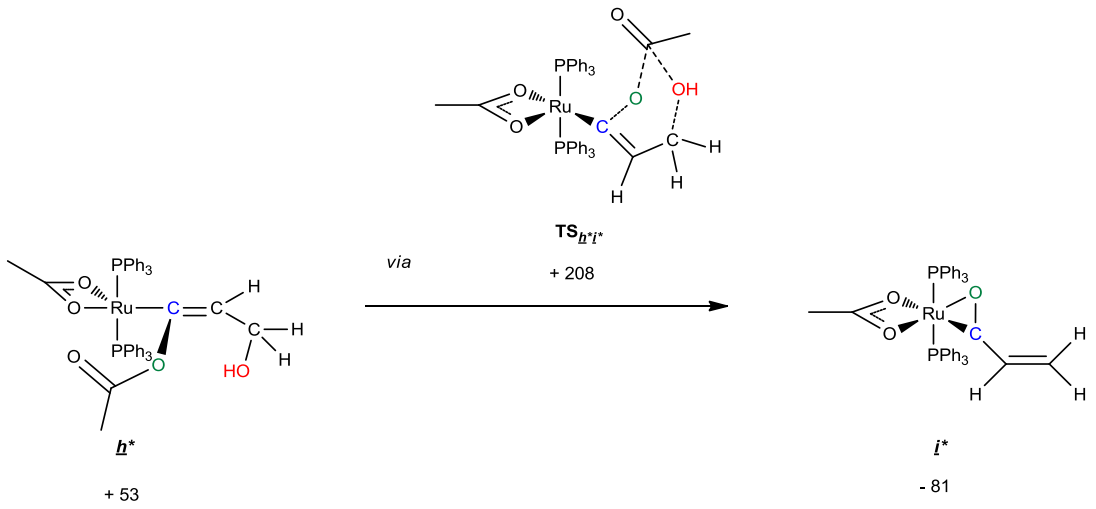

Figure 6.6.8: Conversion of ***h**** to ***i**** *via* **TS**$_{h^*i^*}$

Another alternative considered the concerted intermolecular addition of a water molecule to both ***h*** and ***h****. This proceeded *via* the transition states $\mathbf{TS}_{\underline{hi}(water)}$ and $\mathbf{TS}_{\underline{h}^*\underline{i}^*(water)}$ respectively, however both were again found to present an activation barrier too high to be overcome under the conditions employed experimentally at 166 kJ mol^{-1} and 225 kJ mol^{-1} relative to [**1**+**8h**] (227 kJ mol^{-1} and 286 kJ mol^{-1} relative to ***g***).

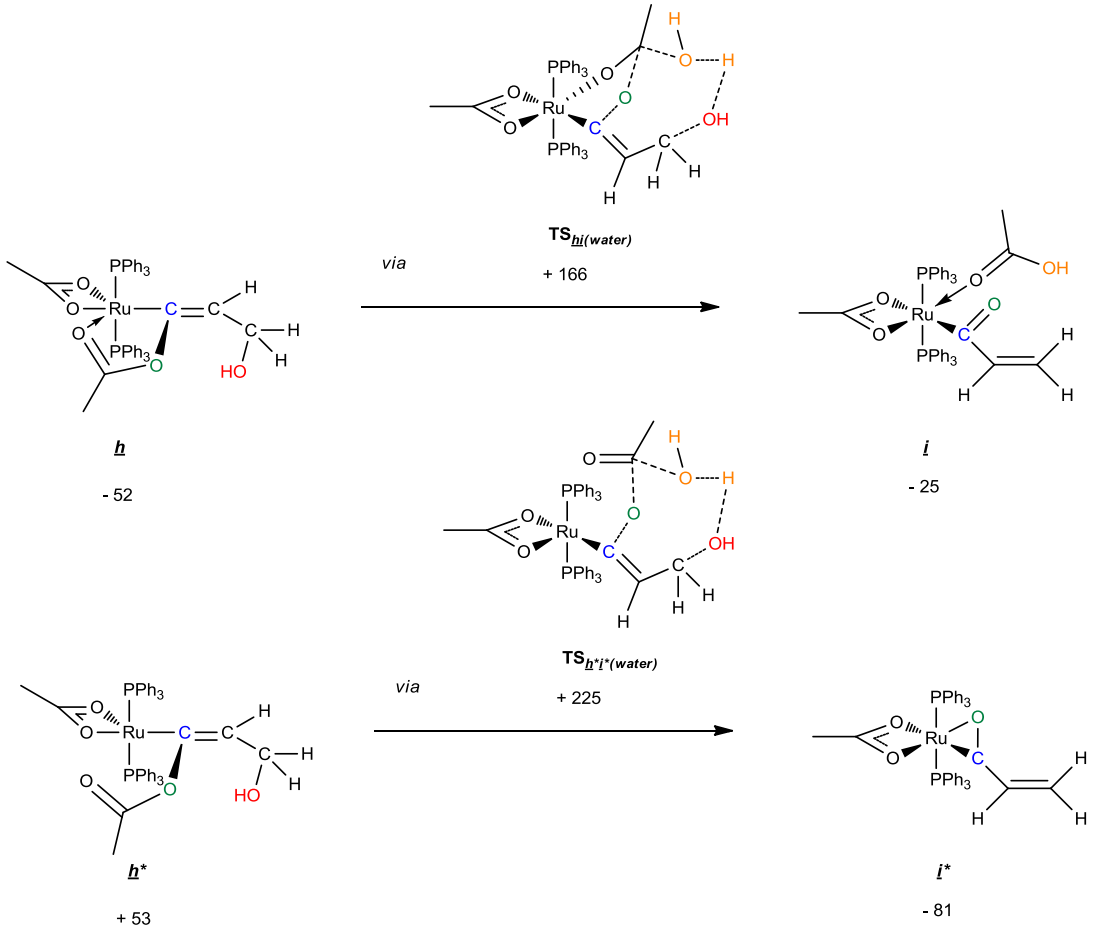

Figure 6.6.9: Conversion of ***h*** to ***i*** *via* $\mathbf{TS}_{\underline{hi}(water)}$ and ***h**** to ***i**** *via* $\mathbf{TS}_{\underline{h}^*\underline{i}^*(water)}$

A final alternative considered an additional alternative to ***h***, in the formation of a complex which contains a coordinated molecule of water. This complex, ***o***, has an energy of +49 kJ mol^{-1} relative to [**1**+**8h**] which is +110 kJ mol^{-1} relative to ***g***. A number of intermediate geometries to a conversion from this complex to a derivative of ***i*** have been attempted, however only one (***p***) has successfully converged. This is shown in Figure 6.6.10. The energy of this intermediate is +79 relative to [**1**+**8h**] and +140 kJ mol^{-1} relative to ***g***. Again, this seems unfavourable so this pathway was not investigated further.

Figure 6.6.10: Conversion of ***o*** to ***p***

It is clear that the pathways which have until now been proposed for the conversion of the hydroxy-vinylidene complexes are incorrect. Following a conversation with Professor Odile Eisenstein of the Université Montpellier 2, an alternative route has been suggested which involves the generation of charged intermediates, as shown in Figure 6.6.11.

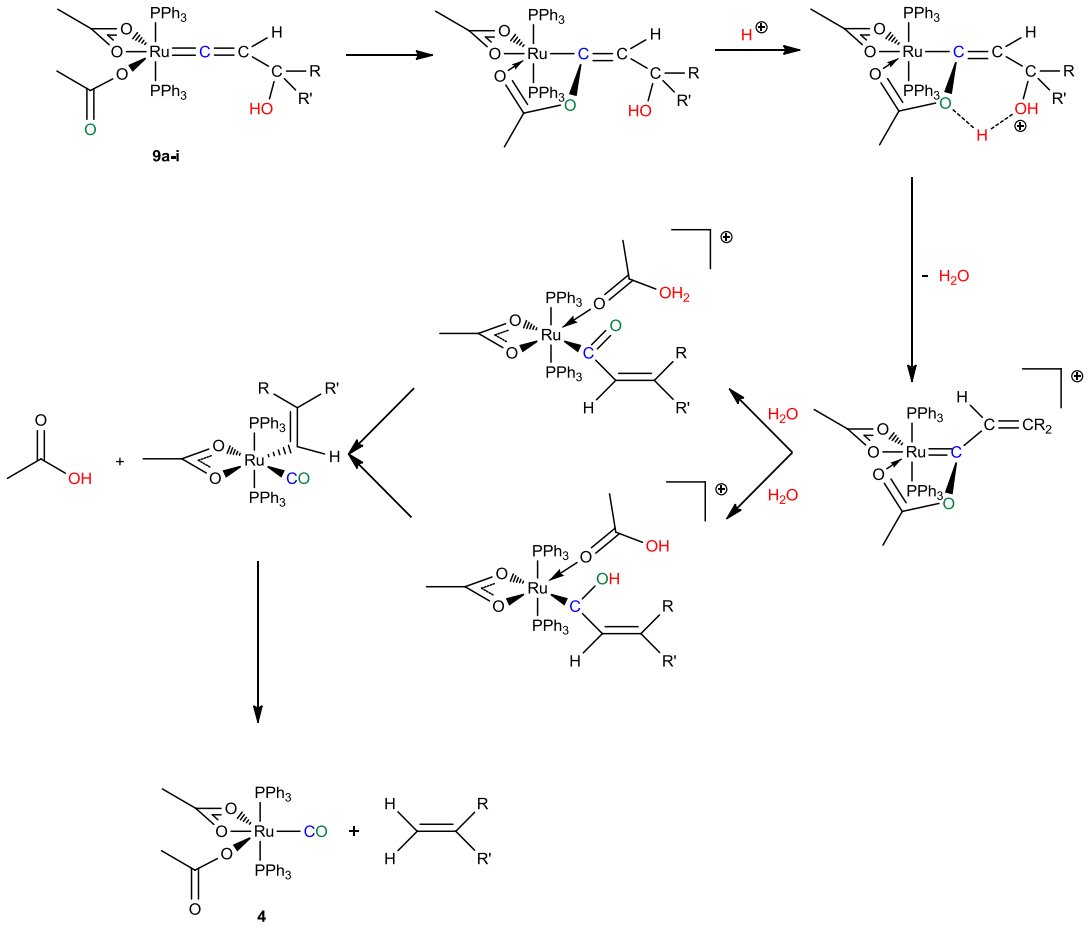

Figure 6.6.11: Alternative mechanism (**VIII**) involving the formation of charged species.

This mechanism (**VIII**) involves the addition of a proton to promote the loss of a water molecule from a metallo-enolester derivative. This results in the formation of a cationic carbene intermediate. The addition of water to this species may then result in the formation of acetic acid and the vinyl complex analogous to **10** *via* either of the two intermediates indicated in Figure 6.6.11 (both are currently under investigation). The ultimate formation of carbonyl complex **4** and the appropriate alkene may then occur with the liberation of the vinyl ligand by acetic acid. It is thought that the proton which instigates this pathway may arise from the DCM solvent used in the reactions as the formation of trace quantities of HCl in DCM is well-known. This mechanism is consistent with the experimental evidence described in this Chapter and may explain the facile nucleophilic substitution of propargylic substrates at C_γ in the apparent absence of an allenylidene species.

Efforts are currently underway to pinpoint the energies of the various intermediates and transition states on the PES for this pathway in the case of the propargylic alcohols. Interestingly, a crystal structure of the cationic intermediate $[Ru(\kappa^2\text{-}OAc)(=C(OAc)CH=CPh_2)(PPh_3)_2]BF_4$ has recently been obtained by Elizabeth Smith , who is continuing the experimental research on this project.

It is clear that the mechanisms initially proposed based upon experimental work (**VI** and **VII**) must be discounted based upon the results obtained by the DFT investigation. At the time of writing, theoretical and experimental work is ongoing in an attempt to determine the mechanism by which a hydroxy-vinylidene complex converts to a carbonyl complex with the concomitant formation of an alkene.

6.7: Conclusions

The family of vinylidene complexes derived from complex **1** has been extended to include the phenoxy-vinylidene complex **9j**, as well as additional substituted vinylidene complexes **9k**, **9l** and **9m**. These complexes were shown to undergo a slightly different conversion process to the hydroxy-vinylidene complexes **9a-i**. Instead of the formation of an alkene and the carbonyl complex **4**, a vinyl complex **10** and another organic product were observed. In the case of **9j**, these products could be isolated and individually characterised. The conversion process was also observed to occur more rapidly in the case of these vinylidene complexes than for complexes **9a-i**.

The identification of this vinyl complex **10** provided some indication as to the nature of the conversion mechanism, and complexes **11** and **12** were subsequently synthesised and characterised. These complexes appeared to be 'trapped' forms of intermediates in a potential conversion mechanism. To understand the potential mechanisms more fully, further experimental work was conducted. It was established that propargylic substitution at C_γ of the vinylidene complexes is possible, and that the exchange of an acetate ligand for an alternative carboxylate ligand such as benzoate is possible. An ^{18}O-labelling study successfully demonstrated that the acetate ligands again play an important role in this mechanism, and a kinetic study indicated that the conversion is first order with respect to the ruthenium complex. Activation parameters were also obtained from this kinetic study though further analysis may be needed as the associated errors are large and the observed rate constant had to account for a number of elementary steps. A theoretical DFT study, which is currently ongoing, has established that a number of pathways initially considered involve transition states with energy barriers that are larger than is deemed experimentally realistic. Experimental and computational work is continuing on this system in an attempt to understand this conversion mechanism, and it is unfortunate that a complete picture cannot be presented here. Future work is expected to focus on an alternative reaction pathway involving the formation of charged intermediates.

It has been successfully demonstrated that the decarbonylation of propargylic alcohols to alkenes mediated by complex **1** occurs *via* a novel reaction pathway. It has also been shown that the acetate ligands again assist in this transformation.

6.8: References

1. Selegue, J. P., *Organometallics* **1982**, *1*, 217.
2. Cadierno, V., Gimeno, J., *Chem. Rev.* **2009**, *109*, 3512.
3. Bruneau, C., Dixneuf, P. H., Eds. *Metal Vinylidenes and Allenylidenes in Catalysis: From Reactivity to Applications in Synthesis*, **2008**, Wiley VCH: Weinheim, Germany.
4. Selegue, J. P., *Coord. Chem. Rev.* **2004**, 248, 1543.
5. Rigaut, S., Touchard, D., Dixneuf, P. H., *Coord. Chem. Rev.* **2004**, *248*, 1585.
6. Bruce, M. I., *Chem. Rev.* **1998**, *98*, 2797.
7. Cadierno, V., Gamasa, M. P., Gimeno, J., *Eur. J. Inorg. Chem.* **2001**, 571.
8. Touchard, D., Dixneuf, P. H., *Coord. Chem. Rev.* **1998**, *178-180*, 409.
9. Bustelo, E., Dixneuf, P. H., *Adv. Synth. Catal.* **2005**, *347*, 393.
10. Bustelo, E., Dixneuf, P. H., *Adv. Synth. Catal.* **2007**, *349*, 933.
11. Hocking, R. K.; Hambley, T. W. *Organometallics* **2007**, 26, 2815.
12. Cannadine, J. C.; Hill, A. F.; White, A. J. P.; Williams, D. J.; Wilton-Ely, J. D. E. T. *Organometallics* **1996**, *15*, 5409.
13. Hill, A. F.; White, A. J. P.; Williams, D. J.; Wilton-Ely, J. D. E. T. *Organometallics* **1998**, *17*, 4249.
14. Matas, L.; Muniente, J.; Ros, J.; Alvarez-Larena, Á.; Piniella, J.F.; *Inorg. Chem. Commun.* **1999**, *2*, 364.
15. Roper, W. R.; Taylor, G. E.; Water, J. M.; Wright, L. J. *J. Organomet. Chem.* **1979**, *182*, C46.
16. Sanford, M. S.; Valdez, M. R.; Grubbs, R. H. *Organometallics* **2001**, *20*, 5455.

17. Shaffer, E. A.; Chen, C-L.; Beatty, A. M.; Valente, E. J.; Schanz, H-J. *J. Organomet. Chem.* **2007**, *692*, 5221.

18. Kawano, H.; Masaki, Y.; Matsunaga, T.; Hiraki, K.; Onishi, M.; Tsubamara, T. *J. Organomet. Chem.* **2000**, *601*, 69.

19. Esteruelas, M. A.; Lahoz, F. J.; López, A. M.; Oñate, E.; Oro, L. A. *Organometallics* **1994**, *13*, 1669.

20. Werner, H.; Daniel, T.; Mahr, N.; Braun, T. *Organometallics* **1993**, *12*, 1475.

21. Yi, C. S.; Gao, R. *Organometallics* **2009**, *28*, 6585.

22. Comparison with an authentic sample of β-styryl acetate.

23. Mitchell, R. W.; Spencer, A.; Wilkinson, G. *J. Chem. Soc. Dalton Trans.* **1973**, 846.

24. Kikukawa, K.; Kono, K.; Nagira, K.; Wada, F.; Matsuda, T. *J. Org. Chem.* **1981**, *46*, 4413.

25. Herzberg, G., *Molecular Spectra & Molecular Structure Vol II – Infrared and Raman Spectra of Polyatomic Molecules*, **1991** reprint of 1945 ed., Kreiger Publishing Company.

26. Jordan, R. B., *Reaction Mechanisms of Inorganic and Organometallic Systems*, 3rd Ed., **2007**, Oxford University Press.

27. Günther, H., *NMR Spectroscopy: Basic Principles, Concepts and Applications*, 2nd Ed., 1995, Wiley.

28. Kuzmic, P. (1996) *Anal. Biochem.* **237**, 260.

29. Nishibayashi, Y.; Milton, M. D.; Inada, Y.; Yoshikawa, M.; Wakiji, I.; Hidai, M.; Uemura, S. *Chem. Eur. J.* **2005**, *11*, 1433.

30. Lynam, J. M.; Welby, C. E.; Whitwood, A. C. *Organometallics* **2009**, *28*, 1320.

31. Comparison with an authentic sample of acetic anhydride.

32. Comparison to data of 4-methoxyphenylacetate: Qiu, R.; Zhang, G.; Ren, X.; Xu, X.; Yang, R.; Luo, S.; Yin, S. *J. Organomet. Chem.* **2010**, *695*, 1182.

33. *N*,*N*-dimethylacetamide: Comparison with simulated NMR spectrum in ALDRICH online NMR library.

34. Hiett, N. P.; Lynam, J. M.; Welby, C. E.; Whitwood, A. C. *J. Organomet. Chem.* **2011**, *696*, 378.

6.9: Experimental

General:

All experimental procedures were performed under an atmosphere of dinitrogen or argon using standard Schlenk Line and Glove Box techniques. DCM, pentane and hexane were purified with the aid of an Innovative Technologies anhydrous solvent engineering system. The CD_2Cl_2 used for NMR experiments was dried over CaH_2 and degassed with three freeze-pump-thaw cycles. The solvent was then vacuum transferred into NMR tubes fitted with PTFE Young's taps. The DCM used for the ^{18}O-labelling studies was dried and degassed in a similar fashion to CD_2Cl_2. NMR spectra were acquired on a Bruker AVANCE 500 (Operating Frequencies ^{1}H 500.23 MHz, ^{31}P 202.50 MHz, ^{13}C 125.77 MHz). ^{31}P and ^{13}C spectra were recorded with proton decoupling. Mass spectrometry measurements were performed on a Thermo-Electron Corp LCQ Classic (ESI) instrument or Waters GCT Premier Acceleration TOF MS (LIFDI). IR spectra were acquired on a Thermo-Nicolet Avatar 370 FTIR spectrometer using either CsCl solution cells or as KBr discs. CHN measurements were performed using an Exeter Analytical Inc. CE-440 analyser. The proportion of DCM in CHN samples was confirmed by a ^{1}H NMR spectrum of a sample used for CHN analysis in d_8-toluene. Relative integration of the peak at δ_H 4.31 (CH_2Cl_2) to that of the vinylidene proton indicates the proportion of DCM in that sample. Structural characterisation of complexes **10**, **11** and **12** was conducted using a Bruker Smart Apex diffractomer with Mo-K_α radiation (λ = 0.71073 Å) with a SMART CCD camera. Diffractometer control, data collection and initial unit cell determination was performed using SMART. Frame integration and unit-cell refinement software was carried out with Saint+. Absorption corrections were applied by SADABS (v 2.03, Sheldrick). Structures were solved by direct methods using SHELXS-97, and refined by full-matrix least-squares using SHELX-97. All non-hydrogen atoms were refined anisotropically. Hydrogen atoms were placed using a "riding model" and included in the refinement at calculated positions. Substrates **h** and **j-n**, HO-C_6H_4-OMe (Sigma-Aldrich), ^{t}BuOH, CH_3COOH (Fisher Scientific) and $CH_3C^{18}O^{18}OH$ (Isotec: Sigma-Aldrich) were used as supplied without further purification. Complex **1** was prepared according to the published literature procedure.[30]

Key to NMR abbreviations:

s (singlet); br s (broad singlet); d (doublet); dd (doublet of doublets); ad (apparent doublet); t (triplet); dt (doublet of triplets); tt (triplet of triplets); at (apparent triplet); q (quartet); aq (apparent quartet); qn (quintet), aqn (apparent quintet); sp (septet); asp (apparent septet); m (multiplet)

(H_2-Ph) or (H_2-PPh_3) refers to the proton in the *ortho*-position of a phenyl ring

(H_3-Ph) or (H_3-PPh_3) refers to the proton in the *meta*-position of a phenyl ring

(H_4-Ph) or (H_4-PPh_3) refers to the proton in the *para*-position of a phenyl ring

General Procedure for the synthesis of complexes 9a-i

Approximately one equivalent of the alkyne was added to a Schlenk vessel containing a solution of **1** in CH_2Cl_2. After stirring for one hour the product was precipitated by addition of pentane/hexane. After filtration of the solvent by a cannula wire fitted with a filter-paper tip, the solid powder was washed twice more with pentane/hexane and dried *in vacuo*.

6.9.1: Synthesis and Characterisation of 9j

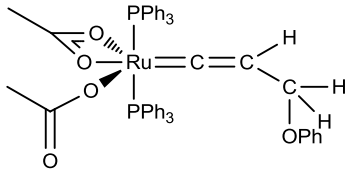

The same general procedure was followed for the synthesis of **9j** as for **9a-i** (see also Section 6.9) 0.14 g **9j** (40.0 %) was obtained as a yellow powder from 0.30 g (0.40 mmol) **1** and 52.0 μL (0.40 mmol) HC≡CCH$_2$OPh in 30 mL CH_2Cl_2. 40 mL pentane was used to precipitate the product, and it was washed further with 2 x 20 ml portions of pentane.

NMR Spectra CD_2Cl_2:

^{1}H δ_H 0.87 (s, 6H, C*H*$_3$COO), 4.41 (m, 1H, [Ru]=C=C*H*), 4.46 (br s, 1H, [Ru]=C=CHC*H*$_A$H$_B$), 4.48 (br s, 1H, [Ru]=C=CHCH$_A$*H*$_B$), 6.70 (d, 8.2 Hz, 2H, *H*$_2$-O*Ph*), 6.93 (at, 7.3 Hz, 1H, *H*$_4$-O*Ph*), 7.03 (t, 8.5 Hz, 2H, *H*$_3$-O*Ph*), 7.37 (at, 7.3 Hz, 12H, *H*$_3$-P*Ph*$_3$), 7.44 (t, 7.1 Hz, 6H, *H*$_4$-P*Ph*$_3$), 7.53 (m, 12H, *H*$_2$-P*Ph*$_3$)

^{31}P δ_P 35.2 (s, 2.0P, *P*Ph$_3$)

^{13}C δ_C 21.6 (s, *C*H$_3$COO), 61.5 (s, Ru=C=CH–*C*OPh), 103.6 (m, Ru=*C*=C), 114.9 (s, Ru=C=C–C(Ph)–*C*$_3$), 121.8 (s, Ru=C=C–C(Ph)–*C*$_4$), 127.9 (t, $^3J_{PC}$ + $^5J_{PC}$ = 9.2 Hz, PPh$_3$–*C*$_3$), 129.5 (s, Ru=C=C–C(Ph)–*C*$_2$), 129.9 (s, PPh$_3$–*C*$_4$), 130.2 (t, $^1J_{PC}$ + $^3J_{PC}$ = 43.2 Hz, PPh$_3$–*C*$_1$), 134.8 (t, $^2J_{PC}$ + $^4J_{PC}$ = 12.2 Hz, PPh$_3$–*C*$_2$), 159.0 (Ru=C=C–C(Ph)–*C*$_1$), 179.8 (s, CH$_3$*C*OO)

IR (KBr) 1359 cm^{-1} (κ^1-OCO$_{sym}$), 1432 cm^{-1} (P–Ph), 1457 cm^{-1} (κ^2-OCO$_{sym}$), 1537 cm^{-1} (κ^2-OCO$_{asym}$), 1597 cm^{-1} (κ^1-OCO$_{asym}$), 1651 cm^{-1} (C=C), $\Delta\nu_{(uni)}$ 238 cm^{-1}, $\Delta\nu_{(chelate)}$ 80 cm^{-1}; (CH_2Cl_2) 1366 cm^{-1} (κ^1-OCO$_{sym}$), 1436 cm^{-1} (P–Ph), 1458 cm^{-1} (κ^2-OCO$_{sym}$), 1538 cm^{-1} (κ^2-OCO$_{asym}$), 1598 cm^{-1} (κ^1-OCO$_{asym}$), 1652 cm^{-1} (C=C), $\Delta\nu_{(uni)}$ 232 cm^{-1}, $\Delta\nu_{(chelate)}$ 80 cm^{-1}.

MS (ESI) m/z 877.1733 (Expected for $^{101}RuP_2O_5C_{49}H_{45}$ $[MH]^+$ = 877.1786)

CHN: not obtained as complex found to degrade rapidly even in the solid state.

6.9.2: General procedure for monitoring the conversion of complexes 9j-m to 10 by NMR Spectroscopy:

The same general procedure as for **9a-i** was followed to prepare the samples (see section 5.6.10). The ^{1}H NMR data of the organic conversion products are described for each complex and the integrations of the appropriate peaks are measured relative to the three acetate protons of **10** at δ_H 0.71. The ^{1}H and ^{31}P NMR data of complexes **9k**, **9l** and **9m** are included in addition to the ^{1}H NMR data of the organic degradation products. References 22 and 31-33 correspond to literature data for the isolated organic compounds.

9j[22]

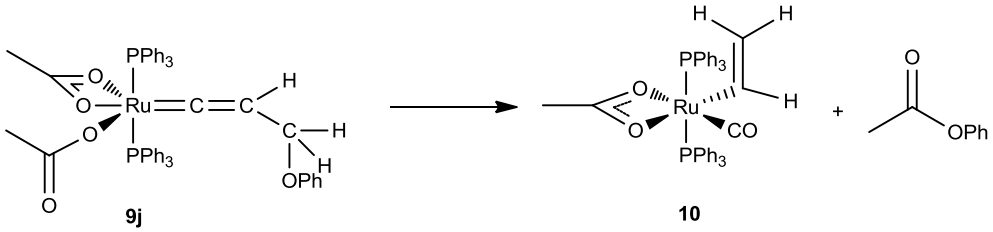

9j **10**

Phenyl Acetate: ^{1}H δ_H 2.32 (s, 3H, CH_3COOPh), Ph resonances are obscured by PPh_3

9k[31]

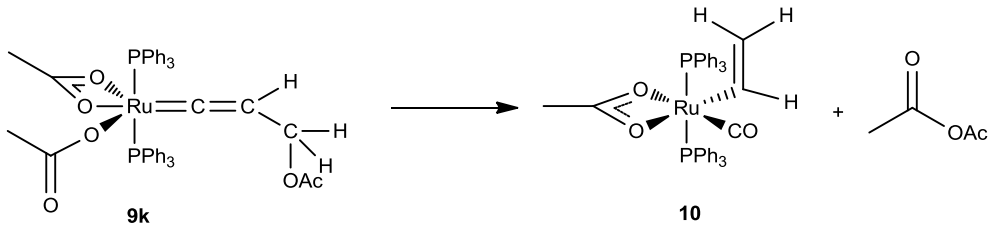

9k **10**

On addition of HC≡CCH_2OAc to **1**, the vinylidene forms and decomposes at such a rapid rate that obtaining spectroscopic data of pure **9k** was extremely difficult.

9k: ^{1}H δ_H 0.85 (s, 9H, CH_3COO), 4.35 (m, 1H, [Ru]=C=CH), 4.44 (br s, 1H, [Ru]=C=CHCH_AH$_B$), 4.46 (br s, 1H, [Ru]=C=CHCH$_A$$H_B$), PPh$_3$ obscured.

9k: ^{31}P δ_P 35.3 (s, 2PPh$_3$)

Acetic anhydride: ^{1}H δ_H 2.24 (s, 3H, CH_3COOCOCH_3)

9l[32]

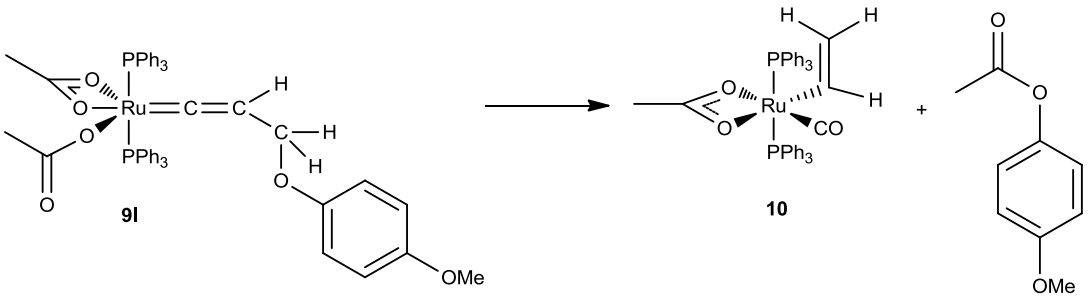

9l: ^{1}H δ_H 0.86 (s, 6H, CH_3COO), 3.79 (s, 3H, OCH_3), 4.36 (m, 1H, [Ru]=C=CH), 4.42 (br s, 1H, [Ru]=C=CHCH_AH$_B$), 4.43 (br s, 1H, [Ru]=C=CHCH$_A$$H_B$), 6.61 (ad, J = 8.9 Hz, 2H, H_2- or H_3-Ph); 6.79 (ad, J = 8.9 Hz, 2H, H_2- or H_3-Ph), 7.37 (at, 7.7 Hz, 12H, H_3-PPh_3), 7.44 (t, 7.3 Hz, 6H, H_4-PPh_3), 7.53 (m, 12H, H_2-PPh_3);

9l: ^{31}P δ_P 35.2 (s, 2PPh$_3$)

4-methoxyphenyl acetate: ^{1}H δ_H 2.26 (s, 3H, CH_3COO), 3.83 (s, 3H, OCH_3), 6.93 (ad, J = 9.1 Hz, 2H, H_2- or H_3-Ph); 7.03 (ad, J = 9.2 Hz, 2H, H_2- or H_3-Ph)

9m[33]

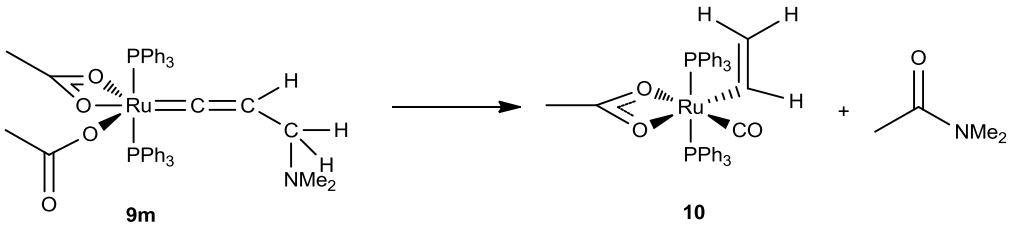

9m: ^{1}H δ_H 0.83 (s, 6H, CH_3COO), 1.71 (s, 6H N(CH_3)$_2$), 2.91, (br s, 1H, [Ru]=C=CHCH_AH$_B$), 2.93 (br s, 1H, [Ru]=C=CHCH$_A$$H_B$), 4.07 (m, $^{4}J_{HP}$ = 3.7 Hz, 1H, [Ru]=C=CH), 7.32 – 7.54 (m, 30H, PPh_3)

9m: ^{31}P δ_P 35.3 (s, 2*P*Ph_3)

N,*N*,-dimethylacetamide: ^{1}H δ_H 2.06 (s, 3H, C*H*$_3$CON(CH_3)$_2$), 2.92 (s, 3H, CH_3CON(C*H*$_3$)(CH_3)), 3.01 (s, 3H, CH_3CON(CH_3)(C*H*$_3$))

6.9.3: Synthesis and Characterisation of 10

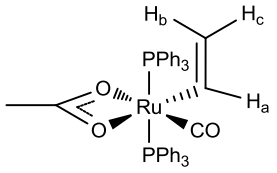

10

One equivalent (83.0 μL, 0.65 mmol) $HC{\equiv}CCH_2OPh$ was added to a Schlenk vessel containing a solution of **1** (0.50 g, (0.67 mmol) in 40 mL CH_2Cl_2. After stirring for 22 hours the product was precipitated by addition of 50 mL pentane. After filtration, the yellow-grey powder was washed twice more with 2 x 40 ml portions of pentane before drying *in vacuo*. Yield 0.31 g (63.2 %)

NMR Spectra CD_2Cl_2:

^{1}H δ_H 0.59 (s, 3H, C*H*$_3$COO), 4.78 (ad, $^{3}J_{HaHb}$ = 16.5 Hz, 1H, *H$_b$*), 4.98 (dt, $^{4}J_{HP}$ = 2.2 Hz, $^{3}J_{HaHc}$ = 9.0 Hz, 1H, *H$_c$*), 7.33 (qt, $^{4}J_{HP}$ = 2.0 Hz, $^{3}J_{HaHc}$ = 8.9 Hz, $^{3}J_{HaHb}$ = 16.4 Hz, 1H, *H$_a$*), 7.47 (m, 30H, P*Ph*$_3$)

^{31}P δ_P 38.5 (s, 2.0P, *P*Ph$_3$)

^{13}C δ_C 22.2 (s, *C*H$_3$COO), 117.2 (m, Ru–C=*C*), 128.1 (t, $^{3}J_{PC}$ + $^{5}J_{PC}$ = 9.2 Hz, PPh$_3$–*C*$_3$), 130.0 (s, PPh$_3$–*C*$_4$), 131.7 (t, $^{1}J_{PC}$ + $^{3}J_{PC}$ = 43.2 Hz, PPh$_3$–*C*$_1$), 134.5 (t, $^{2}J_{PC}$ + $^{4}J_{PC}$ = 11.5 Hz, PPh$_3$–*C*$_2$), 157.7 (t, $^{2}J_{PC}$ = 11.2 Hz, Ru–*C*=C), 182.7 (s, CH$_3$*C*OO), 206.7 (t, $^{2}J_{PC}$ = 15.3 Hz, Ru–*C*O)

IR (KBr) 1432 cm^{-1} (P–Ph), 1455 cm^{-1} (κ^2-OCO$_{sym}$), 1526 cm^{-1} (κ^2-OCO$_{asym}$), 1625 cm^{-1} (C=C), 1916 cm^{-1} (CO), $\Delta\nu_{(chelate)}$ 71 cm^{-1}; (CH_2Cl_2) 1435 cm^{-1} (P–Ph), 1457 cm^{-1} (κ^2-OCO$_{sym}$), 1531 cm^{-1} (κ^2-OCO$_{asym}$), 1622 cm^{-1} (C=C), 1914 cm^{-1} (CO), $\Delta\nu_{(chelate)}$ 74 cm^{-1}.

MS (LIFDI) m/z 740 (Expected for $^{101}RuP_2O_3C_{41}H_{36}$ $[M\text{-}H]^+$ = 740.1)

CHN Anal. for $RuP_2O_3C_{41}H_{37}$ + (0.20 CH_2Cl_2) (calc), C 65.39, H 4.85; (found) C 65.41, H 4.86

Crystal data and structure refinement for 10.

Identification code	jml0915m	
Empirical formula	$RuP_2O_3C_{41}H_{36}$	
Formula weight	739.71	
Temperature	110(2) K	
Wavelength	0.71073 Å	
Crystal system	Monoclinic	
Space group	P2(1)/c	
Unit cell dimensions	a = 17.531(4) Å	α= 90°.
	b = 9.769(2) Å	β= 106.076(4)°.
	c = 20.833(5) Å	γ = 90°.
Volume	3428.5(14) $Å^3$	
Z	4	
Density (calculated)	1.433 Mg/m^3	
Absorption coefficient	0.589 mm^{-1}	
F(000)	1520	
Crystal size	0.23 x 0.06 x 0.04 mm^3	
Theta range for data collection	2.03 to 25.00°.	
Index ranges	-20<=h<=20, -11<=k<=11, -24<=l<=24	
Reflections collected	26085	
Independent reflections	6036 [R(int) = 0.0646]	
Completeness to theta = 25.00°	99.8 %	
Absorption correction	Semi-empirical from equivalents	
Max. and min. transmission	0.980 and 0.696	
Refinement method	Full-matrix least-squares on F^2	
Data / restraints / parameters	6036 / 0 / 429	
Goodness-of-fit on F^2	0.993	
Final R indices [I>2sigma(I)]	R1 = 0.0377, wR2 = 0.0832	
R indices (all data)	R1 = 0.0746, wR2 = 0.0995	
Largest diff. peak and hole	0.734 and -0.851 $e.Å^{-3}$	

6.9.4: Synthesis and Characterisation of 11

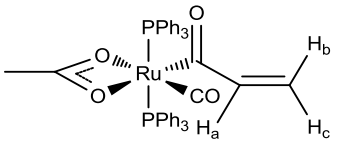

One equivalent (121 μL, 0.94 mmol) HC≡CCH$_2$OPh was added to a Schlenk vessel containing a solution of **1** (0.70 g, (0.94 mmol) in 30 mL CH_2Cl_2. After stirring for 22 hours the product was precipitated by addition of 40 mL pentane. After filtration, the powder was washed twice more with 2 x 30 ml portions of pentane and dried *in vacuo*. At this stage, the dark yellow powder was redissolved in 15 mL CH_2Cl_2 and the atmosphere of Ar partially removed *in vacuo*. The solution was put under a CO atmosphere and stirred for 1 hour (IR spectra were periodically recorded and showed the reaction had gone to completion after this time) and the solvent removed *in vacuo*. Yield 0.40 g (55.6 %)

^{1}H δ_H 0.56 (s, 3H, C*H*$_3$COO), 4.21 (dd, $^2J_{HbHc}$ = 2.6 Hz, $^3J_{HaHc}$ = 10.3 Hz, 1H, *H*$_c$), 4.56 (dd, $^2J_{HbHc}$ = 2.7 Hz, $^3J_{HaHb}$ = 17.0 Hz, 1H, *H*$_b$), 7.21 (dd, $^3J_{HaHc}$ = 10.3 Hz, $^3J_{HaHb}$ = 17.0 Hz, 1H, *H*$_a$), 7.43 – 7.51 (m, 30H, P*Ph*$_3$)

^{31}P δ_P 36.7 (s, 2.0P, *P*Ph$_3$)

^{13}C δ_C 21.9 (s, *C*H$_3$COO), 111.8 (s, Ru–COC=*C*), 128.2 6 (t, $^3J_{PC}$ + $^5J_{PC}$ = 9.5 Hz, PPh$_3$–*C*$_3$), 130.4 (s, PPh$_3$–*C*$_4$), 130.8 (t, $^1J_{PC}$ + $^3J_{PC}$ = 44.3 Hz, PPh$_3$–*C*$_1$), 134.5 (t, $^2J_{PC}$ + $^4J_{PC}$ = 11.1 Hz, PPh$_3$–*C*$_2$), 138.4 (s, Ru–CO*C*=C), 182.1 (s, CH$_3$*C*OO), 204.6 (t, $^2J_{PC}$ = 15.0 Hz, Ru–*C*O), 243.6 (t, $^2J_{PC}$ = 7.9 Hz, Ru–*C*OC=C)

IR (KBr) 1433 cm^{-1} (P–Ph), 1453 cm^{-1} (κ^2-OCO$_{sym}$), 1531 cm^{-1} (κ^2-OCO$_{asym}$), 1573 cm^{-1} (acyl CO), 1613 cm^{-1} (C=C), 1941 cm^{-1} (CO), $\Delta\nu_{(chelate)}$ 78 cm^{-1}. (CH_2Cl_2) 1434 cm^{-1} (P–Ph), 1452 cm^{-1} (κ^2-OCO$_{sym}$), 1535 cm^{-1} (κ^2-OCO$_{asym}$), 1576 cm^{-1} (acyl CO), 1612 cm^{-1} (C=C), 1943 cm^{-1} (CO), $\Delta\nu_{(chelate)}$ 83 cm^{-1}.

MS (ESI) m/z 750.1 (Expected for $^{101}RuP_2O_2NC_{42}H_{36}$ [M - OAc^- + MeCN]$^+$ = 750.1265)

CHN Anal. for $RuP_2O_4C_{42}H_{36}$ + (1.40 CH_2Cl_2) (calc), C 58.79, H 4.41; (found) C 58.43, H 4.36

Crystal data and structure refinement for 11.

Identification code	jml0920m	
Empirical formula	$RuP_2O_4Cl_4C_{44}H_{40}$	
Formula weight	937.57	
Temperature	110(2) K	
Wavelength	0.71073 Å	
Crystal system	Monoclinic	
Space group	P2(1)/c	
Unit cell dimensions	a = 9.5629(6) Å	α= 90°.
	b = 22.8704(13) Å	β= 00.2740(10)°.
	c = 19.7241(11) Å	γ = 90°.
Volume	4244.6(4) $Å^3$	
Z	4	
Density (calculated)	1.467 Mg/m^3	
Absorption coefficient	0.738 mm^{-1}	
F(000)	1912	
Crystal size	0.27 x 0.18 x 0.09 mm^3	
Theta range for data collection	1.78 to 30.01°.	
Index ranges	-13<=h<=13, -31<=k<=31, -27<=l<=27	
Reflections collected	47967	
Independent reflections	12221 [R(int) = 0.0240]	
Completeness to theta = 30.01°	98.7 %	
Absorption correction	Semi-empirical from equivalents	
Max. and min. transmission	0.936 and 0.800	
Refinement method	Full-matrix least-squares on F^2	
Data / restraints / parameters	12221 / 0 / 525	
Goodness-of-fit on F^2	1.014	
Final R indices [I>2sigma(I)]	R1 = 0.0297, wR2 = 0.0714	
R indices (all data)	R1 = 0.0372, wR2 = 0.0756	
Largest diff. peak and hole	0.827 and -0.481 $e.Å^{-3}$	

6.9.5: Synthesis and Characterisation of 12

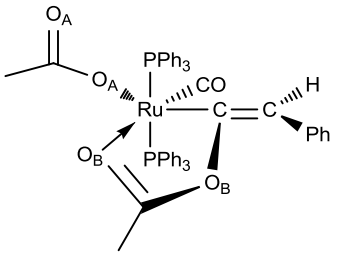

One equivalent (30.0 μL, 0.27 mmol) HC≡CPh was added to a Schlenk vessel containing a solution of **1** (0.20 g, (0.27 mmol) in 15 mL CH_2Cl_2. After stirring for 1 hour to prepare **2a** *in situ*, the atmosphere of Ar was partially removed *in vacuo*. The solution was then put under a CO atmosphere and stirred for 1 hour (IR spectra were periodically recorded and showed the reaction had gone to completion after this time). The solvent was finally removed *in vacuo* to leave a yellow-green crystalline material. Yield 0.17 g (74.0 %)

^{1}H δ_H 1.15 (s, 3H, C*H*$_3$COO), 1.63 (s, 3H, C*H*$_3$COO), 6.25 (t, $^{4}J_{HP}$ = 2.8 Hz, 1H, C=C*H*Ph), 7.09 (at, 7.6 Hz, 1H, *H*$_4$-CH*Ph*), 7.12 (ad, 7.9 Hz, 2H, *H*$_2$-CH*Ph*), 7.24 (at, 7.7 Hz, 2H, *H*$_3$-CH*Ph*), 7.34 (at, 7.6 Hz, 12H, *H*$_2$-P*Ph*$_3$), 7.41 (at, 7.3 Hz, 6H, *H*$_4$-P*Ph*$_3$), 7.60 – 7.66 (m, 12H, *H*$_3$-P*Ph*$_3$)

^{31}P δ_P 30.7 (s, 2.0P, *P*Ph$_3$)

^{13}C δ_C 18.5 (s, *C*H$_3$COO), 24.0 (s, *C*H$_3$COO), 122.3 (t, $^{3}J_{PC}$ = 4.5 Hz Ru–C=*C*HPh), 124.7 (s, CH*Ph*-*C*$_4$), 127.9 (t $^{3}J_{PC}$ + $^{5}J_{PC}$ = 9.3 Hz, PPh$_3$–*C*$_3$), 129.7 (s, PPh$_3$–*C*$_4$), 130.0 (s, CH*Ph*-*C*$_{2/3}$), 132.2 (s, CH*Ph*-*C*$_{3/2}$), 132.6 (t, $^{1}J_{PC}$ + $^{3}J_{PC}$ = 40.7 Hz, PPh$_3$–*C*$_1$), 134.4 (t, $^{2}J_{PC}$ + $^{4}J_{PC}$ = 10.7 Hz, PPh$_3$–*C*$_2$), 136.9 (br s, CH*Ph*-*C*$_1$), 177.9 (s, CH$_3$*C*OO), 180.5 (s, CH$_3$*C*OO), 193.2 (t, $^{2}J_{PC}$ = 17.8 Hz, Ru–*C*), 205.8 (t, $^{2}J_{PC}$ = 12.7 Hz, Ru–*C*O)

IR (KBr) 1367 cm^{-1} (κ^1-O$_A$CO$_{A\ sym}$), 1394 cm^{-1} (κ^1-O$_B$CO$_{B\ sym}$), 1434 cm^{-1} (P–Ph), 1571 cm^{-1} (κ^1-O$_B$CO$_{B\ asym}$), 1593 cm^{-1} (κ^1-O$_A$CO$_{A\ asym}$), 1616 cm^{-1} (C=C), 1963 cm^{-1} (CO), $\Delta\nu_{A(uni)}$ 227 cm^{-1}, $\Delta\nu_{B(uni)}$ 177 cm^{-1}. (CH_2Cl_2) 1373 cm^{-1} (κ^1-O$_A$CO$_{A\ sym}$), 1396 cm^{-1} (κ^1-O$_B$CO$_{B\ sym}$), 1435 cm^{-1} (P–Ph), 1572 cm^{-1} (κ^1-O$_B$CO$_{B\ asym}$), 1594 cm^{-1} (κ^1-O$_A$CO$_{A\ asym}$), 1613 cm^{-1} (C=C), 1963 cm^{-1} (CO), $\Delta\nu_{A(uni)}$ 221 cm^{-1}, $\Delta\nu_{B(uni)}$ 176 cm^{-1}.

MS (ESI) m/z 875.1 (Expected for $^{101}RuP_2O_5C_{49}H_{43}$ $[M]^+$ = 875.1629), 856.1 (Expected for $^{101}RuP_2O_3NC_{49}H_{42}$ [M – HOAc + MeCN]$^+$ = 856.1683), 815.1 (Expected for $^{101}RuP_2O_3C_{47}H_{39}$ [M – HOAc] = 815.1418)

CHN Anal. for $RuP_2O_5C_{49}H_{43}$ + (0.1 CH_2Cl_2) (calc), C 66.76, H 4.93; (found) C 66.78, H 4.85

Crystal data and structure refinement for 12.

Identification code	jml0923m	
Empirical formula	$RuP_2O_5C_{49}H_{42}$	
Formula weight	873.84	
Temperature	110(2) K	
Wavelength	0.71073 Å	
Crystal system	Monoclinic	
Space group	P2(1)/n	
Unit cell dimensions	a = 10.1668(6) Å	α= 90°.
	b = 19.0026(11) Å	β= 95.8070(10)°.
	c = 21.4366(13) Å	γ = 90°.
Volume	4120.2(4) Å^3	
Z	4	
Density (calculated)	1.409 Mg/m^3	
Absorption coefficient	0.506 mm^{-1}	
F(000)	1800	
Crystal size	0.12 x 0.10 x 0.06 mm^3	
Theta range for data collection	1.44 to 30.02°.	
Index ranges	-14<=h<=14, -26<=k<=25, -29<=l<=30	
Reflections collected	46626	
Independent reflections	11878 [R(int) = 0.0361]	
Completeness to theta = 30.02°	98.6 %	
Absorption correction	Semi-empirical from equivalents	
Max. and min. transmission	0.970 and 0.855	
Refinement method	Full-matrix least-squares on F^2	
Data / restraints / parameters	11878 / 0 / 520	
Goodness-of-fit on F^2	1.018	
Final R indices [I>2sigma(I)]	R1 = 0.0324, wR2 = 0.0742	
R indices (all data)	R1 = 0.0461, wR2 = 0.0808	
Largest diff. peak and hole	0.710 and -0.387 e.Å^{-3}	

6.9.6: Addition of CH_3COOH to 10, 11, 12 and ^{13}C-12

General procedure for NMR scale reactions involving addition of CH_3COOH:

A portion of the relevant complex was added to an NMR tube fitted with a PFTE Young's tap. The complex was then dissolved in CD_2Cl_2 transferred into the tube by vacuum distillation. Approximately one equivalent of CH_3COOH was then added to the solution under a N_2 or Ar atmosphere.

6.9.6.1: Addition of CH_3COOH to 10

The general procedure for an NMR scale reaction was followed using 13.2 mg **10** (17.8 μmol) and 1.0 μL CH_3COOH (17.5 μmol). After one day, resonances due to complex **10** and acetic acid began to be replaced by those due to complex **4** and ethene.

6.9.6.2: Addition of CH_3COOH to 11

The general procedure for an NMR scale reaction was followed for **11** and 0.8 μL CH_3COOH (2 equivalents: 14.0 μmol). After one day, resonances due to complex **11** and acetic acid began to be replaced by those due to ethene and [Ru(κ^1-OAc)$_2$(PPh$_3$)$_2$(CO)$_2$].

[Ru(κ^1-OAc)$_2$(PPh$_3$)$_2$(CO)$_2$] ^{1}H NMR (CD_2Cl_2) δ_H: 1.18 (s, 6H, C*H*$_3$COO), 7.46 (at, *J* = 7.2 Hz, 12H, *H*$_3$-P*Ph*$_3$), 7.50 (at, *J* = 7.2 Hz, 6H, *H*$_4$-P*Ph*$_3$), 7.50 (m, 12H, *H*$_2$-P*Ph*$_3$)

6.9.6.3: Addition of CH_3COOH to 12

The general procedure for an NMR scale reaction was followed using 18.9 mg **12** (21.6 μmol) and 1.2 μL CH_3COOH (21.6 μmol). After one day, resonances due to complex **12** and acetic acid were replaced by those due to complex **4** and (*Z*)-*β*-styryl acetate.

(*Z*)-*β*-styryl acetate: ^{1}H NMR (CD_2Cl_2) δ_H: 2.27 (s, 3H, C*H*$_3$), 5.75 (d, $^3J_{HH}$ = 7.2 Hz, 1H, C=C*H*) Other alkene proton is obscured by Ph resonances

6.9.6.4: Addition of CH_3COOH to ^{13}C-12

The general procedure for an NMR scale reaction was followed using 25.0 mg **^{13}C-12** (28.6 μmol) and 1.6 μL CH_3COOH (28.6 μmol). After one day, resonances due to complex **12** and acetic acid were replaced by those due to complex **4** and ^{13}C-(*Z*)-*β*-styryl acetate.

^{13}C-(*Z*)-*β*-styryl acetate: ^{1}H NMR (CD_2Cl_2) δ_H: 2.30 (s, 3H, C*H*$_3$), 5.76 (t, $^3J_{HH} = J_{HC}$ = 7.0 Hz, 1H, C=C*H*), Other alkene proton is obscured by Ph resonances; ^{13}C NMR: significant enhancement observed at δ_C 134.1 (s, CH_3COO^{13}*C*H=CHPh)

6.9.7: Reaction of 9d with CO.

19.8 mg complex **1** (26.9 μmol) was added to an NMR tube fitted with a PFTE Young's tap. The complex was then dissolved in CD_2Cl_2 transferred into the tube by vacuum distillation. One equivalent HC≡CC(H)(Ph)(OH) (**d**: 3.3 μL, 26.9 μmol) was then added under Ar atmosphere and the solution permitted to stand to allow for full vinylidene formation. Once the mixture had changed from red to bright yellow, the solution was degassed by three freeze-pump-thaw cycles. The sample was then placed under an atmosphere of CO and NMR spectra were immediately recorded.

6.9.8: Synthesis of complexes 13, 15a, 16d and 17

Procedures conducted by Mr. Nicholas Hiett (MChem student, JML group, 2008-2009). See also reference 34

6.9.9: Reaction between complexes 1 and 13

Approximately 5 mg of **1** (6.72 μmol) and 5 mg of **13** (5.76 μmol) were dissolved in 5 mL CD_2Cl_2. The composition of the solution was monitored by NMR spectroscopy over the course of 4 days.

Assignments:

^{31}P NMR δ_P 63.6 (**1**), 63.3 (**19**), 62.9 (**13**)

Ratios of integration:

Immediate:	**1**: 1.00; **19**: 0.55; **13**: 0.93
1 day after addition:	**1**: 1.00; **19**: 1.85; **13**: 0.88
4 days after addition:	**1**: 1.00; **19**: 1.80; **13**: 0.75

6.9.10: Addition of alkynes 8j, 8m and 8n to 13 and 1.

General procedure for NMR scale reactions involving addition of alkynes:

A portion of the relevant complex was added to an NMR tube fitted with a PFTE Young's tap. The complex was then dissolved in CD_2Cl_2 transferred into the tube by vacuum distillation. Approximately one equivalent of the appropriate alkyne was then added to the solution under a N_2 or Argon atmosphere. Complex **13** was prepared by Mr Nicholas Hiett

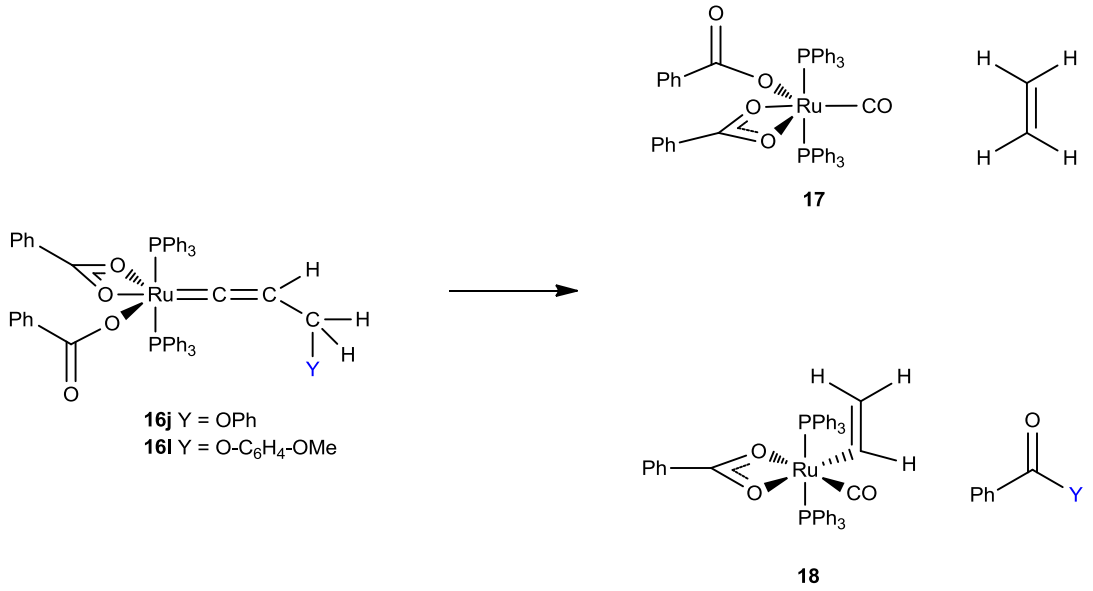

6.9.10.1: Reaction of 8j ($HC{\equiv}CCH_2OPh$) with 13

The general procedure for an NMR scale reaction was followed using 10.0 mg **13** (11.5 μmol) and 1.5 μL **8j** (11.7 μmol). After five days, resonances due to complex **16j** were replaced by those due to complexes **17**, **18** and ethene.

16j: ^{1}H NMR δ_H 4.51 (br s, 3H, [Ru]=C=C*H*C*H*$_2$), 6.73 (ad, J_{HH} = 7.8 Hz, 2H, O*Ph*), 6.96 (tt, J_{HH} = 1.0 Hz, 7.4 Hz, 1H, O*Ph*), 7.07 – 7.58 (m, ~ 40H, O*Bz*, P*Ph*$_3$); ^{31}P NMR δ_P 34.1

After 5 days: **17**: ^{31}P NMR δ_P 38.2; ethene: ^{1}H NMR δ_H 5.45 (s); **18**: ^{1}H NMR δ_H 4.81 (ddt, $^2J_{HbHc}$ = 0.7, $^4J_{HP}$ = 2.1 Hz, $^3J_{HaHa}$ = 16.5, 1H, *H*$_b$), 5.05 (dtt, $^2J_{HbHc}$ = 0.8, $^4J_{HP}$ = 2.2 Hz, $^3J_{HaHc}$ = 9.0 Hz, 1H, *H*$_c$), ^{31}P NMR δ_P 37.9

6.9.10.2: Reaction of 8l (HC≡CCH$_2$O-C$_6$H$_4$-OMe) with 13

The general procedure for an NMR scale reaction was followed using 15.2 mg **13** (17.5 μmol) and 2.9 μL **8l** (17.5 μmol). After five days, resonances due to complex **16l** were replaced by those due to complexes **17**, **18** and ethene.

16l: ^{1}H NMR δ_H 3.81 (s, 3H, OC*H*$_3$), 4.47 (br s, 3H, [Ru]=C=C*H*C*H*$_2$), 6.65 (ad, *J* = 9.0 Hz, 2H, *H*$_2$- or *H*$_3$-Ph); 6.82 (ad, *J* = 9.1 Hz, 2H, *H*$_2$- or *H*$_3$-Ph), 7.00 – 7.62 (m, ~ 42H, *Ph*/O*Bz*, P*Ph*$_3$); ^{31}P NMR δ_P 34.1

After 5 days: Resonances for complex **17**, **18** and ethene are observed identical to those in Section 6.9.8.1. In addition, two singlet resonances are observed at δ_H 3.77 and 3.87, presumably due to PhOCO-C$_6$H$_4$-OMe and perhaps HO-C$_6$H$_4$-OMe.

6.9.10.3: Reaction of 8n (HC≡CCH$_2$OBz) with 13

The general procedure for an NMR scale reaction was followed using 23.3 mg **13** (26.9 μmol) and 3.9 μL **8n** (26.9 μmol). Immediately upon addition of the alkyne resonances due to complex **16n** were observed along with those of complex **17,** ethene and a number of unidentified resonances, the majority of which have been excluded for simplicity.

^{1}H NMR δ_H 4.55 (m, 1H, [Ru]=C=C*H*, **16n**), 4.81 (m, 2H, [Ru]=C=CHC*H*2, **16n**), 5.45 (s, ethene)

^{31}P NMR δ_P 34.2 (s, **16n**), 35.8 (s, unknown), 38.2 (s, **17**)

6.9.10.4: Reaction of 8n (HC≡CCH$_2$OBz) with 1

The general procedure for an NMR scale reaction was followed using 18.4 mg **1** (24.7 μmol) and 3.6 μL **8n** (24.9 μmol). Immediately after addition resonances due to complex **9n** and **9k** were observed. Two days later these resonances had disappeared and those due to complexes **4**, **10**, **17**, **18** and **20**, and compounds ethene, acetic anhydride and benzoic acetic anhydride were observed.

Assignments of acetate and phenyl/benzoate resonances have not been attempted as many peaks overlap in these regions.

9n:: ^{1}H δ_H 0.85 (6H, s, C*H*$_3$COO), 4.40 (m, 1H, [Ru]=C=C*H*), 4.49 (br s, 1H, [Ru]=C=CHC*H*$_A$H$_B$), 4.50 (br s, 1H, [Ru]=C=CHCH$_A$*H*$_B$),

9n: ^{31}P δ_P 34.8 (s, 2*P*Ph$_3$)

Benzoic acetic anhydride: ^{1}H δ_H 2.40 (s, C*H*$_3$COOCOPh)

9k and acetic anhydride: resonances identical to those described in 6.9.2; **4:** see section 3.8.2; **10**: see Section 6.9.3; **17**, **18** and ethene: see section 6.9.9.1

20: ^{31}P δ_P 38.8 (s, 2*P*Ph$_3$)

6.9.10.5: Reaction of 9j with HO-C$_6$H$_4$-OMe

The general procedure for an NMR scale reaction was followed using 10.0 mg **1** (13.4 μmol) and 1.7 μL **8j** (13.2 μmol) to initially prepare **9j**. After standing for 10 minutes (to allow for full formation of the vinylidene complex), 1.7 mg (13.7 μmol) HO-C$_6$H$_4$-OMe was added under N_2. The sample was sealed and analysed immediately by NMR spectroscopy. Resonances identical to those observed for complexes **9j** (6.9.1) and **9l** (6.9.2) were immediately observed. After one day, these resonances had been replaced by those due to complex **10** (6.9.3), phenyl acetate (6.9.2) and 4-methoxyphenyl acetate (6.9.2) were observed.

6.9.11: Synthesis of $[Ru(\kappa^2\text{-}^{18}OAc)_2(PPh_3)_2]$ ^{18}O-1

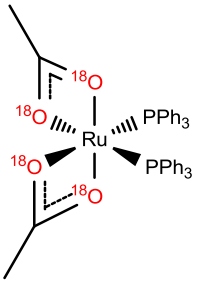

7.00 mL ^{t}BuOH (liquid, m.p. 25 °C) was added to a warm Schlenk tube containing 0.176 g KO^tBu (1.57 mmol) and a stirrer bar under N_2. 90.0 µL $CH_3C^{18}O_2H$ (1.57 mmol) was added and the mixture vigorously stirred at 35 °C for 5 minutes to give a cloudy suspension of $K^{18}O_2CH_3$. 0.15 g $[RuCl_2(PPh_3)_3]$ (0.156 mmol) was added and the mixture heated with stirring at 90 °C for 45 minutes. Over this time the mixture changed from a black to orange-red suspension. The mixture was allowed to cool to leave an orange-red precipitate which was filtered through a warm sintered funnel and flask. The orange-red filtrate, still containing $K^{18}O_2CH_3$, was immediately collected and transferred to another Schlenk tube and degassed by bubbling with N_2 for 10 minutes. The orange-red precipitate was washed with H_2O (5 ml), MeOH (3 mL) and Et_2O (2 mL). 22.8 mg (**^{18}O-1a**, 19.8 % yield) of an orange-red powder was obtained in this way.

To optimize yield, the small amounts of product embedded in the sintered funnel were washed through into another Schlenk tube by addition of DCM. The DCM was immediately removed *in vacuo* to leave a dark-red residue (**^{18}O-1b**, 22.4 mg).

To the degassed filtrate, 70.5 mg $[RuCl_2(PPh_3)_3]$ (0.07 mmol) was added and the mixture once more heated at 90°C for 30 minutes to give an orange-red suspension. The mixture was again filtered though a warm sintered funnel and washed with small portions of H_2O (3 ml), MeOH (2 mL) and Et_2O (1 mL). 5.9 mg (**^{18}O-1c**, 10.7 % yield) was obtained as an orange-red powder.

The procedure used to obtain **^{18}O-1b** was repeated to yield a further 1.1 mg (**^{18}O-1d**) of a dark-red residue. **^{18}O-1b** and **^{18}O-1d** were combined in a small ampoule and dissolved in DCM. Slow diffusion of pentane into this solution yielded 43.1 mg (**^{18}O-1e**, 25.0 % yield) of the product as red crystals. Overall yield of **^{18}O-1**: 71.8 mg, 41.6 %.

NMR (CD_2Cl_2) Resonances in ^{1}H and $^{31}P\{^{1}H\}$ identical to those of **1**

IR (CH_2Cl_2) 1435 cm^{-1} (P-Ph), 1482 cm^{-1} (P-Ph and κ^2-$^{18}OC^{18}O_{asym}$)

MS (LIFDI) m/z 752.1 (Expected for $^{101}RuP_2{}^{18}O_4C_{40}H_{36}$ $[M]^+$ = 752.1302)

6.9.12: Synthesis of [Ru(κ^2-^{18}OAc)(C^{18}O)(CH=CH$_2$)(PPh$_3$)$_2$] ^{18}O-10

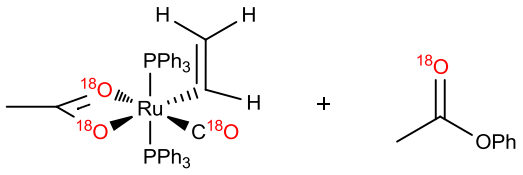

^{18}O-10

7.1 mg **^{18}O-1** (9.45 μmol) was dissolved in 1 mL CH_2Cl_2 (dried over CaH_2 and distilled under reduced pressure) in an ampoule with a stirrer bar. 1.2 μL HC≡CCH_2OPh was then added and the mixture stirred for 18 h. The mixture initially changed from pale orange to pale yellow on addition of the alkyne, but after 18 h had darkened to a brown-orange. The mixture was then analysed by LIFDI- and GC-EI-MS and IR.

NMR (CD_2Cl_2) Resonances in ^{1}H and ^{31}P{^{1}H} identical to those of **10**

IR (CH_2Cl_2) 1434 cm^{-1} (P-Ph), 1480 cm^{-1} (P-Ph), 1493 cm^{-1} (κ^2-^{18}OC^{18}O$_{asym}$), 1594 cm^{-1} (C=C), 1722 cm^{-1} (ester C=^{18}O), 1875 cm^{-1} (Ru-C^{18}O)

LIFDI-MS m/z 746.1 (Expected for $^{101}RuP_2{}^{18}O_3C_{41}H_{36}$ $[M-H]^+$ = 746.1311)
EI-MS m/z 138.1 (Expected for $[CH_3C^{18}O^{16}OPh]^+$ = 138.06), 94.0, (Expected for $[H^{16}OPh]^+$ = 94.04), 45.0 (Expected for $[CH_3C^{18}O]^+$ = 45.03)

6.9.13: Synthesis of [Ru(κ^2-^{18}OAc)(C^{18}O)(CH=CH$_2$)(PPh$_3$)$_2$] ^{18}O-4

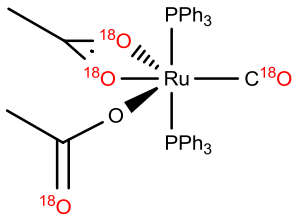

5.6 mg **^{18}O-1** (7.45 µmol) was dissolved in 900 µL CH_2Cl_2 (dried over CaH_2 and distilled under reduced pressure) in an ampoule with a stirrer bar. 0.4 µL HC≡CCH_2OH was then added and the mixture stirred for 18 h. The mixture initially changed from orange to yellow on addition of the alkyne, but after 18 h had changed to a dark-yellow. The mixture was then analysed by LIFDI-MS and IR.

IR (CH_2Cl_2) 1434 cm^{-1} (P-Ph), 1480 cm^{-1} (P-Ph), 1493 cm^{-1} (κ^2-^{18}OC^{18}O$_{asym}$), 1905 cm^{-1} (Ru-C^{18}O)

LIFDI-MS m/z 818.1 (?) 774.1 (Expected for $^{101}RuP_2{}^{16}O_4{}^{18}OC_{41}H_{36}$ $[M-H]^+$ = 774.1124); 746.1 (Expected for $^{101}RuP_2{}^{18}O_3C_{41}H_{36}$ [**^{18}O-10** - H]$^+$); 718.1 (Expected for $^{101}RuP_2{}^{18}O_2{}^{16}OC_{39}H_{34}$ $[M\text{-}OAc^-]^+$ = 718.1112)

6.9.14: Kinetic Studies

General Procedure for monitoring the degradation of vinylidene complexes 9j and 9h by NMR spectroscopy

20 mg **1** (26.9 μmol) was added to an NMR tube fitted with a PTFE Young's tap. 500 μL CD_2Cl_2 was added *via* microliter syringe under N_2. TMS and was added as internal standard and the ^1H and $^{31}P\{^1H\}$ NMR spectra recorded at the temperature to be monitored. One equivalent of the appropriate alkyne (3.5 μL **8j**, 26.9 μmol; 1.60 μL **8h**, 26.9 μmol) was then added to the NMR tube whilst immersed in a water bath thermostatted to the appropriate temperature. The sample was shaken vigourously before being placed into the NMR spectrometer. A ^1H NMR spectrum was recorded periodically over a number of hours as indicated below. All temperatures reported are uncalibrated.

290 K: ^1H NMR spectra recorded at 20 m intervals over 6 h

295 K: ^1H NMR spectra recorded at 20 m intervals over 4 h

300 K: ^1H NMR spectra recorded at 20 m intervals over 16 h

305 K: ^1H NMR spectra recorded at 15 m intervals over 16 h

310 K: ^1H NMR spectra recorded at 8 m intervals over 16 h

315 K: ^1H NMR spectra recorded at 10 m intervals over 16 h

320 K: ^1H NMR spectra recorded at 5 m intervals over 16 h

Addition of Bu_4NOAc: 8.1 mg (26.9 μmol) Bu_4NOAc was added to the NMR tube at the same point as the TMS internal standard.

Addition of PhOH: 2.5 mg (26.9 μmol) PhOH was added to the NMR tube at the same point as the TMS internal standard.

7: Synthesis and Characterisation of novel Ruthenium Oxacyclocarbene complexes.

7.1: Introduction

The preceding chapters have described how complex **1** is highly reactive towards terminal alkynes resulting in the rapid formation of vinylidene and hydroxy-vinylidene complexes. Hydroxy-vinylidene complexes were obtained upon addition of propargylic alcohols of the general form HC≡CCRR'OH to complex **1**. It was proposed that this work be extended towards terminal alkynes containing longer alkyl chains, such as $HC{\equiv}C(CH_2)_n(OH)$. These substrates, also known as *ω*-alkynols, may react with transition-metal centres of groups 6 – 10 to give another type of carbene ligand: an oxacyclocarbene.[1] These complexes are thought to form *via* the intramolecular nucleophilic attack of the OH group onto the electrophilic C_α of an intermediate vinylidene complex,[2-4] as demonstrated in Figure 7.1.1:

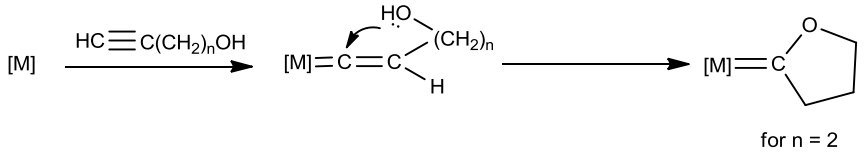

Figure 7.1.1: Formation of an oxacyclocarbene complex.

These carbene ligands are technically Fischer-type carbenes, which have been known since the 1970s. The most commonly observed forms contain five or six[5-7] membered rings, though examples of seven[4,8,9] membered rings are known. Attempts have been made to utilise this cycloisomerisation catalytically, with positive results obtained in generating either *endo*- or *exo*-products.[10-13] It is thought that the *endo*-cycloisomerisation reaction occurs *via* a vinylidene intermediate undergoing *anti*-Markovnikov intramolecular attack of the OH group, as observed in the formation of oxacyclocarbene shown in Figure 7.1.1.[14] Such a transformation has been made catalytic using $[Ru(N_3P)(OAc)]BPh_4$, which is derived from complex **1** (N_3P = *N*,*N*-bis[(pyridine-2-yl)methyl][2-(diphenylphosphino)phenyl]methanamine). The *exo*-cycloisomerisation is thought to proceed *via* the Markovnikov addition of the OH moiety onto the C_β of the π-

bound alkyne; this has been utilised in the formation of furan derivatives by $[RuCl_2(p\text{-cymene})(PPh_3)]$.[15] Both mechanisms are illustrated in Figure 7.1.2.

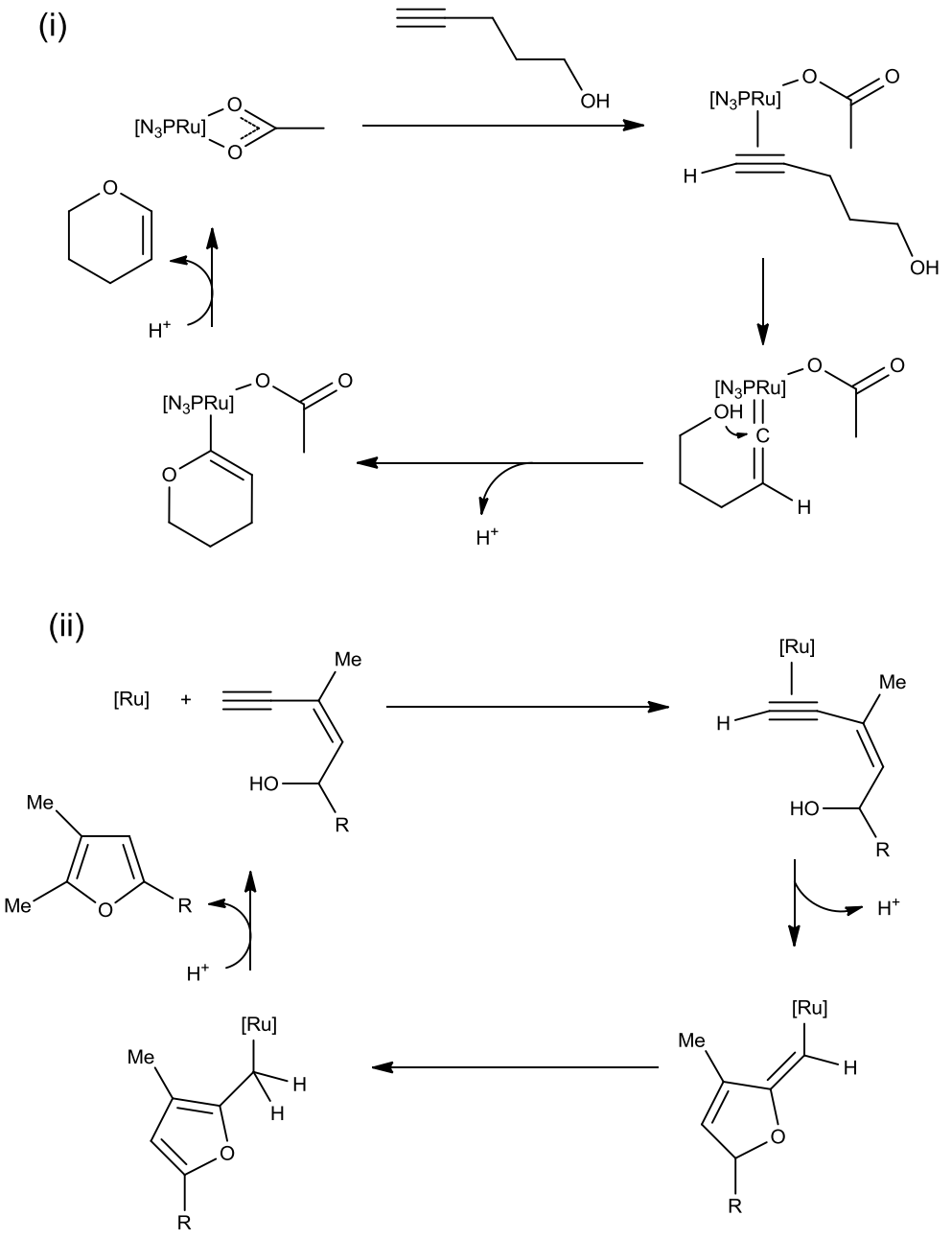

Figure 7.1.2: *Anti*-Markovnikov (**i**) and Markovnikov (**ii**) pathways for the *exo*- and *endo*-cycloisomerisation of alkynols.

As complex **1** has proven to exhibit high selectivity towards terminal alkynes, the reaction of complex **1** with ω-alkynols was considered a natural extension of this chemistry. Consequently, attempts were made to synthesise five, six and seven-membered oxacyclocarbene ligands.

7.2: Synthesis and Characterisation of Five- Six and Seven-Membered Oxacyclocarbene Complexes.

The addition of the ω-alkynols $HC{\equiv}C(CH_2)_nOH$ where n = 2 or 3 to a solution of complex **1** in DCM resulted in the rapid formation of the oxacyclocarbene complexes **21a** and **21b**, incorporating five and six membered rings respectively. The reaction is rapid, and no trace of an intermediate hydroxy-vinylidene complex could be detected when the reaction was conducted on a NMR scale. The complexes are reasonably stable in solution; analysis of a NMR sample of **21a** after two days revealed that little change had occurred.

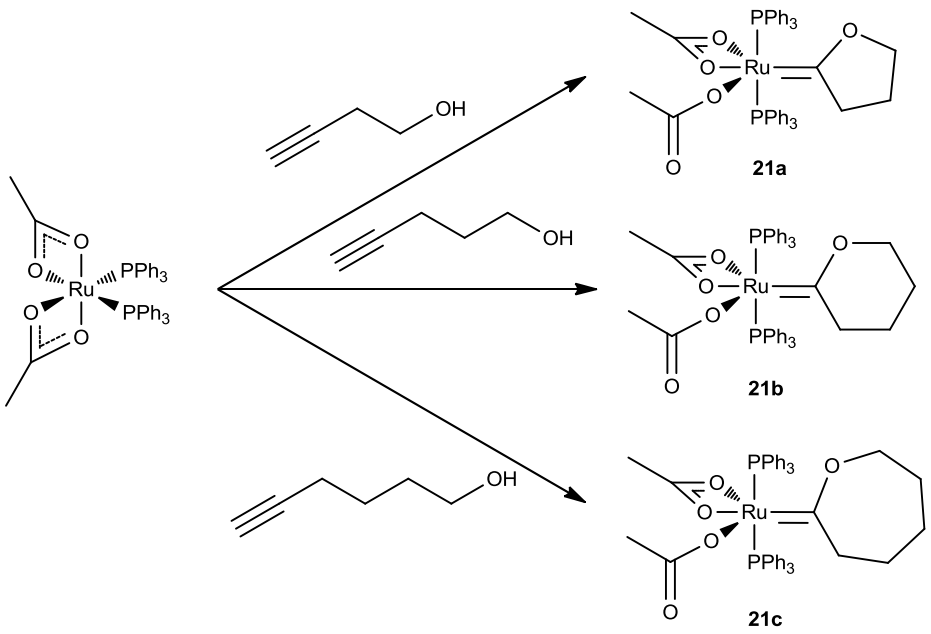

Figure 7.2.1: Formation of oxacyclocarbene complexes **21a-c**.

The formation of the seven membered oxacyclocarbene complex **21c** required a longer reaction time: addition of the ω-alkynol $HC{\equiv}C(CH_2)_4OH$ to a CD_2Cl_2 solution of complex **1** resulted in the gradual formation of **21c**, as shown by NMR spectroscopy. Resonances assigned to complex **1** and $HC{\equiv}C(CH_2)_4OH$ in the ^1H and $^{31}P\{^1H\}$ NMR spectra were gradually replaced by those due to **21c** over a period of 24 hours. Despite this slow rate of reaction, a hydroxy-vinylidene intermediate could not be detected. A slower rate of formation of 7-membered oxacyclocarbenes has been noted by another group.[9] Gamasa has suggested "…that the intramolecular attack of the hydroxy group on the vinylidene group to generate the oxacyclocarbene complexes takes place at a rate similar for 3-butyn-1-ol and 4-pentyn-1-ol and

becomes increasingly disfavoured for 5-hexyn-1-ol…" They were also able to isolate an intermediate hydroxy-vinylidene complex for this transformation.

These complexes also exhibit characteristic NMR and IR spectroscopic features. These are summarised in Tables 7.2.1, 7.2.2 (NMR) and 7.2.4 (IR).

Complex	^{1}H δ_H CH_3COO	^{31}P δ_P PPh_3	^{13}C δ_C C_α	^{13}C $^{2}J_{CP}$/Hz
21a	0.82	35.9	304.7	11.8
21b	0.83	35.4	306.8	11.7
21c	0.84	34.2	311.0	11.8

Table 7.2.1: Common characteristic NMR features of complexes **21a-c**.

	^{1}H δ_H OCH_2	^{1}H δ_H =CCH_2	^{1}H δ_H CH_2	^{13}C δ_C OCH_2	^{13}C δ_C =CCH_2	^{13}C δ_C CH_2
21a	3.90 (t, 7.3 Hz)	2.48 (t, 7.7 Hz)	0.93 (qn, 7.5 Hz)	79.2	52.8	22.6
21b	3.85 (t, 5.8 Hz)	2.61 (t, 6.9 Hz)	1.02 (qn, 6.1 Hz) 0.77 (qn, 6.9 Hz)	72.3	47.2	17.0, 22.6
21c	3.85 (t, 4.2 Hz)	2.72 (br s)	0.67 (m) 0.91 (m) 1.16 (m)	74.6	50.8	20.4, 28.4, 29.2

Table 7.2.2: ^{1}H and ^{13}C{^{1}H} NMR features for the oxacyclocarbene rings of **21a-c**[ii]

The NMR features observed for complexes **21a-c** are consistent with those observed for similar complexes in this thesis. A singlet resonance is observed at δ_H 0.82-0.84 for the protons of the acetate ligand in the ^{1}H NMR spectrum, once more suggesting the two ligands are undergoing an exchange that is rapid on the NMR timescale. Resonances due to the oxacyclocarbene ring protons were assigned based on the literature convention[16,4,9] that the most deshielded resonance corresponds to the OCH_2 protons whilst the second most deshielded resonance observed corresponds to the =CCH_2 protons. Rossi[4] confirmed these assignments based on a number of 1D and 2D NMR data on his compounds [$ReCl_2(\eta^1$-*N*-$N_2COPh)(=C\{CH_2\}_nCHRO)(PPh_3)_3$] (n = 1, 2; R = H, Me).

ii NMR spectra of complexes **21a** and **21b** were recorded on a Bruker Avance 500 MHz spectrometer whereas **21c** was recorded on a JEOL 400 MHz machine

The chemical shift values of the PPh_3 ligands in the $^{31}P\{^1H\}$ NMR spectrum again indicate that the two equivalent phosphine ligands adopt a mutually *trans*-orientation. The C_α of the carbene ligand is typical for a carbene of this type, and is observed at a lower δ_C value than vinylidene complexes **2a-d** and **9a-n** (both ca. δ_C 350), due to the greater electrophilic character of the hydroxy-vinylidene ligand. The resonance is again observed as a triplet with a $^2J_{PC}$ of 11.7 / 11.8 Hz. As for the ^1H NMR spectrum, the assignments for the carbon atoms of the oxacyclocarbene ligand are observed in a trend in which the carbon adjacent to the oxygen atom is at a higher chemical shift than the others, whilst the $=C\mathit{C}H_2$ atom is second most deshielded. It has been suggested that the chemical shift values of C_α are sensitive to ring size, with the value increasing with ring size.[5] Complexes **21a-c** conform to this trend, as do others reported in the literature,[4,8,9] as demonstrated in Table 7.2.3.

[M]	**^{13}C δ_C C_α [M]=C_4H_6O**	**^{13}C δ_C C_α [M]=C_5H_8O**	**^{13}C δ_C C_α [M]=$C_6H_{10}O$**
$[Ru(OAc_2)_2(PPh_3)_2]$	304.7	306.8	311.0
$[RuTp(PPh_2{}^iPr)]Cl$	313.2	318.3	323.7
$[RuTp(PPh_3)]Cl$	314.4	320.2	325.0
$[Ru(\eta^5\text{-}C_9H_7)(PPh_3)_2]$	296.3	302.5	306.8
$[Ru(\eta^5\text{-}C_9H_7)(PMe_2Ph)_2]$	295.1	302.5	306.7
$[Ru(\eta^5\text{-}C_9H_7)(dppm)]$	300.3	308.1	312.5
$[Ru(\eta^5\text{-}C_9H_7)(PPh_3)(PMe_3)]$	296.8	303.9	307.5
$[Re(triphos)(CO)_2]BF_4$	293.4	303.0	310.8

Table 7.2.3: Comparison of δ_C value of the C_α of 5-, 6-, and 7-membered oxacyclocarbene complexes (triphos = $MeC\{CH_2PPh_2\}_3$).

The IR spectra of complexes **21a-c** exhibit symmetric and asymmetric stretches for both monodentate and chelate coordination modes that are consistent with those observed for other complexes reported in this thesis with a similar structure. The magnitude of κ^2-$\Delta\upsilon$ is the largest reported in this thesis. A further comparison of these features is discussed in Chapter 8.

Complex	P–Ph	κ^1-OCO_{sym}	κ^1-OCO_{asym}	κ^1-$\Delta\upsilon$	κ^2-OCO_{sym}	κ^2-OCO_{asym}	κ^2-$\Delta\upsilon$
21a (DCM)	1433	1375	1615	240	1448	1540	92
21a (KBr)	1433	1368	1616	248	1447	1541	94
21b (DCM)	1434	1375	1613	238	1447	1545	98
21b (KBr)	1432	1375	1615	240	1446	1549	103
21c (DCM)	1433	1382	1607	225	1452	1548	96
21c (KBr)	1433	1382	1608	225	1450	1546	96

Table 7.2.4: Common characteristic IR features of complexes **21a-c**.

A low temperature NMR study was also conducted on these complexes. Coalescence of the singlet resonance due to the six acetate protons in the ^{1}H NMR spectrum was observed at approximately 190 – 215 K for complexes **9a**, **9d**, **9e** and **9g** (see Section 5.2). Upon cooling solutions of complexes **21a** and **21b** in CD_2Cl_2 to 185 K, the resonance due to the acetate protons broadened and eventually coalesced. Using equations 5.2.1 and 5.2.4, the rate of coalescence (k_{coal}) and energy barrier to exchange ($\Delta G^{\ddagger}$) could be calculated. The values obtained are shown in Table 7.2.4 and are similar to those obtained for the hydroxy-vinylidene and vinylidene complexes. For **21c**, cooling to 195 K resulted in the broadening of the resonance due to the acetate protons; however as for complexes **9f** and **9i**, other resonances in the region began to obscure the peak of interest so the extent of coalescence could not be determined.

Complex	δ_v at T_c / s^{-1}	T_c / K	k_{coal} / s^{-1}	$\Delta G^{\ddagger}$ / kJ mol^{-1}
21a	203.0	185	451.0	35.2
21b	146.5	185	325.4	35.7

Table 7.2.4: Temperature of coalescence, rate and free energy of exchange for compounds **21a** and **b**.

Crystals of complexes **21a-c** suitable for X-ray diffraction were grown by the slow diffusion of pentane into DCM solutions of these complexes. ORTEP figures of the resulting structures are given in Figures 7.2.2, 7.2.3 and 7.2.4 for complexes **21a**, **21b** and **21c** respectively, along with relevant bond lengths and angles in Tables 7.2.5, 7.2.6 and 7.2.7.

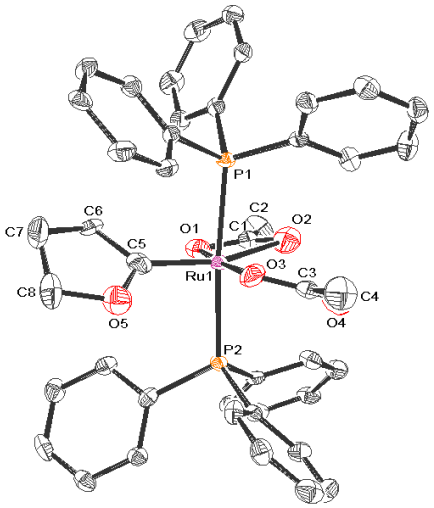

Figure 7.2.2: ORTEP diagram of **21a**, thermal ellipsoids at the 50 % probability level. Hydrogen atoms and two molecules of DCM omitted for clarity.

Bond Length	**(Å)**	**Bond Angle**	**(deg / °)**
Ru – P(1)	2.3840(14)	P(1) – Ru – P(2)	173.69(5)
Ru – P(2)	2.3642(14)	P(1) – Ru – O(1)	97.81(10)
Ru – O(1)	2.204(4)	P(1) – Ru – O(2)	85.53(11)
Ru – O(2)	2.355(4)	P(1) – Ru – O(3)	82.52(11)
Ru – O(3)	2.058(4)	O(1) – Ru – O(2)	56.40(15)
Ru – C(5)	1.878(6)	O(1) – Ru – O(3)	170.95(16)
C(5) – O(5)	1.343(7)	O(2) – Ru – O(3)	114.74(16)
C(5) – C(6)	1.474(8)	P(1) – Ru – C(5)	89.88(17)
		P(2) – Ru – C(5)	92.92(17)
		O(1) – Ru – C(5)	96.6(2)
		O(2) – Ru – C(5)	151.5(2)
		O(3) – Ru – C(5)	92.4(2)
		Ru – C(5) – O(5)	124.0(4)
		Ru – C(5) – C(6)	126.5(4)

Table 2.2.5: Selected Bond Lengths and Angles for **21a**.

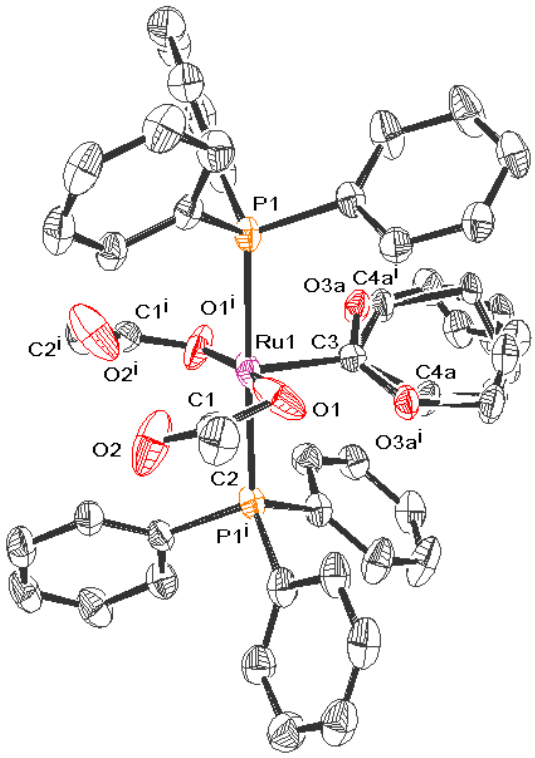

Figure 7.2.3: ORTEP diagram of **21b**, thermal ellipsoids at the 50 % probability level. Hydrogen atoms and one molecules of DCM omitted for clarity.

Bond Length	**(Å)**	**Bond Angle**	**(deg / °)**
Ru – P(1)	2.3734(5)	P(1) – Ru – O(1)	84.71(5)
Ru – O(1)	2.104(2)	P(1) – Ru – C(3)	89.30(2)
Ru – C(3)	1.865(3)	O(1) – Ru – C(3)	95.45(7)
C(3) – O(3a)	1.357(4)	P(1) – Ru – O(1^{i})	95.43(5)
C(3) – C(4a)	1.488(8)	P(1) – Ru – P(1^{i})	178.60(4)
		O(1) – Ru – O(1^{i})	169.10(13)
		C(4a) – C(3) – Ru	129.4(2)
		O(3a) – C(3) – Ru	113.1(2)

Table 2.2.6: Selected Bond Lengths and Angles for **21b**.

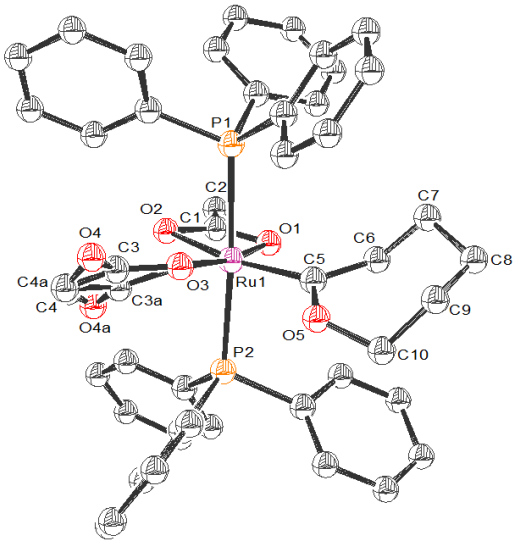

Figure 7.2.4: ORTEP diagram of **21c**, thermal ellipsoids at the 50 % probability level. Hydrogen atoms omitted for clarity.

Bond Length	**(Å)**	**Bond Angle**	**(deg / °)**
Ru – P(1)	2.3891(8)	P(1) – Ru – P(2)	175.91(3)
Ru – P(2)	2.3591(8)	P(1) – Ru – O(1)	92.03(6)
Ru – O(1)	2.126(2)	P(1) – Ru – O(2)	84.79(6)
Ru – O(2)	2.325(2)	P(1) – Ru – O(3)	82.38(6)
Ru – O(3)	2.086(2)	O(1) – Ru – O(2)	58.92(8)
Ru – C(5)	1.902(3)	O(1) – Ru – O(3)	170.96(9)
C(5) – O(5)	1.317(4)	O(2) – Ru – O(3)	113.25(8)
C(5) – C(6)	1.498(4)	P(1) – Ru – C(5)	96.05(9)
		P(2) – Ru – C(5)	87.67(9)
		O(1) – Ru – C(5)	98.29(11)
		O(2) – Ru – C(5)	157.19(11)
		O(3) – Ru – C(5)	89.40(12)
		Ru – C(5) – O(5)	121.5(2)
		Ru – C(5) – C(6)	120.6(2)

Table 2.2.7: Selected Bond Lengths and Angles for **21c**.

The structure obtained for complex **21a** is very similar to the majority of crystal structures reported in this thesis in that the κ^2-OAc ligand places constraints on the structure so it adopts that of a distorted octahedron. The Ru – C(1) bond length of 1.865(3) Å is similar to those of other ruthenium complexes containing a five-membered oxacyclocarbene. Kirchner reported a Ru=C bond length of 1.921(2) Å in the complex $[RuTp(PPh_3)_2(=C_4H_6O)]$[8] whilst Whiteley reported a distance of 1.92(1) Å for the complex $[RuCp(dppe)(=C_4H_6O)]PF_6$.[16] Leung reported a carbene bond length of 1.870(13) Å for the complex $[Ru(L_{OEt})(PPh_3)_2(=C_4H_6O)]PF_6$[17] whilst Jia has recently reported a bond length of 1.906(4) for the complex $[Ru(N_3P)(\kappa^1$-OAc$)(=C_4H_6O)]BPh_4$ (where L_{OEt} = $[CoCp\{P(O)(OEt)_2\}_3]$ and N_3P = *N*,*N*-bis[(pyridin-2-yl)methyl][2-diphenylphopshino)phenyl]methanamine))[18]

The structure obtained for complex **21b** is unlike any other reported in this thesis. The complex crystallises in the orthorhombic space group *Aba2*, whilst the majority of structures reported in this thesis are in either the triclinic space group *P-1* or the monoclinic space groups *P2(1)/c* or *P2(1)/n*. The asymmetric unit contains half the molecule, consisting of a ruthenium atom bonded to one PPh_3 ligand and one κ^1-OAc ligand, and the six-membered oxacyclocarbene ligand. The ORTEP diagram shown in Figure 7.2.3 illustrates the complete molecule, with atoms labelled with a superscript ^{i} being generated by symmetry. The structure indicates that both OAc ligands must be monodentate; the Ru – O(2) is measured to be 2.748 Å which is significantly longer than the Ru – O(1) distance of 2.104(2). This conflicts with the NMR and IR characterisation data recorded in both solid and solution state reported earlier in this section which indicates that **21b** contains both κ^1- and κ^2-OAc ligands. It is therefore proposed that the structure obtained is merely the form of the complex in the crystal selected for structural characterisation. It was also noted that the oxacyclocarbene ligand was disordered by a mirror plane and in the C(5) and C(6) position. Consequently, these positions were modelled in a refined occupancy of 27:23. This disorder also makes it difficult to determine if the six-membered ring adopts a 'chair-' or 'boat-'like conformation.

The carbene bond length observed in complex **21b** is comparable to that of **21a** and also to other ruthenium complexes containing a six-membered oxacyclocarbene; Whiteley reported that $[RuCp(dppe)(=C_5H_8O)]PF_6$[16] exhibits a Ru=C bond length of 1.938(4) Å.

The structure obtained for **21c** is also that of a distorted octahedron with a small O(1) – Ru – O(2) angle of 58.92(8) °. The Ru – C(5) distance of the oxacyclocarbene ligand is slightly longer than those observed for complexes **21a** and **21b** at 1.902(3) Å, but is still well within an acceptable range for an oxacyclocarbene ligand. Only one other crystal structure containing a seven-membered oxacyclocarbene ligand could be located in the literature, reported by Gamasa in 2002.[9] The complex $[Ru(=C_6H_{10}O)(\eta^5\text{-}C_9H_7)(PPh_3)_2]PF_6$ exhibits a Ru=C distance of 1.89(1) Å, which is only slightly shorter than that observed in **21c**. The κ^1-OAc ligand exhibits some disorder so has been modelled in two positions with a refined occupancy ratio of 82.2:17.8. The seven-membered ring also appears to adopt a "pseudochair"-like conformation.

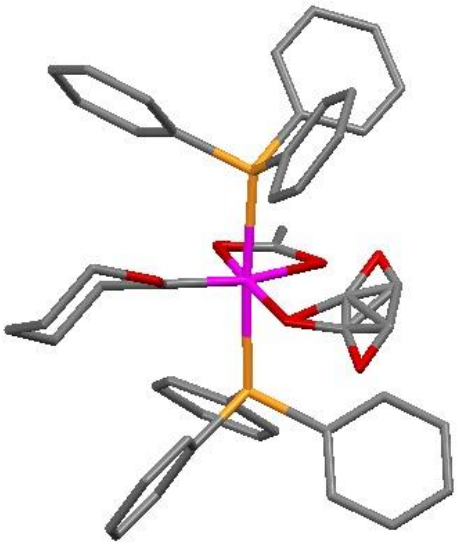

Figure 7.2.5: The "pseudochair" orientation of the oxacyclocarbene ligand of **21c**.

At this point, it becomes pertinent to discuss and compare the orientation of the vinylidene and oxacyclocarbene ligands of this system. The crystal structures obtained of complexes **2a**, **2b**, **2c**, **9a**, **9c** and **9e** all demonstrate that the vinylidene ligand adopts the expected horizontal orientation (see Section 1.2). However the oxacyclocarbene ligands of complexes **21a-c** deviate significantly from the predicted vertical orientation of the carbene ligand. Complex **21a** deviates by 48.9 ° from the vertical plane in which the phosphine ligands sit, whilst complex **21b** displays a larger deviation of 64.5 °. Complex **21c** exhibits an almost horizontal oxacyclocarbene ligand which has deviated from the vertical plane by 70.3 °. This

deviation is not uncommon and other oxacyclocarbene complexes have also shown a similar aberration, for example Gamasa's $[Ru(=C_6H_{10}O)(\eta^5\text{-}C_9H_7)(PPh_3)_2]PF_6$ exhibits a deviation of 29.7(5) °. As noted in Section 1.2, the R-substituents of vinylidene ligands typically adopt a horizontal orientation whilst those of carbene and allenylidene ligands adopt a vertical configuration with respect to the metal-ligand plane. An interesting exception to this has been probed extensively by Whiteley, who has shown that the relative orientations of carbene, vinylidene and allenylidene ligands in the $[Mo(\eta^7\text{-}C_7H_7)(L)_2]$ fragment are the reverse of those found in Ru and Fe half-sandwich analogues.[5]

By virtue of containing carbene ligands, complexes **21a**, **21b** and **21c** exhibit slightly longer Ru=C bonds than complexes that contain vinylidene or hydroxy-vinylidene ligands. The following chapter provides a full comparison of the common and interesting structural and spectroscopic features of all acetate-containing complexes reported in this thesis.

7.3: Conclusions

Three novel oxacyclocarbene complexes (**21a-c**) containing five-, six- and seven-membered rings were synthesised upon addition of the appropriate *ω*-alkynol to the precursor complex **1**. It is thought that these complexes form *via* an intermediate hydroxy-vinylidene complex; however such a complex was not detected in the course of our studies. These complexes exhibited a number of spectroscopic and structural features that were similar to those exhibited by other acetate-containing complexes reported in this thesis. As such, a full comparison of all novel complexes derived from the precursor complex **1** over the course of this PhD is provided in the following chapter.

7.4: References

1. Weyershausen, B.; Dötz, K. H. *Eur. J. Inorg. Chem.* **1999**, 1057.
2. Bruce, M. I.; Swincer, A. G.; Thomson, B. J.; Wallis, R. C.; *Aust. J. Chem.* **1980**, *33*, 2605.
3. Dötz, K. H.; Sturm, W. *Organometallics* **1987**, *6*, 1424.
4. Bianchini, C.; Marchi, A.; Mantovani, N.; Marvelli, L.; Masi, D.; Peruzzini, M.; Rossi, R. *Eur. J. Inorg. Chem.* **1998**, 211.
5. Grime, R. W.; Helliwell, M.; Hussain, Z. I.; Lancashire, H. N.; Mason, C. R.; McDouall, J. J. W.; Mydlowski, C. M.; Whiteley, M. W. *Organometallics* **2008**, *27*, 857.
6. Marvelli, L.; Mantovani, N.; Marchi, A.; Rossi, R.; Brugnati, M.; Peruzzini, M.; Barbaro, P.; de los Rios, I.; Bertolasi, V. *Dalton Trans.* **2004**, 713.
7. Beddoes, R. L.; Grime, R. W.; Hussain, Z. I.; Whiteley, M. W. *J. Chem. Soc. Dalton. Trans.* **1996**, 3893.
8. Pavlik, S.; Mereiter, K.; Puchberger, M.; Kirchner, K. *J. Organomet. Chem.* **2005**, *690*, 5497.
9. Gamasa, M. P.; Gimeno, J.; Martín-Vaca, B. M.; Isea, R.; Vegas, A. *J. Organomet. Chem.* **2002**, *651*, 22.
10. Marchal, E.; Uriac, P.; Legouin, B.; Toupet, L.; van deWeghe P. *Tetrahedron*, **2007**, *63*, 9979.
11. Geier, M. J.; Vogels, C. M.; Decken, A.; Westcott, S. A. *Eur. J. Inorg. Chem.* **2010**, 4602.
12. Varela-Fernández, A.; García-Yebra, C.; Varela, J. A.; Esteruelas, M. A.; Saá, C.; *Angew. Chem. Int. Ed*. **2010**, *49*, 4278.
13. Jiménez-Tenorio, M., Puerta, M. C., Valerga, P., Moreno-Dorado, F.J.; Guerra, F. M.; Massanet, G. M. *Chem. Commun.* **2001**, 2324.

14. Liu, P. N.; Su, F. H.; Wen, T. B.; Sung, H. H.-Y.; Williams, I. D.; Jia, G. *Chem. Eur. J.* **2010**, *16*, 7889.

15. Seiller, B.; Bruneau, C.; Dixneuf, P. H. *J. Chem. Soc. Chem. Commun.* **1994**, 493.

16. Beddoes, R.L.; Grime, R. W.; Hussain, Z. I.; Whiteley, M. W. *J. Organomet. Chem.* **1996**, *526*, 371.

17. Leung,W-H.; Chan,E. Y. Y.; Williams,I D.; Wong W-T. *Organometallics* **1997**, *16*, 3234.

18. Liu, P.N.; Wen, T. B.; Ju, K. D.; Sung, H. H.-Y.; Williams, I. D.; Jia, G. *Organometallics* **2011,** *30*, 2571.

19. Dolomanov, O. V.; Bourhis, L. J.; Gildea, R. J.; Howard J. A. K.; Puschmann, H. *J. Appl. Cryst. 2009*, **42**, 339.

7.5: Experimental

General:

All experimental procedures were performed under an atmosphere of dinitrogen or argon using standard Schlenk Line and Glove Box techniques. DCM, pentane and hexane were purified with the aid of an Innovative Technologies anhydrous solvent engineering system. The CD_2Cl_2 used for NMR experiments was dried over CaH_2 and degassed with three freeze-pump-thaw cycles. The solvent was then vacuum transferred into NMR tubes fitted with PTFE Young's taps. NMR spectra were acquired on a Bruker AVANCE 500 (Operating Frequencies ^{1}H 500.23 MHz, ^{31}P 202.50 MHz, ^{13}C 125.77 MHz) with the exception of the ^{13}C NMR spectrum of **21c** recorded on a JEOL 400 (^{1}H 399.78 MHz, ^{13}C 100.53 MHz). ^{31}P and ^{13}C spectra were recorded with proton decoupling. Mass spectrometry measurements were performed on a Thermo-Electron Corp LCQ Classic (ESI) instrument or Waters GCT Premier Acceleration TOF MS (LIFDI). IR spectra were acquired on a Thermo-Nicolet Avatar 370 FTIR spectrometer using either CsCl solution cells or as KBr discs. CHN measurements were performed using an Exeter Analytical Inc. CE-440 analyser. The proportion of DCM in CHN samples was confirmed by recording a ^{1}H NMR spectrum of a sample used for CHN analysis in d_8-toluene. Relative integration of the peak at δ_H 4.31 (CH_2Cl_2) to that of the vinylidene proton indicates the proportion of DCM in that sample. Structural characterisation of complexes **21a-c** was conducted using a Bruker Smart Apex diffractomer with Mo K_α radiation (λ = 0.71073 Å) with a SMART CCD camera. Diffractometer control, data collection and initial unit cell determination was performed using SMART. Frame integration and unit-cell refinement software was carried out with Saint+. Absorption corrections were applied by SADABS (v 2.03, Sheldrick). Structures **21a** and **21b** were solved by direct methods using SHELXS-97, and refined by full-matrix least-squares using SHELX-97. The structure of **21c** was solved and refined using Olex2[19] implementing SHELX algorithms. All non-hydrogen atoms were refined anisotropically. Hydrogen atoms were placed using a "riding model" and included in the refinement at calculated positions. Alkynes $HC{\equiv}C(CH_2)_nOH$ n = 2,3,4 (Sigma-Aldrich) were used as supplied without further purification.

Key to NMR abbreviations:

s (singlet); br s (broad singlet); d (doublet); dd (doublet of doublets); ad (apparent doublet); t (triplet); dt (doublet of triplets); tt (triplet of triplets); at (apparent triplet); q (quartet); aq (apparent quartet); qn (quintet), aqn (apparent quintet); sp (septet); asp (apparent septet); m (multiplet)

(H_2-Ph) or (H_2-PPh_3) refers to the proton in the *ortho*-position of a phenyl ring

(H_3-Ph) or (H_3-PPh_3) refers to the proton in the *meta*-position of a phenyl ring

(H_4-Ph) or (H_4-PPh_3) refers to the proton in the *para*-position of a phenyl ring

General Procedure for the synthesis of complexes 21a-c

Approximately one equivalent of the alkyne was added to a Schlenk vessel containing a solution of **1** in CH_2Cl_2. After stirring for one hour* at room temperature the product was precipitated by addition of pentane/hexane. After filtration of the solvent by a cannula wire fitted with a filter-paper tip, the solid powder was washed twice more with pentane/hexane and dried *in vacuo*.

Minor modifications were made to this procedure for **21c**: * the mixture was stirred for 28 hours at room temperature and the CH_2Cl_2 solvent was entirely removed *in vacuo* before the product was washed with pentane.

7.5.1: Synthesis of [Ru(κ^1-OAc)(κ^2-OAc)(=CO(CH$_2$)$_3$)(PPh$_3$)$_2$] 21a.

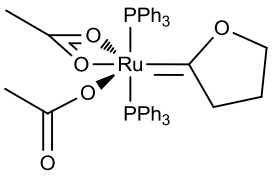

0.04 g **21a** (19.0 %) was obtained as a bright yellow powder from 0.20 g (0.27 mmol) **1** and 20.0 μL (0.26 mmol) HC≡C(CH$_2$)$_2$OH in 15 mL DCM. After reducing the volume of the solution by half *in vacuo*, 40 mL pentane was used to precipitate the product, and it was washed further with 2 x 20 ml portions of pentane. Crystals for X-ray diffraction were obtained from a CH_2Cl_2/pentane solution.

NMR Spectra CD_2Cl_2:

^{1}H δ_H 0.82 (s, 6H, C*H*$_3$COO), 0.93 (qn, $^3J_{HH}$ = 7.5 Hz, 2H, C*H*$_2$), 2.48 (t, $^3J_{HH}$ = 7.7 Hz, 2H, =CC*H*$_2$), 3.90 (t, $^3J_{HH}$ = 7.3 Hz, 2H, OC*H*$_2$), 7.37 (at, 7.2 Hz, 12H, *H*$_3$-P*Ph*$_3$), 7.42 (t, 7.1 Hz, 6H, *H*$_4$-P*Ph*$_3$), 7.54 (m, 12H, 12H, *H*$_2$-P*Ph*$_3$)

^{31}P δ_P 35.9 (s, 2.0P, *P*Ph$_3$)

^{13}C δ_C 21.9 (s, *C*H$_3$COO), 22.6 (s, *C*H$_2$), 52.8 (s, =C*C*H$_2$), 79.2 (s, O*C*H$_2$), 127.8 (t, $^3J_{PC}$ + $^5J_{PC}$ = 9.3 Hz, PPh$_3$–*C*$_3$), 129.4 (s, PPh$_3$–*C*$_4$), 132.9 (t, $^1J_{PC}$ + $^3J_{PC}$ = 39.3 Hz, PPh$_3$–*C*$_1$), 134.4 (t, $^2J_{PC}$ + $^4J_{PC}$ = 11.8 Hz, PPh$_3$–*C*$_2$), 180.0 (s, CH$_3$*C*OO), 304.7 (t, $^2J_{PC}$ = 11.8 Hz, [Ru]=*C*)

IR (KBr) 1368 cm^{-1} (κ^1-OCO$_{sym}$), 1433 cm^{-1} (P–Ph), 1481 cm^{-1} (κ^2-OCO$_{sym}$), 1541 cm^{-1} (κ^2-OCO$_{asym}$), 1616 cm^{-1} (κ^1-OCO$_{asym}$), $\Delta\nu_{(uni)}$ 248 cm^{-1}, $\Delta\nu_{(chelate)}$ 60 cm^{-1}; (CH_2Cl_2) 1375 cm^{-1} (κ^1-OCO$_{sym}$), 1433 cm^{-1} (P–Ph), 1483 cm^{-1} (κ^2-OCO$_{sym}$), 1540 cm^{-1} (κ^2-OCO$_{asym}$), 1615 cm^{-1} (κ^1-OCO$_{asym}$), $\Delta\nu_{(uni)}$ 240 cm^{-1}, $\Delta\nu_{(chelate)}$ 57 cm^{-1}.

MS (ESI) m/z 796.1615 (Expected for $^{101}RuP_2O_3NC_{44}H_{42}$ [M - OAc$^-$ + MeCN]$^+$ = 796.1683); (LIFDI) m/z 814 (Expected for $^{101}RuP_2O_5C_{44}H_{42}$ [M]$^+$ = 814.1551)

CHN Anal. for $RuP_2O_5C_{44}H_{42}$ + (0.20 CH_2Cl_2) (calc), C 63.90, H 5.14; (found) C 63.90, H 5.14.

Crystal data and structure refinement for 21a.

Identification code	jml0911m	
Empirical formula	$RuP_2O_5Cl_4C_{46}H_{46}$	
Formula weight	983.64	
Temperature	110(2) K	
Wavelength	0.71073 Å	
Crystal system	Monoclinic	
Space group	P2(1)/n	
Unit cell dimensions	a = 14.328(2) Å	α= 90°.
	b = 21.311(3) Å	β= 105.083(3)°.
	c = 15.088(2) Å	γ = 90°.
Volume	4448.4(12) $Å^3$	
Z	4	
Density (calculated)	1.469 Mg/m^3	
Absorption coefficient	0.710 mm^{-1}	
F(000)	2016	
Crystal size	0.21 x 0.06 x 0.03 mm^3	
Theta range for data collection	1.69 to 25.03°.	
Index ranges	-17<=h<=17, -25<=k<=25, -17<=l<=17	
Reflections collected	34027	
Independent reflections	7825 [R(int) = 0.0891]	
Completeness to theta = 25.03°	99.7 %	
Absorption correction	Semi-empirical from equivalents	
Max. and min. transmission	0.979 and 0.822	
Refinement method	Full-matrix least-squares on F^2	
Data / restraints / parameters	7825 / 0 / 525	
Goodness-of-fit on F^2	1.015	
Final R indices [I>2sigma(I)]	R1 = 0.0592, wR2 = 0.1288	
R indices (all data)	R1 = 0.1070, wR2 = 0.1514	
Largest diff. peak and hole	1.278 and -1.124 e.$Å^{-3}$	

7.5.2: Synthesis of [Ru(κ^1-OAc)(κ^2-OAc)(=CO(CH$_2$)$_4$)(PPh$_3$)$_2$] 21b.

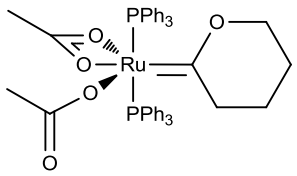

0.03 g **21b** (11.1 %) was obtained as a bright yellow powder from 0.25 g (0.33 mmol) **1** and 32.0 μL (0.34 mmol) HC≡C(CH$_2$)$_3$OH in 30 mL DCM. After reducing the volume of the solution by half *in vacuo*, 20 mL pentane was used to precipitate the product, and it was washed further with 2 x 20 ml portions of pentane. Crystals for X-ray diffraction were obtained from a CD_2Cl_2/ pentane solution.

NMR Spectra CD_2Cl_2:

^{1}H δ_H 0.77 (qn, $^3J_{HH}$ = 6.9 Hz, 2H, C*H*$_2$), 0.83 (s, 6H, C*H*$_3$COO), 1.02 (qn, $^3J_{HH}$ = 6.1 Hz, 2H, C*H*$_2$), 2.61 (t, $^3J_{HH}$ = 6.9 Hz, 2H, =CC*H*$_2$), 3.85 (t, $^3J_{HH}$ = 5.8 Hz, 2H, OC*H*$_2$), 7.38 (at, 7.18 Hz, 12H, *H*$_3$-P*Ph*$_3$), 7.42 (t, 7.1 Hz, 6H, *H*$_4$-P*Ph*$_3$), 7.56 (m, 12H, 12H, *H*$_2$-P*Ph*$_3$)

^{31}P δ_P 35.4 (s, 2.0P, *P*Ph$_3$)

^{13}C δ_C 17.0 (s, *C*H$_2$), 21.6 (s, *C*H$_3$COO), 22.6 (s, *C*H$_2$), 47.2 (s, =C*C*H$_2$), 72.3 (s, O*C*H$_2$), 127.8 (t, $^3J_{PC}$ + $^5J_{PC}$ = 9.4 Hz, PPh$_3$–*C*$_3$), 129.4 (s, PPh$_3$–*C*$_4$), 133.3 (t, $^1J_{PC}$ + $^3J_{PC}$ = 39.6 Hz, PPh$_3$–*C*$_1$), 134.5 (t, $^2J_{PC}$ + $^4J_{PC}$ = 11.3 Hz, PPh$_3$–*C*$_2$), 179.8 (s, CH$_3$*C*OO), 306.8 (t, $^2J_{PC}$ = 11.7 Hz, [Ru]=*C*)

IR (KBr) 1375 cm^{-1} (κ^1-OCO$_{sym}$), 1432 cm^{-1} (P–Ph), 1481 cm^{-1} (κ^2-OCO$_{sym}$), 1549 cm^{-1} (κ^2-OCO$_{asym}$), 1615 cm^{-1} (κ^1-OCO$_{asym}$), Δν$_{(uni)}$ 240 cm^{-1}, Δν$_{(chelate)}$ 68 cm^{-1}; (CH_2Cl_2) 1375 cm^{-1} (κ^1-OCO$_{sym}$), 1434 cm^{-1} (P–Ph), 1481 cm^{-1} (κ^2-OCO$_{sym}$), 1545 cm^{-1} (κ^2-OCO$_{asym}$), 1613 cm^{-1} (κ^1-OCO$_{asym}$), Δν$_{(uni)}$ 238 cm^{-1}, Δν$_{(chelate)}$ 64 cm^{-1}.

MS (ESI) m/z 810.1825 (Expected for $^{101}RuP_2O_3NC_{45}H_{44}$ [M - OAc$^-$ + MeCN]$^+$ = 810.1840)

CHN Anal. for $RuP_2O_5C_{45}H_{44}$ + (1.80 CH_2Cl_2) (calc), C 57.32, H 4.89; (found) C 57.60, H 4.90.

Crystal data and structure refinement for 21b.

Identification code	jml0905a	
Empirical formula	$RuP_2O_5Cl_4C_{47}H_{48}$	
Formula weight	997.66	
Temperature	110(2) K	
Wavelength	0.71073 Å	
Crystal system	Orthorhombic	
Space group	A b a 2	
Unit cell dimensions	a = 18.2165(18) Å	α= 90°.
	b = 16.3759(16) Å	β= 90°.
	c = 15.0598(15) Å	γ = 90°.
Volume	4492.5(8) $Å^3$	
Z	4	
Density (calculated)	1.475 Mg/m^3	
Absorption coefficient	0.704 mm^{-1}	
F(000)	2048	
Crystal size	0.31 x 0.25 x 0.10 mm^3	
Theta range for data collection	2.15 to 28.31°.	
Index ranges	-24<=h<=24, -21<=k<=21, -20<=l<=20	
Reflections collected	22618	
Independent reflections	5538 [R(int) = 0.0168]	
Completeness to theta = 28.31°	99.9 %	
Absorption correction	Semi-empirical from equivalents	
Max. and min. transmission	0.932 and 0.799	
Refinement method	Full-matrix least-squares on F^2	
Data / restraints / parameters	5538 / 4 / 317	
Goodness-of-fit on F^2	1.055	
Final R indices [I>2sigma(I)]	R1 = 0.0293, wR2 = 0.0693	
R indices (all data)	R1 = 0.0309, wR2 = 0.0705	
Absolute structure parameter	0.00(3)	
Largest diff. peak and hole	0.423 and -1.230 $e.Å^{-3}$	

7.5.3: Synthesis of [Ru(κ^1-OAc)(κ^2-OAc)(=CO(CH$_2$)$_4$)(PPh$_3$)$_2$] 21c.

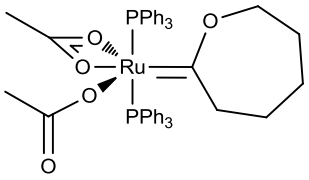

0.09 g **21c** (52.9 %) was obtained as an orange powder from 0.15 g (0.19 mmol) **1** and 21.4 μL (0.19 mmol) HC≡C(CH$_2$)$_4$OH in 10 mL DCM. After removing the solvent *in vacuo*, the product was washed with 3 x 20 mL portions of pentane. Crystals for X-ray diffraction were obtained from a CH_2Cl_2/pentane solution.

NMR Spectra CD_2Cl_2:

^{1}H δ_H 0.67 (m, 2H, CH_2), 0.84 (s, 6H, C*H*$_3$COO), 0.91 (m, 2H, CH_2), 1.16 (m, 2H, CH_2), 2.72 (br s, 2H, =CC*H*$_2$), 3.85 (t, *J* = 4.2 Hz, 2H, OC*H*$_2$), 7.36 – 7.43 (m, 18H, P*Ph*$_3$), 7.59 – 7.61 (m, 12H, P*Ph*$_3$)

^{31}P δ_P 34.2(s, 2.0P, *P*Ph$_3$)

^{13}C δ_C 20.4 (s, *C*H$_2$), 22.5 (s, *C*H$_3$COO), 28.4 (s, *C*H$_2$), 29.2 (s, *C*H$_2$), 50.8 (s, =C*C*H$_2$), 74.6 (s, O*C*H$_2$), 127.7 (t, $^3J_{PC}$ + $^5J_{PC}$ = 9.2 Hz, PPh$_3$–*C*$_3$), 129.4 (s, PPh$_3$–*C*$_4$), 133.2 (t, $^1J_{PC}$ + $^3J_{PC}$ = 38.8 Hz, PPh$_3$–*C*$_1$), 134.5 (t, $^2J_{PC}$ + $^4J_{PC}$ = 11.5 Hz, PPh$_3$–*C*$_2$), 179.6 (s, CH$_3$*C*OO), 311.0 (t, $^2J_{PC}$ = 11.8 Hz, [Ru]=*C*)

IR (KBr) 1382 cm^{-1} (κ^1-OCO$_{sym}$), 1433 cm^{-1} (P–Ph), 1450 cm^{-1} (κ ^{2}-OCO$_{sym}$), 1546 cm^{-1} (κ ^{2}-OCO$_{asym}$), 1608 cm^{-1} (κ ^{1}-OCO$_{asym}$), Δν$_{(uni)}$ 225 cm^{-1}, Δν$_{(chelate)}$ 96 cm^{-1}; (CH_2Cl_2) 1382 cm^{-1} (κ ^{1}-OCO$_{sym}$), 1433 cm^{-1} (P–Ph), 1452 cm^{-1} (κ ^{2}-OCO$_{sym}$), 1548 cm^{-1} (κ ^{2}-OCO$_{asym}$), 1607 cm^{-1} (κ ^{1}-OCO$_{asym}$), Δν$_{(uni)}$ 225 cm^{-1}, Δν$_{(chelate)}$ 96 cm^{-1}.

MS (ESI) m/z 843.1936 (Expected for $^{101}RuP_2O_5C_{46}H_{47}$ $[M+H]^+$ = 843.1942)

CHN Anal for $RuP_2O_5C_{46}H_{46}$ + (0.30 CH_2Cl_2): (calc) C 64.11, H 5.42; (found) C 64.17, H 5.50

Crystal data and structure refinement for 21c.

Identification code	jml1026_twin1_hklf4
Empirical formula	$RuP_2O_5C_{46}H_{46}$
Formula weight	841.84
Temperature / K	110.0
Crystal system	monoclinic
Space group	$P2_1/c$
a / Å, b / Å, c / Å	23.3069(7), 15.8366(3), 10.6439(2)
α/°, β/°, γ/°	90.00, 92.537(2), 90.00
Volume / $Å^3$	3924.85(15)
Z	4
ρ_{calc} / mg mm^{-3}	1.425
μ / mm^{-1}	0.528
F(000)	1744
Crystal size / mm^3	0.2284 × 0.1714 × 0.0766
2Θ range for data collection	6.22 to 60.08°
Index ranges	$-32 \leq h \leq 28$, $-20 \leq k \leq 20$, $-6 \leq l \leq 14$
Reflections collected	16799
Independent reflections	9876[R(int) = 0.0367]
Data/restraints/parameters	9876/3/500
Goodness-of-fit on F^2	1.043
Final R indexes [I>2σ (I)]	R_1 = 0.0481, wR_2 = 0.0989
Final R indexes [all data]	R_1 = 0.0739, wR_2 = 0.1054
Largest diff. peak/hole / e $Å^{-3}$	1.139/-1.818

8: A Comparison of Structural and Spectroscopic Features of Acetate-Containing Complexes derived from $[Ru(\kappa^2\text{-}OAc)_2(PPh_3)_2]$.

8.1: Introduction

It has become clear that the majority of acetate-containing complexes reported in this thesis fit into one of two main classes of structure; Structure **8A** and Structure **8B** (Figure 8.1.1). In both, the two PPh_3 ligands are mutually *trans*. In Structure **8A**, two acetate ligands and one other (**XX'**) ligand are present, whilst in Structure **8B**, one acetate and two other ligands (**YY'** and **ZZ'**) are present.

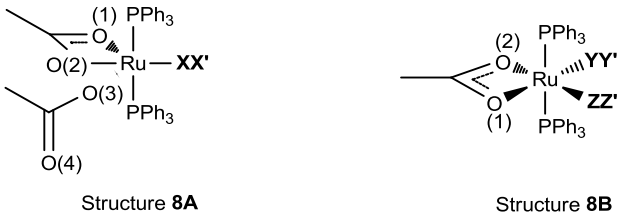

Figure 8.1.1: Two common structural motifs: **8A** and **8B** for complexes reported in this thesis.

Structure **8A** is common to the vinylidene complexes **2a-d** $[Ru(\kappa^1\text{-}OAc)(\kappa^2\text{-}OAc)(PPh_3)_2(=C=CHR)]$ and **9a-n** $[Ru(\kappa^1\text{-}OAc)(\kappa^2\text{-}OAc)(PPh_3)_2(=C=CHCRR'OH)]$ (where **X** = C and **X'** = CHR) and for the CO- and NO-containing complexes **4** $[Ru(\kappa^1\text{-}OAc)(\kappa^2\text{-}OAc)(PPh_3)_2(CO)]$ (**X** = C; **X'** = O) and **5** $[Ru(\kappa^1\text{-}OAc)(\kappa^2\text{-}OAc)(PPh_3)_2(NO)]BF_4$ (**X** = N; **X'** = O). It is also applicable to the oxacyclocarbene complexes **21a-c** $[Ru(\kappa^1\text{-}OAc)(\kappa^2\text{-}OAc)(PPh_3)_2(=C_nH_{2n-2}O)]$ (**XX'** = COR).

Structure **8B** is a general structure for the acetylide complexes **6** $[Ru(\kappa^2\text{-}OAc)(C\equiv CPh)(CO)(PPh_3)_2]$ (**YY'** = CO; **ZZ'** = C≡CPh) and **7** $[Ru(\kappa^2\text{-}OAc)(C\equiv CPh)(NO)(PPh_3)_2]BF_4$ (**YY'** = NO; **ZZ'** = C≡CPh), the vinyl complex **10** $[Ru(\kappa^2\text{-}OAc)(CH=CH_2)(CO)(PPh_3)_2]$ (**YY'** = CO; **ZZ'** = $CH=CH_2$) and the acyl complex **11** $[Ru(\kappa^2\text{-}OAc)(COCH=CH_2)(CO)(PPh_3)_2]$ (**YY'** = CO; **ZZ'** = $COCH=CH_2$).

In compiling the common crystallographic characteristics as well as pertinent NMR and IR spectroscopic features of complexes of structure types **8A** and **8B**, it became apparent that not only was there a significant similarity, but that some,

particularly for complexes of structure **8A**, acted as a sensitive probe of the different ligand effects present.

The bonding interaction between an acetylide ligand and a metal centre is considered to be almost purely σ-donor, as the large energy gap between the metal fragments HOMO and the ligand π* LUMO prevents a significant interaction. Carbonyl, nitrosyl and carbene ligands are all considered to be 'σ-donor, π-acceptor' ligands, however the relative strength of these bonding properties varies. For these ligands, the σ-donor interaction arises from the donation of a lone pair of electrons from a ligand orbital into a d-orbital of the metallic fragment of corresponding symmetry and similar energy. The π-acceptor interaction arises from the donation of electron density from a filled metal d-orbital into a vacant orbital of appropriate symmetry (p or π) of similar energy. When the π-acceptor interaction involves the donation of electrons into a ligand antibonding orbital, the result is a net weakening of the overall bond order. Figure 8.1.2 and 8.1.3 illustrate the bonding between a transition metal fragment [M] and these ligands.

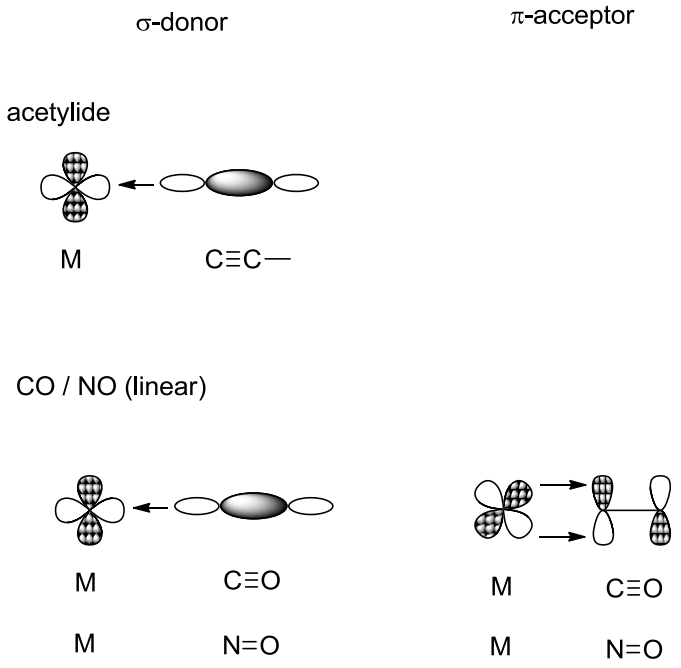

Figure 8.1.2: Bonding interactions between the ML_5 fragment and CO, NO and acetylide ligands.

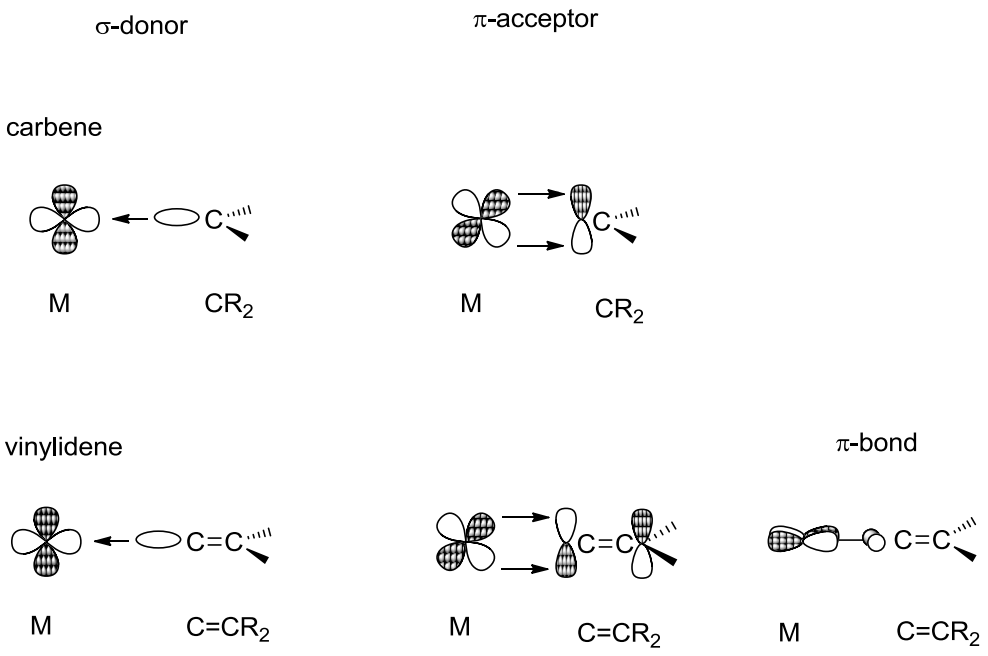

Figure 8.1.3: Bonding interactions between the ML_5 fragment and carbene and vinylidene ligands.

It has been established that the nitrosyl ligand is a weaker σ-donor, but stronger π-acceptor ligand than the carbonyl ligand.[1] This was demonstrated by Hedburg[2] in 1985 who used gaseous electron diffraction studies of the isoelectronic series of complexes $[Ni(CO)_4]$, $[Co(CO)_3(NO)]$, $[Fe(CO)_2(NO)_3]$, $[Mn(CO)(NO)_3]$ and $[Cr(NO)_5]$ to determine the relative trends in bond orders. It was noted that, for complexes in which both nitrosyl and carbonyl ligands were present, the M – N bond orders were substantially greater than the M – C bond orders, indicating that the nitrosyl ligand is a better π-acceptor.

As noted in Section 1.2, contradictory reports exist on the comparable π-acceptor strength of the vinylidene and carbonyl ligands; Antonova[3] used force constants of the $[MnCp(CO)_2L]$ (L = CO; C=CHPh) derivative to determine that the vinylidene ligand is a better π-acceptor than the carbonyl ligand whilst Werner[4] used a combination of DFT, IR and Raman spectroscopic studies to demonstrate that the opposite was true for $[Rh(X)(L)(P^iPr_3)_2]$.

In their pivotal paper, Kostić and Fenske[5] compared the ability of vinylidene and Schrock carbene ligands to undergo nucleophilic and electrophilic attack by discerning the localisation of molecular orbital density within the metal-ligand fragments. Whilst the donor/acceptor properties of these ligands were not explicitly

alluded to in this paper, it was established that the M=C bond order of the vinylidene fragment [$MpCCH_2$] is typically between two and three whilst for a carbene the M=C bond order is formally two (Mp = [$Mn(Cp)(CO)_2$]). This is due to the vinylidene ligand having two orbitals able to accept electron density from the metal whilst the carbene ligand has only one, which is perpendicular to the ligand plane. As noted in Section 1.2, this feature also has implications for the conformational preferences of these ligands when bound to half-sandwich complexes and their ability to rotate. The electrophilic characters of the C_α atoms of the vinylidene, carbene and acetylide ligands were also established by these authors using a Mulliken population analysis to understand the gross atomic charges. It was shown that the C_α atom of the $[Fp'CCH_2]^+$ fragment (Fp' = $[Fe(Cp)(PH_3)_2]$) had a larger positive character (0.19) and was therefore more electrophilic than the corresponding C_α atom of the analogous carbene complex $[Fp'CH_2]^+$ (0.02).

The oxacyclocarbene ligands reported in this thesis are Fischer carbene ligands, and as such may be considered to be a weaker π-acceptor ligand than a vinylidene ligand. This is due to the additional π-interaction between the p-orbital (LUMO) of the carbene carbon and a p-orbital of the oxygen atom of similar symmetry and energy. Consequently, the π-back bonding interaction between the metal and the carbene carbon is smaller.[6]

The effects of these bonding properties can be seen upon examining common structural and spectroscopic features of complexes derived from **1**. In particular, the Ru – O(2) bond distance and the $^4J_{PC}$ coupling constant observed in complexes of structure type **8A** are suggestive of the relative π-acceptor strength of these ligands.

8.2: Structure 8A

For those complexes for which structural characterisation were possible, all bar one adopted the structure of a distorted octahedron. It is proposed that this is due to the presence of the κ^2-OAc ligand, which restricts the O(1) – Ru – O(2) angle to approximately 60 ° and causes a deviation from 90 ° of angles involving ligands in the same plane about the ruthenium atom. The exception to this is complex **21b**, which crystallised in a different space group (*Aba2*) with the asymmetric unit comprising half the molecule, containing only one κ^1-OAc ligand. Tables 8.2.1 and 8.2.2 summarise common structural features suitable for comparison, using the nomenclature system shown in Figure 8.1.1.

Table 8.2.1 illustrates how similar a number of common features are for these complexes. Of the vinylidene complexes, the Ru=C and C=C distances are within expected values[7] and are highly uniform. The shortest Ru=C distance is observed for the CO_2Me-substituted vinylidene complex **2b** and the longest exhibited by the hydroxy-vinylidene complex **9e** containing a cyclopentanol substituent. Of the C=C bond lengths, the shortest is again observed for complex **2b**, whilst the longest is observed for **2c** containing a pyrene-substituted vinylidene ligand. As noted in Section 7.2 the Ru=C bond lengths for the vinylidene complexes are shorter than those observed for the oxacyclocarbene complexes **21a** and **21b**, reflecting the differences in bond order between the two types of carbene (between two and three for the vinylidene and formally two for the carbene). This phenomenon is also mirrored in the lower δ_C values observed for C_α in the $^{13}C\{^1H\}$ NMR spectra of the oxacyclocarbene complexes compared to the vinylidene and hydroxy-vinylidene complexes, which is thought to be due to the more electrophilic character of the vinylidene/hydroxy-vinylidene ligands.[5]

	Ru – X	X – X'	Ru – O(1)	Ru – O(2)	Ru – O(3)
2a	1.786(3)	1.318(4)	2.1139(17)	2.2863(18)	2.0699(17)
2b	1.766(6)	1.296(8)	2.102(4)*	2.282(4)*	2.063(4)
2c	1.7863(16)	1.325(2)	2.1116(11)	2.2465(12)	2.0160(11)
9a	1.8027(15)	1.312(2)	2.1100(11)	2.2588(11)	2.0344(11)
9c	1.7959(18)	1.316(2)	2.1141(13)	2.2620(13)	2.0179(12)
9e	1.805(3)	1.297(4)	2.1119(19)	2.3259(19)	2.088(2)
21a	1.878(6)	n.a.	2.204(4)	2.355(4)	2.058(4)
21b	1.865(3)	n.a.	n.a.	n.a.	2.104(2)
21c	1.902(3)	n.a.	2.126(2)	2.325(2)	2.086(2)
4	1.8318(17)	1.146(2)	2.1466(11)	2.1897(11)	2.0365(11)
5	1.739(2)	1.137(3)	2.1336(19)	2.0744(19)	1.9966(19)

Table 8.2.1: Summary of pertinent bond lengths (Å) exhibited by complexes conforming to structure **8A** (n.a. = not applicable) *: assignments have been reversed from real data set.

It appears that the Ru – O(3) bond length of the κ^1-OAc ligand is typically the shortest of the Ru–O distances. The Ru – O(1) and Ru – O(2) bond lengths of the κ^2-OAc ligand illustrate that it is bound in an asymmetric manner; the Ru – O(1) distance is slightly shorter than the Ru – O(2). It has been suggested that the Ru – O(2) distance may be affected by the strength of the labilising effect of the ligand *trans* to it.[8,9] As such, it can be noted that the Ru – O(2) distance of complex **5**, in which this bond is *trans* to the strong π-acceptor ligand NO, is the shortest at 2.0744(19) Å. Conversely, it can be shown that the longest Ru – O(2) bond lengths are observed for the oxacyclocarbene complex **21a** (2.355(4) Å) and the hydroxy-vinylidene complex **9e** at (2.259(19) Å), which may be considered weaker π-acceptor '**X**' ligands.

Table 8.2.2 contains pertinent bond angles reported for complexes conforming to structure **8A**. The majority of bond angles are reasonably similar, though less uniform than observed for the bond lengths. The Ru – X – X' moiety in structure **8A** is expected to be linear in all cases except the oxacyclocarbene complexes **21a** and **21b**. Inspection of this data reveals there is only a slight deviation from 180 °, the largest observed for complex **2b** at 173.6(5) °. The P(1) – Ru – P(2) angle is also

close to linear in all examples, with the largest deviation (173.647(14) °) observed for the diphenyl-substituted hydroxy-vinylidene complex **9a**. The O(1) – Ru – O(2) is approximately 60 ° for all complexes, and it is this constraint which gives rise to the distortion observed in other angles in the same plane, which may deviate by up to 10 – 30 °.

	Ru – X – X'	O(1) – Ru – X	O(2) – Ru – X	O(3) – Ru – X
2a	176.5(2)	97.81(9)	155.65(9)	93.90(9)
2b	173.6(5)	97.5(2)*	154.7(2)*	94.1(2)
2c	174.72(14)	101.92(6)	161.77(6)	102.72(6)
4	175.02(15)	104.71(6)	164.49(6)	99.45(6)
5	176.5(2)	106.75(9)	168.00(9)	102.25(10)
9a	175.16(13)	101.35(6)	161.05(6)	101.59(6)
9c	178.10(16)	103.64(6)	162.68(6)	104.95(7)
9e	178.2(3)	98.99(10)	155.45(10)	92.52(10)
21a	n.a.	96.6(2)	151.5(2)	92.4(2)
21b	n.a.	95.45(7)	n.a.	n.a.
21c	n.a.	98.29(11)	157.19(11)	89.40(12)

	P(1) – Ru – P(2)	O(1) – Ru – O(2)	O(1) – Ru – O(3)	O(2) – Ru – O(3)
2a	178.89(3)	59.08(6)	168.17(7)	109.09(7)
2b	178.20(6)	58.78(14)	168.40(15)*	109.67(15)*
2c	174.126(15)	59.86(4)	154.87(5)	95.49(4)
4	176.545(15)	60.42(4)	155.62(5)	95.71(5)
5	176.05(2)	61.55(8)	150.64(9)	89.64(8)
9a	173.647(14)	59.79(4)	156.68(4)	97.36(4)
9c	177.844(17)	59.78(5)	151.04(5)	92.05(5)
9e	178.45(3)	58.45(7)	168.47(7)	110.09(7)
21a	173.69(5)	56.40(15)	170.95(16)	114.74(16)
21b	178.60(4)	n.a.	169.10(13)	n.a.
21c	175.91(3)	58.92(8)	170.96(9)	113.25(8)

Table 8.2.2: Summary of pertinent bond angles (°) exhibited by complexes conforming to structure **8A** (n.a. = not applicable) *: assignments have been reversed c.f. real data set.

Tables 8.2.3-5 summarise NMR features common to complexes that are analogous to structure **8A**. Table 8.2.6 summarises common IR features.

Complex	^{1}H δ_H [Ru]=C=C*H*	^{1}H $^{4}J_{HP}$/Hz	^{1}H δ_H CH_3COO	^{31}P δ_P PPh_3
2a	5.14	3.7	0.81	34.1
2b	5.41	3.2	0.78	34.8
2c	6.20	3.6	0.95	33.8
2d	3.74	3.7	0.74	35.5
4	n.a.	n.a.	0.64	39.1
5	n.a.	n.a.	0.82	34.7
9a	4.73	3.9	0.71	34.0
9b	4.32	3.9	0.77	34.1
9c	4.56	3.9	0.81	34.3
9d	4.14	3.8	0.86	34.9
9e	4.38	3.8	0.83	34.3
9f	4.39	3.7	0.82	34.4
9g	4.56	3.8	0.82	33.9
9h	4.11	3.7	0.85	35.1
9i	4.48	3.7	0.75	35.5
9j	4.41	3.6*	0.87	35.2
9k	4.35	n.d.	0.85	35.3
9l	4.36	n.d.	0.86	35.2
9m	4.07	n.d.	0.83	35.3
9n	4.40	n.d.	0.85	34.8
21a	n.a.	n.a.	0.82	35.9
21b	n.a.	n.a.	0.83	35.4
21c	n.a.	n.a.	0.84	34.2

Table 8.2.3: Common ^{1}H and ^{31}P{^{1}H} NMR features of complexes that fit structural motif **8A**. (n.d. = not detected; n.a. = not applicable, * = simulated value).

Collating the data in this way allows for similar characteristics to be spotted easily, anomalies identified and perhaps accounted for. Comparing the resonances observed in the ^{31}P{^{1}H} spectra for these complexes shows that there is only a small variation in chemical shift. It has been shown throughout this thesis that complexes derived from **1** exhibit a NMR resonance around δ_P 60-65 when the phosphine ligands are mutually *cis*, and between δ_P 30-40 when they are mutually *trans*. All vinylidene and oxacyclocarbene complexes exhibit a resonance at approximately δ_P 34; as does the NO-containing complex **5**. The CO-complex **4** is an exception in that

it exhibits a resonance at a very different chemical shift (δ_P 39.1). It can be seen that the resonances for the vinylidene proton of complexes **2a-d** and **9a-n** are mostly uniform, particularly with regard to the substituted vinylidene complexes **9a-n**. There appears to be a greater variation in chemical shift for the vinylidene complexes **2a-d**. The pyrene-substituted vinylidene complex **2c** and the TMS-substituted vinylidene complex **2d** are two extremes with a δ_H of 6.20 and 3.74 respectively. There is little deviation in the coupling constants reported for the $^4J_{HP}$ interaction.

The singlet resonance assigned to the six protons of the two acetate ligands has consistently demonstrated that these ligands are undergoing an exchange process that is rapid on the NMR timescale. In some instances it has been possible to observe decoalescence of the two environments upon cooling, although it was not possible to reach the low temperature limit for any example. Table 8.2.4 summarises the exchange parameters calculated for those complexes for which decoalescence was observed. This shows that although there is some variation in the rate of exchange (k_{coal}), the energy barrier ($\Delta G^{\ddagger}$) to this exchange for each complex is quite similar. The highest barrier is observed for the NO-containing complex **5**, which also exhibits the shortest Ru – O(2) distance as noted earlier. The chemical shift of this resonance again shows little variation; the CO-containing complex **4** displays the lowest δ_H value (δ_H 0.64) whilst **2c** exhibits the highest (δ_H 0.95).

Complex	$\boldsymbol{\delta_v}$ **/ s^{-1}**	$\mathbf{T_c}$ **/ K**	$\boldsymbol{k_{coal}} \leq$ **/ s^{-1}**	$\boldsymbol{\Delta G^{\ddagger}} \leq$ **/ kJ mol^{-1}**
4	173.7	195	385.6	37.4
5	183.9	235	408.3	45.3
9a	291.3	215	646.7	40.5
9d	270.4	190	600.2	35.7
9e	175.8	195	390.2	37.4
9g	138.7	195	307.8	37.8
21a	203.0	185	451.0	35.2
21b	146.5	185	325.4	35.7

Table 8.2.4: T_c, k_{coal} and $\Delta G^{\ddagger}$ of complexes for which coalescence is observed.

Table 8.2.5 summarises the notable features observed in the $^{13}C\{^{1}H\}$ NMR spectra of these complexes.

Complex	^{13}C δ_C [Ru]=C_α	^{13}C $^{2}J_{CP}$/Hz	^{13}C δ_C [Ru]=C=C_β	^{13}C $^{3}J_{CP}$/Hz	^{13}C δ_C CH_3COO	^{13}C δ_C CH_3COO
2a	355.6	16.8	112.1	4.4	179.6	21.9
2b	345.2	n.d.	104.4	3.9	179.8	21.8
2c	n.d.	n.d.	109.4	4.6	179.8	22.0
2d	337.6	15.4	94.0	3.9	179.6	22.2
4	207.4	13.2	n.a.	n.a.	181.4	29.1
5	n.a.	n.a.	n.a.	n.a.	n.d.	21.1
9a	347.6	16.2	117.2	4.7	179.6	21.7
9b	352.0	16.3	118.4	4.8	179.5	22.0
9c	350.4	16.0	117.6	4.3	179.6	21.8
9d	345.1	16.2	112.5	4.7	179.9	21.8
9e	352.0	16.3	116.3	4.6	179.6	21.9
9f	352.2	16.5	117.5	4.7	179.5	21.9
9g	349.3	16.1	113.7	4.6	179.6	21.9
9h	345.7	16.3	106.5	5.0	179.7	21.8
9i	352.0	16.2	114.4	4.6	179.5	21.7
9j	n.d.	n.d.	103.6	n.d.	179.8	21.6
9k	n.d.	n.d.	n.d.	n.d.	n.d.	n.d.
9l	n.a.	n.a.	n.a.	n.a.	n.a.	n.a.
9m	n.a.	n.a.	n.a.	n.a.	n.a.	n.a.
9n	n.a.	n.a.	n.a.	n.a.	n.a.	n.a.
21a	304.7	11.8	n.a.	n.a.	180.0	21.9
21b	306.8	11.7	n.a.	n.a.	179.8	21.6
21c	311.0	11.8	n.a.	n.a.	179.6	22.5

Table 8.2.5: Common $^{13}C\{^{1}H\}$ NMR features of complexes that fit structural motif **8A**. (n.d. = not detected; n.a. = not applicable).

Of those that contain a vinylidene ligand (**2a-d** and **9a-n**), the characteristic C_α resonance is typically observed at a very high field.[7] Furthermore, all resonances are observed as a triplet due to the coupling of the C_α to the two PPh_3 ligands. In 1990, Fenske professed that "the results not only reemphasize the inadequacy of traditional shielding arguments in the analysis of NMR spectra for atoms other than hydrogen but also direct one's attention to the key elements in the paramagnetic term that are principally responsible for the chemical shifts."[10] All other resonances for the C_β of the vinylidene complexes are observed at a similar chemical shift. The coupling

constants observed between the PPh_3 ligands and both C_α and C_β of the vinylidene ligands are fairly uniform and are typical of this system. The $^2J_{PC}$ values of the vinylidene (**2a-d**) and hydroxy-vinylidene (**9a-i**) complexes are larger than the $^2J_{PC}$ of complex **4**, which is in turn larger than the $^2J_{PC}$ of the oxacyclocarbene complexes **21a-c**. This is indicative of the vinylidene ligand being more tightly bound to the ruthenium centre, as also evidenced by the shorter Ru – X distances observed on structural characterisation and the expected relative bond orders. The C_α resonance of the oxacyclocarbene complexes **21a-c** is observed at a lower chemical shift than the corresponding C_α of the vinylidene complexes. This is thought to be due to the stronger electrophilic character of a vinylidene ligand compared to a Fischer carbene.[5] The singlet resonances observed for both carbon atoms of the acetate ligand for all complexes are remarkably uniform and there is very little variation in the chemical shift across the complexes listed. The single exception to this is complex **4**, in which, as also observed in the $^{31}P\{^1H\}$ NMR spectrum, the resonances are shifted to a slightly higher chemical shift.

Table 8.2.6 summarises the common IR spectroscopic features. The short lifetime of complexes **9k-n** meant that IR spectra of these complexes would be contaminated by peaks due to complex **10** so have been excluded. Ambiguity also exists for the assignments of peaks in the IR spectra of complex **5**, as previously noted (see Section 3.4). As mentioned earlier in Section 2.2, the difference ($\Delta\upsilon$) between the symmetric and asymmetric stretches is characteristic of the coordination mode of the acetate ligand; a larger $\Delta\upsilon$ is observed for a κ^1-OAc ligand than for a κ^2-OAc ligand. Robinson has proposed that for a monodentate acetate ligand, the difference is typically in the region of 210 – 270 cm^{-1} whilst for a chelating acetate ligand it is 40 – 120 cm^{-1}.[11]

Complex	C=C	κ^1-OCO_{sym}	κ^1-OCO_{asym}	κ^1-Δυ	κ^2-OCO_{sym}	κ^2-OCO_{asym}	κ^2-Δυ
2a (DCM)	1630	1366	1594	228	1462	1531	69
2a (KBr)	1635	1360	1595	235	1459	1534	75
2b (DCM)	1696	1365	1600	235	1460	1533	73
2b (KBr)	1684	1365	1600	235	1466	1535	69
2c (DCM)	1610	1360	1587	227	1458	1536	78
2c (KBr)	1607	1366	1590	224	1462	1530	68
2d (DCM)	1633	1361	1611	250	1463	1521	58
2d (KBr)	1636	1366	1616	250	1459	1531	72
4 (DCM)	n.a.	1374	1603	229	1468	1520	52
4 (KBr)	n.a.	1368	1607	239	1466	1520	54
5 (DCM)	n.a.	n.d.	n.d.	n.d.	n.d.	n.d.	n.d.
5 (KBr)	n.a.	1364	1636	272	n.d.	n.d.	n.d.
9a (DCM)	1649	1371	1598	227	1463	1531	68
9a (KBr)	1654	1378	1595	217	1465	1527	62
9b(DCM)	1653	1366	1623	257	1459	1539	80
9b (KBr)	1648	1362	1619	257	1460	1533	73
9c (DCM)	1652	1367	1601	234	1463	1533	70
9c (KBr)	1649	1361	1601	240	1458	1536	78
9d (DCM)	1647	1373	1596	223	1455	1538	83
9d (KBr)	1648	1369	1592	223	1454	1537	83
9e (DCM)	1656	1364	1584	220	1457	1533	76
9e (KBr)	1654	1364	1590	226	1458	1536	78
9f (DCM)	1648	1368	1600	232	1461	1536	75
9f (KBr)	1646	1366	1591	225	1458	1538	80
9g (DCM)	1646	1367	1606	239	1463	1531	68
9g (KBr)	1636	1367	1597	230	1463	1534	71
9h (DCM)	1651	1368	1605	237	1456	1538	82
9h (KBr)	1655	1372	1595	223	1457	1533	76
9i (DCM)	1652	1372	1616	244	1458	1538	80
9i (KBr)	1649	1374	1620	246	1456	1530	74
9j (DCM)	1652	1366	1598	232	1458	1538	80
9j (KBr)	1651	1359	1597	238	1457	1537	80
21a (DCM)	n.a.	1375	1615	240	1448	1540	92
21a (KBr)	n.a.	1368	1616	248	1447	1541	94
21b (DCM)	n.a.	1375	1613	238	1447	1545	98
21b (KBr)	n.a.	1375	1615	240	1446	1549	103
21c (DCM)	n.a.	1382	1607	225	1452	1548	96
21c (KBr)	n.a.	1382	1608	225	1450	1546	96

Table 8.2.6: Common IR features of complexes that fit structural motif **8A**. (n.d. and n.a. as before).

Upon inspection of the data it was noted that there appears to be a larger variation in the stretching frequency range recorded for the κ^1-OAc_{asym} stretch than for the κ^1-OAc_{sym} stretch. The highest κ^1-OAc_{asym} stretch recorded was for **9b** at 1623 cm^{-1} whilst the lowest was for **9e** (1584 cm^{-1}); spanning a range of 39 cm^{-1}. For the corresponding κ^1-OAc symmetric stretch there is a variation of 23 cm^{-1} (1359 cm^{-1} {**9j**} – 1382 cm^{-1} {**21c**}). For the κ^2-OAc stretches the variation in the symmetric stretch is 22 cm^{-1} (1446 cm^{-1} {**21b**} – 1468 cm^{-1} {**4**}) whilst for the asymmetric it is 29 cm^{-1} (1520 cm^{-1} {**4**} – 1549 cm^{-1} {**21b**}). It was noted in the preceding section (7.2) that the oxacyclocarbene complexes exhibit the largest κ^2-OAc $\Delta\upsilon$ values recorded in this thesis. If these are excluded then the variation in the κ^2-OAc_{sym} becomes 14 cm^{-1} and the κ^2-OAc_{asym} 19 cm^{-1}. For the vinylidene complexes **2a-d** and **9a-j**, the C=C stretch is observed at approximately 1640 cm^{-1}. The highest recorded stretch is observed for complex **2d**, the TMS-substituted vinylidene complex, at 1696 cm^{-1} (DCM).

A trend becomes apparent upon inspection of the κ^2-$\Delta\upsilon$ values of these complexes. The values recorded in both solution and solid state for the CO-containing complex **4** (52 and 54 cm^{-1} respectively) are noticeably lower than those for the vinylidene complexes, which span a range from 58-83 cm^{-1}. The complexes containing the oxacyclocarbene ligands are, as noted previously, significantly higher at approximately 90 cm^{-1}. This trend appears to follow the trend of ligand π-acceptor strength, where a smaller κ^2-$\Delta\upsilon$ is observed for the better π-acceptor ligands. It may be predicted that, were the pertinent features observable in the IR, that complex **5** would exhibit a κ^2-$\Delta\upsilon < 50$.

It has been shown that a number of complexes reported in this thesis share a common structural motif which is accompanied by the observation of similar NMR and IR spectroscopic features. The following section will consider how these features compare with those of other acetate-containing complexes of structure **8B**.

8.3: Structure 8B

Crystals of complexes **6**, **10** and **11** were obtained and again, due to the presence of a κ^2-OAc ligand, adopt a distorted octahedron structure. Tables 8.3.1 and 8.3.2 summarise the pertinent bond lengths and angles of interest. For these complexes, **YY'** corresponds to a CO ligand, whilst for complex **7** (for which a crystal structure was not obtained) **YY'** corresponds to a NO ligand.

	Ru – Y	**Y – Y'**	**Ru – Z**	**Ru – O(1)**	**Ru – O(2)**
6	1.824(3)	1.138(3)	2.002(3)	2.1829(18)	2.1959(18)
10	1.841(4)	1.158(5)	1.987(4)	2.190(3)	2.265(3)
11	1.8344(16)	1.152(2)	1.9935(16)	2.1612(11)	2.3502(11)

Table 8.3.1: Summary of pertinent bond lengths (Å) exhibited by complexes of structure **8B**.

As for complexes of structure **8A**, the κ^2-OAc ligand is again coordinated in an asymmetric fashion. Figure 7.3.1 illustrates how the O(1) atom is *trans* to a good π-acceptor CO ligand in complexes **6**, **10** and **11**, which accounts for the shorter bond length of Ru – O(1) compared to Ru – O(2). The Ru–Y and Y–Y' distances are all consistent with expectations for a CO ligand,[13] and are similar to those observed for complex **4** (structure **8A**). The Ru–Z distance is also considered as having mainly single bond character for complexes **6**, **10** and **11**, which agrees with the distances observed.

The bond angles summarised in Table 8.3.2 are also consistent with most observed for complexes of structure **8A**. The P(1) – Ru – P(2) angle is close to linear, as is the Ru – Y – Y' angle. The O(1) – Ru – O(2) angle observed for each is slightly below 60 °, and the remaining angles between ligands in the same plane are distorted accordingly with deviations ion the range of 10 – 25 °. It should be noted however, that Y – Ru – Z angle is least distorted from the ideal 90 °.

	Ru – Y – Y'	P(1) – Ru – P(2)	O(1) – Ru – O(2)	Y – Ru – Z
6	178.3(2)	178.15(3)	59.91(7)	92.42(12)
10	172.5(4)	179.03(4)	58.67(10)	91.92(18)
11	178.64(16)	172.714(14)	57.95(4)	89.80(7)

	O(1) – Ru – Y	O(2) – Ru – Y	O(1) – Ru – Z	O(1) – Ru – Z
6	166.69(9)	107.40(9)	100.37(10)	160.16(10)
10	169.53(14)	111.08(15)	98.46(14)	156.74(14)
11	171.73(6)	113.78(6)	98.47(6)	156.40(6)

Table 8.3.2: Summary of pertinent bond angles (°) exhibited by complexes of structure **8B**.

As for complexes of structure **8A**, a comparison of common NMR and IR spectroscopic features is included in Tables 8.3.3 and 8.3.4 respectively.

Complex	^{1}H δ_H C***H***$_3$COO	^{31}P δ_P PPh$_3$	^{13}C [Ru]-***C***O	^{13}C $^{2}J_{CP}$/Hz	^{13}C δ_C CH$_3$***C***OO	^{13}C δ_C ***C***H$_3$COO
6	0.61	38.6	204.9	13.9	185.4	22.5
7	0.70	32.8	n.a.	n.a.	191.7	22.4
10	0.59	38.5	206.7	15.3	182.7	22.2
11	0.56	36.7	204.6	15.0	182.1	21.9

Table 8.3.3: Common ^{1}H, ^{31}P{^{1}H} and ^{13}C{^{1}H} NMR features of complexes that fit structural motif **8B**. (n.a. = not applicable).

The NMR features of these complexes appear to be mostly similar; the singlet resonance due to the three protons of the acetate ligand of each complex is observed at a comparable chemical shift, although this is noted to be lower than those generally observed for complexes of structure **8A**. The chemical shift of the resonance in the ^{31}P{^{1}H} NMR spectrum due to the phosphine ligands of complex **7** is observed at a slightly lower chemical shift than the other three complexes. The chemical shifts observed for the triplet resonances due to the CO ligands of complexes **6**, **10** and **11** are typical of these ligands and are comparable to that of complex **4** (δ_C 207.4). As in structure **8A**, there is very little change in the chemical shift of the two resonances due to the two carbon atoms of the acetate ligand. The single exception to this is that of complex **7**, which is observed at a higher chemical shift (δ_C 191.7). In general, the chemical shifts of these resonances are observed slightly higher than those observed for structure **8A** at *circa*. δ_C 180. However, it

should be noted that the acetate ligands of complexes conforming to structure **8A** are undergoing a rapid exchange whilst those of structure **8B** are not.

Complex	CO	κ^2-OCO_{sym}	κ^2-OCO_{asym}	κ^2-$\Delta\upsilon$
6 (DCM)	1947	1464	1521	57
6 (KBr)	1947	1463	1521	58
7 (DCM)*	n.a.	1464	1513	49
7 (KBr)*	n.a.	1463	3 possible peaks	-
10 (DCM)	1914	1457	1531	74
10 (KBr)	1916	1455	1526	71
11 (DCM)	1943	1452	1535	83
11 (KBr)	1941	1453	1531	78

Table 8.3.4: Common IR features of complexes that fit structural motif **8A**. (n.a. = not applicable)

*: stretches due to a possible κ^1-OAc ligand are also observed in these spectra.

This table once more illustrates how uniform the IR features are for these acetate-containing complexes. The symmetric and asymmetric stretches of the κ^2-OAc ligand are observed at similar wavenumbers in each complex, and compare very favourably with those observed for the complexes of structure **8A**. Again a trend is visible in the value of κ^2-$\Delta\upsilon$ which may be connected to the change in the π-acceptor properties of the ligands. The value for the NO-containing acetylide complex **7** is smaller at 49 cm^{-1} than the analogous CO-containing acetylide complex **6**.

It has been noted previously in Section 3.4 that the IR spectra of complexes containing both NO and acetate ligands cannot be unambiguously assigned; it is possible that the NO ligand and the acetate ligands may be altering their coordination mode rapidly. The CO stretches of these complexes are highly characteristic, although it has been previously noted that the CO stretch of complexes **4** (1946 cm^{-1}) and **6** (1947 cm^{-1}) are coincident.

This comparison demonstrated how these complexes may be divided into two subsets of common structure; **8A** and **8B**. A comparison of structural features obtained by X-ray crystallography studies demonstrated how some features are highly conserved. It was shown that all but one complex characterised by X-ray diffraction adopted a distorted octahedron structure which was attributed to the presence of a κ^2-OAc ligand. A comparison of pertinent NMR and IR spectroscopic features also demonstrated how some features are highly uniform. Complexes conforming to structure type **8A** also exhibited a number of features that were sensitive to the donor/acceptor properties of the ancillary ligands.

8.4: Thesis Conclusions

An investigation into the non-innocent role of the acetate ligand in the formation and subsequent reactivity of ruthenium complexes derived from complex **1** has been conducted. Starting from this easily prepared complex, a number of novel organometallic complexes have been synthesised and the acetate ligand has been shown to facilitate their formation. For example, their fluxional nature allows them to make a coordination site available when required by an incoming ligand. This property has been utilised in the synthesis of carbonyl (**4**), nitrosyl (**5**), carbene (**21a-c**), vinylidene (**2a-d**;**9a-n**) and acetylide derivatives of complex **1**, the vast majority of which were previously unknown compounds, or compounds which had been synthesised by alternative routes.

This family of complexes have been characterised as fully as possible, and in doing so a number of common structural and spectroscopic features became apparent. This allowed for the classification of these complexes into one of two different structures, and the distinction was dependent on the number of acetate ligands and their coordination mode. In one structure (**8A**), two acetate ligands were coordinated to the ruthenium centre in a fluxional κ^1-κ^2 mode. In the other (**8B**), only a single κ^2-OAc ligand was present. Analysis of the common structural and spectroscopic features led to the identification of several important features that were able to act as a 'sensor' for the donor/acceptor properties of the ancillary ligands. For example, the relative π-acceptor strength can be seen in the varying lengths of the *trans*-Ru – O(2) distances.

The acetate ligands also play a significant role in the formation of vinylidene and hydroxy-vinylidene complexes (**2a-d** and **9a-n**) from terminal alkynes. Not only do their fluxional properties allow a vacant site to be created at the metal centre, but they are then able to behave as both acid and base, acting as a proton shuttle to deprotonate the η^2-alkyne intermediate and reprotonate the acetylide intermediate. In an extensive DFT computational investigation, it was shown that this pathway is lower in energy than the alternatives.

This ability to act as an internal base was also shown to facilitate the formation of an acetylide ligand. The syntheses of complexes **6** and **7** were shown to require two equivalents of HC≡CPh and also resulted in the formation of an organic by-product (styryl acetate) from a coupling between acetic acid and the alkyne. A theoretical study again confirmed the role of the acetate ligand in facilitating this transformation.

This work has been developed further by Luke Shilling who has been able to adapt this stoichiometric synthesis to catalytically produce the organic by-product using complexes **4** and **5**. Interestingly, the *Z* vs. *gem* (Markovnikov vs. *anti*-Markovnikov) selectivity can vary when using a catalytic amount of complex **4**. Alkynes with electron-withdrawing groups in the *para*-postion of a phenyl ring favour a Markovnikov product whilst electron-donating favour *anti*-Markovnikov.

This work could also be extended towards the synthesis of a pyrene-substituted acetylide complex. Whilst it was shown that the vinylidene complex **2c** is not luminescent, it would have been interesting to investigate the potential photochemical properties of an acetylide derivative.

The acetate ligands were also found to play an important role in the decarbonylation of propargylic alcohols (HC≡CCRR'OH). The hydroxy-vinylidene complexes **9a-i** were all observed to convert over time to the carbonyl complex **4** with concomitant formation of an alkene ($HC{=}CR_2$). A conversion to the vinyl complex **10** and an acetate-derived organic by-product was also observed for the vinylidene complexes **9j-n**. A number of stoichiometric reactions allowed other potential intermediates to be identified and based on these data two possible mechanisms were proposed. Further experimental investigation using a benzoate analogue of complex **1** (**13**) discovered that the carboxylate ligands could undergo intermolecular exchange and that propargylic substitution at the γ-position of the coordinated ligand was possible. An ^{18}O-labelling study confirmed the involvement of the acetate ligands, by the synthesis of the quadruple-labelled complex **^{18}O-1**, derived from $CH_3C^{18}O^{18}OH$. A kinetic study confirmed that the mechanism was first order with respect to the ruthenium complex, ruling out a potential bimolecular pathway. The addition of an alcohol (PhOH) to the stoichiometric reaction also accelerated the conversion. Activation parameters were also established for the

conversion, which confirmed that the mechanism is dissociative, and that the activation barrier is around 100 kJ mol^{-1}.

Recently, results obtained by Elizabeth Smith have revealed that there is an induction period for the conversion of [Ru(κ^1-OAc)(κ^2-OAc)(P^iPr_3)$_2$(=C=CHCPh_2OH)] to [Ru(κ^1-OAc)(κ^2-OAc)(CO)(P^iPr_3)$_2$] and H_2C=CPh_2. Monitoring this conversion *in situ* by IR has shown that the conversion is complete within a matter of hours, whilst the full conversion of **9a** requires approximately two weeks.

Based on these experimental results, a DFT computational study was begun to map the PES of this conversion. The two possible mechanisms that had been compiled based on experimental evidence were soon shown to involve large activation barriers, which made them unrealistic. A number of modifications to these mechanisms were also shown to involve large activation barriers. Recently, attention has turned towards a pathway involving charged intermediates, which had not previously been considered. This pathway is appearing more likely as a result of promising results obtained in the ongoing experimental and theoretical study.

This project is currently being extended by two experimental workers; Elizabeth Smith and Oliver Pickup. They are attempting to study the change (if any) in reactivity of complexes analogous to **1** containing different phosphine and carboxylate ligands towards terminal alkynes. It has already been mentioned that Elizabeth has managed to synthesise a P^iPr_3-containing analogue that exhibits enhanced reactivity in the decarbonylation of propargylic alcohols. Ultimately, efforts will focus on making the production of alkenes in this way catalytic.

The theoretical results have indicated that the allenylidene derivative of complex **9h** is 47 kJ mol^{-1} higher in energy. Whilst attempts to obtain such a derivative *via* the traditional dehydration process have failed, Guy Bertrand has demonstrated that it is possible to transmetallate an allenylidene ligand from silver to ruthenium.[13] The ruthenium complex selected was [$RuCl_2(PPh_3)_3$]; it would be interesting to see if such a transmetallation could be replicated with complex **1**.

Stoichiometric reactions have shown that propargylic substitution of a coordinated propargylic substrate is facile with complex **1**. This work could also be extended to investigate the potential for this process to be made catalytic, or whether the decarbonylation process would act as an inhibitive competitor.

This thesis has described the synthesis and characterisation of a number of novel complexes and the importance of acetate ligands in their formation and subsequent reactivity. Extensive experimental studies have allowed for a novel reaction mechanism to be proposed for the decarbonylation of propargylic alcohols to alkenes. Whilst the fact that some avenues of research reported in this thesis remain incomplete means that a full picture of the reactivity of complex **1** cannot be drawn, the scope for further research into this system is encouraging.

8.5: References

1. Richter-Addo, G. B.; Legzdins, P. *Metal Nitrosyls*, **1992**, Oxford University Press.

2. Hedburg, L.; Hedburg, K.; Satija, S. K.; Swanson, B. I. *Inorg. Chem.* **1985**, *24*, 2766.

3. Antonova, A.B.; Kolobova, N.E.; Petrovsky, P.V.; Lokshin B.V.; Obezyuk, N.S. *J. Organomet. Chem.* **1977**, *137*, 55.

4. Moigno, D.; Callejas-Gasper, B.; Gil-Rubio, J.; Werner, H.; Kiefer, W. *J. Organomet. Chem*. **2002**, *661*, 181.

5. Kostić, N. M.; Fenske, R. F. *Organometallics* **1982**, *1*, 974.

6. Elsenbroich, C. *Organometallics*, **2006**, Wiley-VCH.

7. Bruce, M. I. *Chem. Rev*. **1991**, *91*, 197.

8. Matas, L.; Muniente, J.; Ros, J.; Alvarez-Larena, Á.; Piniella, J. F. *Inorg. Chem. Commun.* **1999**, *2*, 364.

9. Sfinchez-Delgado, R. A.; Thewalt, U.; Valencia, N.; Andriollo, A.; Márquez-Silva, R-L.; Puga, J.; Schollhorn, H.; Klein, H-P.; Fontal, B. *Inorg. Chem.* **1986**, *25*, 1097.

10. Czech, P. T.; Xe, X.-Q.; Fenske, R. F. *Organometallics* **1990**, *9*, 2016.

11. Robinson, S.D., Uttley, M.F., *J. Chem. Soc. Dalton. Trans.*, **1973**, 1912.

12. Hocking, R. K.; Hambley, T. W. *Organometallics* **2007**, 26, 2815.

Abbreviations

Å	Angstrom
AMLA	Ambiphilic Metal Ligand Activation
bpy	bispyridine
Bu	Butyl
°C	Degrees Celsius
cm^{-1}	Wavenumber
CMD	Concerted Metalation Deprotonation
COD	1,5-Cyclooctadiene
Cp	Cyclopentadienyl
Cp*	Pentamethylcyclopentadienyl
Cp’	Methylcyclopentadienyl
CuAAC	Copper Azide-Alkyne Cycloaddition
Cy	Cyclohexyl
DBU	1,8-Diazabicycloundec-7-ene
DCE	Dichloroethane
DCM	Dicholoromethane
δ	Chemical shift in ppm
depe	Diethylphosphinoethane
DEPT	Distortionless Enhancement by Polarisation Transfer
DFT	Density Functional Theory
dippe	Diisopropylphosphinoethane
dmpe	Dimethylphosphinoethane

dppb	Diphenylphosphinobutane
dppe	Diphenylphosphinoethane
dppf	Diphenylphosphinoferrocene
dppm	Diphenylphosphinomethane
EI	Electron Ionisation
ESI	Electrospray Ionisation
Et	Ethyl
Et_2O	Diethyl ether
EtOH	Ethanol
FTIR	Fourier Transform Infrared
Fc	Ferrocene
Fp	$[FeCp(CO)_2]$
Fp’	$[FeCp(PH_3)_2]$
g	gram
(g)	Gas
GC	Gas Chromatography
HOMO	Highest Occupied Molecular Orbital
IMes	1,3-Dimesityl-imidazol-2-ylidene
IPr	1,3-Bis(2,6-diisopropylphenyl)imidazole-2-ylidene
^{i}Pr	Isopropyl
IR	Infrared
J	Joules
J	Coupling constant (in Hertz)

kJ	kilojoules
(l)	Liquid
LAPS	Ligand-Assisted Proton Shuttle
LIFDI	Liquid Injection Field Desorption Ionisation
LUMO	Lowest Unoccupied Molecular Orbital
Me	Methyl
MeOH	Methanol
mg	milligram
mL	millilitre
mmol	millimol
m.p.	Melting Point
Mp	$[MnCp(CO)_2]$
MS	Mass Spectrometry
m/z	mass/charge ratio
$NaBAr^F$	Sodium tetrakis[3,5-bis(trifluoromethyl)phenyl]borate
NHC	N-Heterocyclic Carbene
NMR	Nuclear Magnetic Resonance
OA	Oxidative Addition
OAc	Acetate
OBz	Benzoate
OTf	Triflate
p-BQ	*para*-Benzoquinone
PES	Potential Energy Surface

Ph	Phenyl
phen	Phenanthroline
PhOH	Phenol
Pr	Propyl
PTFE	Polytetrafluoroethylene (Teflon)
Py	Pyridine
Pz	Pyrazolylborate
RCM	Ring Closing Metathesis
ROMP	Ring Opening Metathesis Polymerisation
(s)	Solid
SBM	Sigma Bond Metathesis
^{t}Bu	*tert*-Butyl
^{t}BuOH	*tert*-Butyl alcohol (*t*-butanol)
TEA	Triethylamine
THF	Tetrahydrofuran
TMS	Trimethylsilyl
TOF	Time-of-Flight
Tp	Trispyrazolylborate [$HB(C_3N_2H_3)_3$]
µL	microliter
µmol	micromole
VT	Variable Temperature

List of References

Chapter 1:

1. Bruce, M. I. *Chem. Rev*. **1991**, *91*, 197.
2. Bruce, M. I. *Chem. Rev*. **1998**, *98*, 2797.
3. Bruneau, C.; Dixneuf, P. H. *Acc. Chem. Res*. **1999**, *32*, 311.
4. Katayama, H.; Ozawa, F. *Coord. Chem. Rev*. **2004**, *248*, 1703.
5. Lynam, J. M., *Chem. Eur. J*. **2010**, *16*, 8238.
6. Cadierno, V., Gimeno, J., *Chem. Rev*. **2009**, *109*, 3512.
7. King, R. B. (ed). Coord. *Chem. Rev*. **2004**, *248*, 1531.
8. Bruneau, C., Dixneuf, P. H., Eds. *Metal Vinylidenes and Allenylidenes in Catalysis: From Reactivity to Applications in Synthesis*, **2008**, Wiley VCH: Weinheim, Germany.
9. Dykstra, C. E.; Schaefer, H. F., III, *J. Am. Chem. Soc*. **1978**, *100*, 1378.
10. Silvestre, J., Hoffmann, *Helv. Chim. Acta*. **1985**, *68*, 1461.
11. Stanton, J. F.; DePinto, J. T.; Seberg, R. A.; Hodges, J. A.; McMahon, R. J. *J. Am. Chem. Soc*. **1997**, *119*, 429.
12. Sherrill, C. D.; Brandow, C. G.; Allen, W. D.; Schaefer, H. F., III *J. Am. Chem. Soc*. **1996**, *118*, 7158.
13. Hehre, W. J.; Pople, J. A.; Lathan, W. A.; Radom, L.; Wasserman, E.; Wasserman, Z. R. *J. Am. Chem. Soc*. **1976**, *98*, 4378.
14. Mills, O. S.; Redhouse, A. D. *Chem. Commun*. **1966**, 444.
15. Mills, O. S.; Redhouse, A. D. *J. Chem. Soc. A*. **1968**, 1282.
16. King, R. B.; Saran, M. S. *Chem. Commun*. **1972**, 1053.
17. Fischer, E. O.; Kalder, H. J.; Frank, A.; Köhler, F. H.; Huttner, G. *Angew. Chem. Int. Ed*. **1976**, *15*, 623.

18. Berke, H. *Angew. Chem. Int. Ed.* **1976**, *15*, 624.

19. Zhu, J.; Lin, Z. Theoretical Aspects of Metal Vinylidene and Allenylidene Complexes (Chapter 4) *Metal Vinylidenes and Allenylidenes in Catalysis: From Reactivity to Applications in Synthesis*, (Bruneau, C., Dixneuf, P. H., Eds.) **2008**, Wiley VCH: Weinheim, Germany.

20. Wakatsuki, Y. *J. Organomet. Chem*. **2004**, *689*, 4092.

21. Kostić, N. M.; Fenske, R. F. *Organometallics* **1982**, *1*, 974.

22. Bianchini,C.; Casares, J. A.; Peruzzini, M.; Romerosa, A.; Zanobini, F. *J. Am. Chem. Soc*. **1996**, *118*, 4585.

23. Bruce, M. I.; Swincer, A. G.; Wallis, R. C. *J. Organomet. Chem*. **1979**, *171*, C5.

24. Jiménez-Tenorio, M. A.; Jiménez-Tenorio, M.; Puerta, M. C.; Valerga, P. *Organometallics* **1997**, *16*, 5528.

25. Wolf, J.; Werner, H. *J. Organomet. Chem*. **1987**, *336*, 413.

26. Wolf, J.; Zolk, R.; Schubert, U.; Werner, H. *J. Organomet. Chem*. **1988**, *340*, 161.

27. Werner, H.; Wolf, J.; Muller, G.; Kruger, C. *J. Organomet. Chem*. **1988**, *342*, 381.

28. Delbecq, F. *J. Organomet. Chem*. **1991**, *406*, 171.

29. Carvalho, M. F. N. N.; Henderson, R. A.; Pombeiro, A. J. L.; Richards, R. L. *J. Chem. Soc. Chem. Commun*. **1989,** 1796.

30. Hohn, A.; Werner, H. *Angew. Chem. Int. Ed*. **1986**, *25*, 737.

31. Moigno, D.; Callejas-Gasper, B.; Gil-Rubio, J.; Werner, H.; Kiefer, W. *J. Organomet. Chem*. **2002**, *661*, 181.

32. Schilling, B. E. R.; Hoffmann, R.; Lichtenberger. D. L. *J. Am. Chem. Soc*. **1979**, *101*, 585.

33. Gamasa, M. P.; Gimeno, J.; Lastra, E.; Martin, B. M.; Anillo, A.; Tiripicchio, A. *Organometallics* **1992**, *11*, 1373.

34. Miller, D. C.; Angelici, R. J. *Organometallics* **1991**, *10*, 79.

35. Bruce, M. I.; Dean, C.; Duffy, D. N.; Humphrey, M. G.; Koustsantonis, G. A. *J. Organomet. Chem*. **1986**, *314*, 213.

36. Consiglio, G.; Morandini, F.; Ciani, G. F.; Sironi, A. *Organometallics* **1986**, *5*, 1976.

37. Beddoes, R. L.; Bitcon, C.; Grime, R. W.; Ricalton A.; Whiteley, M. W. *J. Chem. Soc. Dalton Trans*. **1995**, 2873.

38. Consiglio, G.; Morandini, F. *Inorg. Chim. Acta*. **1987**, *127*, 79.

39. Yang, S. Y.; Wen, T. B.; Jia, G.; Lin, Z. *Organometallics* **2000**, *19*, 5477.

40. Ariafard, A.; Zare, K. *Inorg. Chem. Commun*. **2004**, *7*, 999.

41. Esteruelas, M. A.; Gómez, A. V.; López, A. M.; Modrego, J.; Oñate, E. *Organometallics* **1997**, *16*, 5826.

42. Cadierno, V.; Gamasa, M. P.; Gimeno, J.; López-González, M. C.; Borge, J.; García-Granda, S. *Organometallics* **1997**, *16*, 4453.

43. Grime, R. W.; Helliwell, M.; Hussain, Z. I.; Lancashire, H. N.; Mason, C. R.; McDouall, J. J. W.; Mydlowski, C. M.; Whiteley, M. W. *Organometallics* **2008**, *27*, 857.

44. Bruce, M. I.; Wallis, R. C. *J. Organomet.Chem*. **1978**, *161*, C1.

45. Nesmeyanov, A. N.; Aleksandrov, G.G.; Antonova, A.B.; Anisimov, K.N.; Kolobova, N.E.; Struchkov, Y.T. *J. Organomet. Chem*. **1976**, *110*, C36.

46. Antonova, A.B.; Kolobova, N.E.; Petrovsky, P.V.; Lokshin B.V.; Obezyuk, N.S. *J. Organomet. Chem*. **1977**, *137*, 55.

47. Kolobova, N.E.; Antonova, A.B.; Khitrova, O.M.; Antipin M.Y.; Struchkov, Y.T. *J. Organomet. Chem*. **1977**, *137*, 69.

48. Bellerby, J.M.; Mays, H. J. *J. Organomet. Chem*. **1976**, *117*, C21.

49. Bruce, M. I., Wong, F. S., Skelton, B. W., White, A. H., *J. Chem. Soc. Dalton. Trans*. **1982**, 2203.

50. Bullock, R. M., *J. Chem. Soc. Chem. Commun*. **1989**, 165.

51. Haquette, P., Pirio, N., Touchard, D., Toupey, L., Dixneuf, P. H., *J. Chem. Soc. Chem. Commun*. **1993**, 163.

52. Touchard, D., Haquette, P., Pirio, N., Toupet, L., Dixneuf, P. H., *Organometallics* **1993**, *12*, 3132.

53. Bruce, M. I., Hall, B. C., Zaitseva, N. N., Skelton, B. W., White, A. H., *J. Organomet. Chem*. **1996**, *522*, 307.

54. Bruce, M. I., Hall, B. C., Zaitseva, N. N., Skelton, B. W., White, A. H., *Dalton Trans*. **1998**, 1793.

55. Wakatsuki, Y., Koga, N., Yamazaki, H., Morokuma, K., *J. Am. Chem. Soc*. **1994**, *116*, 8105.

56. Braunstein, P.; Naud, F. *Angew. Chem. Int. Ed*. **2001**, *40*, 680.

57. Werner, H., Stark, A., Schulz, M., Wolf, J., *Organometallics* **1992**, *11*, 1126.

58. Selegue, J. P., *Organometallics* **1982**, *1*, 217.

59. Bustelo, E., Jiménez-Tenorio, M., Puerta, M. C., Valerga, P., *Organometallics* **1999**, *18*, 4563.

60. Aneetha, H., Jiménez-Tenorio, M., Puerta, M. C., Valerga, P., *Organometallics* **2003**, *22*, 2001.

61. Cadierno, V., Gamasa, M. P., Gimeno, J., González-Cueva, M., Lastra, E., Borge, J., García-Granda, S., Pérez-Carreño, E., *Organometallics* **1996**, *15*, 2137.

62. Werner, H., Rappert, T., Wiedemann, R., Wolf, J., Mahr, N., *Organometallics* **1994**, *13*, 2721.

63. Bustelo, E., Jiménez-Tenorio, M., Puerta, M. C., Valerga, P., *Eur. J. Inorg. Chem*. **2001**, 2391.

64. Martín, M.; Gevert. O.; Werner, H. *Dalton Trans.* **1996**, 2275.

65. Cadierno, V.; Gamasa, M. P.; Gimeno, J.; Borge, J.;García-Granda, S. *Organometallics* **1997**, *16*, 3178.

66. Cadierno, V.; Conejero, S.; Gamasa, M. P.; Gimeno, J.; Rodríguez, M. A. *Organometallics* **2002**, *21*, 203.

67. Fischer, H.; Szesni, N. *Coord. Chem. Rev*. **2004**, *248*, 1659.

68. Cadierno, V.; Crochet, P.; Gimeno, J. Preparation and Stoichiometric Reactivity of Metal Allenylidene Complexes (Chapter 2) *Metal Vinylidenes and Allenylidenes in Catalysis: From Reactivity to Applications in Synthesis*, (Bruneau, C., Dixneuf, P. H., Eds.) **2008**, Wiley VCH: Weinheim, Germany.

69. Bruce, M. I., Wallis, R. C., *Aust. J. Chem*. **1979**, *32*, 1471.

70. Kelley, C.; Lugan, N.; Terry, M. R.; Geoffroy, G. L.; Haggerty, B. S.; Rheingold, A.L. *J. Am. Chem. Soc*. **1992**, *114*, 6735.

71. Bruce, M.I. Preparation and Stoichiometric Reactivity of Mononuclear Metal Vinylidene Complexes (Chapter 1) *Metal Vinylidenes and Allenylidenes in Catalysis: From Reactivity to Applications in Synthesis*, (Bruneau, C., Dixneuf, P. H., Eds.) **2008**, Wiley VCH: Weinheim, Germany.

72. Baya, M.; Esteruelas, M. A. *Organometallics* **2002**, *21*, 2332.

73. Werner, H.; Baum, M.; Schneider, D.; Windmiiller, B. *Organometallics*, **1994**, *13*, 1089.

74. Katayama, H.; Onitsuka, K.; Ozawa, F. *Organometallics* **1996**, *15*, 4642.

75. Connelly, N. G.; Geiger, W. E.; Lagunas, M. C.; Metz, B.; Rieger, A. L.; Rieger, P. H.; Shaw, M. J. *J. Am. Chem. Soc*. **1995**, *117*, 12202.

76. Sakurai, H.; Fujii, T.; Sakamoto, K. *Chem. Lett*. **1992**, 339.

77. Naka, A.; Okazaki, S.; Hayashi, M.; Ishikawa, M. *J. Organomet. Chem*. **1995**, *499*, 35.

78. Ilg, K.; Paneque, M.; Poveda, M. L.; Rend_on, N.; Santos, L. L.; Carmona, E.; Mereiter, K. *Organometallics* **2006**, *25*, 2230.

79. Venkatesan, K.; Blacque, O.; Fox, T.; Alfonso, M.; Schmalle, H. W.; Kheradmandan, S.; Berke, H. *Organometallics* **2005**, *24*, 920.

80. Venkatesan, K.; Fox, T.; Schmalle, H. W.; Berke, H. *Eur. J. Inorg. Chem*. **2005**, 901.

81. Miller, D. C.; Angelici, R. J. *Organometallics* **1991**, *10*, 79.

82. Miura, T.; Iwasawa, N. *J. Am. Chem. Soc*. **2002**, *124*, 518.

83. Ikeda, Y.; Yamaguchi, T.; Kanao, K.; Kimura, K.; Kamimura, S.; Mutoh,Y.; Tanabe,Y.; Ishii, Y. *J. Am. Chem. Soc*. **2008,** *130*, 16856.

84. Mutoh,Y.; Ikeda,Y.;Kimura,Y.; Ishii,Y. *Chem.Lett*. **2009,** *38*, 534.

85. Mutoh, Y.; Imai, K.; Kimura, Y.; Ikeda, Y.; Ishii, Y. *Organometallics* **2011**, *30*, 204.

86. P. C. Ting, Y. C. Lin, G. H. Lee, M. C. Cheng, Y. Wang, *J. Am. Chem. Soc*. **1996**, *118*, 6433.

87. Sato, M.; Kawata, Y.; Shintate, H.; Habata, Y.; Akabori, S.; Unoura, K.; *Organometallics* **1997**, *16*, 1693.

88. Sato, M.; Shintate, H.; Kawata, Y.; Sekino, M.; Katada, M.; Kawata, S. *Organometallics* **1994**, *13*, 1956.

89. Sato, M.; Iwai, A.; Watanabe, M. *Organometallics* **1999**, *18*, 3208.

90. Olivan, M.; Clot, E.; Eisenstein, O.; Caulton, K. G. *Organometallics* **1998**, *17*, 3091.

91. Johnson, D. G.; Lynam, J. M.; Slattery, J. M.; Welby, C. E. *Dalton Trans*. **2010**, *39*, 10432.

92. De Angelis, F.; Sgamellotti, A.; Re, N. *Organometallics* **2002**, *21*, 2715.

93. De Angelis, F.; Sgamellotti, A.; Re, N. *Organometallics* **2002**, *21*, 5944.

94. Höhn, A.; Werner, H. *J. Organomet. Chem*. **1990**, *382*, 255.

95. Bianchini, C.; Peruzzini, M.; Vacca, A.; Zanobini, F. *Organometallics* **1991**, *10*, 3697.

96. Wakatsuki, Y.; Koga, N.; Werner, H.; Morokuma, K. *J. Am. Chem. Soc*. **1997**, *119*, 360.

97. Grotjahn, D. B.; Zeng, X.; Coosky, A. L. *J. Am. Chem. Soc*. **2006**, *128*, 2798.

98. Grotjahn, D. B.; Zeng, X.; Cooksy, A. L.; Kassel, W. S.; DiPasquale, A. G.; Zakharov, L. N.; Rheingold, A. L. *Organometallics* **2007**, *26*, 3385.

99. Cowley, M. J.; Lynam, J. M.; Slattery, J. M. *Dalton Trans*. **2008**, 4552.

100. De Angelis, F.; Sgamellotti, A.; Re, N. *Organometallics* **2007**, *26*, 5285.

101. De Angelis, F.; Sgamellotti, A.; Re, N. *Dalton Trans*. **2004**, 3225.

102. de Los Ríos, I.; Jiménez-Tenorio, M.; Puerta, M. C.; Valerga, P. *J. Am. Chem. Soc*. **1997**, *119*, 6529.

103. Tokunaga, M.; Suzuki,T.; Koga, N.; Fukushima, T.;Horiuchi, A.; Wakatsuki, Y. *J. Am. Chem. Soc*. **2001**, *123*, 11917.

104. Weyershausen, B.; Dötz, K. H. *Eur. J. Inorg. Chem*. **1999**, 1057.

105. Bruce, M. I.; Swincer, A. G.; Thomson, B. J.; Wallis, R. C.; *Aust. J. Chem*. **1980**, *33*, 2605.

106. Dötz, K. H.; Sturm, W. *Organometallics* **1987**, *6*, 1424.

107. Bianchini, C.; Marchi, A.; Mantovani, N.; Marvelli, L.; Masi, D.; Peruzzini, M.; Rossi, R. *Eur. J. Inorg. Chem*. **1998**, 211.

108. Gamasa, M. P.; Gimeno, J.; Martín-Vaca, B. M.; Isea, R.; Vegas, A. *J. Organomet. Chem*. **2002**, *651*, 22.

109. Hussain, Z. I.; Whiteley, M. W. *J. Chem. Soc. Dalton. Trans*. **1996**, 3893.

110. Varela-Fernández, A.; García-Yebra, C.; Varela, J. A.; Esteruelas, M. A.; Saá, C. *Angew. Chem. Int. Ed*. **2010**, *49*, 4278.

111. Harlow, K. J.; Hill, A. F.; Wilton-Ely, J. D. E. T. *J. Chem. Soc. Dalton Trans.* **1999**, 285.

112. Touchard, D.; Guesmi, S.; Bouchaib, M.; Haquette, P.; Daridor, A.; Dixneuf, P. H. *Organometallics* **1996**, *15*, 2580.

113. Fürstner, A.; Hill, A. F.; Liebl, M.; Wilton-Ely, J. D. E. T. *Chem. Commun.* **1999**, 601.

114. Schanz, H-J.; Jafarpour, L.; Stevens, E. D.; Nolan, S. P. *Organometallics* **1999**, *18*, 5187.

115. Fürstner, A.; Guth, O.; Düffels, A.; Seidel, G.; Liebl, M.; Gabor, B.; Mynott, R. *Chem. Eur. J.* **2001**, *7*, 4811.

116. Boeda, F.; Clavier, H.; Nolan, S. P. *Chem. Commun*. **2008**, 2726.

117. Malacea, R.; Dixneuf, P. H. Ruthenium Allenylidenes and Indenylidenes as Catalysts in Alkene Metathesis (Chapter 8) *Metal Vinylidenes and Allenylidenes in Catalysis: From Reactivity to Applications in Synthesis*, (Bruneau, C., Dixneuf, P. H., Eds.) **2008**, Wiley VCH: Weinheim, Germany.

118. Castarlenas, R.; Dixneuf, P. H. *Angew. Chem. Int. Ed.* **2003**, *42*, 4524.

119. Castarlenas, R.; Vovard, C.; Fischmeister, C.; Dixneuf, P. H. *J. Am. Chem. Soc*. **2006**, *128*, 4079.

120. Shaffer, A.; Chen, C-L.; Beatty, A. M.; Valente, E. J.; Schanz, H-J. *J. Organomet. Chem.* **2007**, *692*, 5221.

121. Jung, S.; Brandt, C. D.; Werner, H. *New J. Chem.* **2001**, *25*, 1101.

122. Bustelo, E.; Jiménez-Tenorio, M.; Mereiter, K.; Puerta, M. C.; Valerga, P. *Organometallics* **2002**, *21*, 1903.

123. Cadierno, V.; Diéz, J.; García-Garrido, S. E.; Gimeno, J. *Organometallics* **2005**, *24*, 3111.

124. Rigaut, S.; Touchard, D.; Dixneuf, P. H. *Organometallics* **2003**, *22*, 3980.

125. Bigeault, J.; Giodano, L.; Buono, G. *Angew. Chem. Int. Ed.* **2005**, *44*, 4753.

126. Seregin, I. V.; Gevorgyan, V. *J. Am. Chem. Soc.* **2006**, *128*, 12050.

127. Himo, F.; Lovell, T.; Hilgraf, R.; Rostostsev, V. V.; Noodleman, L.; Sharpless, K. B.; Fokin, V. V. *J. Am. Chem. Soc.* **2005**, *127*, 210.

128. Nishibayashi, Y.; Milton, M. D.; Inada, Y.; Yoshikawa, M.; Wakiji, I.; Hidai, M.; Uemura, S. *Chem. Eur. J.* **2005**, *11*, 1433.

129. Doucet, H.; Höfer, J.; Bruneau, C.; Dixneuf, P. H. *J. Chem. Soc. Chem. Commun.* **1993**, 850.

130. Doucet, H.; Matin-Vaca, B.; Bruneau, C.; Dixneuf, P. H. *J. Org. Chem.* **1995**, *60*, 7247.

131. Gemel, C; Trimmel, G.; Slugovc, C.; Kremel, S.; Mereiter, K.; Schmid, R.; Kirchner, K. *Organometallics* **1996**, *15*, 3998.

132. Mitsudo, T.; Hori, Y.; Yamazaki, Y.; Watanabe, Y. *J. Org. Chem.* **1987**, *52*, 2230.

133. Bruneau, C. *Anti*-Markovnikov Additions of *O*-, *N*-, *P*-Nucleophiles to Triple Bonds with Ruthenium Catalysts (Chapter 10) *Metal Vinylidenes and Allenylidenes in Catalysis: From Reactivity to Applications in Synthesis*, (Bruneau, C., Dixneuf, P. H., Eds.) **2008**, Wiley VCH: Weinheim, Germany.

134. Alonso, F.; Beletskaya, I. P.; Yus, M. *Chem. Rev.* **2004**, *104*, 3079.

135. Tokunaga, M.; Wakatsuki, Y. *Angew. Chem. Int. Ed.* **1998**, *37*, 2867.

136. Suzuki, T.; Tokunaga, M.; Wakatsuki, Y. *Org. Lett.* **2001**, *3*, 735.

137. Devanne, D.; Ruppin, C.; Dixneuf, P. H. *J. Org. Chem.* **1988**, *53*, 925.

138. Bruneau, C.; Kabouche, Z.; Neveux, M.; Seiller, B.; Dixneuf, P. H. *Inorg. Chim. Acta.* **1994**, *222*, 154.

139. Darcel, C.; Bruneau, C.; Dixneuf, P. H.; Neef, G. *J. Chem. Soc. Chem. Commun.* **1994**, 333.

140. Costin, S.; Rath, N. P.; Bauer, E. B. *Adv. Synth. Catal.* **2008**, *350*, 2414.

141. Nishibayashi, Y.; Wakiji, I.; Hidai, M. *J. Am. Chem. Soc.* **2000**, *122*, 11019.

142. Ammal, S. C.; Yoshikai, N.; Inada, Y.; Nishibayashi, Y.; Nakamura, E. *J. Am. Chem. Soc.* **2005**, *127*, 9428.

143. Fürstner, A.; Picquet, M.; Bruneau, C.; Dixneuf, P. H. *Chem. Commun.* **1998**, 1315.

144. Picquet, M.; Touchard, D.; Bruneau, C.; Dixneuf, P. H. *New. J. Chem.* **1999**, *23*, 141.

145. Picquet, M.; Bruneau, C.; Dixneuf, P. H. *Chem. Commun.* **1998**, 2249.

146. Sémeril, D.; Le Nôtre, J.; Bruneau, C.; Dixneuf, P. H.; Kolomiets, A. F.; Osipov, S. *New. J. Chem.* **2001**, *25*, 16.

147. Castarlenas, R.; Sémeril, D.; Noels, A. F.; Demnoceau, A, Dixneuf, P. H. *J. Organomet. Chem.* **2002**, *663*, 235.

148. Antonucci, A.; Bassetti, M.; Bruneau, C.;Dixneuf, P. H.; Pasquini, C. *Organometallics* **2010**, *29*, 4524.

149. Dorta, R.; Kelly III, R. A.; Nolan, S. P. *Adv. Synth. Catal.* **2004**, *346*, 917.

150. Jafarpour, L.; Schanz, H-J.; Stevens, E. D.; Nolan, S.P. *Organometallics* **1999**, *18*, 5416.

151. Mitchell, R. W.; Spencer, A.; Wilkinson, G. *J. Chem. Soc., Dalton Trans.* **1973**, 846.

152. Lynam, J. M.; Welby, C. E.; Whitwood, A. C. *Organometallics* **2009**, *28*, 1320.

153. Ford, C. E.; Final Year MChem report, *Synthesis and Reactivity of an η^3-Butenynyl Towards CO, ^{t}BuNC and XylNC. Formation of a Novel Diacetate-Substituted Vinylidene Compound,* University of York, **2007**.

154. Zhang, L.; Chen, X.; Xue, P.; Sun, H. H. Y.; Williams, I. D.; Sharpless, K. B.; Fokin, V. V.; Jia, G. *J. Am. Chem. Soc.* **2005**, *127*, 15998.

Chapter 2:

1. Bruce, M. I. *Chem. Rev*. **1991**, *91*, 197.
2. Bruneau, C.; Dixneuf, P. H. *Acc. Chem. Res*. **1999**, *32*, 311.
3. Katayama,H.; Ozawa, F. *Coord. Chem. Rev*. **2004**, *248*, 1703.
4. Lynam, J. M., *Chem. Eur. J.* **2010**, *16*, 8238.
5. Tokunaga, M.; Suzuki, T.; Koga, N.; Fukushima, T.; Horiuchi, A.; Wakatsuki, Y. *J. Am. Chem. Soc.* **2001**, *123*, 11917.
6. Bruneau, C.; Dixneuf, P. H. *Angew. Chem. Int. Ed*. **2006**, *45*, 2176.
7. Puerta, M. C.; Valerga, P. *Coord. Chem. Rev*. **1999**, *193-195*, 977.
8. Jiménez Tenorio, M. A.; Jiménez Tenorio, M.; Puerta, M. C.; Valerga, P. *Organometallics* **2000**, *19*, 1333.
9. Katayama, H.; Ozawa, F.; *Chem. Lett*. **1998**, 67.
10. Opstal, T.; Verpoort, T. *J. Mol. Catal. A*. **2003**, *200*, 49.
11. Silvestre, J., Hoffmann, *Helv. Chim. Acta.* **1985**, *68*, 1461.
12. Y. Wakatsuki, *J. Organomet. Chem*., **2004**, *689*, 4092.
13. Johnson, D. J., Lynam. J. M., Slattery, J. M., Welby, C. E., *Dalton Trans*. **2010**, *39*, 10432.
14. Le Lagadec, R.; Roman, E.; Toupet, L.; Muller, U.; Dixneuf, P. H. *Organometallics* **1994**, *13*, 5030.
15. Touchard, D.; Haquette, P.; Daridor, A.; Romero, A.; Dixneuf, P. H. *Organometallics* **1998**, *17*, 3844.
16. Bruce, M. I.; Hall, B. C.; Zaitseva, N. N.; Skelton, B. W.; White, A. H. *J. Organomet. Chem*. **1996**, *522*, 307.
17. Bruce, M. I.; Hall, B. C.; Zaitseva, N. N.; Skelton, B. W.; White, A. H.; *Dalton Trans*. **1998**, 1793.

18. Werner, H.; Stark, A.; Schulz, M.; Wolf, J. *Organometallics* **1992**, *11*, 1126.

19. Werner, H.; Schulz, M.; Windmuller, B. *Organometallics* **1995**, *14*, 3659.

20. Bader, A.; Linder, E. *Coord. Chem. Rev*. **1991**, *108*, 27.

21. Slugovc, C.; Mauthner, K.; Kacetl, M.; Mereiter, K.; Schmid, R.; Kirchner, K. *Chem. Eur. J*. **1998**, *4*, 2043.

22. Lynam, J. M.; Welby, C. E.; Whitwood, A. C. *Organometallics* **2009**, *28*, 1320.

23. All complexes reported in this thesis found to contain mutually *trans* phosphine ligands have δ_P values in the range 30-40 ppm; for those in which the phosphines are mutually *cis*, this range is higher, typically between δ_P 45-70.

24. Robinson, S.D.; Uttley, M.F. *J. Chem. Soc. Dalton. Trans.* **1973**, 1912.

25. Deacon, G.B., Phillips, R.J., *Coord. Chem. Rev.* **1980**, *33*, 227.

26. Katayama, H.; Ozawa, F. *Organometallics* **1998**, *17*, 5190.

27. Wolf, J. Stüer, W; Grünwald, C.; Gevert, O; Laubender, M.; Werner, H. *Eur. J. Inorg. Chem.* **1998**, 1827.

28. Grunwald, C., Laubender, M., Wolf, J., Werner, H., *J. Chem. Soc. Dalton. Trans.* **1998**, 833.

29. Wakatsuki, Y., Koga, N., Yamazaki, H., Morokuma, K., *J. Am. Chem. Soc.* **1994**, *116*, 8105.

30. Boutadla, Y.; Davies, D. L.; Macgregor, S. A.; Poblador-Bahamonde, A. I. *Dalton Trans.* **2009**, 5820.

31. Lapointe, D.; Fagnou, K. *Chem. Lett*. **2010**, *39*, 1118.

32. Wu, W., Wu, W., Ji, S., Guo, H., Zhao, J., *Eur. J. Inorg. Chem.* **2010**, 4470.

33. Werner, H.; Baum, M.; Schneider, D.; Windmuller, B. *Organometallics* **1994**, *13*, 1089.

34. Connelly, N. G.; Geiger, W. E.; Lagunas, M. C.; Metz, M.; Rieger, A. L.; Rieger, P. H.; Shaw, M. J.; *J. Am. Chem. Soc*. **1995**, *117*, 12202.

35. Katayama, H.; Onitsuka, K.; Ozawa, F. *Organometallics* **1996**, *15*, 4642.

36. Werner, H.; Lass, R. W.; Gevert, O.; Wolf, J. *Organometallics* **1997**, *16*, 4077.

37. Venkatesan, K.; Blacque, O.; Fox, T.; Alfonso, M.; Schmalle, H. W.; Kheradmandan, S.; Berke, H. *Organometallics* **2005**, 24, 920.

38. Venkatesan, K.; Fox, T.; Schmalle, H. W.; Berke, H. *Eur. J. Inorg. Chem*. **2005**, 901.

39. Ikeda, Y.; Yamaguchi, T.; Kanao, K.; Kimura, K.; Kamimura, S.; Mutoh, Y.; Tanabe, Y.; Ishii, Y. *J. Am. Chem. Soc*. **2008**, *130*, 16856.

40. Mutoh, Y.; Ikeda, Y.; Kimura, Y.; Ishii, Y. *Chem. Lett*. **2009**, *38*, 534.

41. Sheldrick, G. *Acta Crystallographica Section A* **2008**, *64*, 112-122.

42. Dolomanov, O. V.; Bourhis, L. J.; Gildea, R. J.; Howard J. A. K.; Puschmann, H. *J. Appl. Cryst*. **2009**, *42*, 339.

Chapter 3:

1. Yam, V. W. W. *Acc. Chem. Res.* **2002**, *35*, 555.
2. Long, N. J.; Williams, C. K. *Angew. Chem. Int. Ed.* **2003**, *42*, 2586.
3. Szafert, S.; Gladsyz, J. A. *Chem. Rev.* **2003**, *103*, 4175.
4. Yam, V. W. W. *J. Organomet. Chem.* **2004**, *689*, 1393.
5. D'Alessandro, D. M; Keene, F. R. *Chem. Rev*. **2006**, *106*, 2270.
6. Aguire-Etcheverry, P.; O'Hare, D. *Chem. Rev.* **2010**, *110*, 4839.
7. Hartwig, J. F. *Organotransition Metal Chemistry: From Bonding to Catalysis*, **2010**, University Science Books.
8. Manna, J.; John, K. D.; Hopkins, M. D. *Adv. Organomet. Chem.* **1995**, *38*, 79.
9. Chinchilla, R.; Nájera, C. *Chem. Rev.* **2007**, *107*, 874.
10. Bruce, M. I.; Wallis, R. C. *J. Organomet. Chem.* **1978**, *161*, C1.
11. Bruce, M. I.; Wallis, R. C. *Aust. J. Chem*. **1979**, *32*, 1471.
12. Bullock, R. M. *J. Chem. Soc. Chem. Commun.* **1989**, 165.
13. Touchard, D.; Hacquette, P.; Pirio, N.; Toupet, L.; Dixneuf, P. H.; *Organometallics* **1993**, *12*, 3132.
14. Hacquette, P.; Pirio, N.; Touchard, D.; Toupet, L.; Dixneuf, P. H. *J. Chem. Soc. Chem. Commun.* **1993**, 163.
15. Faulkner, C. W.; Ingham, S. L.; Khan, M. S.; Lewis, J.; Long, N. J.; Raithby, P. R. *J. Organomet. Chem*. **1994**, *482*, 139.
16. Touchard, D.; Marice, C.; Cadierno, V.; Hacquette, P.; Toupet, L.; Dixneuf, P. H. *J. Chem. Soc. Chem. Commun.* **1994**, 859.
17. Martín, M.; Gevert, O.; Werner, H.; *J. Chem. Soc. Dalton. Trans.* **1996**, 2275.

18. Touchard, D.; Hacquette, P.; Guesmi, S.; Le Pichon, L.; Doridor, A.; Toupet, L.; Dixneuf, P. H.; *Organometallics* **1997**, *16*, 3640.

19. Olivier, C.; Kim, B.; Touchard, D.; Rigaut, S., *Organometallics* **2008**, *27*, 509.

20. Experimental information is provided in Thomas Eschermann's Erasmus report.

21. Spencer, A.; Wilkinson, G. *J. Chem. Soc. Dalton. Trans*. **1974**, 786.

22. Lynam, J. M.; Welby, C. E.; Whitwood, A. C. *Organometallics* **2009**, *28*, 1320.

23. Hocking, R. K.; Hambley, T. W. *Organometallics* **2007**, 26, 2815.

24. Robinson, S. D.; Uttley, M. F. *J. Chem. Soc. Chem. Commun*. **1972**, 1047.

25. Robinson, S. D.; Uttley, M. F. *J. Chem. Soc. Dalton. Trans*. **1973**, 1912.

26. Dobson, A.; Robinson, S. D.; Uttley, M. F.; *J. Chem. Soc. Dalton. Trans*. **1975**, 370.

27. Creswell, C. J.; Dobson, A.; Moore, D. S. Robinson, S. D. *Inorg. Chem.* **1979**, *18*, 2055.

28. Richter-Addo, G. B.; Legzdins, P. *Metal Nitrosyls*, **1992**, Oxford University Press.

29. Orpen, A. G.; Brammer, L.; Allen, F. H.; Kennard, O.; Watson, D. G.; Taylor, R. *J. Chem. Soc. Dalton Trans.* **1989**, S1.

30. Literature data for ^{1}H NMR CH_3COOH (authentic sample in CD_2Cl_2).

31. Doucet, H.; Martin-Vaca, B.; Bruneau, C.; Dixneuf, P. H. *J. Org. Chem.* **1995**, *60*, 7247.

32. Manna, J.; John, K. D.; Hopkins, M. D. *Adv. Organomet. Chem.* **1995**, *38*, 79.

33. Wisner, J. M.; Bartczak, T. J.; Ibers, J. A. *Inorg. Chim. Acta.* **1985**, *100*, 115.

34. Bruce, M. I.; Hinterding, P.; Tiekink, E. R. T.; Skelton, B. W.; White, A. H. *J. Organomet. Chem.* **1993**, *450*, 209.

35. Santos, A.; López, J.; Matas, L.; Ros, J.; Galán, A.; Echavarren, A. M. *Organometallics* **1993**, *12*, 4215.

36. Echavarren, A. M.; López, J.; Santos, A.; Romero, A.; Hermoso, J. A.; Vegas, A.; *Organometallics* **1991**, *10*, 2371.

37. Romero, A.; Vegas, A.; Santos, A.; Martinez-Ripoll, M. *J. Organomet. Chem.* **1987**, *319*, 103.

38. Panella, L; Feringa, B. L; de Vries, J. G; Minaard, A. J; *Org. Lett*. **2005**, *7*, 4177.

39. Hiett, N. P.; Lynam, J. M.; Welby, C. E.; Whitwood, A. C. *J. Organomet. Chem.* **2011**, *696*, 378.

Chapter 4:

1 Bruce, M. I. *Chem. Rev*. **1991**, *91*, 197.

2 Zhu, J.; Lin, Z. Theoretical Aspects of Metal Vinylidene and Allenylidene Complexes (Chapter 4) *Metal Vinylidenes and Allenylidenes in Catalysis: From Reactivity to Applications in Synthesis*, (Bruneau, C., Dixneuf, P. H., Eds.) **2008**, Wiley VCH: Weinheim, Germany.

3 Lynam, J. M. *Chem. Eur J.* **2010**, *16*, 8238.

4 Wakatsuki, Y. *J. Organometal. Chem*. **2004**, *689*, 4092.

5 Jensen, F. *Introduction to Computational Chemistry* (2nd Ed.) **2007**, Wiley.

6 Olivan, M.; Clot, E.; Eisenstein, O.; Caulton, K. G. *Organometallics* **1998**, *17*, 3091.

7 Johnson, D. G.; Lynam, J. M.; Slattery, J. M.; Welby, C. E. *Dalton Trans*. **2010**, *39*, 10432.

8 Silvestre, J.; Hoffmann, R. *Helv. Chim. Acta* **1985**, *68*, 1461.

9 Wakatsuki, Y.; Koga, N.; Yamazaki, H.; Morokumal, K. *J. Am. Chem. Soc.* **1994**, *116*, 8105.

10 Cadierno, V.; Gamasa, M. P.; Gimeno, J. Pérez-Carreño, E.; García-Granda, S. *Organometallics* **1999**, *18*, 2821.

11 Cadierno, V.; Gamasa, M. P.; Gimeno, J.; González-Bernardo, C.; Pérez-Carreño, E.; García-Granda, S. *Organometallics* **2001**, *20*, 5177.

12 De Angelis, F.; Sgamellotti, A.; Re, N. *Organometallics* **2002**, *21*, 2715.

13 De Angelis, F.; Sgamellotti, A.; Re, N. *Organometallics* **2002**, *21*, 5944.

14 Bassetti, M.; Cadierno, V.; Gimeno, J.; Pasquini, C. *Organometallics* **2008**, *27*, 5009.

15 Nesmeyanov, A. N.; Aleksandrov, G. G; Antonova, A. B.; Anisimov, K. N.; Kolobova, N. E.; Struchkov, Yu. T. *J.Organomet. Chem.* **1976**, *110*, C36.

16 Antonova, A. B.; Kolobova, N. E.; Petrovsky, P. V.; Lokshin, B. V.; Obezyuk, N. S. *J. Organomet. Chem.* **1977**, *137*, 55.

17 Werner, H.; Baum, M.; Schneider, D.; Windmüller, B. *Organometallics* **1994**, *13*, 1089.

18 Wakatsuki, Y.; Koga, N.; Werner, H.; Morokuma, K. *J. Am. Chem. Soc.* **1997**, *119*, 360.

19 Grotjahn, D. B.; Zeng, X.; Coosky, A. L. *J. Am. Chem. Soc.* **2006**, *128*, 2798.

20 Grotjahn, D. B.; Zeng, X.; Cooksy, A. L.; Kassel, W. S.; DiPasquale, A. G.; Zakharov, L. N.; Rheingold, A. L. *Organometallics* **2007**, *26*, 3385.

21 De Angelis, F.; Sgamellotti, A.; Re, N. *Organometallics* **2007**, *26*, 5285

22 Vastine, B. A.; Hall, M. B. *Organometallics* **2008**, *27*, 4325.

23 Cowley, M. J.; Lynam, J. M.; Slattery, J. M. *Dalton Trans.* **2008**, 4552.

24 De Angelis, F.; Sgamellotti, A.; Re, N. *Dalton Trans.,* **2004**, 3225.

25 Tokunaga, M.; Suzuki,T.; Koga, N.; Fukushima, T.;Horiuchi, A.; Wakatsuki, Y. *J. Am. Chem. Soc.* **2001**, *123*, 11917.

26 Grotjahn,D. B.; Miranda-Soto, V.; Kragulj, E. J.; Lev, D. A.; Erdogan, G.; Zeng, X.; Cooksy, A. L. *J. Am. Chem. Soc*. **2008**, *130*, 20.

27 Bustelo, E.; Jiménez-Tenorio, M.; Puerta, M. C.; Valerga, P. *Organometallics* **1999**, *18*, 4563.

28 Bustelo, E.; Jiménez-Tenorio, M.; Puerta, M. C.; Valerga, P. *Organometallics* **1999**, *18*, 950.

29 Aneetha, H.; Jiménez-Tenorio, M.; Puerta, M. C.; Valerga, P.; Mereiter, K. *Organometallics* **2003**, *22*, 2001.

30 Lafrance, M.; Rowley, C. N.; Woo, T. K.; Fagnou, K. *J. Am. Chem. Soc.* **2006**, *128*, 8754.

31 Davies, D. L.; Donald, S. M. A.; Macgregor, S. A.*J. Am. Chem. Soc.* **2005**, *127*, 13754.

32 Lapointe, D.; Fagnou, K. *Chem. Lett*. **2010**, *39*, 1118.

33 Boutadla, Y.; Davies, D. L.; Macgregor, S. A.; Poblador-Bahamonde, A. I. *Dalton Trans.*, **2009**, 5820.

34 Adapted from Davies, D. L.; Macgregor, S. A.; Poblador-Bahamonde, A. I. *Dalton Trans.* **2010**, 10520.

35 Esteruelas, M. A., Lahoz, F. J., López, A. M., Oñate, Oro, L. A., *Organometallics* **1994**, *13*, 1669.

36 Shaffer, A.; Chen, C-L.; Beatty, A. M.; Valente, E. J.; Schanz, H-J. *J. Organomet. Chem.* **2007**, *692*, 5221.

37 Daniel, T.; Mahr, N.; Braun, T.; Werner, H. *Organometallics*, **1993**, *12*, 1475.

38 Ropp, J. *J. Am. Chem. Soc*. **1960**, *82*, 842.

39 Mitsudo, T.; Hori, Y.; Yamazaki, Y.; Watanabe, Y. *J. Org. Chem.* **1987**, *52*, 2230.

40 Bruneau, C. *Anti*-Markovnikov Additions of *O*-, *N*-, *P*-Nucleophiles to Triple Bonds with Ruthenium Catalysts (Chapter 10) *Metal Vinylidenes and Allenylidenes in Catalysis: From Reactivity to Applications in Synthesis*, (Bruneau, C., Dixneuf, P. H., Eds.) **2008**, Wiley VCH: Weinheim, Germany.

41 Alonso, F.; Beletskaya, I. P.; Yus, M. *Chem. Rev.* **2004**, *104* , 3079.

42 Lynam, J. M.; Welby, C. E.; Whitwood, A. C. *Organometallics* **2009**, *28*, 1320.

43 Ahlrichs, R.; Baer, M.; Haeser, M.; Horn, H.; Koelmel, C. *Chem. Phys. Lett.*, **1989**, *162*, 165.

44 Arnim M. V.; Ahlrichs, R. *J. Chem. Phys.* **1999**, *111*, 9183.

45 Császár, P.; Pulay, P. *J. Mol. Struct.*, **1984**, *114*, 31.

46 Koga, T.; Kobayashi, H. *J. Chem. Phys.* **1985**, *82*, 1437.

47 Pulay, P. *Chem. Phys. Lett.* **1980**, *73*, 393.

48 Deglmann, P.; May, K.; Furche, F.; Ahlrichs, R. *RI-J Implementation*, **2004**, *384*, 103.

49 Deglmann, P.; Furche, F.; Ahlrichs, R. *Chem. Phys. Lett.* **2002**, *362*, 511.

50 Deglmann, P.; Furche, F. *J. Chem. Phys.* **2002**, *117*, 9535.

51 Treutler, O.; Ahlrichs, R. *J. Chem. Phys.* **1995**, *102*, 346.

52 Eichkorn, K.; Treutler, O.; Oehm, H.; Haeser, M.; Ahlrichs, R. *Chem. Phys. Lett*. **1995**, 240, 283.

53 Eichkorn, K.; Weigend, F.; Treutler, O.; Ahlrichs, R. *Theo. Chem. Acc*. **1997**, 97, 119.

54 Weigend, F. *Phys. Chem. Chem. Phys.* **2006**, *8*, 1057.

Chapter 5:

1. Selegue, J. P. *Organometallics* **1982**, *1*, 217.
2. Cadierno, V., Gimeno, J., *Chem. Rev.* **2009**, *109*, 3512.
3. Bruneau, C., Dixneuf, P. H., Eds. *Metal Vinylidenes and Allenylidenes in Catalysis: From Reactivity to Applications in Synthesis*, **2008**, Wiley VCH: Weinheim, Germany.
4. Selegue, J. P., *Coord. Chem. Rev.* **2004**, 248, 1543.
5. Rigaut, S., Touchard, D., Dixneuf, P. H., *Coord. Chem. Rev.* **2004**, *248*, 1585.
6. Bruce, M. I., *Chem. Rev.* **1998**, *98*, 2797.
7. Cadierno, V., Gamasa, M. P., Gimeno, J., *Eur. J. Inorg. Chem.* **2001**, 571.
8. Touchard, D., Dixneuf, P. H., *Coord. Chem. Rev.* **1998**, *178-180*, 409.
9. Bustelo, E., Jiménez-Tenorio, M., Puerta, M. C., Valerga, P., *Organometallics* **1999**, *18*, 950.
10. Le Lagadac, R., Roman., E., Toupet, L., Müller, U., Dixneuf, P. H., *Organometallics* **1994**, *13*, 5030.
11. Bustelo, E., Jiménez-Tenorio, M., Puerta, M. C., Valerga, P., *Organometallics* **1999**, *18*, 4563.
12. Aneetha, H., Jiménez-Tenorio, M., Puerta, M. C., Valerga, P., *Organometallics* **2003**, *22*, 2001.
13. Cadierno, V., Gamasa, M. P., Gimeno, J., González-Cueva, M., Lastra, E., Borge, J., García-Granda, S., Pérez-Carreño, E., *Organometallics* **1996**, *15*, 2137.
14. Werner, H., Rappert, T., Wiedemann, R., Wolf, J., Mahr, N., *Organometallics* **1994**, *13*, 2721.

15. Bustelo, E., Jiménez-Tenorio, M., Puerta, M. C., Valerga, P., *Eur. J. Inorg. Chem.* **2001**, 2391.

16. Schanz, H-J.; Jafarpour, L.; Stevens, E. D.; Nolan, S. P. *Organometallics* **1999**, *18*, 5187.

17. Fürstner, A.; Guth, O.; Düffels, A.; Seidel, G.; Liebl, M.; Gabor, B.; Mynott, R. *Chem. Eur. J.* **2001**, *7*, 4811.

18. Castarlenas, R.; Dixneuf, P. H. *Angew. Chem. Int. Ed.* **2003**, *42*, 4524.

19. Castarlenas, R.; Vovard, C.; Fischmeister, C.; Dixneuf, P. H. *J. Am. Chem. Soc*. **2006**, *128*, 4079.

20. Rigaut, S., Touchard, D., Dixneuf, P. H., *Coord. Chem. Rev.***2004**, *248*, 1585.

21. Fürstner, A.; Picquet, M.; Bruneau, C.; Dixneuf, P. H. *Chem. Commun.* **1998**, 1315.

22. Picquet, M.; Touchard, D.; Bruneau, C.; Dixneuf, P. H. *New. J. Chem.* **1999**, *23*, 141.

23. Picquet, M.; Bruneau, C.; Dixneuf, P. H. *Chem. Commun.* **1998**, 2249.

24. Sémeril, D.; Le Nôtre, J.; Bruneau, C.; Dixneuf, P. H.; Kolomiets, A. F.; Osipov, S. *New. J. Chem.* **2001**, *25*, 16.

25. Castarlenas, R.; Sémeril, D.; Noels, A. F.; Demnoceau, A, Dixneuf, P. H. *J. Organomet. Chem.* **2002**, *663*, 235.

26. Bruneau, C., Dixneuf, P. H., *Angew. Chem. Int. Ed.* **2006**, *45*, 2176.

27. Castarlenas, R., Fischmeister, C., Bruneau, C., Dixneuf, P. H., *J. Mol. Catal. A: Chem.* **2004**, *213*, 31.

28. Winter, R. F., Záliš, S., *Coord. Chem. Rev.* **2004**, *248*, 1565.

29. Bruce, M. I. *Chem. Rev.* **1991**, *91*, 197.

30. Desiraju, G. R.; Steiner, T. *The Weak Hydrogen Bond: In Structural Chemistry and Biology*; **1999**, Oxford Science Publications.

31. Günther, H., *NMR Spectroscopy: Basic Principles, Concepts and Applications*, 2nd Ed., **1995**, Wiley.

32. Personal communication from T.A.D. Former MS service Technician, University of York.

33. Berke, H. *Z. Naturforsch., B: Anorg Chem., Org. Chem.* **1980**, *35B*, 86.

34. Martín, M.; Gevert. O.; Werner, H. *Dalton Trans.* **1996**, 2275.

35. Bustelo, E., Dixneuf, P. H., *Adv. Synth. Catal.* **2005**, *347*, 393.

36. Bustelo, E., Dixneuf, P. H., *Adv. Synth. Catal.* **2007**, *349*, 933.

37. Datta, S.; Chang, C-L.; Yeh, K-L.; Liu, R-S. *J. Am. Chem. Soc.* **2003**, *125*, 9294.

38. Haak, E. *Eur. J. Org. Chem.* **2007**, 2815.

39. Schmitt, H. J.; Singer, H. *J.Organomet. Chem.* **1978**, *153*, 165.

40. Chen, X.; Xue, P.; Sung, H. H. Y.; Williams, I. D.; Peruzzini, M.; Bianchini, C.; Jia, G. *Organometallics* **2005**, *24*, 4330.

41. Trost, B. M.; Chan, C.; Rühter, G. *J. Am. Chem. Soc.* **1987**, *109*, 3486.

42. Trost, B. M.; Sorum, M. T.; Chan, C.; Harms, A. E.; Rühter, G. *J. Am. Chem. Soc.***1997**, *119*, 698.

43. Daniels, M.; Kirss, R. U. *J. Organomet. Chem.* **2007**, *692*, 1716.

44. Ohshita, J.; Furumori, K.; Matsuguchi, A.; Ishikawa, M. *J. Org. Chem.* **1990**, *55*, 3277.

45. Slugovc, C.; Mereiter, K.; Zobetz, E.; Schmid, R.; Kirchner, K. *Organometallics* **1996**, *15*, 5275.

46. Katayama, H.; Nakayama, M.; Nakano, T.; Wada, C.; Akamatsu, K.; Ozawa, F. *Macromolecules*, **2004**, *37*, 13.

47. Katayama, H.; Yari, H.; Tanaka, M.; Ozawa, F. *Chem. Commun*. **2005**, 4336.

48. Echavarren, A. M.; López, J.; Santos, A.; Montoya, J. *J. Organomet. Chem.* **1991**, *414*, 393.

49. Ohmura, T.; Yorozuya, S-i.; Yamamoto, Y.; Miyaura, N.; *Organometallics* **2000**, *19*, 365.

50. Yi, C. S.; Liu, N. *Organometallics* **1996**, *15*, 3968.

51. Fossatelli, M.; van der Kerk, A. C. T. H. M.; Vasilevsky, S. F.; Brandsma, L. *Tett. Lett.* **1992**, *33*, 4229.

52. Provencal, D. P.; Leahy, J. W. *J. Org. Chem.* **1994**, *59*, 5496.

53. Bruneau, C., Dixneuf, P. H., *Chem. Commun.* **1997**, 1201.

54. Suzuki, T., Tokunaga, M., Wakatsuki, Y., *Tett. Lett.*, **2002**, *43*, 7531.

55. Cadierno, V., García-Garrido, S. E., Gimeno, J., *Adv. Synth. Catal.* **2006**, *348*, 101.

56. Puerta, M. C.; Valerga, P. *Coord. Chem. Rev.* **1999**, *193-195*, 977.

57. Katayama, H., Ozawa, F., *Coord. Chem. Rev*. **2004**, *248*, 1703.

58. Katayama, H., Ozawa, F., Tanaka, M., Yari, H., *Chem. Commun*. **2004**, *248*, 1703.

59. Olivier, C., Kim, B-S., Touchard, D., Rigaut, S., *Organometallics* **2008**, *27*, 509.

60. Bianchini, C., Peruzzini M., Zanobini, F., Frediani, P., Albinati, A., *J. Am. Chem. Soc*. **1991**, *113*, 5453.

61. Bianchini, C., Frediani, P., Masi, D., Peruzzini, M., Zanobini, F., *Organometallics* **1994**, *13*, 4616.

62. Bianchini, C., Innocenti, P., Peruzzini, M., Romerosa, A., Zanobini, F., *Organometallics*. **1996**, *15*, 272.

63. Nolan, S. P., Yang, C., *J. Org. Chem*. **2002**, *67*, 591.

64. Hou, Z., Nishiura, M., Miyayoto, T., Wakatsuki, Y., Yamaki, T., *J. Am. Chem. Soc*. **2003**, *125*, 1184.

65. Trost, B. M., Crawley, M. L., *Chem. Rev*. **2003**, *103*, 2921.

66. Ishii, Y., Hirabayashi, T., Sakaguchi, S., *Adv. Synth. Catal*. **2005**, *347*, 872.

67. Yi, C. S., Jiu, N., *Organometallics* **1998**, *17*, 3158.

68. Katayama, H., Ozawa, F., Taniguchi, K., Wada, C., *Organometallics* **2002**, *21*, 3285.

69. Wakatsuki, Y., Yamazaki, H., Kumegawa, N., Satoh, T., Satoh, J. Y., *J. Am. Chem. Soc*. **1991**, *113*, 9604.

70. Mitsudo, T.; Hori, Y.; Yamazaki, Y.; Watanabe, Y. *J. Org. Chem.* **1987**, *52*, 2230.

71. Devanne, D.; Ruppin, C.; Dixneuf, P. H. *J. Org. Chem.* **1988**, *53*, 925.

72. Bruneau, C.; Kabouche, Z.; Neveux, M.; Seiller, B.; Dixneuf, P. H. *Inorg. Chim. Acta.* **1994**, *222*, 154.

73. Darcel, C.; Bruneau, C.; Dixneuf, P. H.; Neef, G. *J. Chem. Soc. Chem. Commun.* **1994**, 333.

74. Costin, S.; Rath, N. P.; Bauer, E. B. *Adv. Synth. Catal.* **2008**, *350*, 2414.

75. Bruneau, C. *Anti*-Markovnikov Additions of *O*-, *N*-, *P*-Nucleophiles to Triple Bonds with Ruthenium Catalysts (Chapter 10) *Metal Vinylidenes and Allenylidenes in Catalysis: From Reactivity to Applications in Synthesis*, (Bruneau, C., Dixneuf, P. H., Eds.) **2008**, Wiley VCH: Weinheim, Germany.

76. Hiett, N. P.; Lynam, J. M.; Welby, C. E.; Whitwood, A. C. *J. Organomet. Chem.* **2011**, *696*, 378.

77. Comparison with authentic sample of diphenylethylene.

78. Comparison with simuated spectrum provided by Scifinder.

79. Pondey, S. K., Greene, A. E., Poisson, J-F., *J. Org. Chem.* **2007**, *72*, 7769.

80. Styrene: ALDRICH online NMR library.

81. Methylenecyclopentane: ALDRICH online NMR library.

82. Methylenecyclohexane: ALDRICH online NMR library.

83. Cho, B. P., *Tett. Lett.* **1995**, *36*, 2403.

84. Ethene: Comparison with simulated NMR spectrum in ALDRICH online NMR library.

85. Macdonald, B. S., Sykes, P. J., Adhikary, P. M., Harkness, R. A., *Steroids* **1971**, *18:6*, 753.

86. Templeton, J. F., Jackson, C. J. C., *Steroids* **1983**, *41*, 485.

87. Shimizu, I., Sugiura, T., Tsuji, J., *J. Org. Chem.* **1985**, *50*, 537.

88. Pettigrew, J. D., Cadieux, J. A., So, S. S. S., Wilson, P. D., *Org. Lett.* **2005**, *7*, 467.

89. Ye, J., Ge, J., Chen, X., Zhao, Z., Lu, P., *Tetrahedron* **2007**, *63*, 11040.

Chapter 6:

1. Selegue, J. P., *Organometallics* **1982**, *1*, 217.
2. Cadierno, V., Gimeno, J., *Chem. Rev.* **2009**, *109*, 3512.
3. Bruneau, C., Dixneuf, P. H., Eds. *Metal Vinylidenes and Allenylidenes in Catalysis: From Reactivity to Applications in Synthesis*, **2008**, Wiley VCH: Weinheim, Germany.
4. Selegue, J. P., *Coord. Chem. Rev.* **2004**, 248, 1543.
5. Rigaut, S., Touchard, D., Dixneuf, P. H., *Coord. Chem. Rev.* **2004**, *248*, 1585.
6. Bruce, M. I., *Chem. Rev.* **1998**, *98*, 2797.
7. Cadierno, V., Gamasa, M. P., Gimeno, J., *Eur. J. Inorg. Chem.* **2001**, 571.
8. Touchard, D., Dixneuf, P. H., *Coord. Chem. Rev.* **1998**, *178-180*, 409.
9. Bustelo, E., Dixneuf, P. H., *Adv. Synth. Catal.* **2005**, *347*, 393.
10. Bustelo, E., Dixneuf, P. H., *Adv. Synth. Catal.* **2007**, *349*, 933.
11. Hocking, R. K.; Hambley, T. W. *Organometallics* **2007**, 26, 2815.
12. Cannadine, J. C.; Hill, A. F.; White, A. J. P.; Williams, D. J.; Wilton-Ely, J. D. E. T. *Organometallics* **1996**, *15*, 5409.
13. Hill, A. F.; White, A. J. P.; Williams, D. J.; Wilton-Ely, J. D. E. T. *Organometallics* **1998**, *17*, 4249.
14. Matas, L.; Muniente, J.; Ros, J.; Alvarez-Larena, Á.; Piniella, J.F.; *Inorg. Chem. Commun.* **1999**, *2*, 364.
15. Roper, W. R.; Taylor, G. E.; Water, J. M.; Wright, L. J. *J. Organomet. Chem.* **1979**, *182*, C46.
16. Sanford, M. S.; Valdez, M. R.; Grubbs, R. H. *Organometallics* **2001**, *20*, 5455.

17. Shaffer, E. A.; Chen, C-L.; Beatty, A. M.; Valente, E. J.; Schanz, H-J. *J. Organomet. Chem.* **2007**, *692*, 5221.

18. Kawano, H.; Masaki, Y.; Matsunaga, T.; Hiraki, K.; Onishi, M.; Tsubamara, T. *J. Organomet. Chem.* **2000**, *601*, 69.

19. Esteruelas, M. A.; Lahoz, F. J.; López, A. M.; Oñate, E.; Oro, L. A. *Organometallics* **1994**, *13*, 1669.

20. Werner, H.; Daniel, T.; Mahr, N.; Braun, T. *Organometallics* **1993**, *12*, 1475.

21. Yi, C. S.; Gao, R. *Organometallics* **2009**, *28*, 6585.

22. Comparison with an authentic sample of β-styryl acetate.

23. Mitchell, R. W.; Spencer, A.; Wilkinson, G. *J. Chem. Soc. Dalton Trans.* **1973**, 846.

24. Kikukawa, K.; Kono, K.; Nagira, K.; Wada, F.; Matsuda, T. *J. Org. Chem.* **1981**, *46*, 4413.

25. Herzberg, G., *Molecular Spectra & Molecular Structure Vol II – Infrared and Raman Spectra of Polyatomic Molecules*, **1991** reprint of 1945 ed., Kreiger Publishing Company.

26. Jordan, R. B., *Reaction Mechanisms of Inorganic and Organometallic Systems*, 3rd Ed., **2007**, Oxford University Press.

27. Günther, H., *NMR Spectroscopy: Basic Principles, Concepts and Applications*, 2nd Ed., 1995, Wiley.

28. Kuzmic, P. (1996) *Anal. Biochem.* **237**, 260.

29. Nishibayashi, Y.; Milton, M. D.; Inada, Y.; Yoshikawa, M.; Wakiji, I.; Hidai, M.; Uemura, S. *Chem. Eur. J.* **2005**, *11*, 1433.

30. Lynam, J. M.; Welby, C. E.; Whitwood, A. C. *Organometallics* **2009**, *28*, 1320.

31. Comparison with an authentic sample of acetic anhydride.

32. Comparison to data of 4-methoxyphenylacetate: Qiu, R.; Zhang, G.; Ren, X.; Xu, X.; Yang, R.; Luo, S.; Yin, S. *J. Organomet. Chem.* **2010**, *695*, 1182.

33. *N*,*N*-dimethylacetamide: Comparison with simulated NMR spectrum in ALDRICH online NMR library.

34. Hiett, N. P.; Lynam, J. M.; Welby, C. E.; Whitwood, A. C. *J. Organomet. Chem.* **2011**, *696*, 378.

Chapter 7:

1. Weyershausen, B.; Dötz, K. H. *Eur. J. Inorg. Chem.* **1999**, 1057.
2. Bruce, M. I.; Swincer, A. G.; Thomson, B. J.; Wallis, R. C.; *Aust. J. Chem.* **1980**, *33*, 2605.
3. Dötz, K. H.; Sturm, W. *Organometallics* **1987**, *6*, 1424.
4. Bianchini, C.; Marchi, A.; Mantovani, N.; Marvelli, L.; Masi, D.; Peruzzini, M.; Rossi, R. *Eur. J. Inorg. Chem.* **1998**, 211.
5. Grime, R. W.; Helliwell, M.; Hussain, Z. I.; Lancashire, H. N.; Mason, C. R.; McDouall, J. J. W.; Mydlowski, C. M.; Whiteley, M. W. *Organometallics* **2008**, *27*, 857.
6. Marvelli, L.; Mantovani, N.; Marchi, A.; Rossi, R.; Brugnati, M.; Peruzzini, M.; Barbaro, P.; de los Rios, I.; Bertolasi, V. *Dalton Trans.* **2004**, 713.
7. Beddoes, R. L.; Grime, R. W.; Hussain, Z. I.; Whiteley, M. W. *J. Chem. Soc. Dalton. Trans.* **1996**, 3893.
8. Pavlik, S.; Mereiter, K.; Puchberger, M.; Kirchner, K. *J. Organomet. Chem.* **2005**, *690*, 5497.
9. Gamasa, M. P.; Gimeno, J.; Martín-Vaca, B. M.; Isea, R.; Vegas, A. *J. Organomet. Chem.* **2002**, *651*, 22.
10. Marchal, E.; Uriac, P.; Legouin, B.; Toupet, L.; van deWeghe P. *Tetrahedron*, **2007**, *63*, 9979.
11. Geier, M. J.; Vogels, C. M.; Decken, A.; Westcott, S. A. *Eur. J. Inorg. Chem.* **2010**, 4602.
12. Varela-Fernández, A.; García-Yebra, C.; Varela, J. A.; Esteruelas, M. A.; Saá, C.; *Angew. Chem. Int. Ed*. **2010**, *49*, 4278.
13. Jiménez-Tenorio, M., Puerta, M. C., Valerga, P., Moreno-Dorado, F.J.; Guerra, F. M.; Massanet, G. M. *Chem. Commun.* **2001**, 2324.

14. Liu, P. N.; Su, F. H.; Wen, T. B.; Sung, H. H.-Y.; Williams, I. D.; Jia, G. *Chem. Eur. J.* **2010**, *16*, 7889.

15. Seiller, B.; Bruneau, C.; Dixneuf, P. H. *J. Chem. Soc. Chem. Commun.* **1994**, 493.

16. Beddoes, R.L.; Grime, R. W.; Hussain, Z. I.; Whiteley, M. W. *J. Organomet. Chem.* **1996**, *526*, 371.

17. Leung,W-H.; Chan,E. Y. Y.; Williams,I D.; Wong W-T. *Organometallics* **1997**, *16*, 3234.

18. Liu, P.N.; Wen, T. B.; Ju, K. D.; Sung, H. H.-Y.; Williams, I. D.; Jia, G. *Organometallics* **2011,** *30*, 2571.

19. Dolomanov, O. V.; Bourhis, L. J.; Gildea, R. J.; Howard J. A. K.; Puschmann, H. *J. Appl. Cryst. 2009*, **42**, 339.

Chapter 8:

1. Richter-Addo, G. B.; Legzdins, P. *Metal Nitrosyls*, **1992**, Oxford University Press.
2. Hedburg, L.; Hedburg, K.; Satija, S. K.; Swanson, B. I. *Inorg. Chem.* **1985**, *24*, 2766.
3. Antonova, A.B.; Kolobova, N.E.; Petrovsky, P.V.; Lokshin B.V.; Obezyuk, N.S. *J. Organomet. Chem.* **1977**, *137*, 55.
4. Moigno, D.; Callejas-Gasper, B.; Gil-Rubio, J.; Werner, H.; Kiefer, W. *J. Organomet. Chem*. **2002**, *661*, 181.
5. Kostić, N. M.; Fenske, R. F. *Organometallics* **1982**, *1*, 974.
6. Elsenbroich, C. *Organometallics*, **2006**, Wiley-VCH.
7. Bruce, M. I. *Chem. Rev*. **1991**, *91*, 197.
8. Matas, L.; Muniente, J.; Ros, J.; Alvarez-Larena, Á.; Piniella, J. F. *Inorg. Chem. Commun.* **1999**, *2*, 364.
9. Sfinchez-Delgado, R. A.; Thewalt, U.; Valencia, N.; Andriollo, A.; Márquez-Silva, R-L.; Puga, J.; Schollhorn, H.; Klein, H-P.; Fontal, B. *Inorg. Chem.* **1986**, *25*, 1097.
10. Czech, P. T.; Xe, X.-Q.; Fenske, R. F. *Organometallics* **1990**, *9*, 2016.
11. Robinson, S.D., Uttley, M.F., *J. Chem. Soc. Dalton. Trans.*, **1973**, 1912.
12. Hocking, R. K.; Hambley, T. W. *Organometallics* **2007**, 26, 2815.